THE UNIVERSITY
of EDINBURGH

Mechanisms responsible for 'scarless' tissue repair in the endometrium

Phoebe Maud Kirkwood

Medical Research Council

Centre for Inflammation Research

The Queen's Medical Research Institute

Edinburgh, EH16 4TJ

Thesis submitted to the University of Edinburgh for the degree of

Doctor of Philosophy

August 2018

Declaration

I, Phoebe Maud Kirkwood declare that this thesis was composed by myself and the studies presented within were completed unaided except where acknowledgement is made by reference. The work described in this thesis has not been previously accepted for, or is not currently being submitted for any other qualification.

Phoebe Maud Kirkwood

August 2018.

Acknowledgements

I have absolutely loved my PhD which would not have been possible without the endless support and enthusiasm from my supervisor Philippa Saunders. Thank you Philippa for taking me on and designing such an exciting and fruitful research project with me, it has been an excellent learning experience and I have been so lucky to have you guiding me. You truly are an inspiration and I hope I have done you proud as a student.

Everyone in the Saunders lab group has contributed to my PhD in one way or another whether it be in helping with an experiment, discussing my results or just making it a joy to be in the lab. Thank you to Frances, Arantza, Yanni, Pete and past members Fiona and Bianca. A very special thanks goes to my Olympia who has helped me with every single mouse experiment, you have truly been my saving grace, especially on FACS Tuesdays! Lastly, to Doug who has been the most incredible mentor I could have ever hoped for, helping me with every aspect of my PhD life and making sure I achieved as much as I could. Doug you have been such an inspiration to me, you are a fountain of knowledge, a brilliant scientist and one of the most encouraging people I know. I cannot thank the Saunders team enough.

I have thoroughly enjoyed the Tissue Repair PhD and would like to thank the course organisers Stuart Forbes and Caterina Becker for giving me a place on the programme, and the management team Kelly and Marieke for keeping me on track over the past four years. I would like to thank my Tissue Repair peers who have made the journey all the more enjoyable; Annalucia, Tess, Chandrika and especially Isaac. Lucy and Tess thank you for our fun times outside of the lab especially our night's out where the wine truly flowed! Isaac you have been my partner in PhD crime since day 1 when we were paired together for the PCR training and our friendship has blossomed through a love of bake off, partying, eating lunch (!), badly-done acrobatic tricks, ridickulous memorabilia and of course pericytes! I could not have made it through the PhD without you and I will always treasure the fun times– especially the never ending weeks in the library writing up our theses! Thank you to all the other Tissue Repairers who are excellent students and fantastic scientists.

Thank you to my second supervisor Neil Henderson for giving me invaluable guidance through the world of transgenic mouse lines and sequencing technologies. Your input took my project to new and exciting levels and your patience and encouragement has been so much appreciated over the years. To those in Neil's group who have also helped with various aspects of my project; thank you Jamie, Ross and Beth.

Thank you to my third supervisor Jane Norman who showed me support throughout and to Lesley Forrester and Jurgen Swarze who were on my Thesis Committee and gave me excellent advice regarding both my PhD research and my future career. A huge thank you to everyone in the CIR who shared resources and expertise expanding my research horizons: Steve, Jenna, Calum and Prakash, and to all the PhD students who were a constant source of support. A special thanks to my Lady Lobster Jenni. Jenni you are incredible and truly enriched my latter two years of the PhD, showing me what it means to be an excellent scientist and still live the crazy life outside the lab!

I would like to acknowledge the technical help from Will Ramsey, Shonna Johnston and Mari Patterson who helped me design and carry out my flow cytometry and FACS experiments, your efforts are very much appreciated. To Pam and Linda for your support and patience regarding PCR and Labchip techniques and to Doreen Chambers at the Western General for allowing me to use the Maxwell extractor. To those at Edinburgh Genomics who supported my sequencing studies from planning through to bioinformatics, with which I would have struggled otherwise; thank you Colin Sharp, Jonathan Manning, Frances Turner and Donald

Dunbar. To the technicians in the animal house facility who have supported my animal work: Sandra, Duncan, Will, John and Larraine you have been a great help. I would especially like to thank Sandra for looking after my animal colonies so well, providing me will the best advice on how to manage them and for becoming a friend who brightened up every single trip to the animal house. I would also like to mention that none of this work would have been possible without the mice and I thank them for their contribution to my research.

I would like to take a moment to thank my incredible family, each and every one of whom have contributed to my success. My parents supported me through University and have given me the richest life possible, always encouraging me to grab every opportunity; thank you Mummy and Daddy for everything. To my older sisters Harriet, Matilda and Jemima, you have been amazing role models, thank you for always being there to help solve my problems and pick me up when things got tough. Thank you to my brothers Arthur and Toby who have made my time in Edinburgh really fun and well-protected! My beautiful nieces Maisie, Clodah and my god-daughter Arrietty for being the most delightful little girls and providing me with a childish escape from the stresses of grown-up life.

To my absolutely wonderful little sister Augusta who has been with me through thick and thin, experiencing everything life has to offer and bringing sunshine into each and every day. Thank you Gussie for always showing interest in my research, offering a helpful ear when I had presentations to practise and creating beautiful schematics with your artistic flare. Thank you for keeping me sane during the writing months and bringing me endless treats: blueberry cheesecake Frappuccino's, chocolate eclairs, coffees, peanut M&Ms and your fantastic sense of humour.

A very special thank you goes to my lovely Tree-ancé who I met on the first night of University and has been by my side ever since supporting me through all of my ventures. Andy you are truly my best friend and your constant care and encourangement has allowed me to achieve my PhD dreams. I know it has been a struggle at times but if we can survive the PhD then our marriage should be a breeze, I love you and I cannot wait to marry you!

I would also like to thank best friend Lauren who I also met 8 years ago at the induction to our undergraduate course here in Edinburgh. Not only did you make the four years of 'Medical Sciences' a complete joy you have carried me through my PhD while tackling your own in Dundee, and I will forever be grateful for the countless days together celebrating our successes and navigating our difficulties. You are the most inspirational and hard working person I know and you deserve every success in the future.

Finally, thank you to my examiners who are about to read this thesis. I truly hope you enjoy reading it as much as I have enjoyed my time researching and generating this data.

Thank you.

Dedication

This thesis is dedicated to Mummy, without whom I could not have come so far in academia and life. She has supported me throughout every venture and shows endless enthusiasm about my research. This thesis would not have been written if Mummy hadn't been there for me, always encouraging me to do my best and follow my dreams.

Thank you Mummy for your support, encouragement and love, you are the most important person in my life and I hope I have made you proud.

Abstract

The endometrium is the inner lining of the uterine cavity, composed of distinct epithelial and stromal cell compartments with the latter containing fibroblasts, a vascular compartment and fluctuating populations of immune cells. The endometrium is a highly dynamic tissue that undergoes cycles of proliferation and stromal cell differentiation (decidualisation) followed by tissue shedding (menstruation) and rapid repair/remodelling, all under control of fluctuating concentrations of steroid hormones secreted from the ovaries. This is known as the menstrual cycle.

In response to the 'injury' inflicted as a consequence of decidual breakdown and shedding, the endometrium exhibits a unique capacity to restore tissue architecture by rapid tissue repair. This repair process is tightly regulated to ensure that the endometrium heals consistently every month throughout a woman's reproductive lifespan, without the accumulation of fibrotic scar tissue which could have a negative impact on fertility.

The initiation of menstruation is triggered by the withdrawal of progesterone as a consequence of the demise of the corpus luteum within the ovaries which precipitates an increase in production of inflammatory mediators, focal hypoxia and activation of matrix metalloproteinase enzymes culminating in endometrial shedding. In contrast the cellular and molecular mechanisms responsible for the rapid and scar-free tissue repair of endometrium remain poorly understood. Parallels can be drawn between the repair process of the endometrium and that of the foetal skin and oral mucosa which also exhibit 'scarless' healing, including rapid reepithelialisation, widespread cellular proliferation and migration and a short time to wound closure. However endometrial repair also shares key features of the wound healing experienced by adult tissues that exhibit scarring including extensive angiogenesis and a substantial inflammatory response. The endometrium appears to be unique, fitting in a gap between tissues that typically undergo 'scarless' or 'scarring' tissue repair.

In women, endometrial shedding is considered an inflammatory event and the culmination of a cascade of inflammatory signals result in the accumulation of a diverse population of immune cells within the tissue. Whilst we believe immune cells play a key role in regulating spatial and temporal tissue breakdown and shedding their

role in repair and restoration of tissue homeostasis remains poorly understood. One process essential for endometrial repair is restoration of the luminal epithelial cell layer (re-epithelialisation) and imaging studies have demonstrated that this appears not only to be rapid but also to occur synchronously with tissue degeneration and shedding. Re-epithelialisation was previously thought to be governed by proliferation and migration of glandular epithelial cells in the basal (unshed) tissue compartment, however new data suggest a role for trans-differentiation of stromal cells into epithelial cells which merits further investigation. In addition to role(s) for immune and stromal cells in regulation of endometrial tissue function, a role for somatic stem/progenitor cells capable of differentiating into mature endometrial cells to regenerate the tissue has also been claimed.

In summary, whilst progress has been made in understanding the processes governing endometrial decidualisation, breakdown and shedding the regulation and roles of the different cell types that participate in scar-free repair of the tissue remain poorly defined. The studies in this thesis set out to address this gap by addressing three key aims:

Aim 1. To investigate the phenotype and location of immune cell populations during scarless tissue repair.

Aim 2. To identify and characterise a putative population of mesenchymal stem/progenitor cells in endometrium.

Aim 3. To investigate the contribution of putative mesenchymal stem/progenitor cells to endometrial tissue repair.

The aims were addressed using a recently refined and extensively characterised mouse model in which endometrial shedding ('menstruation') and repair occurs over a 48 hour period following removal of a progesterone stimulus. Importantly the Saunders' group have already demonstrated that this model recapitulates the key features of human menses including overt vaginal bleeding, immune cell influx, tissue necrosis, transient hypoxia, re-epithelialisation and most importantly simultaneous breakdown and repair. Uterine tissues recovered 12, 24, and 48hrs after removal of progesterone and were investigated using immunohistochemistry (spatial organisation), flow cytometry (quantitation of cell subpopulations), FACS sorting (isolation of

subpopulations) and molecular profiling (qPCR, RNAseq and single cell sequencing) with additional insights from bioinformatic analysis.

To address Aim 1 endometrial shedding and repair was studied in Macgreen® mice: in this transgenic line all the cells of the mononuclear phagocyte lineage (monocytes, monocyte-derived macrophages) express green fluorescent protein. Immunohistochemistry revealed striking spatio-temporal changes in both numbers and location of GFP+ cells during endometrial breakdown and repair, the most prominent changes occurring 24hrs after removal of progesterone. Flow Cytometry quantified several immune cell populations with a significant increase in GFP+ cells during repair, the majority of which were GR1+F4/80- (inflammatory monocytes). These novel data provided compelling evidence to support a role for inflammatory monocytes in endometrial repair and provide the platform for future studies on the role of these cells in scarless healing.

To address Aims 2 and 3 *Pdgfrβ-BAC-eGFP*® transgenic mice in which GFP was expressed under control of promoter elements of the *Pdgfrβ* gene was used to identify putative mesenchymal progenitor cells and investigate their role in endometrial repair. GFP+ cells were located exclusively within the endometrial stromal compartment and examination of tissue sections revealed that two subpopulations could be distinguished based on the both the intensity of GFP and expression of CD146 (Mcam). Characterisation by immunohistochemistry, flow cytometry and qPCR identified a GFP^{bright} subpopulation located adjacent to CD31+ endothelial cells that were classified as pericytes based on location and phenotype (NG2+, CD146+, CD31-).

When menstruation was stimulated in *Pdgfrβ*-BAC-eGFP® mice detailed analysis using flow cytometry revealed an increase in the perivascular pericyte subpopulation during active healing (24hrs) and also identified a new previously unidentified sub-population of GFP+ cells which had a unique phenotype during repair. Evidence that GFP+ cells contribute to restoration of epithelial repair was obtained with an increase in expression of the epithelial cell marker EpCAM and GFP+ cells in the renewed epithelial cell layer. RNAseq and single cell sequencing combined with bioinformatics complemented these findings by identifying novel changes in gene expression in both endometrial fibroblasts and pericyte populations consistent with induction of novel

pathways and trans-differentiation of stromal cells by a mesenchymal-to-epithelial transition (MET).

In conclusion, using a mouse model of endometrial breakdown and repair a heterogeneous population of myeloid cells and a putative population of endometrial progenitors (pericytes) have been characterised, quantified and novel changes in gene expression identified. Adaptation of these cell types to the insult of endometrial shedding appears to play a key role in temporal and spatial regulation of rapid, scar-free endometrial tissue repair. These novel findings may inform the development of new approaches to treating gynaecological disorders associated with aberrant endometrial repair such as heavy menstrual bleeding, Asherman's syndrome and endometriosis as well as other disorders associated with excessive fibrosis and scar formation.

Lay Abstract

The endometrium is a complex multicellular tissue that forms the inner lining of the womb (uterus). During each menstrual cycle the endometrium changes in preparation for a the arrival of a new embryo however if a woman does not get pregnant this tissue is no longer required so it breaks down and is shed from the uterus at menstruation an event experienced by the woman as her 'period'. Thus 'periods' are the result of endometrial tissue loss resulting in a bloody 'wound' inflicted on the luminal layer of endometrium not dissimilar to wounds found elsewhere in the body following serious injury. However unlike other tissues such as the skin, that respond to a wound by developing a scar, the endometrium has an amazing ability to completely and rapidly repair over just a few without the accumulation of any scar tissue. This is incredible and unparalleled scarless healing process may happen ~400 times during a woman's reproductive life and is of course absolutely essential to the continued reproductive success of the uterus… and our species!

Although the hormonal regulation of the menstrual cycle has been the focus of many scientific studies, the precise factors that ensure scarless healing of the endometrium are not well understood. In the current study, the contribution that two types of cells play in endometrial tissue repair were investigated – these were immune cells and a putative population of endometrial progenitor (stem) cells called pericytes. We selected these two cell types because immune cells are claimed to be instrumental in clearing up debris in other injured tissues and their numbers have been reported to increase during menstruation. Stem cells are specialised cells that can transform into any other cell types; tissue resident stem/progenitors may provide a tissue with a reservoir from which it can replenish lost cells. Stem cells have been identified in the endometrium although their identity has also been questioned and their contribution to scarless repair remains the subject of debate.

In the lab we artificially induced menstruation (periods) in mice that were genetically modified so that immune cells and stem cells were labelled for ease of identification. In the mice we documented dynamic, time dependent changes in the populations of immune cells during scarless healing with a striking influx in one particular population known as monocytes during active healing. A population of putative endometrial stem

cells was identified close to the blood vessels and not only did we unexpectedly find an increase in their numbers during repair but also evidence to show that these cells have the ability to transform into difference types of cells to help replenish the lost tissue and return the endometrium to its normal state.

In summary novel findings obtained during these studies revealed that both immune cells and stem cells have fundamental roles to play in scarless endometrial healing. We are excited by these results because we believe this new knowledge can open the door to developing new treatments for gynaecological conditions where repair does not work properly and fertility is compromised, but also for other tissues of the body where excess scar formation is a huge clinical problem.

Publications relating to this thesis

Cousins, F. L. & Kirkwood, P. M., Saunders, P. T. & Gibson, D. A. (2016) Evidence for a dynamic role for mononuclear phagocytes during endometrial repair and remodelling. *Sci Rep,* 6, 36748 (Appendix 6).

Cousins, F.L., Kirkwood, P. M., Murray, A. A., Collins, F. Gibson, D.A. & Saunders, P.T (2016) Androgens regulate scarless repair of the endometrial "wound" in a mouse model of menstruation. *FASEB J,* 30, 2802-11.

Publications during this thesis

Haideri. S.S., McKinnon, A.C., Taylor, A.H., Kirkwood, P.M., Starkey-Lewis, P.J., O'Duibhir, E., Vernay, B., Forbes, S. & Forrester, L.M. (2017) Injection of embryonic stem cell derived macrophages ameliorates fibrosis in a murine model of liver injury. *Npj Regenerative Medicine,* 2, 14

Presentations relating to this thesis

Immune cell dynamics in endometrial tissue breakdown and repair. Oral and poster presentation at the ENII 11th Annual Summer School on Advanced Immunology, Sardinia, May 2016.

Identification of mesenchymal progenitor cells in endometrial tissue. Oral presentation at Society for Reproduction and Fertility (SRF) Annual Meeting, Winchester, July 2016. Student prize session.

Characterisation of mesenchymal progenitor cells and their role in endometrial tissue repair. Oral and poster presentation at the Fertility Annual Conference, Edinburgh, January 2017.

Characterisation of uterine macrophage populations and their role in endometrial breakdown and repair. Poster presentation at the Society for

Reproductive Investigation (SRI) 64th Annual Scientific Meeting, Orlando, Florida, March 2017.

Profiling endometrial pericytes reveals roles in endometrial repair. Invited oral presentation at the Society for Reproductive Investigation (SRI) 64th Annual Scientific Meeting, Orlando, Florida, March 2017.

"And when I get that feeling, I wan't scarless healing". Pint of Science, science communication event, Edinburgh, May 2017.

Characterisation of endometrial progenitor cells and their role in 'scarless' endometrial repair and regeneration. Oral and poster presentation at the British Inflammation Research Association (BIRAS) Fibrosis: Mechanisms and New Treatments conference, Alderly Park, Manchester, March 2018. Young Investigator Award.

Characterisation of uterine macrophage populations and their role in endometrial repair and remodelling: a comparison of three different transgenic mouse lines. Oral presentation at Macrophages: a cell for all seasons Satellite Meeting, Edinburgh, April 2018.

"The secrets of scarless healing". University of Edinburgh 3 Minute Thesis competition, Edinburgh, April 2018 College of Medicine and Veterinary Medicine– First runner up, June 2018 UoE Final- Winner.

Characterisation of endometrial progenitor cells and their role in 'scarless' endometrial repair. Oral presentation at the EMBO Workshop: The molecular and cellular basis of regeneration and tissue repair, Malta, September 2018.

Table of Contents

List of Figures

Figure 5-14. Ranked gene list generated using GSEA based on transcript abundance, as determined by CPM, in mesenchymal cells (total GFP+ cells from Pdgfrβ-BAC-eGFP uterus) in naïve and repairing samples.

Figure 5-15. Expression of genes upregulated in GFP+ mesenchymal cells generated from Pdgfrβ-BAC-eGFP endometrial tissue during homeostasis (naïve) and repair (24hrs; repairing) to validate NGS results.

Figure 5-16. Expression of genes upregulated in in isolated subpopulations of mesenchymal cells (GFP^{dim} stromal fibroblasts and GFP^{bright} pericytes) generated from Pdgfrβ-BAC-eGFP endometrial tissue during homeostasis (naïve) and repair (24hrs; repairing).

Figure 5-17. LabChip GX Touch analysis of cDNA quantity and quality for samples generated for single cell sequencing by Edinburgh Genomics.

Figure 5-18. Visualisation of the single cell dataset naïve uterine mesenchymal cells.

Figure 5-19. Expression of Pdgfrβ in naïve uterine mesenchymal cells.

Figure 5-20. Heat map of differentially expressed genes that distinguish five mesenchymal cell clusters in naïve uterine tissue as determined by single cell sequencing.

Figure 5-21. tSNE plots exhibiting the distribution of differentially expressed genes that distinguish each cell cluster in the single cell sequencing dataset of naïve endometrial mesenchyme (5 clusters as outlined in Figure 5-18).

Figure 5-22. Hypothesised phenotypes of each cell cluster identified in the mesenchyme of the naïve mouse endometrium based on differentially expressed genes.

Figure 5-23. Cluster analysis based on Library ID separating mesenchymal cells from naïve (orange) and repairing (blue) uterine tissue.

Figure 5-24. Cluster analysis based on DE gene expression profiles of mesenchymal cells from both naïve and repairing uterine tissue.

Figure 5-25. Expression of Pdgfrβ mapped onto the t-SNE plot of mesenchymal cells fron naïve and repairing uterine tissue.

Figure 5-26. Heat map of differentially expressed genes that distinguish the nine cell clusters in the aggregate file containing both naïve and repairing mesenchyme single cell datasets.

Figure 5-27. tSNE plots exhibiting the distribution of genes used to identify different cell types present in the naïve endometrial mesenchyme (Figure 5-21) amongst cell clusters in the repairing endometrial mesenchyme.

Figure 5-28. Hypothesised phenotypes of each cell cluster identified in the aggregate file containing both naïve and repairing single cell datatsets of endometrial mesenchyme.

Figure 5-29. The expression of differentially expressed genes that distinguish cluster 5 from all other cell clusters in the aggregate file containing both naïve and repairing single cell datasets of endometrial mesenchyme.

List of Tables

Table 5-4. Top 20 most significantly upregulated genes in repairing samples when compared to naïve samples as determined FDR <0.05. Table displays the mean CPM for each gene in naïve and repairing tissues and the associated LogFC and p-value.

Table 5-5. Top 20 most significantly downregulated genes in repairing samples when compared to naïve samples as determined by FDR <0.05, Table displays the mean CPM for each gene in naïve and repairing tissues and the associated LogFC and p-value.

Table 5-6. Gene Ontology associated with the top 100 up- and down-regulated genes in mesenchymal cells during endometrial repair, fold enrichment scores and associated gene list for each term.

Table 5-7. List of highly expressed genes that were significantly upregulated by mesenchymal cells (total GFP+ cells from *Pdgfrβ-BAC-eGFP* uterus) in repairing samples when compared to naïve samples as determined by LogFC (>2) in mean counts per million (CPM).

Table 5-8. Basic statistics of single cell sequencing data generated for total GFP+ cells isolated from naïve and repairing Pdgfrβ-BAC-eGFP uterine tissue using Cellranger (by Frances Turner). Number of reads, estimated cell number, total genes detected, mean reads per cell, median genes per cell and sequencing saturation values all exceeded threshold requirements, indicating the success of the sequencing.

Table 5-9. Gene Ontology associated with the top 100 upregulated genes in mesenchymal cell types during endometrial repair.

Abbreviations

ACK	Ammonium Chloride Potassium
ACTB	Beta-actin
ANOVA	Analysis of variance
AP	Alkaline phosphatase
AR	Androgen receptor
Arg1	Arginase 1
ARKO	Androgen receptor knock out
AU	Arbitary units
BAC	Bacterial Artificial Chromosome
bFGF	Basic fibroblast growth factor
BM	Bone marrow
BSA	Bovine serum albumin
CC3	Cleaved caspase 3
CCL	Chemokine (C-C motif) ligand
cDNA	Complementary DNA
CFU	Colony forming unit
CL	Corpus luteum
CNS	Central nervous system
COX2	Cyclooxygenase 2
CPM	Counts per million
CSF1	Macrophage colony stimulating factor 1
CSF1R	Colony stimulating factor receptor 1
CSFCS	harcoal stripped foetal calf serum
Ct	Threshold cycle
CXCL	The chemokine (C-X-C motif) ligand 1
D	Dioestrus
DAB	3,3'-diaminobenzidine
DAPI	4', 6-diamidina-2-phenylindole
DC	Dendritic cell
ddh20	Distilled water
DHT	Dihydrotestosterone
DNA	Deoxyribonucleic acid
E2	β-oestradiol
ECM	Extracellular matrix
EDTA	Ethylenediaminetetraacetic acid
eGFP	Enhanced green fluorescent protein
EMT	Epithelial to mesenchymal transition
EpCAM	Epithelial cell adhesion molecule
ER	Oestrogen receptor
ES	Enrichment score
Fabpi	Fatty acid binding protein
FACS	Fluorescence activated cell sorting
FAK	Focal adhesion kinase
FAM	6 carboxy-fluorescein
FBS	Foetal bovine serum

FMO	Fluorescence minus one
FMT	Fibroblast to myofibroblasts transition
FOV	Field of view
FSH	Follicle stimulating hormone
GEM	Gel bead in Emulsion
GFP	Green fluorescent protein
GnRH	Gonadotrophin releasing hormone
GO	Gene ontology
GOI	Gene of interest
GR	Glutocorticoid receptor
H&E	Haematoxylin and Eosin
HCL	Hydrocloric acid
HIF1α	Hypoxia inducible factor 1α
HMB	Heavy menstrual bleeding
HotShot	Hot Sodium Hydroxide and Tris method
HRP	Horseradish peroxidase
ICC	Immunocytochemistry
IFNg	Interferon gamma
IGFBP	Insulin growth factor binding protein
IHC	Immunohistochemistry
IL	Interleukin
IP	Intraperitoneal
IVF	In vitro fertilisation
LEV	Low elution volume
LH	Leutinising hormone
LRC	Label retaining cell
M	Metoestrus
MARKO	Macrophage androgen receptor knock out
MC	Mast cell
MCAM	Melanoma cell adhesion molecule
MET	Mesenchymal to epithelial transition
MHC	Major histocompatibility complex
MIF	Macrophage inhibitory factor
MMP	Matrix metalloproteinase
mRNA	Messenger RNA
MSC	Mesenchymal stem cell
NaOH	Sodium Hydroxide
NAS	Normal animal serum
NFQ	Non-fluorescent quencher
NG2	Neural glial antigen 2
NGS	Next generation sequencing
NSET	Non-surgical embryo transfer device
NTP	Nucleotide peptide
O	Oestrus
OCT	Optimal cutting temperature medium
OHT	4-Hydroxytamoxifen
OPC	Oligodendrocyte progenitor cell

P	Proestrus
P4	Progesterone
PBS	Phosphate-buffered saline
PBS tween	PBS containing 0.05% (v/V) tween20
PCR	Polymerase Chain Reaction
PDGF	Platelet derived growth factor
Pdgfrb	Platelet derived growth factor receptor beta
PET	Pericyte to epithelial transition
PFA	Paraformaldehyde
PG	Prostaglandin
PGDH	Prostaglandin dehydrogenase
PIL	Personal Licence
PPL	Project Licence
PR	Progesterone receptor
PSR	Picro Sirius Red
PTC	Peltier thermal cycler
QMRI	Queen's medical research institute
qPCR	Quantitative PCR
RFP	Red fluorescent protein
RIN	RNA Integrity Number
RNA	Ribonucleic acid
RNA-Seq	RNA sequencing
ROS	Reactive oxygen species
RT	Room temperature
RvT	Reverse transcription
Rxn	Reaction
SEM	Scanning electron microscopy
SP	Side population
SPIA	Single Primer Isothermal Amplification
SURF	Shared University Research Facilities
T	Testosterone
TAE	Tris base, Acetic acid, EDTA
TE	Tris-EDTA
TEM	Transmission electron microscopy
TGFβ	Transforming growth factor β
THAM	Tris (hydroxymethyl) aminomethane
TIMP	Tissue inhibitor of MMPs
TMX	Tamoxifen
TNFα	Tumour necrosis factor α
tPA	Tissue plasminogen activator
Tris-HCL	Tris (hydroxymethyl) aminomethane (THAM) hydrochloride
TSA	Tyramide Signal Amplification
uNK	Terine natural killer cell
uPA	Urokinase-type plasminogen activator
UPL	Universal probe library
VEGF	Vascular endothelial growth factor
WPRE	Woodchuck hepatitis virus post-transcriptional regulatory element

Chapter 1 Introduction

The human endometrium, located in the central portion of the uterus, is a complex multicellular tissue that undergoes repeated cycles of proliferation, degeneration and shedding during each menstrual cycle. The endometrium is unusual amongst adult tissue in that it exhibits an unparalleled capacity for rapid scar-free repair. The studies in this thesis have used the Edinburgh mouse model of simulated 'menses' as a physiological tissue system in which to study the mechanisms contributing to scarless tissue repair. In the following literature review the wound healing response and its possible progression to fibrosis as exhibited by most adult tissues will be discussed to place the studies on endometrium in the context of wound healing. A more detailed assessment of the structure and function of the endometrium, the physiological changes that take place during menstruation and the animal models used to study menstrual physiology will be used to highlight what is known in the field and reveal gaps in the current knowledge.

1.1 Wound healing

1.1.1 Wound healing and tissue repair

Wound healing is an essential physiological process that maintains tissue homeostasis in response to injury, and when impaired, predisposes to various pathologies (Shaw and Martin 2009). Wound healing is a tightly regulated process involving a range of cell types that work together to coordinate the overlapping phases of wound healing: coagulation, inflammation, tissue replacement and resolution (Bodnar et al. 2016, Sorg et al. 2017). Cellular and molecular mechanisms associated with wound healing in the skin are outlined in Figure 1-1. Briefly, following an injury, inflammatory cells are recruited to phagocytose cellular debris and stimulate the proliferation and migration of fibroblasts into the wound bed to synthesis extracellular matrix (ECM) components (Gurevich et al. 2018, Cash and Martin 2016). Rapid cellular proliferation and migration occurs resulting in reformation of the epithelium and new blood vessels (Shaw and Martin 2016). Fibroblasts differentiate into contractile myofibroblasts to contract the edges of the wound and lay down collagens which then form scar tissue.

Resolution involves apoptosis of myofibroblasts and cessation of the inflammatory response (Tomasek et al. 2002, Hinz 2007). Despite relatively rapid wound closure, remodelling of the scar tissue occurs over the following months to years however in severe wounding, correct architecture of the tissue may never be regained. What is more, the tensile strength is only 70% that of normal skin and therefore full function cannot be regained (Larson, Longaker and Lorenz 2010). Cutaneous wound healing therefore is described as a fibroproliferative response resulting in the incomplete regeneration of the original tissue (Shaw and Martin 2016, Shinzawa et al. 2007).

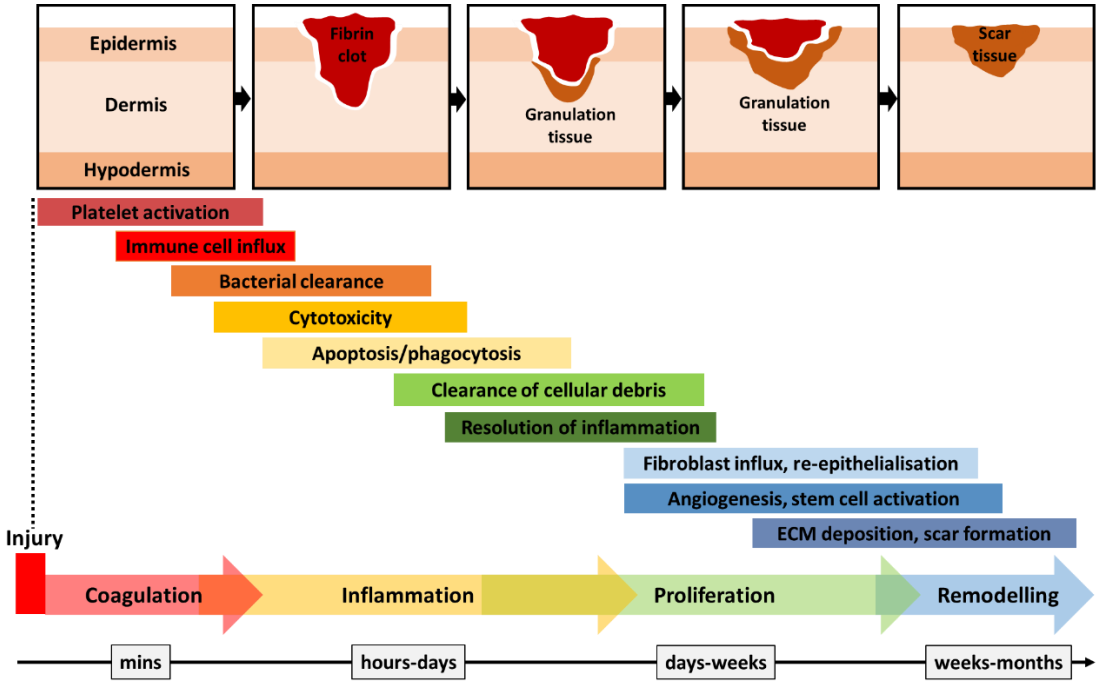

Figure 1-1. Cellular and molecular mechanisms of the wound healing response in the skin, composed of four overlapping phases: coagulation, inflammation, proliferation and remodeling. Wound healing in the skin involves a host of effector cells and signalling pathways leading to the deposition of granulation tissue which matures into scar tissue and takes weeks-months to resolve (based on Shaw and Martin 2009, Diegelmann and Evans 2004).

1.1.2 Mechanisms of normal wound healing with self-limiting fibrosis

1.1.2.1 Coagulation phase

The wound healing response has been most well characterised in the skin with a 'full thickness' wound shown to damage several structures including the epidermal keratinocyte layer, the dermal layer including fibroblasts, blood vessels, hair follicles, sweat glands and the basement membrane (McNeil and Kirchhausen 2005). Trauma to the skin results in ruptured cells and damaged blood vessels which emit both chemical and mechanical 'damage' signals initiating the wound healing response (Shaw and Martin 2009). To stop local haemorrhage, the coagulation cascade is triggered whereby blood components enter the site of injury and platelets interact with exposed collagen and other elements of the extracellular matrix which causes their activation and aggregation (Diegelmann and Evans 2004). Fibrin is formed from fibrinogen by the action of the protease thrombin and together with aggregated platelets, forms a clot made up of a network of insoluble fibrin fibres (Shaw and Martin 2009). This clot plugs damaged blood vessels and serves as a provisional matrix upon which healing events can take place and endothelial cells, smooth muscle cells, fibroblasts, leukocytes, epithelial cells and stem cells can bind and migrate (Diegelmann and Evans 2004). The fibrin network of the clot also binds growth factors to establish chemotactic gradients which facilitate cell recruitment and constitutes a storage pool that can be secondarily released by matrix metalloproteinases (MMPs). Often the outcome of wound healing is influenced by the thickness of fibrin fibres, the number of branch points and the permeability of the clot at the wound site (Nurden et al. 2008).

Platelet degranulation further affects blood vessels by stimulating vasodilation, increasing blood vessel permeability and MMP production influencing the recruitment of inflammatory cells to the site of injury (Duffield et al. 2013). Activated platelets also secrete a number of cytokines and growth factors including PDGF, CXCL4, bFGF, VEGF, RANTES and TGFβ which can influence multiple processes including inflammation, angiogenesis and fibroblast migration (Bahou and Gnatenko 2004). In particular, PDGF is involved in the chemotaxis of macrophages, neutrophils, fibroblasts and smooth muscle cells and stimulates proliferation of fibroblasts and

smooth muscle cells while TGFβ stimulates macrophages to release cytokines such as FGF, PDGF, TNFα and IL1, enhances fibroblast and smooth muscle cell chemotaxis and modulates collagen and collagenase expression (Diegelmann and Evans 2004).

1.1.2.2 Inflammatory phase

The inflammatory response begins when immune cells escape the vasculature through damaged blood vessels and potentiates in response to increasing levels of cytokines and chemokines secreted by damaged tissue. The first cells to be recruited are mostly neutrophils and this is followed by influx of monocytes (Eming, Krieg and Davidson 2007) both of which have important roles in removing dead, damaged or infected tissue from the wound (Duffield et al. 2013). Neutrophils become activated and have primary roles in killing invading microorganisms and influencing aspects of repair including angiogenesis, resolution of the fibrin clot and re-epithelialisation (Theilgaard-Mönch et al. 2004). Monocytes can differentiate into macrophages upon extravasation from the circulation, initiating distinct gene expression signatures in response to signals coming from the tissue microenvironment (Martinez et al. 2006). Macrophages play a critical role in restoration of tissue integrity by phagocytosing cellular debris, damaged matrix and spent neutrophils. It has been reported that classically activated or 'M1' pro-inflammatory macrophages are present in early phases of wound healing while alternatively activated or 'M2' anti-inflammatory macrophages are seen to persist later in repair (Deonarine et al. 2007). Increased expression of MMPs by inflammatory cells helps to clear tissue debris during early stages of repair (Davis and Saunders 2006). Whether inflammatory cells are an essential requirement for effective wound healing remains an area of intense research interest although it is clear that immune cells play a major role in orchestrating processes such as angiogenesis and fibrogenesis (Martin and Leibovich 2005).

1.1.2.3 Tissue replacement phase

During the tissue replacement phase of skin wound healing closure of the wound gap and reconstitution of lost tissue is achieved. Although this phase begins within hours of wounding the time to wound closure depends upon the size and location of wound and additional factors including age and the health of the tissue (Shaw and Martin

2009). Angiogenesis is essential to a robust wound healing response and involves the sprouting of damaged blood vessels into the wound site to deliver nutrients, oxygen and growth factors to the site of injury (Shaw and Martin 2009). Re-epithelialisation is achieved by the proliferation and migration of keratinocytes in the vicinity of the wound. Injured epithelial cells undergo phenotypic changes to acquire a migratory phenotype known as an epithelial-to-mesenchymal transition (EMT), governed by activation of a gene expression programme including the transcription factor SNAIL (Duffield 2014) and driven by TNFα and IL1β in a TGFβ-dependent mechanism (Fan et al. 2001). During this transition, keratinocytes decrease cell-cell and cell-matrix adhesions to allow 'crawling' over the provisional collagen and fibronectin rich clot and increase expression of MMPs in order to create a pathway at the interface between the scab and viable tissue (Ilina and Friedl 2009). Injured or activated epithelial cells are a potent source of TGFβ and PDGFs which both believed to be important in activating fibroblasts and pericytes during tissue repair (Chen et al. 2011, Liu et al. 2011). Stem cells that reside in the epidermis and region of hair follicles also respond to injury by committing to an epidermal phenotype and migrating to participate in repair (Ito et al. 2005). Epithelial stem cells in the hair follicle bulge region respond to wounding by generating transient amplifying cells that also partake in re-epithelialisation (Ito et al. 2005).

Alongside healing of the epidermis, the damaged dermis must be reconstituted. The fibrin clot formed during the immediate response is replaced by granulation tissue which is a temporary structure laid down by stromal fibroblasts originating from various sources: healthy dermal fibroblasts at the wound edge, circulating fibrocytes, bone marrow derived progenitor cells, multipotent dermal progenitor cells and perivascular pericytes (Hinz 2007, Fernandes et al. 2004, Rajkumar et al. 2006). In addition the mechanical stress in the wound and immune cell secretion of PDGF, TGFβ1 and IL13 stimulates mesenchymal cells such as fibroblasts and pericytes to differentiate into myofibroblasts (Wynn and Barron 2010). Myofibroblasts express alpha smooth muscle actin (αSMA) and form stress bundles which have contractility properties promoting connective tissue contraction and closure of the wound edge (Hinz et al. 2012). αSMA is also expressed by vascular smooth muscle cells although their contractions are reversible and short-lived whereas myofibroblasts generate

irreversible and long-lived contractions (Castella et al. 2010). Myofibroblasts also secrete factors that are both mitogenic and chemotactic for epithelial and endothelial cells to stimulate the formation of new ECM, epithelium and blood vessels (Duffield et al. 2013). Fibroblasts and myofibroblasts instigate wound closure and contribute to the synthesis, bundling and alignment of collagen fibres which when not aligned correctly is the main constituent of scar tissue (Bodnar et al. 2016).

Pericytes residing in close proximity to blood vessels are reported to have various roles in wound healing (Crocker, Murad and Geer 1970, Mills, Cowin and Kaur 2013, Murray et al. 2014). For example, during wound healing, pericytes interact with platelets, endothelial cells and inflammatory cells to instigate new vessel growth (Thomas 1999). Pericytes also secrete various cytokines to influence immune cell infiltration and may act as precursors for myofibroblast transition through PDGF-dependent mechanism (Bodnar et al. 2016). *In vitro* pericytes have been shown to migrate towards proteolytic digests of ECM, consistent with the important property of progenitors to migrate to the site of injured tissue for reconstruction (Crisan et al. 2009).

1.1.2.4 Resolution phase

The resolution of wound healing returns cutaneous tissue to pre-injured appearance and full functionality through various changes including refinement and maturation of blood vessel network within the scar (Adams and Alitalo 2007), remodelling of the deposited ECM to correctly align collagen bundles and myofibroblast apoptosis (Hinz 2007, Ulrich et al. 2007). Myofibroblast activation is a normal response to injury and normal wound healing (Hinz et al. 2012) however during the resolution phase myofibroblasts undergo apoptosis and are cleared by immune cells to avoid excessive ECM deposition. The mechanisms responsible for apoptosis in these cells remain unknown but a greater understanding of their regulation may help our understanding of fibrosis (Desmoulière et al. 1995). The inflammatory response resolves upon completion of wound healing through neutrophil apoptosis and clearance by macrophages, or emigration through lymphatics (Eming et al. 2007). Anti-inflammatory cytokines such as resolvin E and annexin I further de-activate immune cells (Shaw and Martin 2009). Wound healing is imperfect with many tissues

not regaining full function or architecture that recapitulates the pre-injured state (Larson et al. 2010).

1.1.2.5 Hormonal regulation of wound healing

Observational studies in elderly men and women have identified endogenous oestrogens and androgens (testosterone; T, dihydrotestosterone; DHT) as being respectively enhancers and inhibitors of repair (Gilliver et al. 2009).

Age exacerbates androgen effects in male keratinocytes which may explain why older males experience wound healing difficulties (Fimmel et al. 2007). These studies have been complemented by studies in rodents in which hormone levels have been manipulated. Acute reductions in androgens (T or DHT) has been linked to reduction in leucocytosis and pro-inflammatory signalling molecules including IL-6, TNFα and MMPs. (Gilliver et al. 2009, Gilliver et al. 2006, Ashcroft and Mills 2002). In the absence of androgens (castration of male mice), inflammatory function of macrophages and fibroblasts are dysregulated with concomitant decreases in IL-1 and IL-6 associated with accelerated wound healing (Nitsch et al. 2004). The use of transgenic mice with targeted deletion of *Ar* in myeloid cells induced by cross-breeding Arflx mice with those carrying a LysMCre (Clausen et al. 1999) has revealed evidence for a role for androgen-dependent signalling in modulating macrophage function (Lai et al. 2009). In the MARKO mice healing was accelerated, a result not recapitulated by *Ar* ablation in other cell types (keratinocyte, fibroblast). In contrast stimulation of macrophage AR increased the inflammatory response and TNFα expression and topical application of a compound that degrades AR resulted in accelerated healing highlighting a potential novel treatment strategy (Lai et al. 2009). Androgen effects are most pronounced during the early stages of wound healing. Androgens can affect the rate of re-epithelialisation by increasing β-catenin expression, but do not affect proliferation of dermal fibroblasts (Ashcroft and Mills 2002). Androgens also inhibit the expression of MMP1, 3 and 7 (Schneikert et al. 1996).

Topical administration of oestrogen to cutaneous wounds in elderly patients can accelerate wound healing and increase wound strength (Ashcroft et al. 1999).

Oestrogens can alter the inflammatory response, inhibiting chemotaxis of polymorphonuclear leucocytes to reduce the number present in the wound (Ito et al. 1995). In particular the neutrophil population is affected with an associated decreased in elastase resulting in reduced degradation of fibronectin and increased collagen deposition. Oestrogens also decrease expression of macrophage migration inhibitory factor (MIF) (Ashcroft et al. 2003): MIF represses the actions of anti-inflammatory cytokines such as IL-6, IL-1β and Il-8 thereby affecting signalling cascades associated with wound repair (Calandra and Bucala 1995, Hardman et al. 2005). Oestrogens have been found to increase the expression of ECM components including procollagen 1, fibrillin 1 and tropoelastin while decreasing MMP1 expression and thereby affecting ECM remodelling (Son et al. 2005). Oestrogens also increase GM-CSF secretion by keratinocytes which in turn increases keratinocyte proliferation and migration whilst also stimulating endothelial and inflammatory cells, accelerating the repair response (Mann et al. 2001). Oestrogen classically binds to one of two receptors: ERα and ERβ, both of which have been found to have differing roles in wound healing. ERα expressed by endothelial cells has been shown to have a role in enhancing angiogenesis (Arnal et al. 2010) and mediating the activity of VEGF (Ashcroft et al. 1999). Oestrogen action via ERβ promotes cutaneous wound healing in mice irrespective of effects on inflammation, while the anti-inflammatory effects of oestrogens are believed to involve both receptor subtypes (Campbell et al. 2010). Finally activation of ERα or ERβ in human keratinocytes enhanced migration and proliferative capacity *in vitro*; ERβ signalling did not increase the expression of TGFβ1 making it a potential target to enhance wound healing without side effects of stimulating a fibrotic response (Merlo et al. 2009).

1.1.3 Mechanisms of chronic wound healing and the progression of fibrosis

When an injury is repeated, the wound healing response may be dysregulated resulting in hyperproliferation, persistence of myofibroblasts and prolonged inflammation with fibrosis and excessive scar formation (Wynn 2008, Fan et al. 2008, Duffield et al. 2013). Fibrosis encompasses various morphological changes in the affected tissue including loss of cellular homeostasis and tissue architecture, ECM deposition and

dysregulated cellular phenotypes. Scar tissue can distort normal tissue architecture and inhibits efficient tissue function. Despite differences in the presentation of fibrosis in different tissues, common mechanisms include sustained secretion of proteolytic enzymes, growth factors, fibrogenic cytokines and angiogeneic factors all of which stimulate excess ECM deposition (Duffield et al. 2013).

Myofibroblasts have been identified as key players in pathogenic fibrosis due to their production of ECM proteins and proteoglycans, making them the focus of various studies investigating their origins, activation, deactivation and apoptosis (Duffield et al. 2013). During fibrosis, myofibroblasts accumulate and produce collagen, EDA-containing fibronectin, various soluble mediators and reactive oxygen species (ROS). They also secrete a variety of lipid mediators, cytokines and chemokines thereby potentiating the inflammatory response (Phan et al. 1999). In normal wound healing myofibroblasts arise from fibroblasts through fibroblast-to-myofibroblast transition (FMT) and are essential for wound closure (Leavitt et al. 2016) however persistence of myofibroblasts at a site of injury associated with resistance to apoptosis results in the continued formation of scar tissue and progression of fibrosis (Hantash et al. 2008, Haldar et al. 2016, Greenhalgh, Iredale and Henderson 2013). The mechanisms underlying development of an apoptosis-resistant phenotype remain unknown (Thannickal and Horowitz 2006). As pericytes have been identified as precursors for fibrotic myofibroblasts, with the first conclusive evidence being generated in the kidney using lineage tracing methods (Humphreys et al. 2010), pericytes have also been implicated in pathological fibrosis. Pericyte-derived myofibroblasts have been identified in kidney fibrosis as collagen-producing cells (Ballhause, Soldati and Mertens 2014, Duffield 2014, LeBleu et al. 2013) and in dermal fibrosis where the majority of collagen producing cells were generated from a pericyte subpopulation (Dulauroy et al. 2012). Notably, treatment of cutaneous wounds with a PDGFRβ inhibitor (imatinib mesylate) delays wound healing causing a reduction in proliferation and differentiation of fibroblasts and pericytes thereby reducing numbers of myofibroblasts (Rajkumar et al. 2006).

Macrophages have also been identified as key players in the progression and persistence of fibrosis through both direct effects on ECM remodelling and indirect

effects by regulating myofibroblast activity and endothelial cells (Lupher and Gallatin 2006, Anders and Ryu). Fibrocytes are a distinct subset of collagen-producing cells derived from peripheral blood monocytes that enter tissues following injury and promote angiogenesis and tissue repair but are also key players in scar formation and chronic inflammation observed during fibrosis (Herzog and Bucala 2010). In the setting of fibrosis, macrophages and fibrocytes are often located in close proximity to collagen-secreting myofibroblasts and produce growth factors and cytokines that can suppress or stimulate myofibroblasts activity (Herzog and Bucala 2010, Koh and DiPietro 2011). Monocytes can promote fibrosis by differentiating into M2a-like macrophages and fibrocytes which in turn secrete fibroblast stimulating factors such as TGFβ1, PDGF, FGF2, IGFBP5, CCL18 and Galectin-3 (Wynn and Vannella 2016). M1 macrophages are also implicated in progression of fibrosis by causing hyperinflammation in neighbouring tissues (Duffield et al. 2005). Notably it is now appreciated that functional heterogeneity within macrophage populations may impact on the progression of fibrosis or its resolution with different subclasses having the potential to impact on tissue repair responses to injury (Hesketh et al. 2017). Recent studies report that many factors can induce a pro-fibrotic phenotype in macrophages e.g. IL-1, Il-13, CSF1, CCL17 and CCL2 and once activated these cells can amplify levels of pro-fibrotic cytokines and growth factors thereby driving and accelerating myofibroblast activation and fibrosis progression (Shapouri-Moghaddam et al. 2018).

1.1.4 Mechanisms of scarless healing

1.1.4.1 Foetal skin

It has been reported that wounds on human foetal skin during the early, but not late, gestational period exhibit scarless wound repair (Gurtner et al. 2008). Although this process is not fully understood some differences between wound healing in the foetal and adult skin have been recorded (Figure 1-2). Foetal skin has much decreased tensile strength which consequently decreases the amount of mechanical signalling from the wound region. This is relevant because the focal adhesion kinase (FAK) pathway has been implicated in linking mechanotransduction with fibrosis (Wong et al. 2011). Furthermore, clinical trials using a device designed to reduce mechanical forces on

healing wounds resulted in reduced scar formation (Longaker et al. 2014). Foetal skin wound healing also has a reduced inflammatory component whereby platelets do not form aggregates, there is less infiltration by neutrophils and decreased secretion of pro-inflammatory cytokines such as TGFβ and interleukins (Leavitt et al. 2016). Foetal wounds express more TGFβ3 than TGFβ1 while adult wounds show greater TGFβ1 expression, a known driver of fibrosis (Leavitt et al. 2016).

Alterations in the phenotype and function of cells in foetal and adult skin have been noted with proteomic analysis of foetal and adult skin fibroblasts revealing differences expression relevant to the wound healing response (Ho, Marçal and Foster 2014). Notably, mid-gestational keratinocytes can modulate the gene expression profile of adult dermal fibroblasts causing increased proliferation and migration and downregulation of precollagen1, collagen 1, TGFβ1, TGFβ2, TIMP2 and TIMP3 and upregulation of precollagen 3, collagen 3, TGFβ3, MMP1, MMP2, MMP3 MMP9 and MMP14, while fibroblasts co-cultured with late-gestational keratinocytes showed a more pro-fibrotic phenotype (Wang et al. 2015). In foetal wounds collagen III and IV are rapidly deposited by fibroblasts in a network that reflects the architecture of uninjured skin while in adult wounds collagen I predominates giving greater strength and rigidity but inhibiting cellular migration. Foetal fibroblasts have greater capacity for migration and there is no evidence for myofibroblast differentiation (Larson et al. 2010). Human foetal skin has been shown to heal without a scar even when transplanted into the subcutaneous tissue of an immunodeficient adult mouse (Larson et al. 2010) suggesting wound healing responses are intrinsic to the tissue.

1.1.4.2 Oral mucosa

An example of an adult tissue that exhibits minimal scarring is the oral mucosa (Figure 1-2). As with foetal skin, the inflammatory component of wound healing in the oral mucosa is diminished (Glim et al. 2015): there are significantly lower numbers of macrophages, neutrophils and T cells observed in oral mucosal wounds when compared to wounds of equivalent size in the adult skin. This is accompanied by decreased expression of the pro-inflammatory cytokines IL-6 and TGFβ1 (Szpaderska, Zuckerman and DiPietro 2003). When compared to the skin, the oral mucosa also displays decreased expression of fibronectin, ED-A fibronectin and chondroitin

sulfate. Myofibroblastic expression of αSMA is dependent on ED-A fibronectin in addition to TGFβ signalling suggesting that the ECM of the oral mucosa is less likely to support myofibroblast differentiation (Leavitt et al. 2016, Tomasek et al. 2002).

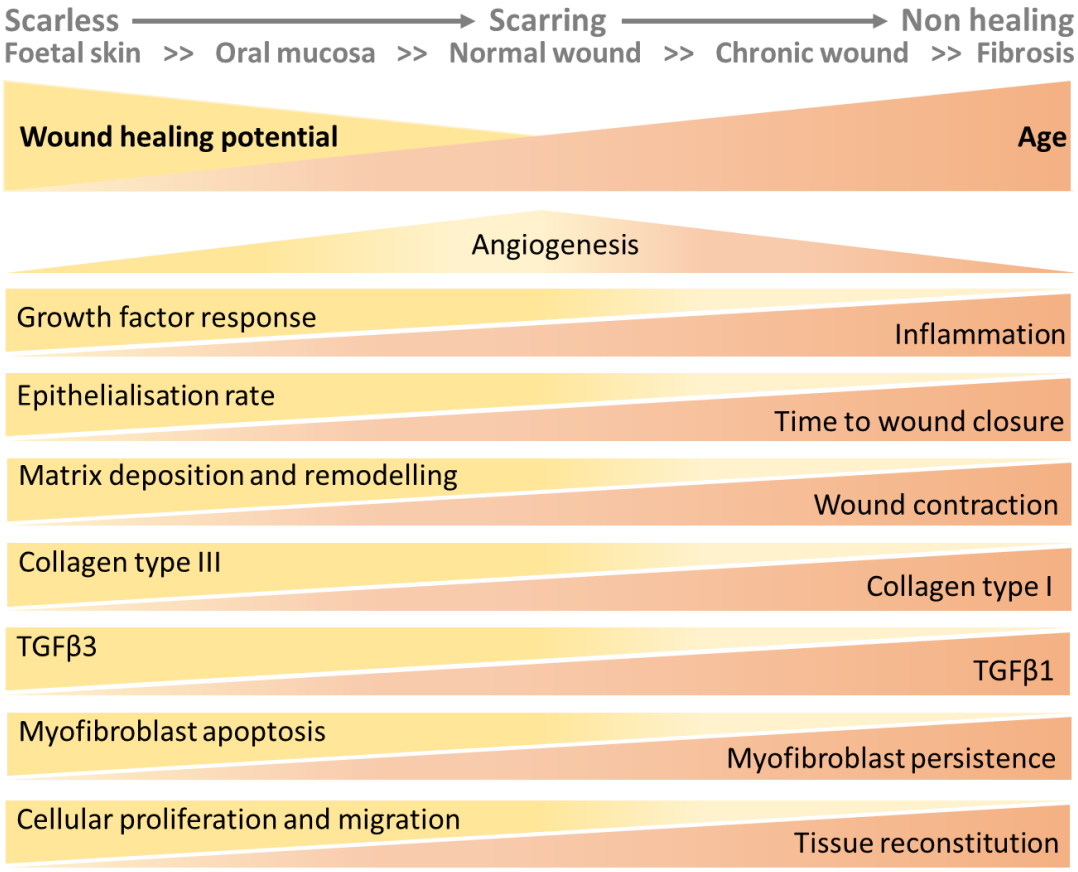

Figure 1-2. Overview of cellular and molecular characteristics of scarless regeneration and scar formation during wound healing. Key processes are displayed as they increase or decrease across the wound healing spectrum: scarless, scarring and non-healing wound repair. Features highlighted include angiogenesis, inflammation, epithelialisation, ECM remodelling, TGFβ signalling and myofibroblasts differentiation (based on Peake et al. 2014, Leavitt et al. 2016).

1.1.5 Summary

Wound healing is a complex interplay of various cell types and signalling pathways that orchestrate a highly regulated process to return a tissue to its pre-injured state. Dysregulated tissue repair results in the accumulation of ECM products and the

development of fibrosis which occurs in most adult tissues upon repeated injury and has severely negative impacts on tissue function. Physiological examples of scarless healing exist in the foetal skin and oral mucosa where a diminished inflammatory response and altered myofibroblast phenotype have been highlighted as key differences. The endometrium is also an example of an adult tissue that can undergo scarless repair and current understanding of this process is discussed below.

1.2 The endometrium

1.2.1 Development of the endometrium

Development of the female reproductive tract occurs prenatally arising from the intermediate mesoderm and differentiating from the embryonic structures known as the Müllerian ducts (Kobayashi and Behringer 2003). Humans and other higher primates have a simplex uterus with a single uterine cavity formed through the fusion of the two Müllerian ducts at approximately 8 weeks of gestation during Carnegie stages 22-23 (Hashimoto 2003, Kobayashi and Behringer 2003). During gestational weeks 16-24 the uterus undergoes extensive growth (Pietryga and Woźniak 1992) and the mesenchyme differentiates into both the stroma and myometrium by gestational week 22: endometrial glands differentiate from columnar luminal epithelium, extending from the lumen to the myometrium (Beckman and Feuston 2003). Primordial germ cells migrate into the genital ridge and populate the developing gonads from around 5-6 weeks of gestation (Makabe and Motta 1989). Subsequent development of the ovary is characterised by proliferation of somatic components, differentiation of the gonadal cortex and differentiation of primordial germ cells into clusters of oocytes (Motta, Makabe and Nottola 1997). This process continues until oocytes reach meiotic arrest in the 22nd gestational week (Makabe and Motta 1989).

The female reproductive tract is controlled by the hypothalamic pituitary ovarian (HPO) axis. Briefly neurons in the hypothalamus produce pulsatile secretions of gonadotrophin-releasing hormone (GnRH) from the onset of puberty binding to GnRH receptors in the pituitary and stimulating production and secretion of luteinising hormone (LH) and follicle stimulating hormone (FSH) (Marshall et al. 1991) (Figure

1-3). These pituitary hormones stimulate the production of steroid hormones oestrogen and progesterone by ovarian tissue. Oestrogens are produced in a two-step process: LH binds to LH receptors on thecal cells on the outer layer of follicles stimulating the conversion of cholesterol to androgens which are transported inwards to granulosa cells; granulosa cells have FSH receptors and upon binding, FSH stimulates the conversion of androgens to oestrogen (Yen 1977) (Figure 1-3). Oestrogen is required to support the development of the oocyte within the follicle and creates a positive feedback loop to the hypothalamus and pituitary gland. After ovulation the follicle undergoes leutinization and becomes the corpus luteum (CL) which synthesizes and secretes progesterone (Bates and Bowling 2013, Timonen et al. 2002). Steroid hormones are essential for the growth and function of the human endometrium and govern cyclical changes that take place during the menstrual cycle (Section 1.2.3).

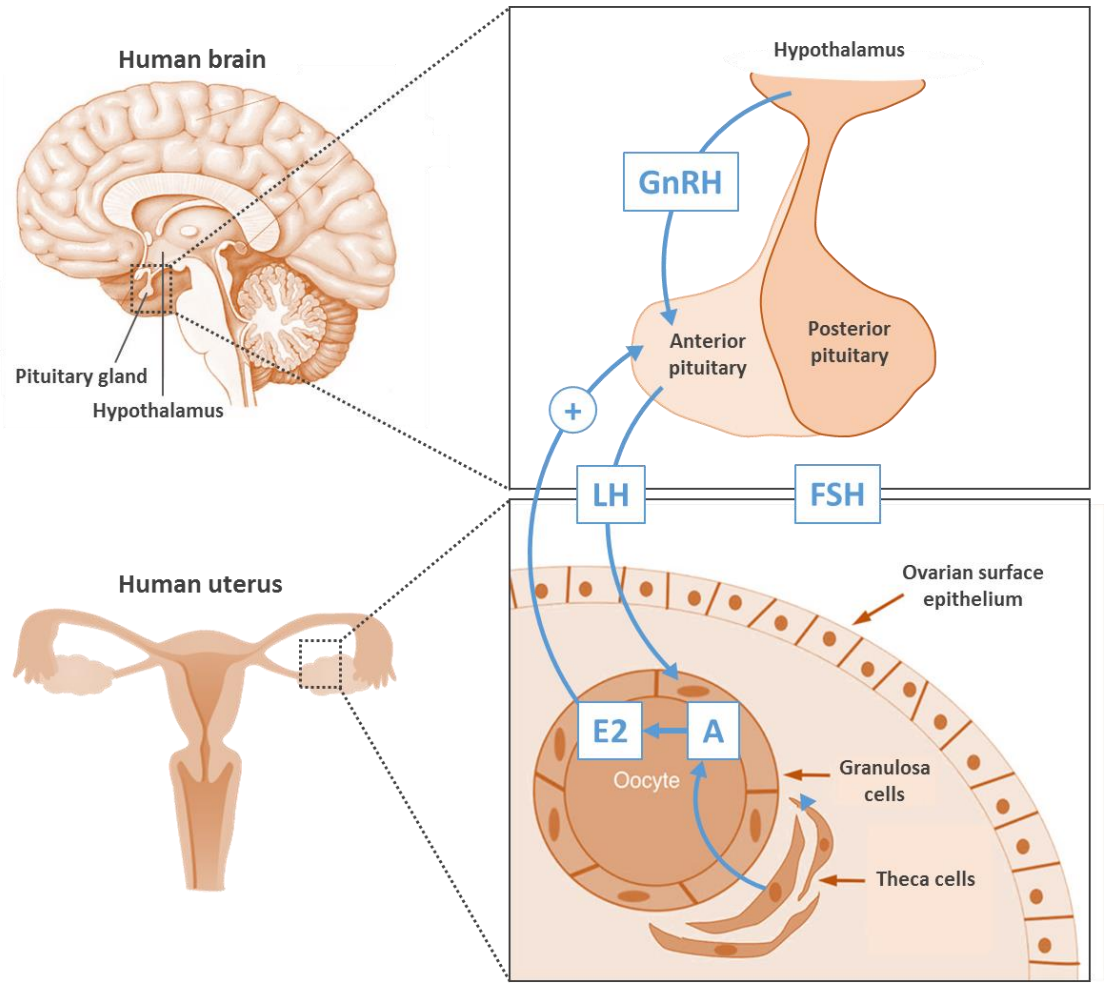

Figure 1-3. Overview of the hypothalamic pituitary ovarian (HPO) axis that governs function of the femal reproductive tract. Gonadotrophin releasing hormone (GnRH) is released from the hypothalamus in the brain which stimulates release of leutinising hormone (LH) and follicle stimulating hormone (FSH) from the pituitary gland. These hormones act on the ovary to regulate follicular development and synthesis of the steroid hormone oestrogen. Rising oestrogen levels activate positive feedback on the pituitary gland resulting in a pre-ovulatory gonadotrophin surge (based on Bates and Bowling 2013, Marshall et al. 1991, Yen 1977).

1.2.2 Tissue architecture of the adult endometrium in women and mouse

The human uterus comprises two principle components: a thick muscular outer layer known as the myometrium and a multicellular internal layer known as the endometrium which lines the internal uterine cavity. The myometrium consists predominantly of muscle fibres interspersed with blood vessels, lymphatics and nerves, and is responsible for uterine contractions during menstruation and parturition (Naftalin and Jurkovic 2009). The endometrium is a dynamic tissue that undergoes monthly cycles of tissue remodelling in response to fluctuating levels of ovarian-derived steroid hormones during the menstrual cycle (Critchley and Saunders 2009). The purpose of the menstrual cycle is to ready the endometrium for implantation of a blastocyst and then further support the development of a foetus throughout pregnancy.

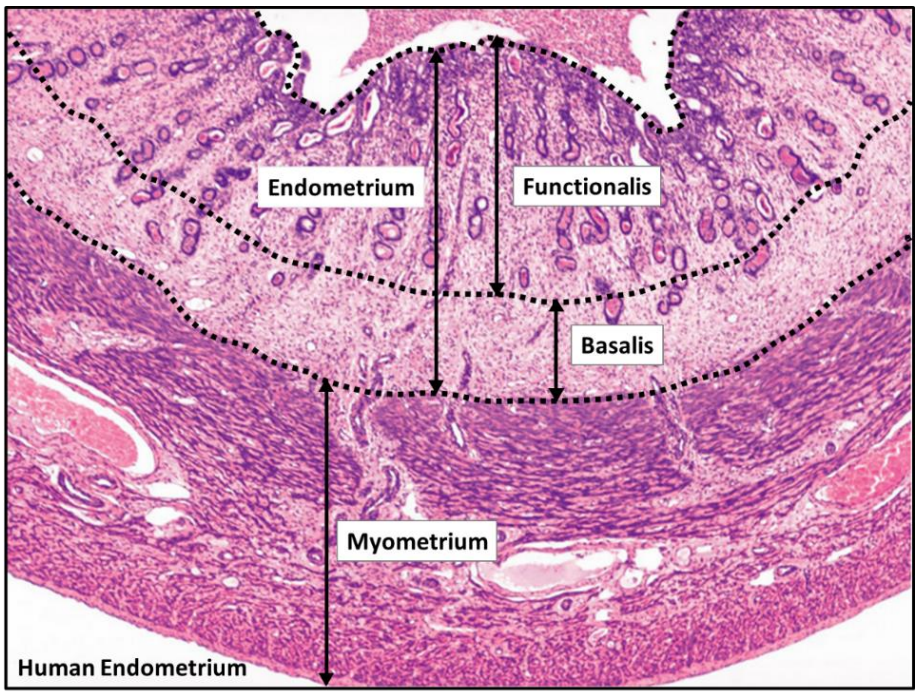

Figure 1-4. Histological appearance of the human uterus. The human uterus is comprised of two principle components: the outer muscular myometrium and the inner multicellular endometrium. The endometrium is composed of two distinct layers: the outer basalis and inner functionalis. Modified image (Original image available at: http://medcell.med.yale.edu/histology/female_reproductive_system_lab/uterus.php).

The human endometrium is composed of two morphologically distinct layers: the basal layer and the functional layer. The outer basal layer is directly adjacent to the surrounding myometrium creating the endometrial-myometrial junction which is highly vascularised (Tetlow et al. 1999) and remains intact throughout the menstrual cycle (Padykula et al. 1989, Naftalin and Jurkovic 2009) (Figure 1-5). The functional layer is luminal to the basal layer and represents a transient tissue which proliferates, degenerates and is shed during menstruation (Figure 1-5). Both layers of the endometrium have a well-defined stromal compartment containing fibroblasts, vasculature (vascular smooth muscle cells, pericytes and perivascular fibroblasts) and immune cells and a distinct epithelial compartment (Garry et al. 2009, Ludwig and Spornitz 1991, Thiruchelvam et al. 2013, Berbic, Ng and Fraser 2014). The luminal surface of the endometrium and the glands are lined with a single layer of columnar epithelial cells. The luminal epithelium represents the interface between the endometrial mucosa and the uterine cavity (Niklaus, Murphy and Lopata 2001) (Figure 1-5).

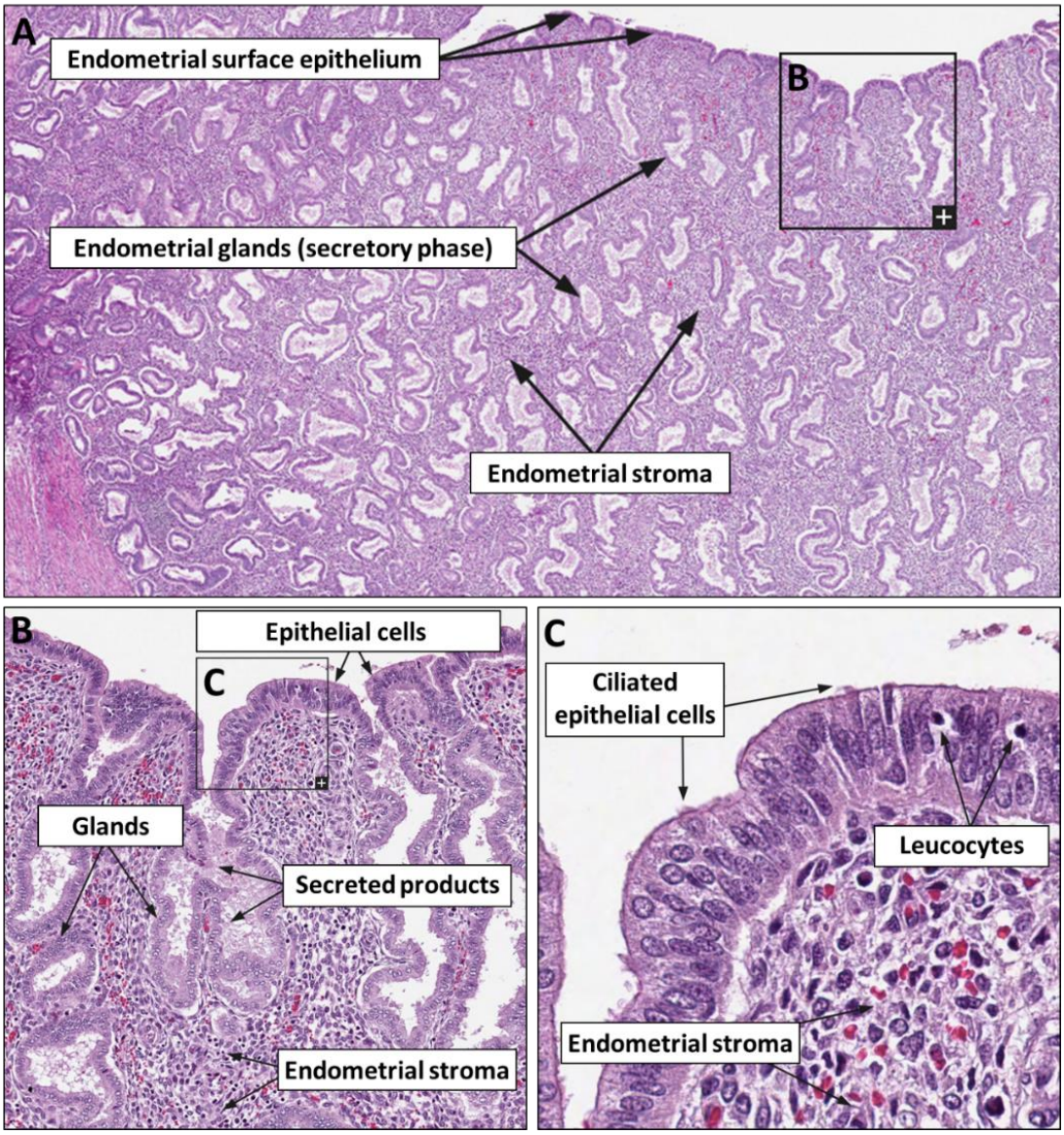

Figure 1-5. Histological assessment of human endometrial structure. The endometrium is composed of two distinct layers (Figure 1-4) comprising both stromal and epithelial compartments. The stroma is composed of fibroblasts, endothelial cells that make up blood vessels and immune cells. The epithelium is composed of epithelial cells that line both the inner lumen and glands (image adapted from the Human Protein Atlas: https://www.proteinatlas.org/; original image available at: https://www.proteinatlas.org/learn/dictionary/normal/endometrium)

1.2.3 The human menstrual cycle

The menstrual cycle is split into three phases governed by changes in circulating hormone concentrations and consequently tissue morphology (Figure 1-6): the menstrual phase involves the degeneration of the functional layer; the proliferative phase involves regeneration of the functional layer; and the secretory phase involves the differentiation of the new functional layer in preparation for the implantation of a blastocyst (Bartelmez 1957, Ferenczy, Bertrand and Gelfand 1979, Garry et al. 2009). Noyes *et al* examined the histology of 8000 human endometrial biopsies to describe the stages of the menstrual cycle which was determined on average to be ~28 days in length. The onset of menstruation is considered to be day 1 and the proliferative phase follows on from days 4-14. Ovulation occurs between days 14-16 and the secretory phase begins on day 16 and is often designated as: the early-secretory phase (days 16-19), the mid-secretory phase (days 20-24) and the late-secretory phase (days 25-28). The cycle ends on day 28 and starts again with the onset of the subsequent menstrual phase (Noyes, Hertig and Rock 1975). The morphological and cellular changes that take place during each phase of the cycle are outlined below.

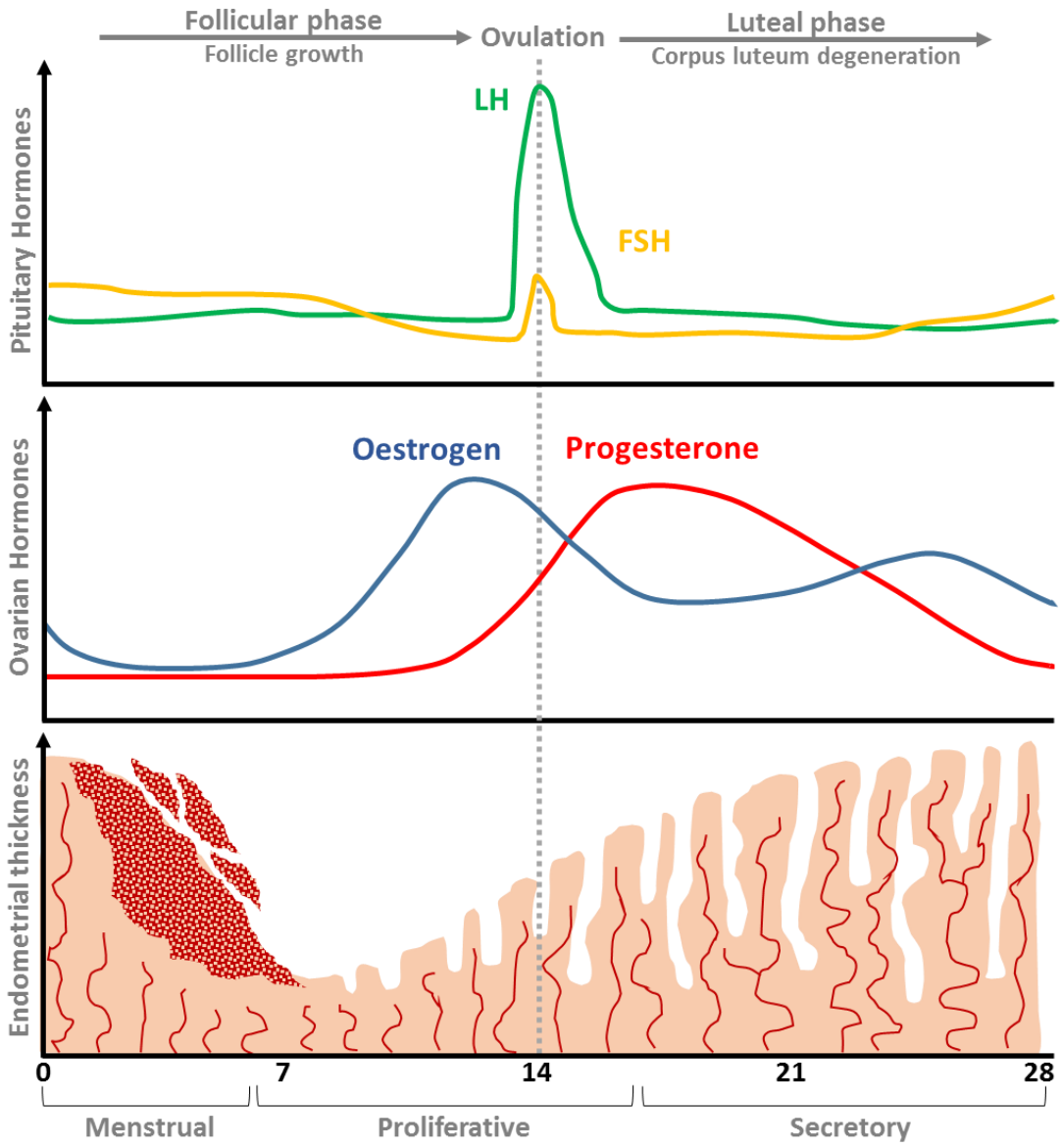

Figure 1-6. Overview of the cyclical changes in circulating hormone levels and morphology of the endometrial functionalis during the human menstrual cycle. LH and FSH secreted from the pituitary stimulate synthesis of steroid hormones. Menstruation occurs on day 0 (hormone depleted environment) and involves sloughing of the functional layer after which the endometrium goes through rapid tissue repair. The oestrogen dominant proliferative phase occurs from days 4-16 of the cycle involving cellular proliferation and angiogenesis. This phase culminates in ovulation in response to the 'LH surge' after which the corpus luteum (derived from the ovulated follicle) secretes progesterone. During the secretory phase at days 20-28, progesterone induces decidualisation of stromal fibroblasts in preparation for the implantation of a blastocyst. In the absence of a blastocyst, progesterone concentrations fall stimulating a cascade of cellular and molecular events that culminate in sloughing of the functional layer during menstruation (based on Bates and Bowling 2013).

1.2.3.1 The proliferative phase

The proliferative phase (follicular phase) is under the control of increasing levels of oestrogens (predominantly E2) secreted by ovarian follicles as they grow and increase the expression of aromatase (Bates and Bowling 2013, Turner et al. 2002). Oestrogens stimulate extensive cellular proliferation in the functional layer and increased mitotic events in epithelial, stromal and vascular cells (Ferenczy et al. 1979), coupled with the development of a voluminous glandular network and extensive blood vessel system (Hess, Nayak and Giudice 2006). Proliferative changes increase the overall thickness of the endometrium from 2mm up to 14mm in just 10 days (Johannisson et al. 1987, McLennan and Rydell 1965, P. Hess et al. 2006). Oestrogen receptor isoform α (ERα) is expressed by stromal cells and epithelial cells of both the lumen and glands (Critchley and Saunders 2009). Human endothelial cells are ERα-/ERβ+ but perivascular cells express both ERα and ERβ: the impact of E2 on the endothelium may be mediated directly through ERβ or indirectly via ERα in perivascular cells (Critchley et al. 2001b). Over the course of the proliferative phase epithelial cells become more ciliated which is important for distributing secretions in the subsequent phase (Campbell et al. 1988). Studies using human explant cultures have identified 3 phases of response to E2 with respect to proliferation and known E2 regulated genes including PR (Platz and Giovannucci 2004).

Studies in transgenic mice have shown E2 dependent signalling via ERα is critically important for stromal-epithelial interactions in the endometrium (Winuthayanon et al. 2010). E2 upregulates the secretion of insulin growth factor 1 by stromal fibroblasts (Igf1) (Zhu and Pollard 2007) that stimulates the proliferation of both stromal fibroblasts and epithelial cells (Walker et al. 2010, Irwin et al. 1993), and expression of epidermal growth factor receptor by epithelial cells which increases binding of EGF a potent mitogenic factor (Watson, Franks and Bonney 1996, Taketani and Mizuno 1988). ERα signalling upregulates progesterone receptor (PR) expression which is essential for priming the endometrium for morphological changes that will occur during the secretory phase (Couse and Korach 1999, de Ziegler et al. 1998).

1.2.3.2 The secretory phase

The secretory phase is also known as the luteal phase (Bates and Bowling 2013): the corpus luteum (CL) formed after ovulation, synthesises high levels of progesterone reducing epithelial and stromal cell proliferation by downregulation of ERα (Felix and Farahmand 1997). Progesterone also further upregulates the expression of PR by stromal and glandular epithelial cells (Wang et al. 1998). From days 17-20 during the early secretory phase glandular epithelial cells accumulate glycogen granules in their cytoplasm and then secrete glycoprotein-rich products into the glandular lumen to fill the uterine cavity. Glands become more tortuous and epithelial cells become highly secretory with a ciliated phenotype (Campbell et al. 1988). From days 20-22 increased vascular permeability results in stromal oedema accompanied by coiling of spiral arterioles in the functional endometrium (Bates and Bowling 2013). On day 22 maximum oedema is reached and this, alongside increasing levels of P4, stimulates stromal fibroblasts to go through a non-reversible differentiation event known as decidualisation. Decidualisation occurs during the mid-secretory phase and is the conversion of spindle-shaped stromal fibroblasts into epithelial-like cells known as decidual cells (Gellersen and Brosens 2014, Dunn, Kelly and Critchley 2003). Decidual cells accumulate collagen and laminin (Church et al. 1996) and secrete insulin-like growth factor binding protein 1 (IGFBP1) which further stimulates progesterone regulated decidualisation (Matsumoto, Sakai and Iwashita 2008). Stromal decidualisation initiates in regions directly under the luminal epithelium and in the perivascular niche around spiral arterioles and then radiates throughout the endometrium (Dunn et al. 2003). This spread is believed to occur through paracrine signalling with cytokines such as IL-11 and activin released from decidualised cells stimulating surrounding fibroblasts (Evans and Salamonsen 2012).

Decidualisation is an essential process to prepare the endometrium for the implantation of a blastocyst (Salker et al. 2010). The endometrium is only receptive to a blastocyst during the mid-secretory phase in the 'window of receptivity' which lasts for ~3 days and is determined by transient expression of adhesion molecules by the epithelium (Acosta et al. 2000). During the late-secretory phase, decidual cells secrete chemokines including CCL7, CCL13, CCL21, CCL22, CXCL8 and CX3CL1 which stimulate

recruitment of leucocytes to the endometrium (Evans and Salamonsen 2012): the numbers of leucocytes in the tissue reach a maximum at days 27-28 and persist into pregnancy if implantation occurs (Salamonsen, Zhang and Brasted 2002). Gene expression studies comparing the transcriptome of human endometrial biopsies from the proliferative and secretory phases have identified genes that may be responsible for the preparation for pregnancy such as apolopoprotein (Apo) E, PGE2 receptor, glucarunytransferase, Dkk-1, IGFBO1, osteopontin (SPP1) and laminin, among others (Kao et al. 2002, Riesewijk et al. 2003). If a pregnancy ensues, decidual cells go on to form the maternal component of the placenta (Moffett and Loke 2006) however if a pregnancy is not established, the CL regresses and menstruation occurs (Jabbour et al. 2006, Critchley and Saunders 2009).

1.2.3.3 The menstrual phase

Regression of the CL (luteolysis) in the late-secretory phase results in a rapid fall in circulating ovarian-derived steroid hormones, notably progesterone, which triggers a series of cellular, molecular and vascular changes that culminate in breakdown and shedding of the functional layer of the endometrium (Salamonsen 2003b, Niswender et al. 2000, Salamonsen 1998). Menstruation is characterised by decidual degeneration, epithelial cell death and blood vessel necrosis resulting in sloughing of endometrial tissue into the uterine lumen which together with tissue exudate and blood are lost via the vagina (Jabbour et al. 2006). Menstruation only occurs in mammals following spontaneous or induced decidualisation (Evans, Kaitu'u-Lino and Salamonsen 2011).

Menstruation has been classified as an inflammatory event because the mechanisms and cellular changes involved are similar to those observed during a physiological inflammatory response; an immediate increase in the expression of prostaglandins, cytokines and chemokines secreted by stromal decidual cells in response to progesterone withdrawal (Maybin et al. 2011b, Jabbour et al. 2006, Evans and Salamonsen 2012, Jones et al. 2004). The production of these factors further stimulates an influx of immune cells into the tissue which release MMPs and proteolytic enzymes to degrade ECM components and facilitate tissue breakdown (Critchley et al. 2001a, Kelly, King and Critchley 2002). Progesterone withdrawal has been shown to induce

the secretion of MMP precursors, urokinase-type plasminogen activator (uPA), tissue-type plasminogen activator (tPA) among other regulatory molecules which may all contribute to a rapid breakdown in tissue architecture (Evans and Salamonsen 2012). At the onset of bleeding the decidualised stroma and associated blood vessels disintegrate without an accompanying haemostatic reaction however within 20hrs blood vessels become partly or totally sealed by intravascular thrombi containing aggregated platelets and fibrin, mirroring the response observed during wound healing in other tissues (Christiaens et al. 1980, Christiaens et al. 1983). Furthermore, vasoconstriction of the spiral arteries prevents local haemorrhage and causes ischemia and focal hypoxia (Garry et al. 2010, Henriet, Gaide Chevronnay and Marbaix 2012, Maybin and Critchley 2015, Cousins et al. 2016d).

Elegant scanning electron microscopy (SEM) studies have revealed that decidual shedding is a piecemeal process with areas of shed endometrium existing beside areas of unshed endometrium, so that tissue repair occurs simultaneously with breakdown. Following the sloughing of the functionalis, the exposed basalis is rapidly covered with a fibrinous mesh within which blood components and other cell types become trapped. This mesh provides a provisional matrix upon which new epithelial cells develop and migrate (Garry et al. 2009). Similarly the expression of fibronectin and various integrins increases in the endometrium during menstruation and subsequent repair most prominently in the uppermost zone of the denuded stroma. Fibronectin interacts with specific integrins and is known to enhance cell adhesion and migration during wound healing (Slayden and Brenner 2006).

In women endometrial breakdown and repair is tightly regulated to prevent excessive blood loss and regain structural integrity of the organ. Individual factors implicated in regulation of endometrial tissue shedding and repair are further detailed in section 1.3.2.

1.2.4 The mouse oestrous cycle

Spontaneous decidualisation and menstruation are limited to the higher-order primates including humans, 4 species of bat, the elephant shrew and a recently described member of the Spiny mouse species (Acomys cahirinus) (Bellofiore et al. 2018). The

majority of rodents including rats and mice have a relatively short reproductive cycle known as the oestrus cycle (Caligioni 2009). The first detailed analysis of the mouse oestrus cycle was by Allen in 1922 who observed both external and internal signs of oestrus in 90 animals. The presence of specific cell types in vaginal lavage was used to define 4 distinct phases: proestrus (P) by nucleated epithelial cells; oestrus (O) by cornified epithelial cells; metoestrus (M) by cornified epithelial cells and leucocytes; and dioestrus (D) by leucocytes (Allen 1922, Caligioni 2009, Byers et al. 2012).

As in women regulation of endometrial function in the mouse is governed by fluctuating levels of ovarian-derived steroid hormones (Figure 1-7 (A)). During the P and O phases the endometrial stroma undergoes extensive proliferation in response to increasing circulating levels of oestrogen. Unlike in the human endometrium however, the stroma does not undergo spontaneous decidualisation in response to increased levels of progesterone during M, rather the presence of a blastocyst is required. In addition, the stroma does not breakdown when progesterone levels drops (D), instead the tissue is reabsorbed before the cycle begins again (Caligioni 2009, Fata, Chaudhary and Khokha 2001, Strassmann 1996). The mouse uterus is composed of two uterine horns (Figure 1-7 (B)) which is morphologically different to the human simplex uterus (Figure 1-7 (C)). Despite additional differences in the cycle, the cellular composition of endometrial tissue is remarkably similar between humans and mice: the outer muscular myometrium encloses the multicellular endometrial stroma containing stromal fibroblasts and blood vessels, and the lumen and glands are lined with epithelial cells (Figure 1-7 (D)) (Fata et al. 2001). Such similarities in structure and the availability of countless transgenic mouse strains, make the mouse an attractive model in which to interrogate mechanisms associated with endometrial function.

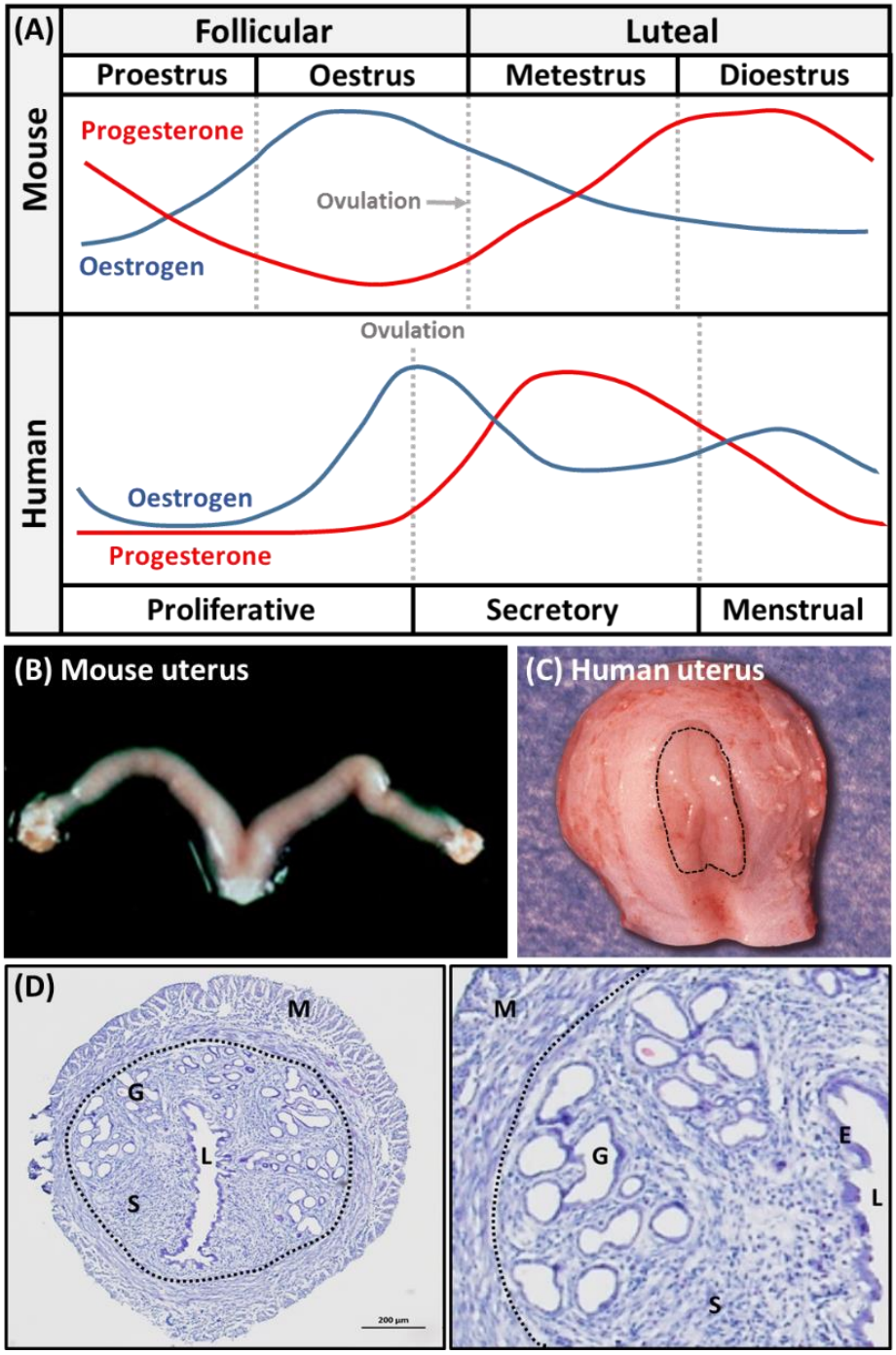

Figure 1-7. Comparison of the mouse oestrus cycle with the human menstrual cycle. (A) Schematic representation of cyclical changes in steroid hormone levels across a 4 day oestrous cycle (mouse) and a 28 day menstrual cycle (human). Both species experience increasing concentrations of oestrogen during the follicular phase with a peak just prior to ovulation. Progesterone concentrations increase during the luteal phase. Anatomical structure of the **(B)** mouse and **(C)** human uterus (Adapted from Gargett, Chan and Schwab 2008, Fata et al. 2001). **(D)** Cross section through a mouse uterine horn displaying the outer muscular myometrium (M), endometrial stroma (S) embedded with glands (G), and the lumen (L) lined with epithelial cells (E) (Author's own H&E images).

1.3 Endometrial repair

1.3.1 Post menstrual repair

It has been postulated that as well as initiating tissue breakdown the withdrawal of progesterone initiates endometrial repair processes. This is supported by microarray analysis of human endometrial explants cultured in the presence or absence of hormonal support *in vitro*, where hormone deprived explants had a gene signature in line with 'wound healing and inflammation' (Gaide Chevronnay et al. 2012). Menstruation is the culmination of vascular, cellular and inflammatory changes which leaves the luminal surface in a 'wounded' state (Maybin and Critchley 2015). In order to limit blood loss and regain tissue function for the subsequent cycle, rapid re-epithelialisation and structural reorganisation is required without the accumulation of any functional damage or fibrotic scar tissue (Salamonsen 2003a, Cousins et al. 2014, Maybin and Critchley 2015). Although the human endometrium is the only adult tissue that undergoes regular and repeated cycles of degeneration and regeneration under normal physiological conditions (Gargett and Masuda 2010) parallels can be drawn between mechanisms of post menstrual endometrial repair and the wound healing response of the skin and oral mucosa (Figure 1.1) (Shaw and Martin 2009, Leavitt et al. 2016, Critchley et al. 2006a). In foetal skin and oral mucosa it is believed scar-free healing is facilitated by a diminished inflammatory response and altered fibroblast phenotype (Szpaderska et al. 2003, Martin and Leibovich 2005, Leavitt et al. 2016). This appears to be in contrast to endometrium which experiences both a significant influx of immune cells and cascade of inflammatory signals during menstruation (Evans and Salamonsen 2012). Hence it appears the endometrium may represent a tissue that sits between scarless and scarring tissue repair and studies on this tissue may therefore shed new light on the mechanisms of each process.

Whilst morphological and cellular changes that occur during the various phases of the menstrual cycle have been well documented less is known about the mechanisms that govern post-menstrual endometrial tissue repair. Decidual shedding and repair was documented as a 'piecemeal process' which occurred simultaneously in regions

throughout the uterine cavity (Figure 1-8), with an important role for the stromal compartment being highlighted (Garry et al. 2009).

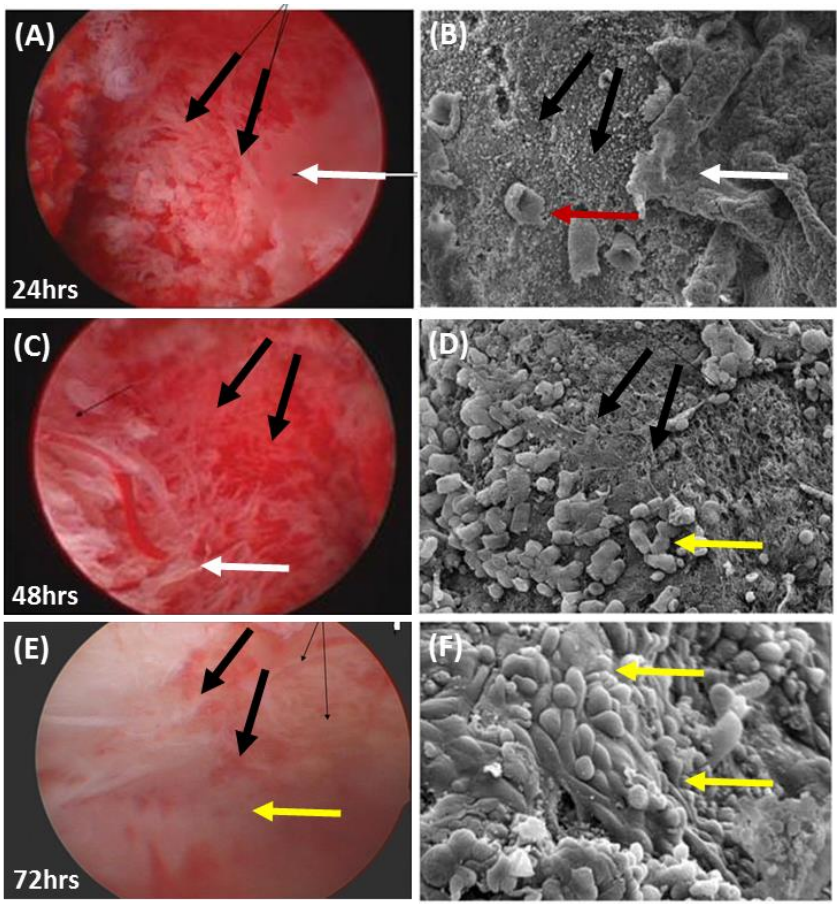

Figure 1-8. Visualisation of the human endometrium during menstruation using hysteroscopy (A, C, E) and scanning electron microscopy (SEM) (B, D, F). Decidual shedding is a progressive piecemeal process with areas of denuded stroma and exposed glands found alongside regions of unshed tissue at 24hrs (A-D, black versus red versus white arrows). At 48hrs new epithelial cells are present (D, yellow arrows) and by 72hrs the luminal surface is almost completely re-epithelialised (F, yellow arrows) (Adapted from Garry et al. 2009).

Endometrial repair occurs in a steroid hormone depleted environment as regression of the CL results in low levels of circulating steroids. Using a mouse model of endometrial breakdown and repair in which mice were ovariectomised (described fully 1.7.5), Kaitu'u-Lino *et al* reported complete healing occurred even if mice were fed a

soya-free diet and treated with an aromatase inhibitor consistent with E2-independence (Kaitu'u-Lino, Morison Nb Fau - Salamonsen and Salamonsen). Similarly, a xenograft technique has been used whereby human endometrial explants are transplanted subcutaneously into mice and menstrual changes induced by administering E2 and P4 to mimic the 28-day human cycle. Upon steroid hormone withdrawal explants are seen to undergo tissue degeneration but return to a proliferative phenotype within 4 days in the absence of hormonal support (Matsuura-Sawada et al. 2005).

1.3.2 Factors reported to regulate menstrual shedding and repair

1.3.2.1 Hypoxia

Progesterone withdrawal is associated with an increase in the synthesis of prostaglandins inducing arteriole vasoconstriction which results in an increase in focal hypoxia and expression of VEGF (Figure 1-9, orange pathway) (Maybin et al. 2011a, Maybin et al. 2011b, Cousins et al. 2016d). Hypoxia is considered an important regulator of endometrial breakdown and repair (Semenza 1998). Hypoxia stabilises hypoxia-inducible factor 1α (HIF1α), a transcription factor that mediates a cell's homeostatic response to reduced oxygen availability (Semenza 1998). In the Edinburgh mouse model of endometrial breakdown (Section1.7.5) striking spatial and temporal fluctuations in hypoxia have been visualised with changes being correlated with changes in gene expression of VEGF and CXCL12 suggesting hypoxia has a role in driving both the angiogenic response and inflammation (Cousins et al. 2016d). In the same model stabilisation of HIF1α has been shown to enhance re-epithelialisation of the denuded stromal surface (Figure 1-9, yellow pathway) with pharmacological reduction in HIF1α delaying complete repair (Maybin et al. 2018). Evidence for stabilisation of HIF1α in human endometrial tissue has been detected during the secretory and menstrual phase and is believed to regulate the expression of genes involved in angiogenesis including IL8 (Maybin et al. 2011b, Maybin et al. 2011a). Using endometrial biopsy specimens it has been shown that *in vitro* P4 withdrawal increased IL8 secretion but only in the presence of hypoxia (Maybin et al. 2011b). Contrasting data were published by Coudyzer *et al* who used a xenograft model of menstruation where fragments of human endometrium were engrafted to

ovariectomised immunodeficient mice: in this model they could not detect evidence for increased HIF1α and concluded that hypoxia is not required to trigger menstrual-like tissue breakdown or repair in human endometrium (Coudyzer et al. 2013).

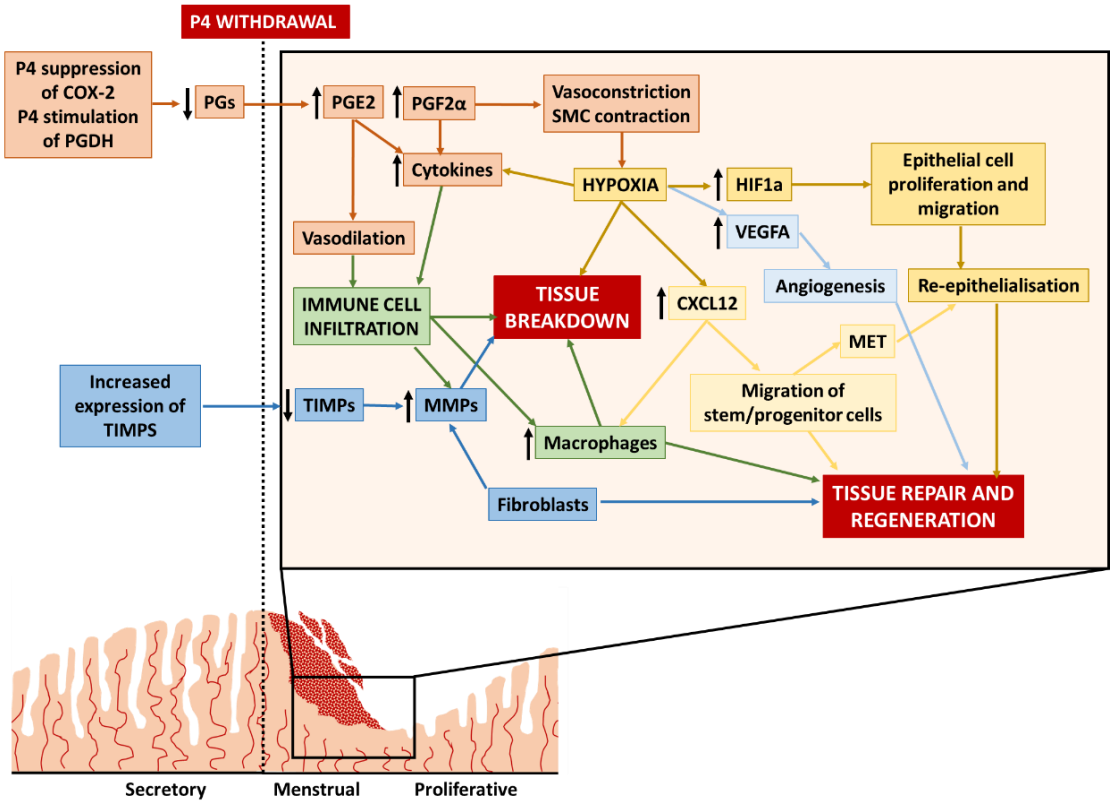

Figure 1-9. Schematic representation of mechanisms that trigger the initation of tissue breakdown and shedding during menstruation. Progesterone withdrawal stimulates an increase of COX1 and a decrease in PGDH which results in an increase in prostaglandin synthesis. This induces hypoxia through PGF2α-stimulated vasoconstriction, and immune cell infiltration through PGE2-stumlated vasodilation (orange pathway). Hypoxia increases expression of HIF1α which stimulates cytokine release (orange pathway) and epithelial cell proliferation and migration (gold pathway). Hypoxia also stimulates release of CXCL12 which enhances macrophage function (green pathway) and the activation of stem/progenitor cells (yellow pathway). Decreased expression of TIMPS and increased expression of MMPs by immune cells and fibroblasts results in breakdown of decidualised tissue (blue pathway). ↑: increase, ↓: decrease, COX2: cyclooxygenase, PGDH: prostaglandin dehydrogenase, PGF2α: prostaglandin F2 alpha, PGE2: prostaglandin E2, MMPs: matrix metalloproteinases, TIMPS: tissue inhibitors of MMPs, HIF1α: hypoxia-inducible factor 1α, VEGFA: vascular endothelial growth factor A, MET: mesenchymal to epithelial transition (Figure compiled by author based on research by Critchley et al. 2006b, Maybin et al. 2011a, Gaide Chevronnay et al. 2012, Salamonsen and Woolley 1999, Punyadeera et al. 2006).

1.3.2.2 Matrix metalloproteinases (MMPs)

MMPs are zinc-dependent endopeptidases that when activated cleave almost all components of ECM (Nagase, Visse and Murphy 2006): TIMPs are endogenous tissue inhibitors of MMPs. The cyclical remodelling and breakdown of ECM observed during the menstrual cycle depends on MMPs the activity of which is tightly controlled to allow for efficient tissue breakdown, concurrent repair and accurate remodelling in preparation for the next cycle (Gaide Chevronnay et al. 2012). The role of MMPs in endometrial breakdown was first described *in vitro* using human endometrial explant cultures to demonstrate oestrogen and progesterone supress the expression of MMP1, 3 and 7 suggesting that hormones regulate MMP expression in endometrial tissue (Marbaix et al. 1996b). This hypothesis was supported by an elegant study in ovariectomized macaques, where progesterone implants were removed at the end of the simulated cycle but replaced at staggered time-points from 12 to 72hrs after initial withdrawal (Slayden and Brenner, 2006). Replacement up to 24hrs after withdrawal prevented menstruation and prevented increases in endometrial MMP1, 2 and 3. Replacement after 36hrs had no effect on menstruation and partially blocked MMP production, with significantly less endometrial MMP2 expression. Other studies have confirmed an immediate increase in MMP1, 3, 7, 9, 11 and 12 in response to progesterone withdrawal (Figure 1-9, blue pathway) (Goffin et al. 2003, Vassilev et al. 2005, Salamonsen and Woolley 1999).

Using an *in vivo* human explant technique Vassilev *et al* demonstrated that high levels of TIMP mRNAs are maintained throughout the menstrual cycle supposedly to regulate the extent of tissue degradation, while various MMPs (MMP-1, MMP-3, MMP-7, MMP-10) were upregulated during menstruation and endometrial repair which apparently overwhelms the actions of TIMPs. Of particular note in this study was that MMP10 was expressed at very high levels during menstruation and located throughout the endometrial stroma, being identified as a menstruation-associated MMP (Vassilev et al. 2005). In a mouse model of endometrial breakdown and repair MMP3, MMP7, MMP9 and MMP13 were significantly upregulated during menstruation and postmenstrual repair but administration of two MMP inhibitors, doxycycline and batimistat, had little effect on endometrial repair suggesting they are

not key mediators (Kaitu'u et al. 2005). The mouse model has been further used to demonstrate integrin-fibronectin interaction and MMP-facilitated cell movement during re-epithelilisation (Evans et al. 2011). In a recent study using the Edinburgh mouse model administration of DHT resulted in delayed restoration of the luminal epithelium associated with changes in expression of MMP3, MMP9, Snai3 and osteopontin, important regulators of MET (Cousins et al. 2016b).

It is believed that leucocytes play an important role in menstruation in part by releasing MMPs (Figure 1-9, green pathway). In a mouse model, MMP7 and 9 colocalised with leucocyte subsets particularly neutrophils (Kaitu'u et al. 2005). In a xenograft model, MMP1, 2 and 9 were increased following progesterone withdrawal concurrent with an infiltrating leucocyte population (Guo et al. 2011); co-culture studies have revealed that BM-derived mast cells and neutrophils release MMPs when cultured with human endometrial stromal cells (Salamonsen et al. 2000). Neutrophils contain high levels of MMPs and have the ability to activate resident MMPs to initiate endometrial breakdown (Gaide Chevronnay *et al.*, 2011) and depletion of granulocytes using an anti-mouse GR-1 antibody (expressed on BM-derived monocytes and neutrophils) decreased the expression of matrix modifying enzymes such as MMP3, 9 and 10 and impaired tissue repair (Menning et al. 2012).

An *in vitro* study of human endometrial stromal fibroblasts demonstrated that activated platelet-rich plasma enhanced cell migration and proliferation and significantly increased the expression of MMP1, MMP3, MMP7, MMP26 and various cytokines specifically in endometrial fibroblasts and MSCs (Aghajanova et al. 2018). The withdrawal of progesterone triggers focal expression of MMPs specifically in regions undergoing lysis, mediated by cytokines such as IL-1α, LEFTY-2 and TNFα (Gaide Chevronnay et al. 2012). It has been reported that MMPs undergo receptor mediated endocytosis through the low density lipoprotein receptor-related protein 1 (LRP-1) which clears active MMPs during the proliferative and secretory phases. Loss of LRP-1 during tissue shedding also enhances MMP activity during endometrial tissue breakdown (Gaide Chevronnay et al. 2012). Active forms of MMP2 and MMP9 are significantly reduced in menstrual endometrium of women with HMB (Malik et al. 2006) further supporting a role of MMPs in efficient endometrial tissue repair.

1.3.2.3 Angiogenesis

Endometrial repair and regeneration requires a substantial angiogenic response. Biosynthesis of VEGF, a signalling molecule that plays a key role in stimulating growth of new blood vessels, is triggered by hypoxia in the menstrual phase and then by oestrogen in the subsequent proliferation phase (Figure 1-9, pale blue pathway) (Punyadeera et al. 2006). In a rhesus macaque model VEGF mRNA is upregulated in the glands and stroma 1-2 days after progesterone withdrawal and VEGFR1 and 2 is increased in endothelial cells immediately below the luminal surface, implicating epithelial-derived VEGF in neoangiongenesis during endometrial regeneration (Nayak and Brenner 2002). Fan *et al* showed that blocking VEGF action (VEGF Trap) during menstruation in both primate and mouse models, completely inhibited neoangiogenesis while not affecting existing vessels. What is more the process of re-epithelialisation was also inhibited and additional *in vitro* studies confirmed that migration of luminal epithelial cells involved signalling through the VEGFR-NP2 on stromal cells. (Fan et al. 2008). In human endometrium changes in VEGF ligands and receptors were associated with increased expression of HIF1α in menstrual and early proliferative phase (Punyadeera et al. 2006) with results obtained that mirrored those in primates extending the understanding of VEGF and the hormonal regulation of VEGFR-NP1 during menstruation (Germeyer et al. 2005).

1.3.2.4 Re-epithelialisation: epithelial proliferation and migration

One of the most fundamental processes of endometrial repair is complete restoration of the luminal epithelial cell layer. In women re-epithelialisation begins on day 2 of menses and full epithelial coverage of the denuded stromal surface is achieved by day 5 (Garry et al. 2009). In depth morphological analysis of the human endometrium during menstruation showed that a fibrinous mesh is rapidly produced that covers the denuded surface of the basalis endometrium. It is upon and within this fibrinous mesh that new epithelial cells develop and migrate to re-epithelialise the surface (Garry et al. 2009). Originally it was believed that new epithelial cells arose from epithelial cells residing in basal glands that were preserved during decidual shedding (Novak 1946). Ferenczy updated the hypothesis in the 1970s by suggesting that new epithelial cells

also arose from proliferation of intact surface epithelium bordering regions of denuded stroma that was not lost during shedding (Ferenczy 1976). When Garry *et al* analysed tissue morphology during active bleeding they discovered that immediately before and during menstruation, epithelial cells of the glands undergo apoptosis and are shed with the decidua to be replaced by small rounded epithelial cells. As these cells did not appear to be proliferating it was hypothesised that some of the new epithelial cells were arising through differentiation of the stromal compartment (Garry et al. 2009).

A study by Kaitu'u *et al* exploring cell proliferation in a mouse model of menstruation showed that during early stages of breakdown and repair extensive luminal epithelial cell proliferation occurred with a population of glandular epithelial cells proliferating during the later repair stage (Kaitu'u-Lino, Ye and Gargett 2010). More recently, using the Edinburgh menses mouse model Cousins *et al* showed epithelial cells of the lumen and glands undergo extensive proliferation during repair while a small amount of proliferation was also detected in the stroma. Detailed immunohistochemistry revealed that epithelial cells in regions of the denuded surface were smaller and more rounded and appearing to 'roll' across the surface of the stroma, in line with a migratory phenotype. To support this data significant increases in stromal mRNAs (Cdh2, Vimentin, Wnt4) were detected in the early repair phase which decreased in later phases while epithelial genes (Cdh1, Wnt7a, Krt18) were decreased in early phases and increased in later phases (Cousins et al. 2014). This suggests that residual epithelial cells undergo a morphological change to exhibit a migratory phenotype, indicative of an epithelial-to-mesenchymal transition (EMT) (Figure 1-10). Interestingly, *in vitro*, human endometrial epithelial cells respond to hypoxia by decreasing expression of E-cadherin and increasing expression of N-cadherin, Vimentin and Snail, changes known to be indicative of EMT. Overexpression of HIF1α induced changes characteristic of EMT under normoxic conditions and it was concluded that hypoxia can stimulate EMT of endometrial epithelial cells, essential to migration (Xiong et al. 2016). As transient focal hypoxia is present in endometrial tissue in the initial phases of tissue breakdown and repair (Maybin et al. 2018) it may be that hypoxia may drive EMT and the acquired migratory phenotype of epithelial cells during initial phases of endometrial repair.

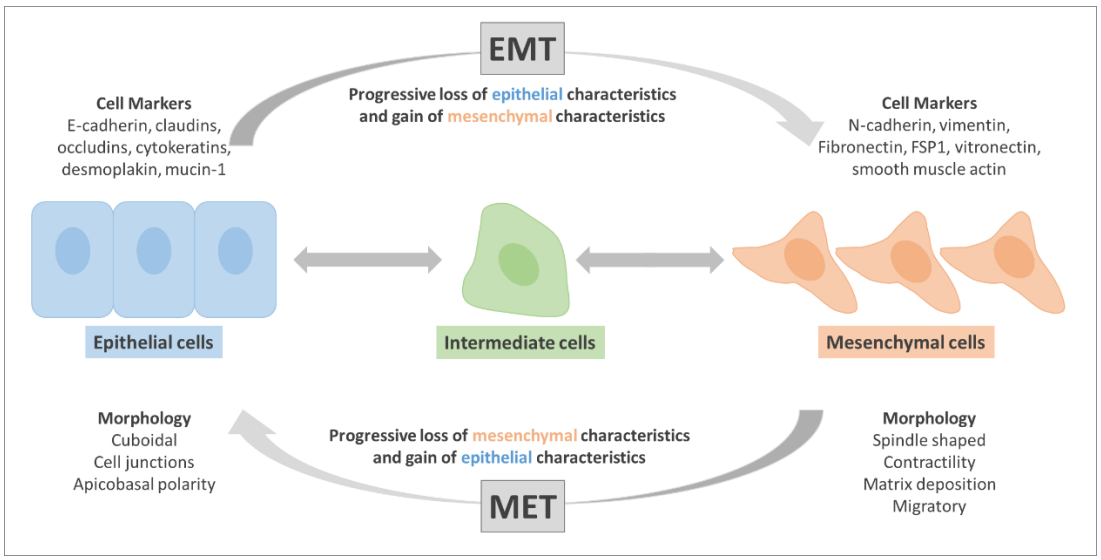

Figure 1-10. Overview of the epithelial to mesenchymal transition (EMT). During EMT, polarised epithelial cells (blue) undergo a functional and morphological transisition into migratory mesenchymal cells (orange). Epithelial cells express markers such as E-Cadherin, Occludins and Cytokeratins while mesenchymal cells express N-cadherin, Vimentint and Fibronectin. Cells of an intermediate phenotype (green) express markers of both epithelial and mesenchymal cells however upon complete transition epithelial markers are lost. The reverse process of mesenchymal to epithelial transition (MET) can also take place whereby mesenchymal cells undergo a transition into an epithelial phenotype (based on Kalluri and Weinberg 2009).

1.3.2.5 Mesenchymal to epithelial transition (MET)

There is a range of evidence suggesting stromal cells have a role to play in re-epithelialisation (Baggish, Pauerstein and Woodruff 1967). Studies using SEM identified groups of newly formed epithelial cells that were not associated with gland structures or residual luminal epithelium (Garry et al. 2009), suggesting stromal cells may be transdifferentiating into epithelial cells a process called mesenchymal-to-epithelial transition (MET) (Kalluri and Weinberg 2009, Maybin and Critchley 2015). Fate mapping studies carried out using Amhr2-Cre;Rosa26-EYFP double transgenic mice in which EYFP is expressed exclusively by the mesenchymal cell compartment detected EYFP in endometrial epithelial cells lining the lumen following parturition or in a pseudopregnancy model of menstruation. These MET cells could also be detected by co-expression of mesenchymal and epithelial cell

markers (vimentin and cytokeratin respectively) (Patterson et al. 2013). Cousins et al provided evidence that re-epithelialisation involved luminal and glandular epithelial cell proliferation and migration and a MET by cells of the stromal compartment in proximity to the denuded surface (Figure 1-11). Using detailed immunohistochemistry, they located cells in the stromal compartment adjacent to areas of denuded stroma that expressed both vimentin (stromal marker) and pan cytokeratin (epithelial marker) indicative of a MET. This study also highlighted dynamic changes in expression of genes implicated in regulation of EMT and MET including WT1, Snai1, Snai2, Snai3, Cdh1, cytokeratin, Wnt1, osteopontin and Vim (Cousins et al. 2014).

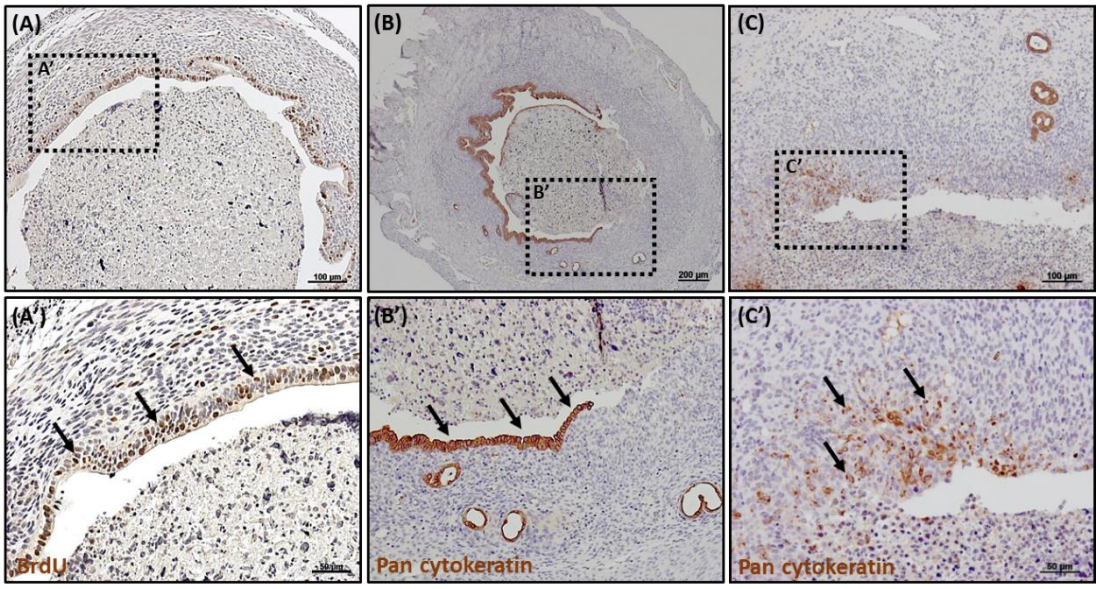

Figure 1-11. Immunohistochemistry demonstrating the three synchronous mechanisms by which re-epithelialisation occurs during endometrial repair in the Edinburgh menses mouse model (24hrs following P4 withdrawal). (A-A') BrdU expression identifies epithelial cell proliferation in luminal epithelial cells (black arrows). **(B-B')** Pancytokeratin expression identified epithelial cells that have a rounded morphology and appear to be migrating over the denuded stromal surface. **(C-C')** Evidence for pancytokeratin expression by mesenchymal cells of the stromal compartment indicative of an MET (Adapted from Cousins et al. 2014).

In summary the current consensus is that three synchronous mechanisms contribute to re-epithelialisation during endometrial repair: glandular epithelial cell proliferation

and migration, luminal epithelial cell proliferation and migration and MET by cells of the endometrial stroma (Garry et al. 2009, Patterson et al. 2013, Cousins et al. 2014) (Figure 1-11). These studies do not discriminate between different stromal cell populations and it has been proposed that stromal LRCs may also have the ability to proliferate and differentiate into epithelial cells during endometrial repair although to date there is no definitive evidence for this.

1.4 Endometrium and inflammation

Inflammation is a key regulator of the wound healing response (Cash and Martin 2016, Gurevich et al. 2018, Vannella and Wynn 2017). However excessive and persistent inflammation is associated with chronic non-healing wounds, fibrosis and abnormal tissue repair (Zhao et al. 2016, Qian et al. 2016) while scar-free tissue repair of foetal skin and oral mucosa is associated with a reduced inflammatory response and cell influx (Martin and Leibovich 2005, Morris et al. 2014, Szpaderska et al. 2003).

Menstruation is now considered to be an 'inflammatory' event as progesterone withdrawal stimulates a cascade of inflammatory signals including increased release of cytokines, chemokines and prostaglandins (Maybin et al. 2011b, Evans and Salamonsen 2012, Critchley et al. 2001a). Similarities between the processes occurring during menstruation and the inflammatory response of normal wound healing was first observed by Finn *et al* using a mouse model of menstruation who noted that the first morphological change in the uterus following P4 withdrawal was an infiltration of leucocytes into the stroma (Finn and Pope 1986). Interactions between these leucocytes and the decidualised stromal cells result in the release of pro-inflammatory mediators which in turn stimulate the production and activation of various degradative enzymes culminating in the rapid breakdown and shedding of the decidua (Evans and Salamonsen 2012). Menstruation has been proposed as a 'model of self-limiting inflammation' (Maybin and Critchley 2015).

A number of inflammatory mechanisms have been highlighted to playing a role in the co-ordination of the menstrual inflammatory response. The activity of reactive oxygen species (ROS) scavenging enzymes (superoxide dismutases) changes in response to fluctuating hormone levels throughout the menstrual cycle and importantly decreases

upon withdrawal of progesterone (Sugino et al. 2002). This results in an increase in ROS which stimulate various downstream signalling pathways including the NFκB pathways culminating in the production of inflammatory cytokines, chemokines and prostaglandins (Sugino et al. 2004). NFκB target genes include MMP9, COX-2, CCL1, CCL3, CCL5, CXCL1, CXCL8, IL-6, IL1β, GM-CSF and TNFα (Evans and Salamonsen 2012).

It is believed that progesterone acts as an anti-inflammatory mediator during the proliferative and secretory phases in part by suppression of the COX-2 enzyme which synthesises prostaglandins from arachidonic acid, and stimulation of prostaglandin 15 dehydrogenase enzyme (PGDH), the enzyme responsible for conversion of prostaglandins to inactive metabolites (Figure 1-9, orange pathway) (Evans and Salamonsen 2012, Catalano et al. 2007). In women taking Mifepristone, a potent antiprogestagen, serum progesterone levels are significantly reduced which results in a decrease in the expression of PGDH and an increase in cyclooxygenase-2 (COX2), consistent with progesterone withdrawal during menstruation stimulating an upregulation in the synthesis of prostaglandins which are key mediators of the inflammatory response (Hapangama et al. 2002, Jensen Dv Fau - Andersen, Andersen Kb Fau - Wagner and Wagner). Different prostaglandins have different roles in the inflammatory response. Specifically, PGF2α promotes vasoconstriction of the spiral arteries and smooth muscle contraction contributing to the hypoxic environment and menstrual shedding respectively (Fan et al. 2008). On the other hand, PGE_2 stimulates vasodilation and therefore may enhance oedema and leucocyte infiltration (Figure 1-9, orange pathway) (Jensen Dv Fau - Andersen et al. , Evans and Salamonsen 2012). Prostaglandins also have roles in mediating the production of cytokines such as CXCL1 and CXCL8 involved in leucocyte recruitment and growth factors such as adrenomedullin and VEGF important to endometrial repair (Evans and Salamonsen 2012). Notably, the ratio of PGF2α:PGE_2 has been found to be significantly lower in the endometrium of women suffering from heavy menstrual bleeding (HMB) suggesting a link between the regulation of prostaglandin synthesis and the extent of bleeding during menstruation (Smith et al. 1981).

1.4.1 Immune cell populations in the endometrium

The immune system has two components: the innate immune system which is non-specific and is stimulated immediately to recruit immune cells including neutrophils, macrophages and natural killer cells to the site of infection/injury; and the adaptive immune system which is more specialised and activated when specific antigens are presented to T cells and an antigen-specific response is generated (Berbic et al. 2014). Cytokines, chemokines and growth factors stimulate leucocyte recruitment to endometrial tissue during the menstrual cycle. For example, progesterone withdrawal upregulates the expression of cytokines and chemokines including CXCL8 which is a neutrophil chemotactic factor (Maybin et al. 2011b) and CCL-2 which is a monocyte chemotactic factor (Jabbour et al. 2006b, Critchley et al. 1999). Several cytokines including CCL2, CXCL1, CXCL8 and CX3CL1 have been found to be expressed perivascularly (Slayden and Brenner 2006, Catalano et al. 2007, Wallace et al. 2009, Jolicoeur et al. 1998) whilst others including TNFα, CXCL12, CXCL8, CCL2, IL-1β, CXCL1 and endothelin are expressed in the epithelium and stroma (Berbic et al. 2014). Leucocytes may also secrete cytokines which can exacerbate the inflammatory response.

Immune cells account for ~10% of cells in endometrial stromal during the proliferative phase, ~25% of cells in the secretory phase and up to 40% of cells in the menstrual phase (Starkey, Clover and Rees 1991, Kamat and Isaacson 1987, Salamonsen and Lathbury 2000, Maybin and Critchley 2015), summarised in Figure 1-12. The major leucocyte populations present in the endometrium during menstruation in women are uterine (u) NK cells and mast cells which proliferate within the tissue, and neutrophils, macrophages, and eosinophils which are recruited from the circulation (Salamonsen and Woolley 1999). Using a xenograft model of menstruation where human endometrial tissue is transplanted subcutaneously to immunocompromised mice, it was shown that human CD45+ cells increased and peaked during the secretory phase while mouse CD45+ cells increased during the menstrual phase and peaked 3 days following progesterone withdrawal, suggesting that tissue resident immune cells are important during endometrial tissue breakdown while immune cells recruited from the circulation have a more prominent role in endometrial repair (Guo et al. 2011).

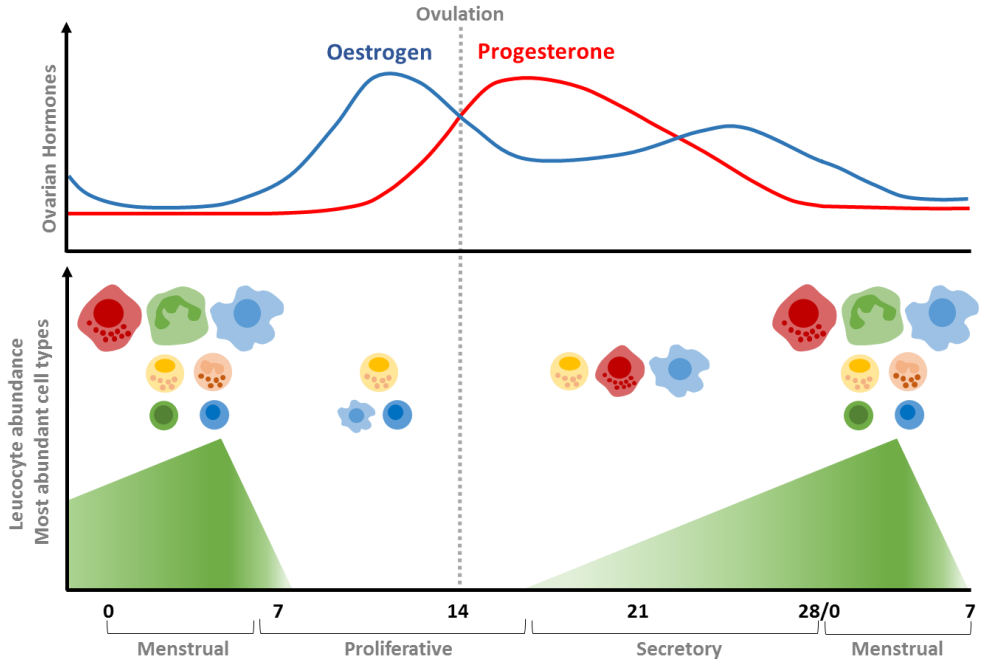

Day of cycle	0-7	10-12	20-26	0-7
Macrophages	+ + +	+	+ +	+ + +
Neutrophils	+ + +	-	-	+ + +
Eosinophils	+ +	-	-	+ +
Mast cells	+ +	+ +	+ +	+ +
T-lymphocytes	+	+	-	+
B-lymphocytes	+	-/+	-/+	+
uNK cells	+ + +	-	+ +	+ + +

- (0) + (1-2) ++ (3-5) +++ (6-15) % of total endometrial cells

Figure 1-12. Schematic representation of cyclical changes in the immune cell population of the endometrium during the menstrual cycle. Top panel represents fluctuations in steroid hormone levels that govern the menstrual cycle. Bottom panel displays the increase in abundance of immune cells during the secretory phase which peaks during menstruation. The contributing immune cells are symbolized with the increasing size relating to relative abundance. The table outlines immune cell populations and present in the endometrium and their relative abundance during different phases of the menstrual cycle as a proportion of total cells present in the endometrium (based on Starkey et al. 1991, Kamat and Isaacson 1987, Salamonsen and Lathbury 2000, Maybin and Critchley 2015).

1.4.2 Role of uNK cells

Natural killer (NK) cells are large, granular lymphocytes which target infected cells by secretion of granular protein such as perforin and granzymes which induce an apoptotic response (Berbic et al. 2014). A specialised subset of uterine NK cells exists in the endometrium, identified as $CD56^{bright}$ which have lower cytotoxic ability but more potent cytokine secretion than their peripheral counterparts. uNK cells increase in number during the secretory phase (Bulmer and Lash 2005) as a result of *in situ* proliferation as demonstrated by expression of Ki67 (Kämmerer et al. 1999). uNK cells ($CD56^{bright}$CD16-) can be distinguished from peripheral blood NK cells ($CD56^{dim}CD16^{bright}$) and account for the majority of leucocytes present in the endometrium during the late secretory phase and through to early pregnancy (Jabbour et al. 2006b). uNK cells have been implicated in vascular remodelling during the menstrual cycle and placentation (Manaster et al. 2008) as they are located in close proximity to spiral blood vessels and have been shown to secrete IFNγ which dilates and thins the walls of spiral arteries to enhance blood flow to the implantation site (Jabbour et al. 2006b). uNK cells accumulate in perivascular regions and express angiogenic factors including placental growth factor, angiopoietin 2 and VEGF-C which stimulates endothelial cell proliferation and migration and are therefore implicated in angiogenesis (Li et al. 2001, Hanna et al. 2006). HMB is associated with altered endometrial vasculature and it has been found that in women with HMB there are reduced numbers of uNK cells during the secretory phase which may impact on vessel development (Biswas Shivhare et al. 2015).

Cyclical changes in uNK cell number are considered consistent with hormonal regulation (Henderson et al. 2003): uNK migration has been shown to be enhanced by administration of E2 *in vitro* and conditioned media from uNK cells treated with E2 can increase angiogenesis by human endometrial endothelial cells, in a CCL2-dependent manner (Gibson et al. 2015). The mRNA for ERβ and GR but not ERα or PR, has been detected in purified human uNK cells and it is believed that oestrogens and glucocorticoids can act directly on uNK cells while progesterone acts indirectly (Henderson et al. 2003) potentially via stromal cell secretion of IL-15 and prolactin. A role for uNK cells in endometrial repair has not been proposed.

1.4.3 Role of neutrophils

Neutrophils are polymorphonuclear cells, representing the most abundant leucocyte in the circulation of human blood with a short life span of only a few hours. In many inflammatory responses, neutrophils are the dominant cell population in the initial leucocyte influx and primary mediators of the inflammatory response, recruited quickly to sites of infection/injury where they persist for days, release pro-inflammatory mediators and phagocytose pathogens and cellular debris (Berbic et al. 2014, Martin and Leibovich 2005). The endometrial neutrophil population shows a dramatic change in numbers during the human menstrual cycle and they are the most prominent leucocyte present during decidual tissue breakdown (Kamat and Isaacson 1987) being reported as 6-15% of total cell number peri-menstrually (Lathbury and Salamonsen 2000). In a recent study immunostaining of human endometrial tissue sections using an antibody directed against neutrophil elastase reported immunopositive staining restricted to samples recovered during active menses (Armstrong et al. 2017). In the endometrium neutrophils influx through spiral arteries in response to chemokines secreted by decidual tissue and the vessels themselves (Jones et al. 2004).

In a mouse model of simulated ‘menstruation’ Kaitu’u-Lino *et al* used anti Ly6B2 antibodies to identify putative neutrophils and reported they were low in number during the proliferative and secretory phase and most abundant 24hrs after progesterone withdrawal. Using the RB6-8C5 antibody to specifically deplete neutrophils from both the circulation and in peripheral tissues, it was shown that there was aberrant tissue breakdown and marked delay in repair, suggesting that the neutrophils are essential for endometrial repair. Authors also reported that F4/80 expressing macrophages were in low abundance and therefore unlikely to contribute to endometrial tissue repair (Kaitu'u-Lino, Morison and Salamonsen 2007). Another study used an anti-mouse GR-1 antibody to target and deplete neutrophils resulting in decreased expression of MMPs and dysregulated endometrial repair (Menning et al. 2012). When human endometrial stromal fibroblasts are cultured with human blood neutrophils there is an increase in the secretion of MMPs identified above as critical mediators of endometrial tissue breakdown (Lathbury and Salamonsen 2000).

Characterisation of the inflammatory response during menstruation in the Edinburgh mouse model demonstrated that Ly6G+ putative neutrophils peaked at 24hrs during active repair (Armstrong et al. 2017).

Neutrophils synthesize and release a wide range of immunoregulatory cytokines and can initiate and orchestrate immune responses (Martin and Leibovich 2005). Neutrophils in the endometrium during menstruation express VEGF-A, an angiogenic factor which plays an important role in the regulation of vascular permeability and new blood vessel formation (Mueller et al. 2000). Neutrophils contain granules which hold a variety of degradative enzymes including neutrophil elastase, cathepsin C, MMP9 and proteinase 3 which can activate latent forms of pro-inflammatory mediators including TNFα and IL-1β (Evans and Salamonsen 2012). Furthermore neutrophils have been shown to express the antiproteinase and antimicrobial molecule elafin during menstruation, a molecule involved in the regulation of proteolytic enzymes (King et al. 2003). Neutrophil granule subsets have specialised functions and their specific release depends on signals from the immediate environment. Some granules contain proMMP8 and proMMP9 released when neutrophils are stimulated, which are then activated by proteolytic cleavage by mast cell tryptase, MMP9 and MMP3. In this way an MMP cascade is initiated which is central to endometrial tissue breakdown and repair highlighting an important role for neutrophils in endometrial repair (Evans and Salamonsen 2012).

1.4.4 Role of macrophages

The mononuclear phagocyte population belongs to the innate immune system and includes monocytes and macrophages which have a longer life span than neutrophils. Upon extravasation from the circulation and migration to the tissue, circulating peripheral blood monocytes differentiate into mature macrophage phenotypes (Martin and Leibovich 2005). In recent years however, the simple view that all macrophages arise through differentiation of circulating monocytes after they extravasate from the blood stream and enter peripheral tissues (Van Furth and Thompson 1971, Martin and Leibovich 2005) has been challenged. New data from lineage tracing experiments in mice suggest there are at least three origins of tissue-resident macrophages: those

arising from haematopoietic stem cells or yolk sac progenitor cells established during development or those being continuously replaced by BM-derived progenitors in response to changes in tissue microenvironment (Ginhoux et al. 2010, Schulz et al. 2012, Wynn, Chawla and Pollard 2013). Furthermore, the circulating monocyte population is heterogeneous and therefore distinct recruitment mechanisms may exist that may vary between tissues (Evans and Salamonsen 2012). The primary role of macrophages in inflammatory responses is to phagocytose and destroy pathogens and cellular debris and secrete inflammatory mediators including cytokines, chemokines and growth factors (Berbic et al. 2014). Macrophages also have roles in maintaining tissue homeostasis and regulating other immune cell populations and are believed to have important roles in wound healing (Wynn and Barron 2010, Wynn and Vannella 2016, Mosser and Edwards 2008). For example macrophage depletion in transgenic mouse model has been shown to delay closure of skin wounds and to impair neoangiognesis (Goren et al. 2009). Tissue-resident macrophages represent highly plastic cell populations that responds to signals in each specific microenvironment and therefore a complex spectrum of activation states and phenotypes exist, reflected by surface receptor expression and secretion of molecules (Mosser and Edwards 2008, Radzun 2015) (Figure 1-13). Despite such variation, all macrophages exert precise roles in the immune response through phagocytosis of apoptotic bodies and modulation of other immune cells through the secretion of inflammatory factors (Stout and Suttles 2004).

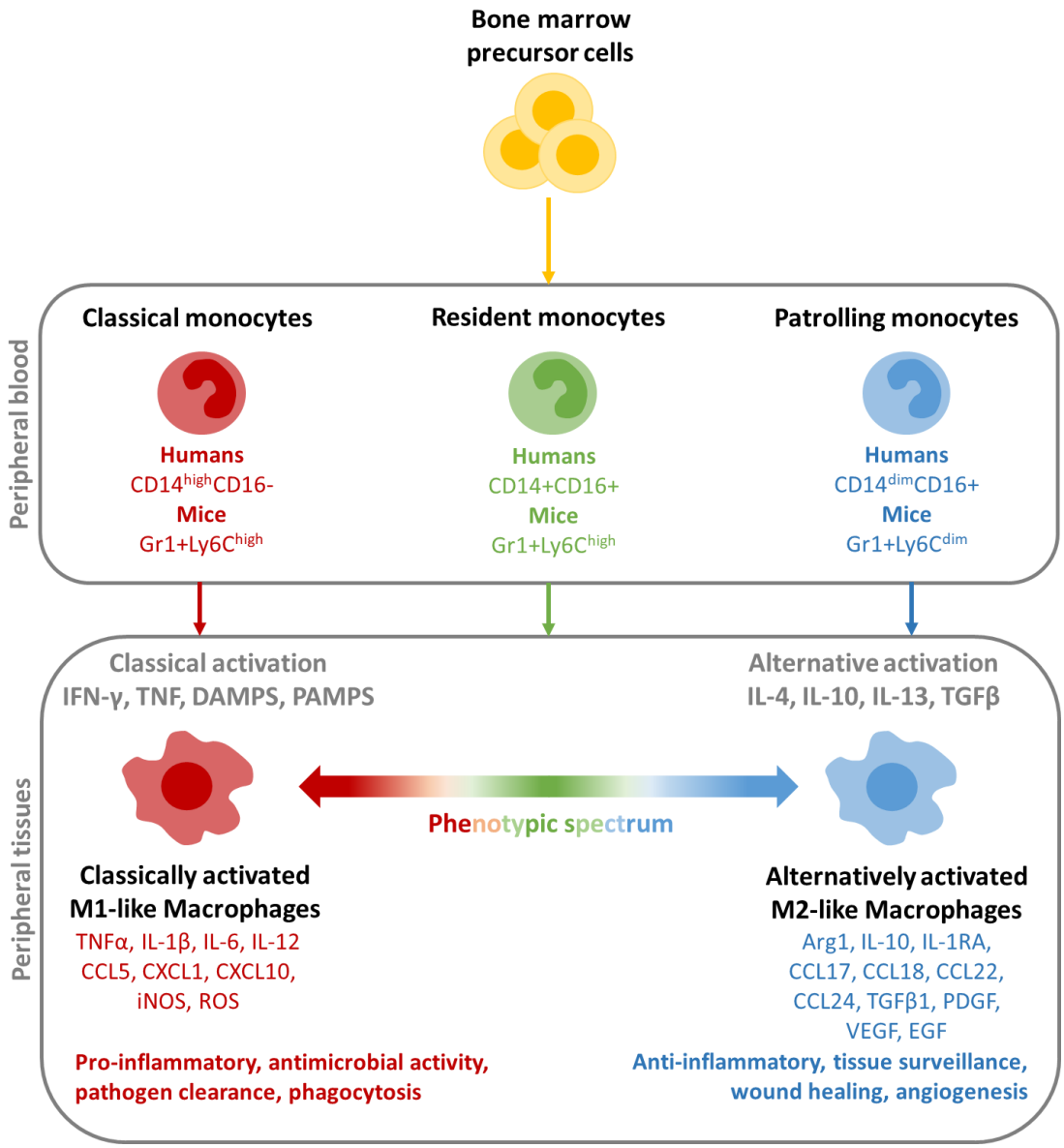

Figure 1-13. The heterogeneous phenotypes of monocytes and macrophages. Monocytes derive form precursor cells found in the bone marrow and can have one of three phenotypes: classical monocytes, resident monocytes or patrolling monocytes each of which display different surface markers. Monocytes differentiate into macrophages upon extravasation of the circulation into peripheral tissues. Macrophages have been described to have either a classically activated M1 phenotype or an alternatively activated M2 phenotype with distinct functional attributes, although it is now believed a phenotypic spectrum exists for this cell type (based on Biswas et al. 2012, Das et al. 2015, Ferrante and Leibovich 2012, Dunster 2016, Dalmas, Clément and Guerre-Millo 2011).

To identify macrophages in human tissues antibodies directed against CD68 are used: using antibodies against CD163 can further differentiate between $CD163^{high}$ tissue-resident macrophages and $CD163^{low}$ vascular-associated macrophages (Tremellen and Russell 2012). Macrophages have been detected in the endometrium throughout the menstrual cycle (Bonatz et al. 1992). Immunostaining for CD68 identifies cells that are most abundant during the late secretory and menstrual phases of the cycle, located predominantly in the decidualised stoma (Garry et al. 2010). Macrophages account for 1-2% of the stromal cells during the proliferative phase which increases to 3-5% during the secretory phase, and reach a peak during the menstrual phase where they account for approximately 6-15% of cells in the tissue (Figure 1-12) (Kamat and Isaacson 1987, Salamonsen, Marsh and Findlay 1999, Salamonsen et al. 2002). Specifically, in the decidua macrophages represent ~20% of the immune cells and two distinct subtypes have been identified: $CD11c^{high}$ and $CD11c^{low}$ which have 379 differentially expressed genes between them as determined by gene expression analysis by RNA microarray. Further analysis showed that genes enriched in $CD11c^{high}$ macrophages were associated with lipid metabolism and inflammation while genes enriched in $CD11c^{low}$ macrophages were associated with ECM formation, muscle regulation and tissue growth. Notably both decidual subsets secrete both pro- and anti-inflammatory cytokines which may represent a phenotype unique to the endometrium which is important in maintaining a balance for foetal-maternal tolerance during pregnancy (Houser et al. 2011). Although macrophage numbers change throughout the menstrual cycle they express ERβ and GR but do not express ERα or PR (Hunt, Miller and Platt 1998). The administration of exogenous oestrogen to women undergoing IVF has been associated with increased macrophage numbers in the endometrium (DeLoia et al. 2002). Treatment of peripheral blood monocyte-derived macrophages with cortisol resulted in secretion of factors that altered endometrial endothelial cell expression of angiogenic genes (Thiruchelvam et al. 2016).

The increase in macrophage numbers over the menstrual cycle is accompanied by a marked increase in immunoexpression of CXCL2 and CXCL8 in human tissues, complemented by *in vitro* cytokine secretion analysis of macrophages differentiated from peripheral blood monocytes (Evans and Salamonsen 2012, Maybin et al. 2018). These chemokines have roles in neutrophil chemotaxis and stimulating phagocytosis

and therefore macrophages are key mediators of the inflammatory response (Biswas et al. 2012). The huge increase in expression of macrophage-derived cytokines and proteases which stimulate the breakdown of collagens and ECM proteins have implicated macrophages in the initiation of decidual breakdown during menstruation (Salamonsen and Woolley 1999, Critchley et al. 2001a, Jeziorska et al. 1996). Furthermore it has been suggested that macrophages, as active phagocytes, have a primary role in apoptotic cell clearance and glandular remodelling (Garry et al. 2010). Production of VEGF by macrophages has implicated them in stimulating neoangiogenesis and revascularisation following tissue breakdown (Jabbour et al. 2006b).

In the endometrium of normal cycling mice, F4/80 immunopositive macrophages are abundant and located throughout the endometrial stroma (Mackler et al. 2000) and have been shown to change in number during the oestrous cycle, accumulating predominantly beneath epithelial cells expressing CSF-1. In op/op mice (recessive mutation in CSF1 gene) uterine macrophages are immature and reduced in number and apoptotic epithelial cells accumulate in the uterine lumen, highlighting a role for macrophages in epithelial cell clearance during oestrous (Shimada-Hiratsuka et al. 2000). In contrast, using a mouse model of simulated 'menstruation' it was reported that F4/80 expressing macrophages do not associate with areas undergoing tissue remodelling were located distal to the lumen (Kaitu'u-Lino et al. 2007). The evidence presented above highlights is consistent with macrophages having the potential to play multiple roles in endometrial tissue function including regulation of breakdown and subsequent repair.

1.4.5 Other immune cell types

1.4.5.1 Mast cells

Mast cells (MC) are granulocytes with roles in inflammatory processes. Human mast cells can classically differentiate into MCt or MCtc sub-types which express tryptase (t) only or tryptase and chymase (tc) respectively (Jabbour et al. 2006b). Both subtypes of MC have been identified in the human endometrium although in small numbers, with MCt preferentially located to the functionalis and MCtc preferentially located in

the basalis (Jeziorska et al. 1996, Sivridis et al. 2002). Recently our understanding of the MC phenotypes present in the endometrium was expanded to include three protease-specific phenotypes: MCt, MCtc and MCc, however the functional significance of distinct phenotype remains to be determined (De Leo et al. 2017). Endometrial MCs express ERβ and GR but not PR (Jabbour et al. 2006b). Notably the numbers of MCs do not changed dramatically according to cycle state although MCs do become activated prior to and during menstruation (Jeziorska et al. 1996, Drudy, Sheppard and Bonnar 1991). When MCs are activated they degranulate and release pre-formed mediators such as histamine, tryptase, bradykinin, heparin and proteoglycans. They can also release newly-synthesised mediators including platelet-activating factor, prostaglandins and leukotrienes (Berbic et al. 2014). Such mediators control cytokine action and activate MMP cascades and activation of other proteolytic enzymes resulting in the degradation of ECM essential to endometrial tissue breakdowns (Salamonsen et al. 2000, Berbic et al. 2014, Zhang et al. 1998). MCs can secrete precursors of MMP2 and MMP9 (Evans and Salamonsen 2012) and alter vascular permeability through release of histamine (Berbic et al. 2014, Menzies et al. 2011). These results suggest MCs might play a role in menstrual tissue breakdown but this requires confirmation.

1.4.5.2 Eosinophils

Eosinophils are cells of the innate immune system that are resident in mucosal tissue and arise from a common progenitor shared with basophils (Hogan et al. 2008). Eosinophils contribute to various physiological and pathological processes and can be a source of both regulatory and pro-inflammatory cytokines depending on their activation state (Kita 2011, Hogan et al. 2008). Eosinophils have only been identified in the human endometrium just prior to the onset of menstruation (Jeziorska et al. 1996). Eosinophils are immunopositive for ER and GR (Peterson et al. 1981) but negative for PR (Aerts, Christiaens and Vandekerckhove 2002) mirroring other endometrial immune cell populations. Eosinophils can be detected by expression of eosinophil cationic proteins (ECP1 and ECP2) and when these proteins are extracellular the eosinophils are deemed to be activated (Acharya and Ackerman 2014). Eosinophils express VEGF and MMPs when activated (Okada et al. 1997)

and endometrial eosinophils have been shown to express MMP9 (Jeziorska et al. 1996). A full characterisation of these cells and functions during the menstrual cycle remain to be determined.

1.4.5.3 Dendritic cells

Dendritic cells (DCs) are a heterogeneous population of leucocytes that play an essential role in modulation of the immune response, functioning primarily as antigen-presenting cells (Inaba and Inaba 2005). DCs patrol through peripheral tissues and upon capture of foreign antigens, undergo maturation which alters their phenotype and function. Activated DCs migrate to lymph nodes and present processed antigens to T cells via MHC proteins. This activates T cells and launches the adaptive immune response (Bonasio and von Andrian 2006). Although DCs have been identified in the endometrium, phenotype and functions are poorly characterised. One study reported there are significantly more immature DCs in the endometrium when compared to mature DCs with mature DCs mostly located in the basal stroma in both the proliferative and secretory phases. The functional significance of these findings remain unknown although it is suggested DCs may enhance localised regulatory mechanisms related to the immune response (Schulke et al. 2008) during pregnancy DC behaviour is altered to maintain tolerance (Tagliani and Erlebacher 2011). DCs express PR and progesterone appears to regulate DC function in the endometrium by limiting secretion of pro-inflammatory cytokines (Butts et al. 2008). A role in menstruation has not been described.

1.4.5.4 T and B lymphocytes

Lymphocytes such as B cells and T cells have crucial roles in the adaptive immune response. B cells are involved in the humoral immune response whereby they secrete antibodies against specific antigens, and then internalise and destroy the antigens. T cells (CD8+ cytotoxic T cells, CD4+ helper T cells, FOXP3+ regulatory T cells) are involved in the cellular immune response launched upon presentation of specific antigens through release of cytotoxins (Berbic et al. 2014). Following antigen-specific responses, specialised B and T cells retain a memory against that specific antigen and

therefore upon subsequent invasion, are rapidly activated to clear the antigen (Berbic et al. 2014).

During the menstrual cycle the endometrium contains very few B cells (Thiruchelvam et al. 2013), which are thought to have a more prominent role in the maintenance of foetal tolerance during pregnancy by secreting immunomodulatory molecules such as IL-10, and fighting against infection (Fettke et al. 2014). While increases in differential lymphocyte count in the blood during the secretory phase can be attributed to increases in cytotoxic T cells, helper T cells and uNK cells (Tikare, Das and Dhundasi 2008) such changes are not reflected within the endometrial tissue itself. Both cytotoxic T cells and regulatory T cells (Tregs) are seen to decrease between the proliferative and secretory phase while γδ T cells remain unchanged, which is thought to promote a permissive environment at the time of implantation (Flynn et al. 2000). Tregs are a distinct subtype of T cells that play crucial roles in immunological regulation and suppression. Tregs have been shown to influence the proliferation and activation of a wide range of immune cells to alter cytokine release. Tregs ensure that immunological responses are tightly regulated (Berbic et al. 2014). To date no roles in endometrial repair have been asigned to either T or B cells.

1.5 Endometrial progenitor cells

1.5.1 Identification of stem/progenitor cells in human endometrium

The endometrium exhibits an extensive regenerative capacity and it has been proposed that this is faciliated by tissue resident stem/progenitor cells (Dimitrov et al. 2008, Gargett, Schwab and Deane 2016). The concept of endometrial stem/progenitor cells was first introduced in 1978 by Prainishnikov (Prianishnikov 1978) however the first real evidence for the existence of stem/progenitor cells came from Chan *et al* who identified rare clonogenic cells (CFUs) in purified human endometrial cells (Chan, Schwab and Gargett 2004). Since then, a growing body of work has developed for the identification and functional classification of stem/progenitor cells some of which is detailed in the following sections.

A number of terms have been used to describe functions of adult stem/ progenitor cells: proliferation potential is the number of times a cell population doubles from a single cell (Gargett, Chan and Schwab 2007); self-renewal is a cell's ability to divide and produce identical progeny (Bach, Renehan and Potten 2000). In contrast differentiation is defined as the ability of a cell to completely change phenotype and gene expression profile to take on the appearance and function of a different type(s) of cell (Figueira et al. 2011). Tissue reconstitution is the ability of a pure population of cells to give rise to multiple cell types of a tissue become organised to recapulate the architecture of the tissue *in vivo* (Gargett and Masuda 2010). A recent review by Gargett and colleagues has highlighted the importance of using functional assays and informative identification markers to identify endometrial stem progenitors (Gargett et al. 2016).

1.5.1.1 Epithelial stem/progenitor cells

During menstruation the glands in the basal compartment remain intact while both glands and surface epithelium in the functional layer are shed leaving a denuded stromal surface (Clancy 2009, Maybin and Critchley 2015). It has been reported that the basal glands contain a population of epithelial progenitor cells that can generate new epithelial cells to re-epithelialise the exposed surface (Gargett et al. 2007, Cousins et al. 2014). Epithelial progenitor cells have been also been identified by in cell suspensions derived from hysterectomy specimens (Chan et al. 2004, Schwab, Chan and Gargett 2005, Gargett et al. 2009). In these studies epithelial CFU showed stem cell properties such as self-renewal, proliferation, and differentiation into gland like structures composed of cells expressing cytokeratin in 3D culture with a stromal feeder layer (Gargett et al. 2009). Furthermore the Hoechst exclusion assay identified side population cells in the epithelial fraction of endometrium with stem cell properties (Cervelló et al. 2011, Kato et al. 2007, Kato 2012). Kato *et al* showed that epithelial SP cells aggregated into glad-like structures when cultured in Matrigel which had positive expression of epithelial cell markers e-cadherin and CD9 (Kato et al. 2007) which supported evidence generated for clonogenic epithelial cells (Gargett et al. 2009).

A study investigating specific cell markers for identifying endometrial epithelial progenitor cells compared the gene profile of magnetic bead selected EpCAM+N-cadherin+ with EpCAM+N-cadherin- epithelial cells. N-cadherin+ cell were found to be more clonogenic, underwent more population doublings than N-cadherin- cells, differentiated into cytokeratin+ gland-like structures *in vitro*, and were localised to epithelial cells in the base of glands in the basalis. Authors concluded that N-cadherin can be used to isolate human endometrial epithelial progenitor cells and may recognise a more primitive cell population (SSEA-1 positive) suggestive of an epithelial hierarchy in the basalis (Nguyen et al. 2017). Similarly, using single cell sequencing technologies Wu *et al* reported transcriptomic profiles of uterine epithelial from neonatal to sexually mature mice *in vivo*. This study identified and characterised ALDH1A1 as a marker that enriched for a population with stem/progenitor properties during early development with high proliferative and self-renewal capacity with the ability to undergo EMT and located mainly in newly formed basal glands (Wu et al. 2017). Despite clear progress being made in identifying markers expressed by epithelial stem/progenitor cells, none have been shown to be exclusive to this population alone. The discovery of distinct epithelial stem/progenitor cell markers is a necessary prerequisite for prospective isolation and further characterisation.

1.5.1.2 Stromal (mesenchymal) stem/progenitor cells

Mesenchymal stem cells (MSCs) are multipotent cells that have been found to reside in many adult tissues and can produce more than one type of differentiated cell. MSCs have been identified in many adult tissues including the bone marrow, adipose tissue, dental pulp, pancreas, placenta, dermis and skeletal muscle, most predominantly located in the perivascular niche (Crisan et al. 2008, Feng et al. 2011, Hwang et al. 2009, Marquez-Curtis et al. 2015, Murray et al. 2014, Phinney and Prockop 2007, Hass et al. 2011, Kalinina et al. 2011). MSCs represent a rare population of undifferentiated cells that have several properties that make them ideal candidates for regulating tissue homeostasis, including self-renewal, proliferative potential, multilineage differentiation and immunomodulatory activity (Crisan et al. 2008, Feng et al. 2011). During cell division MSCs undergo asymmetric cell division and thereby maintain the stem cell populations whilst also giving rise to differentiated progenitor cells which

are responsible for producing differentiated progeny called transit-amplifying cells (Kalinina et al. 2011) (Figure 1-14).

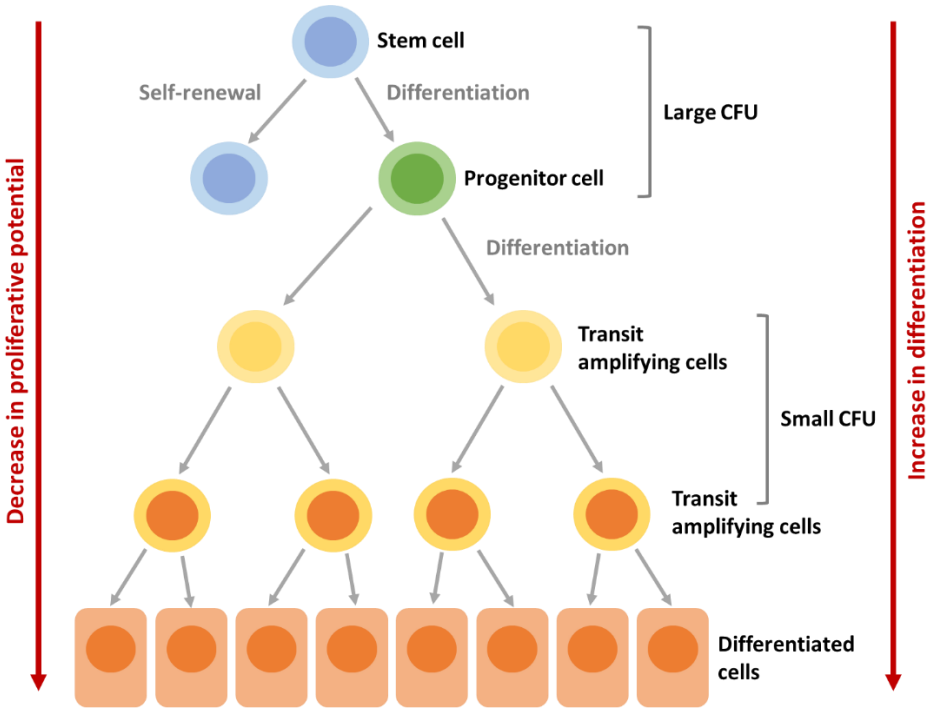

Figure 1.14. Schematic representation of the hierarchy of stem-cell differentiation. Stem cells can undergo self-renewal or differentiate into progenitor cells. Progenitor cells can proliferate extensively and give rise to more differentiated transit amplifying cells which finally differentiate into terminally differentiated functional cells with low proliferative capacity. CFU assays with human endometrial cells produce both large and small colonies. It is believed that the large colonies arise from stem/progenitor cells while the small colonies arise from transit amplifying cells (based on Chan et al. 2004).

In general MSCs are reported as plastic adherent cells that can differentiate *in vitro* into adipocytes, osteoblasts and chondrocytes (Crisan et al. 2008, Crisan et al. 2009), and express the following cell surface markers: CD29, CD44, CD73, CD90 and CD105 (Dimitrov et al. 2008) whilst being completely distinguishable from cells expressing CD31, CD34 or CD45.

1.5.2 Identification of putative MSCs in the endometrium

1.5.2.1 Human endometrium

Chan *et al* discovered a small population of colony forming cells in single cell suspensions of both epithelial and stromal cells isolated from human hysterectomy samples. They showed *in vitro* that 0.22±0.07% and 1.25±0.18% of epithelial and stromal cells respectively formed individual colonies following a 15 day culture period, identifying both large and small resulting colonies. It was hypothesised that large colonies had arisen from true stem/progenitor subpopulations which have a greater self-renewal capacity whilst the smaller colonies had arisen from transit-amplifying cells (Figure 1-14) (Chan et al. 2004). A further study reported that proportions of clonogenic cells did not change across the menstrual cycle (Schwab et al. 2005). Further investigation has shown that clonogenic endometrial stromal cells exhibit properties of MSCs including self-renewal, a high proliferative potential and capacity multilineage differentiation *in vitro* into four mesodermal lineages at the single cell level: adipocytes, chondrocytes, osteoblasts and smooth muscle cells (Dimitrov et al. 2008, Gargett et al. 2009) however the proportions and preference for lineage differentiation is unknown at present.

Other studies have used the Hoechst exclusion assay to detect side population (SP) cells which relies on the fact that stem cells have the ability to extrude the DNA binding dye Hoechst 33342 due to their increased expression of the ATP-binding cassette transporter protein ABCG2/Bcrp. Using this method the human endometrium has been shown to contain up to 5% SP cells in freshly isolated and short-term cultures of endometrial cells thought to represent a mixture of epithelial and stromal stem/progenitor cells (Cervelló et al. 2011, Hu et al. 2010, Kato et al. 2007, Kyo, Maida and Inoue 2011). It has been shown that the percentage of SP cells varies between subjects (0-5.11%) and higher percentages of SP cells were detected in both the proliferative and menstrual phases of the cycle (Masuda et al. 2015, Kato et al. 2007, Tsuji et al. 2008, Masuda et al. 2010). SP cells in the endometrial stroma were located in both the basalis and functionalis and predominantly found in proximity to blood vessels (Kato et al. 2007). Characterisation of stromal SPs confirmed they

expressed markers of undifferentiated cells including c-kit/CD117 and Oct4 (Cervelló et al. 2011) and were negative for the stromal cell differentiation CD13, however when cultured in Matrigel aggregates of stromal-like cells formed which expressed CD13 consistent with differentiation (Kato et al. 2007). In long-term cultures of SP cells they proliferated slowly and were able to form CFU which was in contrast to non-SP cells that became senescent after 3 months (Masuda et al. 2010).

SP cells have also been shown to differentiate into multiple mesodermal lineages *in vitro* and upon engraftment under the kidney capsule of immuno-comproimised mice, reconstitute endometrial-like tissue *in vivo* (Cervelló et al. 2011) (Miyazaki et al. 2012). In another study, flow cytometry analysis indicated that endometrial SP cells were a mixed population as 51% expressed CD31 (endothelial), 27% expressed EpCAM (epithelial) and 10-14% expressed CD10 or Pdgfrβ (stromal) (Miyazaki et al. 2012). Although isolation of SP cells is believed to enrich for endometrial stem/progenitor populations it is unclear whether these populations are heterogeneous with only a subset of cells possessing stem cell-like properties.

1.5.2.2 Mouse endometrium

The Hoechst exclusion assay has only been used to identify SP cells in postpartum mouse endometrium but not in tissue from mice experiencing oetrous cycles. In these assays SP cells were enriched in clonogenic cells and differentiated in culture although their exact identity was not determined (Hu et al. 2010). The label retaining cell (LRC) method is more commonly used to identify stem/progenitor cells and their *in vivo* location in rodents. This method is based on the finding that stem/progenitor cells undergo less cell divisions than 'fast cycling' differentiated cell populations and therefore retain DNA integrated labels (eg. BrdU) for longer (Gargett et al. 2007). Using this technique, LRC cells have been identified as 3% of epithelial cells and 6-9% of stromal cells in the mouse endometrium (Chan and Gargett 2006b, Kaitu'u-Lino et al. 2012, Cao, Chan and Yeung , Patterson and Pru 2013). The LRC method has identified a putative endometrial stem/progenitor cell population cells in both the epithelium and in the stroma adjacent to blood vessels (Figure 1-15 (B)) (Gargett et al. 2016). Further methods of identification were therefore required to compliment current knowledge and fully characterise mouse endometrial stem/progenitor cells.

In summary, labelling and clonogenic assays have been used to identify putative endometrial epithelial and mesenchymal stem/progenitor cells in human and mouse endometrium (Figure 1-15 (A-B)) with the latter located predominantly in a perivascular region (Schwab and Gargett 2007).

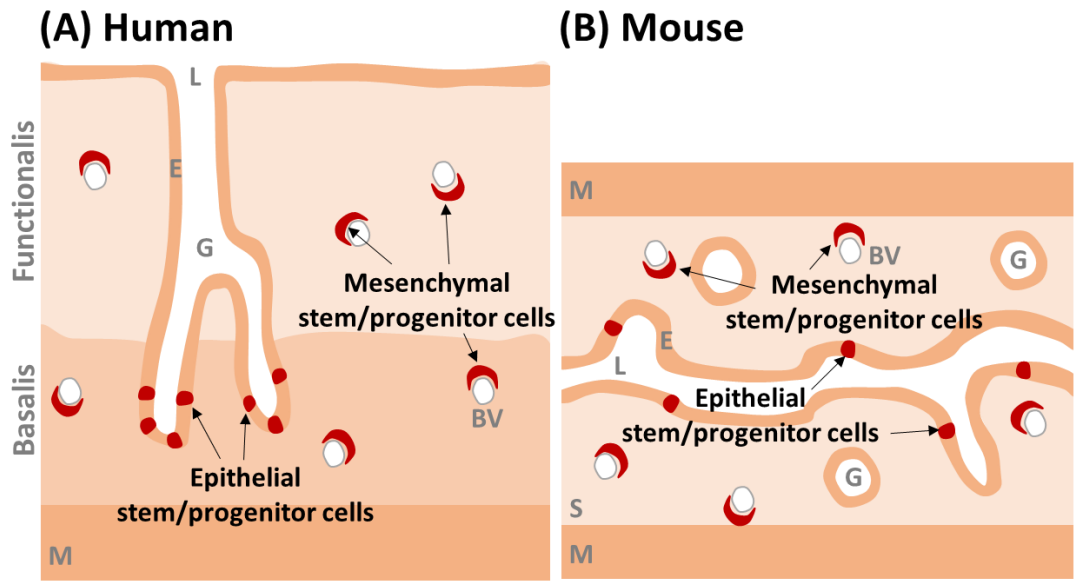

Figure 1-15. Hypothesised location of stem/progenitor cells in human and mouse endometrium. (A) In human endometrium epithelial progenitor cells are located in the base of glands in the basalis while MSCs are located near blood vessels. Human endometrial MSCs have been identified as clonogenic or SP cells. **(B)** In mouse endometrium, LRC hypothesised to be stem/progenitor cells are located in the luminal epithelium and near blood vessels in the stroma (based on Gargett and Masuda 2010).

1.5.3 Identification of cell surface markers on putative endometrial mesenchymal stem cells

1.5.3.1 Human endometrium

The expression of typical stem cell markers such as Oct4, c-kit, CD90, CD44, CD73, CD166 (Cho et al. 2004, Cervelló et al. 2007, Indumathi et al. 2013) and MSC markers such as CD29, SUSD2 and CD105 (Schwab and Gargett 2007, Dimitrov et al. 2008,

Phinney and Prockop 2007, Hwang et al. 2009, Marquez-Curtis et al. 2015) have been confirmed in human endometrial MSCs (studies using immunohistochemistry and flow cytometry on cells identified by the clonogenic and SP techniques). When analysing clonogenic stromal cells by flow cytometry Gargett *et al* reported they expressed MSC markers CD29, CD44, CD73, CD90, CD105, CD140b and CD146 but did not express endothelial or immune cell markers such as CD31, CD34 and CD45, although these were also present in other cell types and hence not MSC specific (Gargett et al. 2009).

In another study, the RNA binding protein Musashi-1 which is known to be involved in the control of asymmetric cell division of neural and epithelial progenitor cells, was found to be more highly expressed in the human endometrium than the myometrium, and more abundant in the basalis when compared to the functionalis. Cells expressing Musashi-1 also expressed Notch1 and telomerase and were concluded to be endometrial MSCs (Götte et al. 2008). The same group reported that there was an upregulation of Musashi-1 expressing cells during the proliferative and menstrual phases of the cycle and increased numbers detected in lesions of endometriosis and endometrial carcinoma (Götte et al. 2008).

When culturing human endometrial stromal cells, it was also noted that they only formed colonies when PDGF-BB was present in the culture medium which lead to the hypothesis that endometrial MSCs expressed Pdgfrβ (Chan et al. 2004, Schwab et al. 2005). Notably Pdgfrβ and the adhesion molecule CD146 are expressed by MSCs in bone marrow, dental pulp and other tissues (Shi and Gronthos 2003, Bühring et al. 2007, Armulik, Genové and Betsholtz 2011). In a study by Schwab and Gargett, cells co-expressing Pdgfrβ and CD146 were isolated from human endometrial biopsies and compared to Pdgfrβ-CD146- cells. The Pdgfrβ+CD146+ cells represented 1.5% of the sorted population and were enriched 8-fold for CFU when compared to Pdgfrβ-CD146- counterparts (7.7±1.7% versus 0.7±0.2%, $p<0.0001$). They also had the ability to differentiate into various mesodermal lineages including adipogenic, chondrogenic, osteogenic and myogenic. Immunohistochemistry located cells co-expressing Pdgfrβ and CD146 to the perivascular niche and showed that Pdgfrβ was also expressed by stromal fibroblasts while CD146 could also be detected in myometrial tissues. The

authors hypothesised that co-expression of these markers identified perivascular pericytes which were responsible for mesenchymal differentiation (Schwab and Gargett 2007).

Further to this, a study was undertaken to identify a single marker for purifying MSCs from the human endometrium using an antibody panel with novel specificities. The protein SUSD2 (sushi domain containing-2) which is identified by the W5C5 antibody was found on the previously identified endometrial MSC population. SUSD2+ cells represented 4.2±0.6% of the total endometrial stromal cells, were located in the perivascular niche and when xenografted under the kidney capsule of immunocompromised mice, gave rise to endometrial stromal tissue (Masuda et al. 2012). Immunohistochemistry and flow cytometry revealed they all expressed CD146 and the majority also expressed Pdgfrβ. Once isolated SUSD2+ cells exhibited significant potential for clonogenicity (3.8%, 14.7 fold increase over W5C5- cells), self-renewal and multilineage differentiation *in vitro* when compared to their SUSD2- counterpart (Masuda et al. 2012). Notably, SUSD2+CD146+ cells generated more CFUs than Pdgfrβ+CD146+ cells and were more highly increased during the proliferative phase of the cycle (Masuda et al. 2012). This study was the first to report a single marker which could be used to identify MSCs in the human endometrium: RNA sequence analysis of cultured endometrial SUSD2+ and SUSD2- confirmed that SUSD2+ cells had a gene signature consistent with a pericyte phenotype (Murakami et al. 2014).

1.5.3.2 Mouse endometrium

Putative MSCs in the mouse endometrium using the LRC method have been located near to CD31+ endothelial cells of blood vessels and have been shown to express c-kit/CD117 and Oct4 (Cervelló et al. 2007) and other typical MSC markers including Pdgfrβ, CD146, CD44, CD90 and Sall4 (Chan and Gargett 2006b). They were negative for CD45 (leucocyte marker), and positive for αSMA (myofibroblast marker) leading to the hypothesis that they are perivascular cells or pericytes (Chan and Gargett 2006b).

A study by Deane *et al*, (Deane et al. 2016) investigated the expression of mouse telomerase reverse transcriptase (mTert) as a putative stem cell marker. Rare mTert expressing cells were located in the endometrial stromal and epithelial compartments and showed morphological heterogeneity. The subpopulations of mTert+ cells also expressed epithelial (EpCAM+), endothelial (CD31+) and haematological (CD45+) markers hence as with traditional LRC techniques mTert identified a heterogeneous population of cells in the endometrium and was not specific to MSCs. In a more recent study a cell population co-expressing Pdgfrβ and CD146 was identified in mouse endometrium in a perivascular location, as these two markers were also expressed by mouse embryonic stem cells the authors concluded these cells might play an important role in human endometrial development (Parasar et al. 2017).

In summary evidence for a cell-specific marker for stromal MSC/stem/progenitor cells in the mouse endometrium remains limited although comparing results from mouse and human suggest the stromal MSC may have a perivascular location and exhibit expression of Pdgfrβ and CD146 suggestive of a pericyte phenotype (Gargett et al. 2016).

1.5.4 Perivascular pericytes in the endometrium

Pericytes are mural cells that sit on the outer surface of blood cells in close contact with underlying endothelial cells, often encapsulated in the same basement membrane (Mills et al. 2013, Ansell and Izeta 2015, Bodnar et al. 2016, Spitzer et al. 2012). They have a fibroblast-like morphology with a prominent cell body and large nucleus and several long cytoplasmic processes which allow them to be in contact with more than one endothelial cell through adhesion molecules such as fibronectin, N-cadherin and β-catenin (Mills et al. 2013, Armulik et al. 2011), outlined in Figure 1-16.

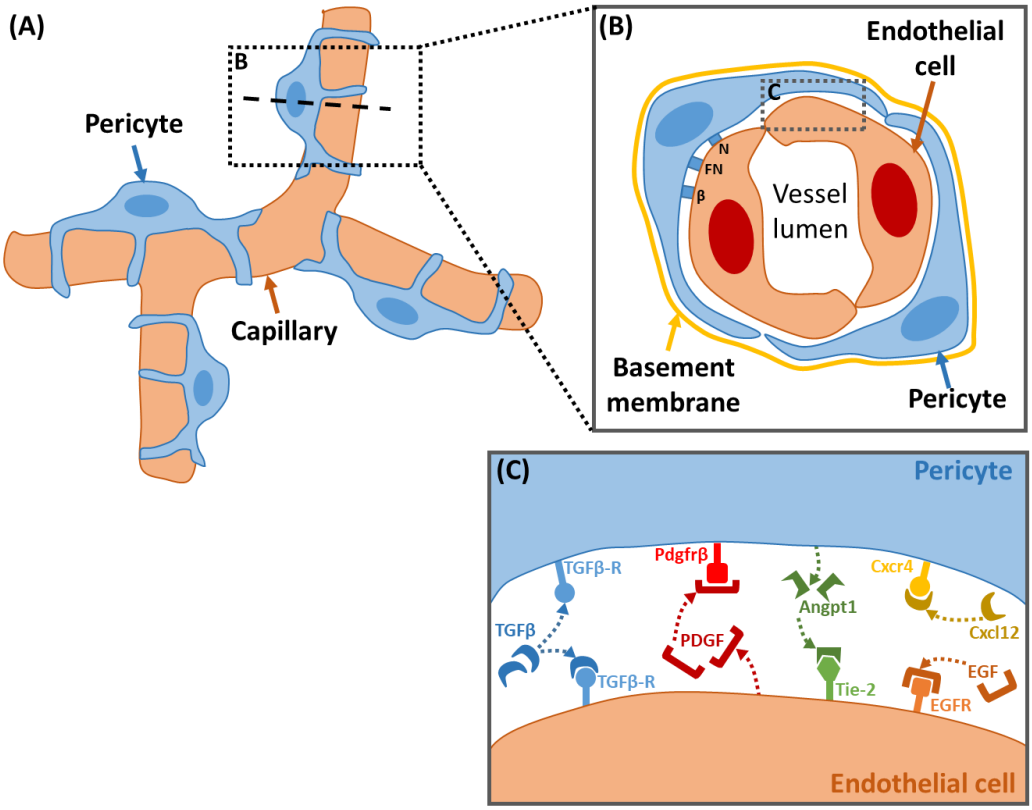

Figure 1-16. Schematic representation of the structure and function of pericytes. (A) Pericytes are cells that have membranous processes that wrap around endothelial cells of blood vessels. **(B)** Pericytes are embedded in the basement membrane of blood vessels and kept in close contact with endothelial cells through adhesion molecules such as N-cadherin (N), fibronectin (FN) and β-catenin **(C)** Pericytes and endothelial cells are in close proximity and release factors to regulate each others function (proliferation, migration, maturation) including PDGF and Angpt1. Other factors that regulate pericyte and endothelial cell function include TGFβ, EGF and Cxcl12 (based on Armulik et al. 2011, Ribatti, Nico and Vacca 2015).

Pericyte-endothelial cell communication is fundamental to the survival and function of each cell type. When PDGF is knocked out in mice it is embryonically lethal and the embryos exhibited vessels that were completely denuded of pericytes resulting in severe haemorrhage (Holmgren et al. 1991). This study suggests pericyte proliferation and migration is regulated by endothelial cells and vice versa (Armulik et al. 2011). Pericytes are present to varying degrees, in every human tissue with primary roles in regulating blood flow, perfusion of fluids, cells and proteins between capillaries and tissues, and supporting vascular development (Mills et al. 2013, Ansell and Izeta 2015, Bodnar et al. 2016, Spitzer et al. 2012). The most well described function of pericytes

is to regulate vessel tone and permeability of mature vessels as well as modulating angiogenesis (Ahmed and El-Badri 2017). Pericyte coverage is variable between tissues with the relative density proposed to be related to specific functions in each tissue. In the retina and central nervous system (CNS) the pericyte to endothelial ratio is 1:1 offering tight support to these regions of high blood pressure whereas in the skeletal muscle this is as low as 1:100 in vasculature that experiences much lower blood pressure (Bodnar et al. 2016).

Pericytes have previously identified as having putative stem-cell functions as they are clonogenic and capable of giving rise to cells of the mesodermal lineages including chondrocytes, adipocytes and osteoblasts (Mills et al. 2013, Murray et al. 2014, Feng et al. 2011). Moreover it has been suggested by several groups that pericytes are MSCs as they express the MSC markers CD105, CD73 and CD90 (Bodnar et al. 2016), or that all MSCs are pericytes (Caplan 2008, Cano, Gebala and Gerhardt 2017, de Souza et al. 2016). Pericytes express Pdgfrβ and CD146 which supports the hypothesis that they represent MSC like cells. Other receptors expressed by pericytes include Egfr, αSMA, Desmin, NG2, Rgs5 (Mills et al. 2013), Angpt2, Igf, Ngf and Pdgf (Ansell and Izeta 2015, Crisan et al. 2008) some of which have been found to be expressed by stem/progenitor cells in the human endometrium (Spitzer et al. 2012, Ansell and Izeta 2015, Crisan et al. 2008, Crisan et al. 2009). Murine pericyte markers include Pdgfrβ, NG2, CD13, αSMA and Desmin (Armulik et al. 2011).

Although the markers detailed above can be used to identify pericytes in human and mouse tissues, none of them are exclusive for pericytes (Bodnar et al. 2016) nor are they expressed uniformly by pericytes in all tissues consistent with adaptation of cells to local tissue environments (Mills et al. 2013). Expression of these markers can also vary depending on the type of vessel they are surrounding for example NG2+/αSMA+ pericytes surround arterioles while NG2-/αSMA+ pericytes surround venules and NG2+/αSMA- pericytes surround capillaries, and αSMA expression has been found to correlate with the extent of vasoconstriction in a vessel (Crisan et al. 2012). Although, Pdgfrβ and CD146 are considered to be ubiquitously expressed by pericytes in all tissues (Bodnar et al. 2016) these markers are also expressed by a number of other cell types.

In summary, there is some limited evidence related to the characterisation of pericytes as MSCs in uterine tissues although it has been suggested that endometrial MSCs may be similar to vSMC, pericytes or even endothelial cells since MSC progeny appear to share common markers with these cell types (Gargett et al. 2007).

1.5.5 Role of endometrial stem/progenitor cells in endometrial repair

Although stem-like cells have been identified in the human endometrium the precise contribution of these cells to endometrial repair and remodelling remains unclear (Schwab et al. 2005, Schwab and Gargett 2007, Cervelló et al. 2007) although some evidence has come from use of xenograft and LRC experiments. Using unfractionated single-cell suspensions of endometrium from hysterectomy tissue that were grafted under the kidney capsule of immunocompromised mice, Masuda and colleagues were able to generate endometrial like tissue which expressed markers of stromal cells (vimentin, CD10, CD13), glandular epithelial cells (CD9) and endothelial cells (CD31), some of which had associated αSMA+ vascular smooth muscle cells with a functional response to oestrogen and progesterone inducing a menstrual-like cycle (Masuda et al. 2007). Engraftment of purified SP cells also resulted in formation of endometrial tissue comprising both stromal and epithelial compartments with an associated establishment of vasculature (Cervelló et al. 2011, Masuda et al. 2015). These results indicate that a population of putative stem/progenitor cells exist in endometrial tissues that have the ability to regenerate endometrial tissue *in vivo*, however their phenotype was not further defined.

A study by Kaitu'u *et al* used the LRC technique in mice to identify putative stem/progenitor cells during endometrial repair with results suggesting that a population of epithelial progenitor cells might reside in the basal glands and that stromal LRC could have an active role to play in endometrial repair (Kaitu'u-Lino et al. 2012). Similarly, a LRC study looking at postpartum endometrial repair showed that stromal LRC numbers were maintained throughout pregnancy, located at the inter-implantation/placental loci, and upon parturition were shown to proliferate (BrdU+Ki67+) with stromal LRC returned to a prepartum pattern of distribution by postpartum day 7 (Cao, Chan and Yeung 2015). Using more sophisticated genetic fate

mapping, Patterson *et al* have shown that during postmenstrual and postpartum endometrial repair in mice, stromal cells have the ability to undergo a mesenchymal-to-epithelial transition, demonstrated by EYFP expression in the endometrial epithelium of Amhr2-Cre;Rosa-Stop$^{fl/fl\text{-}eYFP}$ mice (mesenchymal specific) (Patterson et al. 2013). This result has been recapitulated by others (Cousins et al. 2014) confirming a role for mesenchymal cells in both post menstrual and postpartum repair. Despite current knowledge, the precise phenotypes of the cells described in each of these different studies remain unknown.

As almost every study based on identifying and characterising stem/progenitor cells in the endometrium have localised them to the perivascular niche, it has been postulated that the endometrial stem/progenitor cells in the stroma may be the same as the perivascular pericytes described above (Tintut et al. 2003, Gargett et al. 2016). Notably cells isolated from endometrial tissue by co-expression of Pdgfrβ and CD146 had colony forming ability and multilineage differentiation potential when cultured in adipogenic, osteogenic, myogenic and chondrogenic induction medium. Putative MSCs/pericytes expressed gene signatures associated with self- renewal, multipotency, differentiation and immunomodulation (Spitzer et al. 2012) and expressed high levels of CXCR4 which when bound by CXCL12 is known to stimulate the migration of MSCs suggesting they are poised to respond to chemotactic signals released during endometrial injury and repair (Spitzer et al. 2012). Although it is speculated that endometrial pericytes may contribute to the regeneration of endometrial tissue following menstruation, their precise contribution is unknown.

A few studies have suggested bone marrow progenitor cells could contribute to endometrial repair. Using a mouse model where HLA-mismatched bone marrow transplants were undertaken, donor-derived cells were detected in the endometrial tissue accounting for 0.2-48% of epithelial cells and 0.3-51% of stromal cells suggesting that BM cells might make a small contribution to endometrial tissues (Taylor 2004). In a further BM transplant study, BM cells were harvested from a transgenic donor (ubiquitous GFP expression) and injected into irradiated mice. GFP+ cells were found in the endometrial stroma as soon as 3 months post-transplant comprising 47.3-72.2% of the total BMDCs in the stroma by 12 months. BMDCs were

not detected in the epithelial compartment until 12 months (Morelli, Rameshwar and Goldsmith 2013). Gene expression profiling and *in vitro* assays have been performed to compare human endometrial MSCs with BM-MSCs which found a large degree of similarity between the two cell types although endometrial MSCs were found to have greater population doubling. 52 core genes were shared including those associated with stemness, self-renewal and members of the Notch, TGFβ, FGF and Wnt signalling pathways. 16 genes were significantly downregulated in eMSCs including VCAM1 and IGF and 16 genes were significantly upregulated including the following cytokines and growth factors: G-CSF, GM-CSF, VWF, IL1β, GDF15 and KDR. Differences suggest endometrial MSCs are better suited to have roles in angiogenesis, cell adhesion, proliferation, migration and differentiation (Gaafar et al. 2014). Definitive roles remain to be determined.

1.6 Disorders of the endometrium that might be associated with aberrant endometrial repair or regeneration

It is believed that abnormalities in the regulation of physiological endometrial repair during the menstrual cycle may contribute to disorders of the endometrium including endometriosis, endometrial cancer, heavy menstrual bleeding (HMB) and Asherman's syndrome (Dimitrov et al. 2008). Although these conditions are prevalent and pose a substantial health burden, little is known about their pathogenesis (Gargett and Chan 2006) and it is possible that alterations in the number, function, regulation and location of endometrial stem/progenitor cells and/or immune cell populations may be involved in the aetiology of these conditions (Chan and Gargett 2006b, Gargett and Chan 2006, Du and Taylor 2007). In addition, in all these conditions a putative link to the malfunction in macrophage behaviour has been suggested and therefore careful characterisation of macrophage phenotype and function in physiological endometrial repair and proliferative disorders is required. Thus if the contribution(s) of stem/progenitor cells and/or macrophages to the scar-free repair process exhibited by endometrial tissue can be determined such knowledge could inform the development of cell-based therapies or treatments that would manipulate an abnormal cell response to treat endometrial disorder such as those outlined below.

1.6.1 Heavy menstrual bleeding

Heavy menstrual bleeding (HMB) is defined as abnormal menstrual bleeding in excess of 80ml per cycle affecting in 1 in 3 women in the perimenopausal period (Hapangama and Bulmer 2016). An excessive or unresolved inflammatory response is often associated with delayed healing and is thought to underpin the pathophysiology of HMB. It has been shown that the endometrium of women suffering from HMB displays an increased inflammatory response with increased levels of pro-inflammatory TNFα expression (Malik et al. 2006) and increased expression of COX 1 and COX-2 which promote excess synthesis of prostaglandins (Smith, Jabbour and Critchley 2007). HMB was also found to be associated with a shift in the PGF2α/PGE_2 ratio with increased concentrations of PGE_2 measured in menstrual blood which may impact on vessel stabilisation during endometrial repair (Smith et al. 2007). In a study by Biswas *et al*, endometrial leucocyte populations were compared in the endometrium of women with and without HMB suggesting dysregulated NK number and function may contribute to the disorder possibly by adverse impacts on vascular maturation (Biswas Shivhare et al. 2015).

It is well known that endometrial macrophages are key players in regulating the initiation of menstruation and have been localised to regions of endometrial repair and remodelling (Thiruchelvam et al. 2013, Salamonsen et al. 2002). In women complaining of unscheduled bleeding, Clarke *et al* found that there was an increase in the number of macrophages and associated cytokines in the endometrium (Clark et al. 1996) and therefore dysregulation of macrophages may have roles in abnormal endometrial bleeding although mechanisms are poorly understood.

Pericytes are known to have roles in regulating endothelial and blood vessel function including angiogenesis, vasoconstriction and regulation of blood flow (Armulik et al. 2011). It has been shown that women with HMB have increased blood flow during menstruation when compared to healthy controls which is suggestive of a decreased hypoxic response and lack of vascular smooth muscle function (Hurskainen et al. 1999). In one study the association of pericytes and blood vessels in endometrial tissues was compared in healthy controls and women suffering from HMB and it was

concluded that low pericyte coverage of endometrial vessels found in the endometrium from women suffering from HMB may contribute to vessel fragility and excessive blood loss during menstruation (Andersson et al. 2015). Irregular bleeding is also observed in up to 60% of women using HRT with significant differences in endometrial blood vessels including a decreased density of endothelial cells, decreased organisation of endothelial cells and significantly reduced number of pericytes supporting vessel structure in women taking HRT. This study suggests that irregular bleeding can be attributed to dysfunctional blood vessels which may in part be due to loss of pericyte support (Hickey et al. 2003, Hickey et al. 2008).

Although the precise mechanisms responsible for the origin of HMB are unknown, links to defective blood vessel and pericyte function and an aberrant inflammatory response have been drawn. Understanding mechanisms that drive endometrial repair may highlight important roles for immune cells and putative stem/progenitor cells and manipulation of these cell populations may provide novel strategies in the management and/or treatment of this common disorder.

1.6.2 Asherman's syndrome

Asherman's syndrome (AS) is characterised by a thin atrophic endometrium and intrauterine adhesions and scars composed of fibrous tissue; it presents with symptoms including amenorrhea, pregnancy complications and infertility, occurring in 13% of women undergoing routine infertility evaluation (Gargett and Healy 2011). AS most frequently arises following damage to the basal layer of the endometrium as a result of infection or trauma especially in the postpartum period which is thought to deplete the endogenous stem/progenitor cell population (Kodaman and Arici 2007, Sahin Ersoy et al. 2017). The application of stem/progenitor cells as a therapeutic option to treat AS is under consideration. Notably it has been shown that post-injury delivery of BM-MSCs in a mouse model of AS improved reproductive outcome (Alawadhi et al. 2014). Ersoy *et al* showed that intrauterine administration of CXCL12 resulted in increased engraftment of endogenous BM-MSCs into the uterus in a mouse model of AS which resulted in a shorter time to conceive and larger litter sizes, restoring

reproductive outcome to be comparable to controls. Notably a decrease in fibrosis and return to normal uterine structure was also observed (Sahin Ersoy et al. 2017)

In a human trial with a patient suffering from severe AS, adult autologous stem cells were isolated from the patient's own bone marrow and endometrial angiogenic stem cells separated using immunomagnetic isolation and antibodies against CD9, CD44 and CD90. A total of 39 million marker-positive cells were administered to the patient's uterine cavity under ultrasound guidance after curettage, and subsequently the patient was given cyclical hormonal therapy; 14-19 days later there was an increase in endometrial thickness detected and good vascularity with the presence of mature spiral vessels. IVF was later performed and a pregnancy was established (Nagori, Panchal and Patel 2011). A similar trial was carried out by Gargett and Healy during which the thin endometrium of an AS patient was successfully treated by transplantation of BM fibroblasts and MSCs to the uterine cavity with concurrent curettage. The authors argue that both methods may have independently or synergistically promoted endometrial growth: BM cells by promoting angiogenesis and tissue growth through the secretion of trophic factors; and the curettage by stimulating endogenous stem/progenitor cell populations to regenerate endometrial tissue (Gargett and Healy 2011).

Improved understanding of the mechanisms of physiological endometrial repair might improve treatment of AS without the requirement of stem-cell transplantation but more investigations are required.

1.6.3 Endometriosis

Endometriosis is a condition where endometrial-like tissue grows outside the uterus primarily on the peritoneum, ovaries and rectovaginal septum (Giudice and Kao 2004, Giudice 2010). It affects 6-10% of women of reproductive age and is associated with severe pelvic pain and irregularities in menstruation and is present in up to 50% of women presenting with infertility (Giudice 2010, Sensky and Liu 1980). The most widely accepted theory for why some women develop endometriosis is based on transit of endometrial cells and tissue fragments into the peritoneal cavity during

menstruation which attach to the peritoneum, invade into the tissue and establish a nerve and blood supply (Sampson 1927, Corwin 1997, Giudice 2010). A role for both inflammation and endometrial progenitor/stem cells in the aetiology of the disorder has been proposed by multiple authors (reviewed by Vercellini et al. 2014).

The activation of macrophages has been reported in both peritoneal fluid and ectopic endometriotic lesions and a significant increase in macrophage cell numbers has also been detected in the intra-uterine endometrium of women with endometrosis (Berbic et al. 2009). Expression of fractaline/CX3CR1 was also increased. This factor important for lymphocyte and monocyte chemotaxis that has been shown to enhance stromal cell proliferation and invasion (Hou et al. 2016). These studies suggests a link between immune changes in the eutopic endometrium and the pathophysiology of endometriosis and associated pain and infertility, however it is still unclear whether these changes are primary or secondary to the establishment of disease (Jolicoeur et al. 1998, Berbic et al. 2009, Akoum et al. 2006, Hou et al. 2016)

In a study using a mouse model of endometriosis in combination with MacGreen reporter mice as donors and recipients (reciprocal transfers) Greaves *et al* reported that macrophages from both the recipient peritoneum and donor menstrual endometrial tissue contribute to the inflammatory microenvironment of the endometriotic lesion (Greaves et al. 2014). Bacci *et al* reported that macrophage in patients with endometriosis were alternatively activated (expressed high levels of CCL63/CD206) and that adoptive transfer of alternatively activated macrophages enhanced lesion formation in mice (Bacci et al. 2009). Mei *et al* found that peripheral blood-derived monocyte (PBMC)-driven macrophages co-cultured *in vitro* with endometrial stromal cells from women with endometriosis displayed lower phagocytic activity and an immunosuppressive phenotype when compared to healthy controls.

It has also been proposed that stem/progenitor cells in menstrual tissue contribute to formation of endometriosis lesions: there is evidence to show that women with endometriosis have a more extensive basal compartment in their endometrium to start with (Leyendecker et al. 2002, Leyendecker, Wildt and Mall 2009, Hufnagel et al. 2015). Some endometriotic lesions are monoclonal suggesting a single cell origin

whilst others are polyclonal and believed to originate from stromal cells, BM-MSCs and stem/progenitor cells from retrograde menstrual tissue (Kao et al. 2003). Human endometrial MSCs isolated from women undergoing laparoscopy were shown to express MSC markers including CD73, CD90, CD105 and CD166 and differentiate into osteoblasts, adipocytes and chondrocytes *in vitro* and have high tropism to endometriotic tissues *in vivo* (Cheng et al. 2017). When endometrial MSCs isolated from eutopic and ectopic endometrial tissue from women with endometriosis were cultured with HUVECs a subpopulation of MSCs was found to express CD31 and form tube like structures. These cells had increased expression of VEGFR2, TEK receptor tyrosine kinase and vascular endothelial-cadherin mRNAs and unchanged expression of c-myc, Vimentin, N-cadherin and SUSD2. This suggests that MSCs have the ability to undergo endothelial differentiation and may be involved in the development of vascular support for endometriotic lesions (Canosa et al. 2017).

Whilst the proportion of different stromal cell types in the endometrium in women with or without endometriosis appear to be similar (CD90+ fibroblasts, αSMA+ myofibroblasts) (Konrad et al. 2017), changes in the epithelial cell phenotype has been noted with both K19 and MUC1 being significantly decreased and vimentin increased in endometriotic lesions suggestive of an EMT transition (Konrad et al. 2018). In ovarian endometriosis increased expression of genes associated with EMT including vimentin, slug and N-cadherin was noted in association with an increase in Mmp7.

Matsuzaki *et al* also hypothesised that EMT-like and MET-like processed are involved in the pathogenesis of endometriosis. By analysing molecular markers of EMT such as cytokerain, E-cadherin, N-cadherin, Vimentin and β-catenin in various forms of endometriosis they showed that epithelial cells of ‘red’ lesions showed decreased expression of epithelial markers and increased expression of mesenchymal markers while epithelial cells of ‘black’ lesions had increased expression of epithelial cell markers and some expression of mesenchymal cell markers. This suggested that the regulation of EMT and MET may be important in the pathophysiology and progression of endometriosis (Matsuzaki and Darcha 2012). The activity of endometrial stem/progenitor cells may be important in establishing lesions so understanding how stem/progenitor cells give rise to endometrial tissue during repair may highlight ways

to hinder lesion development. Further to this as it has been shown that endometrial MSCs show significant tropism for endometriotic lesion tissue when applied both *in vitro* and *in vivo* (Cheng et al. 2017) and therefore may have potential in serving as vectors for targeted delivery of therapeutics. By increasing our understanding of how specific immune cell and stem/progenitor cell populations respond in normal endometrial repair novel targets may be identified and therapeutic strategies developed.

1.7 Model systems for studying endometrial repair

Studies seeking a greater understanding of the mechanisms responsible for endometrial breakdown and repair carried out by examining tissue samples recovered from endometrium across the menstrual cycle have been complemented and enhanced using *ex vivo* human tissue explants/xenografts and animal models. Developing informative animal models recapitulating the mechanisms of endometrial shedding/repair has not been easy as menstruation is only a natural process in a few Old World Primates (Finn 1987, Emera et al. 2012a), bat species (Rasweiler 1991, Rasweiler and de Bonilla 1992, Rasweiler, Badwaik and Mechineni 2011) and the recently discovered Spiny mouse (Bellofiore et al. 2017, Bellofiore et al. 2018). Although menstruation does not occur naturally in laboratory mice 'menstrual' models based on induction of artificial decidualisation and hormonal manipulation are attractive as they can benefit from availability of a large number of transgenic lines. These different models are discussed below.

1.7.1 Xenograft models

One of the most striking examples of the use of endometrial explants were the studies by Markee (1940) who transplanted endometrium from rhesus macaques into the anterior chamber of the eye and was then able to directly observe changes in tissue architecture and vascular constriction (Markee 1978).

By manipulating the steroid microenvironment, the human menstrual cycle can be mimicked in tissue xenografts that can be maintained long-term in immune compromised mice as recipients. For example changes consistent with menstruation

can be induced by treatment with oestradiol-17β for 14 days followed by treatment with oestradiol-17β plus progesterone for 14 days followed by cessation of hormonal support (Matsuura-Sawada et al. 2005). Interestingly when samples from the functional layer of human endometrium were transplanted and stimulated to undergo a simulated menstrual event, hormonal withdrawal induced a rapid decrease in graft volume which was stopped when oestrogen was applied again however the grafts did not increase in size thereafter (Coudyzer et al. 2015). These data would be consistent with a role for basal endometrium in endometrial regeneration.

In other studies mouse CD31+ cells were detected in both transplanted and host tissues consistent with the establishment of a blood supply. An increase in the number of human CD45+ immune cells has also been noted, showing a peak during the simulated secretory phase. In contrast, a peak in mouse CD45+ cells was seen 3 days following P4 withdrawal and surpassed the number of human CD45+ cells indicating that recruitment of immune cells from the circulation is an important response to endometrial tissue breakdown: the expression of MMP1, 2 and 9 were also significantly increased after P4 withdrawal consistent with endometrial tissue breakdown (Guo et al. 2011). A role for hypoxia has also been investigated using this method with authors reporting they did not find significant HIF1-α immunostaining after hormone withdrawal concluding that hypoxia was not essential to trigger menstrual-like tissue breakdown in human endometrial xenografts (Coudyzer et al. 2013). Human endometrial tissue has also been regenerated from endometrial clonogenic (Chan et al. 2004), SP cells (Cervelló et al. 2011) and perivascular SUSD2+ cells (endometrial MSCs) when transplanted beneath the kidney capsule in immunocompromised mice (Gurung et al. 2018) extending studies on endometrial tissue fragments and supporting a role for stem/progenitor cells in tissue regeneration.

1.7.2 Non-human primate models

The rhesus macaque is an example of a non-human primate that undergoes spontaneous decidualisation and menstruation during a 28 day cycle and this species has been widely used for studying the process of menstruation (Demers et al. 1972). Rhesus macaques have the advantage of being trained to allow for vaginal swabs to

detect bleeding and the insertion of tampons to quantitate blood loss. In addition, naturally cycling macaques often display spontaneous menstrual disorders making them ideal for clinically relevant studies of conditions like heavy menstrual bleeding (Brenner and Slayden 2012). The structure of the macaque uterus is morphologically similar to the human uterus and contains the same cellular compartments: luminal epithelium, functionalis, basalis and myometrium which undergoes similar processes of decidualisation and spiral artery formation in preparation for pregnancy (Brenner et al. 1996). To reduce variability in bleeding patterns, macaques can be ovariectomised and treated with a hormone regime that recapitulates the cycle allowing for consistent collection of tissues from the premenstrual, menstrual and postmenstrual phases (Brenner and Slayden 2012, Brenner et al. 1996).

In this species dynamic roles for MMPs and TIMPS in endometrial breakdown and repair have been demonstrated (Brenner et al. 1996). Significant increases in the expression of fibronectin, Itga5 and Itgb1 were also noted during menstruation, concentrated in the glandular epithelium and stroma of the functionalis (Cao et al. 2007). Notably VEGF mRNA was upregulated 1-2 days after progesterone withdrawal and in the healing epithelium during repair which was accompanied an increase in VEGFR1 and 2 in endothelial cells immediately below the luminal surface, implicating epithelial-derived VEGF in neoangiongenesis during endometrial regeneration (Nayak and Brenner 2002). Further to this, Fan *et al* demonstrated that blocking VEGF action during menstruation completely inhibited neoangiogenesis and disrupted the process of re-epithelialisation. These studies provided key insights into the importance of VEGF in postmenstrual endometrial repair (Fan et al. 2008, Germeyer et al. 2005).

A critical window for the duration of progesterone withdrawal has been identified by adding the progesterone secreting pellet back at multiple time points between 12 and 72hrs following withdrawal. Notably menses could be blocked if progesterone was added back 12 and 24hrs after removal, but rescue was reduced at 30hrs and menstruation proceeded if add back of progresterone was 36hrs or later indicating that a critical period of progesterone withdrawl exists and lasts approximately 36hrs in the macaque. Notably progesterone replacement significantly inhibited the expression of

MMP1, 2 and 3 further implicating upregulation of MMPs as critical to the induction of menses (Slayden and Brenner 2006).

1.7.3 Spiny mouse

Recently, natural menstruation has been reported in the spiny mouse (*Acomys Cahirinus*) a species of rodent originating in desert areas in Northern Africa (Bellofiore et al. 2018). To investigate the menstrual cycle in these mice, vaginal sampling was performed for two complete cycles revealing that mean menstrual cycle length was 8.7±0.4 days with red blood cells observed over 3.0±0.2 of the days, and the endometrium was thickest when plasma progesterone concentrations peaked (Bellofiore et al. 2017). The spiny mouse menstrual cycle displayed both ovarian and uterine phases as in other menstruating species: during the follicular phase the endometrium was thin; during the luteal phase angiogenesis and decidualisation were observed; and the onset of cytological and haemorrhagic changes coincided with regression of the CL and a drop in plasma progesterone concentration (Bellofiore et al. 2017). The spiny mouse also displays unique physiological traits such as scar-free wound healing in the skin (Mamrot et al. 2017). Although not yet fully investigated this rodent offers potential as non-primate model in which to study physiological mechanisms of endometrial breakdown, shedding and repair (Bellofiore et al. 2017).

1.7.4 Mouse pseudopregnancy model

Pseudopregnancy can be achieved by mating female mice to vasectomised males and four days later administering an intrauterine injection of oil to artificially induce a decidualisation response. Progesterone withdrawal is achieved by ovariectomy two days following decidualisation: decidual tissue breakdown and shedding was reported to be complete by 24 hours following P4 withdrawal and complete re-epithelialisation was observed by 48 hours (Fan et al. 2008). Using this model, Fan *et al* demonstrated that VEGF is essential for neoangiogenesis, regulating vessel stability and re-epithelialisation during endometrial repair by administering a pharmacological VEGF inhibitor at the time of steroid withdrawal. Mice treated with the inhibitor failed to fully repair and dysfunction in the vasculature was observed (Fan et al. 2008). This

pseudopregnancy model has been used in combination with inhibition of Wnt7a where there is a failure of re-epithelialisation and degradation of the basal gland complementing studies in primates that localized WNT7a to newly formed luminal epithelium and upper glands during endometrial repair (Fan et al. 2012).

In a modified version of the pseudopregnancy mouse model Rudolph *et al* administered the potent progesterone receptor antagonist mifepristone two days after induced decidualisation instead of performing ovariectomy. This blockade mimicked progesterone withdrawal and stimulated decidual tissue breakdown. Bleeding was evaluated by vaginal lavage however blood was also visible at the opening of the vagina (Rudolph et al. 2012).

1.7.5 Mouse model of simulated 'menses'

A mouse model of 'menstruation' based on hormone manipulation and artificial decidualisation was first described in 1984 by Finn and Pope. Mice were ovariectomised to deplete endogenous steroid hormone production and then primed with a hormone schedule to mimic the fluctuating hormones experienced by women during the menstrual cycle: ovariectomy and seven days rest; two days of oestradiol (100ng/100µl); three days of rest, three days of oestradiol (20ng/100µl) and progesterone (1mg/100µl) followed by an intraluminal injection of oil 4-6h later. In rodents, unlike humans, decidualisation only occurs naturally in response to blastocyst implantation. The decidualisation reaction has been likened to the formation of granulation tissue in response to the presence of a foreign body (the implanting blastocyst) and so it is believed that the insertion of oil into the uterine lumen mimics this physiological event. The exact mechanism by which this occurs however is largely unknown (Finn and Keen 1963, Finn and Pope 1984). One problem with this model was variation in the extent of decidualisation however if decidualisation had occurred, removal of progesterone resulted in tissue breakdown and a 'menses like' which shared key features of human menstruation incluiding tissue necrosis, inflammation and luminal shedding (Finn and Pope 1984).

The model was updated by the Salamonsen Group who modified the protocol to use inbred mice and to include a silastic progesterone-secreting pellet to replace injections which ensured a steadily increasing concentration of circulating progesterone, considered to be more comparable to what happens in women (Brasted et al. 2003). Using this model decidualisation was successfully induced in the uterine horns and endometrial breakdown was initiated 12-16hrs following progesterone withdrawal. The entire decidua was detached and shed at 24hrs and re-epithelialisation of the luminal surface was almost complete by 36hrs, while restoration of endometrial tissue architecture was achieved by 48hrs. The authors also demonstrated changes in CD45+ leucocyte numbers cellular apoptosis as determined by TUNEL staining in the endometrium during tissue shedding (Brasted et al. 2003). Notably this study was the first to define the endometrial breakdown and repair phase as being complete 48hrs following withdrawal of progesterone. A further refinement to this model led to the establishment of the Edinburgh model (Cousins et al 2014; 2016): specific differences were use of a transvaginal route to induce decidualisation (reduction in number of surgeries) and an increase in exposure to the progesterone secreting pellet from 2 to 4 days ensuring a more robust and reproducible decidualisation response. In common with other reports shedding was maximal at 24hrs after progesterone withdrawal and tissue restored at 48hrs. (Figure 1-17).

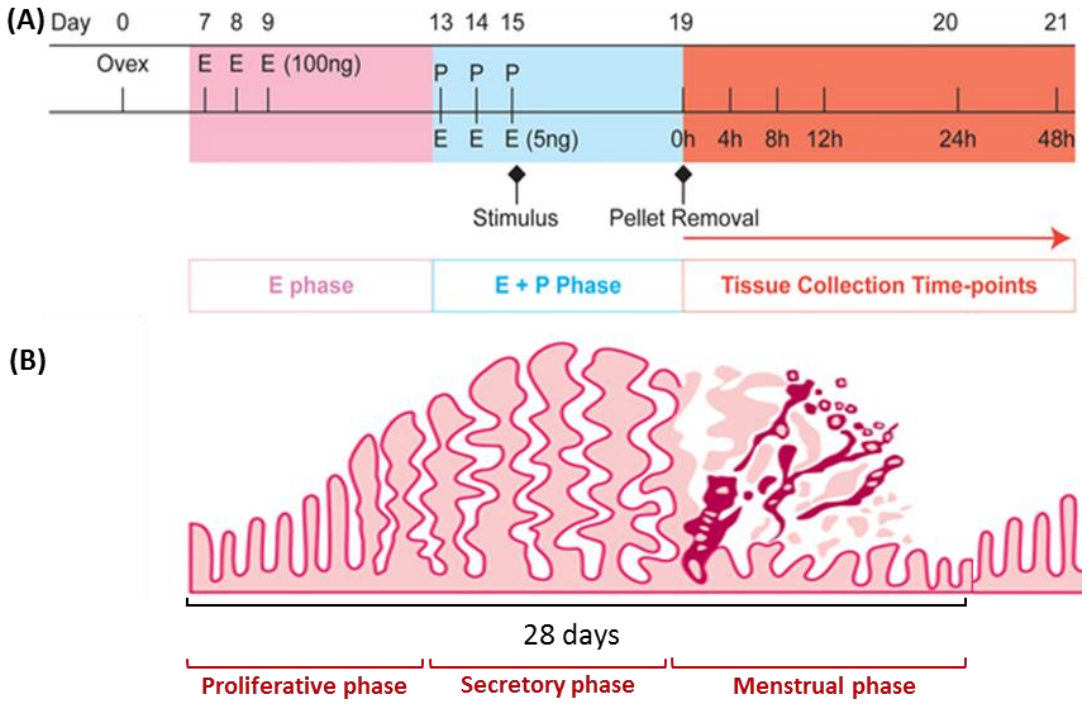

Figure 1-17. Schematic of the Edinburgh menses mouse model. (A) The pink box represents the oestrogen dominant proliferative phase, the blue box represents the progesterone dominant secretory phase and the red box represents the menstrual phase of the model. Tissue breakdown and shedding is stimulated by removal of progesterone and complete endometrial repair is observed within 48hrs of this. **(B)** Respresentative image of the phases of the human menstrual cycle recapitulated by the Edinburgh menses mouse model. Ovex: ovariectomy, E: β-oestradiol at 100ng/100µl then 5ng/µl, P: progesterone (adapted from Cousins et al. 2014).

These mouse models have been widely used to study mechanisms associated with endometrial tissue breakdown and repair: Wang *et al* showed that replacement of progesterone at 8 and 12hrs blocked menstrual-like bleeding while replacement at 16-24 hrs had no effect on bleeding (Wang et al. 2013). This study identified the critical window to be within the first 12hrs following P4 withdrawal, a lot shorter than that of the macaque model. Kaitu'u *et al* maintained females on a soy-free diet with additional administration of the aromatase inhibitor letrozole demonstrating repair in the absence of measurable oestrogens (Kaitu'u-Lino et al.). Hypoxia has been found to be an important regulator of endometrial breakdown and repair (Semenza 1998). Striking spatial and temporal fluctuations in hypoxia were displayed using Hypoxyprobe™ detection system with the epithelium exposed to hypoxic conditions during endometrial repair. The changes in hypoxia were correlated with changes in gene expression of VEGF and CXCL12 suggesting hypoxia has a role in driving both the

angiogenic response and inflammation (Cousins et al. 2016d). Furthermore, hypoxia has been shown to stabilise HIF1α and drive endometrial repair where pharmacological reduction of HIF1α delays complete repair and pharmacological stabilisation rescues the delay. This study identifies HIF1α as a potential therapeutic target for HMB (Maybin et al. 2018).

A study by Kaitu'u *et al* used the LRC technique and a mouse model to show that BrdU signal in the luminal epithelium rapidly decreased during post menstrual repair indicative of extensive proliferation while glandular epithelium remained constant. In contrast during the later repair phase glandular epithelial cells decreased BrdU expression suggesting that a population of epithelial progenitor cells reside in the basal glands that are important during postmenstrual repair (Kaitu'u-Lino et al. 2010). Cousins *et al* later demonstrated that re-epithelialisation occurred through three synchronous mechanisms: luminal and glandular epithelial cell proliferation and migration and a mesenchymal to epithelial transition (MET) by cells of the stromal compartment in proximity to the denuded surface (Cousins et al. 2014). Stromal LRC were also identified throughout endometrial breakdown and repair although this was significantly decreased during endometrial repair indicative of proliferation in response to wounding (Kaitu'u-Lino et al. 2012).

The inflammatory response has also been the subject of many studies. Depletion of granulocytes using an anti-mouse GR-1 antibody (expressed on BM-derived monocytes) decreased the expression of matrix modifying enzymes such as MMP3, 9 and 10 and impaired tissue repair (Menning et al. 2012). Another study where neutrophils were specifically depleted by application of the RB6-8C5 antibody, confirmed a delay in endometrial repair in the absence of neutrophils. The authors reported that F4/80 expressing macrophages were in low abundance and therefore unlikely to contribute to endometrial tissue repair (Kaitu'u-Lino et al. 2007). Further characterisation of the inflammatory response during menstruation revealed that Ly6G+ neutrophils peaked in number at 24hours associated with significant increase in the expression of cytokines and chemokines including CXCL1, TNF, CCL2 and IL-6. These dynamic changes were recapitulated in human tissue samples at corresponding phases of the cycle thereby validating the use of this mouse model to

recapitulate inflammatory processes during human menstruation (Armstrong et al. 2017).

The distribution of MMPs has been examined by Kaitu'u *et al* revealing important roles for MMP7 and MMP9 during endometrial tissue breakdown and MMP3 and MMP7 during re-epithelialisation. The application of two MMP inhibitors did not affect endometrial breakdown or repair processes suggesting that while MMPs are important, they are not the key mediators during post-menstrual repair (Kaitu'u et al. 2005). The mouse model has been further used to demonstrate dynamic expression and functional importance of ECM interactions (Evans et al. 2011) and the expression of activin A in specific epithelial and stromal cell populations which may have a role in regulating re-epithelialisation (Kaitu'u-Lino et al. 2009). Furthermore an important role for androgens has been recognized in regulating repair processes whereby administration of DHT resulted in delayed restoration of the luminal epithelium associated with changes in expression of MMP3, MMP9, Snai3 and osteopontin, important regulators of MET (Cousins et al. 2016b).

1.8 General conclusions and aims of the study

The endometrium is a complex multicellular tissue that experiences cyclical episodes of ECM remodelling, inflammation, hypoxia, vascular changes and tissue repair in response to menstruation, all of which may have important roles to play in scar-free regeneration (Spitzer et al. 2012, Salamonsen 2003b). Strict regulation of cyclical 'injury' and 'repair' episodes is an unparalleled physiological response that is essential to successful reproductive function (Maybin and Critchley 2015). Despite knowledge on cellular and molecular changes that govern endometrial tissue breakdown during menstruation, the precise mechanisms that underpin rapid scar-free healing are yet to be fully elucidated. Progress is hindered by the fact that it is very difficult to obtain tissue samples of defined stages of the menstrual cycle and the onset of vaginal bleeding, which is considered to be the start of menstruation, actually only occurs when the endometrial surface and blood vessels are breached while initiation of molecular and cellular events happen well before that (Evans et al. 2011). Tissue breakdown and repair also occur simultaneously and therefore human endometrial

samples are likely to contain a mix of pre-menstrual tissue, tissue that is degrading and tissue that has repaired (Garry et al. 2009), making it difficult to tease apart mechanisms associated with each. The development of robust mouse models of endometrial breakdown and repair that mimic the events of the human menstrual cycle provide a platform for initial investigations which can later be translated to human tissues.

Endometrial macrophage numbers increase in the endometrial tissue during the secretory and menstrual phase with prominent roles in regulating tissue breakdown (Thiruchelvam et al. 2013) however their presence and function during subsequent tissue repair is at present unknown. Tissue resident macrophages are highly plastic cells that exhibit diverse phenotypes in response to signals in their local microenvironment (Das et al. 2015). The current study aimed to phenotype and characterise macrophage populations specific to the endometrium during homeostasis and in response to the 'wound' inflicted during menstruation. In-depth characterisation of endometrial macrophages could lead to new insights into the role of macrophage heterogeneity in the regulation of scar-free endometrial tissue repair.

The striking regenerative capacity of the endometrium has led to the hypothesis that a population of stem/progenitor cells exist in the basal endometrium that are not lost during menstruation but instead are are mobilised to differentiate and reconstitute lost tissues (Gargett et al. 2016). A population of stem/progenitor cells has been identified as clonogenic or SP cells in the human endometrium and as LRC in the mouse endometrium. These cells share properties and characteristics of MSCs and can be further identified through co-expression of Pdgfrβ and CD146 (Schwab and Gargett 2007). Recently it has been proposed that endometrial stem/progenitor cells may be perivascular pericytes which have stem-cell properties, however the physiological role for these cells remains undetermined. This study aims to further characterise endometrial stem/progenitor cells and investigate how this population responds during endometrial breakdown and repair with the aim of highlighting a role in scar-free tissue repair exhibited by the endometrium.

It is clear that a balance in tissue degradative and tissue repair mechanisms is key to regulating endometrial regeneration during the menstrual cycle. Further understanding of this balance and how it may be tipped to one or the other side may provide important insight into regulatory mechanisms of scar-free tissue repair with potential to identify new therapeutic targets for both gynaecological conditions and conditions associated with scar formation elsewhere in the body.

1.9 Hypothesis

The endometrium can provide a model system in which to investigate the mechanisms of physiological scarless wound healing.

1.10 Aims

1. To investigate the relationship between tissue resident and transient immune cell populations in endometrial repair.
2. To identify and characterise a putative population of mesenchymal progenitor cells in endometrium.
3. To investigate the role of mesenchymal progenitor cells in endometrial repair and regeneration.

Chapter 2 Materials and Methods

2.1 Animal Work

All animal procedures were carried out according to best practise and in line with the Home Office Animals (Scientific Procedures) Act 1986 under the project licence numbers PPL60/4208 and PPL70/8945 held by Professor Philippa TK Saunders, and personal licence number PIL IE9547CC3.

Animals were housed in standard conditions with a constant light cycle of 12hours and food and water provided *ad libitum*.

Wildtype C57BL/6 mice were bred in house from available breeding stocks.

2.1.1 Transgenic mice

2.1.1.1 The *Pdgfrβ-BAC-eGFP* knock-in reporter mouse line

Platelet derived growth factor receptor beta (*Pdgfrβ*), also known as CD140b is a cell surface receptor belonging to the family of receptor tyrosine kinases which transmit signals from the cell surface to the cell interior once stimulated by PDGF (Hewitt et al. 2012). This ligand-receptor interaction is important for a variety of essential mesenchymal cellular processes including proliferation, growth, de-differentiation, movement and development, whilst also having roles in many diseases such as cancer (reviewed by(Raica and Cimpean 2010). In general, Pdgfrβ has been found on cells of mesenchymal origin including stromal cells such as fibroblasts and pericytes which support the function of parenchymal cells and secrete ECM to maintain tissue architecture (Hewitt et al. 2012).

Pdgfrβ-BAC-eGFP reporter mice (C57BL/6 background) carry one copy of a bacterial artificial chromosome (BAC) construct in which an enhanced green fluorescent protein (eGFP) reporter gene, followed by a polyadenylation sequence, is inserted into a BAC clone (RP23-10L16) at the initiating ATG codon of the first coding exon of the Pdgfrβ gene. Therefore eGFP expression is driven by the regulatory sequences of the Pdgfrβ gene resulting in mesenchymal cell specific expression of eGFP. Founder stocks were obtained from Professor Neil Henderson (Centre for Inflammation Research, University of Edinburgh) [Originally obtained from GENSAT (Gene

Expression Nervous System Atlas) and deposited in MMRRC (Mutant Mouse Regional Resource Centre- STOCK Tg(*Pdgfrβ*-EGFP)JN169Gsat/Mmucd, 031796-UCD) (Henderson et al. 2013)].

2.1.1.2 The *Csf1r*-eGFP 'MacGreen' reporter mouse line

Macrophage colony stimulating factor receptor 1 (CSF1r, CD115) is expressed by cells of the mononuclear phagocyte system and regulates differentiation, proliferation and cell survival. The gene is expressed selectively in monocyte and trophoblast cell lineages but has also been found to be expressed by some granulocytes. CSF1r is encoded by the *c-fms* (*Csf1r*) proto-oncogene (Sasmono and Williams 2012). The fms-eGFP 'MacGreen' reporter mice (C57BL/6 background) have a reporter gene construct containing 3.5-kb of 5' flanking sequence of exon 2 and the entire intron 2 sequence of the *Csf1r* gene driving expression of eGFP to cells expressing CSF1R, namely cells of the mononuclear phagocyte system. The generation of these mice has been previously described (Sasmono et al. 2003) and founder stocks were obtained from Dr. Bernadette Dutia and Professor David Hume (Roslin Institute, University of Edinburgh- STOCK Tg(Csf1r-EGFP)1Hume)(Cousins et al. 2016c).

2.1.1.3 The *Csf1r*-mApple 'MacApple' reporter mouse line

Macrophage colony stimulating factor receptor 1 (CSF1r, CD115) is expressed by cells of the mononuclear phagocyte system and is encoded by the *c-fms* (*Csf1r*) proto-oncogene (Sasmono and Williams 2012). The *Csf1r* reporter construct used to generate the Csf1r-eGFP 'MacGreen' transgenic mouse line, described above (Sasmono et al. 2003), and a construct encoding the fluorescent protein *Csf1r*-mApple (Balic et al. 2014) were ligated with T4 ligase to create a *Csf1r-mApple/Csf1r-rtTA* construct. This construct was used to generate the *Csf1r*-mApple reporter mouse line at the University of Edinburgh's Central Biological Services Transgenic Core facility by microinjection of the transgene into the pronuclei of fertilised oocytes from C57BL/JOlaHsd mice. The resulting mApple expression is in cells of the mononuclear phagocyte system (Hawley et al. 2018). Stock mice (female) were obtained from Dr Steve Jenkins (MRC Centre for Inflammation Research, University of Edinburgh, STOCK- *Csf1r-mApple/Csf1r-rtTA*).

2.1.1.4 The *hCD68-GFP* reporter mouse line

CD68 is a transmembrane protein with roles in antigen processing and as a scavenger protein however, the exact function is yet to be confirmed. CD68 is expressed by myeloid cells, specifically monocytes and macrophages (Iqbal et al. 2014). To generate the hCD68-GFP reporter mouse line, a complementary DNA fragment encoding eGFP (pEGFP-N1 vector, Invitrogen) was cloned into the 1265 vector containing the promoter and intron one of human CD68 (2.9kb). DNA was excised from the cloning vector and injected into C57Bl/6J mouse oocyte. This generated mice in which GFP is expressed under control of CD68, expressed therefore by myeloid lineage cells (Iqbal et al. 2014). Stock mice (female) were obtained from Dr Jenna Cash (MRC Centre for Inflammation Research, University of Edinburgh), originally obtained from The Jackson laboratory- STOCK- Tg(Cd68-EGFP)1Drg).

2.1.1.5 The NG2-CreER^{TM} BAC tamoxifen-inducible mouse line

Neural/glial antigen 2 (NG2) also known as chondroitin sulfate proteoglycan 4 (Cspg4), is an integral membrane proteoglycan found on many cell types including oligodendrocyte progenitor cells (OPCs), chondroblasts, myoblasts and pericytes (Ozerdem, Monosov and Stallcup 2002). NG2 may be either membrane bound or secreted and associated with the extracellular matrix and is believed to have functions in cell adhesion, cell-ECM communication, proliferation, migration, axonal growth and regeneration. NG2 expressing cells are most prominently described as oligodendrocyte progenitor cells in the central nervous system (Zhu et al. 2011).

NG2-CreER^{TM} BAC mice carry once copy of a 208kb BAC construct containing the entire NG2 (Cspg4) gene with 60kbp of 5' and 114kbp of 3' flanking sequences, and a CreER^{TM} fusion gene, where cre recombinase is fused to a G525R mutant form of the mouse oestrogen receptor ligand binding domain followed by a rabbit beta-globin polyA signal, inserted into the first exon of the NG2 gene. The mutant oestrogen receptor does not bind its natural ligand (17β-oestradiol) but binds with the synthetic oestrogen receptor ligand 4-hydroxytamoxifen (OHT or tamoxifen). When NG2Cre-ER^{TM} BAC transgenic mice are bred with mice containing *loxP*-flanked sequences (Ai14 reporter mouse outlined below), tamoxifen-inducible cre-mediated recombination is expected to result in deletion of the floxed sequences in the NG2

expressing cells specifically. Founder stocks were obtained from The Jackson laboratory- STOCK B6.Cg-Tg(Cspg4-cre/Esr1*)BAkik/J).

2.1.1.6 The Ai14 reporter mouse line

Ai14 reporter mice are a Cre reporter strain. They contain a Rosa-CAG-LSL-tdTomato-WRPE targeting vector designed with a CMV-IE enhancer/chicken beta-actin/rabbit beta-globin hybrid promoter (CAG), an FRT site, a loxP-flanked STOP cassette, tdTomato sequence (DsRed fluorescent protein), a woodchuck hepatitis virus post-transcriptional regulatory element (WPRE), a polyA signal and an attB/attP-flanked PGK-FRT-Neo-PolyA cassette. This entire construct was inserted between exons 1 and 2 of the ubiquitously expressed Gt(ROSA)26Sor locus. The loxP-flanked STOP cassette is designed to prevent transcription of the tdTomato. When bred to mice that express Cre recombinase, the resulting offspring will have the STOP cassette deleted specifically in the cre-expressing tissues or cells, resulting in robust tdTomato fluorescence. Stock mice (female) were obtained from Professor Neil Henderson (MRC Centre for Inflammation Research, University of Edinburgh) [Originally obtained from The Jackson Laboratory- STOCK *Gt(ROSA)26Sor*$^{tm14(CAG-tdTomato)Hze}$] (Henderson et al. 2013).

2.1.1.7 Tamoxifen induction of NG2-CreER^{TM} BAC transgenic mice

Tamoxifen (Sigma, Cat. #T5648-1G) (TMX) was dissolved in sesame seed oil to a concentration of 20mg/ml and left overnight on a roller at 37°C (light protected). For TMX administration, an intraperitoneal (IP) injection of 125µl was given to each mouse (standard 25g weight) for 5 consecutive days (TMX dose 100mg/kg).

2.1.2 Genotyping transgenic reporter mice

2.1.2.1 Preparation of Stock buffers

Stock buffers of 0.5M Ethylenediaminetetraacetic acid (EDTA) and 1M Sodium Hydroxide (NaOH) were prepared using the reagents in Table 2-1, and kept at room temperature (RT).

Table 2-1. Volume of reagents required for stock solutions of EDTA and NaOH

Reagent Stock	Supplier, Cat. No.	Volume for 100ml stock 0.5M EDTA	Volume for 100ml stock 1M NaOH
EDTA (g)	Sigma, E5134-500g	18.62	0
NaOH (g)	Sigma, L4390-100g	2.028	4
Distilled water (ddH_2O, ml)	Baxter, UK17114	88.95	100

2.1.2.2 Preparation of digestion buffers

A working solution of an alkaline lysis reagent was prepared by mixing 2.5ml of stock NaOH with 40µl of stock EDTA, and made up to 100ml with ddH_2O. A working solution of a neutralising reagent was prepared by dissolving 630mg of Tris (hydroxymethyl) aminomethane (THAM) hydrochloride (Tris-HCL, 40mM) in 100ml ddH_2O. Working solutions were kept at RT.

2.1.2.3 DNA extraction from mouse ear biopsy using Hot Sodium Hydroxide and Tris (HotShot) method

The 'HotShot' (Sodium Hydroxide and Tris) method was used to extract DNA from each mouse ear biopsy. For each reaction, 75µl of the alkaline lysis reagent was added to the mouse ear biopsy and heated at 95°C for 30 minutes. Solutions were cooled to 4°C for 5 minutes and then 75µl of the neutralising reagent was added. Suspensions were kept on ice or stored at -20°C until PCR analysis could be completed. The combination of the alkaline lysis reagent and neutralising reagent yields a buffer of pH 8.1, 20mM Tris-HCL and 0.1M EDTA, similar to Tris-EDTA (TE) buffer which is commonly used for extracting DNA.

2.1.2.4 PCR for transgenes in DNA sample from mouse ear biopsy

PCR (polymerase chain reaction) can be used to target and amplify a specific segment of DNA. A typical a reaction requires a DNA template, two primers specific to the gene to be amplified, a DNA polymerase, dNTPs and a buffer solution capable of providing an optimal chemical environment to maintain the activity and stability of the DNA polymerase. During PCR complimentary base pairing primers attach to a denatured double stranded template thereby defining a location at the 3' end of

opposite strands facilitating attachment of a thermostable form of DNA polymerase. DNA polymerase is a naturally occurring complex of proteins whose function is to copy a cell's DNA before it undergoes division by adding complimentary nucleotides (adenine, guanine, cytosine and thymine) to the primers (SantaLucia 2007).

To genotype the *Pdgfrβ-BAC-eGFP* knock-in reporter mice and MacGreen reporter mice, primers specific to a region of the eGFP transgene were used to identify transgenic animals. Fatty acid binding protein 2 (*Fabpi*) was used as an internal control in each reaction, to confirm both the success of the PCR reaction and the quality of the resulting DNA. Primer sequences are shown in Table 2-2. To genotype the NG2-CreER^{TM} BAC transgenic mice, primers specific to a region of the generic Cre transgene were used alongside an internal control, Table 2-2. Primers for each gene of interest (GOI) and associated controls were designed using the Universal Probe Library Assay Design Centre (Roche Applied Science) and purchased from Eurofins (Germany).

Table 2-2. Primer sequences for eGFP, Fabpi, Cre and a control used to genotype *Pdgfrβ-BAC-eGFP*, Macgreen and NG2-CreER^{TM} BAC transgenic mice

Primer	Associated Transgenic	Primer Sequence
eGFP Forward Primer	*Pdgfrβ-BAC-eGFP*, MacGreen	5' GCA CGA CTT CTT CAA GTC CGC CAT GCC 3'
eGFP Reverse Primer	*Pdgfrβ-BAC-eGFP*, MacGreen	5' GCG GAT CTT GAA GTT CAC CTT GAT GCC 3'
Fabpi Forward Primer	*Pdgfrβ-BAC-eGFP*, MacGreen	5' CCT CCG GAG AGC AGC GAT TAA AAG TGT CAG 3'
Fabpi Reverse Primer	*Pdgfrβ-BAC-eGFP*, MacGreen	5' TAG AGC TTT GCC ACA TCA CAG GTC ATT CAG 3'
Cre Forward Primer (oIMR1084)	NG2-CreER^{TM} BAC	5' GCG GTC TGG CAG TAA AAA CTA TC 3'
Cre Reverse Primer (oIMR1085)	NG2-CreER^{TM} BAC	5' GTC AAA CAG CAT TGC TGT CAC TT 3'
Control Forward Primer (oIMR7338)	NG2-CreER^{TM} BAC	5' CTA GGC CAC AGA ATT GAA AGA TCT 3'
Control Reverse Primer (oIMR7339)	NG2-CreER^{TM} BAC	5' GTA GGT GGA AAT TCT AGC ATC ATC C 3'

Each PCR reaction was prepared by mixing 2x BioMix Red (Bioline, London, UK) with 100µm stocks of primers for the GOI and appropriate control using volumes outlined in Table 2-3. 2x BioMix Red is a reaction mix containing a stable Taq DNA polymerase and an additional red dye permitting easy visualisation and direct loading onto a gel. Using this mix reduces the time required to set up reactions, minimising the risk of contamination by reducing the number of pipetting errors that may occur. A positive control (known transgenic positive animal), a negative control (known transgenic negative animal) and a water control (no DNA) were prepared in parallel for each genotyping reaction.

PCR amplification was carried out on a Peltier Thermal Cycler (PTC-200) under the following conditions: 35 cycles of 94°C for 30 seconds (denaturation); 65°C for 30 seconds (annealing); 72°C for 1 minute (elongation) then 72°C for 7 minutes (final elongation) and finally 10°C for ten minutes (final hold). Samples were then put in a fridge at 4°C for later processing. Principles of the PCR reaction are outlined in the Figure 2-1.

Table 2-3. Final concentration and reaction volumes for each component of the PCR master mix.

Reagent Stock	Final Concentration	Volume per 10µl reaction (µl)
2x Biomix Red	1x	5
GOI Forward Primer 100µm	100nm	0.1
GOI Reverse Primer 100µm	100nm	0.1
Control Forward Primer 100µm	100nm	0.1
Control Reverse Primer 100µm	100nm	0.1
ddH_2O	X	3.6
DNA template	X	1
	Total Volume	10

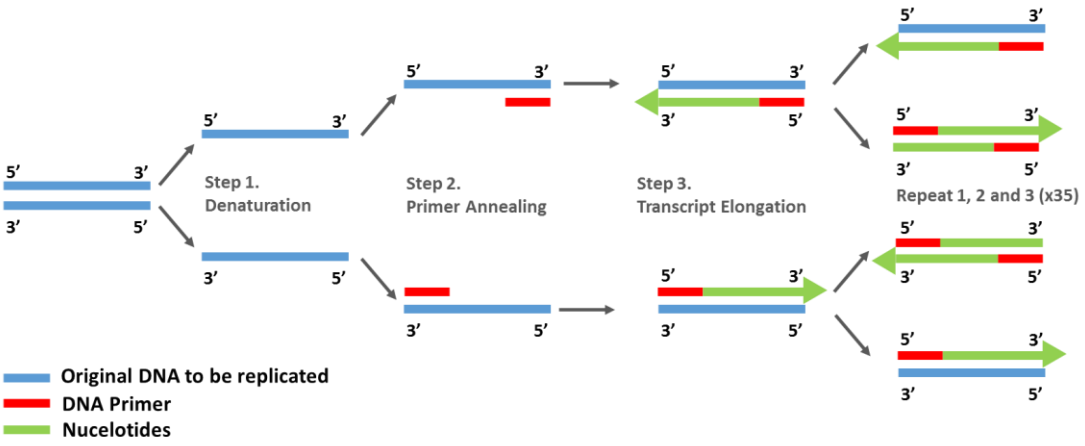

Figure 2-1. Schematic representation of the principles of the polymerase chain reaction (PCR). **Step 1:** Denaturation is the first essential step in the reaction and required to disrupt the hydrogen bonds between complimentary bases, yielding single stranded DNA molecules. **Step 2:** Thereafter the temperature is reduced to favour annealing of the primers (which are in excess) to the DNA strands. Careful design of primers is essential to ensure this read is specific to the target of interest. **Step 3:** Elongations follows governed by the optimal activity temperature of the DNA polymerase which synthesizes a new DNA strand complimentary to the template by adding dNTPs in the 5' to 3' direction. Final elongation ensures that any remaining single stranded DNA is fully extended and the final hold is for an indefinite time to allow for short term storage of the reaction (based on SantaLucia 2007))

2.1.2.5 DNA fragment analysis on agarose gels

PCR products were separated by electrophoresis on a 2% (w/v) agarose gel, prepared by heating 1g powdered agarose in 50ml 1xTAE (Tris base, Acetic acid, EDTA mix) and setting the gel in a mould and comb with 5µl SYBR safe DNA gel stain (Invitrogen, Cat. #S33102) for visualisation. The percentage of agarose gel needs to be adjusted depending on the size of product being analysed, in general the smaller size of product correlates to a larger percentage agarose. Samples were electrophoresed at 120V and 300mA alongside an aliquot (5µl) of DNA Hyperladder IV (1000kb) (Bioline, London, UK) in one lane. The size of DNA fragments for each transgenic can be seen in Figure 2-2, in each case the detection of two bands was consistent with a positive transgenic animal (Figure 2-2).

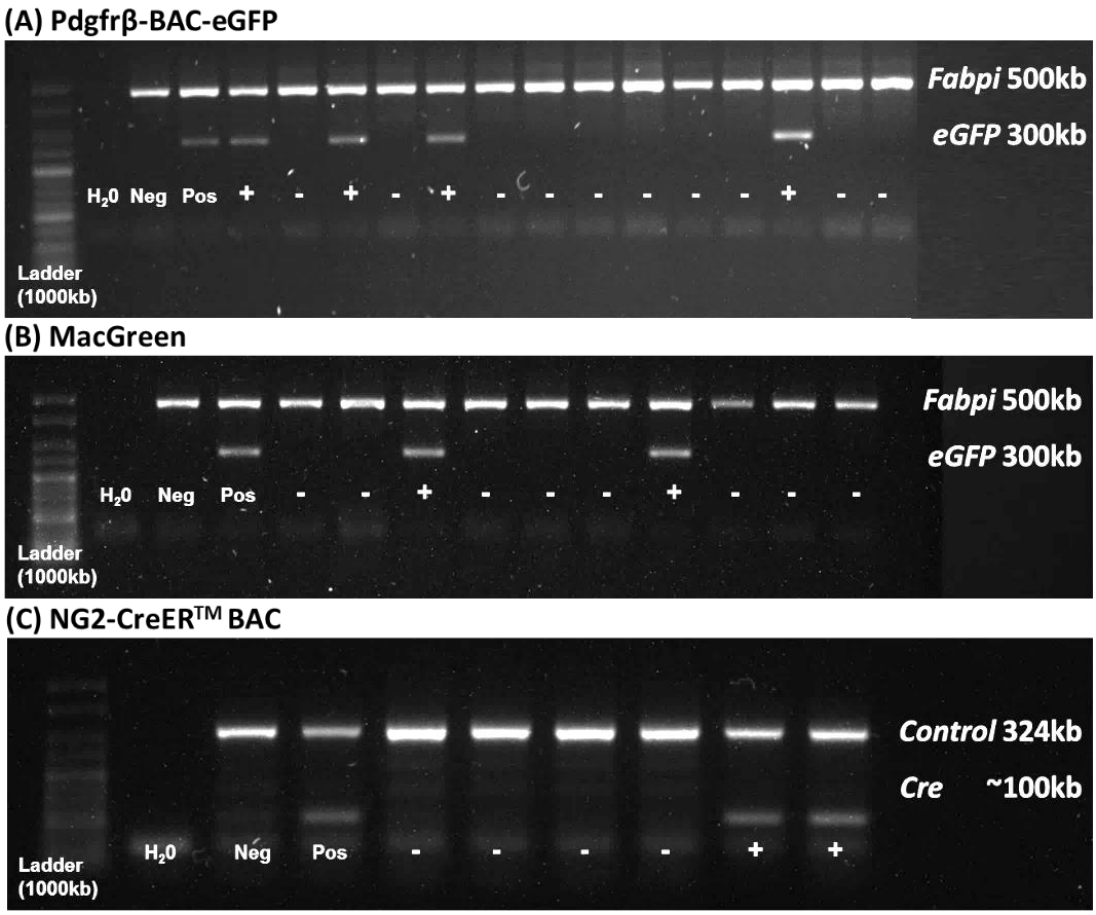

Figure 1-2: Gel image of typical DNA fragment analysis using the agarose gel method for (A) *Pdgfrβ-BAC-eGFP*, (B) MacGreen and (C) NG2-CreER^{TM}BAC transgenic mouse lines. Hyperladder IV in lane 1, H_20 control in lane 1, negative control in lane 3, positive control in lane 4. The remaining lanes show both transgenic positive (+) and transgenic negative (-) animals (Author's own images)

2.2 Investigating uterine tissue in mice

2.2.1 Collection of uterine tissue from intact/naïve mice

Normal mouse uterine tissue samples were gathered to investigate cell populations of interest in endometrial tissue during homeostasis. Uterine tissues were collected from cycling adult female mice (8-10 w/o, all strains) denoted as naïve tissues and, unless stated otherwise, used as comparative controls in the experiments of this thesis. Mice were culled by asphyxiation by carbon dioxide gas and death confirmed by cervical dislocation. Oestrous stage was confirmed by vaginal smears as follows: phosphate-buffered saline (PBS) (50µl) was introduced into the vagina and vaginal

cells collected onto a glass slide. Vaginal smears were air dried and then fixed by immersion in ice cold methanol and air dried four times. Fixed slides were stained with haematoxylin and eosin (H&E staining, Section 2.4.1) and the stage of oestrus cycle determined by comparing the composition of cells in the smear with a reference figure, see Figure 2-3 (Caligioni 2009).

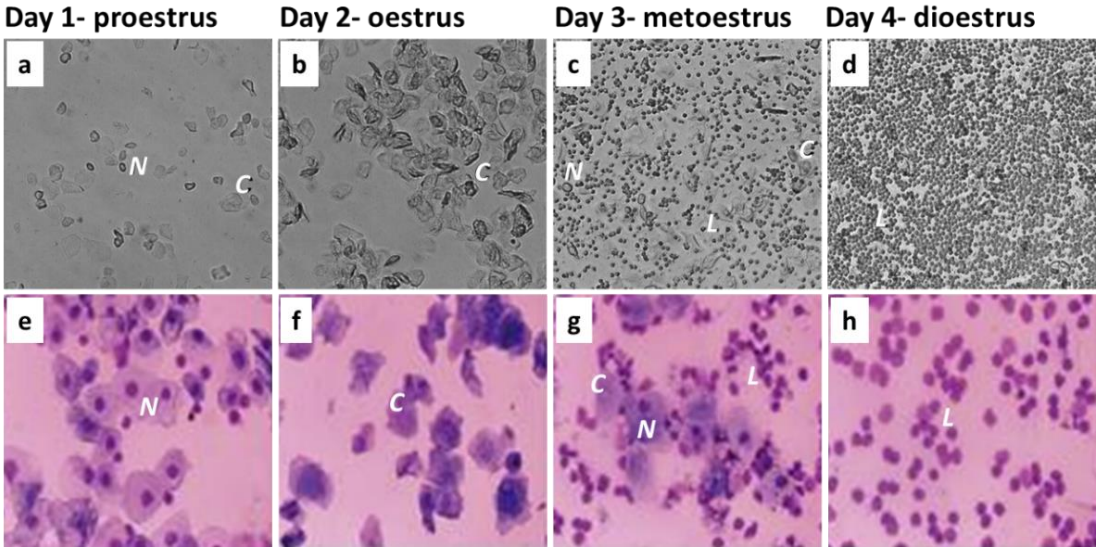

Figure 2-3. Photomicrographs (a-d) and haematoxylin and eosin staining (e-h) of vaginal smears taken at various stages of the mouse oestrus cycle. Mice were culled and vaginal smears collected to identify the stage of the oestrous cycle. **(a/e)** Proestrus stage consists predominantly of nucleated epithelial cells (*N*). **(b/f)** Oestrus stage consists of enucleated cornified epithelial cells (*C*). **(c/g)** Metoestrus stage consists of nucleated and cornified enucleated epithelial cells and leukocytes (*L*). **(d/h)** Dioestrus consists predominantly of leukocytes (Adapted from Caligioni, 2010 and Mettus & Rane, 2003).

Uteri from naïve female mice were dissected from the peritoneal cavity and separated from the ovaries, cervix and surrounding adipose tissue. Uteri were weighed and collected into RNAlater (QIAGEN) and stored thereafter at -80°C, or fixed in 4% paraformaldehyde (PFA) for two hours followed by overnight storage in 18% sucrose and embedding in OCT (optimal cutting temperature) medium for downstream histological analysis. Uteri were collected in this way to generate control samples for each of the transgenic mouse lines outlined in Section 2.1.1 and also from C57BL/6 mice for use as transgene negative samples.

2.2.2 The Edinburgh menses mouse model

Laboratory mice do not spontaneously decidualise or menstruate however studies in the Saunders group have refined and extended studies by others (Brasted et al. 2003, Kaitu'u-Lino et al. 2007, Kaitu'u et al. 2005, Finn and Pope 1984)**,** and established a robust mouse model of simulated menstruation in which endometrial breakdown and shedding can be detected as overt vaginal bleeding. Briefly, ovariectomised mice are treated with a hormonal schedule (exogenouse E2 followed by P4) and decidualisation of the endometrial stroma is induced after an intrauterine injection of oil. Thereafter endometrial breakdown occurs simulated by the withdrawal of progesterone. Validation of this model has confirmed it shares key features with menstruation and scarless endometrial repair in women including focal hypoxia (Cousins et al. 2016d), tissue breakdown, epithelial repair (Cousins et al. 2014) and dynamic changes in immune cell populations (Cousins et al. 2016c).

All animal procedures carried out in this thesis were done so with assistance from Olympia Kelepouri (PIL: IFAF4370C).

2.2.2.1 Preparation of oestrogen for injections

A 1mg/ml stock solution of β-oestradiol (E2) was prepared by dissolving 1mg crystallised β-estradiol (Sigma, Cat # E8875, Mw 272.38 g/mol) in 100% ethanol (VWR Prolabo, France), from which a further 50µg/ml stock solution was made. Working solutions of 100µg/100µl and 5µg/100µl were prepared by diluting stock solutions by 1/1000 into sesame seed oil (Sigma, Cat # S3547) and mixed overnight at RT, Figure 2-4.

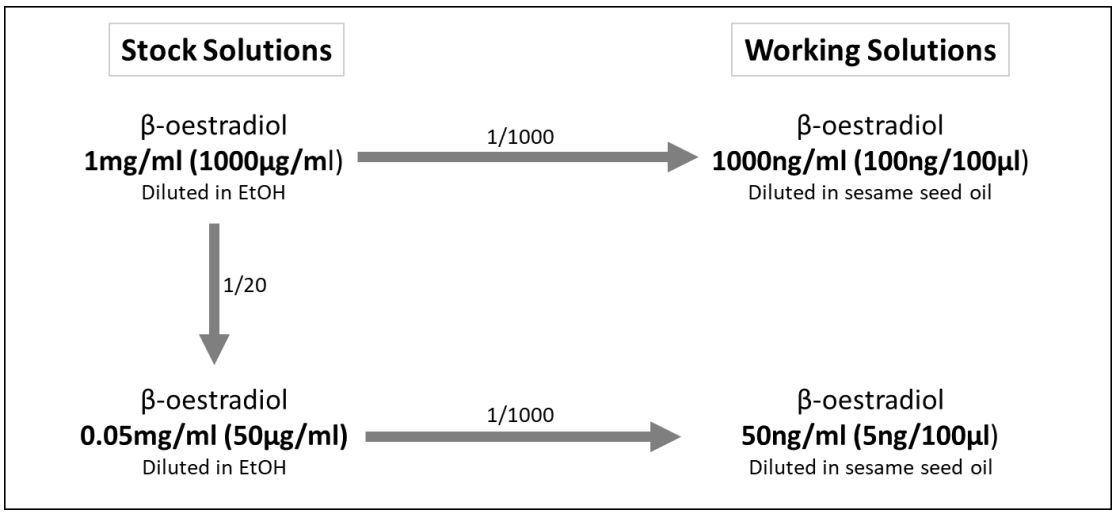

Figure 2-4. Stock solutions and working solutions of β-oestradiol used in the mouse model of endometrial breakdown and repair. Stock solutions (1mg/ml and 0.05mg/ml) were prepared by dissolving E2 in 100% ethanol. Working solutions of E2 (100ng/100µl and 5ng/100µl) were prepared by diluting stock solutions by 1/1000 into sesame seed oil (Author's own image).

2.2.2.2 Preparation of progesterone secreting pellets

Dow corning silastic tubing (Cat #508-008, 1.57mm ID x 3.18mm OD) was washed in 70% ethanol, rinsed in distilled water and air dried, before10mm lengths were cut. Multipurpose sealant (Dow Corning multipurpose sealant 732) was used to seal one end of each tube and then the pellets were filled with crystalline progesterone (P4, Sigma, Cat #P0130) and the other end was sealed; 24 hours prior to insertion, P4 pellets were incubated in PBS with 1% charcoal stripped foetal calf serum (CSFCS) at 37℃.

2.2.2.3 Induction of endometrial tissue proliferation, decidualisation, breakdown and repair

A review of the refined model is shown in Figure 2-5 and the key steps outlined in Table 2-4. On day 0, female mice between 8-10 weeks of age were ovariectomised under iso-fluorane induced anaesthesia (Merial) and given a post-operative injection of an analgesic, buprenorphine (Buprecare, 0.1mg/kg, Alstoe animal health). Mice were monitored and allowed to recover for 7d allowing for the complete depletion of endogenous ovarian-derived steroids. Mice received daily sub-cutaneous injections

(0.1ml) E2 in sesame oil (100ng/100µl) on days 7-9 followed by the sub-cutaneous insertion of a P4-secreting pellet on day 13, under iso-fluorane induced anesthesia. Mice also received daily sub-cutaneous injections (0.1ml) of E2 in sesame oil (5ng/100µl). On day 15, endometrial decidualisation was induced in one uterine horn by administering sesame seed oil (20µl) into the uterine lumen via the cervix using a non-surgical embryo transfer device (NSET) (Datesand Ltd, Manchester, UK). This procedure was performed under iso-fluorane induced anesthesia and the contralateral horn was left untreated to act as an unstimulated control (Figure 2-6). P4 'withdrawal' was induced 90 hours after decidualisation by removal of the P4-secreting pellet (designates time 0 of induced shedding).

For subsequent tissue recovery, mice were culled by asphyxiation using carbon dioxide gas and death confirmed by cervical dislocation. In the majority of slides in this thesis tissue was recovered 24hrs after steroid withdrawal but in some cases recovery was at other time points (12hrs, 48hrs). Uteri were dissected, weighed and collected into RNAlater (QIAGEN) and stored thereafter at -80°C, or fixed in 4% PFA for 2hrs as in Section 2.3. In general, uteri collected from this mouse model were either non-decidualised/unstimulated or fully decidualised/stimulated as displayed in Figure 2-6.

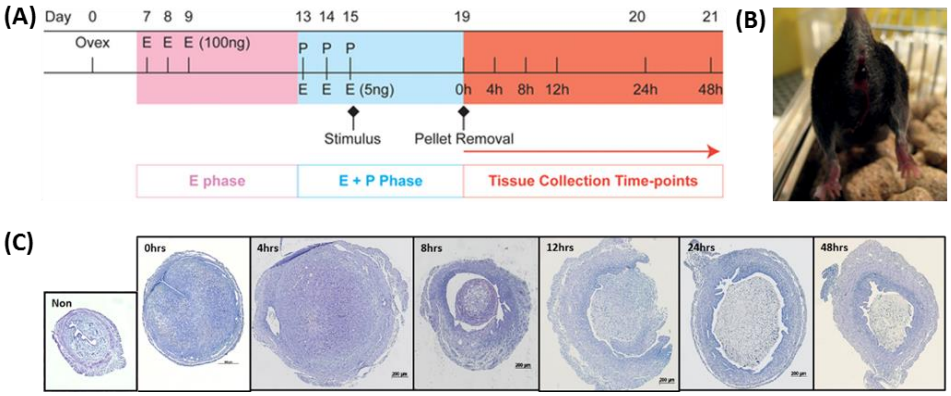

Figure 2-5: The Edinburgh menses mouse model. (A) Schematic of mouse model of menstruation. Following ovariectomy (ovex), addition of exogenous hormones mimics the human menstrual cycle; 'proliferative phase' (pink), 'secretory phase' (blue), 'menstrual phase' (red). Decidualisation is stimulated by introduction of oil into the luminal cavity of the uterus. The contralateral uterine horn serves as control (non-decidualised). Menstrual-like tissue shedding is induced via removal of P4 pellet on day 19. **(B)** Induction of menses and endometrial shedding can be detected as overt vaginal bleeding. **(C)** Histological tissue morphology of uterine horns 0, 4, 8, 12, 24 and 48hrs following P4 withdrawal. E= oestradiol, P= progesterone (adapted from Cousins et al. 2014)).

Table 2-4. Summary of key steps in the Edinburgh menses mouse model

Day of Model	Procedure
0	Ovariectomy
7	E2 injection 100ng/100µl
8	E2 injection 100ng/100µl
9	E2 injection 100ng/100µl
13	P4 pellet insertion + E2 injection 5ng/100µl
14	E2 injection 5ng/100µl
15	E2 injection 5ng/100µl + Oil into lumen for decidualisation
19	P4 pellet removal
20	24hrs tissue recovery
21	48hrs tissue recovery

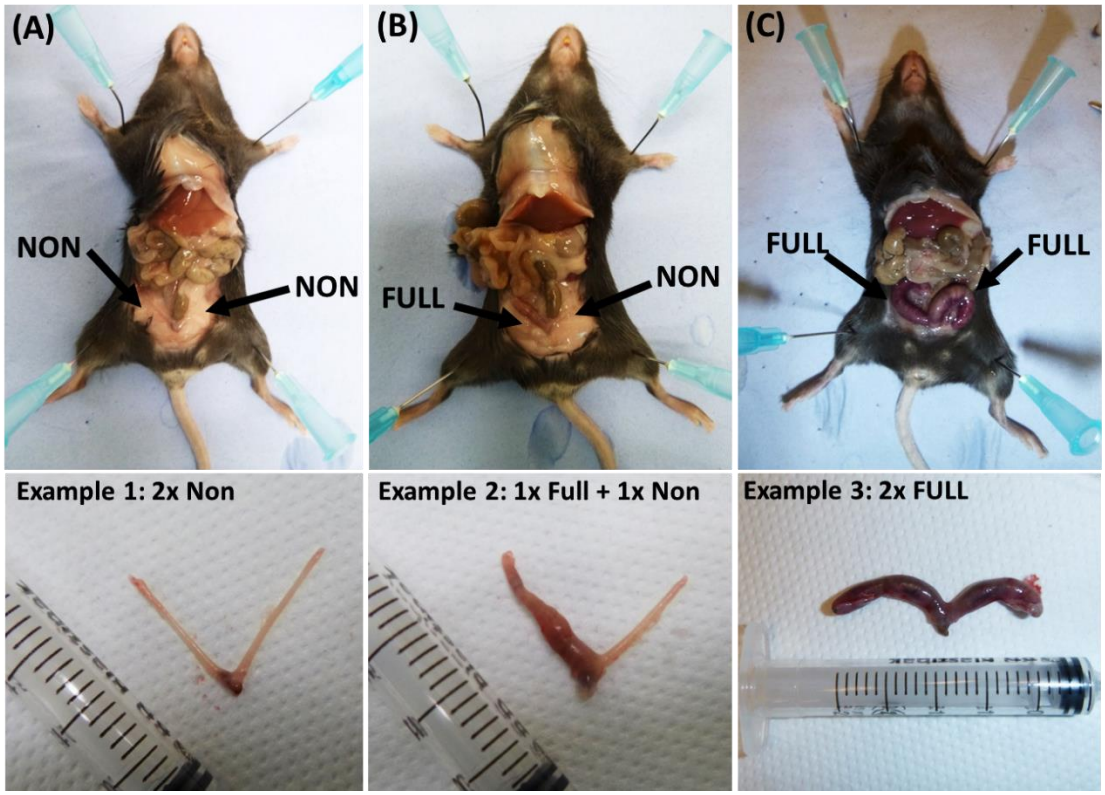

Figure 2-6: Gross Anatomy of mouse uterine tissues after manipulation by the Edinburgh menses mouse model. (A) Two non-decidualised/unstimulated (Non) uterine horns considered to be the unmanipulated control for this model. **(B)** One decidualised/stimulated (Full) uterine horn and on non-decidualised/unstimulated uterine horn. **(C)** Two decidualised/stimulated uterine horns considered to be experimental tissues (Author's own images).

2.3 Tissue processing

Tissue samples were fixed in 4% (w/v) PFA for 2hrs at 4°C, rinsed thoroughly in PBS and stored overnight in 18% (w/v) sucrose at 4°C to replace water in the tissue. Approximately 24hrs later samples were rinsed in PBS and snap frozen in optimal cutting temperature (OCT) medium, carefully orientated in the cold block so that cross sections of the uterine horn could be cut.

Thin sections (5µm) were cut using a Leica Cryostat CM onto X-tra adhesive pre-cleaned micro slides (Surgipath, Leica Biosystems, Peterborough, UK) and left to air dry for 2hrs prior to staining at RT, or stored in a freezer at -20°C if required for future use.

2.4 Histological examination of uterine sections

2.4.1 Haematoxylin and eosin staining

The most commonly used staining system in histology uses two dyes called Haematoxylin and Eosin (H&E). Haematoxylin is a basic dye which binds to acidic structures such as DNA and RNA and therefore highlights the nucleus in a purple colour, while eosin is an acidic dye while stains basic structures such as proteins, intracellular membranes and extracellular fibres in the cytoplasm, highlighting the cytoplasmic compartment in red or pink (Fischer et al. 2008).

H&E staining was carried out on 5µm uterine tissue sections cut on the cryostat and left to air dry at RT for 2hrs (Section 2.3). Sections were washed in PBS to remove any residual OCT medium and further washed in distilled water before submersion in Shandon™ Harris Haematoxylin (ThermoFischer Scientific, Cat. #6765002) for 5 minutes to stain cell nuclei. Following this, slides were washed in distilled water, dipped in 1% acid alcohol (1% hydrochloric acid in 70% ethanol) to remove non-specific background staining and washed in water again. Slides were submerged in Scott's tap water for 20 seconds to convert haematoxylin to a dark blue colour, washed in water and passed through Shandon™ Eosin (ThermoFischer Scientific, Cat. #10483750) for 10 seconds to stain non-nuclear elements, before a final wash in water. Slides were dehydrated through ascending concentrations of alcohols to remove all

traces of water then rinsed in several baths of xylene to remove any residual alcohol. Sections were protected using Pertex (CellPath) and coverslips (VWR Prolabo).

2.4.2 Picrosirius red staining

Picrosirius red (PSR) staining is a histological technique used to detect collagen I and III fibres in tissue sections. PSR stain is viewed using standard light microscopy where collagen is red and the background is yellow, or polarised light resulting in birefringence of the collagen fibres to distinguish between type I (yellow/orange) and type III fibres (green).

The PSR staining in this thesis was performed by the SuRF Histology and imaging laboratory, QMRI. The PSR stain was prepared by mixing one part of 0.5% Direct Red (Sigma, Cat. #365548) with nine parts of picric acid, saturated aqueous solutions (Sigma, Cat. #P6744-1GA) and stored in a light protected bottle. PSR staining was carried out on 5µm uterine tissue sections cut on the cryostat and left to air dry at RT for 2hrs (Section 2.3). Sections were washed in PBS to remove any residual OCT medium and further washed in distilled water before submersion in the PSR solution for 2-4hrs. Sections were rinsed in 100% alcohol, cleared in xylene and mounted using a Shandon Thermo Scientific^{TM} ClearVue^{TM} Coverslipper.

2.4.3 Immunohistochemical staining

Immunohistochemistry (IHC) is the process used to detect and visualise antigens/proteins within cells of a tissue section using the principle of specific antibody-antigen binding. The technique was first implemented in 1941 by Albert Coons (Coons, Creech and Jones 1941) and since has been widely used in a number of applications to: assist in medical diagnoses and prognoses; investigate specific cellular events of interest such as proliferation or apoptosis; assess biomarker localisation; visualise differentially expressed proteins in different tissues; and investigate the pathogenesis of disease (Ramos-Vara and Miller 2014). There are various methods of IHC which can be broadly separated into two categories: the direct method uses one labelled antibody (fluorescent conjugate) which binds directly to the specific antigen on interest; and the indirect method uses a primary antibody which binds directly to the specific antigen of interest and a labelled secondary antibody that binds to the primary antibody, Figure 2-7. The direct method is rapid and simple

however the sensitivity is relatively low whereas the indirect method is more sensitive as it allows greater amplification of the signal (Ramos-Vara and Miller 2014). In this thesis, IHC was used to visualise cell specific markers used in cell phenotyping and cell differentiation using both direct and indirect methods.

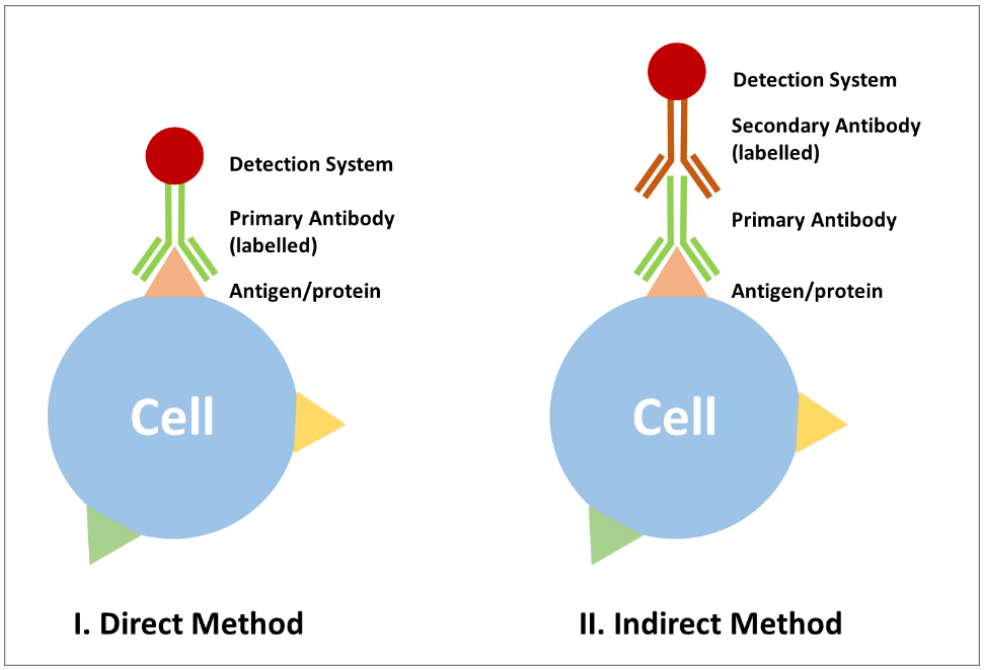

Figure 2-7. Schematic representation of the principles of direct and indirect IHC methods. The cellular antigen is detected by application of a specific labelled primary antibody (direct, I), or a specific unlabelled primary antibody followed by a labelled secondary antibody (indirect, II). The detection system can be by chromogenic antigen detection or by fluorescently-conjugated antibodies, discussed in Sections 2.4.3.2 and 2.4.3.3 (based on Ramos-Vara & Miller, 2013).

2.4.3.1 IHC examination of antigens

IHC was carried out on 5µm uterine tissue sections cut on the cryostat and air dried for approximately 2hrs, according to the protocol outlined in Table 2-5. Unless otherwise stated, all wash steps included one 5 minute wash with PBS containing 0.05% (v/v) tween20 (PBS tween) and two further 5 minute washes in PBS alone. An antigen retrieval step was not required for frozen sections as tissue fixation was brief and the process would damage the tissues. Controls included a positive tissue control, a primary antibody negative control, a secondary antibody negative control where each was replaced with normal animal serum (NAS).

Table 2-5. IHC protocol for antigen detection in uterine tissue sections

Step	Description	Purpose
Day 1		
1	Wash sections twice in PBS	Remove residual OCT
2	Incubate sections in 3% (v/v) hydrogen peroxide in methanol for 30 minutes at RT	Inactivation of any endogenous peroxidase enzymes that would otherwise interfere with desired HRP activity: reduce non-specific background staining
3	Wash sections	
4	Incubate sections in 20% (v/v) normal animal serum (NAS: PBS containing 20% animal serum and 0.05% (w/v) bovine serum albumin (BSA)) for 30 minutes at RT	Saturate non-specific antigen binding sites to prevent non-specific binding of either primary or secondary antibody. Use serum from the secondary host
5	Wash sections	
6	Incubate sections with primary antibody at an optimised dilution in NAS overnight at 4°C	Primary detection of antigen of interest (unconjugated)
Day 2		
7	Wash sections	
8	Incubate sections with HRP-conjugated secondary antibody at an optimised dilution in NAS for 30 minutes at RT	Secondary detection of primary antibody (conjugated). Enzyme label is HRP which reacts with a substrate to yield a detection signal
9	Wash sections	
10	Detection systems: see section 2.4.2.2 and 2.4.2.3	Amplification of detection signal: DAB or Tyramide (see section 2.4.2.2 and 2.4.2.3)
11	Wash sections	
12	Nuclear counterstain: see section 2.4.2.4	Detection of cell nuclei by Haematoxylin or DAPI (see section 2.4.2.4)
13	Wash sections	
14	Protect sections using Pertex for DAB detection (CellPath) or permafluor for fluorescent detection (Immunotech) and mount with coverslips (VWR Prolabo).	Protection of sections for long term storage and later microscopy

A complete list of primary antibodies and associated working dilutions used in this thesis are outlined in Table 2-6 and a complete list of secondary antibodies and associated working dilutions are outlined in Table 2-7.

Table 2-6. Primary antibodies and associated working dilutions used in the IHC detection of antigens in uterine tissue sections

Antibody Name	Supplier and Cat. No. (concentration)	Dilution	Serum block
Polyclonal rabbit anti-GFP	Abcam, ab6556 (0.5mg/ml)	1/1000	Goat
Polyclonal rabbit anti-MCSF (Csfr1)	Abcam, ab21544 (1mg/ml)	1/500	Horse
Monoclonal rat anti-CD45	ThermoFisher Scientific 14-0451-81 (0.5mg/ml)	1/500	Goat
Monoclonal rat anti-F4/80	eBioscience, 14-4801 (0.5mg/ml)	1/2000	Goat
Rabbit anti-CD11b (clone EPR1344)	Abcam, 133357	1/1000	Goat
Polyclonal rat anti-GR1	AbD Serotec, MCA2387PET	1/500	Goat
Polyclonal rabbit anti-RFP	Rockland, 600-401-379 (1mg/ml)	1/2000	Goat
Rabbit anti-cleaved caspase 3 (Asp175)	Cell Signalling Technology, #9661S (0.25mg/ml)	1/600	Goat
Monoclonal rabbit anti-Pdgfrβ	Abcam, ab32570 (0.15mg/ml)	1/1000	Goat
Monoclonal rabbit anti-CD146 (Mcam)	Abcam, ab75769 (0.123mg/ml)	1/1000	Goat
Polyclonal Rabbit anti-NG2 (Cspg4)	Abcam, ab12905	1/600	Goat
Monoclonal mouse anti-αSMA	Sigma, A-2547	1/10K	Horse
Polyclonal rabbit anti-CD31	Abcam, ab28364 (1mg/ml)	1/500	Goat
Polyclonal rabbit anti-EpCAM	Abcam, ab71916 (1mg/ml)	1/2000	Goat

Table 2-7. Secondary antibodies and associated working dilutions used in the immunohistochemical detection of antigens in uterine tissue sections

Antibody name	Supplier and Catalogue No. (concentration)	Dilution
Goat F(ab) anti-rabbit IgG H&L (HRP)	Abcam, Ab7171 (1mg/ml)	1/500
Goat F(ab) anti-mouse IgG H&L (HRP)	Abcam, ab6823 (1mg/ml)	1/500
ImmmPRESS™ reagent anti-rat IgG (mouse absorbed) (serum=goat)	Vector laboratories, MP-7444	N/A (1 drop per slide)
ImmmPRESS™ reagent anti-rabbit IgG (mouse absorbed) (serum=horse)	Vector laboratories, MP-7401	N/A (1 drop per slide)
ImmmPRESS™ reagent anti-mouse IgG (mouse absorbed) (serum=horse)	Vector laboratories, MP-7402	N/A (1 drop per slide)

2.4.3.2 Enzyme mediated chromogenic antigen detection by 3,3' diaminobenzidine (DAB)

The enzyme mediated chromogenic antigen detection method is based on the production of a coloured reporter molecule upon interaction of an enzyme and its substrate that can be easily visualised by microscopy. The enzymes most commonly used as labels are alkaline phosphatase (AP) and horseradish peroxidase (HRP) and a variety of substrates are available including DAB which produces a brown staining when the enzyme is bound (Ramos-Vara and Miller 2014). In this thesis secondary antibodies conjugated to HRP (Table 2-7) and DAB were used as the preferred enzyme-substrate interaction.

Sections were incubated with chromogen DAB (Vector, Peterborough, UK) (Figure 2-8) for 5 minutes or until the brown colour was detectable. Sections were immersed in water to cease the enzymatic reaction. The staining protocol continued as in Table 2-5, step 11.

2.4.3.3 Fluorochrome antigen detection

Fluorochrome antigen detection relies on a fluorescent signal which can be used in multiplex immunohistochemistry to detect co-localisation of antigens. The tyramide signal amplification (TSA) system (PerkinElmer, Massachusetts, USA) is a method

used to amplify the signal to increase sensitivity of detection and spatial resolution, whilst keeping background staining to a minimum. In this amplification method, HRP (conjugated to the secondary antibody) reacts with the phenolic part of tyramine to produce quinone-like structures that carry a radical on the C2 groups. This reactive intermediate covalently binds to electron rich amino acids in nearby tissue proteins resulting in a localized deposition of the fluorescently-conjugated tyramide derivative at the location of the antigen-antibody reaction (Figure 2-8) (Ramos-Vara and Miller 2014).

For detection by TSA, sections were incubated with tyramide solution diluted 1/50 in the kit diluent for 10 minutes at RT in the dark. Both the red cyanine-3 fluorophore and green cyanine-5 fluorophore were used in single and double IHC stains. The staining protocol continued as in Table 2-5, step 11, with sections protected from the light using aluminium foil to avoid photo bleaching during each subsequent wash and incubation steps.

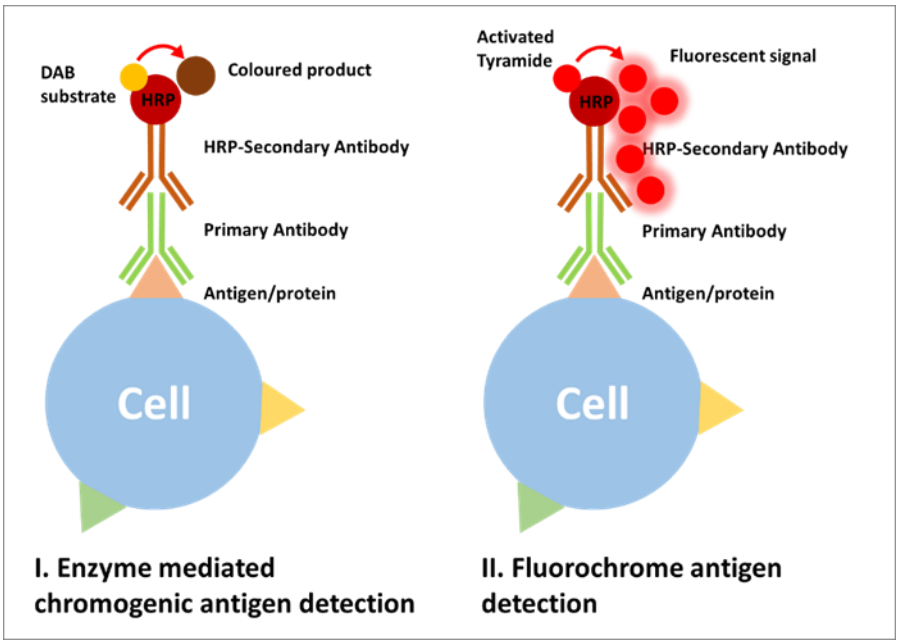

Figure 2-8. Schematic representation of the principles of enzyme mediated chromogenic antigen detection and fluorochrome antigen detection used in standard IHC methods. The cellular antigen is detected by application of a specific primary antibody followed by a HRP-conjugated secondary antibody. Antigen detection can be achieved by application of (I) DAB substrate and visualisation of the coloured product or (II) Tyramide and visualisation of the fluorescent signal (based on Ramos-Vara and Miller 2014)).

2.4.3.4 Nuclear counterstaining

After chromogenic detection, sections were counterstained with haematoxylin for 5 minutes, dipped in1% acid alcohol (1% hydrochloric acid in 70% ethanol) and washed thoroughly in water. Sections were passed through an increasing alcohol gradient from 70%, 85%, 95% and 100% before immersion in xylene. Sections were protected using Pertex (CellPath) and coverslips (VWR Prolabo).

After TSA detection, sections were incubated with DAPI (4', 6-diamidina-2-phenylindole) (Sigma, D9542) which binds to DNA therefore staining cell nuclei blue. Sections were incubated with DAPI diluted to 1/1000 in PBS for 10 minutes at RT. The staining protocol continued as in Table 2-5, step 13, with sections protected from the light using aluminium foil to avoid photo bleaching during the subsequent wash step. Sections were protected using permaflour (Immunotech, Marseille, France) and coverslips (VWR Prolabo).

2.4.4 Microscopy and Image analysis

2.4.4.1 Brightfield microscopy

Bright field images of H&E sections and DAB positive sections were obtained using AxioVision 4.8 Software (Carl Zeiss, Cambridge, UK) and a Leica light microscope (Olympus Optical, London, UK) with an attached Canon DS126131 camera.

2.4.4.2 Confocal miscroscopy

Images of fluorescent sections were obtained using Zen 2009 software (Carl Zeiss, Cambridge, UK) and a Zeiss LSM 510 Meta Confocal microscope (Carl Zeiss, Cambridge, UK).

2.4.4.3 Transmission Electron Microscopy (TEM)

TEM is a very powerful technique where a high energy beam of electrons is shone through a very thin layer of tissue and the interactions between the electrons and the atoms can be observed and imaged. TEM therefore gives structural information at the subcellular level (Burghardt and Droleskey 2006). For TEM, uterine tissue samples were fixed in 3% glutaraldehye in 0.1M Sodium Cacodylate buffer (pH 7.3) for 2hrs then washed in 0.1M Sodium Cacodylate for 10minutes three times. The following steps were carried out by Dr Stephen Mitchell at the Centre Optical Instrumentation Laboratory (COIL) in King's Buildings. Tissues were post-fixed in 1% Osmium

Tetroxide in 0.1M Sodium Cacodylate for 45 minutes at RT then washed in 0.1M Sodium Cacodylate for 10minutes three times. The tissues were dehydrated through increasing concentrations of ethanol: 50%, 70%, 90% and 100% ethanol for 15 minutes each then immersed in two 10 minute changes in Propylene Oxide.

Samples were embedded in TAAB 812 resin. Sections (1μm) were cut on a Leica Ultracut ultramicrotome, stained with Toluidine Blue, and viewed in a light microscope to select suitable areas for investigation. Ultrathin sections (60nm) thick were cut from selected areas, stained in Uranyl Acetate and Lead Citrate then viewed in a JEOL JEM-1400 Plus TEM. Representative images were collected on a GATAN OneView camera by thesis author. This technique was carried out with support from the Wellcome Trust Multi User Equipment Grant (WT104915MA).

2.5 Flow Cytometry and Fluorescence Activated Cell Sorting (FACS)

Flow cytometry is a powerful method used to interrogate cell characteristics and phenotype. Flow cytometry combines fluidics and optics whereby cells are sensed as they move in a liquid stream through a laser and can be characterised based on the light-scattering property (size, granularity) and colour-discriminated fluorescence from antibodies of dyes. In-depth phenotypic information can be gathered based on whether a cell is carrying fluorescent molecules conjugated to antibodies designed against specific cell surface or intracellular components. Flow cytometry is most commonly used therefore to identify different cell types present in a heterogeneous population and provides a basis to separate and isolate cells of interest for downstream analysis such as an *in vitro* culture or gene expression analysis (Macey, 2007).

2.5.1 Uterine tissue digest

Uterine horns from adult mice were dissected and placed immediately into ice cold PBS (2ml per horn) in standard laboratory bijous tubes before being transferred to the laboratory for processing. Thereafter uterine tissues were cut into small fragments using scalpels (Swann Morten, Cat #0503) in a petri dish with a small volume of PBS to avoid the tissues drying out. The dissociated tissue was transferred back to the bijous

containing PBS then collagenase (10mg/ml) and DNase (10mg/ml) were added. Tissue samples were incubated with digestive enzymes for 30 minutes at 37°C on a rocking incubator (Figure 2-9). The tissue samples were further dissociated using an 18G needle (BD Microlance^{TM}, Cat. #2022-12) and 2ml syringe (BD Plastipak, Cat. #2022-02). Dissociated tissue samples were passed through a series of cell strainers (70µm and 40µm) to remove debris, undigested tissue clumps and large epithelial cells. Each cell strainer was rinsed through with 'FACS' buffer (PBS Ca_2-Mg_2-, 5% charcoal stripped fetal calf serum (CSFCS), 2mM EDTA) to rinse off any remaining cells. The resulting cell suspensions were centrifuged at 400rcf for 5 minutes and the supernatant discarded. Cell pellets were re-suspended in 1ml ACK lysing buffer (Gibco, Cat. #A10492-01) for 1 minute to remove any residual red blood cells, then by 5ml of 'FACS' buffer was added to stop the reaction. Cell suspensions were centrifuged for a second time at 400rcf for 5 minutes and the supernatant discarded. Cell pellets were re-suspended in 200µl of 'FACS' buffer and transferred to 1.5ml Eppendorf tubes and placed on ice for antibody staining (Section 2.5.2).

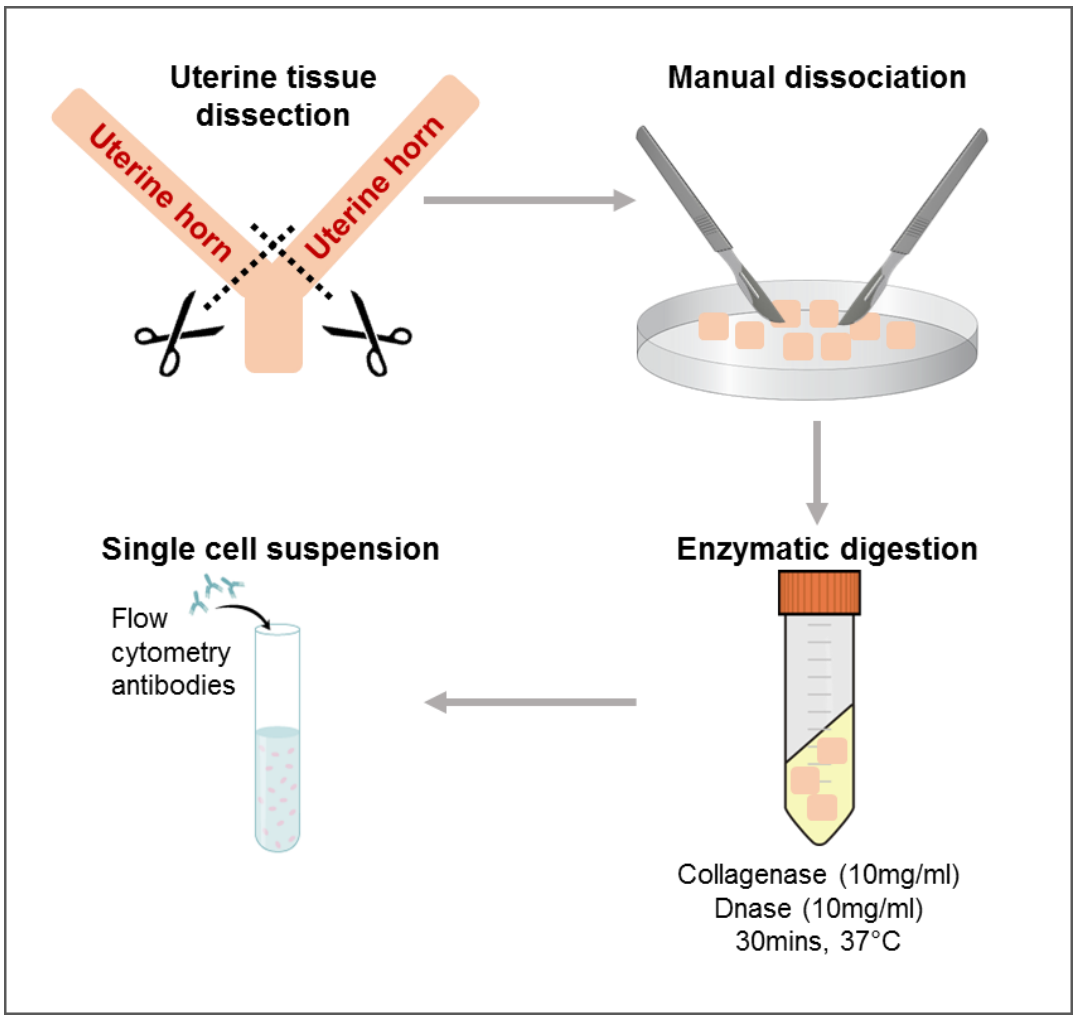

Figure 2-9: Optimised uterine tissue digest protocol to generate single cell suspensions for both Flow Cytometry and FACS. Mouse uterine horns were dissected into ice cold PBS and manually dissociated before being incubated with Collagenase (10mg/ml) and DNase (10mg/ml) for 30minutes at 37°C. Single cell suspensions were generated and stained with fluorescently conjugated flow cytometry antibodies as outlined in Table 2-8 and 2-9 (Author's own image)

2.5.2 Flow cytometry antibody staining and analysis

Flow cytometers are multiparametric so they can record several measurements of each cell at once. Different flow cytometer instruments are set up with the capacity to analyse a set number of different fluorochromes, with current instruments able to detect as many as 18 colours. This allows for the extensive differentiation of specific cell types within a heterogeneous population. Flow cytometry antibody panels need to be carefully designed with the emission and excitation spectra of each flourochrome accounted for to avoid overlap and minimise compensation (Macey, 2007).

In the current thesis, two separate flow cytometry antibody panels were designed to investigate immune cell populations and mesenchymal cell populations using reagents outlined in Table 2.8 and Table 2.9 respectively. Single cell suspensions were prepared (Section 2.5.1) and incubated with fluorescently conjugated flow cytometry antibodies for 30 minutes on ice.

Table 2-8. Flow cytometry antibody panel designed to interrogate myeloid immune cell populations in uterine tissue

Antibody name	Supplier Cat. No. (concentration)	Excitation wavelength	Emission wavelength	Dilution
V450 anti-mouse CD45	Fischer scientific, BDB560501 (0.2mg/ml)	404nm	448nm	1/100
PE anti-mouse Gr1	Abd Serotec, MCA2387PET	496nm	578nm	1/20
APC anti-mouse F4/80	Bio-rad, MCA497APC	650nm	660nm	1/20
BV605 anti-mouse Ly6C	BioLegend, 128035 (0.2mg/ml)	405nm	603nm	1/100
AF488 anti-mouse CD68	BioLegend, 137011 (0.2mg/ml)	495nm	519nm	1/100
BV650 anti-mouse MHCII	BioLegend 107641 (0.2mg/ml)	407nm	650nm	1/100

Table 2-9. Flow cytometry antibody panel designed to interrogate mesenchymal cell populations in uterine tissue

Antibody name	Supplier Cat. No. (concentration)	Excitation wavelength	Emission wavelength	Dilution
BV421 anti-mouse CD31 (Pecam1)	BioLegend, 102423 (0.2mg/ml)	405nm	421nm	1/200
V450 anti-mouse CD45: 30-F11	Fischer scientific, BDB560501 (0.2mg/ml)	404nm	448nm	1/100
PE anti-mouse CD146 (Mcam)	BioLegend, 134704 (0.2mg/ml)	496nm	578nm	1/200
BV605 anti-mouse CD326 (EpCAM)	BioLegend, 118227 (0.2mg/ml)	405nm	603nm	1/400
APC anti-mouse CD140b (Pdgfrβ)	BioLegend, 136008, (0.2mg/ml)	650nm	660nm	1/100
AF488 anti-mouse NG2	Merck, AB5320A4	495nm	519nm	1/100
APC anti mouse CD146 (Mcam)	BioLegend, 134712, (0.2mg/ml)	650nm	660nm	1/200

Flow cytometry controls included an unstained and fully stained control, single antibody stains and fluorescence minus one (FMO) stains for each antibody represented in Table 2-10. Controls were set up for each individual experiment using both cell samples and OneComp ebeads™ compensation beads (ThermoFisher Scientific, Cat. # 01-1111-41) to ensure reliable adjustment of cytometer compensations and consistent set up of the analysis template.

Table 2-10. Representative set up of flow cytometry analysis controls samples

Control (cells and beads)	Antibody 1	Antibody 2	Antibody 3
Unstained	✗	✗	✗
All stains	✓	✓	✓
Single Antibody 1	✓	✗	✗
Single Antibody 2	✗	✓	✗
Single Antibody 3	✗	✗	✓
FMO Antibody 1	✗	✓	✓
FMO Antibody 2	✓	✗	✓
FMO Antibody 3	✓	✓	✗

Following antibody incubation, 1ml PBS was added to each suspension and the suspensions were centrifuged for 5 minutes at 400rcf at 4°C to pellet the cells. The supernatant was discarded and cells were then re-suspended in 500µl PBS and kept on ice until analysis by flow cytometry could take place (< 30 minutes). To exclude dead cells, DAPI (1/10K) was added prior to flow cytometry analysis. Flow cytometry was performed using a BD 5L LSR Fortessa instrument and BD FACSDiva software (BD Biosciences). Analysis templates were set up using control samples with guidance from core technical staff (Dr Shonna Johnston, Dr William Ramsay, Dr Mari Pattison). Data was analysed using FlowJo analysis software (Flowjo LLC, Oregon USA).

2.5.3 Uterine cell isolation by Fluorescence Activated Cell Sorting

Fluorescence activated cell sorting (FACS) is a technique used to separate cells of interest from a heterogeneous population based on fluorescent labelling: single cell suspensions are stained with fluorescently-conjugated antibodies and are separated from each other based on the combination of fluorophores they possess (Macey, 2007). The principles of the FACS method are detailed in Figure 2-10.

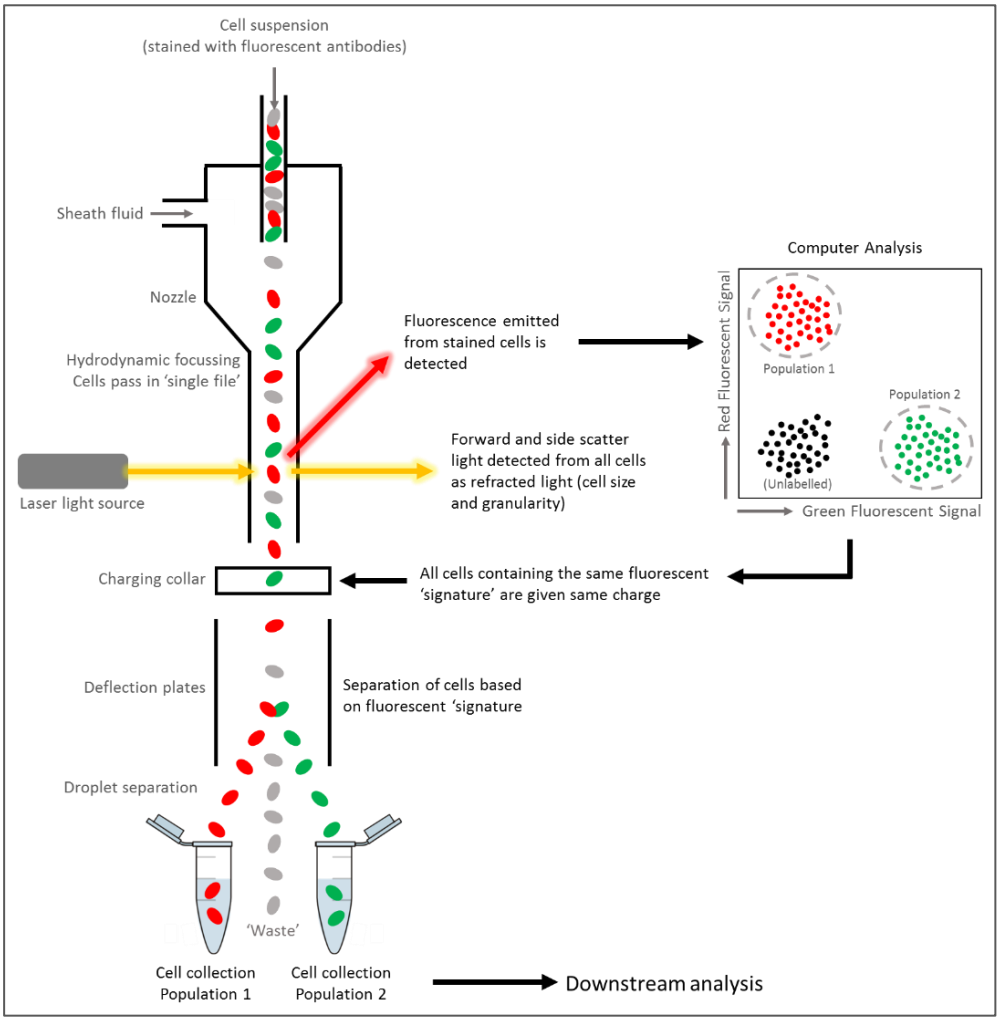

Figure 2-10. Schematic representation of Fluorescence Activated Cell Sorting (FACS). A mixed cell population stained with fluorescently-conjugated antibodies enters a liquid stream and each cell becomes encapsulated within a single droplet. Droplets are passed through a laser (light amplification by stimulated emission of radiation) and the relative scatter of light and colour-discriminated fluorescence of each cell is measured. Information is passed to a computer system that collects data from each droplet. Analysis and differentiation of the cells is based on size, granularity and fluorescence and populations of interest defined. Droplets pass through a charging collar where all cells containing the same fluorescent signature are given the same charge. Cells are then separated by the deflection plates and are collected into Eppendorfs for downstream analysis (based on Macey, 2007).

Using the principles described in Sections 2.5.1 and 2.5.2, single cell suspensions were prepared from mouse uterine tissues and stained with fluorescently-conjugated antibodies. FACS was performed using a FACS Aria II instrument and BD FACSDiva software (BD Biosciences). Analysis templates were set up using control samples with guidance from core technical staff (Dr Shonna Johnston, Dr William Ramsay, Dr Mari Pattison). Data files were gathered during FACS and analysed using FlowJo analysis software (Flowjo LLC, Oregon USA).

2.5.4 Immunocytochemical staining

2.5.4.1 Cytospin

Cells were isolated from uterine tissues by FACS (Section 2.5.3), sorted into Eppendorf's containing PBS+2% foetal bovine serum (FBS) and placed on ice. Eppendorf's were centrifuged at 400rcf for 5 mins at 4°C and the supernatant discarded. Cell pellets were re-suspended in PBS+2% FBS to a concentration of approximately $5x10^5$ cells/ml. The cytocentrifuge was prepared with labelled slides, cuvettes (chambers) and blotter papers mounted in the metal holders for each sample being examined. Cytospins were carried out by adding 200µl of each cell suspension to a slide cuvette and centrifuging at 800rpm for 5 minutes. Slides were carefully removed from the cytocentrifuge and allowed to air dry for at least 30 minutes prior to staining.

2.5.4.2 Fixation and immunocytochemical staining

Slides were air dried for at least 30 minutes then fixed by immersing in ice cold methanol and air dried four times. Fixed slides were either stained with H&E, Section 2.4.1, or taken through an IHC protocol following the method described in Section 2.4.3. Slides were visualised using brightfield and confocal microscopy, see Section 2.4.4.

2.6 RNA extraction

The extraction of ribonucleic acid (RNA) from tissues and cells is a crucial starting point for many downstream techniques of molecular biology. RNA is a macromolecule that is transcribed from deoxyribonucleic acid (DNA) to produce copies of the genetic

information necessary for cell growth, differentiation and survival. Ribosomes translate RNA into functional proteins including structural components, enzymes and signalling molecules. RNA therefore is responsible for regulating the abundance of protein that can be made from a gene at any one time and is a useful readout of gene expression profiles in both tissue and cells (reviewed by (Tan and Yiap 2009)).

2.6.1 RNA extraction using the Qiagen RNeasy mini kit

The RNeasy Mini Kit offers an efficient RNA extraction method to yield high-quality RNA from tissues and cells using silica-membrane RNeasy spin columns (binding capacity 100µg RNA) (QIAGEN).

2.6.1.1 Workspace Preparation

The workspace and pipettes were cleaned with RNAzap to degrade environmental RNase, and new filter pipette tips used throughout the protocol. A lab coat and gloves were worn throughout and gloves changed frequently. The RNeasy protocol was carried out as per the manufacturer's instructions (QIAGEN) at RT in a class II fume hood and all waste disposed of correctly. Details are given in the following sections.

2.6.1.2 Tissue homogenisation

Tissue samples previously preserved in RNAlater were removed from -80°C and weighed. Tissues were cut so that approximately 20mg fragments could be placed in a tube containing a ball bearing to which 1000µl TriReagent (Sigma, Cat. #T9424) was added. Any remaining tissue was stored in RNAlater at -80°C. Tissues were homogenised using a tissue lyser (QIAGEN) for two rounds of three minutes at 25Hz and then incubated at RT for a further 5 minutes. Samples (1ml) were centrifuged for 15 minutes at 14,000 rcf at 4°C. Lysates were transferred to 2ml PhaseLock Heavy Gel tubes (Invitrogen, Cat #A33248), pelleted at 12,000-16,000 rcf for 20 to 30 seconds prior to use. Chloroform (200µl) was added to the lysates (1.2ml), and the tubes vortexed for 15 seconds. Lysates were incubated for 2 to 3 minutes at RT and centrifuged for 15 minutes at 14,000 rcf at 4°C. The aqueous layer (~550µl) was aspirated into a new Eppendorf and stored at -80°C. PhaseLock Heavy gel tubes were discarded appropriately.

2.6.1.3 RNA extraction protocol

Samples were taken from -80°C and equilibrated to RT. To each sample 1 volume (~550µl) of 70% ethanol was added which was then mixed by gentle pipetting. RNA extraction was carried out as per manufacturer's instructions (QIAGEN), briefly outlined in Table 2-11. Unless otherwise stated all centrifuge steps were performed at 8,000 rcf at RT. Resultant RNA samples were stored at -80°C until further use.

Table 2-11. RNA extraction protocol from RNeasy Mini Kit (QIAGEN).

Step	Description
1	Transfer approximately 700µl aqueous layer/ethanol mix to RAeasy spin columns (QIAGEN) and centrifuge 15 seconds. Discard flow through
2	Repeat with remaining 400µl of sample
3	Add 350µl Buffer RW1 and centrifuge 15 seconds. Discard flow through
4	Add 80µl of DNase mix (10ul DNase and 70ul buffer RDD (QIAGEN)) and incubate for 15 minutes at RT
5	Add 350µl Buffer RW1 and centrifuge 15 seconds. Discard flow through
6	Add 500µl Buffer RPE and centrifuge 15 seconds. Discard flow through
7	Add 500µl Buffer RPE and centrifuge 2 minutes. Discard flow through
8	Place columns in new collection tubes and centrifuge for 1 minute
9	Place columns were in 1.5ml Eppendorf tubes and add 30µl RNAse-free water directly to the membrane
10	Centrifuge 1 minute to elute RNA. Discard columns

2.6.2 Measuring RNA concentration by Nanodrop

The total concentration of each RNA sample was determined using a Nanodrop ND-100 Spectrophotometer (ThermoFischer Sscientific) using nuclease-free water as the blank measurement. The Nanodrop measures the absorbance of eluted RNA (1µl of each sample) to determine concentration. RNA samples were diluted to a concentration of 100ng/µl using nuclease-free water to create standardised stock solutions for downstream applications (qPCR).

2.6.3 RNA extraction using the SimplyRNA Cells Maxwell® 16 LEV kit

For many of the studies in this thesis a small number of cells were isolated from tissues by FACS (section 2.5.3) however the quality of RNA extracted using the RNeasy Mini Kit (QIAGEN) was not sufficient for downstream applications. A paper by Jeffries *et al* (2014) compared the performance of five commercially available RNA extraction kits using small tissue samples (<15mg), the RNeasy Mini Kit from QIAGEN as one of them. Results from this paper show that although each kit was capable of extracting ~5µg RNA from each sample there were noticeable differences in the quality of RNA as determined by RNA integrity number (RIN), therefore care needs to be taken when selecting extraction methods to generate RNA and should be tailored to the requirements of downstream analyses. The study highlighted two superior kits: RNeasy Plus Mini Kit (QIAGEN) and SimplyRNA Maxwell® 16 LEV kit (Promega, Wisconsin, USA) to yield RNA with consistently higher RIN (>7) than that of the other kits (Sellin Jeffries et al. 2014). In this thesis the SimplyRNA Cells Maxwell® 16 LEV (low elution volume) kit (Promega, Cat. #AS1270) was used as per manufacturer's instructions (Promega), to extract good quality RNA from a small number of cells.

2.6.3.1 Sample preparation

Cells were isolated from mouse uterine tissue using the tissue digestion and FACS isolation protocol described in Section 2.5. To prepare the cells for RNA extraction, cells were collected into PBS at 4°C and stored on ice (<2hrs). Cell suspensions were centrifuged at 400 rcf for 5 minutes at 4°C and the supernatant carefully aspirated. Cell pellets were re-suspended in 200µl homogenisation solution (20µl of 1-Thioglycerol per ml of homogenisation solution stock) from the Maxwell® SimplyRNA cells kit (Promega, Wisconsin, USA) and lysates stored on ice at 4°C until the RNA extraction was performed (<1h). Shortly before adding cell lysates to the Maxwell® cartridge (Promega) 200µl of lysis solution was added to each sample and vortexed for 15 seconds.

2.6.3.2 Maxwell® Cartridge preparation

Maxwell® cartridges were places in the Maxwell® 16 LEV cartridge rack (Cat. #AS1251) with the label side facing away from the elution tubes and the seals were carefully peeled off. An LEV (low elution volume) plunger was placed in well #8 of each cartridge. A 0.5ml elution tube was placed in front of the appropriate cartridge for each cell lysate and 30µl of nuclease free water was added. The DNase I solution (275µl of nuclease-free H_20+lyophilized DNase I+5µl blue dye from Maxwell® SimplyRNA cells kit (Cat. #AS1270)) was added to well #5 of each cartridge (5µl). All 400µl of cell lysate was transferred to well #1 of the Maxwell® 16 LEV Cartridge, Figure 2-11.

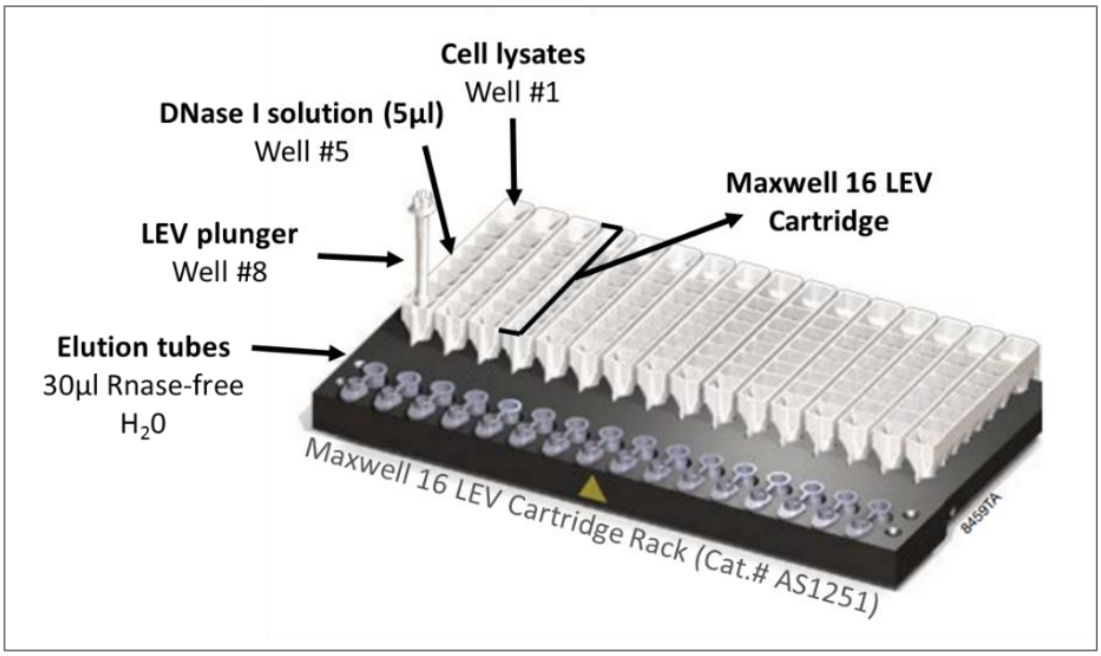

Figure 2-11. Schematic of the Maxwell® cartridges placed in the Maxwell® 16 LEV cartridge rack. Each cartridge has 8 wells. A LEV plunger is placed in well #8 and a 0.5ml elution tube in well #1 with 30µl of nuclease-free water for RNA elution. Cell lysates (400µl) are added to well #1 just prior to running the Maxwell® Instrument (Adapted from the manufacturer's instructions, Promega, Wisconsin, USA).

2.6.3.3 Maxwell® 16 Instrument Run

The Maxwell® 16 LEV cartridge rack containing prepared Maxwell® cartridges, was transferred to the Maxwell® 16 Instrument (Cat. #AS2000) configured with the Maxwell® 16 High Strength LEV Magnetic Rod and Plunger Bar Adaptor (Cat. #SP1070). The SimplyRNA cells protocol was run using the Maxwell® 16 firmware version 4.95 with the 'LEV' hardware configuration and 'Rsch' operational mode settings. The following selections were made on the instrument: Run > RNA > simplyRNA > simplyRNA > OK > Run/Stop. The Maxwell® 16 Instrument performed the automated RNA extraction protocol as outlined in Figure 2-12. Upon completion of the protocol, elution tubes containing total RNA were removed from the Maxwell® cartridge and stored at -80°C. Maxwell® cartridges were discarded.

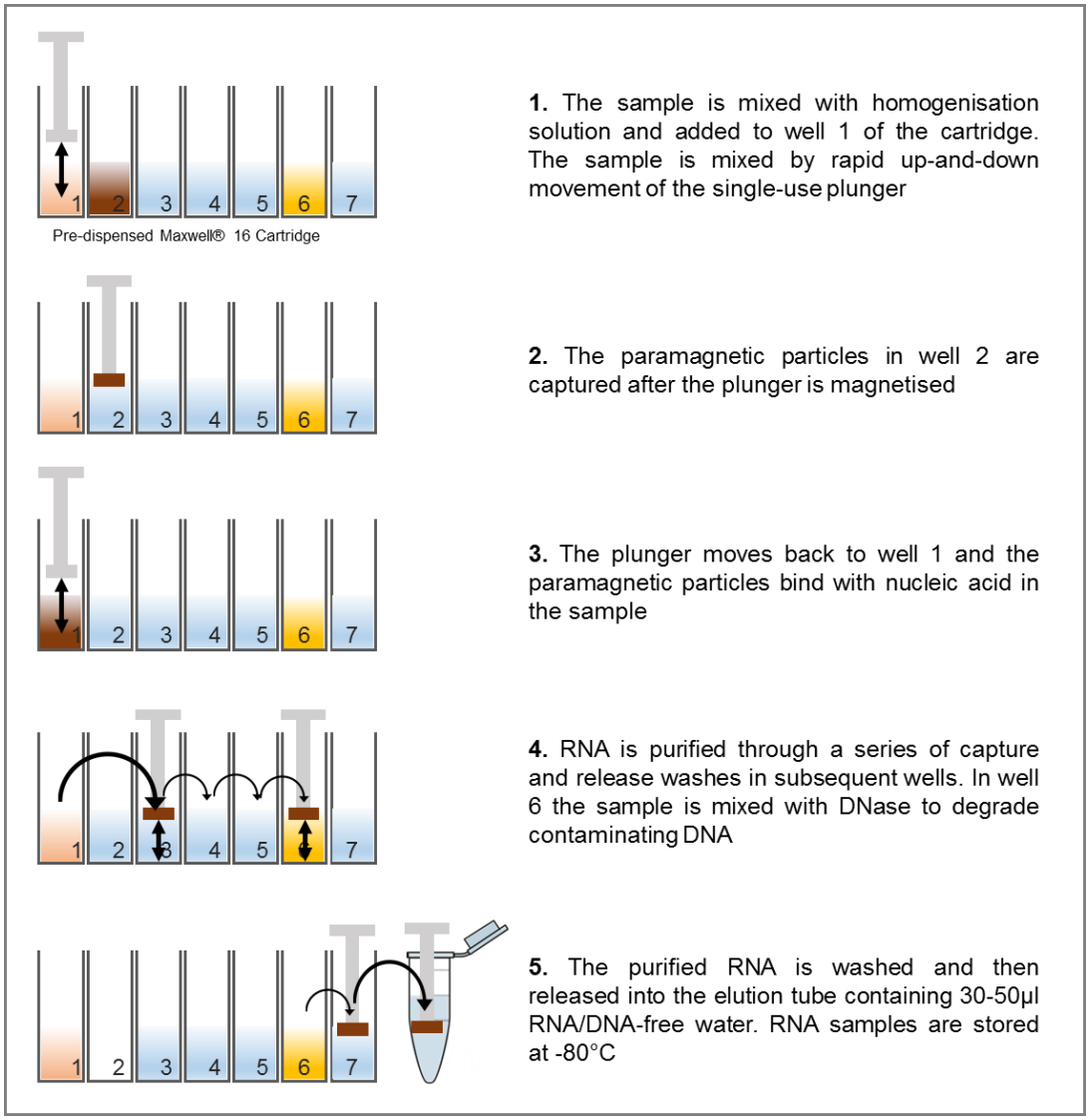

Figure 2-12. Schematic representation of RNA extraction protocol using the Maxwell® 16 LEV Instrument (Cat. #AS2000) and SimplyRNA Cells kit. The Maxwell® 16 LEV simplyRNA Cells Kit(a) (Cat.# AS1270) is used with the Maxwell® 16 Instrument (Cat.# AS2000) configured with the Maxwell® 16 High Strength LEV Magnetic Rod and Plunger Bar Adaptor (Cat.# SP1070) to purify RNA from cell lysates. This RNA extraction method is automated and the LEV is used to generate concentrated high-quality RNA suitable for use in downstream applications **(**based on manufacturer's instructions, Promega, Wisconsin, USA).

2.6.4 Measurement of RNA yield and purity using the LabChip GX Touch Nucleic Acid Analyser

Robust measurement of RNA concentration and quality is an essential requirement for many downstream applications. The LabChip GX Touch Nucleic Acid Analyser is an automated electrophoresis system which gives precise nucleic acid quantification and RNA integrity numbers (RIN) as an assessment of sample quality. This system saves time and money by replacing the use of conventional agarose gels and imaging with a re-usable LabChip which has a long sample life and an automated data collection. The RNA Pico Sensitivity Assay is a rapid and high throughput method which allows the detection and quantification of RNA samples as low as 250pg/µl (PerkinElmer).

2.6.4.1 RNA Pico Sensitivity Assay

Analysis of RNA concentration and quality was determined using the RNA Pico Sensitivity Assay Reagent Kit (Perkin Elmer, Cat. #CLS960012) as per manufacturer's instructions, and loaded into the DNA 5K/RNA/Charge Variant Assay LabChip (LabChip) (Perkin Elmer, Cat. #760435) to be read using the LabChip GX Touch Nucleic Acid Analyser (Perkin Elmer, Cat. #CLS138162). Reagent kit components can be seen in Table 2-12. The chip and reagents were allowed to equilibrate to RT for 20 minutes before use, RNA samples were thawed on ice.

Table 2-12. RNA Pico Sensitivity Assay Reagent Kit components (Perkin Elmer)

Reagent	Quantity/ Volume
Pico RNA Dye Concentrate	1 vial, 0.5ml
Chip Storage Buffer	5 vials, 1.8ml
RNA Pico Gel Matrix	5 vials, 0.51ml
RNA Pico Ladder (Part No. CLS760652)	2 vials, 0.04ml
RNA Pico Marker	1 vial, 0.8ml
10x RNA Sample Buffer Concentrate	3 vials, 2.0ml

2.6.4.2 Preparation of Gel-Dye Solution

The Pico RNA Dye Concentrate (0.5ml) was vortexed for 20 seconds and then 90µl was added to 1 vial of the RNA Pico Gel Matrix (0.51ml). The solution was vortexed until it was well mixed and centrifuged for a few seconds to remove any debris. The supernatant was transferred into a spin filter and centrifuged at 93,000rcf for 5minutes at RT. The filter was removed and the Gel-Dye Solution kept at 4°C on ice.

2.6.4.3 LabChip Preparation

The LabChip GX Touch chip has six active wells (1, 3, 4, 7, 8 and 10) and four inactive wells (2, 5, 6 and 9). Each active well was rinsed and aspirated twice with nuclease-free water to clean before use. Using a reverse pipetting technique, 50µl of the prepared Gel-Dye was added to wells # 3, 7, 8 and 10 and 50µl of the RNA Pico Marker was added to well #4, Figure 2-13 (A). Both sides of the LabChip window were cleaned with the clean room cloth supplied with the kit which was dampened with 70% isopropanol before loading it onto the LabChip GX Touch Nucleic Acid Analyser, Figure 2-13 (B).

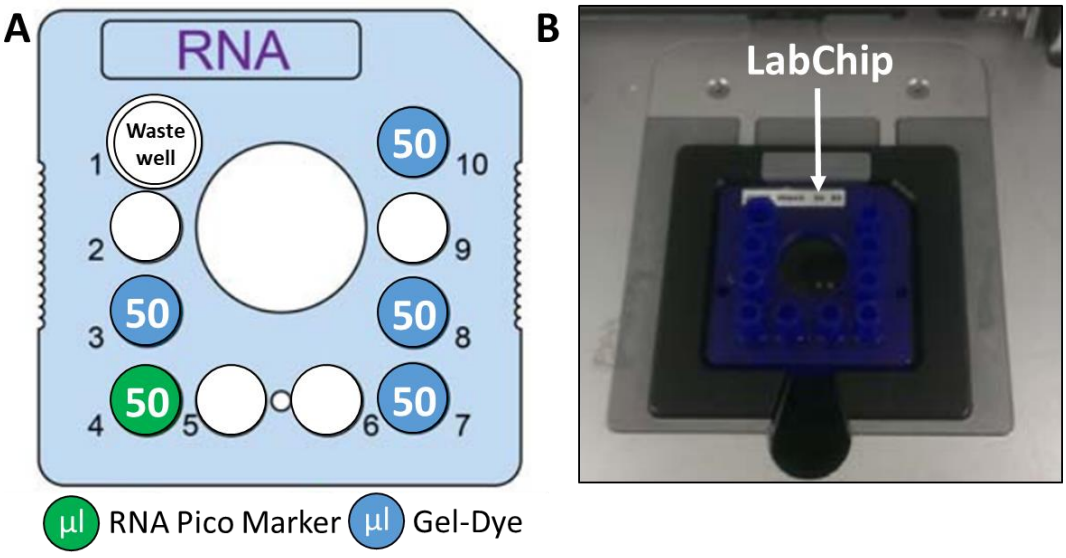

Figure 2-13. Preparation of the DNA 5K/RNA/Charge Variant Assay LabChip. (A) Schematic representation of the LabChip: 50µl Gel-Dye was added to wells 3, 7, 8 and 10 and 50µl RNA Pico Marker was added to well 4. **(B)** LabChip loaded into the LabChip GX Touch Nucleic Acid Analyser (adapted from the manufacturer's instructions).

2.6.4.4 Sample Preparation

Sample buffer was prepared by adding 200µl RNA Sample Buffer Concentrate (10x solution) to 1800µl to nuclease-free water. 8µl of Sample Buffer was pipetted into each well on a 96 well plate that was due to receive samples thereafter. 2µl of each sample was added to an individual well and mixed with the sample buffer by pipetting. The plate was tightly sealed and centrifuged at 10,000rcf for 2 minutes at RT. The RNA samples were denatured by heating to 70°C for 2mins then immediately snap cooled on ice for 5 minutes and centrifuged at 10,000rcf for 2 minutes at RT.

2.6.4.5 Preparation of RNA Ladder

The RNA Ladder (0.04ml) (Cat. #CLS760652) was centrifuged and heat denatured at 70°C for 2 minutes. Immediately afterwards, the tubes were snap cooled on ice for 5 minutes and then aliquoted (4µl) in to nuclease-free tubes and stored at -70°C. Upon use, an aliquot of the RNA ladder was thawed and 116µl Sample Buffer was added. The resulting solution was mixed thoroughly and transferred to the provided 'Ladder Tube' while 750µl Sample Buffer alone was transferred to the provided 'Buffer Tube'.

2.6.4.6 LabChip GX Touch Nucleic Acid Analyser setup

The RNA samples (96 well plate), RNA Ladder and Sample Buffer were prepared as above and loaded onto the LabChip GX Touch Nucleic Acid Analyser (Perkin Elmer, Cat. #CLS138162), to perform the HT RNA Pico Sensitivity Assay, Figure 2-14. Electropherograms were obtained for each sample as seen in Figure 2-15. Upon completion of the assay, the LabChip was removed from the LabChip GX Touch Nucleic Acid Analyser, each well cleaned with nuclease-free water and returned to the LabChip storage container.

LabChip techniques were carried out with assistance from Dr Pamela Brown.

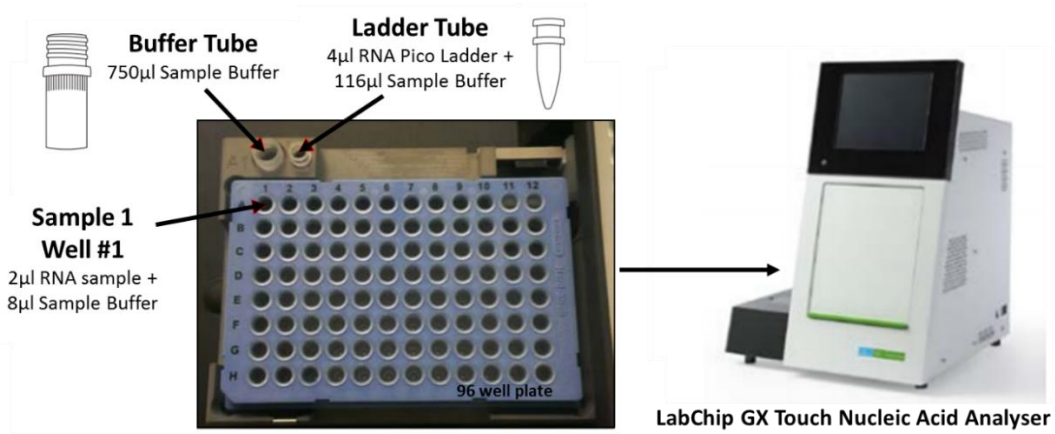

Figure 2-14. Preparation of RNA samples, Sample Buffer and RNA Pico Ladder for RNA Pico Sensitivity Assay on the LabChip GX Touch Nucleic Acid Analyser. RNA samples were prepared as in Section 2.6.4.4 in a 96 well plate and loaded onto the LabChip GX Touch Nucleic Acid Analyser. Sample Buffer and the RNA ladder were loaded in the appropriate tubes (adapted from manufacturers' instructions).

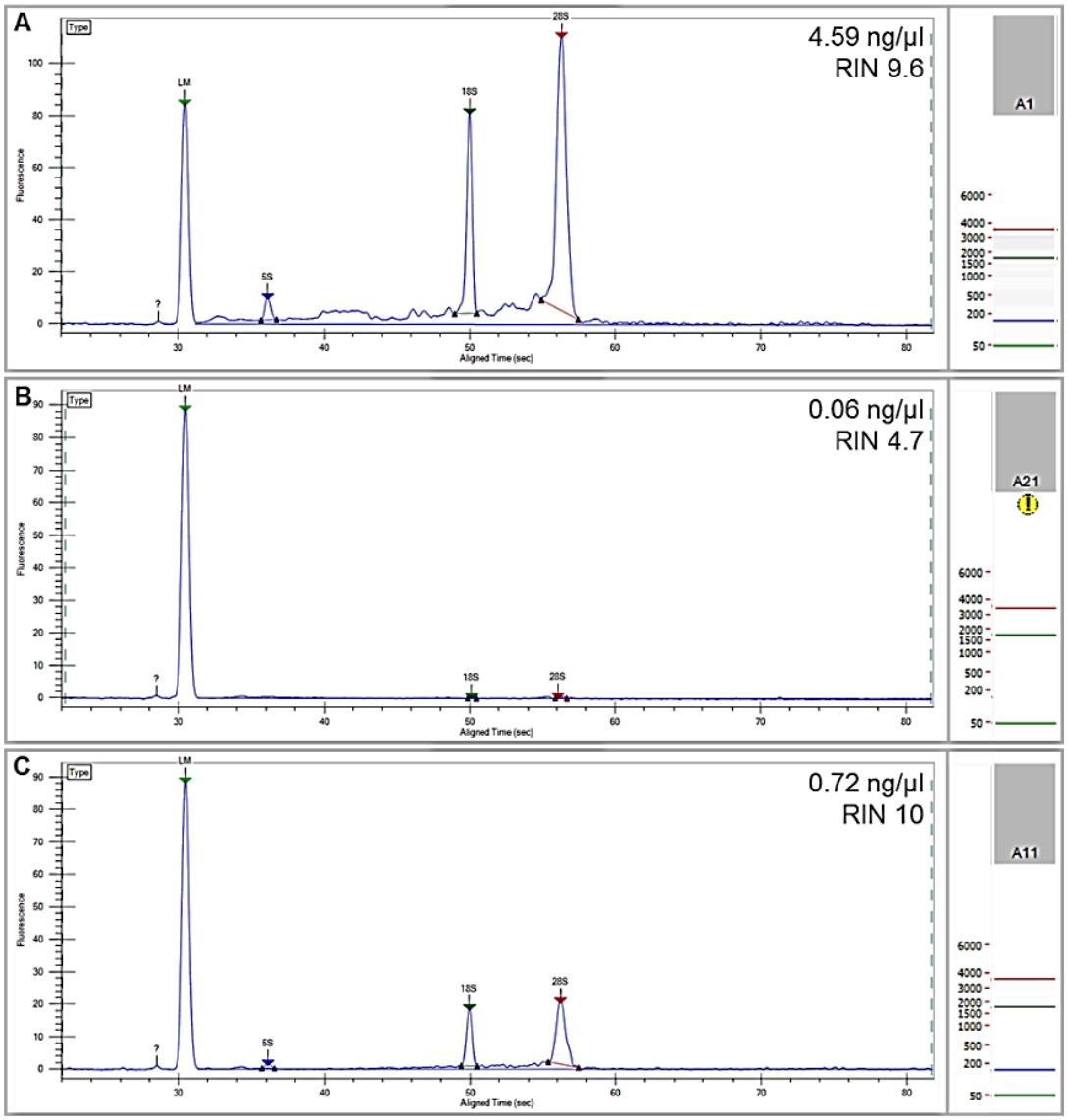

Figure 2-15: Sample RNA concentration and RNA Integrity Number (RIN /10) as determined by LabChip GX Touch Nucleic Acid Analyser and the RNA Pico Sensitivity Assay. (A) Example of a high concentration sample with good RNA integrity. Note peaks at 5S, 18S and 28S corresponding to tRNA and ribosomal RNA. **(B)** Example of a low concentration sample with poor RNA integrity (no ribosomal RNA peaks). **(C)** Example of a low concentration sample with good RNA integrity. The LabChip GX Touch Nucleic Acid Analyser was used to assess RNA concentration and quality of every sample (Author's own images).

2.7 Synthesis of complimentary DNA

Reverse transcription is used to synthesis complementary DNA (cDNA) from an RNA template using a reverse transcriptase enzyme and short primers complementary to the 3' end of the RNA. This method facilitates the cloning of low copy genes and produces a cDNA library that can be used directly as a template for quantitative polymerase chain reaction (qPCR) thereby obtaining information about corresponding gene expression.

2.7.1 cDNA synthesis using the Superscript VILO cDNA Synthesis Kit

2.7.1.1 RNA sample preparation

The concentration of stock RNA samples was determined using the Nanodrop ND-1000 Spectrophotometer (Section 2.6.2) or the LabChip GX Touch Nucleic Acid Analyser (Section 2.6.4). Stock RNA samples were diluted in nuclease-free water to obtain a working concentration of 100ng/µl in a final volume of 30µl and kept on ice.

2.7.1.2 cDNA synthesis master mix preparation

A master mix solution was prepared, the total volume of which was determined by the number of samples to be run in duplicate, using reagents of the Superscript VILO™ cDNA Synthesis Kit (InVitrogen, Cat. #11754-250) outlined in Table 2-13.

Table 2-13. Volumes of reagents used to prepare the cDNA synthesis master mix

Component	Concentration	Volume for 1 reaction/sample
5X VILO mix	1x	4 µl
10x superscript enzyme mix	0.125x	0.25 µl
H_20	NA	14.75 µl
	Total Volume	**19 µl**

Individual master mixes were also prepared for each of the three controls using reagents in Table 2-13. The positive control contained 5X VILO mix, 10x superscript enzyme mix, H_20 and control RNA (supplier); the negative control contained 5X VILO mix, 10x superscript enzyme mix, H_20 and no RNA (replaced by H_20); the 'no enzyme'

control contained 5X VILO mix, H_20 and control RNA (10x superscript enzyme replaced by water).

2.7.1.3 cDNA Synthesis

Nuclease-free PCR tubes (0.2ml) (Applied Biosystems) were labelled appropriately and 19µl master mix added to each followed by the addition of 1µl of RNA sample (100ng/µl) to make a final volume of 20µl. Tubes were placed in a Peltier Thermal Cycler (PTC-200) and the reaction performed using the following parameters: 25°C for 1 minute; 42°C for 60 minutes; 85°C for 5 minutes: 4°C 'hold'. Once completed, cDNA samples were stored at -20°C. The concentration of resultant cDNA was measured using the Nanodrop ND-1000 Spectrophotometer (Section 2.6.2).

2.7.2 cDNA synthesis using the NuGEN Ovation RNA-Seq System V2

In some cases, the concentration of RNA was relatively low and therefore standard methods of cDNA synthesis could not be used. The NuGEN Ovation RNA-Seq System V2 (NuGEN, Cat. #7102-32) provides a rapid and sensitive RNA amplification process to make amplified cDNA from a starting RNA concentration as low as 500pg-100ng, suitable for downstream applications including RNA-Seq and qPCR. For RNA-seq studies in this thesis the NuGEN Ovation RNA-Seq System V2 (NuGEN, Cat. #7102-32) was used as outlined below.

2.7.2.1 Workspace set up

Two separate areas were set up: a pre-amplification workspace and a post-amplification workspace with dedicated consumables and equipment to minimise the risk of contamination in the samples. All surfaces, instrumentation and equipment were cleaned with RNase*Zap* (ThermoFischer Scientific, Cat. #AM9780) to reduce environmental RNases followed by DNA-OFF (MP Biomedicals, Cat. #QD050) to avoid any previously amplified cDNA from contaminating the new amplification. All reagents quoted below were from NuGEN Ovation RNA-Seq System V2 (Cat. #7102-32).

2.7.2.2 Programming the Thermal Cycler

Programmes were prepared as outlined in Table 2-14 following the operating instructions provided by the manufacturer (NuGEN) on a thermal cycler with a heat block designed for 0.2ml tubes, equipped with a heated lid and with 100µl reaction volume.

Table 2-14. Thermal Cycler Programming for the NuGEN Ovation RNA-Seq System V2 (Cat. #7102-32)

First Strand cDNA Synthesis	
Programme 1: Primer Annealing	65°C 2 mins, hold at 4°C
Programme 2: First Strand Synthesis	4°C 1 min, 25°C 10 minx, 42°C 10 mins, 70°C 15mins, hold at 4°C
Second Strand cDNA Synthesis	
Programme 3: Second Strand Synthesis	4°C 1 min, 25°C 10 mins, 50°C 30 mins, 80°C 20mins, hold at 4°C
SPIA Amplification	
Programme 4: SPIA Amplification	4°C 1 min, 47°C 60 mins, 80°C 20mins, hold at 4°C

2.7.2.3 First Strand cDNA Synthesis

Prior to starting the reaction, the First Strand Primer Mix (A1), First Strand Buffer Mix (A2), First Strand Enzyme Mix (A3) and water were retrieved from the -20°C freezer, thawed at RT, centrifuged briefly and placed on ice. The nuclease-free water was kept at RT; 2µl of A1 and 5µl of total RNA sample (500pg-100ng) was added to each 0.2ml PCR tube and mixed by pipetting 5 times, briefly centrifuged and placed on ice. All tubes containing samples were placed in a pre-warmed thermal cycler and Programme 1 was run as outlined in Table 2-14.

Samples were removed and placed on ice. A master mix was prepared by combining the First Strand Buffer Mix (A2: 2.5µl per reaction) and the First Strand Enzyme Mix (A3: 0.5µl per reaction) multiplied depending upon the number of samples being analysed, in a 0.5ml capped tube. To each sample, 3µl of the master mix was added to make a final volume of 10µl, mixed by pipetting 5 times and briefly centrifuged. Tubes

were placed in a pre-cooled thermal cycler and Programme 2 was run as outlined in Table 2-14. Once complete samples were centrifuged and placed on ice.

2.7.2.4 Second Strand cDNA Synthesis

The Second Strand Buffer Mix (B1) and the Second Strand Enzyme Mix (B2) were retrieved from -20°C, thawed at RT, centrifuged and placed on ice. A master mix was prepared by combining the Second Strand Buffer Mix (B1: 9.7µl per reaction) and the Second Strand Enzyme Mix (B2: 0.3µl per reaction) multiplied depending upon the number of samples being analysed, in a 0.5ml capped tube. To each sample, 10µl of the Second Strand master mix was added to make a final volume of 20µl, mixed by pipetting 5 times and briefly centrifuged. Tubes were placed in a pre-cooled thermal cycler and Programme 3 was run as outlined in Table 2-14. Once complete samples were centrifuged and placed at RT on the bench.

2.7.2.5 Purification of cDNA

The Agencourt purification beads (NuGEN, Cat. #7102-32) were retrieved from 4°C storage, placed on the bench top and allowed to reach RT. The beads were suspended by inverting and tapping the tube several times. At RT 32µl of the resulting bead suspension was added to each reaction and mixed by pipetting 10 times, then incubated for 10 minutes. The tubes were transferred to a DynaMag^{TM} PCR magnet (Invitrogen, Cat. #49-2025) and left to stand for 5 minutes to completely clear the solution of beads. Carefully to minimize bead loss, 45µl of the solution was removed and discarded. With the tubes still on the magnet, 200µl of freshly prepared 70% ethanol solution was added and allowed to stand for 30 seconds. This ethanol 'wash' was removed using a pipette and the wash step was repeated twice more. Beads were air dried on the magnet for 15 to 20 minutes and each tube was inspected carefully to ensure all the ethanol was evaporated before continuing with the protocol below.

2.7.2.6 Single Primer Isothermal Amplification (SPIA) Amplification

The SPIA Primer Mix (C1), SPIA Buffer Mix (C2) and SPI Enzyme Mix (C3) were retrieved from -20°C storage, thawed at RT, centrifuged and placed on ice. A master mix was prepared by sequentially combining the SPIA Buffer Mix (C2: 20µl per reaction, the SPIA Primer Mix (C1: 10µl per reaction) and the SPIA Enzyme Mix (C3: 10µl per reaction) multiplied depending upon the number of samples being analysed,

in an appropriately sized capped tube. To each sample 40µl of the resulting SPIA Master Mix was added which should now contain double stranded cDNA bound to the dried beads. Samples were removed from the magnet and mixed thoroughly by pipetting at least 8-10 times. Each tube was placed in a pre-cooled thermal cycler and Programme 4 was run as outlined in Table 2-14. Once complete samples were centrifuged and placed at RT on the bench in the post-amplification workspace. Importantly, samples were not take back into the pre-amplification workspace but instead all remaining steps were carried out in the post-amplification workspace using dedicated post-amplification consumables and equipment. The tubes were transferred to the magnet and left to stand for 5 minutes to completely clear the solution of beads; thereafter 40µl of cleared supernatant containing the SPIA cDNA was carefully transferred to a fresh tube.

2.7.2.7 Purification of SPIA cDNA

The QIAGEN QIAquick PCR Purification Kit (QIAGEN, Cat. #28104) was used for the purification of the amplified SPIA cDNA produced with the Ovation RNA-Seq System V2. Briefly, for each sample 250µl of Buffer PB from the QIAGEN kit was added to a clean 1.5ml microcentrifuge tube and the entire volume (40µl) of the individual SPIA reaction was added. Samples were vortexed for 5 seconds and centrifuged briefly before loading into a QIAquick spin column placed in a collection tube. Samples were centrifuged for 1 minute at maximum speed in a microcentrifuge, the flow through from the column was discarded and the column replaced in the collection tube. To each column, 700µl of freshly prepared 80% ethanol solution was added and centrifuged for 1 minute at maximum speed, the flow through again discarded and the column replaced in the collection tube. This ethanol ‘wash’ step was repeated twice more.

The column was centrifuged for a further 2 minutes at maximum speed to remove all residual ethanol. The flow through and collection tube were discarded and the column was blotted onto clean, absorbent paper to remove any residual wash buffer from the tip of the column before placing into a clean 1.5ml microcentrifuge tube. 1X TE solution (30µl per tube) was added to the centre of each column and left to stand for 5 minutes at RT. The columns in their microcentrifuge tubes were centrifuged for 1

minute at full speed then the columns were discarded and the purified SPIA cDNA in each tube (~28µl) was mixed briefly by vortexing, centrifuged and stored at -20°C.

2.7.3 Measuring cDNA concentration and purity by Nanodrop

The total concentration and quality of each synthesised cDNA sample was determined using a Nanodrop ND-1000 Spectrophotometer (ThermoFischer Scientific), as outlined in section 2.6.2. The Nanodrop measures the absorbance of synthesised cDNA (1µl of each sample) to determine concentration. The A260/280 ratios were determined for each sample as a measure of purity and samples were only used for further analysis if they were >1.8.

2.8 Quantitative Real Time PCR- TaqMan method

Quantitative real time polymerase chain reaction (qPCR) is a method which determines and monitors the amplification of a chosen DNA molecule in real time. PCR consists of a series of temperature changes (repeated ~35 times) that allow for the following processes to occur: denaturation of the double stranded DNA molecule; annealing of the specifically designed primers with the DNA template of interest; and extension of the new transcript by DNA polymerase enzyme.

In this thesis, the Applied Biosystems TaqMan method (ThermoFischer Scientific) was used to detect specific PCR products. This method makes use of a pair of unlabelled gene-specific PCR primers (PrimerDesign) and a sequence specific TaqMan probe (Universal Probe Library, Roche) labelled with a FAM (6 carboxy-fluorescein) reporter dye on the 5' end and a non-fluorescent quencher (NFQ) on the 3' end. This probe hybridises to the complementary sequence defined by the primers, quencher activity is released after cleavage by the Taq polymerase resulting in release of the reporter dye (Figure 2-16). qPCR by the TaqMan method is carried out in a thermal cycler with the capacity to illuminate the sample with a beam of light and detect fluorescence emitted by the excited dye in real time.

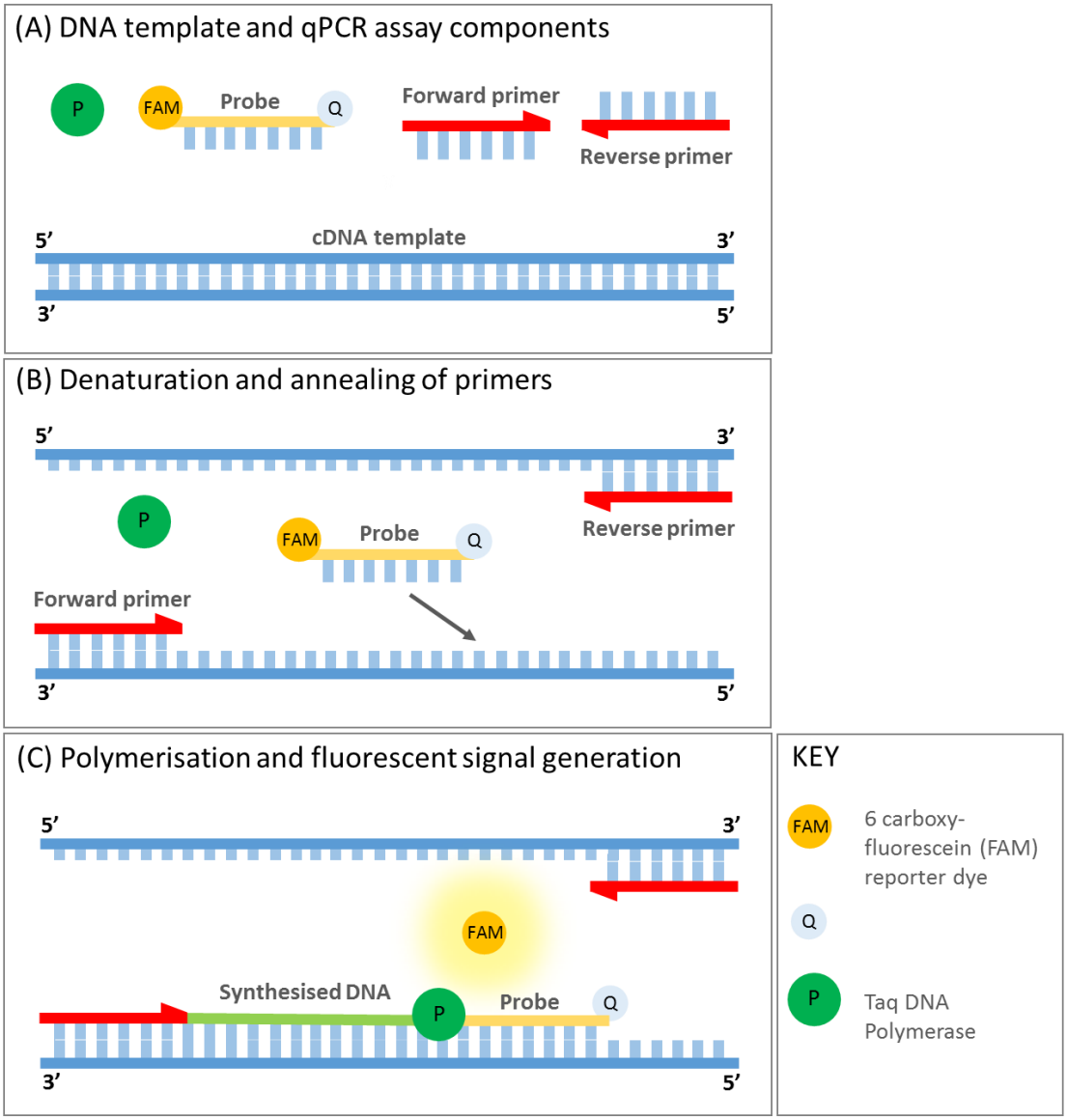

Figure 2-16. Schematic representation of the Applied Biosystems TaqMan qPCR method. (A) Components of the assay include template cDNA, Taq DNA polymerase, forward and reverse primers and a UPL probe. **(B)** The first step of qPCR is to raise the temperature to denature the double stranded cDNA then the temperature is lowered to allow annealing of gene specific forward and reverse primers and sequence specific UPL probe. **(C)** Taq DNA polymerase synthesizes new strands of DNA and when it comes in contact with the probe, its endogenous 5' nuclease activity cleaves the probe separating the FAM dye from the quencher and hence a fluorescent signal is generated. Each cycle generates more dye molecules resulting in an increase in fluorescence intensity proportional to the amount of amplicon synthesised (based on ThermoFisher Scientific).

2.8.1 Preparation of the Taqman mastermix

TaqMan qPCR was used to quantify RNA as a measure of gene expression in samples of cells or tissues. A master mix solution was prepared for each gene being tested, the total volume of which was determined by the number of samples to be run in duplicate, as shown in Table 2-15. Working stock solutions of all primers (20µM) were prepared from stock solutions (100µM) by a 1:5 dilution in nuclease-free water.

Table 2-15. Volumes of reagents used to prepare the TaqMan mastermix.

Stock component	**Supplier**	**Volume per 1 reaction (µl)**
2X express Supermix (+ROX)	InVitrogen, California	7.5
Forward primer (20µM)	Eurofins, Germany	0.15
Reverse primer (20µM)	Eurofins, Germany	0.15
UPL probe (10µM)	Roche	0.15
H20		5.55
Total Volume		**13.5**

13.5µl of the TaqMan mastermix was pipetted into the appropriate number of wells of a 96 well MicroAmp Fast optical reaction plate (Applied Biosystems, California, USA) and 1.5µl cDNA sample added in duplicate wells. The plate was centrifuged and placed on ice before running the PCR amplification on a real time PCR system (Applied Biosystems, 7900HT) using the incubation scheme outlined in Table 2-16.

Table 2-16. Temperature cycles for the TaqMan qPCR method.

Denaturation	
Denaturation	95°C 5 min
cDNA synthesis	
Denaturation	95°C 1 min
Annealing	58°C 1 min
Extension	72°C 1 min
Repeat above three steps	30 cycles
Extension	
Final extension	72°C 10 min, hold at 4°C

2.8.2 PCR primer design

Primers for each gene of interest were designed using the Universal probe Library Assay Design Centre (Roche Applied Science) and purchased from Eurofins (Germany). A complete list of primers used in this thesis can be found in Table 2-17.

Table 2-17. Accession numbers, primer sequences and associated UPL probe numbers for genes of interest investigated in this study

Gene Name	Accession Number	Forward Primer Sequence	Reverse Primer Sequence	UPL Probe Number
Cytokines, chemokines and monocyte/macrophage characterisation panel				
Mus musculus chemokine (C-C motif) ligand 2 (Ccl2)	NM_011333.3	catccacgtgttggctca	gatcatcttgctggtgaatgagt	62
Mus musculus chemokine (C-C motif) receptor 2 (Ccr2)	NM_009915.2	acctgtaaatgccatgcaagt	tgtcttccatttcctttgatttg	27
Mus musculus chemokine (C-C motif) ligand 7 (Ccl7)	NM_013654.3	ttctgtgcctgctgctcata	ttgacatagcagcatgtggat	89
Mus musculus chemokine (C-C motif) ligand 8 (Ccl8)	NM_021443.3	ttctttgcctgctgctcata	gcaggtgactggagccttat	26
Mus musculus Cxcl1 chemokine (C-X-C motif) ligand 1	NM_008176.3	gactccagccacactccaac	tgacagcgcagctcattg	83
Mus musculus Cxcl2 chemokine (C-X-C motif) ligand 2	NM_009140.2	cagaaaatcatccaaaagatactgaa	ctttggttcttccgttgagg	26
Mus musculus Cxcl3 chemokine (C-X-C motif) ligand 3	NM_203320.3	ccccaggcttcagataatca	gggatggatcgcttttctc	69
Mus musculus chemokine (C-X-C motif) ligand 12 (Cxcl12), transcript variant 3	NM_001012477.1	ctgtgcccttcagattgttg	taatttcgggtcaatgcaca	41
Mus musculus colony stimulating factor 1 (macrophage) (Csf1), transcript variant 1	NM_007778	gccattgcactgtgaatactg	catagggatggatgggacag	40
Mus musculus colony stimulating factor 2 (granulocyte-macrophage) (Csf2)	NM_009969	gcatgtagaggccatcaaaga	cgggtctgcacacatgtta	79
Mus musculus chemokine (C-X3-C motif) ligand 1 (Cx3cl1)	NM_009142.3	ctgccagggtcctttcct	gggcaaaggtgagtccttg	108
Mus musculus chemokine (C-X3-C motif) receptor 1 (Cx3cr1)	NM_009987	ggcctagagctcaaagaaatcc	cacagaccttcgatcccagt	16
Mus musculus tumor necrosis factor (Tnf)	NM_013693	ttgtcttaataacgctgatttggt	gggagcagaggttcagtgat	64
Mus musculus interleukin 6 (Il6), transcript variant 1	NM_031168	gctaccaaactggatataatcagga	ccaggtagctatggtactccagaa	6
Mus musculus interleukin 10 (Il10)	NM_010548	cagagccacatgctcctaga	tgtccagctggtcctttgtt	41
Mus musculus arginase, liver (Arg1)	NM_007482	ggcctttgttgatgtcccta	acagaccgtgggttcttcac	17
Mus musculus colony stimulating factor 1 receptor (Csf1r)	NM_001037859	aagcaagatctggacaaagagg	acgtttcgagctgctacgtc	1
Mus musculus CD14 antigen (Cd14)	NM_009841	aaagaaactgaagcctttctcg	agcaacaagccaagcacac	26
Mus musculus Fc receptor, IgG, low affinity III (Fcgr3)	NM_010188	tgtcaccatcactgtccaaga	actagggagaaagcagtgtggta	88

Mus musculus interferon gamma (Ifng)	NM_008337	atctggaggaactggcaaaa	ttcaagacttcaaagagtctgagg	21
Pericyte characterisation panel				
Mus musculus platelet derived growth factor receptor, beta polypeptide (PDGFRβ/CD140b)	NM_001146168.1	tcaagctgcaggtcaatgtc	ccattggcagggtgactc	67
Mus musculus melanoma cell adhesion molecule (MCAM/CD146)	NM_023061.2	aaactggtgtgcgtcttcttg	cttttcctctcctggcacac	27
Mus musculus alpha smooth muscle actin (aSMA/Acta2)	NM_007392.2	ctctcttccagccatctttcat	tataggtggtttcgtggatgc	58
Mus musculus chondroitin sulfate proteoglycan 4 (Cspg4)	NM_139001	cttggccttgttggtcagat	cacctccaggtggttctcc	16
Wound healing factors				
Mus musculus matrix metallopeptidase 2 (Mmp2)	NM_008610.2	taacctggatgccgtcgt	ttcaggtaataagcacccttgaa	77
Mus musculus matrix metallopeptidase 3 (Mmp3)	NM_010809.1	ttgttctttgatgcagtcagc	gatttgcgccaaaagtgc	7
Mus musculus matrix metallopeptidase 9 (Mmp9)	NM_013599.2	acgacatagacggcatcca	gctgtggttcagttgtggtg	19
Mus musculus tissue inhibitor of metalloproteinase 1 (Timp1), transcript variant 1	NM_001044384.1	gcaaagagctttctcaaagacc	agggatagataaacagggaaacact	76
Mus musculus transforming growth factor, beta 1 (Tgfb1)	NM_011577.1	tggagcaacatgtggaactc	gtcagcagccggttacca	72
Mus musculus transforming growth factor, beta 3 (Tgfb3)	NM_009368	gcagacacaacccatagcac	gggttctgcccacatagtaca	1
Mus musculus collagen, type I, alpha 1 (Col1a1)	NM_007742.4	ccgctggtcaagatggtc	ctccagcctttccaggttct	1
Mus musculus collagen, type III, alpha 1 (Col3a1)	NM_009930	gaccaggttgcccatcact	ggaatggacctgcaaaccta	3
Mus musculus fibronectin 1 (Fn1), transcript variant 1	NM_010233	ggaatggacctgcaaaccta	gtagggcttttcccaggtct	3
Validation of RNA-sequencing results				
Mus musculus actin, alpha 2, smooth muscle, aorta (Acta2)	NM_007392.2	ctctcttccagccatctttcat	tataggtggtttcgtggatgc	58
Mus musculus myosin, heavy polypeptide 11, smooth muscle (Myh11), transcript variant 1	NM_013607.2	ttgctgggtttgaaatctttg	ccctctcgctggtactcttc	1
Mus musculus olfactory receptor 78 (Olfr78), transcript variant 1	NM_130866	gcttcctccaaccttctgag	tggagctcgtttcccaaata	42
Mus musculus regulator of G-protein signaling 4 (Rgs4)	NM_009062	tccctcagttaaacaagatgtgc	gtttcatgtcctttgcactcc	4

Mus musculus regulator of G-protein signaling 5 (Rgs5), transcript variant 1	NM_009063.4	cagacagaggcccctaaaga	agacggttccaccaggttc	9
Mus musculus vascular cell adhesion molecule 1 (Vcam1)	NM_011693	tcttacctgtgcgctgtgac	actggatcttcagggaatgagt	47
Mus musculus kit ligand (Kitl), transcript variant 2	NM_001347156.1	cagcgctgcctttccttat	ccttggttttgacaagaggatt	68
Mus musculus potassium inwardly-rectifying channel, subfamily J, member 8 (Kcnj8), transcript variant 2	NM_001330363	gagaaaggcaccatggagaa	ggagaagagaaacgcagacg	109
Mus musculus prostaglandin-endoperoxide synthase 2 (Ptgs2)	NM_011198.4	gatgctcttccgagctgtg	ggattggaacagcaaggattt	45
Mus musculus prune homolog 2 (Drosophila) (Prune2)	NM_181348.4	tgttgaagagtgagaacaactgg	atggcttcaataggaactttgg	69
Mus musculus chemokine (C-X-C motif) ligand 14 (Cxcl14)	NM_019568.2	ttgagaccgttcacagcact	ctctctgagcggaagctttg	1
Mus musculus transforming growth factor, beta induced (Tgfbi)	NM_009369.4	aggtcccaggagagaaaggt	cccacaactcccatggtct	3
Mus musculus runt related transcription factor 1 (Runx1), transcript variant 1	NM_001111021.2	ctccgtgctacccactcact	atgacggtgaccagagtgc	77
Mus musculus patched 1 (Ptch1), transcript variant 1	NM_008957.3	cgactacatgccagagacca	gggaactgagcgtactcgat	3
Mus musculus collagen, type VIII, alpha 1 (Col8a1)	NM_007739.2	gccagccaagcctaaatgt	cagagttcagggaaatgatgaa	3
Mus musculus prickle planar cell polarity protein 1 (Prickle1)	NM_001033217.4	atggattctttggcgttgtc	tgacggtcttggcttgct	58
Mus musculus Wilms tumor 1 homolog (Wt1)	NM_144783.2	cagatgaacctaggagctaccttaaa	tgcccttctgtccatttca	3
Mus musculus tenascin C (Tnc)	NM_011607.3	ccacctcccatgtcctga	ccagggaaggcacttcttc	1

2.8.3 Quantification of gene expression

To quantify gene expression by TaqMan qPCR method, the fluorescence detection is plotted against the number of PCR cycles on a logarithmic scale. The threshold cycle (Ct) is defined from this graph as the number of cycles required for the fluorescent signal to exceed the background signal, Figure 2-17 (A), which is indirectly proportional to the amount of PCR product.

2.8.3.1 Generation of Standard Curve

Gene expression analysis was performed using the Standard Curve method whereby the quantity of each sample was extrapolated from a standard curve and then analysed relative to a control sample. Standard curve samples were generated by pooling an aliquot of each RNA sample (2µl) in any one experiment and performing four 10-fold serial dilutions to produce 4 standard RNA samples of decreasing concentration. The concentration of the first pooled standard was determined using the Nanodrop ND-1000 (section 2.6.2) and the remaining 4 standards calculated as 1/10 dilutions of this value. cDNA synthesis (section 2.7.1) and qPCR (section 2.8) was performed on each serial dilution separately to generate corresponding Ct values for each gene of interest. Ct values were plotted against $\log_{10}$ (RNA concentration) and a straight line fitted. The correlation coefficient on the line was confirmed to be >0.9 (Figure 2-17 (B-C). From this standard curve the relative expression levels of genes of interest in experimental samples can be extrapolated.

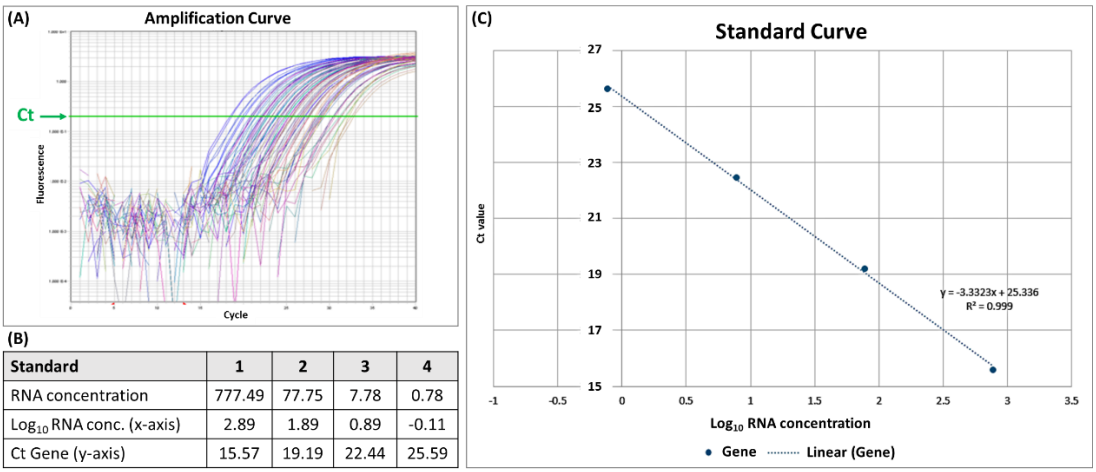

(B)

Standard	1	2	3	4
RNA concentration	777.49	77.75	7.78	0.78
Log_{10} RNA conc. (x-axis)	2.89	1.89	0.89	-0.11
Ct Gene (y-axis)	15.57	19.19	22.44	25.59

Figure 2-17. Generation of a standard curve for qPCR analysis. (A) qPCR graph of the number of cycles plotted against fluorescence with threshold cycle (Ct) denoted with a green arrow**. (B)** RNA concentration and associated Ct value for 4 exemplar standard samples **(C)** Log_{10}RNA concentration plotted against Ct value of 4 exemplar standard samples. Straight line fitted, gradient ~ -3.33 and correlation coefficient >0.9 (Author's own data).

2.8.3.2 Normalisation to a reference gene

It is essential to normalise qPCR data to a fixed control reference, one that is not affected by the experimental conditions. The Primer Only GeNorm 12 Gene Kit (Primer Design, Cat. #ge-SY-12) was used to select the best candidate reference gene for the given experimental samples in this thesis (mouse uterine tissues and cells). The expression of 12 mouse reference genes (*18s*, *Actb*, *Atp5b*, *B2m*, *Canx*, *Cyc1*, *Eif4a2*, *Gapdh*, *Rpl13a*, *Sdha*, *Ubc* and *Ywhaz*) (primers in kit) was assessed in a representative set of cDNA samples by qPCR (Section 2.8) and the results analysed using the qbase+ analysis software (Primer Design) to generate a list in order of stability (Figure 2-18). A report was produced with an output graph which identifies the most stable reference gene for the given samples (*Actb*).

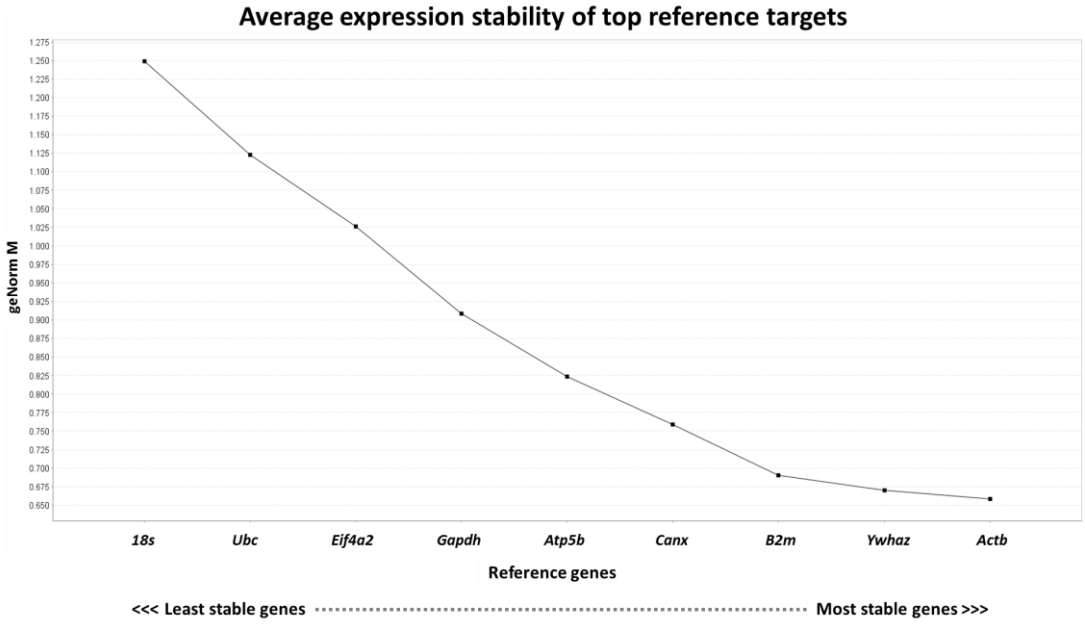

Figure 2-18. Average expression stability of top reference genes in experimental samples (mouse uterine tissues and cells) as determined by geNorm 12 Gene Kit (Primer Design, Cat. #ge-SY-12). Kit included primers against 12 mouse reference genes for including *18s*, *Actb*, *Atp5b*, *B2m*, *Canx*, *Cyc1*, *Eif4a2*, *Gapdh*, *Rpl13a*, *Sdha*, *Ubc* and *Ywhaz* (Author's own data).

The relative quantification result for the gene of interest was normalised to that of the house-keeping gene *Actb* in the same sample. A standard curve was generated for *Actb* and genes of interest normalised to these values. Normalised numbers were then compared between experimental samples and displayed as a fold-change in expression.

2.8.3.3 Statistical Analysis

Statistical analyses were performed using Graphpad Prism software. In data that was normally distributed a student's t-test was performed to determine the significance of a difference between two groups. When comparing the means of more than two groups a one-way ANOVA was used followed by a multiple comparisons test such as Sidak's or Tukey's. All data were presented as mean±SEM and criteria for significance was $p<0.05$.

2.9 Next Generation RNA Sequencing by Edinburgh Genomics

In cells, genetic information is stored as DNA, transcribed into RNA which is translated into proteins. Transcription of genes regulates a cell's biological activity and characterises the phenotype of the cell, therefore understanding the RNA transcriptome gives insight into both development and disease (Wang, Gerstein and Snyder 2009). Over the last 50 years, many techniques and technologies have emerged to facilitate sequencing of DNA and RNA molecules. Next generation sequencing (NGS) or RNA-Seq is a high throughput method that enables RNA analysis through sequencing of cDNA. This gives a more detailed and quantitative assessment of gene expression and how this changes between physiological and pathological conditions (Kukurba and Montgomery 2015).

RNA-Seq uses deep sequencing technologies. In brief, a sample of RNA is converted to a cDNA library with adaptors attached to the ends and these molecules are sequenced to obtain short sequences known as reads (generally 30-400bp). Following sequencing, the reads are aligned to a reference genome to produce a genome-scale transcriptomic map that contains the expression level of each gene (Wang et al. 2009). In this thesis, NGS was used to investigate transcriptomic changes in uterine mesenchymal cells during endometrial tissue repair.

2.9.1 RNA and cDNA sample preparation for Next Generation Sequencing (NGS)

Uterine mesenchymal cells were isolated from endometrial tissues dissected from cycling *Pdgfrβ-BAC-eGFP* mice (naïve) and from *Pdgfrβ-BAC-eGFP* mice at 24hrs of the mouse model of endometrial breakdown and repair (section 2.2.2) by FACS, protocols described in detail in section 2.5. Cells were centrifuged at 400rcf for 5 minutes at 4°C and the cell pellet re-suspended in homogenisation solution. RNA extraction was performed using the SimplyRNA Cells Maxwell® 16 LEV kit and the automated Maxwell® 16 LEV extraction instrument as outlined in section 2.6.3. RNA concentration and RNA Integrity Number (RIN) was measured using the LabChip GX Touch Nucleic Acid Analyser as outlined in section 2.6.4. As RNA samples met minimum quality requirements but failed to reach minimum concentrations, a cDNA

amplification step was included in sample preparation, carried out using the NuGEN Ovation V2 system as outlined in section 2.7.2 and the quality checked by LabChip GX Touch (section 2.6.4) before they were sent to Edinburgh Genomics.

2.9.2 Truseq mRNA sequencing

At Edinburgh Genomics (https://genomics.ed.ac.uk/) TruSeq DNA Nano gel free libraries (350bp insert) were prepared for each sample. Sequence data was generated on the HiSeq 4000 75PE platform to yield at least 290M + 290M reads according to the standard protocols at the facility.

2.9.3 Bioinformatic data analysis

An in-house bioinformatic analysis of the samples was carried out by Jonathan Manning at Edinburgh Genomics and a pdf report outlining the methods used and results was provided. In brief, reads were trimmed using Cutadapt version cutadapt-1.9.dev21. Reads were trimmed for quality at the 3' end using a quality threshold of 30 and for adapter sequences of the NuGen Ovation v2 kit (AGATCGGAAGAGC). After trimming reads were required to have a minimum length of 50. The Mus musculus genome from Ensembl, assembly GRCm38, annotation version 84, was used as the reference for mapping. Reads were aligned to the reference genome using STAR2 version 2.5.2b specifying paired-end reads.

Reads were assigned to exon features grouped by gene ID in the reference genome using 'featureCounts'3, which assigns counts on a 'fragment' basis as opposed to individual reads such that a fragment is counted where one or both of its reads are aligned and associated with the specified features. Strandness was set to 'unstranded' and a minimum alignment quality of 10 was specified. The raw counts table was filtered to remove rows consisting predominantly of near-zero counts, filtering on counts per million (CPM) to avoid artefacts due to library depth. Specifically, a row of the expression matrix was required to have values greater than 0.1 in at least 3 samples, corresponding to the smallest sample group as defined by Group, once any samples were removed (where applicable).

A principal components analysis was undertaken on normalised and filtered expression data to explore observed patterns with respect to experimental factors. The cumulative

proportion of variance associated with each factor was used to study the level of structure in the data, while associations between continuous value ranges in principal components and categorical experimental factors was assessed with an ANOVA test. Points were assigned as outliers in each component if they occurred outside the interquartile range + 1.5. If appropriate due to known experimental difficulties, problematic samples were excluded from downstream analysis. Differential analysis was carried out with EdgeR4 (version 3.16.5), and the quasi-likelihood (QL) F-test using the contrasts desired.

2.9.4 Validation of RNA Sequencing results by qPCR

Validation of RNA sequencing results was done using qPCR on an independent set of cell samples generated from *Pdgfrβ-BAC-eGFP* endometrial tissues (naive, Section 2.2.1 and 24hrs of the mouse model of endometrial breakdown and repair, Section 2.2.2) by FACS (section 2.5). RNA extraction (section 2.6.3), cDNA amplification (section 2.7.1) and qPCR (section 2.8) was performed to analyse the expression of candidate genes in validation samples.

2.10 Chromium Single Cell Gene Expression Analysis- 10x Genomics

Single cell RNA sequencing is a technology designed to elucidate heterogeneity within cell populations thereby revealing *de novo* cellular phenotypes and giving a deeper understanding of biological systems (Hedlund and Deng 2018). Whereas in bulk RNA-Seq subtleties of a heterogeneous cell population are overlooked, single cell sequencing provides a platform to identify subpopulations of cells and interrogate changes in their individual transcriptome due to physiological or pathological conditions (Hedlund and Deng 2018).

The Chromium™ Single Cell Gene Expression technique provides a comprehensive solution for cell characterisation and gene expression profiling with a simplified workflow. In this thesis the Chromium™ system was used to generate samples for single cell sequencing of uterine mesenchymal cells during endometrial tissue repair.

2.10.1. Cell sample preparation for 10x genomics single cell sequencing (ScSeq)

Uterine mesenchymal cells were isolated form endometrial tissues dissected from naive *Pdgfrβ-BAC-eGFP* mice and from *Pdgfrβ-BAC-eGFP* mice at 24hrs of the mouse model of endometrial breakdown and repair (section 2.2) by FACS (section 2.5). Both naïve and 24hrs samples were pooled from uterine tissues of 4 mice (2 horns pooled from each mouse): 25,000 mesenchymal cells (GFP+) from each giving a total number of 100,000 mesenchymal cells (GFP+) for downstream application. Cells were sorted into a 1.5ml Eppendorf with 500µl of PBS+2%FBS added (the Eppendorf was vortexed prior to sorting to ensure the inside was fully coated with buffer). Eppendorfs were kept at 4°C during and after FACS. Cells were immediately centrifuged at 400rcf for 5 minutes at 4°C and the cell pellet re-suspended in PBS+2%FBS and mixed by pipetting. This buffer 'wash' was repeated. In each sample, cells were counted using a TC20^{TM} Automated Cell Counter (Bio Rad, Cat. #1450102), which also gives a viability score (85% threshold value) as determined by a 0.4% trypan blue stain.

2.10.2 Chromium^{TM} Single Cell 3' Library and Gel Beads Kits

The 10x Chromium^{TM} Controller is an instrument which assigns a 10x barcode to each individual cell in a cell suspension by partitioning thousands of cells into nanolitre-scale Gel bead-in-EMulsions (GEMs) so that all cDNA molecules generated by reverse transcription (RvT) share a common 10x barcode. cDNA libraries are generated and sequenced and the 10x barcodes used to associate individual reads back to the individual cells (Figure 2-19 (A)) (10x Genomics, USA).

The Single Cell 3' Protocol is as follows: during GEM RvT, primers containing an Illumina R1 sequence, a 16nt 10x barcode, a 10nt Unique Molecular Identifier (UMI) and a poly-dT primer sequence are mixed with cell lysate and a master mix. Incubation of the GEMs then produces barcoded, full-length cDNA from poly-adenylated mRNA (Figure 2-19). Silane magnetic beads are used to remove leftover biochemical reagents and primers from the resulting solution and barcoded cDNA is amplified by PCR. Enzymatic fragmentation and size selection are used to optimise the cDNA size prior to library construction. The Single Cell 3' protocol produces sequencing libraries with construct structure shown in Figure 2-19 (B).

The Single Cell 3' Reagent Kits used in this thesis were the Chromium™ Single Cell 3' Library & Gel Bead Kit V2. 4 rnx (10x Genomics, Cat. #120267) and the Chromium™ Single Cell A Chip Kit, 16 rnxs (10x Genomics, Cat. #1000009), detailed in Table 2-18. Protocols were carried out as per manufacturer's instructions (10x Genomics, USA).

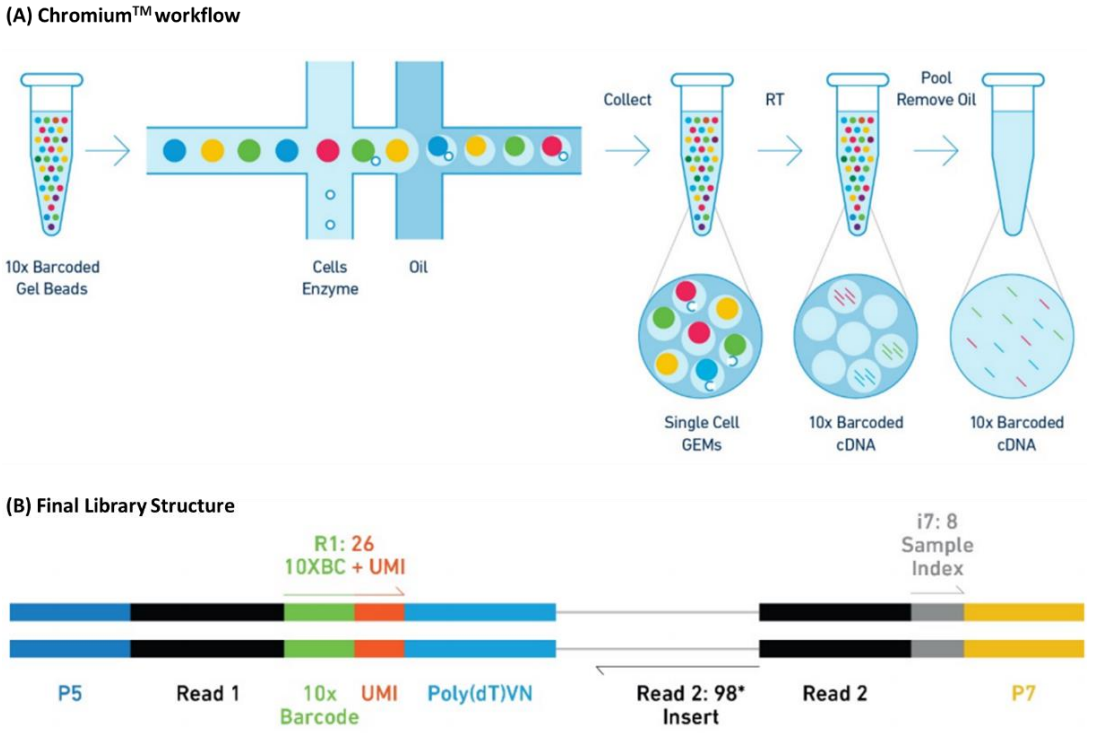

Figure 2-19. **Schematic representation of 10x ChromiumTM workflow and generation of Single Cell cDNA libraries. (A)** GEM production by ChromiumTM Controller, GEM RT incubation and generation of 10x barcoded cDNA molecules. **(B)** Final library construct beginning and ending with P5 and P7 primers, read one encoding the 16bp 10x barcode and 10bp UMI, read two used to sequence the fragment and the i7 Sample Index sequence (adapted from manufacturer's instructions, 10x Genomics, USA).

Table 2-18. Components of the Chromium™ Single Cell 3' Library & Gel Bead Kit V2. 4 rnx and Chromium™ Single Cell A Chip Kit, 16 rxns.

Product	Components	Catalogue Number
Chromium™ Single Cell 3' Library Kit V2, 4 rxns (store at -20°C)		
Reagents Module 1	RvT Reagent Mix	220089
	RvT Enzyme Mix	220127
	Additive A	220074
	RvT Primer	310354
	Buffer Sample Clean Up 1	220020
	Amplification Master Mix	220129
	cDNA Primer Mix	220106
	cDNA Additive	220067
Reagents Module 2	Fragmentation Enzyme Blend	220130
	Fragmentation Buffer	220108
	Ligation buffer	220109
	DNA Ligase	220131
	Adaptor Mix	220026
	SI-PCR Primer	220111
Chromium™ Single Cell 3' Gel Bead Kit V2, 4rxns (store at -80°C)		
	Single Cell 3' Gel Beads	220104
Chromium™ Single Cell A Chip Kit, 16 rxns (store at ambient temperature)		
	Single Cell A Chip (x2)	2000019
	Gaskets	3000072
	Partitioning Oil (x2)	220088
	Recovery Oil (x2)	220016

2.10.3 Preparation of Single Cell Master Mix

Before use (>30mins), Single Cell 3' Gel Beads, the reverse transcriptase (RvT) Reagent Mix and Additive A were equilibrated to RT. Lyophilized RvT Primer was briefly centrifuged and re-suspended in 40µl of low TE buffer, vortexed and centrifuged and left at RT for >30mins prior to use. RvT Enzyme Mix was placed on ice. All reagents used in the following protocol are outlined in Table 2-18.

A master mix was prepared using the reagents in Table 2-19, added in the order shown and mixed by pipetting 15 times and centrifuged briefly. To each well of a PCR 8-tube strip, 66.2µl of the master mix was added and the strip placed on ice.

Table 2-19. Volume of reagents used to prepare the Single Cell Master Mix

Master Mix Component	1 rxn (µl)	4 rxns + 10% xs (µl)
RT Reagent Mix	50.0	220.0
RT Primer	3.8	16.7
Additive A	2.4	10.6
RT Enzyme Mix	10.0	44.0
Total Volume	**66.2**	**291.3**

2.10.4 Loading the Chromium™ Single Cell A Chip

A Single Cell A Chip was placed in a 10xTM Chip Holder (Cat. #330019). As fewer than 8 samples were being processed, a 50% glycerol solution was added to each unused well as follows: 90µl in row #1; 40µl in row #2; and 270µl in row #3 (Figure 2-21).

The appropriate volume of nuclease-free water and single cell suspension of each sample (washed, diluted and mixed well by pipetting), determined from the Cell Suspension Volume Calculator Table (Figure 2-20), was added to the PCR tube strip containing master mix (on ice) (total volume 100µl). Each tube was mixed gently by pipetting and 90µl of the resulting solution was transferred to a corresponding well in row #1 of the Chromium™ Single cell A Chip taking care not to introduce any bubbles (Figure 2-21 (A)).

The Single Cell 3' Gel beads were vortexed for 30 seconds then 40µl was slowly aspirated and dispensed into the bottom of the 'active' wells in row #2 of the Chromium™ Single cell A Chip taking care not to introduce any bubbles (Figure 2-21 (B)).

A total volume of 270µl (2x135µl) of Partitioning Oil was added to the 'active' wells in row #3 of the Chromium™ Single cell A Chip (Figure 2-21 (C)). The 10x™ Gasket (Cat. #3000072) was attached with the notched cut at the top left corner ensuring the holes were aligned with the wells (Figure 2-22 (A)).

Volume of Cell Suspension Stock per reaction (µl) | Volume of Nuclease-Free Water per reaction (µl)											
Cell Stock Concentration (Cells/µl)	**Targeted Cell Recovery**										
	500 cells	1000 cells	2000 cells	3000 cells	4000 cells	5000 cells	6000 cells	7000 cells	8000 cells	9000 cells	1000 cells
100	8.7 25.1	17.4 16.4	n/a	n/a	n/a	n/a	n/a	n/a	n/a	n/a	n/a
200	4.4 29.5	8.7 25.1	17.4 16.4	26.1 7.7	n/a	n/a	n/a	n/a	n/a	n/a	n/a
300	2.9 30.9	5.8 28.0	11.6 22.2	17.4 16.4	23.2 10.6	29.0 4.8	n/a	n/a	n/a	n/a	n/a
400	2.2 31.6	4.4 29.5	8.7 25.1	13.1 20.8	17.4 16.4	21.8 12.1	26.1 7.7	30.5 3.4	n/a	n/a	n/a
500	1.7 32.1	3.5 30.3	7.0 26.8	10.4 23.4	13.9 19.9	17.4 16.4	20.9 12.9	24.4 9.4	27.8 6.0	31.3 2.5	n/a
600	1.5 32.4	2.9 30.9	5.8 28.0	8.7 25.1	11.6 22.2	14.5 19.3	17.4 16.4	20.3 13.5	23.2 10.6	26.1 7.7	29.0 4.8
700	1.2 32.6	2.5 31.3	5.0 28.8	7.5 26.3	9.9 23.9	12.4 21.4	14.9 18.9	17.4 16.4	19.9 13.9	22.4 11.4	24.9 8.9
800	1.1 32.7	2.2 31.6	4.4 29.5	6.5 27.3	8.7 25.1	10.9 22.9	13.1 20.8	15.2 18.6	17.4 16.4	19.6 14.2	21.8 12.1
900	1.0 32.8	1.9 31.9	3.9 29.9	5.8 28.0	7.7 26.1	9.7 24.1	11.6 22.2	13.5 20.3	15.5 18.3	17.4 16.4	19.3 14.5
1000	0.9 32.9	1.7 32.1	3.5 30.3	5.2 28.6	7.0 26.8	8.7 25.1	10.4 23.4	12.2 21.6	13.9 19.9	15.7 18.1	17.4 16.4
1100	0.8 33.0	1.6 32.2	3.2 30.6	4.7 29.1	6.3 27.5	7.9 25.9	9.5 24.3	11.1 22.7	12.7 21.1	14.2 19.6	15.8 18.0
1200	0.7 33.1	1.5 32.4	2.9 30.9	4.4 29.5	5.8 28.0	7.3 26.6	8.7 25.1	10.2 23.7	11.6 22.2	13.1 20.8	14.5 19.3
1300	0.7 33.1	1.3 32.5	2.7 31.1	4.0 29.8	5.4 28.4	6.7 27.1	8.0 25.8	9.4 24.4	10.7 23.1	12.0 21.8	13.4 20.4
1400	0.6 33.2	1.2 32.6	2.5 31.3	3.7 30.1	5.0 28.8	6.2 27.6	7.5 26.3	8.7 25.1	9.9 23.9	11.2 22.6	12.4 21.4
1500	0.6 33.2	1.2 32.6	2.3 31.5	3.5 30.3	4.6 29.2	5.8 28.0	7.0 26.8	8.1 25.7	9.3 24.5	10.4 23.4	11.6 22.2
1600	0.5 33.3	1.1 32.7	2.2 31.6	3.3 30.5	4.4 29.5	5.4 28.4	6.5 27.3	7.6 26.2	8.7 25.1	9.8 24.0	10.9 22.9
1700	0.5 33.3	1.0 32.8	2.0 31.8	3.1 30.7	4.1 29.7	5.1 28.7	6.1 27.7	7.2 26.6	8.2 25.6	9.2 24.6	10.2 23.7
1800	0.5 33.3	1.0 32.8	1.9 31.9	2.9 30.9	3.9 29.9	4.8 29.0	5.8 28.0	6.8 27.0	7.7 26.1	8.7 25.1	9.7 24.1
1900	0.5 33.3	0.9 32.9	1.8 32.0	2.7 31.1	3.7 30.1	4.6 29.2	5.5 28.3	6.4 27.4	7.3 26.6	8.2 25.6	9.2 24.6
2000	0.4 33.4	0.9 32.9	1.7 32.1	2.6 31.2	3.5 30.3	4.4 29.5	5.2 28.6	6.1 27.7	7.0 26.8	7.8 26.0	8.7 25.1

Figure 2-20. Cell Suspension Volume Calculator Table. Grey boxes- volumes that would exceed the allowable water volume in each reaction. Yellow boxes- indicate a low transfer volume that may result in higher cell load variability. Blue boxes- optimal range of cell stock concentration to maximise the likelihood of achieveing the desired cell recovery target (manufacturer's instructions, 10x Genomics, USA)

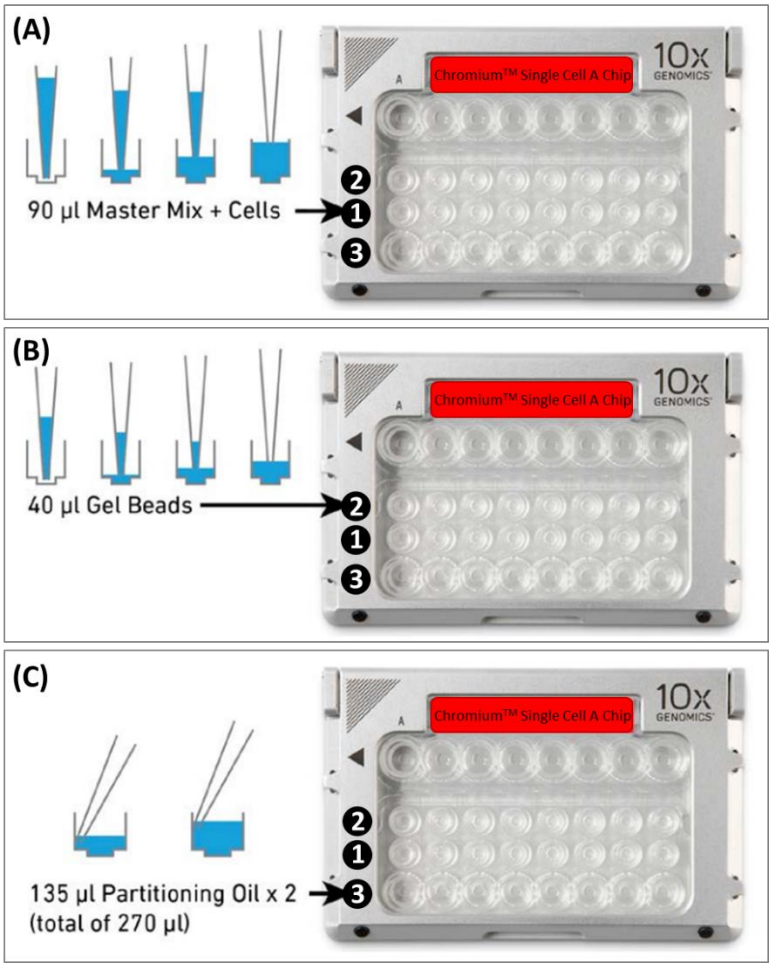

Figure 2-21. Loading the Chromium™ Single Cell A Chip. (A) 90µl of Master Mix and Cell Suspension solution is added to row #1 of the Chip. **(B)** 40µl of the Single Cell 3' Gel beads solution is added to row #2 of the Chip. **(C)** 270µl of Partitioning Oil is added to row #3 of the Chip (adapted from manufacturer's instructions, 10x Genomics, USA).

2.10.5 Running the Chromium™ controller

The assembled Chip, 10x Chip Holder and 10x Gasket was placed on the tray of the Chromium™ Controller (Figure 2-22 (B)) and the tray retracted. It was confirmed that the Chromium Single Cell A programme was shown on the screen and the 'play' button pressed to begin the run (Figure 2-22 (C)). After completion of the run (~6.5 mins) the Chip was removed from the Chromium™ Controller, the gasket removed and the next step of the protocol was immediately undertaken.

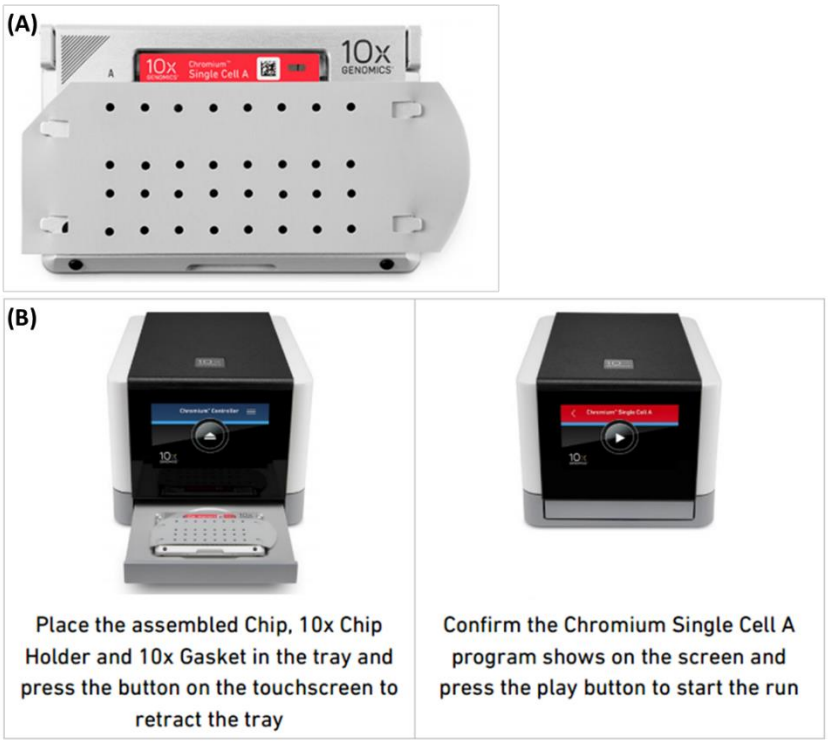

Figure 2-22. Set up of the Chromium™ Controller. (A) Chromium™ Single Cell A Chip with gasket covering. **(B)** Chip placed into the ChromiumTM Controller (adapted from manufacturer's instructions, 10x Genomics, USA).

2.10.6 GEM-RvT Incubation

An emulsion-safe PCR 8-tube strip was placed on ice. The 10x Chip Holder was opened and the lid folded back to expose the wells at a 45° angle. As they have a high viscosity, 100µl GEMs was aspirated slowly from the lowest points of the Recovery Wells with care taken not to introduce bubbles (Figure 2-23 (A)). Samples were verified to have no air in the tips and be uniformly opaque across all channels (Figure 2-23 (B)) and then dispensed into the PCR 8-tube strip and capped. The Single Cell A Chip was discarded. The capped tube strip was loaded into a BioRad C1000 Touch Thermal Cycler and the incubation protocol in Table 2-20 was carried out. Upon completion the tube strip was stored at -4°C (<24hrs) before proceeding to the Post GEM-RvT Clean-up.

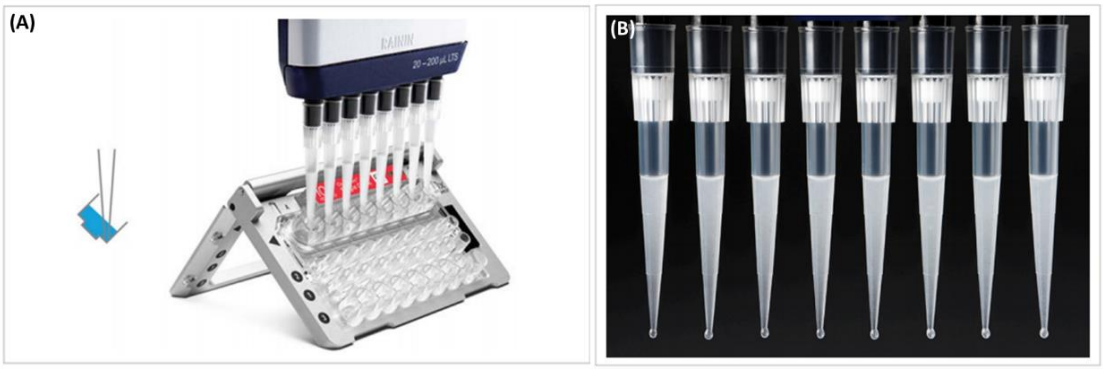

Figure 2-23. Transfer of GEMs for RvT incubation. (A) Aspiration of GEMs from recovery wells. **(B)** Opacity is indicative of a successful Chromium™ Controller run (adapted from manufacturer's instructions, 10x Genomics, USA).

Table 2-20. Temperature cycles for GEM RvT incubation

Specifications		
Lid Temperature	**Reaction Volume**	**Run Time**
53°C	125µl	~55 mins
Protocol		
Step	**Temperature**	**Time**
1	53°C	45 mins
2	85°C	5 mins
3	4°C	Hold

Sections 2.10.2-2.10.5 were carried out with assistance from Dr Ross Dobie, affiliated with Professor Neil Henderson.

2.10.7 Post GEM-RvT Cleanup

Before use (>30mins), DynaBeads® MyOne™ Silane Beads , Additive A, cDNA Additive and cDNA Primer Mix were equilibrated to RT. Buffer Sample Clean Up 1 was thawed at 65°C and kept at RT. An 80% ethanol solution was prepared and the Amplification Master Mix was placed on ice. All reagents used in the following protocol are outlined in Table 2-18.

Recovery Agent (125µl) was added to each well of the PCR 8-tube strip containing post RvT incubation GEMS and incubated for 60 seconds without mixing. The recovered biphasic mixture contained distinct Recovery Agent/Partitioning Oil (Figure 2-24, (A) pink) and aqueous (Figure 2-24, (A) clear) phases with no persisting emulsion. 125µl of the Recovery Agent/Partitioning Oil (pink) was slowly removed from the bottom of the tubes and discarded with care to avoid the clear aqueous sample (Figure 2-24, (B)). DynaBeads MyOne Silane beads were vortexed until fully re-suspended and a DynaBeads Cleanup mix was prepared using reagents in Table 2-21. To each sample, 200µl of amplification master mix was added, mixed by pipetting and incubated at RT for 10 mins (Figure 2-24, (C)).

Figure 2-24. Visualisation of Recovery Agent and DynaBeads. (A-B) The biphasic mixture of Recovery Agent/Partitioning Oil (pink) and aqueous sample (clear). **(C)** Sample re-suspended with DynaBeads MyOne Silane beads (adapted from manufacturer's instructions, 10x Genomics, USA).

Table 2-21. Volume of reagents used to prepare the DynaBeads Cleanup mix

Reagents	**1 rxn (µl)**	**4 rxns +10% xs (µl)**
Nuclease-free water	9	39
Buffer Sample Clean up 1	182	801
DynaBeads MyOne Silane	4	18
Additive A	5	22
Total Volume	**200**	**880**

After incubation, the tube strip was placed into the 10xTM Magnetic Separator (Cat. #230003) (magnet) in the high position until the solution was clear. The supernatant was carefully removed and discarded and 300µl of 80% ethanol added to wash the

pellet for 30 seconds. This ethanol wash was repeated. Ethanol was carefully removed and the samples allowed to air dry for 1 minute.

The Elution Solution I was prepared using reagents in Table 2-22. The tube strip was removed from the magnet and 35.5µl Elution Solution I was added and mixed thoroughly to fully re-suspend the beads. Beads were incubated for 1 minute then returned to the magnetic separator until the solution was clear. A new tube strip was obtained and 35µl of the purified GEM-RT product was transferred into it.

Table 2-22. Volume of reagents used to prepare the Elution Solution I

Reagents	**1 rxn (µl)**	**4 rxns +10% xs (µl)**
Buffer EB	98	392
10% Tween 20	1	4
Additive A	1	4
Total	**100**	**400**

2.10.8 cDNA Amplification Reaction

A cDNA Amplification Reaction Mix was prepared using reagents in Table 2-23, mixed thoroughly and briefly centrifuged. The Amplification Reaction Mix (65µl) was added to each tube containing 35µl of purified GEM-RvT product, mixed by pipetting 15 times and briefly centrifuged. The capped tube strip was loaded into the thermal cycler and the incubation protocol in Table 2-24 was carried out.

Table 2-23 Volume of reagents used for the cDNA Amplification Reaction Mix

Reagent	**1 rxn (µl)**	**4 rxns + 10% xs (µl)**
Nuclease-free water	8	35
Amplification Master Mix	50	220
cDNA Additive	5	22
cDNA Primer Mix	2	9
Total	65	286

Table 2-24. Temperature cycles for the cDNA Amplification Reaction by PCR

Specifications		
Lid Temperature	**Reaction Volume**	**Run Time**
105°C	100µl	~30-45 mins
Protocol		
Step	**Temperature**	**Time**
1	98°C	3 mins
2	98°C	15 secs
3	67°C	20 secs
4	72°C	1 mins
5	**Go to Step 2 for 15 cycles**	
6	72°C	1 min
7	4°C	Hold

2.10.8.1 Post cDNA Amplification Reaction Cleanup- SPRIselect

To carry out the post cDNA Amplification Reaction Cleanup, the SPRIselect Reagent was vortexed until fully re-suspended and 60µl (0.6x) was added to each sample in the tube strip and mixed. Unless otherwise stated, solutions were mixed gently by pipetting 15 times. The tube strip was incubated for 5 mins at RT and then placed on the magnet until the solution was clear. The supernatant was carefully removed and discarded and 200µl 80% ethanol was added to the pellet for 30 seconds. This ethanol wash was repeated. Ethanol was carefully removed and the samples allowed to air dry for 2 minutes. The tube strip was removed from the magnet and 40.5µl Buffer EB was added, mixed and incubated at RT for 2 minutes. The tube strip was returned to the magnet until the solution was clear and 40µl of the sample transferred to a new tube strip and capped and placed on ice. cDNA concentration and quality was measured using a Qubit Fluorometer.

2.10.9 cDNA Library Construction

2.10.9.1 Fragmentation, End Repair and A-tailing

Before use (>30mins) the Fragmentation Buffer, Ligation Buffer, Adaptor Mix, SI-PCR Primer and ChromiumTM i7 Sample Index Plate were equilibrated to RT. The Fragmentation Enzyme Blend, DNA Ligase and Amplification Master Mix were placed on ice. All reagents used in the following protocol are outlined in Table 2-18.

The Fragmentation Mix was prepared on ice using reagents in Table 2-25, mixed thoroughly and briefly centrifuged then 15µl was added to each well of a new PCR 8-tube strip. To individual wells, 35µl of purified cDNA was added and mixed by pipetting 15 times. The tube strip was placed in a pre-cooled thermal cycler and the incubation protocol in Table 2-26 was carried out.

Table 2-25. Volume of reagents used to prepare the Fragmentation Mix

Reagent	1 rxn (µl)	4 rxns + 10% xs (µl)
Fragmentation Buffer	5	22
Fragmentation Enzyme	10	44
Total	**15**	**66**

Table 2-26. Temperature cycles for Fragmentation, End-Repair and A-tailing

Specifications		
Lid Temperature	**Reaction Volume**	**Run Time**
65°C	50µl	~35 mins
Protocol		
Step	**Temperature**	**Time**
1. Pre-cool block	4°C	Hold
2. Fragmentation	32°C	5 mins
3. End Repair & A-	65°C	30 mins
4. Hold	4°C	Hold

2.10.9.2 Double Sided Size Selection- SPRIselect

The SPRIselect Reagent was vortexed until fully re-suspended and 30µl (0.6x) added to each sample in the tube strip, mixed and incubated at RT for 5 mins. The tube strip was placed on the magnet until the solution was clear. The supernatant (75µl) was

added to a new tube strip and 10µl SPRIselect Reagent (0.8x) was added to each sample, mixed and incubated at RT for 5 minutes. The tube was placed on the magnet until the solution was clear. The supernatant (80µl) was carefully removed and discarded and 125µl 80% ethanol was added to the pellet for 30 seconds. This ethanol wash was repeated twice more. Ethanol was carefully removed and the tube strip was removed from the magnet. Buffer EB (50.5µl) was added, mixed and incubated at RT for 2 minutes. The tube strip was returned to the magnet until the solution was clear and 50µl of sample was transferred to a new tube strip which was capped.

2.10.9.3 Adaptor Ligation

The Adaptor Ligation Mix was prepared by adding the reagents in Table 2-27 and 50µl was added to each tube containing 50µl sample, mixed by pipetting 5 times and briefly centrifuged. The sample was placed in a thermal cycler and the incubation protocol in Table 2-28 was carried out.

Table 2-27. Volume of reagents used to prepare the Adaptor Ligation Mix

Reagent	**1 rxn (µl)**	**4rxns + 10% xs (µl)**
Nuclease-free water	17.5	77
Ligation Buffer	20	88
DNA Ligase	10	44
Adaptor Mix	2.5	11
Total	**50**	**220**

Table 2-28. Temperature cycles for Adaptor Ligation

Specifications		
Lid Temperature	**Reaction Volume**	**Run Time**
30°C	100µl	15 mins
Protocol		
Step	**Temperature**	**Time**
1	20°C	15 mins

2.10.9.4 Post Ligation Cleanup- SPRIselect

The SPRIselect Reagent was vortexed until fully re-suspended and 80µl (0.8x) was added to each sample, mixed and incubated at RT for 5 minutes. The tube strip was placed on the magnet until the solution was clear. The supernatant was carefully removed and discarded and 200µl 80% ethanol was added to the pellet for 30 seconds. This ethanol wash was repeated twice more. Ethanol was carefully removed and the samples allowed to air dry for 2 minutes. The tube strip was removed from the magnet and 30.5µl Buffer EB added, mixed and incubated at RT for 2 minutes. The tube strip was returned to the magnet until the solution was clear and 30µl of the sample was transferred to a new tube strip.

2.10.9.5 Sample Index PCR

A Sample Index PCR Mix was prepared by adding the reagents in Table 2-29, mixed thoroughly and briefly centrifuged and 60µl added to each tube containing 30µl purified Post Ligation sample. To each sample an individual Chromium i7 Sample Index (10µl) was added and the assignment recorded. Samples were mixed by pipetting 15 times, centrifuged briefly and placed in a thermal cycler and the incubation protocol in Table 2-30 was carried out.

Table 2-29. Volume of reagents used to prepare a Sample Index PCR Mix

Reagent	**1 rxn (µl)**	**4 rxns + 10% xs (µl)**
Nuclease-free water	8	35
Amplification Master	50	220
SI-PCR Primer	2	9
Total	**60**	**264**

Table 2-30. Temperature cycles for the Sample Index PCR incubation

Specifications		
Lid Temperature	**Reaction Volume**	**Run Time**
105°C	100µl	~25-40 mins
Protocol		
Step	**Temperature**	**Time**
1	98°C	45 secs
2	98°C	20 secs
3	54°C	30 secs
4	72°C	20 secs
5	Go to Step 2 for 16 cycles	
6	72°C	1 min
7	4°C	Hold

2.10.9.6 Post Sample Index PCR Double Sided Size Selection- SPRIselect

The SPRIselect Reagent was vortexed until fully re-suspended and 60µl (0.6x) was added to each sample, mixed and incubated at RT for 5 minutes. The tube strip was placed on the magnet until the solution was clear. The supernatant (150µl) was carefully removed and transferred to a new tube strip. 20µl SPRIselect Reagent (0.8x) was added to each sample, mixed and incubated at RT for 5 minutes. The tube strip was placed on the magnet until the solution was clear. The supernatant (165µl) was carefully removed and discarded and 200µl 80% ethanol was added to the pellet for 30 seconds. This ethanol wash was repeated twice more. The tube strip was removed from the magnet and 35.5µl Buffer EB added, mixed and incubated at RT for 2 minutes. The tube strip was returned to the magnet until the solution was clear and 35µl of the sample was transferred to a new tube strip and capped. Purified cDNA samples were stored at -20°C.

2.10.9.7 Post Library Construction Quantification

cDNA concentration and quality was measured using the LabChip GX Touch Nucleic Acid Analyser as outlined in section 2.6.4 with assistance from Pamela Brown. cDNA samples met the minimum requirements and were sent to Edinburgh Genomics.

Sections 2.10.7-2.10.10 were carried out with assistance from Dr Beth Henderson, affiliated with Professor Neil Henderson.

2.10.10 10x genomics single cell RNA-seq library sequencing

At Edinburgh Genomics (https://genomics.ed.ac.uk/) quality control of the cDNA libraries was performed and sequence data generated on the Illumina NovaSeq platform using an S1 flowcell using the bespoke 10x parameters (28/8/91 cycle setup) to yield a minimum of 350M reads per library, according to the standard protocols at the facility.

2.10.11 Bioinformatic analysis

An in-house bioinformatic analysis of the samples was carried out by Frances Turner at Edinburgh Genomics and a pdf report outlining the methods used and results was provided. An additional analysis was carried out by Dr Richard Taylor, affiliated with Professor Neil Henderson.

In brief, Commands from 10X Genomics' 'Cellranger' tool (version 2.0.1) were executed as follows: FASTQ files were generated using 'Cellranger mkfastq' specifying 'SI-GA' indices associated with each sample. 'Cellranger count' was performed for each sample, using the 'Cellranger mkfastq' files, the 'SI-GA' indices and the transcriptome 'refdata-cellranger-mm10-1.2.0' as supplied by 10x genomics. An aggregated final dataset was created using the 'Cellranger aggr' command, supplying a .cvs file describing the outputs of 'Cellranger count' and the associated sample groups.

Summary tables of the basic statistics, quality control statistics and mapping statistics were delivered with the pdf report. Other output files included Loupe™ Cell Browser files (files for input to the 10x 'Loupe' browser), clustering analysis results, differential expression analysis results, principle components analysis (PCA) results and t-SNE (t-distributed Stochastic Neighbour Embedding) projection results. Loupe files were analysed on the Loupe™ Cell Browser be the author.

Chapter 3 Investigation of the relationship between tissue resident and transient immune cell populations during endometrial repair

3.1 Introduction

3.1.1 Inflammation and the endometrium

Inflammation is a regulator of normal wound healing in most tissues with macrophages being implicated in regulation of repair processes (Cash and Martin 2016, Vannella and Wynn 2017). Excessive and prolonged inflammation is associated with fibrosis, chronic wounds, abnormal wound healing and deposition of scar tissue (Zhao et al. 2016, Qian et al. 2016). When recruitment of immune cells is ablated in experimental mouse models, for example mice which lack macrophages and neutrophils, rapid and scar-free wound healing of the skin occurs. Notably physiological wound healing of human foetal skin (Martin and Leibovich 2005) and the oral mucosa (Szpaderska et al. 2003) is also scar-free and characterised by a significantly reduced inflammatory component. In contrast, repair of endometrium during menstruation does not fit neatly into these categories as although the tissue undergoes rapid and scar-free wound healing this is accompanied by a substantial inflammatory response characterised by a large number of immune cells (Salamonsen et al. 2002, Kats et al. 2005, Maybin and Critchley 2015). Although menstruation has been cited as 'a model of self-limiting inflammation' by Maybin and Critchley (2015) the role played by these inflammatory processes/immune cells in restoration of tissue homeostasis remains poorly understood.

3.1.2 Immune cells in the endometrium

The endometrium hosts a diverse population of immune cells, the abundance and composition of which changes throughout the menstrual cycle. Some immune cell types can proliferate within the tissue and are considered resident populations, while others are recruited from the circulation in response to chemotactic stimuli (Evans and Salamonsen 2012, Maybin and Critchley 2015). Immune cells are present in relatively low numbers during the proliferative phase but there is a striking increase in leucocyte numbers in both the secretory and menstrual phases of the cycle (Kamat and Isaacson 1987, Salamonsen et al. 2002, King and Critchley 2010, Andreotti et al. 2018).

During the secretory phase there is an increase in the numbers of a unique population of CD56++ natural killer cells (uNK) that play a key role in regulation of vascular remodelling and regulation of menstruation (Bulmer and Lash 2005). These cells appear responsive to steroids (Henderson et al. 2003, Gibson et al. 2015) and some studies have claimed their distribution is altered in women suffering from heavy menstrual bleeding (Biswas Shivhare et al. 2015). Another prominent immune cell population that shows a dramatic change in numbers during the human menstrual cycle are neutrophils which are the most prominent leucocyte present during decidual tissue breakdown (Kamat and Isaacson 1987), reported as 6-15% of total cell number perimenstrually (Lathbury and Salamonsen 2000). In a recent study immunostaining of human endometrial tissue sections using an antibody directed against neutrophil elastase reported immunopostive staining restricted to samples recovered during active menses (Armstrong et al. 2017). Using a mouse model of simulated 'menstruation' Kaitu'u-Lino *et al* used anti Ly6B2 antibodies to identify putative neutrophils and reported they were most abundant at 24h after progesterone withdrawal. They also reported *in vivo* depletion of putative neutrophils using an anti-GR-1 antibody delayed endometrial repair processes suggesting that the neutrophils are essential for endometrial repair (Kaitu'u-Lino et al. 2007).

Macrophages have also been detected in the endometrium throughout the menstrual cycle (Bonatz et al. 1992) with important roles in preparation of the receptive endometrium and subsequent decidualisation of the endometrial stroma being proposed (Lea and Clark 1991, Kats et al. 2005). Given the huge increase in expression of macrophage-derived cytokines and proteases (MMPS) that has been reported in the late secretory phase endometrium, macrophages have also been implicated in the initiation of decidual breakdown (Salamonsen and Woolley 1999, Critchley et al. 2001a). It has been suggested that macrophages, as active phagocytes, could have a role in apoptotic cell clearance and glandular remodelling (Garry et al. 2010). Studies on human endometrium complemented by *in vitro* analysis of macrophages differentiated from peripheral blood monocytes showed they were able to synthesise and release CXCL2 and CXCL8 (Evans and Salamonsen 2012) with these and other results postulating a role in tissue repair (Maybin and Critchley 2012) which required further exploration.

3.1.3 Macrophages and endometrial repair

Macrophages are cells of the innate immune system that derive from myeloid progenitors and are largely responsible for engulfing and destroying pathogens and apoptotic cellular debris (Reviewed by Biswas et al. 2012). In recent years the simple view that all macrophages arise through differentiation of circulating monocytes after they extravasate from the blood stream and enter peripheral tissues (Van Furth and Thompson 1971) has been challenged with data from lineage tracing experiments in mice indicating there are at least three lineages of macrophages arising at varying stages of development from different origins: the yolk sac, the foetal liver and bone marrow (Wynn et al. 2013). Macrophages have been found to be capable of phagocytosis, maintaining tissue homeostasis, regulating wound healing and the function of other immune cell populations (Wynn and Barron 2010). In wound healing in particular, macrophages have several roles including defence against pathogens, clearance of apoptotic cellular debris, regulation of the inflammatory response and support of tissue proliferation and restoration (Mosser and Edwards 2008, Koh and DiPietro 2011). Using an inducible transgenic mouse model (LysM-Cre/DTR), administration of diphtheria toxin was shown to reduce BM-derived macrophage numbers in the skin (CD11b+F4/80^{high} cells) but did not affect circulating monocytes (CD11b+Ly6C^{high} cells). When macrophages were depleted it was reported that skin wounds exhibited both impaired neoangiogenesis and delayed wound closure associated with an increase in neutrophils (Goren et al. 2009). This study suggests that macrophages playing a key role in efficient tissue repair in this species in part due to regulation of neutrophil persistence.

Macrophages identified in human endometrium by immunostaining for CD68 are most abundant during the late secretory and menstrual phases of the cycle (Garry et al. 2010). During the menstrual phase macrophages account for ~10% of cells in the tissue (Nowak, Borkowska and Pawlowski 2016): their presence is paralleled by a marked increase in immunoexpression of CXCL2 (Evans and Salamonsen 2012). It has also been postulated that macrophages in the decidua can secrete both pro- and anti-inflammatory cytokines which may represent a phenotype unique to the endometrial tissue (Houser et al. 2011). In the endometrium of normal cycling mice, F4/80 immunopositive macrophages were located throughout the stroma (Shimada-

Hiratsuka et al. 2000, Mackler et al. 2000). Using a mouse model of simulated 'menstruation' it was reported that F4/80 expressing macrophages do not associate with areas undergoing tissue remodelling but instead were located distal to the lumen and the authors concluded that macrophages did not contribute to endometrial repair (Kaitu'u-Lino et al. 2007). It is therefore a subject of debate whether macrophages have a role in endometrial tissue repair.

3.1.4 Importance of understanding macrophage contribution to endometrial repair

Abnormalities in endometrial repair processes are thought to underpin a number of gynaecological pathologies including heavy menstrual bleeding. Women with HMB most often complain of unscheduled bleeding which is thought to be due to problems in the differentiation of the endometrial tissue and its associated vasculature (Maybin and Critchley 2011, Munro et al. 2011). Clark *et al*, 1996 found that there was an increase in the number of macrophages in the endometrium of women presenting with unscheduled bleeding (Clark et al. 1996). Endometriosis is a condition where endometrial-like tissue embeds in regions out with the uterus causing pelvic pain and infertility (Giudice 2010). Bacci *et al*, 2009 reported that macrophages in patients with endometriosis were alternatively activated and likely to support lesion growth (expressed high levels of CD163/CD206). When macrophages were depleted using clodronate liposomes, blood vessels did not populate the lesions which substantially reduced their growth. Additionally, the adoptive transfer of alternatively activated BM-derived macrophages (mouse) enhanced lesion formation in mice while classically activated macrophages impaired lesion establishment (Bacci et al. 2009). In another study using a syngeneic mouse model of endometriosis in combination with MacGreen reporter mice as donors and recipients Greaves *et al* reported that macrophages from both the peritoneum and donor (menses) endometrium can contribute to lesions (Greaves et al. 2014). Similarly, endometrial cancer is the most common gynaecological cancer in the UK (Ryan et al. 2005) and tumour tissue has been shown to be infiltrated with pro-tumorigenic macrophages which may enhance tumour angiogenesis (Sivridis et al. 2002, Harris et al. 2007).

In each of these conditions a link to the malfunction of macrophage behaviour has been suggested and characterisation of macrophage phenotype and function in physiological

endometrial repair may therefore inform understanding of normal tissue regulation. This may lead to the development of therapies to manage or treat such gynaecological conditions. Further to this, if the contribution of macrophages to scarless wound healing can be determined, then the macrophage population in tissues suffering from chronic inflammation might be a target to induce scarless healing in other tissues.

3.1.5 Transgenic mouse lines to study macrophages

A variety of cell surface markers are used in the identification of myeloid immune cells. In the MacGreen (Sasmono et al. 2003, Sasmono and Williams 2012) and MacApple (Hawley et al. 2018) transgenic reporter mice, eGFP and RFP (respectively) are expressed under control of the *Csf1r* gene promoter, though the insertion locus of the transgene is slightly different for each. CSF1R is a tyrosine-protein kinase that acts as a cell surface receptor for CSF1 and IL34 and regulates proliferation, differentiation and survival of haematopoietic precursor cells, in particular mononuclear phagocytes including monocytes and macrophages (Sasmono and Williams 2012). Therefore these transgenic mice were considered suitable to identify and characterise sub-populations of mononuclear phagocytes in endometrial tissue. In addition the CD68eGFP transgenic reporter mouse was also used, in these mice eGFP is expressed under control of the human CD68 gene promoter (Iqbal et al. 2014). CD68 is a transmembrane glycoprotein highly expressed by monocytes and tissue macrophages (Iqbal et al. 2014) thought to be involved in phagocytic activity, and therefore this mouse line offers an additional way to target mononuclear phagocytes in the endometrium using a discrete marker system.

3.1.6 Summary

Menstruation in women involves concurrent shedding and repair of the inner lining of the endometrium (Garry et al. 2009) and is associated with an increase in both immune cells and inflammatory mediators. Endometrial macrophages are reported to be abundant in endometrial tissue during menstruation but their role if any in regulating repair is not well understood. Tissue resident populations of macrophages exhibit diverse phenotypes depending upon their localisation and we therefore postulated that an in-depth characterisation of endometrial macrophage phenotype and location could lead to new insights into the role of macrophages in the regulation of endometrial tissue repair and scarless healing.

3.2 Aim

To characterise the myeloid immune cell populations in endometrial tissue and to investigate changes in phenotype and location during endometrial tissue repair using a mouse model of endometrial breakdown and repair.

3.3 Experimental Approach

3.3.1 Mouse model of endometrial breakdown and repair

The Edinburgh menses mouse model established and refined in the Saunders' group (Cousins et al. 2014), was used to investigate the dynamic changes in immune cell populations in endometrial tissue during a defined period that included breakdown, repair and restoration of homeostasis (0-48hrs after progesterone withdrawal. The full protocol is outlined in Section 2.2.2 and described in Table 2-4 and Figure 2-5.

3.3.2 Transgenic mouse lines

The results in this chapter were generated using the MacGreen, MacApple and CD68-eGFP reporter mouse lines as detailed in Sections 2.1.1.2, 2.1.1.3 and 2.1.1.4 respectively, to specifically identify cells of the myeloid lineage in endometrial tissue.

3.3.3 Tissue processing and immunohistochemistry

Uterine tissue samples were fixed in 4% PFA for 2 hrs at 4°C, rinsed in PBS and stored overnight in 18% sucrose at 4°C before being embedded in OCT medium and stored at -80°C, as described in Section 2.3. H&E staining and IHC was carried out as in Section 2.4.1 and 2.4.3 respectively. Antibodies used for IHC in this Chapter are outlined in Table 3-1. Images were obtained by both brightfield and confocal microscopy as in Section 2.4.4.

Table 3-1. Antibodies used in IHC to interrogate immune cell populations in mouse endometrial tissue

Antibody Name	Supplier and Cat. No. (concentration)	Dilution	Serum block
Polyclonal rabbit anti-GFP	Abcam, ab6556 (0.5mg/ml)	1/1000	Goat
Polyclonal rabbit anti-Mcsf (Csf1r)	Abcam, ab21544 (1mg/ml)	1/500	Horse
Monoclonal rat anti-CD45	ThermoFisher Scientific 14-0451-81 (0.5mg/ml)	1/500	Goat
Monoclonal rat anti-F4/80	eBioscience, 14-4801 (0.5mg/ml)	1/2000	Goat
Rabbit anti-cleaved caspase 3 (Asp175)	Cell Signalling Technology, #9661S (0.25mg/ml)	1/600	Goat
Rabbit anti-CD11b (clone EPR1344)	Abcam, 133357	1/1000	Goat
Polyclonal rat anti-GR1	AbD Serotec, MCA2387PET	1/500	Goat

3.3.4 Flow Cytometry and FACS

Flow cytometry analysis was used to interrogate the phenotype and proportions of immune cell populations in endometrial tissue using protocols detailed in Section 2.5 and flow cytometry antibodies outlined in Table 3-2. Specific immune cells were isolated from the endometrial tissue using FACS according to the protocol detailed in Section 2.5.3. ICC was carried out as in Section 2.5.4 to confirm their identity.

Table 3-2. Flow cytometry antibody panel designed to interrogate myeloid immune cell populations in uterine tissue

Antibody name	Supplier Cat. No. (concentration)	Excitation wavelength	Emission wavelength	Dilution
V450 anti-mouse CD45	Fischer scientific, BDB560501 (0.2mg/ml)	404nm	448nm	1/100
PE anti-mouse Gr1	Abd Serotec, MCA2387PET	496nm	578nm	1/20
APC anti-mouse F4/80	Bio-rad, MCA497APC	650nm	660nm	1/20
BV605 anti-mouse Ly6C	BioLegend, 128035 (0.2mg/ml)	405nm	603nm	1/100
AF488 anti-mouse Cd68	BioLegend, 137011 (0.2mg/ml)	495nm	519nm	1/100
BV650 anti-mouse	BioLegend 107641 (0.2mg/ml)	407nm	650nm	1/100

3.3.5 RNA extraction and cDNA synthesis

RNA was extracted from isolated cell samples using the Qiagen RNeasy mini kit as outlined in Section 2.6.1 followed by synthesis of cDNA using the standard method as in Section 2.7.1.

3.3.6 Quantitative real time PCR

Quantitative real time PCR (qPCR) was used to determine mRNA expression of specific genes used to characterise immune responses and immune cell phenotypes as detailed in Section 2.8 using primers detailed in Table 2-17. Quantification of gene expression and statistical analysis was performed as outlined in Section 2.8.3.

3.4 Results

3.4.1 Validation of transgenic mouse lines by IHC: MacGreen, MacApple and CD68-eGFP

3.4.1.1 Expression of reporter proteins in MacGreen, MacApple and CD68-eGFP transgenic mouse endometrium

IHC on fixed tissue sections was used to detect the expression of specific antigens on immune cells within the endometrial stroma. To validate each of the transgenic mouse reporter lines (MacGreen, MacApple and CD68-eGFP) the expression of the fluorescent reporter proteins (GFP/RFP) and the native proteins (CSF1R/CD68) was examined in adult uterine tissue sections. In the MacGreen uterus, cells that expressed GFP were dispersed throughout the endometrial stroma and GFP co-localised with expression CSF1R protein (Figure 3-1, arrows). Similarly in the MacApple uterus, cells that expressed RFP were dispersed throughout the stroma and co-localised with expression CSF1R protein (Figure 3-2, arrows). The results from these two transgenic lines appeared identical confirming that the different locus of insertion of the reporter gene had no impact on CSF1R promoter activity and appropriate expression of the reporter proteins.

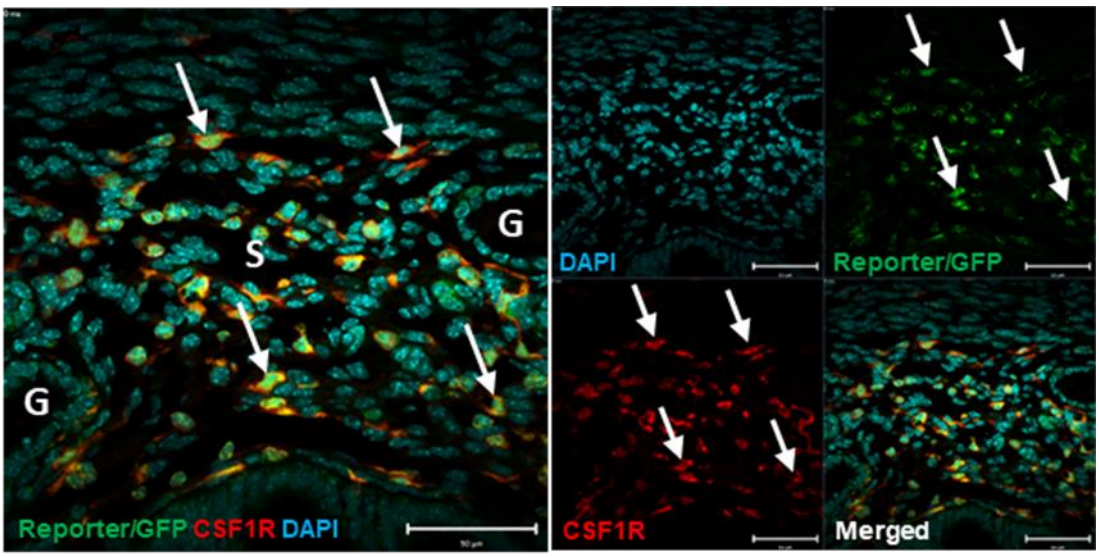

Figure 3-1. Expression of GFP and CSF1R in naïve MacGreen uterine tissue. IHC reveals the expression of the reporter GFP (green) reliably identifies cells that express CSF1R (red) in MacGreen transgenic uterine tissue. GFP/ CSF1R double positive cells (white arrows) are located throughout the endometrial stroma of uterine tissues. Stroma (S), glands (G) (representative image, n=10).

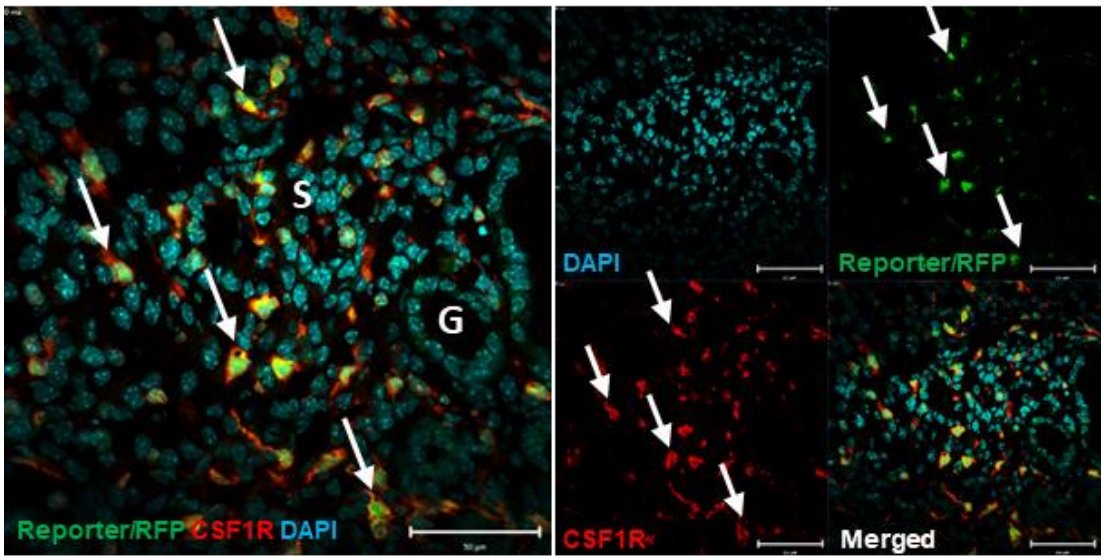

Figure 3-2. Expression of RFP and CSF1R in naïve MacApple uterine tissue. IHC reveals the expression of the reporter GFP (green) reliably identifies cells that express CSF1R (red) in MacApple transgenic uterine tissue. GFP/ CSF1R double positive cells (white arrows) are located throughout the endometrial stroma of uterine tissues. Stroma (S), glands (G) (representative image, n=6).

In CD68-eGFP uterine tissue cells that expressed GFP co-expressed CD68 protein and were dispersed throughout the endometrial stroma (Figure 3-3, arrows) however the staining pattern of the GFP reporter was less distinct than that of MacGreen and MacApple tissues. In this line, it appeared that there were also some reporter+ cells that did not express CD68 (yellow arrows) which may be indicative of background staining due to non-specific reporting. With this in mind, it was concluded that the MacGreen and MacApple lines showed the most reliable reporting of the antigen of interest and since both are based on expression of CSF1R, the MacGreen mouse was chosen for preliminary investigation of mononuclear phagocytes in the endometrium.

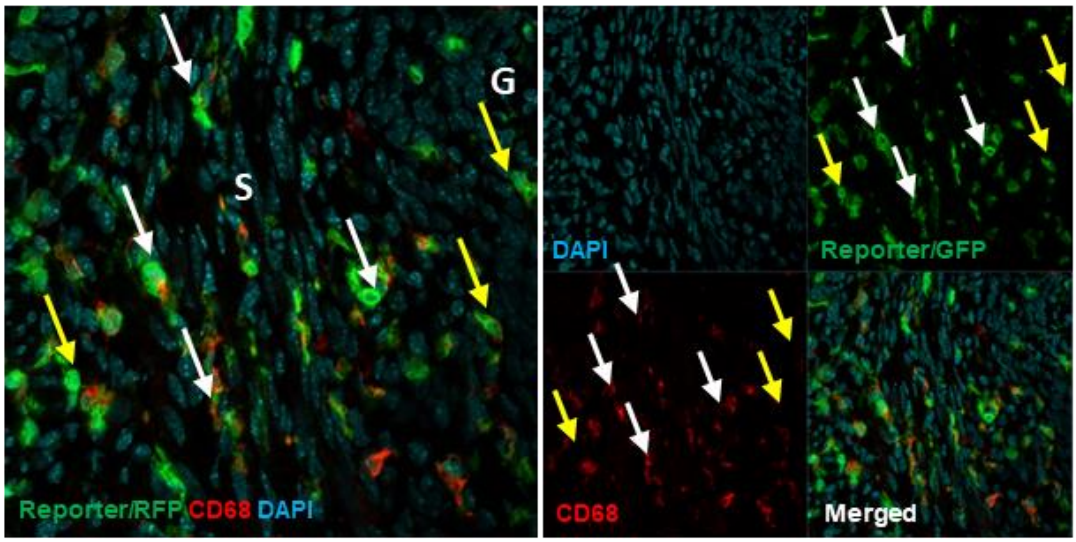

Figure 3-3. Expression of GFP and CD68 in naïve cD68-eGFP uterine tissue. Immunohistochemistry reveals the expression of the reporter GFP (green) identifies cells that express CD68 (red) in CD68-eGFP transgenic uterine tissue. GFP/CD68 double positive cells (white arrows) are located throughout the endometrial stroma of uterine tissues. Cells that express the GFP reporter but not CD68 were also identified (yellow arrows). Stroma (S), glands (G) (representative image, n=4).

3.4.2 Characterisation of myeloid immune cell populations in MacGreen uterine tissue

3.4.2.1 Expression of myeloid cell markers by GFP+ cells in MacGreen uterine tissue

Having established that all GFP+ cells in MacGreen uterus were CSF1R+ and therefore of the myeloid lineage, additional IHC was performed to analyse the expression of other immune cell surface markers CD45, GR1 and CD11b to further characterise the GFP+ cells in uterine tissues from naive MacGreen mice. In line with expectations, all GFP+ cells were CD45+ (Figure 3-4 (A) white arrows). CD45, lymphocyte common antigen, is expressed on all leucocytes (Martin and Leibovich 2005) and therefore the additional presence of GFP-CD45+ cells (Figure 3-4 (A) yellow arrows) was likely to be identifying other immune subtypes in the tissue. Similarly all GFP+ cells were CD11b+ (Figure 3-4 (B) white arrows). CD11b is an integrin involved in various cellular interactions between monocytes, macrophages, granulocytes and other cells and is believed to have a role in phagocytosis (Schulz et al. 2012), therefore the presence of this protein identified GFP+ cells as mononuclear phagocytes.

Interestingly when tissues were stained with an antibody specific for GR1, a granulocyte-associated marker (Yang et al. 2014), two populations were detected. Whilst some cells were GFP+ GR1+ there were also GFP+ GR1- cells (Figure 3-4 (C), white versus yellow arrows). In addition, a sub-population of GFP- GR1+ cells were also detected (Figure 3-4 (C), red arrows). The Gr1 antigen is composed of both Ly6C and Ly6G proteins which are expressed individually by monocytes and neutrophils respectively (Yang et al. 2014, Rose, Misharin and Perlman 2012) therefore it is likely that heterogeneity in expression of Gr1 with respect to GFP expression is related to the identification of different cells types: GFP+ GR1+ monocytes, GFP+ GR1- monocyte/macorphages and GFP- GR1+ neutrophils.

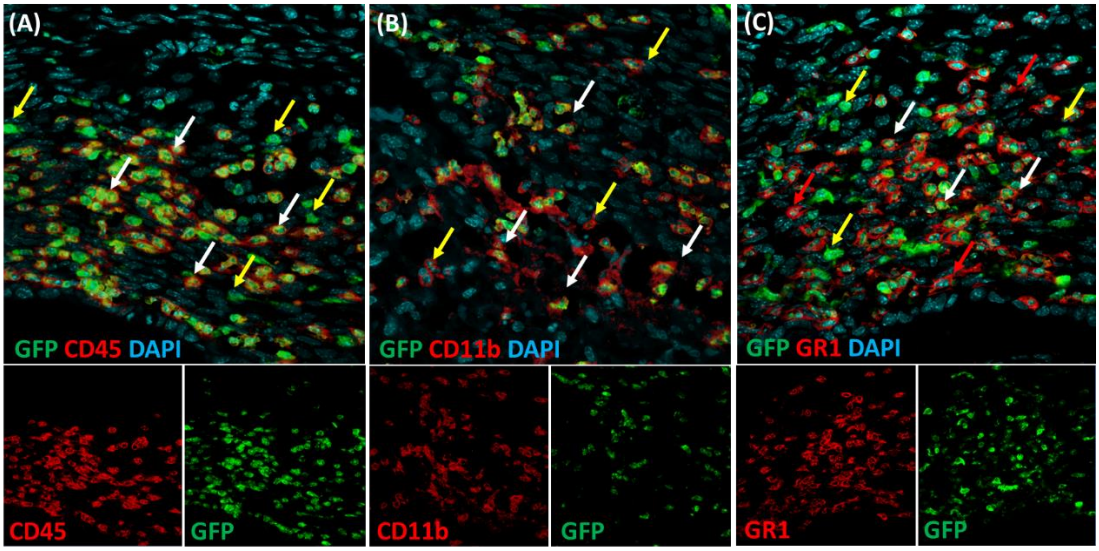

Figure 3-4. The expression of GFP, CD45, GR1 and CD11b in MacGreen uterine tissue. **(A)** Staining for GFP (green) and CD45 (red) identifies GFP+CD45+ cells (white arrows) and GFP-CD45+ cells (yellow arrows). **(B)** Staining for GFP (green) and CD11b (red) identifies GFP+CD11b+ cells (white arrows) and GFP-CD11b+ cells (yellow arrows) **(C)** Staining for GFP (green) and Gr1 identifies GFP+Gr1+ cells (white arrows) GFP+Gr1- cells (yellow arrows) and GFP-Gr1+ cells (red arrows) (representative images, n=4).

3.4.2.2 Expression of myeloid cell markers by GFP+ cells in MacGreen and CD68-eGFP uterine tissues identified by flow cytometry

To further characterise and to quantify GFP+ cell sub-populations in the endometrium, MacGreen and CD68-eGFP uterine tissues were digested and analysed by flow cytometry. Cells were sequentially gated to be within the 'All cells' gate followed by the 'Single cells' gate and then the 'Live' gate as detailed in Figure 3-5 (A). Cells were further analysed for expression of GFP, CD45 and CD11b. In MacGreen and CD68-eGFP uterine tissues GFP+ cells accounted for approximately 49.3±9.38% and 53.1±10.23% of the CD45+ immune cell populations respectively, and all GFP+ cells were CD45+ (Figure 3-5 (B) (D) respectively, upper right quadrant). Furthermore 93.1±3.03% and 98.1±1.23% of GFP+ cells in MacGreen and CD68-eGFP uterine tissues respectively were CD11b+ (Figure 3-5 (C) (E) respectively). Flow cytometry analysis was performed using analytic gates based on an unstained, single stain controls and FMO (fluorescence minus one) controls. Flow cytometry results were in agreement with results of IHC (Figure 3-4) confirming a comparable identity of GFP+ cells in both MacGreen and CD68-eGFP uterine tissues as mononuclear phagocytes.

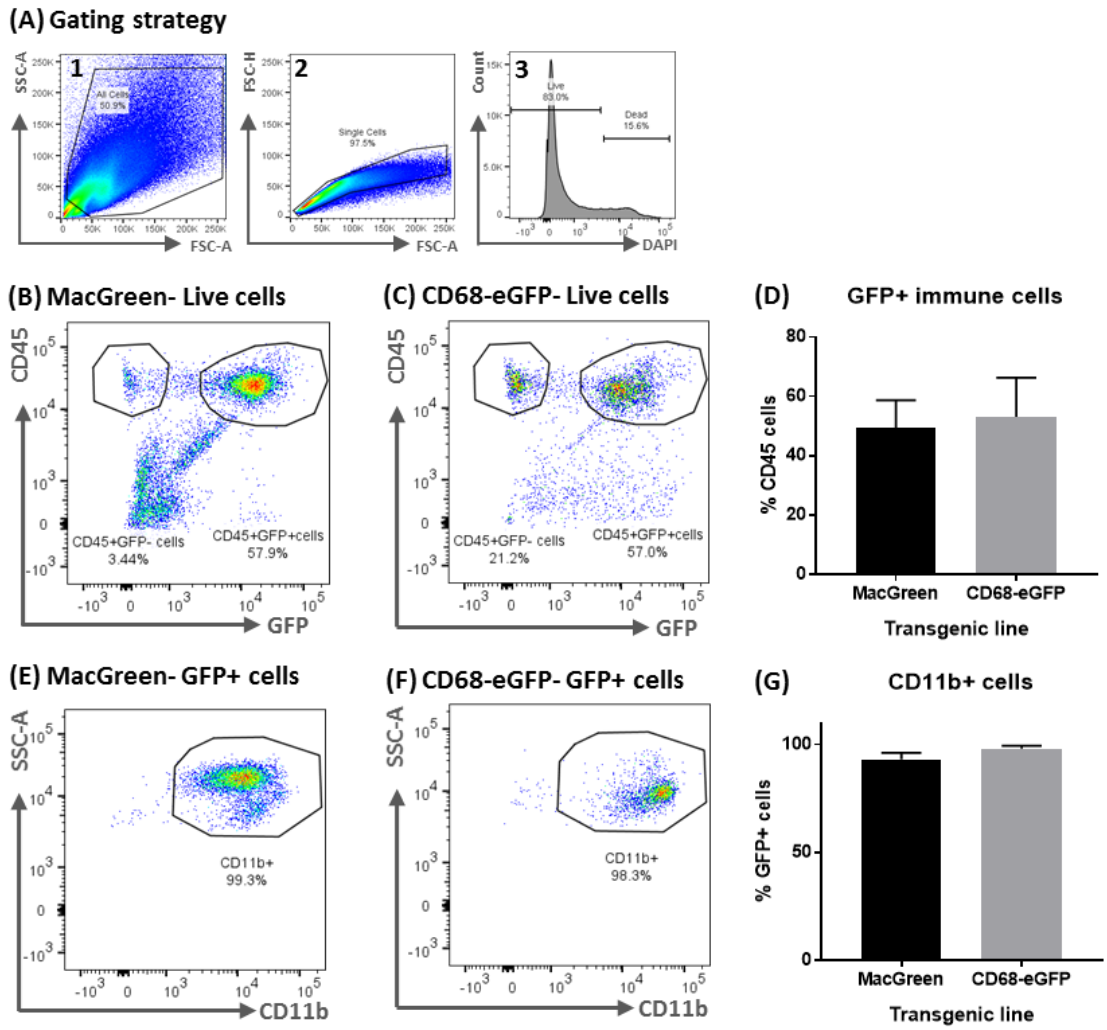

Figure 3-5. Flow cytometry analysis and phenotyping of GFP+ cell populations in naïve MacGreen and CD68-eGFP uterine tissues. (A) Gating strategy employed to analyse GFP+ cell populations in naïve mouse uterine tissue: 1. All cells > 2. Single cells > 3. Live cells > CD45+GFP+ cells > CD11b+ cells, percentages displayed are frequencies of the parent gate. All gates drawn using single stained, unstained and FMO control samples. The proportion of CD45+ leucocytes that are GFP+ in naïve **(B)** MacGreen and **(C)** CD68-eGFP uterine tissues. **(D)** Approximately 49.3±9.38% and 53.1±10.23% of the CD45+ immune cell population is GFP+ in naïve MacGreen and CD68-eGFP uterine tissues respectively. The proportion of GFP+ cells that express CD11b in naïve **(E)** MacGreen and **(F)** CD68-eGFP uterine tissues. (G) Approximately 93.1±3.03% and 98.1±1.23% of GFP+ cells in naïve MacGreen and CD68-eGFP uterine tissues respectively are CD11b+ (representative plots, MacGreen; n=4, CD68-eGFP; n=5).

3.4.2.3 Assessment of morphology of GFP+ cells isolated from MacGreen uterine tissue by FACS

Following analysis by Flow cytometry, the optimised parameters were used to isolate CD45+GFP+ cells from MacGreen uterine tissue by FACS. To confirm the identity of the cells, a cytospin was performed on the isolated cells which were then fixed and stained by H&E or IHC using an antibody against GFP. Isolated cells were found to be mononuclear by H&E (Figure 3-6 (A)) and confirmed to express GFP reporter protein by IHC (Figure 36 (B)) further supporting the identity of the GFP+ cells in the naïve mouse endometrium as mononuclear phagocytes.

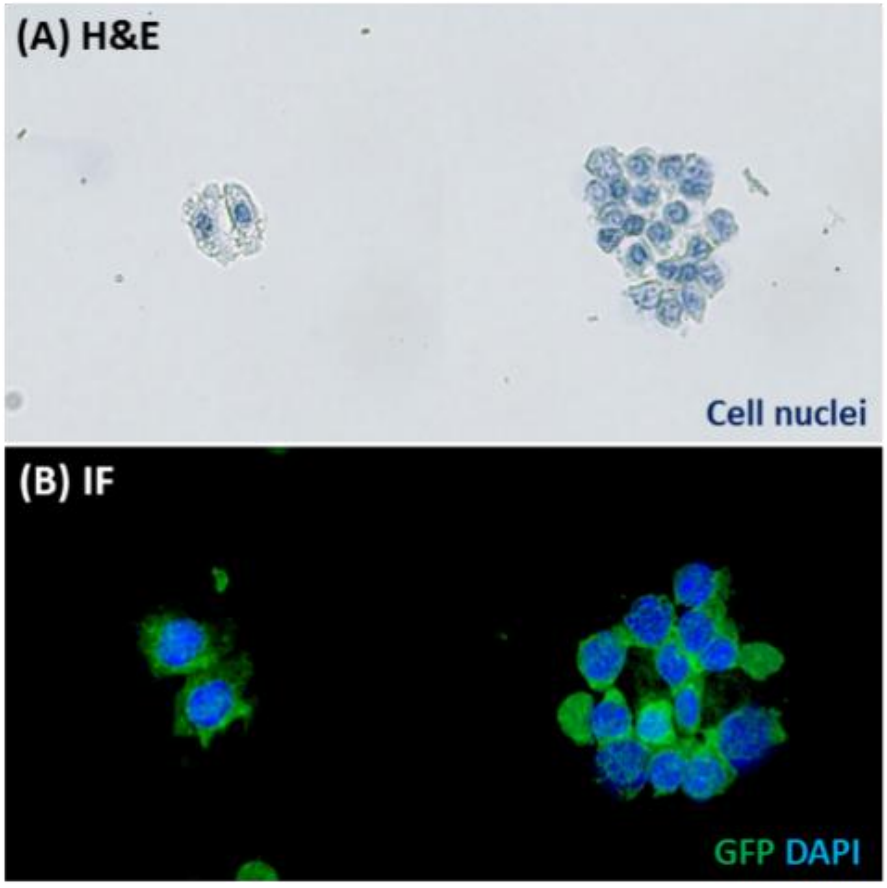

Figure 3-6. Investigation of cell morphology of CD45+GFP+ immune cells isolated from naïve MacGreen uterine tissue. (A) H&E staining of CD45+GFP+ cells indicate the cells are mononuclear. **(B)** IHC of CD45+GFP+ cells show expression of reporter protein GFP (representative images, n=3).

3.4.3 Investigation of myeloid immune cell populations during endometrial breakdown and repair

3.4.3.1 Distribution of GFP+ cells in MacGreen endometrial tissue at various time points during endometrial tissue breakdown and repair

To investigate immune cell dynamics during endometrial repair processes, IHC was used to assess the distribution of GFP+ cells in uterine tissue from MacGreen transgenic mice recovered across the time course of endometrial breakdown and repair (0, 12, 24 and 48hrs). Before tissue breakdown (before P4 withdrawal; 0hrs) very few GFP+ cells were present in the tissue (Figure 3-7 (A), arrows) suggesting that an inflammatory response had not been stimulated. During active tissue breakdown at 12hrs there was a striking increase in the number of GFP+ cells (Figure 3-7 (B), arrows) which were predominantly detected in the endometrial stromal layer in close proximity to the border of decidualised tissue that was undergoing tissue breakdown (Figure 3-7 (B), blue dashed line).

At 24hrs when the endometrial tissue was undergoing synchronous tissue breakdown and repair, an abundance of GFP+ cells was detected in the tissue (Figure 3-7 (C), arrows). Examination of multiple tissue sections generated from different blocks/mice revealed that the majority of the GFP+ cells were located in regions undergoing repair but with some cells also present in the shed tissue (Figure 3-7 (C) arrows) suggesting the cells may have dual roles to play in this process. At 48hrs when tissue repair was complete detected by the fully re-epithelialised lumen (L in Figure 3-7 (D)), there were very few GFP+ cells detected in the endometrial tissue (Figure 3-7 (D), arrows) but a few were present in the shed tissue (Figure 3-7 (D), blue dashed line).

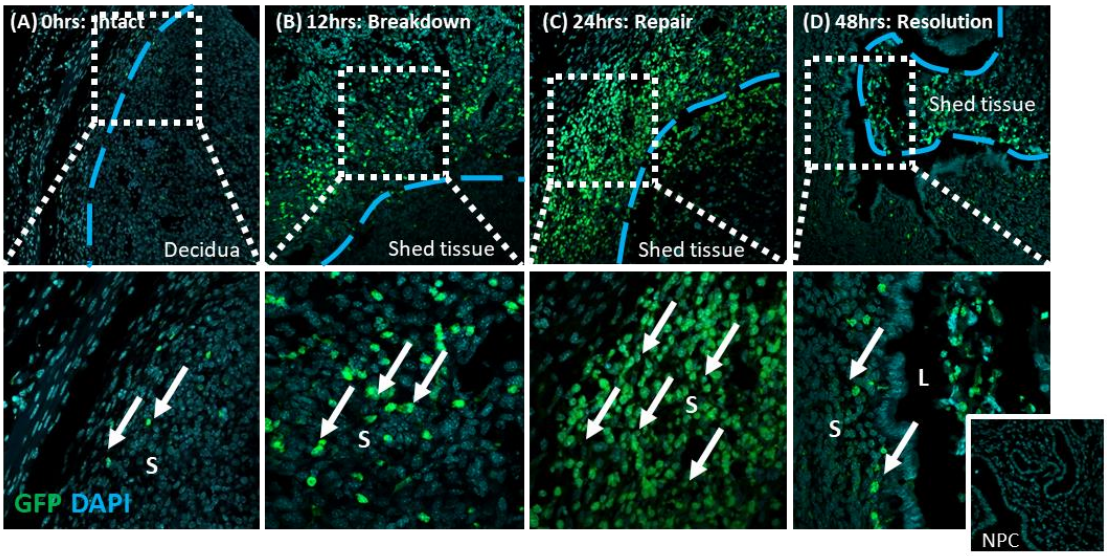

Figure 3-7. Distribution of GFP+ immune cells in MacGreen uterine tissue during endometrial breakdown and repair. IHC reveals dynamic changes in the location and number of GFP+ cells (white arrows) prior to endometrial breakdown (0hrs), during endometrial breakdown (12hrs), and during endometrial repair (24hrs) and the remodelling phases (48hrs). The blue dashed line represents the boundary between decidualised endometrial tissue/shed tissue and the underlying layer of residual endometrial stroma. Stroma (S), lumen (L) (representative image, n=10).

3.4.3.2 Quantification of GFP+ cells in MacGreen endometrial tissue at 24hrs following P4 withdrawal during active tissue repair

As results presented above showed that GFP+ immune cells were most abundant in uterine tissue collected 24hrs following P4 withdrawal (Figure 3-7) further analysis was carried out by flow cytometry at this time point (tissue samples as above). Cells were gated to be within the 'All cells' gate followed by the 'Single cells' gate and then the 'Live' gate as described previously (Figure 3-5 (A)). Analysis of the side scatter profile and GFP expression by live single cells confirmed that whilst there were very few GFP+ cells present in the non-decidualised control uterine horns, i.e. tissue stimulated by hormones but not exposed to oil (Figure 3-8 (A)) there was a prominent GFP+ population in the actively repairing (decidualised) endometrial tissue samples (Figure 3-8 (compare A with B)). The proportion of GFP+ cells in the repairing tissues (24hrs, n=8) accounted for 23.36±3.5% of the live cells whilst in the control tissue (adjacent undecidualised horn) they accounted for only 0.66±0.21% (mean±SEM).

This striking increase in GFP+ cells was significant as determined using an unpaired t-test giving a p value of 0.0033 (Figure 3-8 (C)).

Further phenotyping of the GFP+ cells by analysing expression of F4/80 (a mature macrophage marker) revealed that in naïve endometrial tissue the majority of GFP+ cells were F480+ while there was also a population of GFP-F4/80+ cells (Figure 3-8 (D) Q2 and Q1 respectively). In repairing tissues (24hrs) there was a shift in populations with the majority of the GFP+ cells being F4/80- (Figure 3-8 (E) Q3) and an apparent increase in the numbers of GFP+F4/80+ cells, which appeared to be composed of two subpopulations: $F4/80^{high}$ and $F4/80^{low}$ (Figure 3-8 (E) Q2). There was also a GFP-F4/80+ cell population present in the repairing tissue (Figure 3-8 (E) Q1). Analysis of this additional flow cytometry data confirmed that there was a highly significant increase in GFP+F4/80- cells (16.83±3.27% versus 0.10±0.02%, $p<0.0001$) as well as an increase in GFP+F4/80+ cells (7.35±0.59% versus 1.27±0.15%, $p=0.016$) in the repairing (n=7) versus the non-repairing (n=4) uterine horns. In contrast there is no significant change in the GFP-F4/80+ cell population (0.20±0.06% versus 0.93±0.08%, $p=0.99$) (one-way ANOVA, Sidak's multiple comparisons test) (Figure 3-8 (F)).

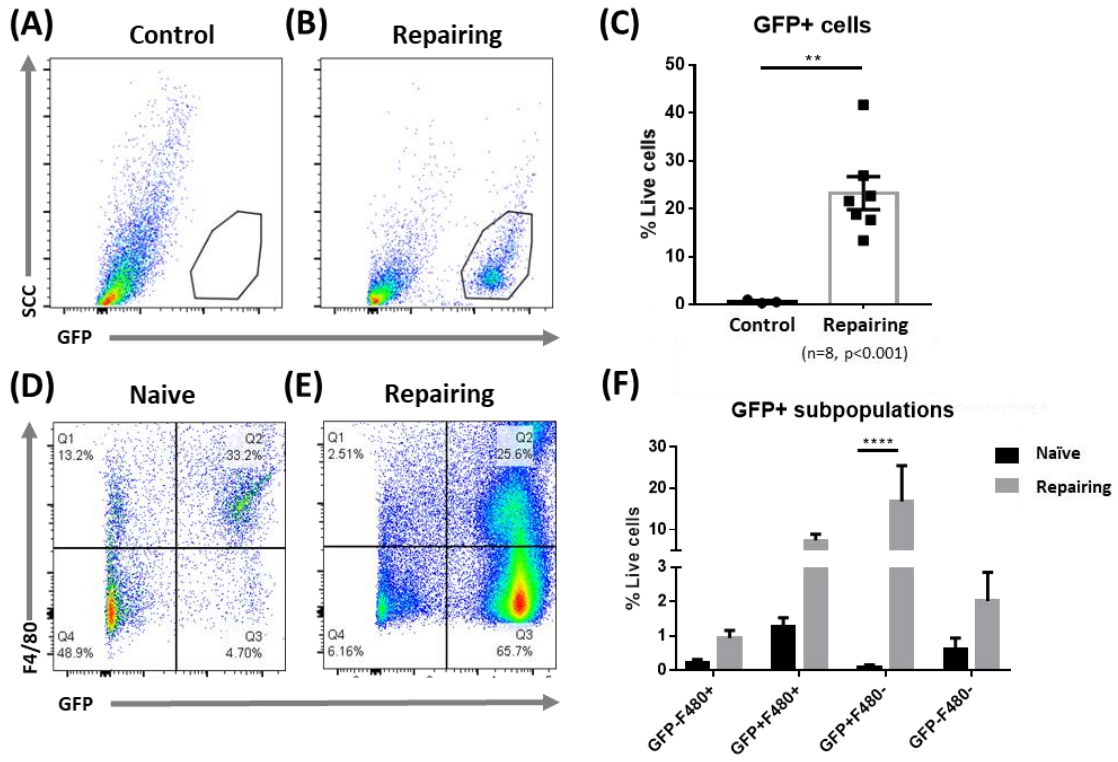

Figure 3-8. Characterisation of GFP+ immune cell populations in MacGreen uterine tissues recovered from control (non-decidualised), naïve and repairing (decidualised) horns 24hrs following progesterone withdrawal by flow cytometry. (A-B) Very few GFP+ cells were detected in the control horns whereas they were abundant in the repairing tissue. **(C)** Summary data showed GFP+ cells represent around 0.66±0.21% of live singlets in control tissue but this increases to 23.36±3.5% of live singlets in repairing tissues (n=8, p<0.001). **(D-E)** The expression of the mature macrophage marker F4/80 was assessed in both naïve and repairing tissues. Three subpopulations of cells were identified: GFP+F4/80- cells (Q3); GFP+F4/80+ cells (Q2); and GFP-F4/80 (Q1), distributed differently when comparing niave and repairing samples. **(F)** Quantification of data showed that the majority of influxing GFP+ cells are F4/80- (~60%) while the remaining cells are F4/80+ (~30%). F4/80+GFP- cell populations were unchanged in niave and repairing tissues (data presented as mean±SEM, representative plots, control: n=4, repairing: n=7).

3.4.3.3 Distribution of GFP and F4/80 expressing immune cell populations in MacGreen uterine tissue at 24hrs

To examine the distribution of discrete immune cell subpopulations as defined by flow cytometry in repairing endometrial tissue, IHC was used to stain MacGreen uterine sections (24hrs after P4 withdrawal) for both GFP and F4/80. Results confirmed the presence of three subpopulations based on these two markers and revealed different patterns of distribution within the repairing tissue (Figure 3-9). GFP+F4/80- cells were

clustered mainly in the shed tissue (Figure 3-9 (A) white arrows) but also abundant in the residual stromal layer (Figure 3-9 (B-C) white arrows). GFP+F4/80+ cells were solely located in the residual stromal layer undergoing tissue repair and not in the shed tissue nor in regions of the tissue already re-epithelialised/repaired (Figure 3-9 (B-C), yellow arrows). In contrast GFP-F4/80+ cells were found to be dispersed throughout the endometrial tissue and the myometrium, seemingly irrespective of regions associated with tissue breakdown and repair (Figure 3-9 (B-C), arrow heads).

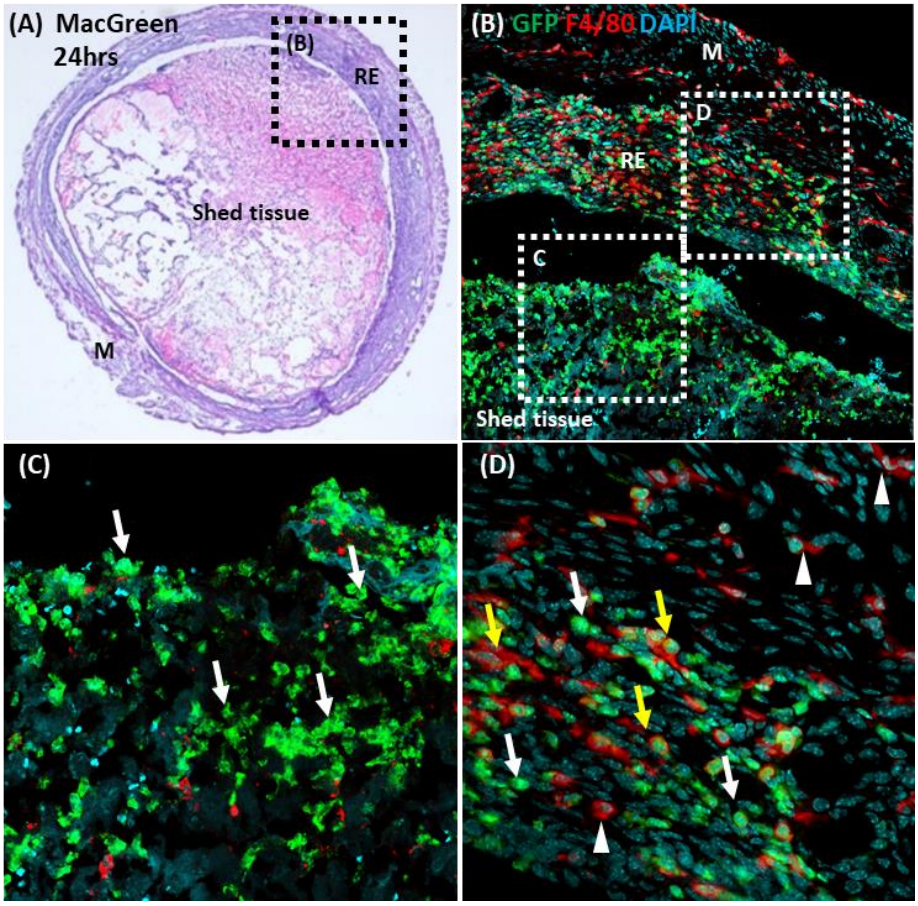

Figure 3-9. Distribution of GFP and F4/80 expressing immune cell populations in MacGreen uterine tissue 24hrs following progesterone withdrawal. (A) H&E cross section of a fully decidualised and actively repairing uterine horn with shed tissue undergoing breakdown in the centre: myometrium (M), residual endometrium (RE). **(B)** IHC looking at the distribution of cells expression GFP and/or F4/80 reveals that **(C)** an influx of GFP+F4/80- cells (white arrows) clustered in regions of shed tissue undergoing breakdown and **(D)** GFP+F4/80+ cells (yellow arrows) are solely located in the underlying residual endometrial layer undergoing active tissue repair. GFP-F4/80+ cells (white arrow heads) are dispersed throughout the residual endometrium and myometrium irrespective of regions associated with tissue breakdown and repair (representative image, n=10).

3.4.3.4 Distribution of subpopulations of GFP and F4/80 expressing immune cells in MacGreen endometrial tissue at various time points of endometrial tissue breakdown and repair

Having identified a heterogeneous population of GFP and F4/80 expressing immune cells in actively repairing tissue (24hrs), the spatio-temporal distribution of these cells was investigated using dual fluorescence across the time course of tissue repair (0-48hrs). At 0hrs (before tissue breakdown) very few GFP+F4/80- cells were present in the tissue and these were only detectable in association with blood vessel structures and not integrated into the tissue (Figure 3-10 (A), white arrows). At this time point GFP-F4/80+ cells were abundant and dispersed throughout the basal layer of endometrium but not so prominent in the decidualised tissue (Figure 3-10 (B), arrows heads). At 12hrs, during active tissue breakdown, these two cell populations were still detectable however there was a greater proportion of GFP+F4/80- cells detectable which appeared to be clustering predominantly near regions of decidual tissue breakdown (Figure 3-10 (C), white arrows). Notably, at this time point the GFP-F4/80+ cell population appeared to be unchanged and was still dispersed throughout the residual endometrium and myometrium (Figure 3-10 (D), arrow heads).

As above, during active tissue repair at 24hrs there was a visible increase in the GFP+F4/80- cells detected in both regions of active breakdown in shed tissue and active tissue repair (Figure 3-10 (E), white arrows). Notably there was also an increase in GFP+F4/80+ cells at 24hrs which had not been detected at earlier time points and these were solely located in the residual endometrium undergoing tissue repair (Figure 3-10 (E), yellow arrows). In the same tissue, but in regions of resolved repair (intact epithelium) there were very few GFP+F4/80+ cells although GFP+F4/80- cells were detected (Figure 3-10 (F), white arrows and white arrow heads respectively). Throughout the tissue GFP-F4/80+ cells were detected and these were distributed as in naive tissues and in tissues from the other time points (Figure 3-10 (F), arrows heads), suggesting they were relatively homeostatic. At 48hrs when tissue repair was complete (intact lumen), there were few detectable GFP+F4/80- cells (shed tissue) and GFP+F4/80+ cells while there was still a prominent GFP-F4/80+ cell population distributed throughout the residual endometrium (Figure 3-10 (G-H)). These IHC results show dynamic changes in the number and location of immune cell populations

during endometrial repair and suggested that GFP+F4/80- monocytes and GFP+F4/80+ monocyte-derived macrophages may have an important role to play in endometrial tissue repair.

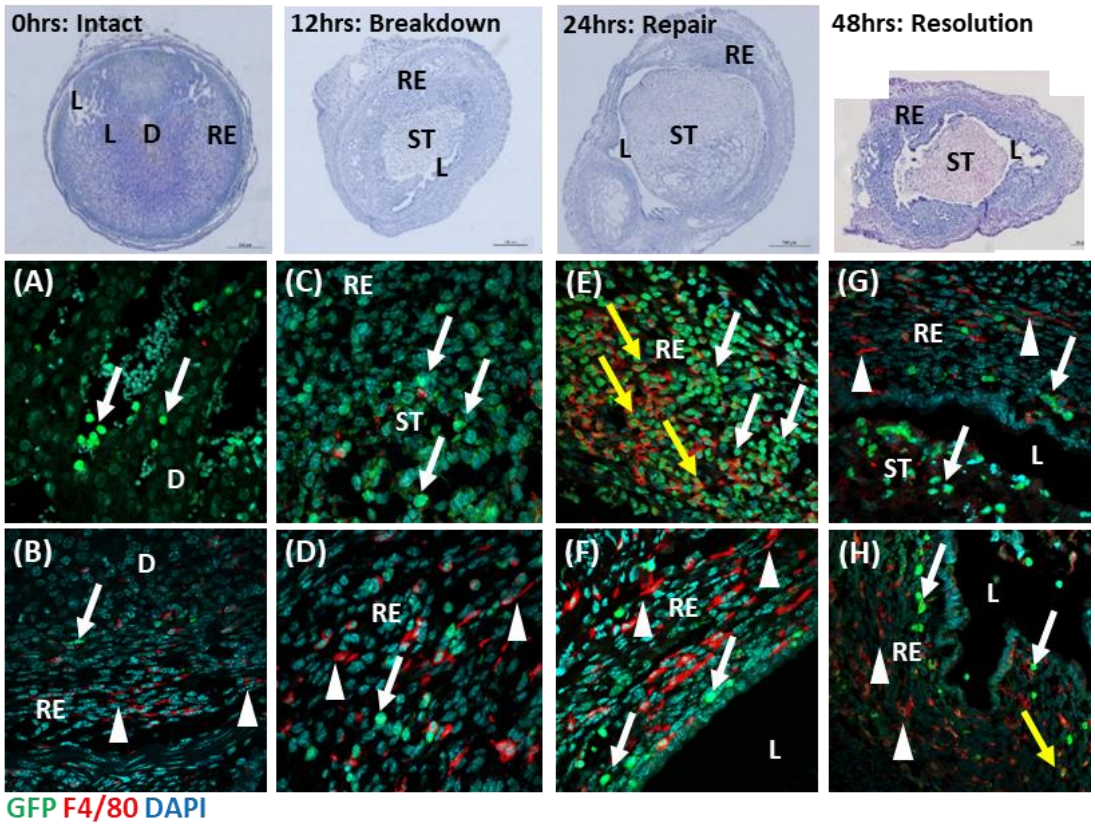

Figure 3-10. Spatio-temporal distribution of GFP+ immune cell subpopulations in Macgreen uterine tissues at various phases of endometrial breakdown (0 and 12hrs) and repair (24 and 48hrs). Note upper panels show a low power view of H&E stained tissue to give an overview of the gross appearance of the decidualised horn in cross section. IHC revealed dynamic changes in populations of immune cells at various phases of endometrial breakdown **(A-D)** and repair **(E-H)** based on the expression of GFP (green) and F4/80 (red) and their location. Three populations of cells exist in the tissue: GFP+F4/80- cells (white arrows), GFP+F4/80+ cells (yellow arrows) and GFP-F480+ cells (white arrow heads). Residual endometrium (RE), Decidualised tissue (D), shed tissue (ST) lumen (L) (representative images, n=10).

3.4.4 Confirmation of the existence of three monocyte/macrophage immune cell subpopulations

Flow cytometry and IHC identified three distinct immune cell populations based on expression of GFP and F4/80 however it was surprising to find cells that were GFP-F4/80+ as the literature states that all populations of macrophages express Csf1r and absolutely require it for cell survival (Dai et al. 2002, Wei et al. 2010, Luo et al. 2013, MacDonald et al. 2010, Jones and Ricardo 2013). In the current study it was initially unclear whether GFP-F4/80+ cells were a true population of macrophages, or whether there was a problem with reporting efficiency in the MacGreen transgenic line in uterine tissues or even if these cells expressed GFP at such a low level it was too difficult to detect using standard methods. Further investigations were therefore undertaken to confirm that GFP-F4/80+ cells were truly CSF1R negative using triple staining and additional transgenic lines (MacApple, CD68-eGFP).

3.4.4.1 Expression of GFP, Csf1r and F4/80 in naïve MacGreen endometrium

Triple IHC was used to analyse the expression of GFP, Csf1r and F480 in naïve MacGreen uterine tissue. Results revealed that cells which expressed GFP also expressed Csf1r (Figure 3-11, white and yellow arrows) and that there was a subset of these which also expressed F4/80 (Figure 3-11, white arrows only). Additionally, the existence of a population of F4/80+ cells which did not express either GFP or Csf1r was confirmed (Figure 3-11, red arrows). This was in agreement with results reported above and consistent with an endometrial macrophage population that existed within the tissue independent of Csf1r signalling.

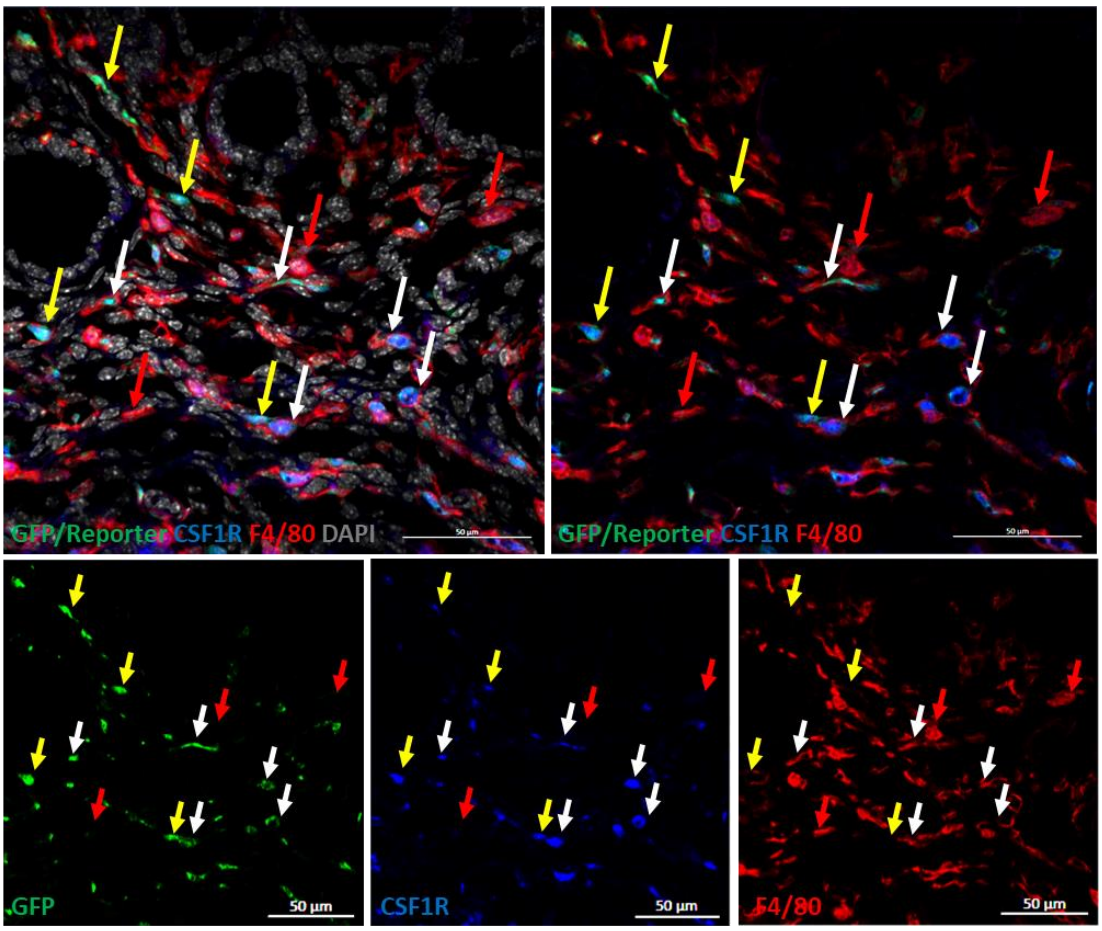

Figure 3-11. Expression of GFP (green), Csf1r (blue) and F4/80 (red) in naive MacGreen uterine tissue. IHC reveals the expression of GFP reliably identifies cells that express Csf1r (white and yellow arrows) with a subset co-expressing F4/80 (red) (white arrows). A population of GFP-Csf1r-F4/80+ cells was detectable (red arrows) (representative image, n=4).

3.4.4.2 Comparison of Reporter+ and F4/80+ cell distribution in MacGreen, MacApple and CD68-eGFP endometrial tissues

To further interrogate the existence of discrete immune cell subpopulations based on expression of GFP and F4/80, additional analysis was carried out using two further transgenic reporter mouse lines: MacApple and CD68-eGFP (described in Section 2.1). The mouse model of endometrial breakdown and repair was performed using both additional lines: MacApple mice (reporter: RFP) and CD68-eGFP mice (reporter: GFP). Uterine tissues were collected at 24hrs in order to draw direct comparisons with results from MacGreen mice (reporter: GFP). In all cases IHC was performed to compare locations of reporter (presented in green for direct comparison of transgenic output) and F4/80 (presented in red) expressing immune cells in the tissues.

In uterine tissues from each transgenic line, collected 24hrs after P4 withdrawal, the same heterogeneity in immune cell populations existed based on detection of fluorescent reporter protein (GFP/RFP) and F4/80 immunoexpression. As before, three populations could be detected, outlines in Figure 3-12 (A-C): Reporter+F4/80- cells (white arrows), Reporter+F4/80+ cells (yellow arrows) and Reporter-F4/80+ (red arrows) cells with similar spatial arrangements in the repairing tissue in all three lines. These discrete populations were also detected in uterine tissues collected from normal cycling adult mice (naïve) of the MacGreen, MacApple and CD68-eGFP transgenic lines (Figure 3-13 (A-C). Taken together, these data support the conclusion that there is a heterogeneous monocyte/macrophage population present in both cycling and repairing endometrial tissues.

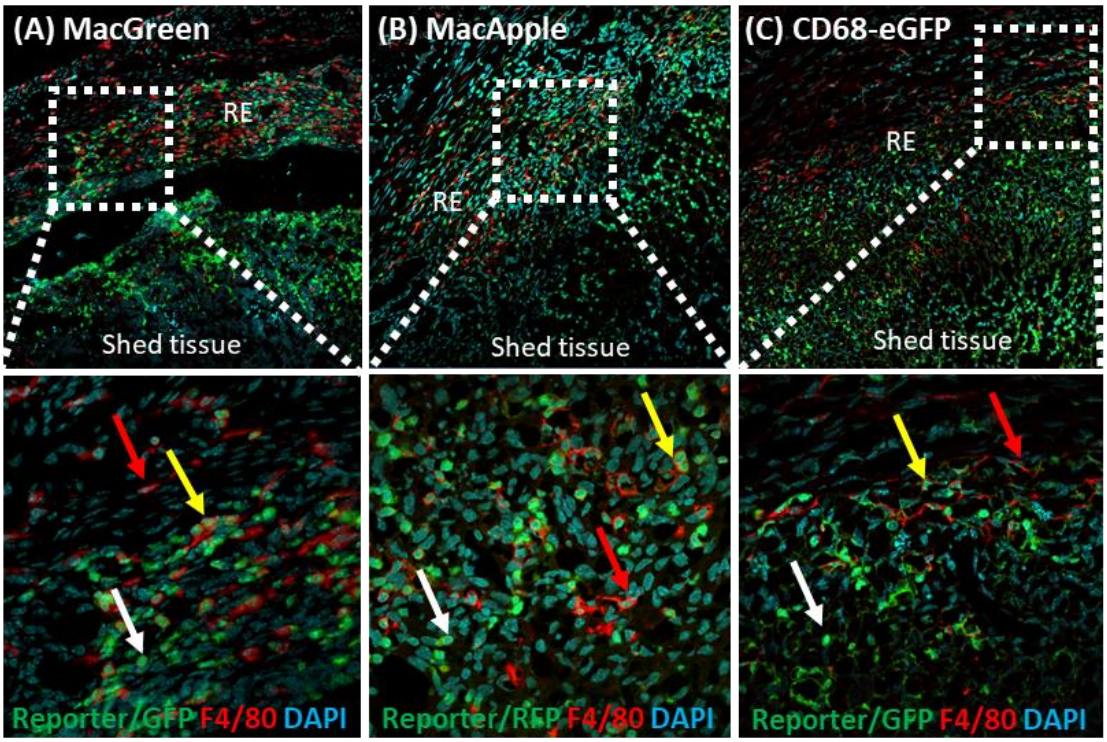

Figure 3-12. Expression of Reporter proteins (green) and F4/80 (red) in MacGreen, MacApple and CD68-eGFP uterine tissues 24h after progesterone withdrawal. IHC confirms that three populations of cells exist in **(A)** MacGreen (n=10), **(B)** MacApple (n=5) and **(C)** CD68-eGFP (n=8) uterine tissues: Reporter+F4/80- cells (white arrows), Reporter+F4/80+ cells (yellow arrows) and Reporter-F480+ cells (red arrows). Residual endometrium (RE).

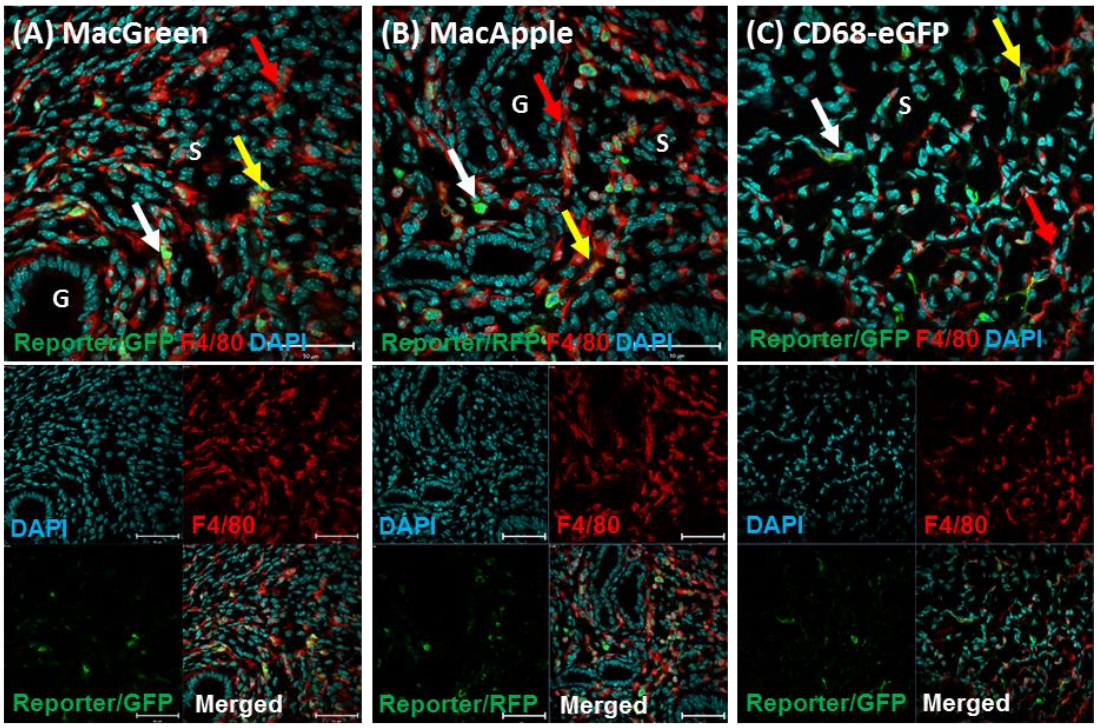

Figure 3-13. Expression of Reporter proteins (green) and F4/80 (red) in naive MacGreen, MacApple and CD68-eGFP uterine tissues. IHC confirms that three populations of immune cells exist within the stromal compartment in **(A)** MacGreen (n=8), **(B)** MacApple (n=4) and **(C)** CD68-eGFP (n=4) uterine tissues: Reporter+F4/80- cells (white arrows), Reporter+F4/80+ cells (yellow arrows) and Reporter-F480+ cells (red arrows). Stroma (S), gland (G).

3.4.4.3 Comparison between GFP+ cells in MacGreen and CD68-eGFP endometrial tissue during active tissue repair (24hrs)

To compliment previous findings, flow cytometry was also used to accurately assess changes in GFP+ immune cell populations during endometrial tissue repair (24hrs) comparing data from MacGreen (Section 3.4.3.2) with data generated using uterine tissues from CD68-eGFP mice. Analysis of the side scatter profile and GFP expression by live single cells from MacGreen uterus showed very few GFP+ cells present in the control (non-decidualised) horn and a distinct GFP+ population present in the samples recovered from the repairing (decidualised) horn after P4 withdrawal (Figure 3-14 (A)). Analysis of cells from the CD68-eGFP uteri showed similar changes between naive and repairing tissues: very few GFP+ cells in the control samples and many GFP+ cells in repairing samples (Figure 3-14 (B)). Analysis of tissues from both reporter lines demonstrated that in MacGreen repairing tissues (24hrs, n=10) GFP+

cells account for 23.36±3.5% of the live cells whilst in the control tissue they account for only 0.66±0.21% (unpaired t-test p=0.003) (Figure 3-14 (C)) and in CD68-eGFP repairing tissues (24hrs, n=8) GFP+ cells account for 23.96±2.59% of the live cells whilst in the control tissue they account for only 1.67±0.39% (unpaired t-test, p<0.0001) (Figure 3-13 (D)).

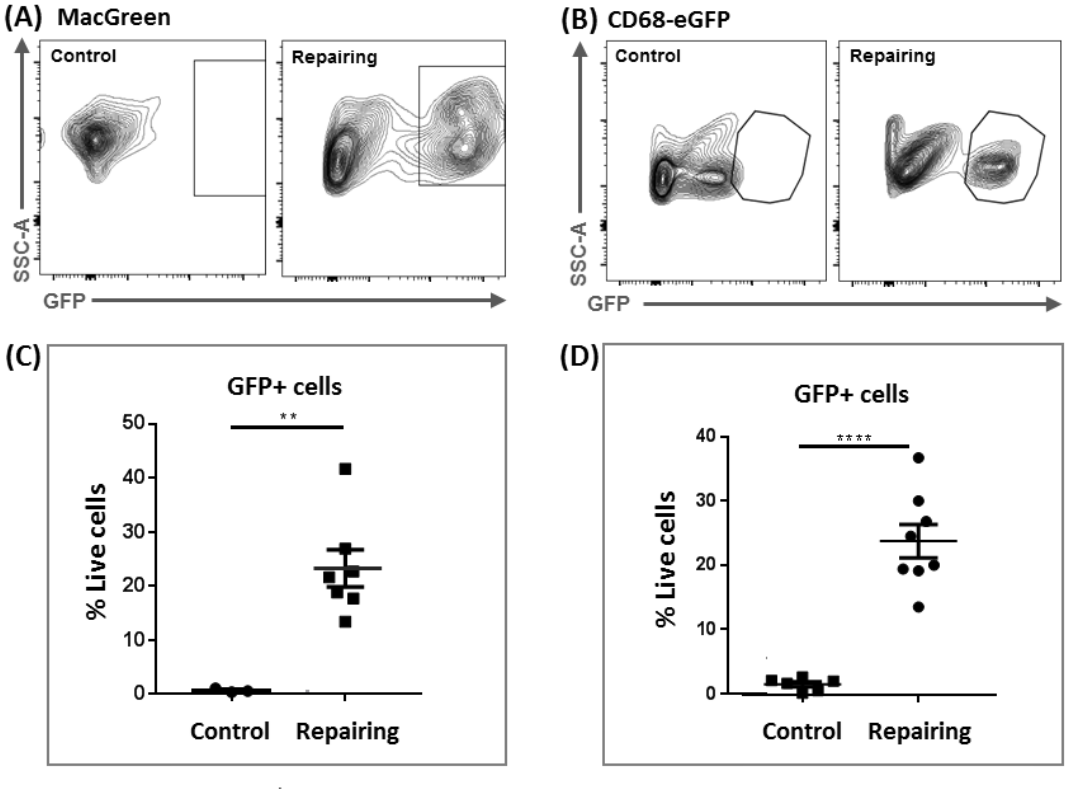

Figure 3-14. Flow Cytometry analysis of MacGreen and CD68-eGFP uterine tissues collected at 24hrs following P4 withdrawal at the time of active tissue repair and compared to non-decidualised control tissues. (A) Flow cytometry plots of control and repairing uterine tissues from MacGreen mice at 24hrs (n=10). **(B)** Flow cytometry plots of control and repairing uterine tissues from CD68-eGFP mice at 24hrs (n=8). **(C)** Assessment of the GFP+ immune cell influx in MacGreen transgenic mice at 24hrs. **(D)** Quantification of the GFP+ immune cell influx in CD68-eGFP transgenic mice at 24hrs (unpaired t-test, **p<0.001, ****p<0.0001).

3.4.5 Spatio-temporal analysis of immune cells and apoptotic cells in endometrial tissue during repair

A primary function of mononuclear phagocytes is to engulf (phagocytose) pathogens, dying/dead cells or cellular debris. To analyse whether GFP+ immune cells were associated with areas of cell death (apoptosis) in the endometrium, double fluorescent IHC was used to identify whether co-expression of cleaved caspase 3 (CC3), an enzyme activated in apoptotic cells, and GFP occurred in MacGreen uterine tissues. Analysis of uterine horns recovered at 0, 12, 24 and 48hrs after progesterone withdrawal revealed dynamic time-dependent changes in expression/co-expression of the proteins. At 0hrs very few CC3+ cells were detected in the tissue consistent with an intact decidualised stroma (Figure 3-15 (A), yellow arrows); as previously described, at 0hrs there were also very few GFP+ immune cells present in the tissue (Figure 3-15 (A), white arrows). By 12hrs after P4 withdrawal active tissue breakdown was underway and CC3+ apoptotic cells could be detected in the decidualised tissue mass which was starting to break down (Figure 3-15 (B), yellow arrows). In areas of tissue with CC3+ cells there was an apparent association with GFP+ immune cells (Figure 3-15 (B) white arrows) although there was no evidence for co-expression of the two proteins in individual cells suggesting active phagocytosis had not yet taken place.

At 24hrs, CC3+ cells were detected throughout the shed tissue consistent with active tissue breakdown and apoptosis (Figure 3-15 (C) yellow arrows). Many GFP+ immune cells were found in close proximity to CC3+ cells (Figure 3-15 (C) white arrows) but there was no evidence for co-expression of the proteins. At 48hrs when tissue repair was complete, CC3+ cells were still present detected within the newly formed epithelium (Figure 3-15 (D)). Notably, the GFP+ immune cells still detected in the residual endometrial stroma co-expressed CC3 (Figure 3-15 (D), white and yellow arrows). GFP+CC3+ cells are either GFP+ immune cells that had phagocytosed CC3+ apoptotic cells or were GFP+ cells that were undergoing apoptosis themselves. With the completion of repair and resolution of inflammation apparent in the endometrial tissue, the latter is considered more likely as it would be a mechanism to explain the rapid reduction in GFP+ cells at 48hrs compared with 24hrs based on previous IHC results (Figures 3-7 and 3-10).

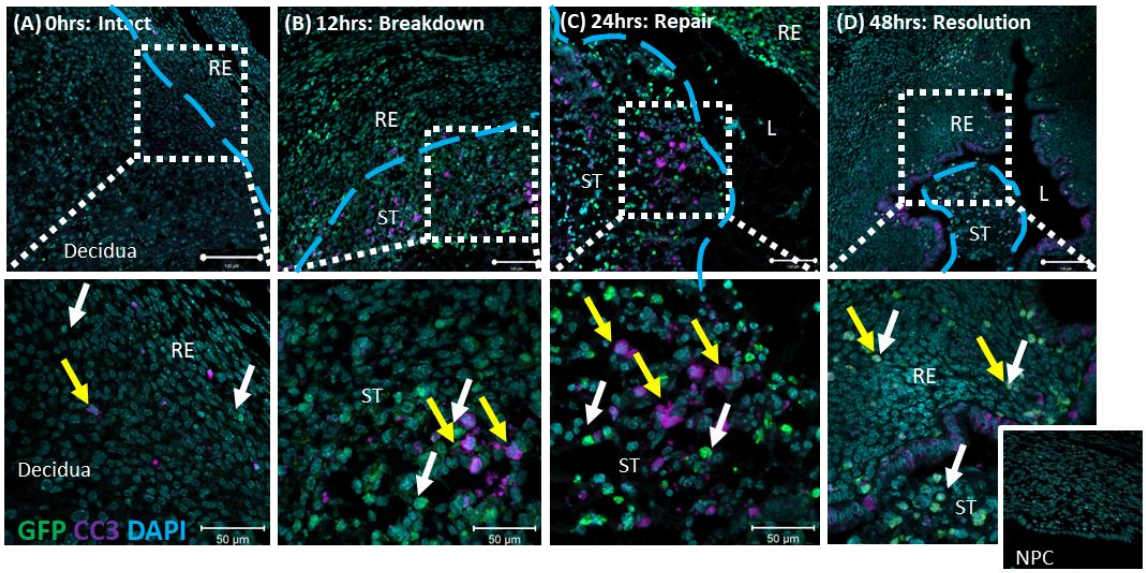

Figure 3-15. Spatio-temporal distribution of GFP+ immune cells and CC3+ apoptotic cells in MacGreen uterine tissues before (0hrs) and at various phases of endometrial breakdown (12hrs) and repair (24-48hrs). IHC reveals dynamic changes in numbers of cells undergoing apoptosis (CC3+) and varying degrees of association with GFP+ immune cells. **(A)** At 0hrs few GFP+ cells (white arrows) and few apoptotic cells (yellow arrows) are present. **(B)** At 12hrs numbers of GFP+ cells increase (white arrows) and apoptotic cells can be detected in the decidua (yellow arroes). **(C)** At 24hrs GFP+ cells peak in numbers (white arrows) and there is a definite association with apoptotic decidual cells (yellow arrows). **(D)** At 48hrs there is evidence for GFP+CC3+ (white and yellow arrows) cells which could be macrophages engulfing apoptotic bodies or undergoing apoptosis themselves. Residual endometrium (RE), shed tissue (ST), lumen (L) (representative images, n=6).

To investigate if the different GFP+ immune cell populations have different phagocytic activities IHC was used to perform a triple stain of MacGreen uterine tissues for GFP, F4/80 and CC3. Notably this more refined examination suggested that in regions of endometrium undergoing active tissue repair there were GFP+F4/80+ cells that were apparently engulfing CC3+ cells (Figure 3-16 (A), yellow arrows) and there was also evidence for GFP-F4/80+ cells engulfing CC3+ cells. No evidence for GFP+F4/80- cells engulfing CC3+ cells (Figure 3-16 (A), red versus white arrows) was found. In regions of shed tissue (undergoing breakdown) there was no evidence for immune cell populations engulfing apoptotic cells however there was a close association of GFP+F4/80- cells with CC3+ (presumptive apoptotic) decidual cells (Figure 3-16 (B), white versus orange arrows). These data suggest that GFP+F4/80- inflammatory monocytes might have a role to play in inducing apoptosis in decidual

cells but that it is only GFP+F4/80+ and GFP-F4/80+ cells (macrophages) that appear capable of phagocytosing cellular debris in the repairing residual endometrial tissue compartment.

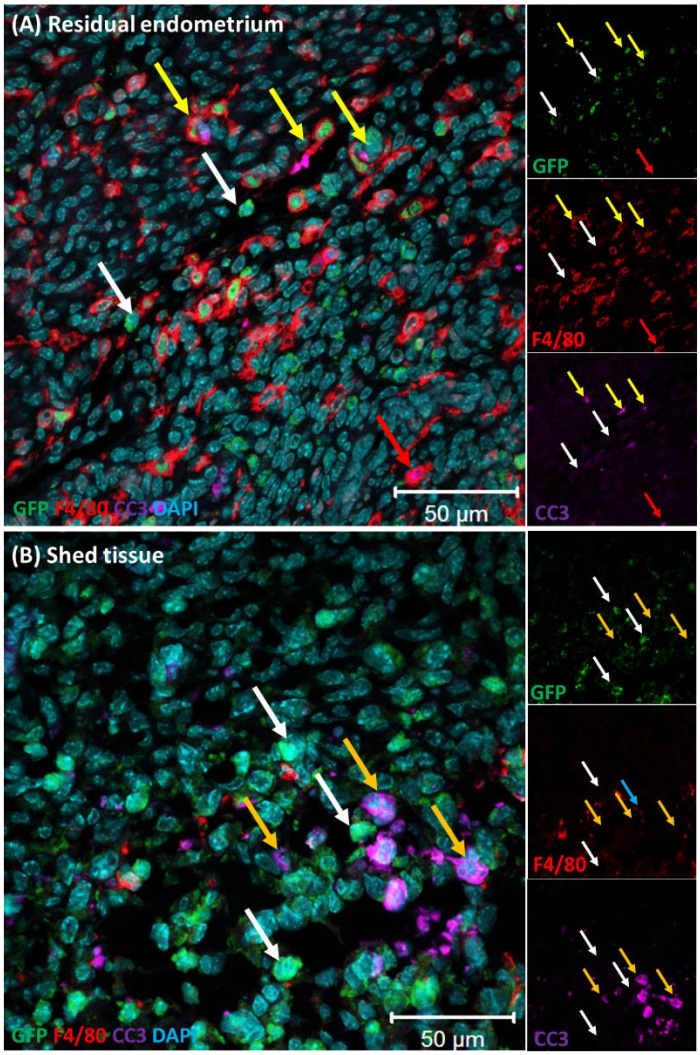

Figure 3-16. Association of immune cells with apoptotic cells in MacGreen uterine tissues during active tissue repair. (A) Expression of GFP, F4/80 and CC3 in residual endometrial tissue **(B)** Expression of GFP, F4/80 and CC3 in shed tissue. Orange arrows represent CC3+ apoptotic cells, white arrows represent GFP+F4/80- cells, yellow arrows represent GFP+F4/80+ cells engulfing a CC3+ cell and red arrows represent GFP-F4/80+ cells engulfing a CC3+ cell. (representative image; n=4).

3.4.6 Expression of signalling molecules and receptors with known roles in monocyte/macrophage function in endometrial tissue

3.4.6.1 qPCR analysis of cytokines and chemokines in endometrial tissue

To investigate mechanisms by which the heterogeneous population of GFP+ immune cells were recruited to the regions of repairing tissue, qPCR was used to analyse mRNA expression of key cytokines and chemokines. mRNA was extracted from whole uterine tissue samples recovered from both the hormone-treated non-decidualised (control) and the decidualised (repairing) uterine horns retrieved between 0 and 48hrs. Results were normalised to mRNA expression of the reference gene *Actb* (Figure 3-17, black versus grey bars respectively).

In uterine tissues mean *Ccl2* mRNA was higher in the decidualised horn compared with the control horn at 0, 12 and 24hrs (Figure 3-17 (A)). However *Ccr2*, a receptor for *Ccl2* which may mediate monocyte chemotaxis to sites of inflammation was reduced at 0 and 12hrs and only higher at 24hrs in the decidualised samples (Figure 3-17 (B)). *Cx3cl1* (fractalkine) mRNA was upregulated in the decidualised horn at 12, 24 and 48hrs suggesting the chemokine will only be secreted after tissue breakdown is initiated but may persist throughout repair (Figure 3-17 (C)). The corresponding receptor *Cx3cr1* was also upregulated in the decidualised tissue at 12hrs and even more so at 24 and 48hrs (Figure 3-17(D)). *Ccl7* (*Mcp3*) mRNA was upregulated in the decidualised horn at 12hrs and further increased at 24hrs (Figure 3-17 (E)). *Ccl8* (*Mcp2*) mRNA was upregulated in the decidualised tissue both before (0hrs) and during tissue breakdowns (12hrs) but no different to controls at 24 and 48hrs (Figure 3-17 (F)). Interestingly, *Csf1* mRNA was upregulated in the decidualised horn at all time points 0, 12, 24 and 48hrs (Figure 3-17 (G)). In contrast, *Csf2* mRNA was exclusively upregulated in the decidualised horn at 24hrs (Figure 3-17 (H)) and comparable to control samples at all other time points.

In uterine tissues both *Cxcl1* and *Cxcl2* mRNA were markedly upregulated only at 24hrs in the decidualised horn (Figure 3-17 (I-J)) which paralleled the time point when there was the highest number of macrophages present in the tissue consistent with these cells being a source of these chemokines. Similarly, *Cxcl3* and *Cxcl12* mRNA were significantly upregulated in decidualised horns exclusively at 24hrs (Figure 3-17 (K-L), ****$p<0.0001$). *Il10* was upregulated in the decidualised horn at 24 and 48hrs

while *Arg1* was only upregulated at 24hrs (Figure 3-17 (M-N)). Notably, both *Il6* and *Tnfa* were significantly upregulated at 24hrs in decidualised uterine horns compared with controls (Figure 3-17 (O-P), ****p<0.0001). All mRNA values (AU) normalised to Actb expression are detailed in Table 3-3.

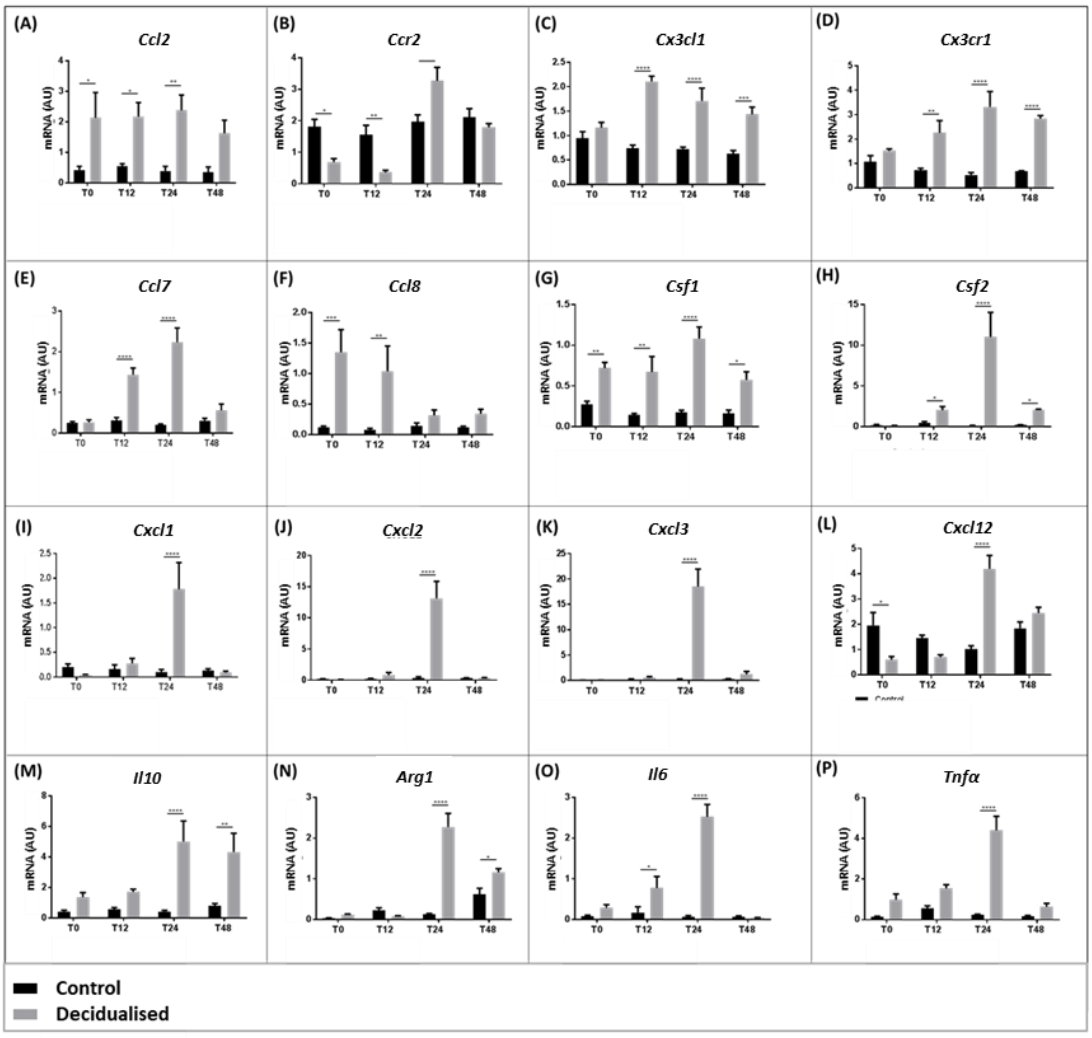

Figure 3-17. qPCR analysis of mRNA encoding key cytokines and chemokines in whole uterine tissue homogenates assessed 0-48hrs in control and decidualised uterine tissues. mRNA expression of **(A)** *Ccl2*, **(B)** *Ccr2*, **(C)** *Cx3cl1*, **(D)** *Cx3cr1*, **(E)** *Ccl7*, **(F)** *Ccl8*, **(G)** *Csf1*, **(H)** *Csf2*, **(I)** *Cxcl1*, **(J)** *Cxcl2*, **(K)** *Cxcl3*, **(L)** *Cxcl12*, **(M)** *Il10*, **(N)** *Arg1*, **(O)** *Il6*, **(P)** *Tnfα* in control (hormone treated, non-decidualised) and repairing tissues (hormone treated, decidualised) (n=5 for each condition and time point). All values normalised to mRNA expression of reference gene (*Actb*). Black bars represent non decidualised uterine tissues, grey bars represent fully decidualised uterin tissues (two-way ANOVA, Sidak's multiple comparison's test, *p<0.05, **p<0.01, ***p<0.001, ****p<0.0001).

Table 3-2. Gene expression values (mRNA; AU) as normalised to *Actb* in control (non-decidualised) and decidualised (repairing) uterine tissues at 0, 12, 24 and 48hrs of the Edinburgh menses mouse model. P values demonstrated significance as analysed using a two-way ANOVA and Sidak's multiple comparison's test.

Gene	0hrs			12hrs			24hrs			48hrs		
	Control	Decidualised	p value	Control	Decidualised	p value	Control	Decidualised	p value	Control	Decidualised	p value
Ccl2	0.42±0.21	2.13±0.83	0.027	0.55±0.08	2.17±0.46	0.039	0.39±0.15	2.38±0.50	0.008	0.35±0.17	1.63±0.42	0.143
Ccr2	1.81±0.24	0.69±0.11	0.014	1.56±0.29	0.36±0.06	0.005	1.97±0.22	3.27±0.24	0.002	2.11±0.27	1.79±0.11	0.832
Cx3cl1	0.95±0.13	1.16±0.11	0.704	0.74±0.06	2.11±0.11	<0.0001	0.73±0.04	1.71±0.62	<0.0001	0.63±0.06	1.43±0.15	0.001
Cx3cr1	1.08±0.24	1.53±0.07	0.771	0.73±0.08	2.26±0.49	0.005	0.53±0.10	3.32±0.63	<0.0001	0.68±0.03	2.84±0.12	<0.0001
Ccl7	0.26±0.03	0.27±0.06	0.999	0.31±0.07	1.44±0.16	<0.0001	0.20±0.03	2.23±0.35	<0.0001	0.31±0.06	0.56±0.15	0.669
Ccl8	0.12±0.02	1.35±0.37	0.001	0.08±0.03	1.04±0.41	0.007	0.14±0.05	0.32±0.09	0.954	0.12±0.02	0.34±0.07	0.904
Csf1	0.27±0.04	0.72±0.07	0.009	0.15±0.02	0.67±0.19	0.002	0.17±0.03	1.08±0.14	<0.0001	0.16±0.04	0.58±0.09	0.018
Csf2	0.17±0.09	0.13±0.02	0.999	0.48±0.15	2.03±0.44	0.779	0.13±0.04	11.03±3.01	<0.0001	0.19±0.04	2.04±0.11	0.654
Cxcl1	0.20±0.07	0.04±0.01	0.971	0.16±0.08	0.28±0.09	0.991	0.10±0.05	1.78±0.54	<0.0001	0.13±0.04	0.09±0.03	0.999
Cxcl2	0.16±0.06	0.07±0.04	0.999	0.16±0.13	0.83±0.39	0.982	0.34±0.21	13.15±2.71	<0.0001	0.30±0.09	0.33±0.08	0.999
Cxcl3	0.02±0.01	0.03±0.01	0.999	0.16±0.15	0.53±0.23	0.999	0.17±0.11	18.52±3.41	<0.0001	0.27±0.08	1.22±0.54	0.971
Cxcl12	1.96±0.51	0.61±0.12	0.012	1.45±0.12	0.70±0.09	0.298	1.01±0.14	4.20±0.52	<0.0001	1.84±0.25	2.45±0.22	0.489
Il10	0.43±0.08	1.38±0.29	0.782	0.58±0.11	1.72±0.16	0.643	0.43±0.07	5.02±1.34	<0.0001	0.81±0.14	4.32±1.23	0.003
Arg1	0.04±0.01	0.12±0.02	0.989	0.23±0.06	0.08±0.02	0.905	0.13±0.02	2.27±0.33	<0.0001	0.62±0.15	1.16±0.08	0.029
Il6	0.08±0.03	0.29±0.08	0.817	0.17±0.14	0.78±0.28	0.044	0.07±0.03	2052±0.31	<0.0001	0.07±0.02	0.04±0.01	0.999
Tnfα	0.14±0.03	0.98±0.28	0.159	0.56±0.13	1.55±0.18	0.069	0.24±0.03	4.38±0.69	<0.0001	0.17±0.04	0.64±0.16	0.671

3.4.6.2 Isolation and characterisation of myeloid immune cell populations during endometrial repair

To further characterise the distinct monocyte/macrophage cell populations identified in repairing endometrial tissue, GFP+F4/80- cells, GFP+F4/80+ cells and GFP-F4/80+ cells were isolated by FACS from MacGreen uterine tissues recovered 24hrs after P4 withdrawal. RNA extraction and cDNA synthesis were performed and qPCR was used to analyse the expression of genes used in previous studies to identify distinct monocyte and macrophage phenotypes in mice (Evans and Salamonsen 2012, Thiruchelvam et al. 2013, Mackler et al. 2000, Martin and Leibovich 2005, Salamonsen et al. 2002, Kamat and Isaacson 1987, Van Furth and Thompson 1971). Cells were isolated from six mice. Total isolated cell numbers are presented in Table 3-4. Notably in all cases the largest number of cells was detected as being in the GFP+F4/80- cell population consistent with results detailed in previous sections (see Figure 3-8).

Table 3-4. Cell numbers of each monocyte/macrophage population isolated by FACS

Sample	GFP+F4/80- cells	GFP+F480+ cells	GFP-F480+ cells
1	97,302	33,025	13,557
2	102,156	52,971	22,988
3	99,373	40,071	24,195
4	218,121	64,579	32,541
5	101,096	42,456	22,222
6	106,430	58,431	22,608

As summarised in Table 3-5, each of these three populations of cells had a distinct gene expression profile. Specifically GFP+F4/80- cells, in agreement with immunohistochemistry (Figure 3-1), expressed *Csf1r* mRNA and also contained readily detectable mRNAs encoded by *Cx3cr1*, *CD14*, and *CD16* all known monocyte markers but had low expression of *Ccr2*, *Arg1* and *Il6*. For ease of comparison macrophages are often considered as having a M1 (classically activated/proinflammatory) or a M2 (alternatively activated/anti-inflammatory) phenotype although it is acknowledged that these are not likely to be discrete phenotypes within a tissue context (Shapouri-Moghaddam et al. 2018, Biswas et al. 2012). Notably, in addition to *Cx3cr1* the GFP+F4/80- cells also expressed some markers considered typical of M2-like macrophages including *Tgfβ1*, *Csf1* and *Il10*

and interestingly a high amount of *Tnfα* mRNA (Table 3-5). These results suggest that the GFP+F4/80- cell population may be heterogeneous, predominantly composed of $Ccr2^{low}$Cx3cr1+ alternative monocytes.

The GFP+F4/80+ cells also expressed high levels of *Cx3cr1* mRNA and lower levels of *Ccr2*, *CD14* and *CD16* mRNA. Notably the GFP+F4/80+ cells also expressed high levels of *Arg1*, *Tgfβ1* and *Il10* mRNAs which usually considered as being M2 macrophage markers (Biswas et al. 2012, Shapouri-Moghaddam et al. 2018). Reassuringly, the purified GFP-F4/80+ cells did not express mRNAs encoded by *Csf1r* in agreement with the IHC and flow cytometry data detailed above. GFP-F4/80+ cells expressed *Ccr2* and showed mixed expression of mRNAs considered typical of M1 (*Il6*, *Tnfα*) and M2 (*Arg1*, *Tgfβ1*, *Csf1*) macrophage phenotypes (Table 3-5), again consistent with a non-typical/intermediate phenotype. In summary, these qPCR results show that although three subpopulations have been identified based on cell surface expression of Csf1r (cytoplasmic GFP) and F4/80, functional heterogeneity exist within each population which requires further investigation.

Table 3-5. Summary of gene expression in three distinct monocyte/macrophage populations in endometrium recovered 24hrs after progesterone withdrawal. All values normalised to mRNA expression of *Actb* (reference gene)

Cell Marker	GFP+F4/80- cells	GFP+F4/80+ cells	GFP-F4/80+ cells
Csf1r	+ +	+ +	-
Ccr2	-	+ +	+ +
Cx3cr1	+ + + +	+ + + +	-
CD14	+ + + +	+ +	-
CD16	+ + + +	+ +	-
Arg1	-	+ + +	+ +
Tgfβ1	+	+	+ +
Csf1	+ + +	-	+ +
Csf2	-	-	-
Il10	+	+	-
Ifnγ	-	-	+
Il6	-	-	+ +
Tnfα	+ + + +	+	+

>20 | 10-20 | 5-10 | 1-5 | >1

mRNA (AU) normalised to *Actb*

3.5 Discussion

3.5.1 Mouse model of endometrial breakdown and repair

During the normal human menstrual cycle, the inner section of the endometrium breaks down and is shed and at the same time a rapid process of scar-free tissue repair takes place (Garry et al. 2009). Menstruation is considered an inflammatory event associated with the sequential recruitment of neutrophils and macrophages that are believed to play key roles in the controlled break down of the tissue and its subsequent shedding (Evans and Salamonsen 2012). We and others have focused on macrophages as one of the immune cells most likely to play a role in regulation of endometrial inflammation and tissue breakdown during menses in part because of the evidence that their numbers peak during menstruation where they account for up to 15% of the total leucocyte population (Salamonsen and Woolley 1999, Thiruchelvam et al. 2013). Macrophages are able to adapt their phenotype so that they can regulate both pro- and anti-inflammatory responses depending upon the tissue environment (Biswas et al. 2012).

Menstruation only occurs naturally in women and a few other species including some higher primates (e.g. macaques: (Brenner and Slayden 2012, Brenner et al. 1996)), some bat species, the elephant shrew and as most recently discovered, the Cairo spiny mouse (Bellofiore et al. 2018, Bellofiore et al. 2017). In order to study mechanisms responsible for breakdown of endometrial tissue a number of models have been developed including the use of human tissue xenografted into immune-suppressed mice (Coudyzer et al. 2013). Whilst this model has the merit of using human tissue it is not suitable for studying the impact of immune cells on the process. A number of investigators have therefore developed protocols to simulate ‘menses’ in non-menstruating rodent species including rats and mice with two approaches most widely used: ovariectomy combined with hormone treatment and mechanical induction of decidualisation (Finn and Pope 1984, Brasted et al. 2003, Kaitu'u et al. 2005); or induction of pseudopregnancy (Rudolph et al. 2012).

In the current study, a mouse model of endometrial breakdown and repair that was a refined and revalidated protocol based on that of the Salamonsen group (Kaitu'u et al.

2005, Kaitu'u-Lino et al. 2007, Kaitu'u-Lino et al. 2009, Kaitu'u-Lino et al. 2010, Kaitu'u-Lino et al. 2012) was used. Using the 'Edinburgh model' we have already demonstrated key parallels with the process of menstruation in women including local hypoxia (Cousins et al. 2016d) which occurs in parallel to simultaneous shedding and repair, expression of matrix metalloproteinases, active angiogenesis and epithelial proliferation and migration in the absence of oestrogen stimulation (Cousins et al. 2014, Cousins et al. 2016b). Given the evidence that monocyte-derived macrophages and paracrine factors secreted by these cells play a key role in regenerating tissues (Das et al. 2015) and in wound repair we used transgenic mice in which these cells could be identified by fluorescent reporter proteins in combination with our mouse model to interrogate their role in endometrial wound healing.

3.5.2 Harnessing the power of mouse transgenics to reveal different subpopulations of endometrial mononuclear phagocytes in the endometrium

Myeloid progenitor cells differentiate into macrophages *in situ* in peripheral tissues, a process that is regulated by macrophage colony-stimulating factor (Csf1) which binds to cells expressing Csf1 receptor (Csf1r) (Dai et al. 2002, Wei et al. 2010, Luo et al. 2013, MacDonald et al. 2010, Jones and Ricardo 2013). Two transgenic mouse lines used in this study are based around this biology: the MacGreen (Sasmono et al. 2003) and MacApple (Hawley et al. 2018) lines express the fluorescent reporter proteins eGFP and RFP (respectively) under control of the Csf1r promoter. Similarly CD68 is expressed by myeloid cells, specifically monocytes and macrophages and another transgenic line, CD68-eGFP, expresses eGFP under control of the CD68 gene promoter (Iqbal et al. 2014).

In the MacGreen endometrium GFP+ cells were found to express CD45 the leucocyte common antigen which is expressed on almost all haematopoietic cells except mature erythrocytes (Martin and Leibovich 2005), confirming their identity as leucocytes. Similarly all GFP+ cells expressed CD11b which is an integrin expressed on the surface of a number of leucocytes including monocytes, natural killer cells and macrophages and in some cases it is believed that varied expression of CD11b relates to diverse functions (Schulz et al. 2012), although both IHC and flow cytometry results in this characterisation did not display this. Interestingly when analysing

immunoexpression of Gr1, an inflammatory monocyte marker, a proportion of the GFP+ cells were GR-1+ while some were Gr1-. It is known that mouse monocyte subsets can be characterised by differential expression of Gr1 where Gr1+ monocytes are CD11b+Csf1r+ and considered to be 'classical' monocytes, while Gr1- monocytes are also CD11b+Csf1r+ but considered to be 'alternative/patrolling' monocytes (Yang et al. 2014).

GFP+ cells were determined to have low granularity as determined by side scatter in flow cytometry analysis, and were mononuclear when examined on cytospins. Taken together these results suggest that GFP+ cells in the MacGreen endometrium represent two subsets of mononuclear phagocytes: Csf1r/GFP+CD11b+Gr1+ 'classical' monocytes and Csf1r/GFP+CD11b+Gr1- 'alternative' monocytes. Notably some previous studies have used Gr1 as a neutrophil specific marker to elucidate essential roles in endometrial physiology (Hestdal et al. 1991, Daley et al. 2008, Menning et al. 2012a, Armstrong et al. 2017). The current dataset suggests the conclusions from those studies may require reinterpretation.

3.5.3 Characterisation of mononuclear phagocytes during endometrial breakdown and repair

Analysis of MacGreen uterine tissue revealed that there was a striking increase in the numbers of GFP+ cells 24hrs after progesterone withdrawal at a time when previous validation studies suggested active decidual tissue breakdown as accompanied with basal endometrial repair (Cousins et al. 2014), shown to parallel with studies in human tissues recovered on day 28/1 of the menstrual cycle (Armstrong et al. 2017). In the current study the use of flow cytometry provided a powerful way of quantifying changes in cell content and revealed that the proportion of GFP+ cells increased from 0.66±0.21% to 23.26±3.46% of live cells in digests of tissue recovered at 24hrs. These findings would appear to be consistent with the extravasation of inflammatory monocytes from the circulation in response to an 'injury' stimulus (Van Furth and Thompson 1971, Das et al. 2015, Hampton et al. 2001, Jones et al. 2004, Yang et al. 2014).

Further characterisation using the mature macrophage marker F4/80, widely used to detect macrophage populations in mouse tissues, identified three putative

subpopulations of monocyte/macrophage present during endometrial repair: GFP+F4/80-, GFP+F4/80+ and GFP-F4/80+ cells. The majority of cells were GFP+F4/80- previously described as inflammatory monocytes while there was also a population of GFP+F480+, which also showed a significant increase in the repairing endometrial tissue with detection of the latter consistent with the differentiation of monocytes into macrophages following extravasation into the endometrial tissue (Van Furth and Thompson 1971, Battersby et al. 2002, Das et al. 2015, Hesketh et al. 2017, Mantovani et al. 2013, Yang et al. 2014). On the basis of flow cytometry alone these subpopulations were therefore characterised as influxing inflammatory monocytes (GFP+F4/80-) and monocyte-derived macrophages (GFP+F4/80+). Notably a third population of GFP-F4/80+ cells were identified the numbers of which appeared to be relatively unchanged during endometrial repair leading to the assumption that these cells would represent a stable tissue-resident macrophage population.

Complementary studies using fixed tissue sections showed the GFP+F480- monocytes were most prominent in areas of decidual tissue breakdown and in areas of repairing tissue. Notably, GFP+F480+ cells were only detected in the regions of residual (unshed) endometrium undergoing active repair and were not associated with regions of repaired tissue. The GFP-F480+ cells, putative tissue-resident macrophages were detected throughout the tissue independent of areas of tissue breakdown and repair. Such distinct locations of immune subpopulations may have significant impacts on their phenotype and function (Schulz et al. 2012). Further analysis of subpopulations revealed dynamic changes in abundance and location across the full time course of endometrial breakdown and repair. Specifically GFP+F480- monocytes were rare before the onset of tissue breakdown (0hrs), increased moderately by 12hrs during tissue breakdown and were highly abundant at 24hrs in regions of both tissue breakdown and repair. By 48hrs these cells were diminished, consistent with successful resolution of inflammation. Interestingly it was noted that the GFP+F4/80+ monocyte-derived macrophage population was abundant at the 24hrs time point but relatively low at all other time points. The GFP-F480+ tissue-resident macrophage population was detected across the time course and appeared relatively homeostatic.

These novel findings documenting for the first time both the temporal and spatial association of three phenotypically identifiable populations of monocytes/macrophages during dynamic endometrial shedding and repair is entirely consistent with the highly plastic nature of these cells and the ability of the local microenvironment to imprint their phenotypic and functional characteristics. An interpretation of these result is summarised in Figure 3-18 showing the most abundant populations of monocytes and macrophages are detected in the mouse endometrium at 24hrs during active endometrial tissue repair.

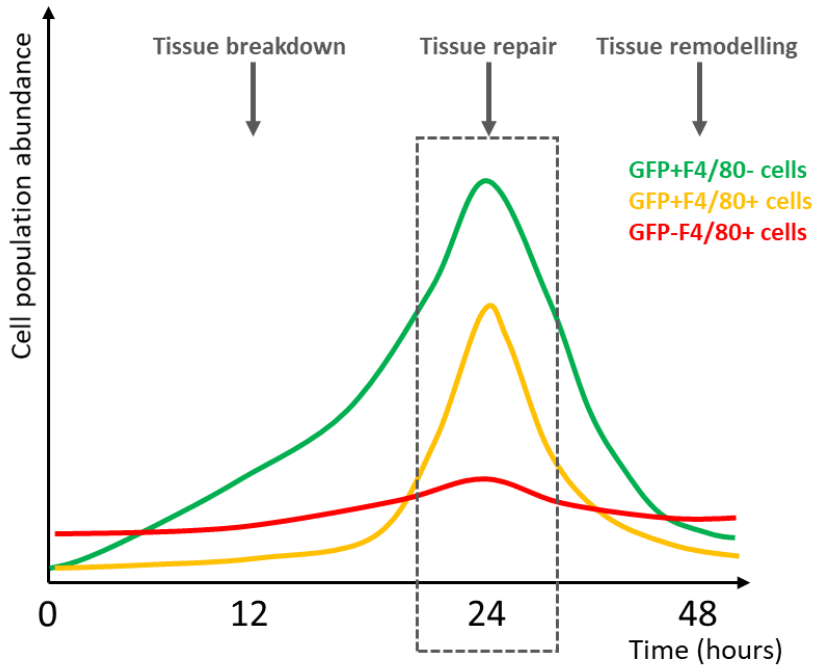

Figure 3-18. Schematic interpretation of changes in immune cell subpopulations during endometrial tissue breakdown and repair based on IHC and flow cytometry results. Before tissue breakdown at 0hrs there are few GFP+F4/80- cells and GFP+F4/80+ cells. GFP+F4/80- cells are more abundant at 12hrs during tissue breakdown and peak at 24hrs during tissue repair. GFP+F4/80+ cells are not detectable at 12hrs but also peak at 24hrs. By 48hrs both GFP+F4/80- and GFP+F4/80+ cells are diminished. GFP-F4/80+ cells are relatively unchanged throughout the cycle of tissue breakdown and repair although show a modest increase in abundance at 24hrs. At 24hrs during active tissue repair GFP+F4/80- cells represent ~ 16%, GFP+F4/80+ cells represent ~7% and GFP-F4/80+ cells represent ~1% of live single cells in the endometrium.

In the case of endometrial repair, monocyte recruitment occurs in response to 'sterile' inflammation. This is similar to the injury response seen in the cardiovascular system where Ly6C^{high} monocytes initially influx into the tissue, postulated to regulate removal of cellular debris, then Ly6C^{low} monocytes influx later to promote tissue repair in a linear bi-phasic progression (Nahrendorf et al. 2007) with the critical difference that during menstruation, simultaneous breakdown and repair is observed. With this in mind it is postulated that inflammatory monocytes (GFP+F4/80-) initially influx into the endometrium and repair-associated monocyte-derived macrophages (GFP+F4/80+) may either arise from this population over time, or differentiate from a second wave of influxing monocytes of the 'alternative' phenotype to take part in repair. This hypothesis requires further investigation. Current results have highlighted clear spatio-temporal regulation of monocytes and macrophage subpopulations, each of which may have distinct functions in endometrial repair.

3.5.4 Confirming the existence of tissue-resident macrophages

In contrast to most tissues in the MacGreen mouse where expression of eGFP corresponds to all F4/80 expressing cells (Sasmono et al. 2003), the endometrium had a population of cells identified as GFP-F4/80+ that were dispersed throughout the tissue and seemingly were not affected by simulated menstrual tissue breakdown and repair. This result was unexpected as it has been reported that macrophages require expression of Csf1r/ Csf1-dependent signalling to proliferate, differentiate and survive (Dai et al. 2002, Wei et al. 2010, Luo et al. 2013, MacDonald et al. 2010, Jones and Ricardo 2013). To confirm that detection of this population was not due to any technical issues with reporting efficiency in the MacGreen transgenic line additional analyses were undertaken. A triple stain revealed that all GFP+ cells were Csf1r+ and a subset of these expressed F4/80. Notably a population of GFP-Csf1r-F4/80+ cells were clearly identified. In addition, using additional transgenic lines, the same three subpopulations of monocyte/macrophage lineage cells were detected in both MacApple and CD68-eGFP endometrial tissue during the repair phase (Reporter+F480-, Reporter+F4/80+, Reporter-F4/80+).

These additional analyses confirmed that GFP-F4/80+ expression identified a true cell population which is consistent with studies suggesting that macrophages are not solely

dependent on Csf1 signalling. For example in mice lacking functional Csf1 (*op/op* mice) (Cecchini et al. 1994) and in mice where Csf1r has been deleted (Dai et al. 2002) there is an incomplete depletion of macrophages (defined as F4/80+). The results of the current study suggest that endometrial tissue-resident macrophages (GFP-F4/80+ cells) do not express Csf1r and given that they appear relatively unchanged during endometrial repair, it is reasonable to speculate that these may represent a quiescent population that persists in the tissue independently of Csf1, although this alternative mechanism is yet to be investigated. This hypothesis can be supported by the fact that a reduction of Csf1 *in vitro* promotes quiescence of BM-derived macrophages (Tushinski and Stanley 1985) and that antibody depletion of Csf1r in MacGreen mice has been shown to diminish GFP expressing macrophages in several tissues but not the uterus (MacDonald et al. 2010). These results suggest that monocytes, monocyte-derived macrophages and tissue-resident macrophages, all present simultaneously in the endometrium during tissue repair, may be phenotypically and functionally distinct from monocyte/macrophage populations in other tissues of the body.

3.5.5 Analysis of immune cells and apoptosis during endometrial repair

To assess the function and fate of the GFP+ immune cells, cellular apoptosis was examined using expression of cleaved caspase 3 (CC3) which plays a central role in cell apoptosis as a key marker. In this study apoptosis was confined to the decidualised tissue undergoing active tissue breakdown at 12 and 24hrs and there was a clear association with GFP+ cells although no clear evidence for phagocytosis (co-expression of GFP and CC3). Additional analysis using triple IHC revealed that in the basal endometrium some GFP+F4/80+ monocyte-derived macrophages and GFP-F4/80+ tissue-resident macrophages did appear to be engulfing CC3+ apoptotic bodies while GFP+F4/80- cells were often associated with CC3+ cells but no colocalisation was detected. At 48hrs, some evidence of apoptotic GFP+CC3+ cells was detected which might be consistent with remaining immune cells undergoing apoptosis to resolve the inflammatory response, perhaps by signals generated by the remodelling tissue itself.

It is well documented that monocytes and macrophages are capable of directing apoptosis in various tissues (Jaffe, Ruggiero and Falcone 1985, Arantes et al. 2000)

however evidence from studies in the human and mouse endometrium suggests that neutrophils are the key functional player in inducing apoptosis of decidual cells during tissue breakdown (Armstrong et al. 2017). Armstrong *et al* detected neutrophils using an anti-Gr1 antibody however Gr1 has been shown by others to be expressed by both granulocytes and monocytes (Rosas et al. 2010, Sasmono and Williams 2012), a result supported by the current study where *Gr1* was detected on GFP+ monocyte/macrophages. As Gr1 is composed of both Ly6C and Ly6G proteins (Yang et al. 2014, Rose et al. 2012) it is likely that Amstrong *et al* detected a missed population of cells and therefore results may need to be reinterpreted. Additionally although an increase in *Il6* and *Tnfα* was noted and attributed to neutrophil function by Armstrong *et al*, these cytokines are often secreted by inflammatory monocytes (Agarwal et al. 1995).

It has been documented that two subsets of macrophages exist in the human decidua during pregnancy: CD14+CD11c^{hi} macrophages (~67%) predominantly involved in inflammation, antigen processing, induction of apoptosis and immune regulation; and CD14+CD11c^{lo} (~33%) macrophages predominantly involved in smooth muscle cell regulation, ECM formation, tissue remodelling and phagocytosis (Houser et al. 2011). Although CD11c expression was not examined in the current study, it can be hypothesised that functional heterogeneity exists in the current data set which may reflect that seen by Houser *et* al: the induction of apoptosis (GFP+F4/80- cells) and subsequent clearance of apoptotic bodies (GFP+F4/80+ cells).

3.5.6 Regulation of monocyte/macrophage trafficking and differentiation

To complement the studies on the immune cell populations, the expression of cytokines and chemokines reported to be involved in the regulation of monocyte and macrophage trafficking and differentiation was measured across the time course of endometrial breakdown and repair. *Ccr2* and *Cx3cr1* are monocyte cell surface receptors which respond to *Ccl2* and *Cx3cl1* respectively to regulate the adhesion and migration of monocytes (Yang et al. 2014). Although *Ccl2* mRNA was upregulated in the endometrium throughout the time course, the corresponding receptor was only upregulated at 24hrs. In contrast both *Cx3cl1* and *Cx3cr1* mRNAs were upregulated in the endometrium at both 12 and 24hrs during tissue breakdown

and repair. These results would suggest that monocyte trafficking in the endometrium might be regulated predominantly through the Cx3cl1/Cx3cr1 alternative axis as opposed to the classic inflammatory axis of Ccr2/Ccl2 (Yang et al. 2014, Ino et al. 2014).

Additional factors examined included: *Ccl7* and *Ccl8* which are cytokines involved in monocyte trafficking; *Csf1* and *Csf2* which are involved in the proliferation, differentiation and survival of monocytes and macrophages; *Cxcl1* and *Cxcl2* which are secreted by macrophages and regulate the function of other immune cells; and *Cxcl3* and *Cxcl12* which are stromal derived factors which control migration, adhesion and activation of monocytes and other leucocytes. Dynamic changes in gene expression of each of these factors were noted in relation to time points of active tissue repair and may be important in orchestrating an immune response associated with scar-free repair. Analysis of anti-inflammatory cytokines (*Il10, Arg1*) associated with M2 or alternative macrophages and pro-inflammatory cytokines (*Il6, Tnfα*) associated with M1 or classical macrophages (Thiruchelvam et al. 2013), indicated that signals associated with pro-repair or alternative monocyte/macrophage populations were more predominant in endometrial tissue during scar-free tissue repair. As qPCR was carried out on whole tissue homogenates however, the spatial regulation of production and secretion of these factors was not realised.

3.5.7 Gene expression profiling of isolated immune cell subpopulations

To complement the analysis of whole tissue homogenates described above, gene expression analysis was carried out on the three isolated immune cell subpopulations uniquely identified in repairing endometrial tissue from MacGreen mice with the results summarised in Table 3-3. Interestingly both monocytes and monocyte-derived macrophages expressed *Csf1r* mRNA while tissue resident macrophages showed minimal expression which is in line with them being GFP- and further reinforces the novel results presented in this chapter. Monocytes (GFP+F4/80-) did not express *Ccr2* mRNA but highly expressed *Cx3cr1* mRNA. Monocytes have been phenotyped by differential expression of *Ccr2* with *Ccr2*+ monocytes having a higher capacity for migration and infiltration and therefore considered to be pro-inflammatory (Yang et al. 2014). More recently the expression

of *Cx3cr1* has been used to further stratify subsets where $Ccr2^{high}Cx3CR1^{low}$ cells are considered to be inflammatory monocytes and $Ccr2^{low}Cx3cr1^{high}$ cells are considered to be alternative monocytes (Yang et al. 2014, Ino et al. 2014).

Similarly GFP+F4/80- cells were found to express equal amounts of *CD14* mRNA and *CD16* mRNA, the ratios of which can also be used to determine monocyte phenotype, with a balance being indicative of intermediate monocytes which differentiate into M2-like macrophages (Mandl et al. 2014). With this in mind, the results of the current study suggest that GFP+F4/80- cells, previously denoted as inflammatory monocytes may represent alternative monocytes that give rise to macrophages with a pro-repair, M2-like phenotype (Thiruchelvam et al. 2013, Biswas et al. 2012, Das et al. 2015, Mantovani et al. 2013). Notably GFP+F4/80- cells expressed both anti-inflammatory (*Tgfβ1*, *Csf1*, *Il10*) and pro-inflammatory (*Tnfα*) cytokines. The use of IHC revealed that GFP+F4/80- cells were located in both the shed tissue and the repairing endometrium consistent with the relative diversity in function that may be attributed to signals in the microenvironment. Furthermore, *Tnfα* which was highly expressed in this subpopulation, is able to induce apoptotic cell death (Agarwal et al. 1995, Oróstica et al. 2016) and thus GFP+F4/80- cells may function in inducing apoptosis of decidualised stromal cells.

Monocyte-derived macrophages (GFP+F4/80+) expressed high levels of *Cx3cr1* mRNA and lower levels of *Ccr2*, *CD14* and *CD16* mRNA, suggesting that they have differentiated from their monocyte precursors as described above. Interestingly these cells also express *Arg1*, *Tgfβ1*, *Csf1* and *Il10* mRNAs which is indicative of a pro-repair, M2-like macrophage phenotype. Tissue resident macrophages expressed *Ccr2* mRNA and mRNAs for both anti-inflammatory (*Arg1*, *Tgfβ1*, *Csf1*) and pro-inflammatory (*Ifnγ*, *Il6*, *Tnfα*). Taken together, qPCR analysis has shown that although three distinct GFP/F4/80 subpopulations can be identified and isolated from endometrial tissue during repair based on surface marker expression, functional heterogeneity may exist within each population, likely to be related to their *in vivo* localisation. This requires further investigation.

3.5.8 Future prospects

To confirm if GFP+ cell become part of the tissue-resident macrophage population, lineage tracing studies are required and care must be taken when choosing which cell markers to use. Further characterisation of the phenotype and function of each subpopulation present in the MacGreen tissue will inform this decision although with current results in mind, *Cx3cr1* can be put forward as a potential target for these technologies. Additional phenotypic characterisation of the same cell populations during earlier (12hrs) and later (48hrs) time points may help uncover the origins of specific cell types and laser capture microdissection would help address the effects of spatial localisation on monocyte/macrophage cell phenotype and function. Studies using isolated cell populations including a comparative phagocytosis assay; phenotypic assessment of the cells using a flow cytometry antibody panel that interrogates multiple immune cell types; and more extensive analysis gene expression profiles and secreted proteins could be employed. Ultimately a single cell sequencing study would be useful in determining subtleties in the heterogeneity of the endometrial monocyte/macrophage population and how these respond during repair processes, not only informing endometrial physiology but also directing future experimentation.

Future functional studies are imperative to confirm if distinct immune cell populations are essential to endometrial repair. This might be achieved using transgenic knock out mice for example by comparison of *Ccr2* KO and *Cx3cr1* KO or by pharmacological inhibition of each subpopulation. It is hoped these studies may inform the development of cell-specific or cell-based therapies for a variety of gynaecological conditions and pathologies in other tissue systems where excessive scar formation is a problem.

3.5.9 Concluding remarks

The novel results obtained in the current study supports the hypothesis that a simple classification of monocytes and macrophages does not accurately reflect the diversity of these populations during tissue homeostasis and following injury, and highlights the limitation of using ‘definitive’ markers described in the literature for identification of immune cell subpopulations. Notably, analysing the inflammatory

response associated with endometrial tissue breakdown and repair in an established mouse model has uncovered novel immune cell subpopulations. A transient population of influxing 'alternative' monocytes and repair-specific monocyte-derived macrophages have been shown to associate with spatio-temporal regulation of endometrial repair and remodelling. In-depth characterisation and phenotyping of these uterine macrophage populations could lead to new insights into the role of macrophage heterogeneity in the regulation of tissue repair and scarless healing.

Chapter 4 Identification and characterisation of a population of putative mesenchymal progenitor cells in mouse endometrium

4.1 Introduction

The extensive regenerative capacity of the endometrium led to the development of a hypothesis proposing that a population of stem/progenitor cells exists in the tissue which may have a role to play in tissue regeneration (Dimitrov et al. 2008). The concept of stem cells in the endometrium was first introduced by Prainishnikov in 1978 however, the first evidence for their existence was only presented in 2004 by Chan *et al* (Chan et al. 2004). Since then, a growing body of work has identified stem/progenitor cells in the endometrium (both human and rodent) which have been shown to have functions important for maintaining tissue homeostasis (Gargett and Masuda 2010). A recent review by Gargett and colleagues highlighted a range of studies and different markers used to identify them (Gargett et al. 2016) highlighting both their potential as a therapeutic target and gaps in our knowledge.

4.1.4 Do mesenchymal stem cells (MSCs) exist in the endometrium?

Mesenchymal stem cells (MSCs) are a rare population of undifferentiated cells that have the ability to self-renew, proliferate and differentiate into several mesodermal lineages including adipocytes, chondrocytes and osteocytes (Cervelló et al. 2007). MSCs have been identified in many adult tissues including the heart, liver, dental pulp, umbilical cord, adipose tissue and the amniotic fluid and found to be crucial for the maintenance of tissue homeostasis (Dimitrov et al. 2008, Marquez-Curtis et al. 2015, Hass et al. 2011, Gargett et al. 2016, Kalinina et al. 2011). MSCs undergo asymmetric cell division to both maintain their own populations whilst also giving rise to more differentiated progenitor cells which are capable of rapid proliferation. These progenitor cells are then responsible for producing more differentiated and mature progeny known as transit-amplifying cells (Kalinina et al. 2011).

MSC are broadly defined as plastic adherent cells which can differentiate into adipocytes, osteoblasts and chondrocytes *in vitro* (Crisan et al. 2008), and express the following markers: CD29, CD44, CD73, CD90 and CD105 (Dimitrov et al. 2008). To

be classified as a MSC, cells must exhibit a capacity for self-renewal, proliferation, migration and multi-lineage differentiation (Spitzer et al. 2012, Phinney and Prockop 2007, Hwang et al. 2009, Takahashi et al. 2018).

Various techniques have been employed in an attempt to identify and characterise cells with a MSC-like phenotype in endometrial tissue and to determine if they represent a resident stem-cell like population (Deane, Gualano and Gargett 2013). These have included assays focussing on clonogenicity and self-renewal; the Hoechst exclusion assay to identify side population cells; the BrdU label retention system to identify label-retaining cells; tissue reconstruction by xenografting techniques; and *in vitro* differentiation assays (Gargett and Masuda 2010).

In 2004, Chan *et al*, identified small populations of both epithelial and stromal cells that had colony forming (CFU) ability *in vitro* (0.22% and 1.25% respectively). Notably their culture media were supplemented by the addition of TGFα, EGF and PDGF-BB (Chan et al. 2004). These clonal cells were found to have properties of self-renewal, a high proliferative potential and capacity for multilineage differentiation *in vitro* (Gargett et al. 2009). Gargett *et al*, suggested that this rare population of clonogenic cells should be identified as the endometrial MSC population.

In other studies, the Hoechst exclusion assay has been used identify side population (SP) cells: this assay relies on the fact that stem cells have the ability to extrude the DNA binding dye Hoechst 33342 due to expression of via the ATP-binding cassette transporter protein ABCG2/Bcrp1 (Cervelló et al. 2011, Hu et al. 2010, Kato et al. 2007). SP cells have been identified in both the epithelial and stromal compartment of the endometrium throughout the basalis and functionalis (Kato et al. 2007). Further characterisation of endometrial SP cells confirmed that SP cells expressed markers of undifferentiated cells including c-kitD/CD117 and Oct-4, could undergo multilineage differentiation and were able to reconstitute endometrial tissue *in vivo* after being engrafted under the kidney capsule of NOD-SCID mice (Cervelló et al. 2011).

A well-known method to identify stem/progenitor cells and their *in vivo* location in rodents is the label retaining cell (LRC) approach. This method is based on the finding that stem/progenitor cells undergo less cell divisions and retain labels integrated into

nuclear DNA (e.g BrdU) for longer than 'fast cycling' cell populations which include many differentiated cell types (e.g. glandular epithelium). LRC have been identified in the mouse endometrium in both the epithelial and stromal cell compartments (Chan and Gargett 2006b, Kaitu'u-Lino et al. 2012, Cao et al. 2015, Patterson and Pru 2013) and have been found to express markers of undifferentiated cell types including c-kit and Oct-4 (Cervelló et al. 2007). Unfortunately, the LRC approach does not definitively identify stem/progenitor cells and functional studies are hindered by the fact that BrdU detection assays require tissue fixation precluding FACS isolation (Gargett et al. 2016). Thus although SP cells and LRCs have been identified in the human and mouse endometrium respectively (Figure 4-1), a definitive MSC could not be identified using these approaches.

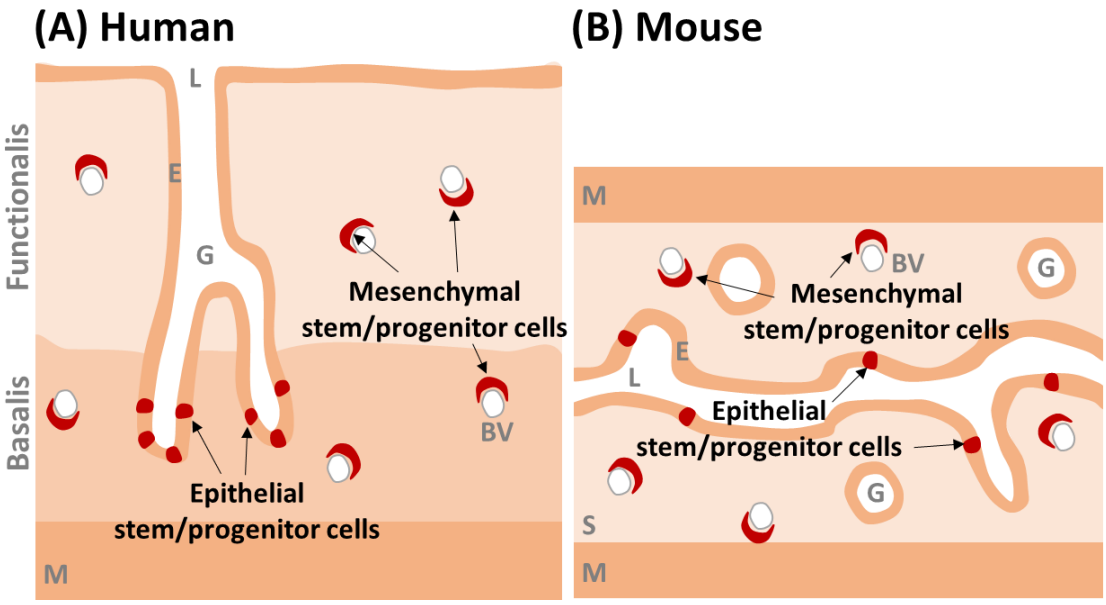

Figure 4-1. Hypothesised location of stem/progenitor cells in human and mouse endometrium. (A) In human endometrium epithelial progenitor cells identified by clonogenic and side population techniques, are located in the base of glands in the basalis while MSCs are located near blood vessels. **(B)** In mouse endometrium, LRC hypothesised to be stem/progenitor cells are located in the luminal epithelium and near blood vessels in the stroma (based on Gargett and Masuda 2010).

4.1.5 Endometrial MSC cell surface markers

To more reliably investigate endometrial MSCs specific cell markers were sought to discriminate between putative MSCs and other cell types in the endometrial tissue. Typical stem cell markers including Oct4, c-kit, CD90, CD44, CD73, and CD166 (Cho et al. 2004, Cervelló et al. 2007, Indumathi et al. 2013, Cheng et al. 2017) and MSC markers CD29, SUSD2 and CD105 (Schwab and Gargett 2007, Dimitrov et al. 2008, Phinney and Prockop 2007, Hwang et al. 2009, Marquez-Curtis et al. 2015) were used to identify putative endometrial MSCs in human (using clonogenic and SP techniques) and mouse endometrium (using LRC technique) through IHC and flow cytometry. A limitation of the results obtained was that these putative MSC specific proteins were also expressed by other cell types and therefore a combination of different markers was required to identify MSC. The challenge therefore was to detect cell surface or other proteins that would specifically identify endometrial MSCs so that they could be purified and separated from other endometrial cell types some of which are detailed below.

The RNA binding protein Musashi-1, known to be associated with control of asymmetric cell division of neural and epithelial progenitor cells, was found to be more highly expressed in the human endometrium than the myometrium (Götte et al. 2008). Further investigation reported that Musashi-1 was co-localised with Notch1 and telomerase (stem cell markers) and concluded that Musashi-1 could be used to identify endometrial MSCs in the human endometrium (Gotte *et al*, 2008). The same group reported an upregulation of putative endometrial stem-cell numbers expressing Musashi-1 in endometriosis and endometrial carcinoma (Götte et al. 2008).

It was also noted that human stromal cells only formed colonies *in vitro* in the presence of PDGF-BB and so it was hypothesised that endometrial MSCs may express Pdgfrβ (Chan et al. 2004, Schwab et al. 2005). To investigate this, Schwab and Gargett assessed the expression of PDGFRβ and the adhesion molecule CD146 (a well-known MSC marker) in human endometrium using IHC and identified cells that co-expressed PDGFRβ and CD146. They isolated these cells by FACS and performed *in vitro* assays to show they had clonogenic and multilineage differentiation potential. Furthermore, some perivascular cells were positive for PDGFRβ and CD146 which led to the

proposal that some or all endometrial MSCs may be perivascular pericytes which may have MSC activity. The lack of cell markers exclusive to pericytes has to date hindered definitive confirmation (Schwab and Gargett 2007). In a subsequent study profiling of $CD146^{+}$/$PDGFRB^{+}$cells, putative endometrial MSCs revealed gene signatures associated with self-renewal, multi-potency, differentiation, migration and immunomodulation. Expression of genes related to Notch, TGFB, IGF, Hedgehog, and G-protein-coupled receptor signalling pathways were increased (Spitzer et al. 2012).

The protein SUSD2 (sushi domain containing-2) identified by the W5C5 antibody, was identified as a novel marker for MSCs in the human endometrium (Masuda et al. 2012). Notably co-localisation studies (IHC) and FACS studies showed that W5C5+ cells were comparable to PDGFRβ+CD146+ cells when analysed, demonstrating clonogenicity, multilineage differentiation and self-renewal consistent with an MSC identity (Masuda et al. 2012, Gargett et al. 2016). Furthermore, these cells also had a perivascular location in both the basal and functional layer of endometrial stroma and when isolated and xenografted under the kidney capsule of NOD-SCID mice, these cells gave rise to endometrial stromal tissue *in vivo* (Masuda et al. 2012). This study was the first to report a single marker (SUSD2) for the identification of MSCs in human endometrial tissue.

Compared to the human tissue, cell surface markers for stem/progenitor cells in the mouse endometrium are less well characterised. Putative MSCs in the mouse endometrium have largely been identified using the LRC method in both the stromal and epithelial cell compartment (Chan and Gargett 2006b, Cervelló et al. 2007, Chan, Kaitu'u-Lino and Gargett 2012, Kaitu'u-Lino et al. 2012, Cao et al. 2015). LRCs have been further characterised by IHC and confirmed to express stem cell markers Oct4 and c-kit (Cervelló et al. 2007) as well as CD44, CD90, Pdgfrβ, CD146 and Sall4 (Chan and Gargett 2006b). Chan and Gargett, (2006) also described LRC as having a close association with CD31 expressing endothelial cells (IHC) in the stroma with their expression of α-SMA (IHC) indicative of a vascular smooth muscle cell or pericyte phenotype. The perivascular location of some of the stromal LRCs (Schwab and

Gargett 2007, Kaitu'u-Lino et al. 2012) parallels results from human eMSCs and to be consistent with a perivascular phenotype in mouse as well as human.

Pericytes are supportive cells that sit in close contact with endothelial cells of blood vessels in most tissues and have functions in regulating blood flow, perfusion of fluids, cells and proteins between capillaries and tissues, and supporting vascular development (Mills et al. 2013). It has been suggested that pericytes may also represent an adult tissue MSC as they are clonogenic and capable of giving rise to other types of mesenchymal cells including chondrocytes, adipocytes, osteoblasts and phagocytes following *in vitro* culture (Mills et al. 2013, Murray et al. 2014). In support of this hypothesis, pericytes express Pdgfrβ and CD146 as well as a number of other markers such as Rgs5, Acta2, Angpt2, Igf, Ngf and Pdgf also identified in stem and progenitor cells (Spitzer et al. 2012). It has been suggested that endometrial MSCs may be similar to vSMC, pericytes or endothelial cells since MSC progeny appear to share common markers with all these cell types (Schwab and Gargett 2007) however, further studies are needed to confirm their identity and function.

4.1.6 Summary

The endometrium experiences cyclical episodes of rapid repair and regeneration. A population of stem/progenitor cells has been identified in human endometrium as clonogenic cells and in mouse endometrium as LRC. These populations which have similar characteristics to MSCs in other tissues and can be further identified by expression of Pdgfrβ and CD146. Endometrial MSCs may have future beneficial implications when used in cell-based therapies for gynaecological pathologies and in regenerative medicine. Recently it has been proposed that MSCs in the human endometrium may be perivascular pericytes however further studies are needed to validate this identity. Various markers have been used to identify stem/progenitor cells in the endometria of women and mice and although SUSD2 (W5C5) has been identified as a specific marker to detect stromal progenitor cells in human endometrium (Masuda et al. 2012), to date no single marker has been found that exclusively identifies putative progenitor cells in the mouse endometrium.

4.2 Aim

To identify and characterise a population of mesenchymal stem/progenitor cells in the endometrium using the *Pdgfrβ-BAC- eGFP* transgenic mouse.

4.3 Experimental Approach

4.3.1 Transgenic mouse lines

The results in this chapter were generated using the *Pdgfrβ-BAC-eGFP* reporter mouse line as detailed in Section 2.1.1.1: in these mice GFP reporter protein is expressed under control of the *Pdgfrβ* gene promoter element. In mice Pdgfrβ is expressed by mesenchymal cells therefore using these mice facilitates identification and isolation of mesenchymal cells.

Further results were gathered using the NG2-CreER^{TM} BAC tamoxifen-inducible mouse line as detailed in section 2.1.1.5. In this line Cre-recombinase is expressed in NG2-expressing cells: results presented in Chapter 4 using the *Pdgfrβ-BAC-eGFP* reporter mouse line, identified NG2+ cells as GFP^{bright} pericytes. When crossed with the Ai14 reporter mouse line (Section 2.1.1.6), TdTomato is expressed in NG2 expressing cells and therefore this mouse allows pericytes to be identified by expression of TdTomato.

4.3.2 Tissue processing and Immunohistochemistry

Uterine tissue samples from *Pdgfrβ-BAC-eGFP* transgenic mice were briefly fixed in 4% PFA for 2 hours at 4°C, rinsed in PBS and stored overnight in 18% sucrose at 4°C before being embedded in OCT medium and stored at -80°C, as described in Section 2.3. H&E staining was carried out as in Section 2.4.1 and IHC performed following the protocols described in Section 2.4.3. Antibodies used for IHC in this Chapter are outlined in Table 4-1. Images were obtained by both brightfield and confocal microscopy as in Section 2.4.4.

Table 4-1. Antibodies used to interrogate mesenchymal progenitor cells in *Pdgfrβ-BAC-eGFP* mouse endometrial tissue

Antibody Name	Supplier and Cat. No. (concentration)	Dilution	Serum block
Polyclonal rabbit anti-GFP	Abcam, ab6556 (0.5mg/ml)	1/1000	Goat
Monoclonal rabbit anti-PDGFRβ	Abcam, ab32570 (0.15mg/ml)	1/1000	Goat
Monoclonal rabbit anti-CD146 (MCAM)	Abcam, ab75769 (0.123mg/ml)	1/1000	Goat
Polyclonal Rabbit anti-NG2 (Cspg4)	Abcam, ab12905	1/600	Goat
Monoclonal mouse anti-αSMA	Sigma, A-2547	1/10K	Horse
Polyclonal rabbit anti-CD31	Abcam, ab28364 (1mg/ml)	1/500	Goat
Polyclonal rabbit anti-EpCAM	Abcam, ab71916 (1mg/ml)	1/2000	Goat

4.3.3 Flow Cytometry and FACS

Flow cytometry analysis was used to interrogate the endometrial mesenchyme using protocols detailed in Section 2.5 and flow cytometry antibodies outlined in Table 4-2. FACS was used to isolate specific mesenchymal cell populations from the endometrial tissue following the protocol in Section 2.5.3

Table 4-2. Flow cytometry antibody panel designed to interrogate mesenchymal cell populations in uterine tissue

Antibody name	Supplier Cat. No. (concentration)	Excitation wavelength	Emission wavelength	Dilution
BV421 anti-mouse CD31 (Pecam1)	BioLegend, 102423 (0.2mg/ml)	405nm	421nm	1/200
V450 anti-mouse CD45: 30-F11	Fischer scientific, BDB560501 (0.2mg/ml)	404nm	448nm	1/100
PE anti-mouse CD146 (MCAM)	BioLegend, 134704 (0.2mg/ml)	496nm	578nm	1/200
BV605 anti-mouse CD326 (EpCAM)	BioLegend, 118227 (0.2mg/ml)	405nm	603nm	1/400
APC anti-mouse CD140b (PDGFRβ)	BioLegend, 136008, (0.2mg/ml)	650nm	660nm	1/100
AF488 anti-mouse NG2	Merck, AB5320A4	495nm	519nm	1/100
APC anti mouse CD146 (MCAM)	BioLegend, 134712, (0.2mg/ml)	650nm	660nm	1/200

4.3.4 Cytospin and Immunocytochemistry

A cytospin was carried out on isolated mesenchymal cells, outlined in Section 2.5.4.1 and immunocytochemical staining performed (Section 2.5.4.2) to analyse expression of key cell surface markers used in the isolation method.

4.3.5 RNA extraction methods and cDNA synthesis

Two RNA extraction methods were used on isolated cell samples: the Qiagen RNease mini kit outlined in Section 2.6.1; and the SimplyRNA Cells Maxwell 16 LEV kit outlined in Section 2.6.3. The resulting yield of RNA from each method was compared using the LabChip GX Touch Nucleic Acid Analyser (Section 2.6.4) and the RNA Pico Sensitivity Assay (Section 2.6.4.1). cDNA samples for qPCR were synthesised from RNA samples using the superscript VILO cDNA Synthesis kit (Section 2.7.1) while cDNA samples for NGS were synthesised using the NuGEN Ovation RNA-Seq System V2 (Section 2.7.2).

4.3.6 Quantitative real time PCR

Quantitative real time PCR (qPCR) was used to determine mRNA expression of specific genes used to identify mesenchymal progenitor cells as detailed in Section 2.8 using primers detailed in Table 2-17. Quantification of gene expression and statistical analysis was performed as outlined in Section 2.8.3.

4.3.7 Next Generation Sequencing

Mesenchymal cells were isolated from *Pdgfrβ-BAC-eGFP* uterine tissues. RNA extraction and cDNA synthesis was carried out as described in Section 2.9.1. Samples were sent to Edinburgh Genomics for sequencing on the HiSeq 4000 75PE platform according to standard protocols at the facility (Section 2.9.2). Bioinformatic analysis of the NGS data was largely carried out by Jonathan Manning at the Edinburgh Genomics facility, as described in Section 2.9.3. Validation of the results was achieved using qPCR on an independent set of cell samples generated from naïve *Pdgfrβ-BAC-eGFP* endometrial tissues (Section 2.9.4).

4.4 Results

4.4.1 Validation of *Pdgfrβ-BAC-eGFP* transgenic mouse line by immunohistochemistry

In the transgenic *Pdgfrβ-BAC-eGFP* reporter mouse, eGFP (green fluorescent protein) is expressed under control of the *Pdgfrβ* gene promoter element. In previous studies Pdgfrβ has been identified as a putative progenitor cell marker in human endometrium (Schwab and Gargett 2007, Spitzer et al. 2012, Bhartiya 2016) therefore the *Pdgfrβ-BAC-eGFP* reporter mouse was considered an ideal choice for these studies to identify putative progenitor cell populations and their distribution in mouse endometrial tissue.

4.4.1.1 Expression of eGFP reporter protein in *Pdgfrβ-BAC-eGFP* endometrial tissue

In uterine tissues from cycling *Pdgfrβ-BAC-eGFP* transgenic mice (n=8), GFP was expressed exclusively in stromal cells distributed throughout all layers of the endometrium and was absent from epithelial cells (glandular and luminal) and myometrial smooth muscle cells of the myometrium (Figure 4-2 (A-D). Based on the intensity of the GFP there appeared to be two subpopulations: GFP^{dim} cells dispersed throughout the stromal compartment and GFP^{bright} cells located in more specific clusters (Figure 4-2, yellow versus white arrows).

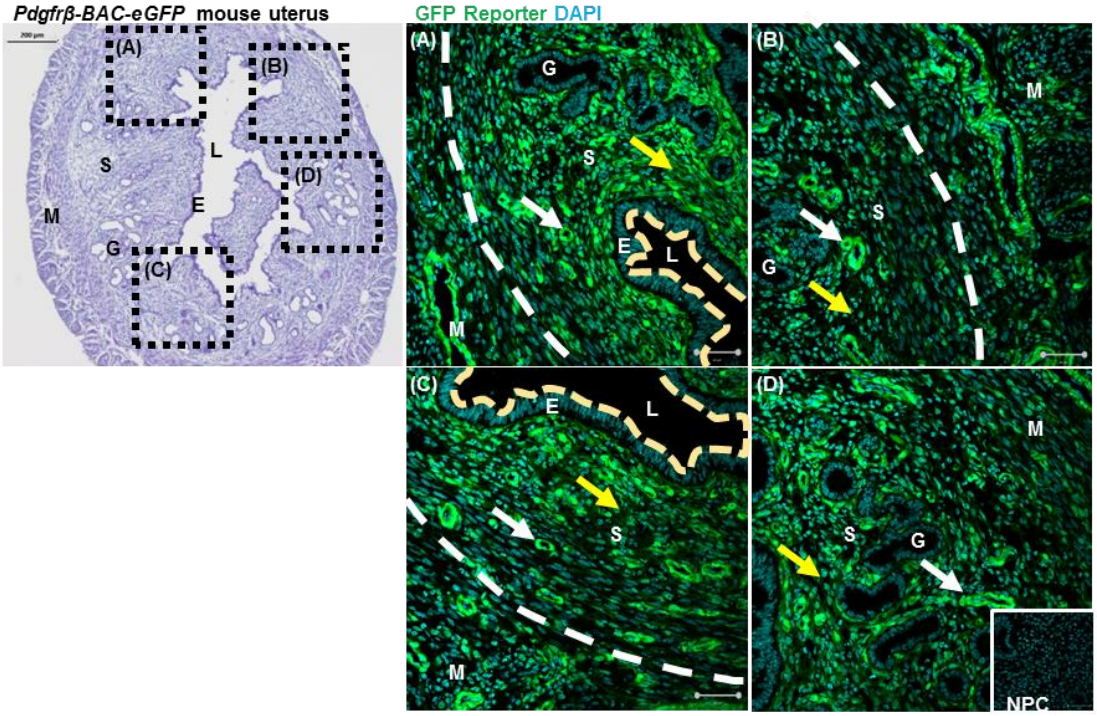

Figure 4-2. Expression of GFP in naïve mouse endometrium from *Pdgfrβ-BAC-eGFP* adult females. (A-D) IHC reveals that GFP is expressed exclusively by cells of the stromal compartment (S) and not expressed by cells of the epithelial compartment be that glandular or luminal (E and G respectively) in the *Pdgfrβ-BAC-eGFP* transgenic uterus. Epithelium (E, yellow dashed line), Glands (G), Stroma (S), and Myometrium (M), stroma-myometrial junction (white dashed line). Two GFP+ cell populations are apparent: GFP^{dim} cells dispersed throughout the stroma (yellow arrows) and GFP^{bright} cells which appear to be more specifically clustered (white arrows) (representative image, n=8, Scale bar 20µm).

4.4.1.2 Expression of Pdgfrβ native protein in *Pdgfrβ-BAC-eGFP* endometrial tissue

As an additional validation of the *Pdgfrβ-BAC-eGFP* transgenic line a double IHC stain was used to detect co-localisation of GFP and endogenous Pdgfrβ expression in endometrial tissues from adult cycling females. As above, two distinct subpopulations of GFP+ cells were apparent: GFP^{dim} and GFP^{bright} cells. Pdgfrβ was detected exclusively in cells of the stromal compartment although in contrast to GFP there was no apparent difference in intensity of Pdgfrβ detected by the antibody in different stromal subpopulations. As there was 100% co-incidence between expression of GFP and Pdgfrβ in cells of the stromal compartment it was concluded GFP is acting as a

reliable reporter for Pdgfrβ gene promoter activity and gene expression in the *Pdgfrβ-BAC-eGFP* transgenic line (Figure 4-3).

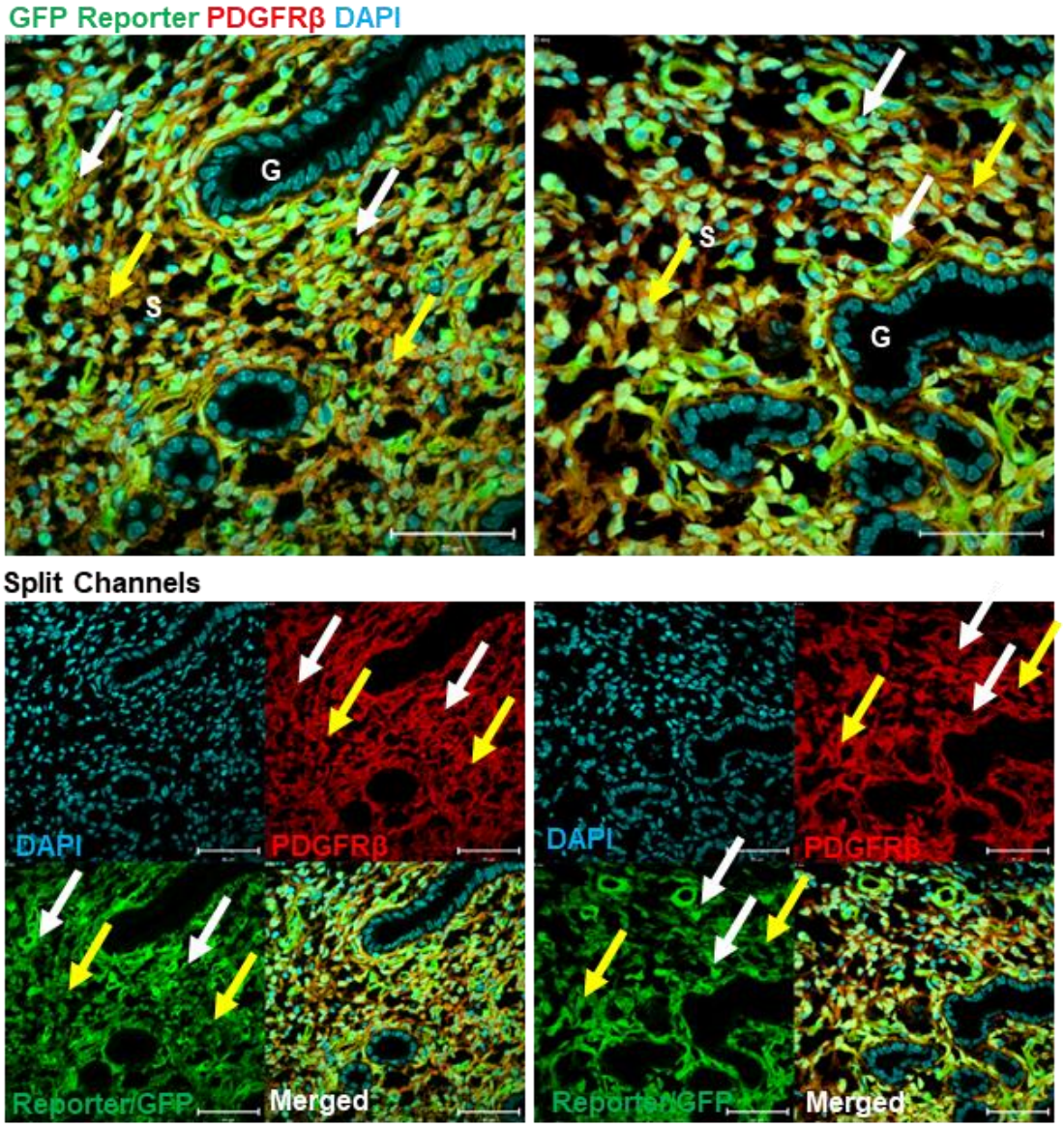

Figure 4-3. Expression of GFP and Pdgfrβ in naive *Pdgfrβ-BAC-eGFP* endometrial tissue. Immunohistochemistry revealed that the expression of the reporter GFP (green) exclusively identifies cells that express Pdgfrβ (red) in cycling *Pdgfrβ-BAC-eGFP* transgenic mouse uterus. Notably the GFP/Pdgfrβ double positive cells (yellow) are located throughout the endometrial stroma (S) but not detected in epithelial cells of the glands (G) in adult cycling uterine tissues. There is not an apparent difference in the expression of Pdgfrβ between GFP^{dim} cells (yellow arrows) and GFP^{bright} cells (white arrows) (representative image, n=8, Scale bar 50μm).

4.4.2 Characterisation of mesenchymal cells in *Pdgfrβ-BAC-eGFP* transgenic endometrial tissue

4.4.2.1 Characterisation of mesenchymal cells based on cell surface marker expression by IHC

Having established that all GFP+ cells were Pdgfrβ+, IHC with antibodies chosen to detect a range of cell marker proteins was used to characterise the two subpopulations of stromal GFP+ cells in *Pdgfrβ-BAC-eGFP* endometrial tissue. The following markers were used based on previous reports of their patterns of expression: CD146 (Mcam) expressed by endothelial cells and smooth muscle cells; NG2 (Cspg4) expressed by smooth muscle cells and pericytes; αSMA (Acta2) expressed by smooth muscle cells; CD31 (Pecam-1) expressed by endothelial cells; and EpCAM (CD326) expressed by epithelial cells. All GFP+ cells were found to be CD31- and EpCAM- distinguishing them from both endothelial and epithelial cells respectively (Figure 4-4 (E-F)). GFP^{dim} cells were confirmed as Pdgfrβ+, CD146-, NG2- and aSMA- indicative of a stromal fibroblast phenotype while GFP^{bright} cells were found to be Pdgfrβ+, CD146+, NG2+ and aSMA+ a phenotype consistent with that of putative pericytes (Figure 4-4 (A-D)).

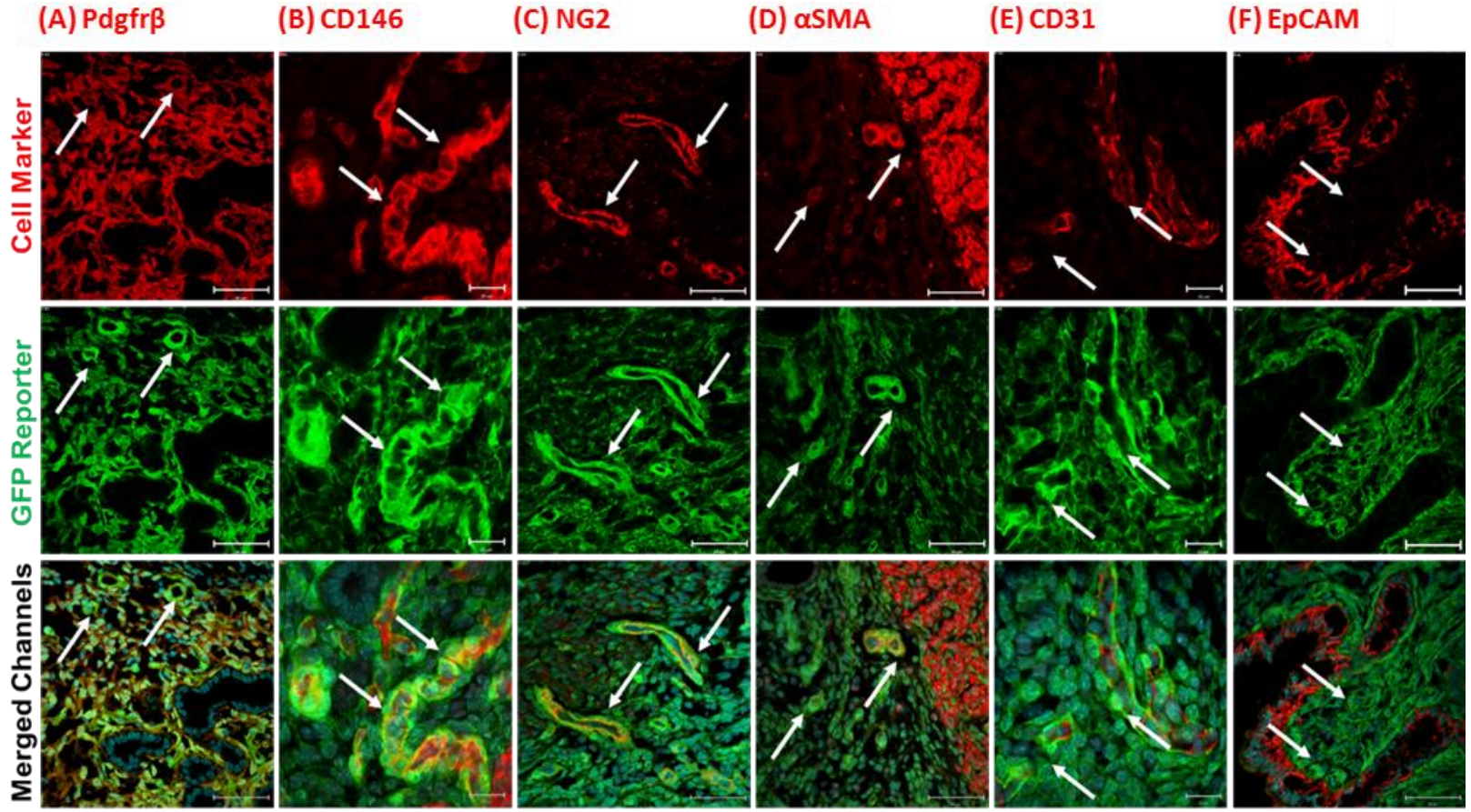

Figure 4-4. Characterisation of GFP^{bright} cells and GFP^{dim} cells in Pdgfrβ-BAC-eGFP uterine tissue. (A-D) Immunofluorescent staining reveals GFP^{bright} cells (white arrows) to be Pdgfrβ+, CD146+, aSMA+, and NG2+ consistent with a perivascular pericyte phenotype while GFP^{dim} cells are Pdgfrβ+, CD146-, aSMA- and NG2- indicative of a stromal fibroblast phenotype. **(E-F)** All GFP^{+} cells are CD31- and EpCAM- distinguishing them from endothelial and epithelial cells respectively (representative images, n=8, Scale bars 50µm).

4.4.2.2 Investigation of endometrial mesenchymal cell types in the perivascular niche

To complement and extend these findings, GFP expression in cells associated with endometrial vasculature was compared to that of the endothelial cell marker CD31 and the putative pericyte marker CD146 using IHC. Notably, GFP^{bright} cells were revealed to be CD146+CD31- and were located in close proximity to CD31+CD146+ endothelial cells. This confirmed their perivascular location and further supported their identity as pericytes which reside in the perivascular niche (Figure 4-5, white arrows).

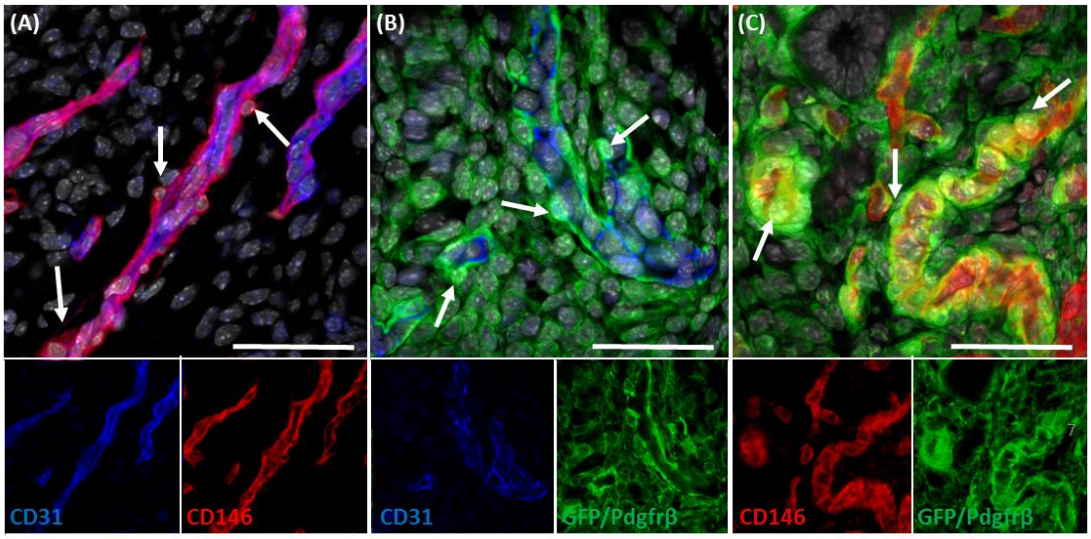

Figure 4-5. Expression of blood vessel markers in association with GFP positive cells in *Pdgfrβ-BAC-eGFP* uterine tissue. Immunohistochemistry using CD31 as an endothelial cell marker, CD146 as a putative pericyte marker and Pdgfrβ as a mesenchymal cell marker reveals **(A)** CD31+CD146+ endothelial cells surrounded by CD31-CD146+ cells (white arrows), **(B)** CD31+GFP- endothelial cells surrounded by CD31-GFP^{bright} cells (white arrows) and **(C)** CD146+GFP- endothelial cells surrounded by CD146+GFP^{bright} cells (white arrow) (representative images, n=8, Scale bars 50µm).

Transmission Electron Microscopy (TEM) was used to look at higher magnifications to examine the ultrastructure of endometrial blood vessels. Blood vessels were identified by the presence of red blood cells in the vessel lumen (Figure 4-6 (A-A')). In the mouse uterine tissues the endometrial blood vessels were found to be composed of endothelial cells that were closely surrounded by perivascular cells that were embedded within a collagenous basement membrane (Figure 4-6), a hallmark of perivascular pericytes (Bergers and Song 2005).

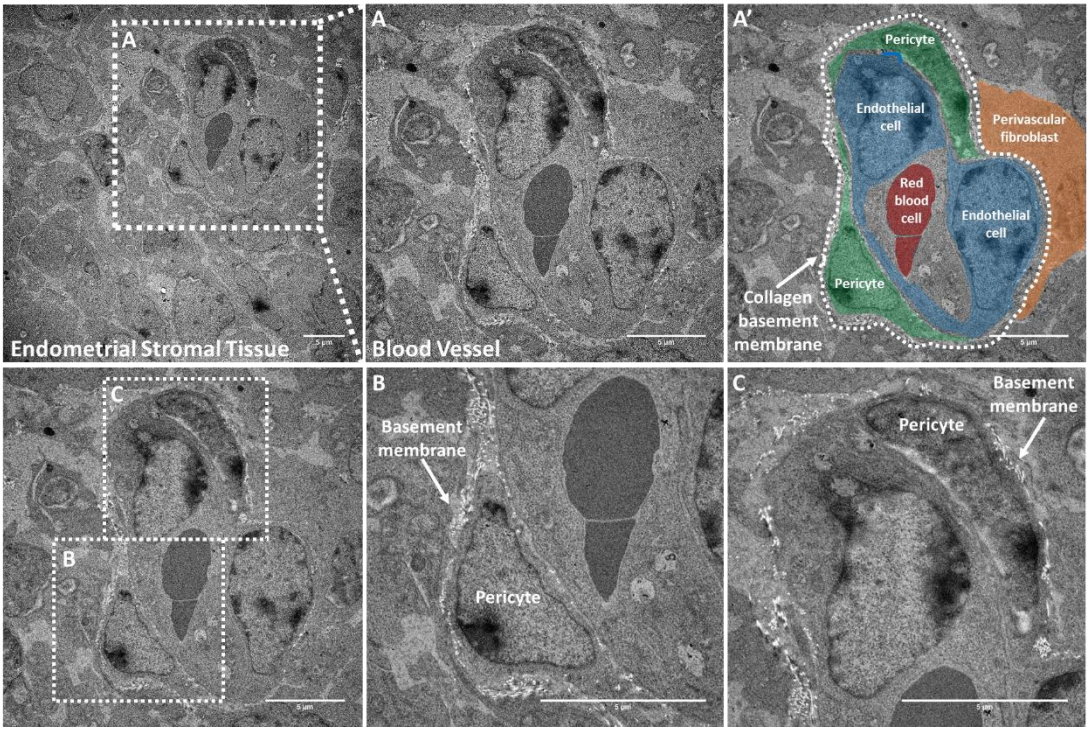

Figure 4-6. Transmission Electron Microscopy (TEM) of naïve murine endometrial tissue. (A) Blood vessel structures can be located in endometrial stromal tissue by the presence of red blood cells which appear as easily identifiable black shapes in the section. **(A')** Blood vessels are composed of endothelial cells (blue overlay) and have red blood cells present in the vessel lumen (red overlay) with perivascular cells (green overlay) surrounding the endothelial cells and perivascular fibroblasts (orange overlay) on close association. **(B-C)** Perivascular cells are located within the collagenous basement membrane of the blood vessel (representative images, n=4, Scale bars 5µm).

4.4.2.3 Semi-quantitative analysis of putative pericytes in mouse endometrial tissue by IHC

Having confirmed that Pdgfrβ was expressed by both stromal fibroblasts (GFP^{dim}) and perivascular pericytes (GFP^{bright}) while CD146 was expressed by both pericytes and endothelial cells (CD31+ cells), it was clear that neither could be used in isolation to identify pericytes. Characterisation by IHC revealed that NG2 was expressed by GFP^{bright} cells (Figure 4-5) and further IHC revealed that NG2+ cells were located in close association with blood vessels, composed of CD31+ endothelial cells (Figure 4-7).

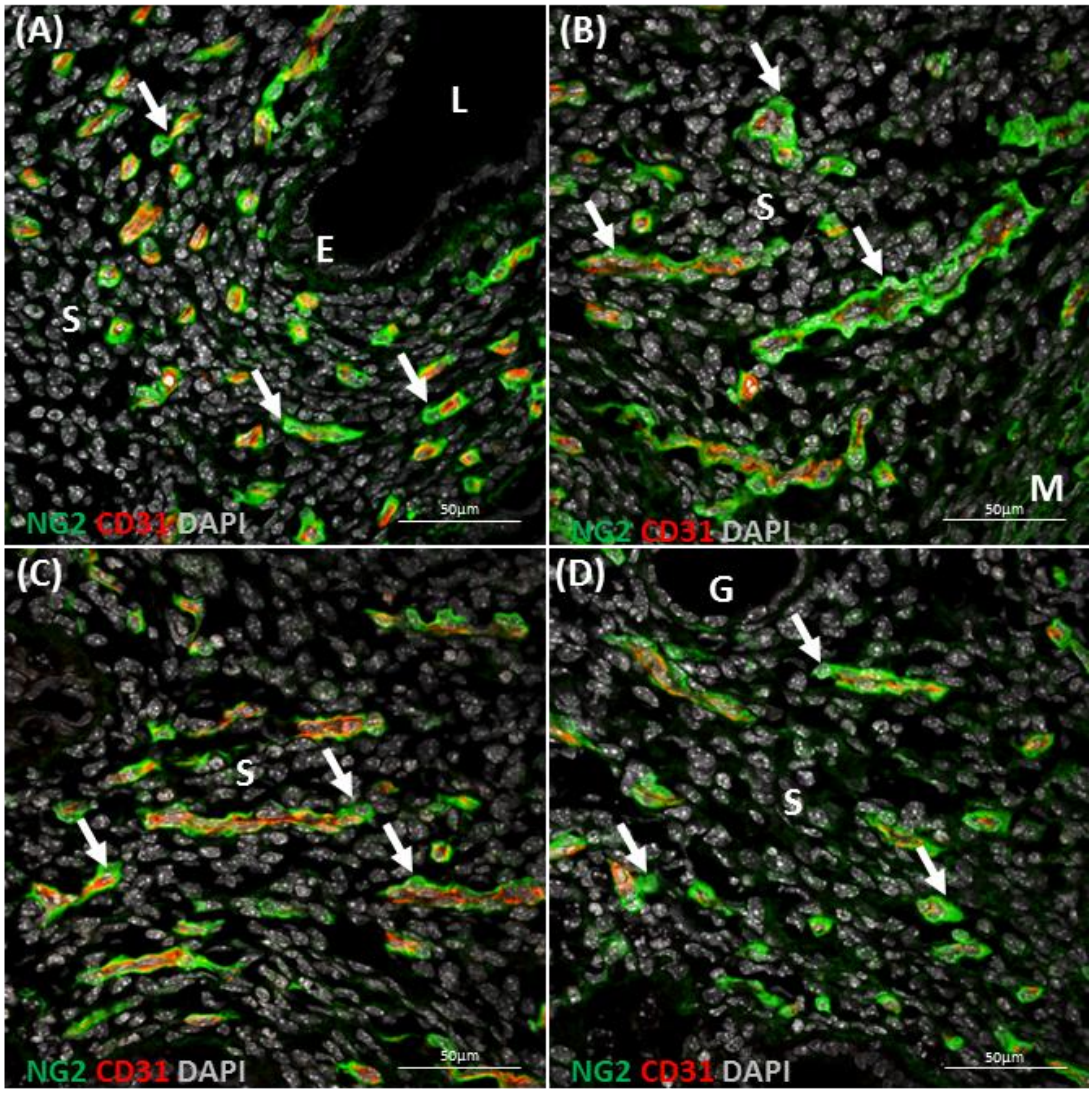

Figure 4-7 IHC analysis of CD31 and NG2 expressing cells in endometrial tissue. (A-D) CD31+ endothelial cells (red) surrounded by NG2+ pericytes (green; white arrows) located in various regions of the endometrial stromal compartment. Stroma (S), Epithelium (E), Lumen (L), Myometrium, (M) and Glands (G) (representative images, n=8, scale bar = 50µm).

To analyse the relationship between pericytes and endothelial cells, cell counting was performed on immunostained sections of mouse uterus to determine the numbers of both CD31+ endothelial cells and NG2+ pericytes per field of view (FOV) in uterine tissue sections. Cells were only counted if there was a visible nucleus associated with positive staining, and distinguished by staining for CD31 and NG2, as outlined in Figure 4-8 (A). In naïve mouse endometrium there was significantly more pericytes

per FOV (38±1.36) than endothelial cells (28.5±1.43) (paired t-test, p<0.0001) (Figure 4-8 (B), resulting in a pericyte:endothelial cell ratio of 1.25±0.02 (Figure 4-7 (C)). Notably all the NG2+ pericytes were found in a perivascular location in close associated to CD31+ endothelial cells (100±0.24%) (Figure 4-8 (D)).

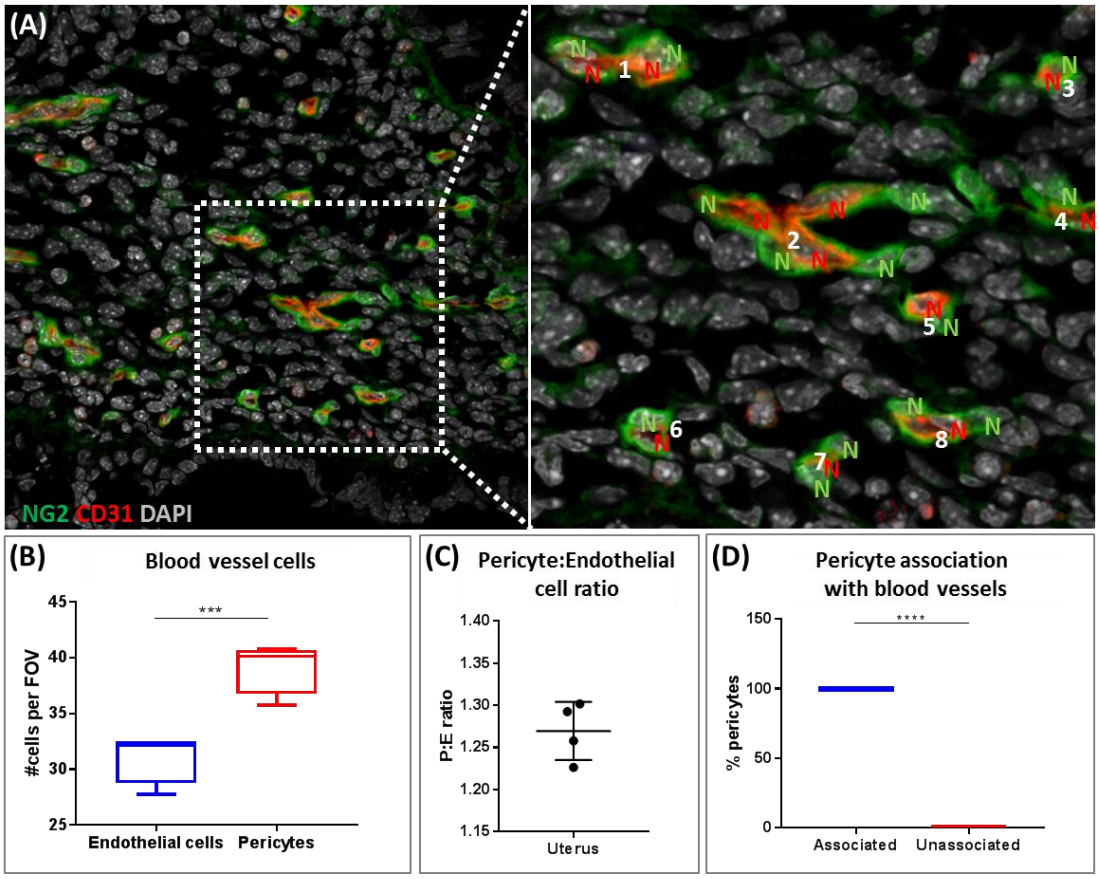

Figure 4-8 Analysis of pericytes and endothelial cells in endometrial tissue. (A) Method employed to count pericytes and endothelial cells: red 'N' represents the nucleus of a CD31+ cell; green 'N' represents the nucleus of an NG2+ cell; numbers are assigned to blood vessel structures identified through presence of CD31+ staining. Uterine tissues were collected from four naïve mice (n=4) and two tissue sections were analysed per mouse (n=8). In each tissue section, two fields of view (FOV) were imaged (n=16). **(B)** CD31+ cells (red N) and NG2+ cells (green N) were counted and presented as the number of cells per FOV (n=4, paired t-test, p<0.001). **(C)** The ratio of pericytes: endothelial cells and **(D)** the proportion of NG2+ pericytes associated with blood vessel structures (determined by positive CD31 staining) was calculated for each FOV (n=4, paired t-test, p<0.0001).

4.4.2.4 Analysis of GFP+ subpopulations in *Pdgfrβ-BAC-eGFP* transgenic endometrial tissue by Flow cytometry

To assess the relative proportions of each GFP+ subpopulations to the stromal compartment, *Pdgfrβ-BAC-eGFP* uterine tissues were digested and flow cytometry performed on single cell suspensions. Flow cytometry analysis was carried out using analytical gates detailed in Figure 4-9.

The unstained control was a single cell suspension generated from age-matched naïve C57BL/6 mouse (GFP-) which was not incubated with any flow cytometry antibodies therefore allowing for the detection of the negative population when assessing the signal for each fluorochrome. The stained control was a single cell suspension generated from a *Pdgfrβ-BAC-eGFP* mouse (GFP+) incubated with all the flow cytometry antibodies to assess the positive population of each and any overlap in signal. Cell suspensions were also prepared for single antibody stains to analyse the positive signal of each fluorochrome. The'fluorescence-minus-one' (FMO) controls contained all the antibodies in a given panel except one which ensured that any spread of the fluorochromes into the channel of interest was properly identified, allowing for the true identification of the negative population. A representation of the setup of flow cytometry controls can be found in Chapter 2, Section 2.5.2, Table 2-10.

Following the establishment of gates from the single and FMO analyses to specifically analyse mesenchymal cells in uterine tissue, a gate was set to exclude both CD31+ and CD45+ cells therefore excluding endothelial and immune cells respectively (Figure 4-9 B lower right). GFP expression was used to identify mesenchymal cells (Figure 4-9 (B,C,D)) and to compare this to the expression of CD146 and EpCAM to determine the proportions of cells with pericyte and epithelial cell phenotypes (Figure 4-9 (C, D).

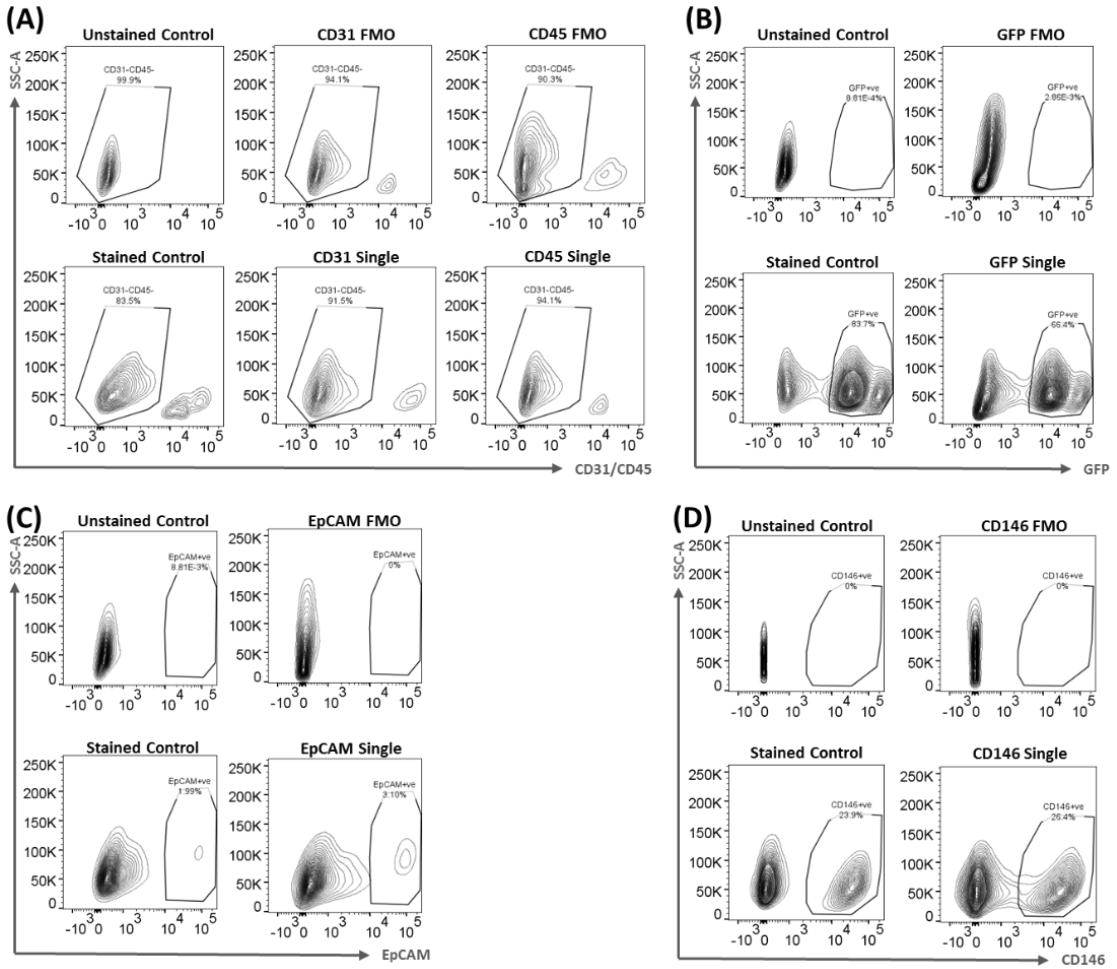

Figure 4-9. Parameters employed to draw analytical gates for flow cytometry analysis of mouse endometrial tissue. A gating strategy was devised to exclude and/or analyse cell populations in naïve *Pdgfrβ-BAC-eGFP* uterine tissues based on unstained, fully stained, singlestained and 'fluorescence minus one' (FMO) controls. **(A)** Antibodies against CD31 and CD45 had similar fluorophores and were used to exclude endothelial cells and immune cells from the analysis. To capture the CD31-CD45- cell population a gate was drawn excluding positive signals derived from the single stains, FMOs and fully stained controls. Analytical gates to capture **(B)** GFP+ cells, **(C)** EpCAM+ cells and **(D)** CD146+ cells were determined against unstained, fully stained, single stained and FMO controls respective to each marker (representative plots, n=3). A full set of controls was prepared for each flow cytometry analysis undertaken in this thesis to ensure accurate gating.

To complement and extend IHC analysis of GFP+ uterine tissues with respect to CD146 and EpCAM, further flow cytometry analysis was undertaken. A sequential gating strategy (Figure 4-10 (A)) was employed to target live and single cells only. Specifically, an 'All cells' gate was drawn to remove data points with low side and

forward scatter (SSC-A and FSC-A respectively) identified as cell debris (Figure 4-10 (A)). A 'Single cell' gate was drawn to capture data points representing single entities and remove potential doublets (Low FSC-H high FSC-A) (Figure 4-10 (B)) and the DAPI signal was used to exclude dead cells (DAPI+) from the data (Figure 4-10 (C)). To further exclude endothelial cells and immune cells from the analysis, a gate was set to capture data points that were both CD31- and CD45- respectively. The antibodies for these two proteins expressed a similar fluorochrome therefore used as an exclusion signal (Figure 4-9 (A) and 4-10 (D)). To analyse mesenchymal cells within the remaining dataset, the expression of GFP was analysed against SSC-A: based on GFP intensity alone two subpopulations of cells were detected: GFP^{dim} and GFP^{bright} cells (Figure 4-10 (E)), confirming IHC results described previously. Further analysis of the relative expression of CD146 by GFP+ cell populations confirmed that GFP^{dim}cells were CD146- while GFP^{bright} cells were CD146+ (Figure 4-10 (F)) identifying them as stromal fibroblasts and pericytes respectively. Plotting these results in histograms displayed the difference in the intensity of GFP expression by mesenchymal sub-populations (Figure 4-10 (G)) and confirmed that GFP^{bright} cells expressed CD146 while GFP^{dim} cells did not express CD146 (Figure 4-10 (H)). Plots in Figure 4-9 (I) and (J) summarise the data showing that in uterine tissue the GFP^{bright}CD146+ cell population accounts for a smaller proportion of total GFP+ mesenchymal cells than the GFP^{dim}CD146- cell population.

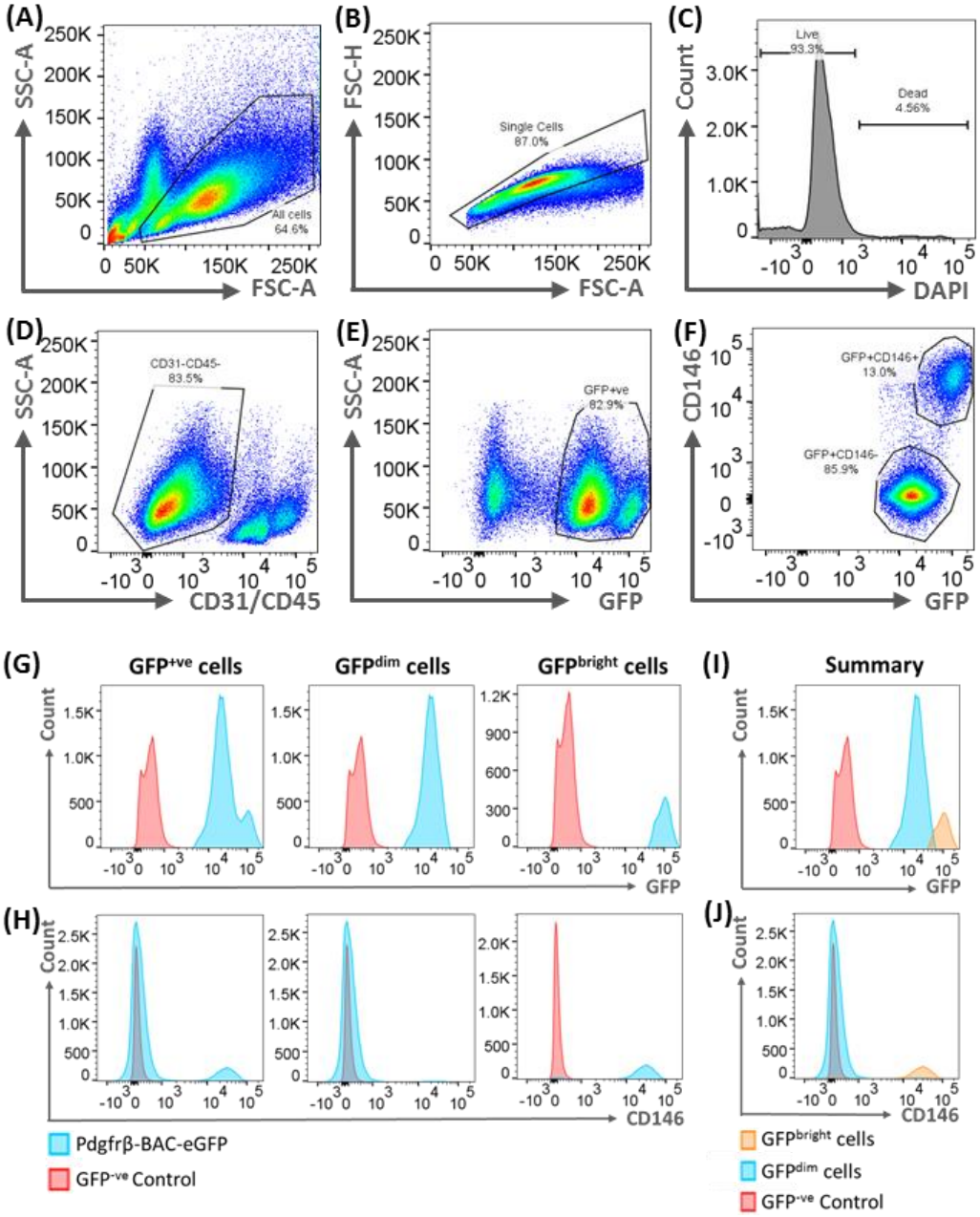

Figure 4-10. Flow cytometry analysis and phenotyping of GFP+ cell populations in naïve *Pdgfrβ-BAC-eGFP* endometrial tissue. Sequential gating strategy employed to analyse GFP/PDGFRβ^{+} cell populations in mouse uterine tissue: **(A)** All cells > **(B)** Single cells > **(C)** Live cells > **(D)** CD31^{-}CD45^{-} cells > **(E)** GFP^{+} cells > **(F)** CD146$^{-/+}$ cells, percentages displayed are frequencies of the parent gate. All gates drawn using single stained, unstained and 'fluorescence minus one' (FMO) control samples (Figure 4-9) (representative plots, n=8). **(G)** Analysis of GFP expression by GFP^{+}, GFP^{dim} and GFP^{bright} cells in *Pdgfrβ-BAC-eGFP* uterus (blue) when compared to C57Bl/6 control uterus (red). **(H)** Analysis of CD146 expression by GFP^{+}, GFP^{dim} and GFP^{bright} cells in *Pdgfrβ-BAC-eGFP* uterus (blue) when compared to C57Bl/6 control uterus (red). **(I)** Summary of GFP expression by GFP^{dim} and GFP^{bright} cells in *Pdgfrβ-BAC-eGFP* uterus. **(J)** Summary of CD146 expression by GFP^{dim} and GFP^{bright} cells in *Pdgfrβ-BAC-eGFP* uterus (representative plots, n=8).

Following this detailed flow cytometry analysis, quantification of the specific cell populations from multiple tissue isolations (8 naïve mice; pooled uterine horns) revealed that GFP^{bright} cells accounted for 17.22±1.26% of the GFP+ mesenchymal cell population while the remaining 82.78±1.29% were GFP^{dim} cells (Figure 4-11 (A)). When results were reanalysed as a frequency of live cells in the tissue, GFP^{bright} cells accounted for 8.33±0.36% while GFP^{dim} cells accounted for 40.05±2.25% (Figure 4-11 (B)).

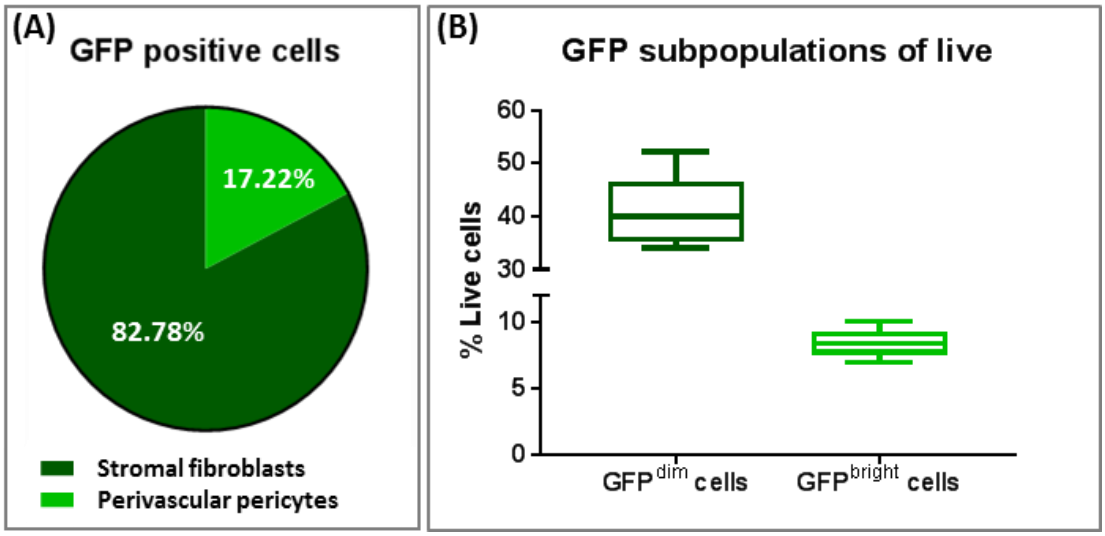

Figure 4-11. Analysis of mesenchymal cell populations in naïve *Pdgfrβ-BAC-eGFP* endometrial tissue by flow cytometry. Uterine tissues were collected from *naïve Pdgrβ-BAC-eGFP* mice (n=8), digested and incubated with flow cytometry antibodies. Based on the gating strategy outlined in Figure 4-10, the proportion of GFP+ subpopulations was calculated. **(A)** Pie chart analyssi of the relative proportions of GFP^{dim} and GFP^{bright} cell populations determined as a frequency of total GFP+ mesenchymal cells. **(B)** Relative proportion of GFP^{dim} and GFP^{bright} cell populations calculated as a frequency of live single cells in naïve mouse endometrium. Data representative of n=8 mice.

4.4.3 Isolation and characterisation of GFP^{dim} and GFP^{bright} cells from *Pdgfrβ-BAC-eGFP* transgenic endometrial tissue

4.4.3.1 Characterisation of GFP+ subpopulations isolated by fluorescent activated cell sorting (FACS) and cytospin

Following the detailed analysis by flow cytometry that identified GFP^{dim} and GFP^{bright} cell populations (stromal fibroblasts and pericytes respectively) the same previously

validated parameters (Figures 4-9, 4-10) were used to isolate GFP+ subpopulations using a Fluorescence Activated Cell Sorter (FACS), based on their relative expression of GFP and CD146. To confirm the identity of the isolated cells, a cytospin was performed and immunocytochemistry used to stain for GFP, Pdgfrβ and CD146 using an independent set of antibodies to those used for Flow and FACS. The cytospins confirmed that the GFP^{bright} cells were GFP+/Pdgfrβ+/CD146+ while GFP^{dim} cells were GFP+/Pdgfrβ-/CD146- in line with previous results (Figure 4-12 (B)). The appearance of the two cell populations was also distinct with the GFP^{dim} cells adopting a clear fibroblastic phenotype (Figure 4-12 (B) lower panels).

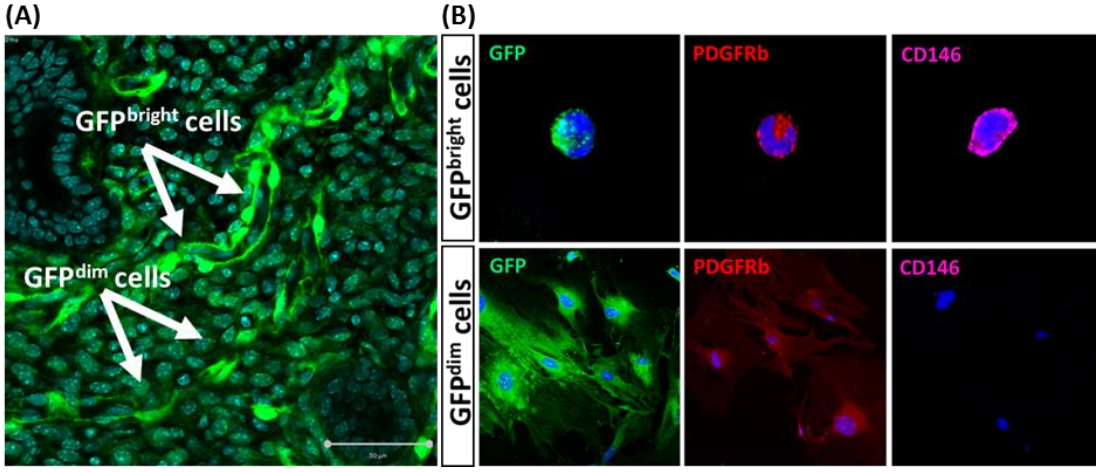

Figure 4-12. Isolation and characterisation of GFP^{dim} stromal fibroblasts and GFP^{bright} pericytes from naive *Pdgfrβ-BAC-eGFP* endometrial tissue. (A) GFP^{dim} and GFP^{bright} cells can be isolated from adult *Pdgfrβ-BAC-eGFP* mouse uterus (Immunohistochemistry, scale bar 50μm) by a fluorescence activated cell sorter (FACS) based on intensity of GFP expression. **(B)** Cytospin and IHC on isolated cells confirms that GFP^{bright} cells are $GFP^{+}Pdgfr\beta^{+}CD146^{+}$ while GFP^{dim} cells are $GFP^{+}Pdgfr\beta^{+}CD146^{-}$, as determined with an independent set of antibodies (n=3).

4.4.3.2 Optimisation of techniques for RNA extraction from isolated cells

RNA extraction was performed using two different techniques to identify the optimal method for a small number of input cells (<20,000): Qiagen RNeasy Mini Kit (manual) and Promega SimplyRNA Cells Maxwell® 16 LEV kit (automated) as described in Chapter 2: Sections 2.7.3 and 2.7.4. The concentration (ng/μl) and integrity (RIN

score) of the RNA samples were analysed by LabChip technology (Chapter 2: Section 2.7.5) to compare the efficiency of each technique. The RNA yield from both GFP^{dim} cells (n=4) and GFP^{bright} cells (n=4) was significantly more with the automated method when compared to the manual method of RNA extraction (GFP^{dim} cells: 14.05±6.15 ng/µl versus 2.65±0.36 ng/µl, unpaired t-test, p=0.02; GFP^{bright} cells: 4.07±0.51 ng/µl versus 2.12±0.31 ng/µl, unpaired t-test, p=0.006) (Figure 4-13 (A)). When analysing RNA yield against input cell number, there was a positive correlation (factor) between the two parameters and the automated method yielded more RNA that the manual method (Figure 4-13 (B)). All GFP^{dim} samples exceeded the minimum RIN requirement (RIN >7) regardless of the RNA extraction method whereas only GFP^{bright} samples where the RNA concentration was >4ng/µl had a suitable RIN score for further analysis (Figure 4-13 (C)).

Based on data obtained it was concluded that the automated system using the SimplyRNA Cells Maxwell® 16 LEV kit with freshly isolated cells was the optimal way to extract RNA from the isolated cell populations that was of sufficient quality for further downstream analysis (Figure 4-13).

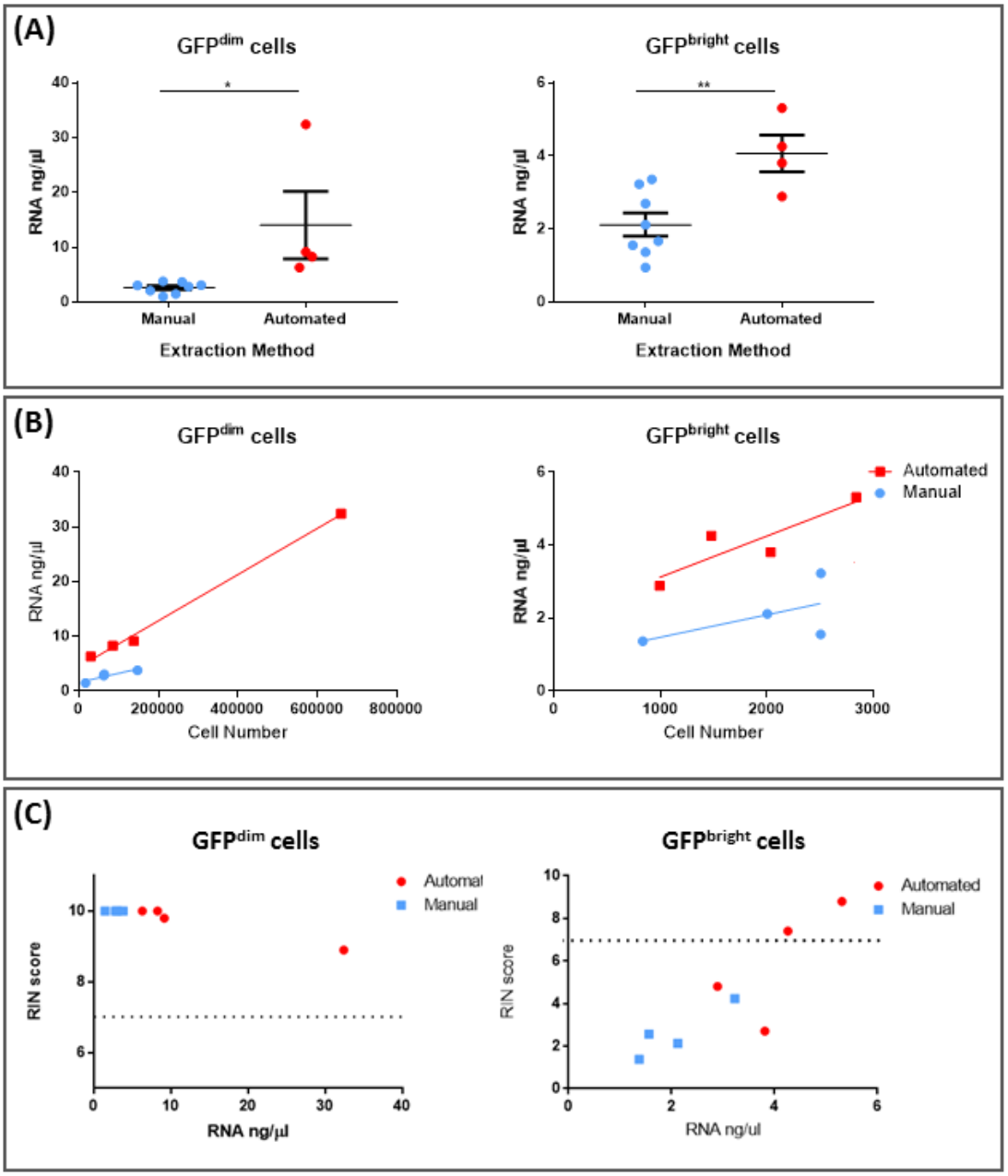

Figure 4-13. Optimisation of RNA extraction techniques. (A) Comparison of RNA yield from GFP^{dim} and GFP^{bright} cells isolated from uterine tissues of naïve Pdgfrβ-BAC-eGFP mice (n=4) after manual or automated RNA extraction (Paired t-test, *p<0.05, **p<0.01). **(B)** RNA yield plotted against starting cell number of both GFP^{dim} and GFP^{bright} cells, comparing manual and automated RNA extraction methods. **(C)** RNA yield plotted against RNA Integrity Number (RIN score) for both GFP^{dim} and GFP^{bright} cells, comparing manual and automated RNA extraction methods, dotted line represents acceptable cut-off score (RIN=7).

4.4.3.3 Analysis of mRNA expression by isolated cells using qPCR

To further investigate the molecular phenotype of GFP+ subpopulations qPCR was used to analyse mRNA expression of the key cell markers *Pdgfrβ, Mcam* (CD146), *Acta2* (αSMA) and *Cspg4* (NG2) in both GFP^{dim} and GFP^{bright} cells isolated from endometrial tissue collected from naïve transgenic *Pdgfrβ-BAC-eGFP* mice (n=4). As detailed in Figure 4-14 (A) both GFP^{bright} cells and GFP^{dim} cells expressed *Pdgfrβ* as expected, however GFP^{bright} cells expressed significantly higher mRNA levels (3.65±0.16 versus 1.51±0.19, p=0.0005). qPCR further revealed that GFP^{bright} cells expressed significantly higher mRNA levels of *Mcam* (CD146) than GFP^{dim} cells (6.14±0.37 versus 0.13±0.01, p=0.0005) (Figure 4-14 (B)). This difference between GFP^{bright} and GFP^{dim} cells was also apparent for the expression on *Acta2* (αSMA) (5.89±0.46 versus 0.01±0.00, p=0.0011) (Figure 4-14 (C)) and *Cspg4* (NG2) (5.25±0.50 versus 0.01±0.00, p=0.0019) (Figure 4-14 (D)). It was notable that in this analysis *Pdgfrβ* mRNA was significantly higher in the isolated GFP^{bright} cells a finding consistent with the intensity of the reporter protein which had not been detected by IHC using antibodies against the native protein on tissue sections (see Figure 4-3).

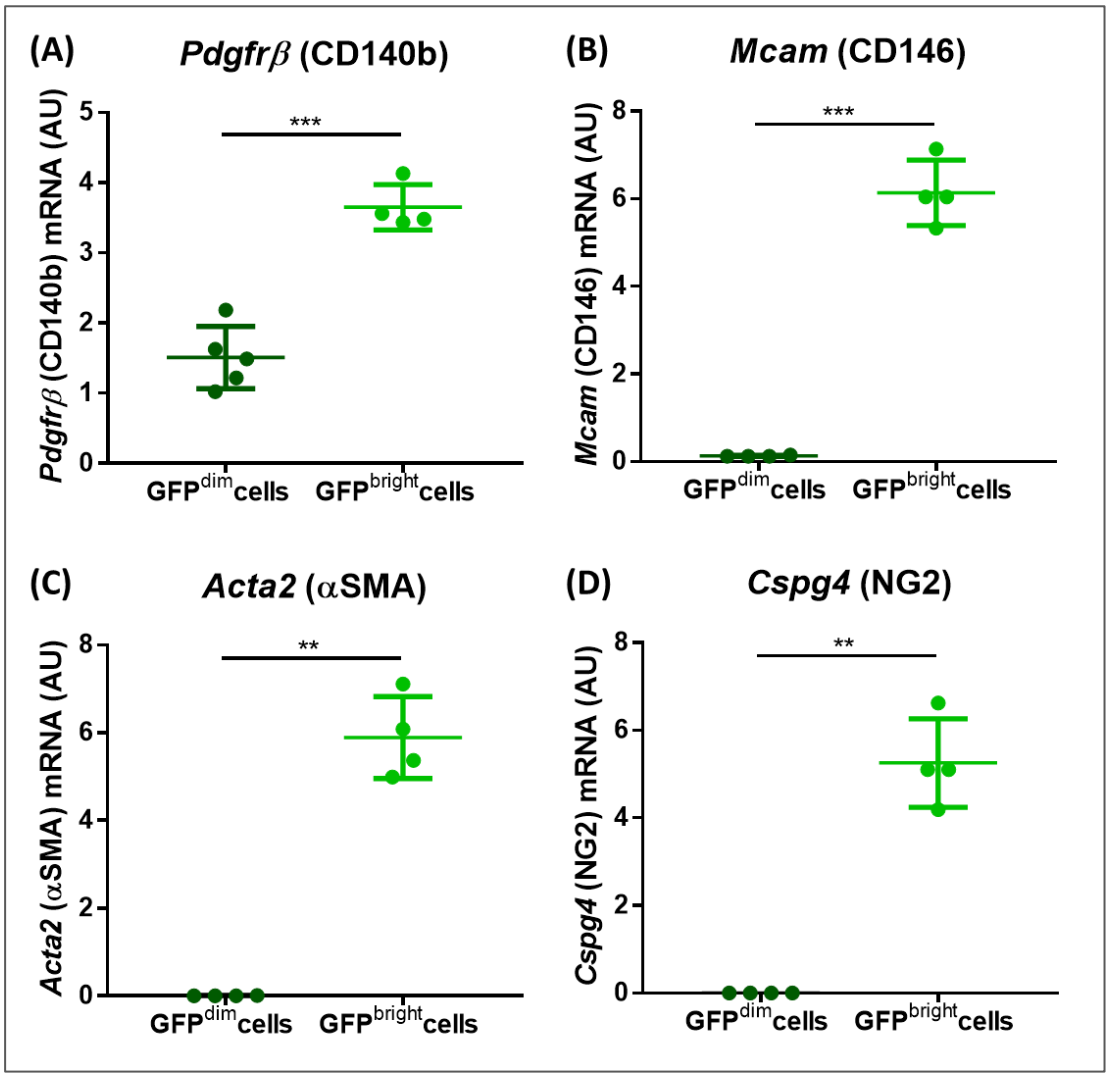

Figure 4-14. qPCR analysis of pericyte marker expression in GFP^{dim} and GFP^{bright} cells isolated from naïve *Pdgfrβ-BAC-eGFP* endometrial tissues by FACS. Expression of **(A)** *Pdgfrβ* **(B)** *Mcam* (CD146) **(C)** *Acta2* (αSMA) **(D)** *Cspg4* (NG2) in isolated GFPdim and GFPbright cells. GFP^{bright} cells; n=4 expressed significantly higher mRNA levels of *Pdgfrβ*, *Mcam* (CD146), *Acta2* (αSMA) and *Cspg4* (NG2) than GFP^{dim} cells; n=4 (paired t-test, *p<0.05, **p<0.01, ***p<0.001, ****p<0.0001).

4.4.4 Profiling GFP^{dim} and GFP^{bright} cells from *Pdgfrβ-BAC-eGFP* endometrial tissue by next generation sequencing (NGS)

4.4.4.1 RNA and cDNA sample preparation

To generate a more comprehensive transcriptomic profile of endometrial pericytes, NGS was undertaken on GFP+ mesenchymal cells isolated from normal adult cycling *Pdgfrβ-BAC-eGFP* mice (naïve). The concentration of RNA extracted from GFP^{bright} pericytes was too low for downstream sequencing applications due to a low numer of

sorted cells. Therefore, total GFP+ cells (GFP^{dim} stromal fibroblasts and GFP^{bright} pericytes combined) and GFP^{dim} cells (stromal fibroblasts alone) were chosen as the comparative samples from which the profile of GFP^{bright} pericytes could be inferred. For presentation of the following results these two samples are labelled as 'naïve' and 'stromal', with only the former containing RNA from pericytes.

RNA concentration and quality were analysed by LabChip GX Touch technique as described previously (Chapter 2: Section 2.6.4). The mean RNA concentration of the naive samples was 12.34±1.651 ng/µl while the mean RNA concentration of the stromal samples was 7.125±2.42 ng/µl and all samples had an RNA Integrity Number (RIN) greater than 8.7. As concentrations did not meet the minimum requirements requested by Edinburgh Genomics (>20ng/µl) a cDNA amplification step was performed as outlined previously (Chapter 2: Section 2.7.2). Following this the mean cDNA concentration of the naïve samples was 123.1±5.342 ng/µl and the mean cDNA concentration of the stromal samples was 137.9± 9.195 ng/µl and all samples had an A260/280 ratio greater than 1.8 (Figure 4-15).

4.4.4.2 TruSeq mRNA Sequencing

All samples were confirmed to meet the minimum criteria for both concentration and quality before being sent to Edinburgh Genomics for RNA sequencing which was conducted by staff within the Genomics Facility (http://genomics.ed.ac.uk/). TruSeq DNA Nano gel free libraries (350bp inserts) were prepared from each of the cDNA samples and sequence data was generated on the HiSeq 4000 75PE platform to yield at least 290M + 290M reads.

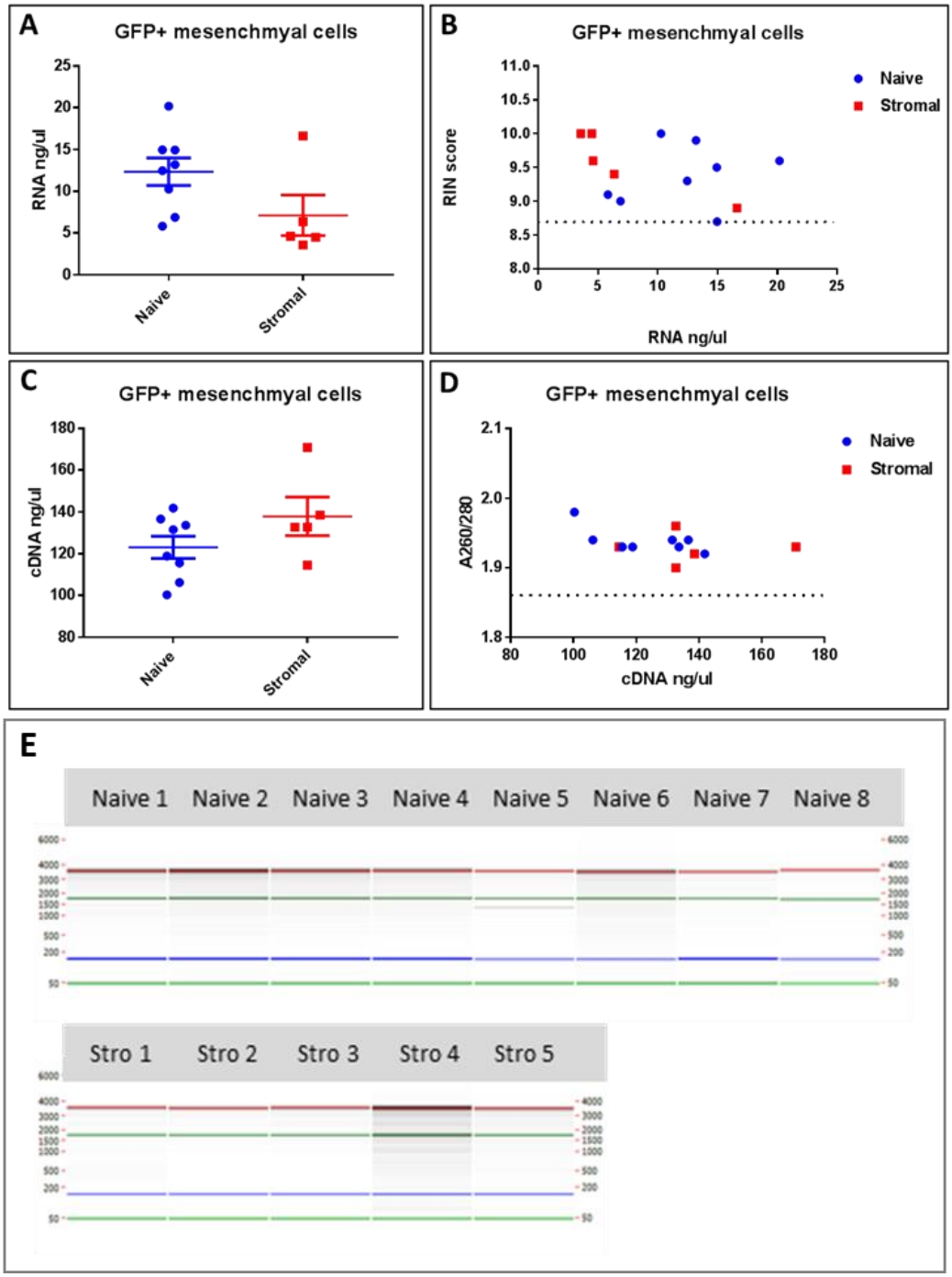

Figure 4-15. LabChip GX Touch analysis of RNA/cDNA quantity and quality for samples generated for RNA sequencing by Edinburgh Genomics. (A) RNA concentrations (ng/ul) of naive and stromal samples. **(B)** RIN score of the naive and stromal samples, dashed line represents the minimum score required by Edinburgh Genomics (8.7). **(C)** cDNA concentrations (ng/µl) of naive and stromal samples after performing cDNA amplification using the NuGEN Ovation V2 system. **(D)** A260/A280 ratios of the naive and stromal samples, dashed line represents the minimum ratio required by Edinburgh Genomics (1.8). **(E)** LabChip GX touch read out gel results for the naïve and stromal (stro) samples: red band represents 18S, green band represents 28s and the blue band represents 5S.

4.4.4.3 Bioinformatic data handling

Initial bioinformatic analysis was performed by Jonathan Manning at Edinburgh Genomics as described in Chapter 2: Section 2.9.3). In brief, reads were trimmed using Cutadept version cutadept-1.9.dev21 at the 3' end using a quality threshold of 30 and for adaptor sequences of the NuGen Ovation V2 kit. Reads were required to have a minimum length of 50. The reference used for mapping was the Mus musculus genome from Ensembl, assembly GRCm38, annotation version 84. Reads were aligned to the reference genome using STAR2 version 2.5.2b specifying paired-end reads. Reads were assigned to exon features grouped by gene ID in the reference genome using 'featureCounts'3. Strandness was set to 'unstranded' and a minimum alignment quality of 10 was specified. Gene names and other fields were derived from input annotation and added to the counts matrix. The raw counts table was filtered to remove rows consisting predominantly of near-zero counts, filtering on counts per million (CPM) to avoid artefacts due to library depth. A summary of key statistics associated with read pair mapping and counting supplied by Edinburgh Genomics can be seen in Table 4-3.

Table 4-3. Summary of key statistics associated with read pair mapping and counting.

Read Mapping		
Total read pairs	28.9-65.2M	
Read pairs after trimming	26.8-60.7M	(90.7 – 94.1%)
Mapped trimmed read pairs	20.7-51.9M	(73.2 – 88.5%)
Mapped read pairs assigned to features for counting	5.5-18.4M	(26.3 – 42.9%)
Derived insert size		
Median	319bp-365bp	
SD	83bp-94bp	
Uncounted mapped reads		
Mapping quality below threshold (10)	0-0M	(0 – 0%)
Not uniquely mapped	0.6-1.4M	(2.3 – 4.4%)
Not mapped to feature	11.4-34.3M	(50.8 – 69.5%)
Ambiguous feature mapping	0.2-0.7M	(0.9 – 2.2%)

4.4.4.4 Principle component analysis

A principal component analysis (PCA) was undertaken by Jonathan Manning on normalised and filtered expression data to explore observed patterns with respect to experimental factors. The cumulative proportion of variance associated with each factor was used to study the level of structure in the data, assessed with an ANOVA test. As seen in Figure 4-16 (A), naïve (GFP^{dim} plus GFP^{bright} cells) and stromal (GFP^{dim} cells only) samples clustered together on the PCA plot reflecting a degree of similarity in the transcriptomic profile of both sample groups which was expected given both contained stromal cells. However this preliminary analysis also hinted at the additional complexity of the naïve group as reflected in them clustering separately to the stromal samples which gave hope that comparisons would reveal differences in gene signatures (Figure 4-16 (A)).

As an extension of this initial PCA analysis I also undertook additional analysis of the data using BioLayout Express 3D software; the correlation between sample groups was determined based on individual gene expression levels. Sample cluster graphs generated (both 2D and 3D) confirm a high correlation in the transcriptomic profiles of both groups (naïve and stromal) (Figure 4-16 (C)).

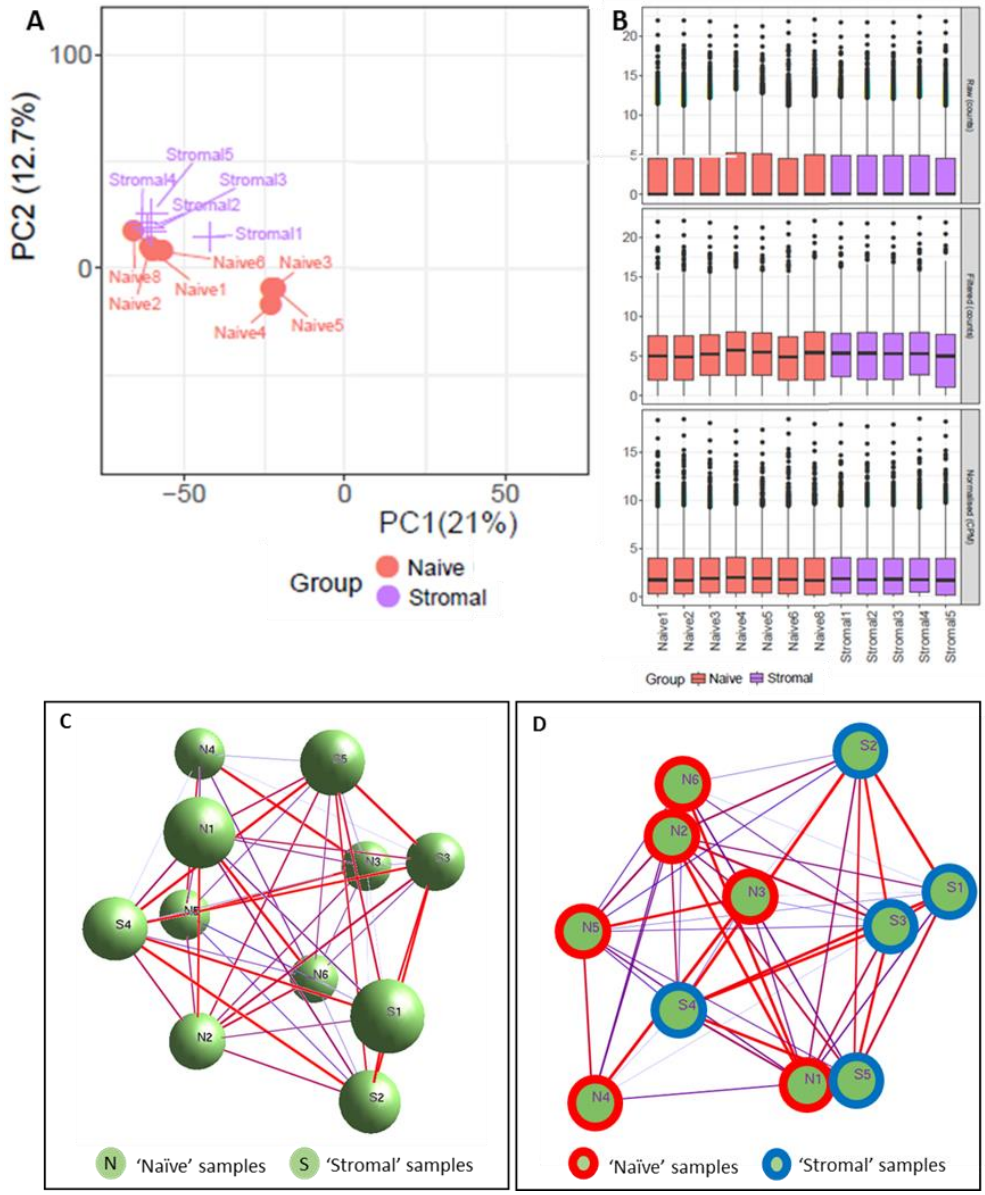

Figure 4-16. Exploratory analysis of the relatedness between the transcriptome of total GFP+ cells (naïve samples) and GFP^{dim} cells (stromal samples). (A) Principle component plot of the first and second components from PCA analysis using selected naive and stromal samples (n=7 and n=5 respectively). **(B)** Boxplots showing expression distributions among samples at different stages of pre-processing (log2 scale), using selected samples. Note that raw and filtered values are expressed in counts, while normalised values are in counts per million (CPM). Points outside whiskers are outliers at 1.5 x IQR where IQR is the inter-quartile range. **(C)** The correlation of RNASeq datasets between naïve and stromal samples was determined in BioLayout Express3D based on individual gene expression levels and a sample cluster graph generated (Pearson's correlation of R>0.8 and intensity >1 of dataset with fold change >2 or <-2 and FDR <0.05). Nodes represent individual samples and edges represent the degree of correlation between them, colour/thickness is equivalent to how similar the samples are. (C) 3D sample cluster graph and **(D)** 2D sample cluster graph displaying a high correlation between the groups (naive n=6; stromal n=5).

4.4.4.5 Differential gene expression analysis

Differential gene expression analysis was carried out with EdgeR4 (version 3.16.5) and the quasi-likelihood (QL) F-test using the contrast between naïve and stromal sample groups (Jonathan Manning, Edinburgh Genomics). The total numbers of differentially expressed genes are outlined in Table 4-4 according to the thresholds on minimum fold-change (2) and maximum false discovery rate (0.05).

Table 4-4. Total numbers of differentially expressed genes between naïve and stromal sample groups

Contrast	Upregulated	Downregulated
Naïve vs Stromal	143	11

Gene expression data can also be visualised as a heatmap, fold change plot or a volcano plot and all of these were used to illustrate the 154 differentially expressed genes between samples (Figure 4-17 (A-C). In the fold change and volcano plots differentially regulated genes are identified as red dots (Figure 4-17 (B-C)). As the naïve sample group was composed of total GFP+ cells while the stromal sample group was composed of a subset of this, GFP^{dim} cells, it was postulated that the 143 genes which appeared to be upregulated in the naïve samples could be attributed to GFP^{bright} cells previously identified as putative pericytes. To confirm this hypothesis the expression data was further analysed to determine whether the candidate pericyte genes already identified in the GFP^{bright} cells were present. Notably in further validation of the RNASeq analysis a clear increase in the mean CPM and LogFC of *Mcam* (CD146), *Cspg4* (NG2), *Acta2* (αSMA) and *Pdgfrβ* was confirmed in naïve compared to stromal samples (Figure 4-17 (D)). The top 100 most significantly upregulated genes in the naïve samples when compared to stromal samples are summarised in Appendix 1.

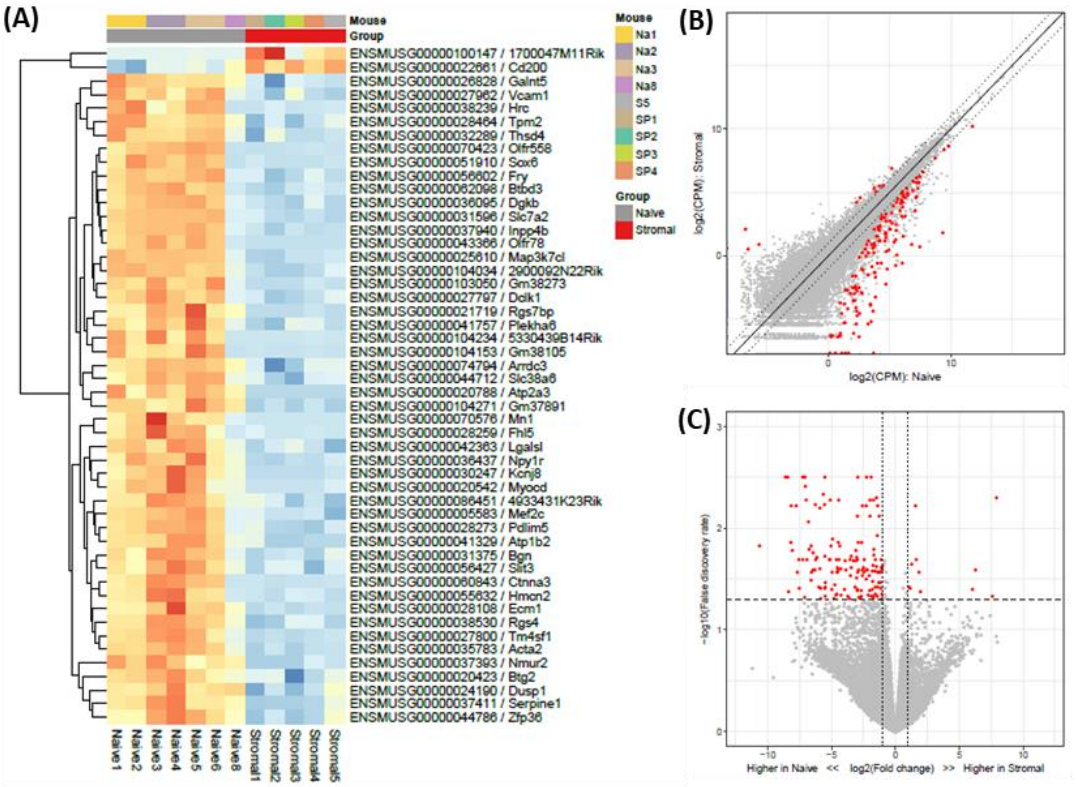

(D)

Gene Name	Mean CPM Naïve (GFPdim+GFPbright)	Mean CPM Stromal (GFPdim)	LogFC
Mcam (CD146)	7.134	0.463	-3.926
Cspg4 (NG2)	7.634	0.572	-3.711
Acta2 (αSMA)	48.625	1.059	-5.508
Pdgfrβ (CD140b)	108.587	59.921	-0.857

Figure 4-17. Differential gene expression analysis between the transcriptome of GFP+ cells (naïve samples) and GFP^{dim} cells (stromal samples). (A) Heatmap showing the top 50 most differentially expressed genes by false discovery rate (FDR <0.05) between the naïve and ntromal groups (11 upregulated genes and 143 downregulated genes in total). **(B)** Fold change and **(C)** volcano plot illustrating differential expression between groups naive and stromal as defined by group. Volcano plots illustrate log(2) fold change vs –log(10) false discovery rate. The horizontal dashed line represents the specified FDR threshold for significance (0.05), dotted lines in both plots represent the specified fold change threshold (2) in both the positive and negative directions. Points passing both thresholds are coloured red and are differentially expressed. **(D)** Table outlining the mean CPM and logFC of target genes previously used to identify and characterise endometrial pericytes, gene expression is validated in the differential gene set.

4.4.4.6 Gene ontology (GO) and Gene Set Enrichment Analysis (GSEA)

Expression data was also analysed using BioLayout Express 3D software and a network map generated based on individual gene expression levels in naïve and stromal samples. Using this methodology three clusters of genes were identified: cluster 1 correlated to genes upregulated in naïve samples while cluster 2 and 3 correlated to genes downregulated in naïve samples when compared to stromal cells alone (Figure 4-18 (A)). Cluster 1 therefore represented putative pericyte associated genes which was further analysed using the online Gene Ontology Consortium to find gene ontology (GO) terms that were over-represented in the differential gene expression data to identifying potential functions of this gene set. GO terms associated with the 143 putative pericyte associated genes included: extracellular matrix assembly; muscle contraction; regulation of blood vessel diameter; angiogenesis; blood vessel morphogenesis; negative regulation of immune system process; cell adhesion; negative regulation of signal transduction; tissue development; and regulation of cell proliferation. This preliminary analysis suggests these key biological processes can be attributed to putative pericytes in the mouse endometrium (Figure 4-18 (B)).

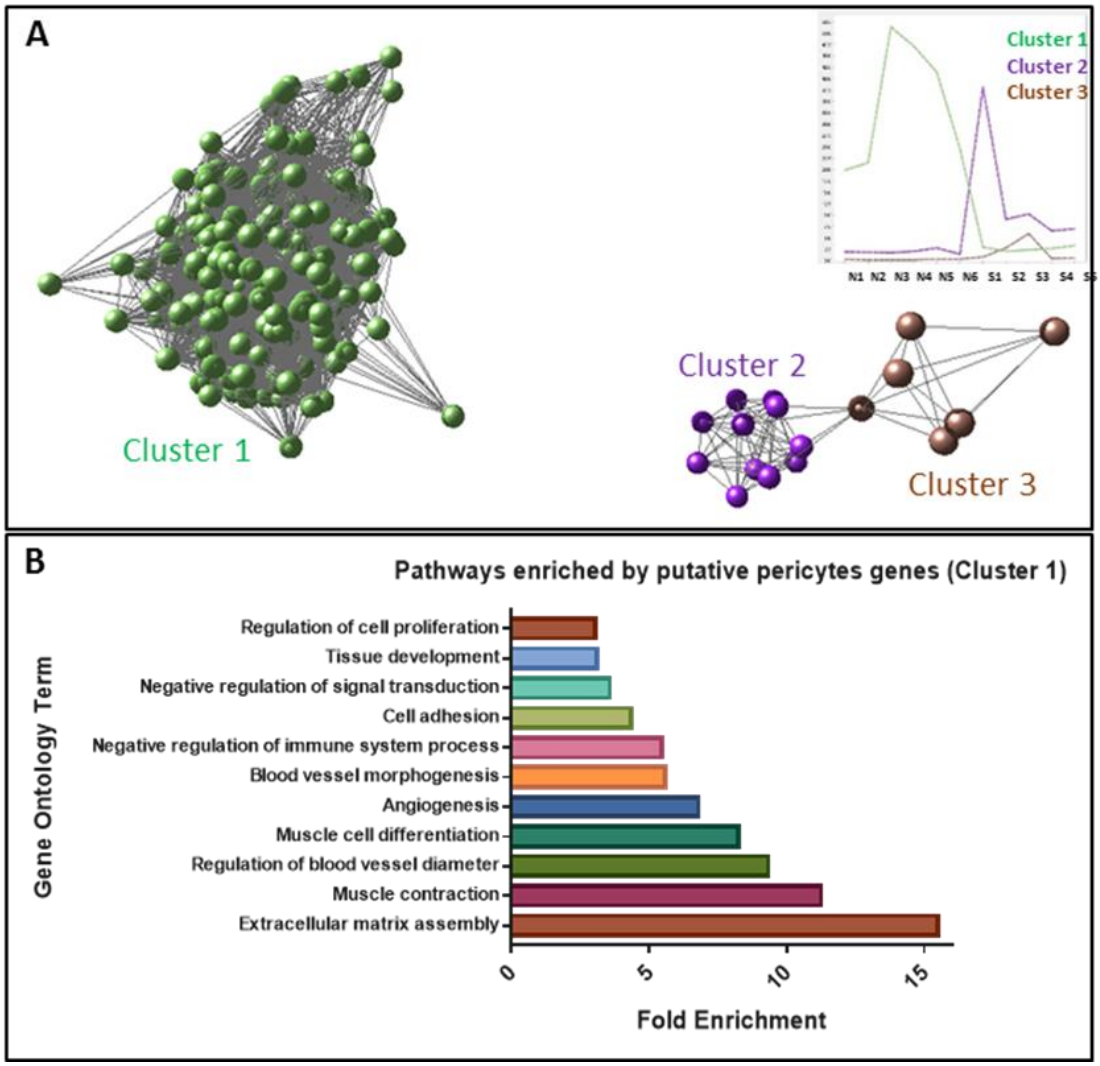

Figure 4-18. Gene ontology analysis of putative pericyte genes. (A) Markov clustering (MCL, inflation= 1.7) was used to identify clusters related to putative pericyte genes (RNASeq results comparing naive' and stromal' samples). Clusters were analysed to create a network map where each node is a gene and each edge the similarity in expression levels between genes, colours of nodes represents membership in a cluster. **(B)** Gene ontology analysis of the putative pericyte genes identifies several key biological processes including blood vessel morphogenesis, regulation of blood vessel diameter, angiogenesis, muscle contraction, regulation of immune cell processes and cell adhesion attributed to pericytes (cluster 1).

Further ontology analysis was performed using the Gene Set Enrichment Analysis (GSEA) software to identify pathways enriched by putative pericyte genes associated with Kyoto Encyclopedia of Genes and Genomes (KEGG) pathways, Canonical Pathways (CP), Biological Process (BP) and Molecular Function (MF). Results of

these analyses are summarised in Figure 4-19 (A-D) respectively. A comparison between the various functions shared between these different pathway analyses highlighted some relevant pathways which included those associated with vasculature function such as vascular smooth muscle contraction (Enrichment score (ES): 2.04), complement and coagulation cascade (1.96), platelet homeostasis (2.28), blood vessel morphogenesis (2.20) and angiogenesis (2.14). Roles in cell adhesion were also highlighted including ECM receptor interaction (2.16), collagen binding (2.26), integrin binding (2.24), cell matrix adhesion (2.20), extracellular structure organisation (2.19), cell adhesion molecule binding (2.01) and ECM glycoproteins (2.07). Functions associated with regulation of the immune system were also noted including integrin cell surface interaction (2.30), regulation of leucocyte migration (2.17), regulation of inflammatory response (2.13), chemokine activity (1.89) and cytokine receptor interactions (1.58).

In summary, simple gene ontology analysis revealed that RNAs over-represented in endometrial pericytes were likely to encode proteins associated with functions of blood vessel regulation, cell adhesion and immune responses all of which would appear consistent with the role(s) played by perivascular pericytes *in vivo*.

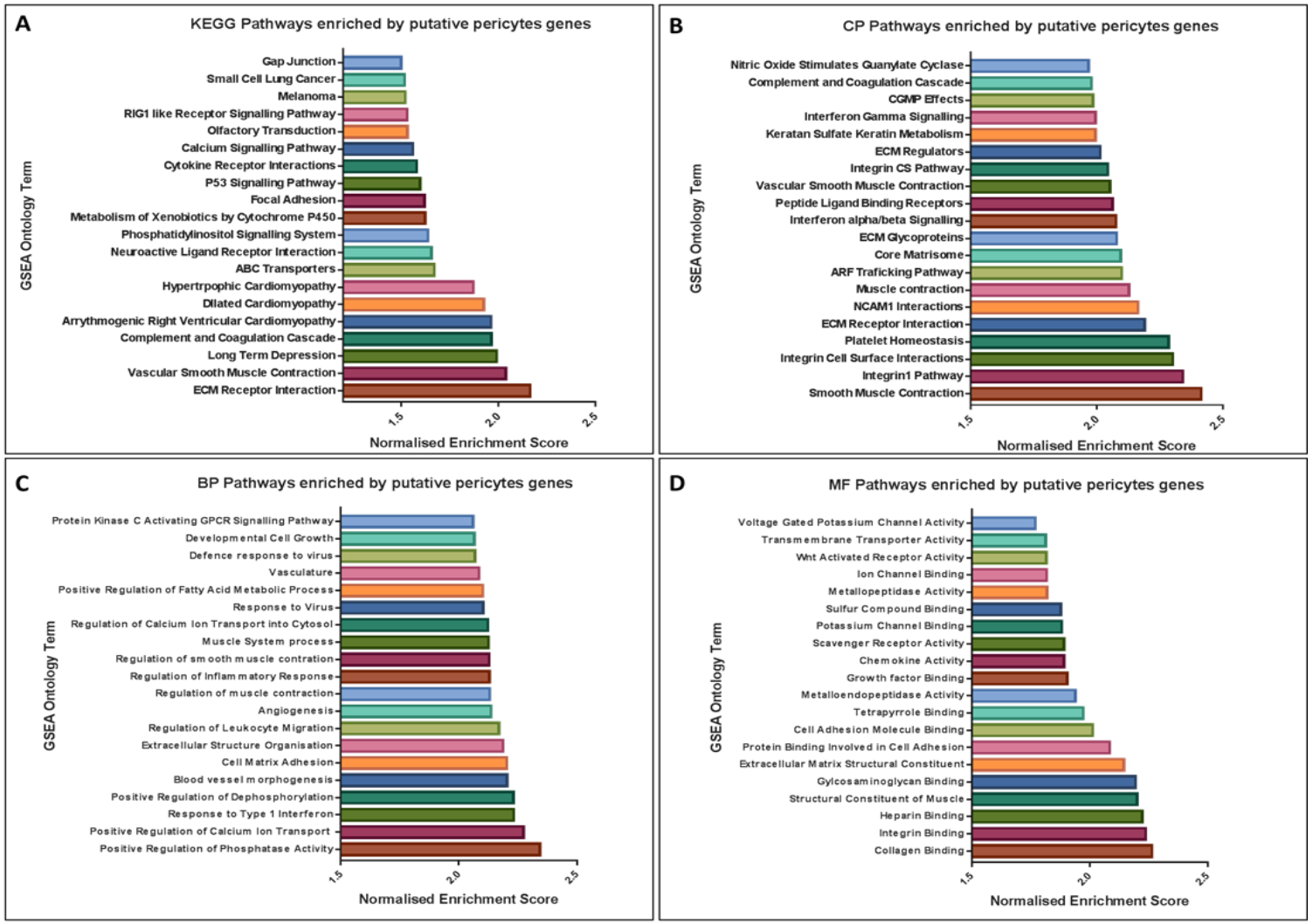

Figure 4-19. Gene Set Enrichment Analysis (GSEA) of putative pericyte genes. Gene ontology analysis as performed using the Gene Set Enrichment Analysis (GSEA) software. Analysis of pathways enriched by putative pericyte genes assessing **(A)** Kyoto Encyclopedia of Genes and Genomes (KEGG) pathways **(B)** Canonical Pathways (CP) **(C)** Biological Process (BP) and **(D)** Molecular Function (MF).

4.4.5 Validation of putative endometrial pericyte-associated gene signature

To provide the platform for further validation of the gene analysis results a ranked gene list was generated using GSEA software to identify the most differentially expressed genes identified as putative pericyte genes (Figure 4-20). This method highlighted 37 genes which had been identified as differentially expressed in the analysis performed by Edinburgh Genomics (LogFC <-2 and FDR <0.05). Taken together these two forms of analysis provided a target list of putative pericyte-associated genes to specifically identify pericytes in the endometrium (Figure 4-20).

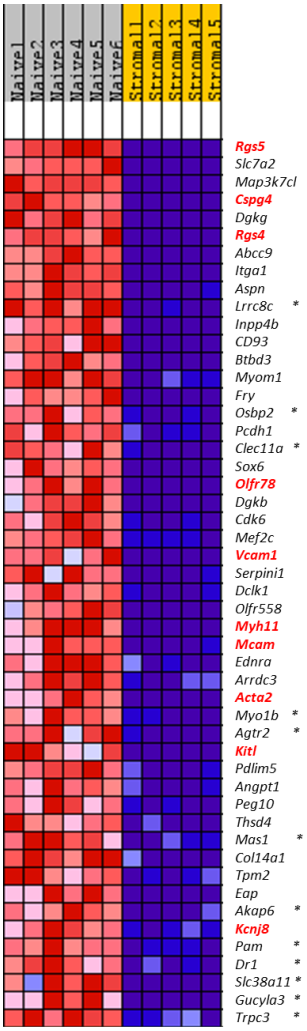

Figure 4-20. Ranked gene list generated using GSEA based on transcript abundance, as determined by CPM, in naïve samples (total GFP+ cells) and stromal samples (GFP^{dim} subset) generated from *Pdgfrβ-BAC-eGFP* uterus. Genes, except for those identified with an *, were also found to be differentially expressed in the dataset by Edinburgh Genomics (logFC >2 and FDR <0.05). Genes highlighted in bold/red were chosen for validation studies.

4.4.5.1 Primary validation of putative endometrial pericyte-associate genes by qPCR

Following identification of a short list of putative mouse endometrial pericyte RNAs validation using qPCR was performed using a new set of samples different to those sent to Edinburgh Genomics. Cells of interest were isolated using FACS and RNA extracted using the Promega SimplyRNA Cells Maxwell® 16 LEV kit as described in Chapter 2: Section 2.6.3. cDNA amplification and qPCR using the Taqman method was performed as described in Chapter 2: Section 2.7.1 and Section 2.8 respectively, using primers designed against ten genes detailed in Table 4-5. In this set of experiments genes were selected for validation based on the LogFC >2, FDR <0.05, mean CPM in naïve samples >5 and mean CPM in stromal samples <4. The availability of reliable primer sequences and antibodies was also used to narrow down genes from the 37 genes considered a priority for validation (Figure 4-20).

Table 4-5. Putative pericyte genes identified through RNA sequencing to be more highly expressed in the naïve samples (total GFP+ cells) than the stromal samples (GFP^{dim} subset) as determined by LogFC (>2) in mean counts per million (CPM).

Gene	Expanded Name	Mean CPM Naive	Mean CPM Stromal	LogFC (>2)
Acta2 (αSMA)	Actin, alpha 2 smooth muscle	48.62480465	1.059755434	5.508426009
Myh11	Myosin heavy polypeptide 11	112.3382175	1.871607608	5.915143007
Cspg4 (NG2)	Neural glial antigen 2	7.623761625	0.572417667	3.710645725
Olfr78	Olfactory receptor 78	13.14954306	0	10.64494967
Rgs4	Regulator of G-protein signalling 4	30.59502037	1.376631718	4.463932917
Rgs5	Regulator of G-protein signalling 5	659.6824379	3.541085656	7.545825823
Vcam1	Vascular cell adhesion molecule 1	18.8761171	2.328397054	3.013912524
Mcam (CD146)	Melanoma cell adhesion molecule	7.13375629	0.463077708	3.925662267
Kitl	Kit ligand	16.11201615	0.682810577	4.552554094
Kcnj8	Potassium channel, subfamily J, member 8	11.43342976	0.028477121	8.418738739

The first set of experiments assessed the expression of mRNAs encoded by these genes in the new set of samples, both naïve (GFP^{dim} and GFP^{bright} cells) and stromal (GFP^{dim} subset) isolated from normal adult *Pdgfrβ-BAC-eGFP* endometrium (Figure 4-21). This validation set was identical to that of the samples sent to Edinburgh Genomics for RNA sequencing. qPCR results were analysed by comparing expression of key genes in naïve samples; n=4 to those of stromal samples; n=4, normalised to a reference gene (*Actb*).

The expression of 6 of the 10 mRNAs were significantly upregulated in the naïve samples when compared to the stromal samples: *Acta2* (0.25±0.003 versus 0.0005±0.0002, p=0.0034), *Myh11* (0.04±0.006 versus 0.0002±6.24E-006, p=0.0027), *Cspg4* (0.53±0.13 versus 1.42E-005± 7.58E-006, p=0.0192), *Rgs4* (0.53±0.13 versus 0.018±0.009, p=0.0218), *Rgs5* (0.15±0.02 versus 0.0002±9.15E-005, p=0.0007) and *Kcnj8* (0.89±0.23 versus 0.002±0.001, p=0.025). There was a trend for the remaining 4 mRNAs to be to be upregulated in naïve samples when compared to stromal samples however these values did not reach significance: *Olfr78* (0.35±0.12 versus 0.0001±1.7E-005), *Vcam1* (0.18±0.03 versus 0.08±0.03), *Mcam* (0.16±0.05 versus 0.001±0.001) and *Kitl* (0.03±0.01 versus 0.001±0.0002) (Figure 4-21). These results were in line with expectations based on the sequencing data and it was notably that only *Vcam1* appeared to be expressed much above baseline in the stromal cells.

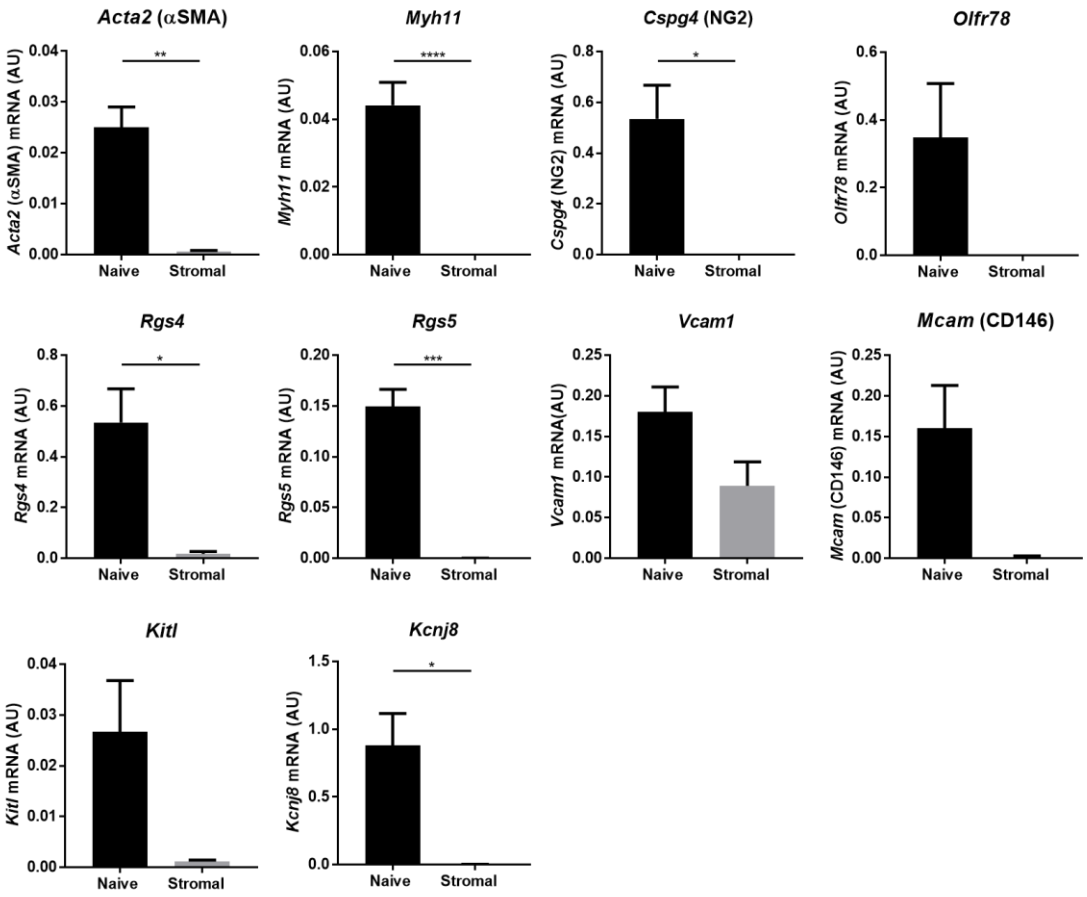

Figure 4-21. Expression of ten putative pericyte genes by qPCR in naïve (total GFP+ cells) and stromal samples (GFP^{dim} subset) generated from *Pdgfrβ-BAC-eGFP* endometrial tissue as samples to validate NGS results. *Acta2* (αSMA), *Myh11*, *Cspg4* (NG2), *Rgs4*, *Rgs5* and *Kcnj8* are all significantly upregulated in naïve samples; n=4 when compared to stromal samples; n=4. Olfr78, Vcam1, Mcam (CD146) and Kitl have a trend for a decrease although this did not reach significance (unpaired t-test,*p<0.05, **p<0.01, ***p<0.001, ****p<0.0001).

4.4.5.2 Further analysis of primary validation of putative endometrial pericyte-associate genes by qPCR

Acta2, *Myh11*, *Cspg4* (NG2), *Olfr78*, *Rgs4*, *Rgs5*, *Vcam1*, *Mcam* (CD146), *Kitl* and *Kcnj8* were identified through RNA sequencing to be overexpressed in naive samples (total GFP+ cells) when compared to stromal samples (GFP^{dim} cell subset) and therefore formed a putative pericyte-specific gene set (GFP^{bright} cells). To provide additional independent verification of cell specific gene expression, qPCR was used to assess the expression of key genes in RNA from purified populations of FACS sorted

cells: GFP^{dim} cells (stromal fibroblasts; n=3); GFP^{bright} cells (pericytes, n=3); and CD31+ cells (endothelial cells, n=4) all of which were isolated from naive *Pdgfrβ-BAC-eGFP* endometrial tissue.

It was notable that all the putative pericyte associated genes identified using the different approaches described in the previous sections were confirmed as being expressed in purified GFP^{bright} cells (pericytes). A key finding was that mRNAs encoded by *Acta2* (*αSMA*) (3.7±1.6 mRNA (AU) normalised to *Actb*; reference gene), *Myh11* (3.25±0.76) and *Cspg4* (*NG2*) (1.79±0.38) were expressed exclusively by the GFP^{bright} cells (pericytes) and undetectable in RNA from either stromal fibroblasts (GFP^{dim}) or endothelial cells. In contrast some expression of *Olfr78* (0.15±0.03), *Rgs4* (0.36±0.08), *Rgs5* (0.07±0.02) and *Kcnj8* (0.36±0.08) was detected in the CD31+ endothelial cells although in all cases expression in this cell type was significantly lower than in the pericytes (Figure 4-22). In contrast three genes were expressed by both GFP^{bright} cells (pericytes) and CD31+ cells (endothelial cells) although RNA levels appeared consistently higher in pericytes: *Vcam1* (4.12±1.61 versus 1.6±0.39), *Mcam* (*CD146*) (3.79±0.37 versus 2.57±0.20) and *Kitl* (2.15±0.65 versus 0.92±0.18). Importantly none of these genes were expressed by GFP^{dim} cells (stromal fibroblasts) providing further validation for the strategy employed to identify a pericyte-specific gene signature (Figure 4-22).

In summary, RNA sequencing and qPCR validation identified *Acta2*, *Myh11*, *Cspg4*, *Olfr78*, *Rgs4*, *Rgs5*, and *Kcnj8* as genes expressed specifically in endometrial pericytes in *Pdgfrβ-BAC-eGFP* mice which may be useful in downstream studies to specifically target pericytes. *Cspg4* (NG2) was identified as a pericyte specific marker in endometrial tissues by IHC, NGS and qPCR and was therefore chosen as the marker to target in further studies.

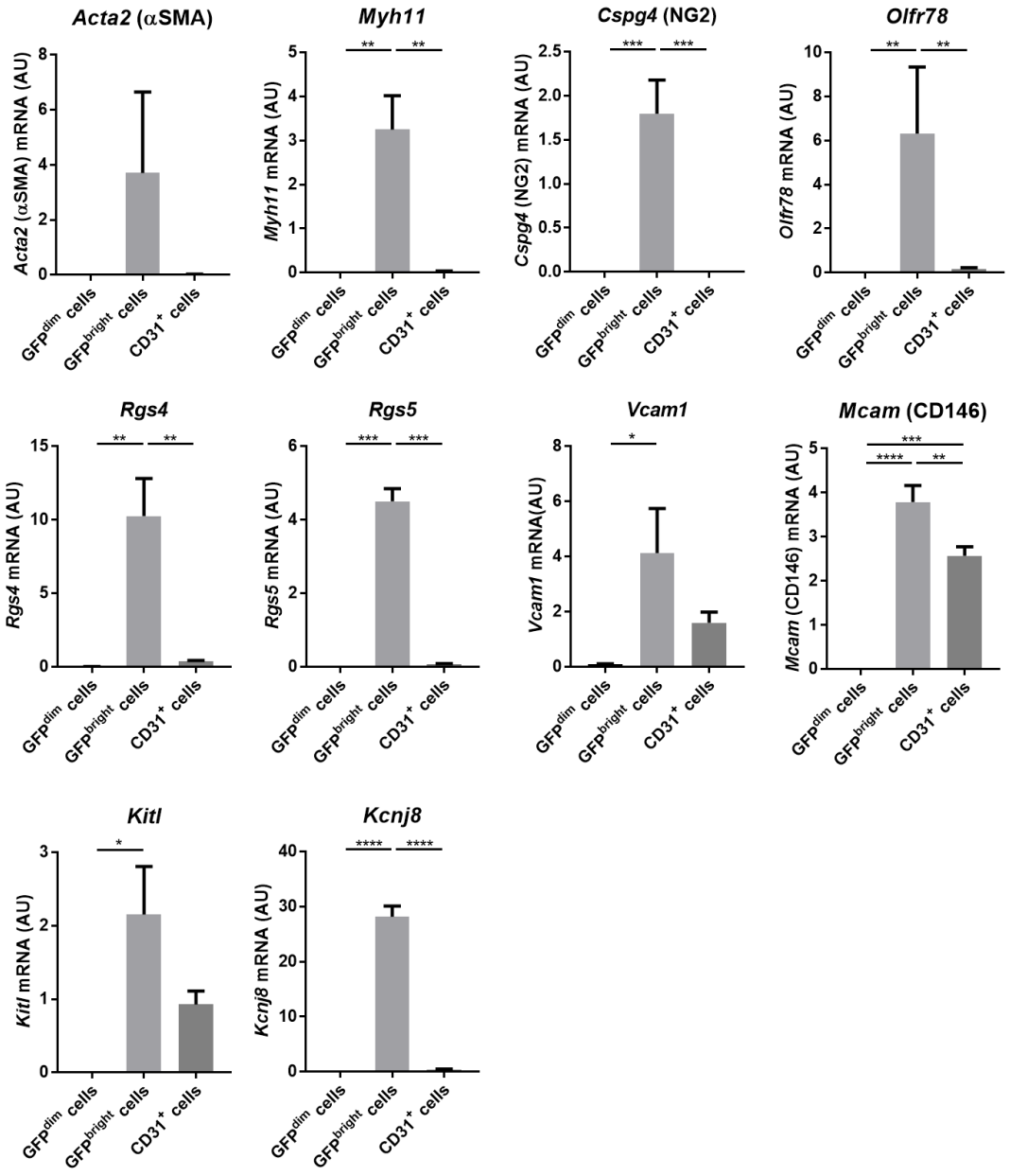

Figure 4-22. Expression of putative pericyte genes by qPCR in GFP^{dim} stromal cells, GFP^{bright} pericytes and CD31^{+} endothelial cells isolated from naive *Pdgfrβ-BAC-eGFP* endometrial tissue to further validate NGS results. *Acta2*, *Myh11*, *Cspg4* (NG2), *Olfr78*, *Rgs4*, *Rgs5*, *Vcam1*, *Mcam* (CD146), *Kitl* and *Kcnj8* are all expressed by GFP^{bright} pericytes (n=3) and not expressed by GFP^{dim} stromal cells (n=3) while *Vcam1*, *Mcam* (CD146) and *Kitl* were also expressed by CD31+ endothelial cells (n=4) (One-way ANOVA, Holm-Sidak's multiple comparisons test,*p<0.05, **p<0.01, ***p<0.001, ****p<0.0001).

4.4.6 Identification of NG2+ pericytes using an inducible transgenic mouse line

Lineage tracing is a biological technique for tracing the progeny of a single cell or group of cells over time; a cell is 'marked' (tattooed) in such a way that this mark will be transmitted to all progeny. Transgenic mice have been developed to exploit this technique using the Cre/lox site-specific recombination system which allows spatial control of gene activity in a cell type of interest. With the development of ligand-dependent induction of specific Cre recombinases, temporal control was gained as Cre recombinase expression was only stimulated by administration of the ligand.

In the preceding sections GFP expression in the *Pdgfrβ-BAC-eGFP* was not pericyte specific, however further analysis suggested that NG2 (encoded by *Cspg4*) was identified as a pericyte-specific gene. To advance studies on the role of endometrial pericytes we purchased an NG2-CreER^{TM} BAC tamoxifen-inducible mouse line (available from Jackson Laboratories detailed in Section 2.1.1.5). These mice were cross-bred with an Ai14 reporter mouse line engineered to contain a loxP-flanked STOP cassette upstream of a TdTomato (DsRed fluorescent protein) sequence, detailed in Section 2.1.1.6. Mice were given injections of tamoxifen (TMX), and the expression of the red fluorescent protein TdTomato examined.

4.4.6.1 Expression of TdTomato in NG2-CreER^{TM} BAC uterine tissue after tamoxifen administration

To investigate the efficiency of recombination by the NG2-CreER^{TM} BAC tamoxifen-inducible mouse line, it was crossed with the Ai14 reporter mouse line (Chapter 2; Section 2.1.1.6). NG2-Cre/Ai14 offspring were generated in which TdTomato is only expressed in NG2 expressing cells. To assess this reporting, uterine tissues were collected from adult cycling mice after administration of TMX and tissue sections observed for TdTomato expression. TdTomato was expressed by cells located within the endometrial stromal compartment (Figure 4-23 (A-B) arrows) and was not expressed by epithelial cells of the lumen (L) (Figure 4-23 (A-B), dashed line). Observation at a higher magnification showed that TdTomato+ cells had cellular morphology consistent with a pericyte phenotype: fat cell bodies and long membranous processes wrapping around blood vessel structures (Figure 4-23 (C) arrows).

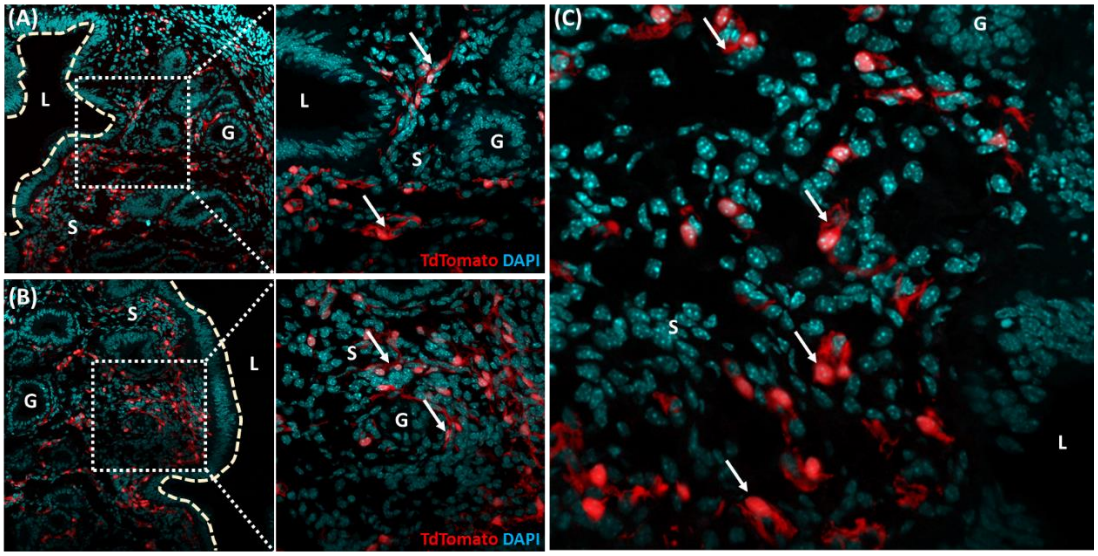

Figure 4-23. TdTomato expression in naïve NG2-Cre/Ai14 uterine tissue after administration of tamoxifen. (A-B) TdTomato expressing cells (arrows) were located throughout the endometrial stromal compartment and not associated with the epithelium (cream dashed line). **(C)** TdTomato expressing cells (arrows) exhibit pericyte-like morphology. Stroma (S), gland (G), lumen (L) (representative images, n=4).

4.4.6.2 Characterisation of TdTomato expressing cells in naïve NG2-Cre/Ai14 uterine tissue by IHC

To confirm that TdTomato+ cells in naïve NG2-Cre/Ai14 uterine tissue were pericytes, IHC was used with antibodies raised against a range cell marker proteins. The following markers were used based on previous reports and the results outlined in Figure 4.24: NG2 (Cspg4) expressed by smooth muscle cells and pericytes; CD146 (Mcam) expressed by endothelial cells and smooth muscle cells; Pdgfrβ expressed by mesenchymal cells; CD31 (Pecam-1) expressed by endothelial cells; and EpCAM (CD326) expressed by epithelial cells. TdTomato+ cells were confirmed as NG2+, CD146+ and Pdgfrβ+ a phenotype consistent with that of pericytes (Figure 4-24 (A-C) arrows). All TdTomato+ cells were CD31- and EpCAM- distinguishing them from both endothelial and epithelial cells respectively (Figure 4-24 (D-E) arrows). These results are consistent with TdTomato expressing cells being identified at pericytes.

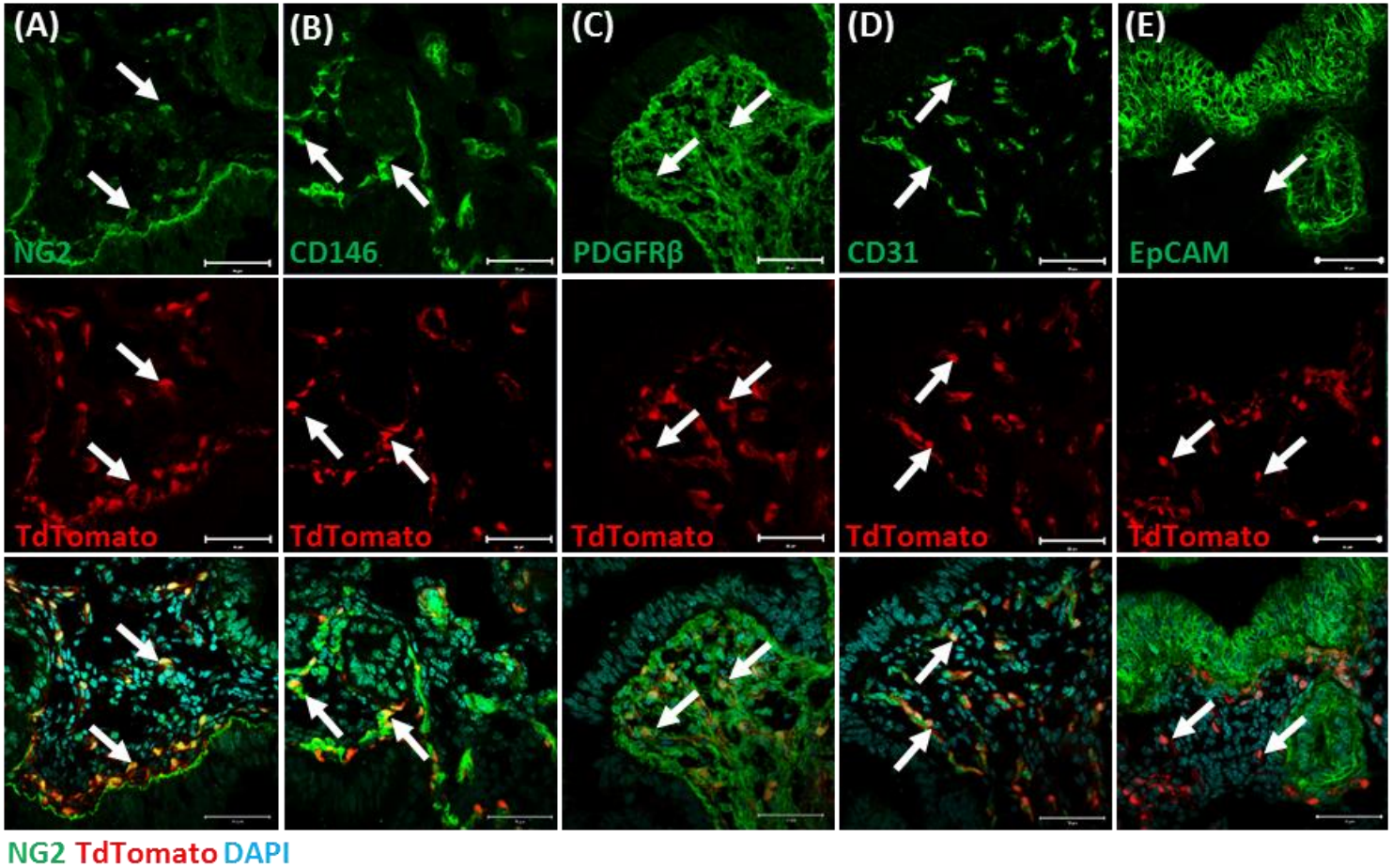

Figure 4-24. Characterisation of TdTomato+ cells in naïve NG2-Cre/Ai14 uterine tissue by IHC. Expression of TdTomato (red; white arrows) and **(A)** NG2 **(B)** CD146 **(C)** Pdgfrβ **(D)** CD31 and **(E)** EpCAM (green) in uterine tissue. Co-localisation of TdTomato with NG2, CD146 and Pdgfrβ was detected. TdTomato positive cells did not express CD31 or EpCAM (representative images; n=4 mice, scale bar = 50μm).

To assess the contribution of TdTomato+ cells to the stromal compartment, naïve NG2-Cre/Ai14 uterine tissues were collected from adult mice after tamoxifen administration and analysed by flow cytometry. Analytical gates were set up using an unstained controls, single stains and FMO's of all the included antibodies and single live cells analysed (Figure 4-25 (A)). There was a population of TdTomato + cells that accounted for 4.12±0.23% of the total live cells in the tissue (Figure 4-25 (B and E). When analysed further it was found that 85.71±1.79% of the TdTomato+ cells expressed CD146 and 58.82±3.87% expressed NG2 (Figure 4-25 (C) and (F)) while TDTomato+ cells did not express either CD31 (2.46±0.36%) or EpCAM (4.85±1.09%) (Figure 4-25 (D) and (F)). TdTomato+ cells were however located in close proximity to CD31+ blood vessels indicative of a perivascular phenotype (Figure 4-25 (D)). These results were in line with the characterisation by IHC and further confirm the pericyte phenotype of TdTomato+ cells.

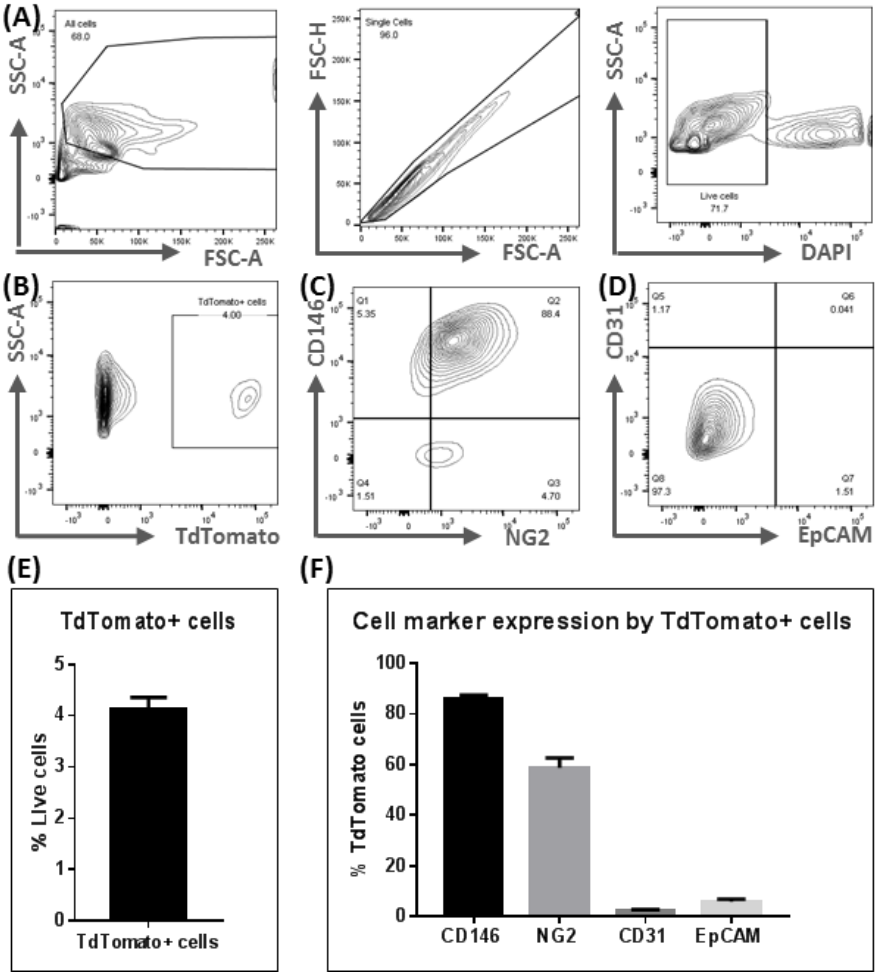

Figure 4-25. Characterisation of TdTomato+ cells in NG2-Cre/Ai14 uterine tissue by flow cytometry. (A) Gating strategy to analyse live single cells**:** All cells > Single cells > Live cells**. (B)** Plot showing TdTomato against SSC-A and the presence of the TdTomato+ cell population. **(C)** Expression of NG2 and CD146 by TdTomato+ cells. **(D)** Expression of CD31 and EpCAM by TdTomato+ cells. **(E)** Quantification of TdTomato+ cells as a frequency of live single cells **(F)** Quantification of cell marker expression by TdTomato+ cells as a frequency of TdTomato+ cells (representative plots, n=4).

In summary, IHC and flow cytometry have confirmed that TdTomato expressing cells in the NG2-Cre/Ai14 uterus can be identified as perivascular pericytes. The results mirror data generated from *Pdgfrβ-BAC-eGFP* transgenic mouse line, where GFP^{bright} cells were previously characterised as perivascular pericytes. This confirms use of the a rationale for using these mice in future studies related to endometrial repair although the further work is needed to determine the independent impact of tamoxifen (an anti-oestrogen) on uterine responsiveness before these can be undertaken.

4.5 Discussion

4.5.1 Characterisation of endometrial mesenchymal cells

Current knowledge on the characterisation of endometrial stem/progenitor cells has been gathered from *in vitro* studies on heterogeneous populations of stromal cells, however this method does not exclude contamination from other cell types and both gene expression and cellular function are likely to be altered by culture conditions (Masuda et al. 2012). It is therefore imperative that new studies focus on use of methods that can identify progenitor cell specific markers using cells recovered from their native environment to provide the tools necessary for reliable isolation of pure cell populations for studies that will enable them to be properly characterised. In the human endometrium, co-expression of Pdgfrβ and CD146 (Schwab and Gargett 2007) and specific expression of SUSD2 (previously known as W5C5) (Masuda et al. 2012) have been used to identify and isolate stromal MSCs consistent with Pdgfrβ+CD146+ cells representative of putative pericytes, while SUSD2+ cells representing true MSCs (Gargett et al. 2016)

Based on these previous findings in the human endometrium, the current study started by identifying and locating cells that co-expressed Pdgfrβ and CD146 in the mouse endometrium and by capitalising on the opportunity to conduct studies in the *Pdgfrβ-BAC-eGFP* transgenic mouse line, previously used to identify pericytes in the liver and kidney (Henderson et al. 2013). Before embarking on studies to isolate putative pericytes a variety of methods were used to demonstrate that in the *Pdgfrβ-BAC-eGFP* transgenic mouse line the promoter-dependent expression of GFP mirrored that of the native Pdgfrβ protein. GFP and Pdgfrβ were both exclusively detected in the stromal compartment. A novel finding during this analysis was that there were two subpopulations present in the endometrial tissue based on the intensity of GFP expression alone: GFP^{dim} cells and GFP^{bright} cells. As GFP expression is a readout of Pdgfrβ gene promoter activity (Henderson et al. 2013) this indicated that the *Pdgfrβ* is more active in the GFP^{bright} cells and that Pdgfrβ protein would be more abundant in these cells and that two populations of stromal GFP+ cells could be easily distinguished. These results confirmed the use of the *Pdgfrβ-BAC-eGFP* transgenic mouse in investigating cells of the endometrial mesenchyme (Pdgfrβ+), and suggested

that there was previously unknown functional heterogeneity within this cell population in the endometrium based on Pdgfrβ signalling.

Further characterisation of the GFP positive cell populations revealed that GFP^{bright} cells expressed Pdgfrβ, CD146, αSMA and NG2 suggesting they had a pericyte phenotype as these markers have been used to identify pericytes in a variety of other tissues including heart, skeletal muscle, brain, spinal cord, retina, adipose tissue, bone marrow, lymph node, skin, aorta, lungs, kidney and pancreas (Guimarães-Camboa et al. 2017). In contrast, GFP^{dim} cells expressed Pdgfrβ but did not express CD146, αSMA or NG2 consistent with a stromal fibroblast phenotype (Schwab and Gargett 2007). Flow cytometry confirmed that two GFP+ subpopulations were present in naive *Pdgfrβ-BAC-eGFP* endometrial tissue and showed that they could be separated based on relative expression of CD146: GFP^{dim} cells were CD146- and GFP^{bright} cells were CD146+ once again confirming a pericyte phenotype (Spitzer et al. 2012).

These results appear in agreement with previously published papers in which co-expression of Pdgfrβ and CD146 has been detected in human endometrial pericytes which may have MSC-like functions (Schwab and Gargett 2007, Kaitu'u-Lino et al. 2012, Spitzer et al. 2012). However it is notable that Pdgfrβ and CD146 are apparently expressed by more than one cell type so cannot be described as pericyte specific and therefore a combination of these markers is required. In the current study αSMA and NG2 appeared to be pericyte specific markers although further investigation showed αSMA was not detected in every pericyte and was also expressed by smooth muscle cells of the myometrium. Notably, this is the first report of increased expression of Pdgfrβ by GFP^{bright} cells (pericytes) compared with stromal cells had not been previously described and warrants further investigation into cell-specific regulation of the promoter.

4.5.2 Investigating the perivascular niche

Both IHC and flow cytometry showed GFP+ cells did not express EpCAM or CD31 demonstrating they were distinct from epithelial and endothelial cells. This is in line with previous data from studies in human endometrial tissue which describes endometrial MSCs as expressing CD29, CD44, CD73, CD90, CD102 and CD146 but not STRO-1, CD31, CD45 or EpCAM (Gargett and Masuda 2010, Guimarães-Camboa

et al. 2017). In the current study the GFP^{bright} cells were located in close proximity to CD31+ cells surrounding blood vessels, and could therefore be described as 'perivascular'. This fits with LRC studies where many endometrial LRCs were located near to blood vessels in the stroma and hypothesised to be either pericytes or vascular smooth muscle cells (Cervelló et al. 2007, Chan and Gargett 2006a, Patterson and Pru 2013). Similarly in other studies where human endometrial MSCs were detected in tissue sections by either co-expression of Pdgfrβ and CD146 (Kaitu'u-Lino et al. 2012, Bergers and Song 2005) or sole expression of SUSD2 (Masuda et al. 2012), they were described as occupying a perivascular niche.

The perivascular location of endometrial pericytes in the mouse endometrium was also investigated using transmission electron microscopy (TEM): endothelial cells were directly adjacent to the vessel lumen with large nuclei, and perivascular cells with smaller nuclei and evidence for membranous processes were found wrapping around these vessel structures. The latter were identified as pericytes and shown to be encapsulated within the collagenous basement membrane of the vasculature, a hallmark of the pericyte phenotype (Bergers and Song 2005). Further studies are needed to confirm their identity using immunogold labelling with an antibody against a pericyte specific marker such as NG2.

Analysis of CD31+ and NG2+ revealed that every NG2+ pericyte in the endometrial tissue was located in close proximity to a CD31+ endothelial cell (100±0.24%) thereby occupying a perivascular niche in endometrial tissue. The ratio of pericytes:endothelial cells was calculated to be 1.25:1 (±0.02). In the literature, pericyte coverage is described as dense or sparse and is thought to be related to the extent of substance transfer between blood vessels in different tissues. For example the retina has a high ratio of 1:1 while the peripheral vasculature has a low ratio of 1:100 (Andersson et al. 2015). A higher ratio is believed to be related to greater regulation of blood flow and more frequent remodelling of microvessels, as well as being a sign of vessel maturity (Andersson et al. 2015). Similarly *in vitro* co-culture studies using a decreasing pericyte (primary human muscle) to endothelial cell (dHMECs) ratio (1:1, 10:1, 20:1) have shown that pericytes 'home' to endothelial cells and there is a decrease in endothelial cord area as pericyte:endothelial cell ratio decreases. At a ratio of 1:1 there

was an inhibition of endothelial cell proliferation which decreased as the ratio decreased believed to be due to an inability of pericytes to communicate with the increasing number of endothelial cells (Bodnar et al. 2016).

Various studies conclude that all endometrial vessels consist of endothelial cells with supporting basal lamina and pericytes (Hickey and Fraser 2000, Hickey et al. 2003). In a paper studying the role of pericyte coverage in endometrial tissue from women suffering from HMB, control subjects were rarely found to exhibit endothelial tubes without associated pericytes while those with HMB had greatly reduced numbers (Andersson et al. 2014). Similarly it has been shown that HRT users have reduced pericyte coverage which coincides with increased vascular fragility and associated unexplained bleeding (Hickey et al. 2003). The current study has demonstrated that endometrial vasculature has a dense coverage of pericytes and this would be consistent with an important role in the regulation of blood flow and control of substance transfer. Considering the endometrium is a highly dynamic tissue that is constantly undergoing regeneration and degeneration with associated changes in vasculature (Gargett et al. 2016) a substantial pericyte population is probably required for regulation of endothelial cell function during angiogenesis and tissue remodelling (Chan et al. 2004). Interestingly it has been shown that while pericytes are associated with all vascular capillaries and post-capillary venules in the human endometrium, there are spatially organised differences in pericyte phenotype (based on vSMC differentiation markers) however the functional significance of this has yet to be determined (Rogers and Abberton 2003). Results of the current study are in agreement that all endometrial vessels (mouse) have a close association with perivascular pericytes which likely have various influences over vascular function in the endometrium.

Pericytes associated with spiral arteries have been found to be more highly proliferative than those of other vessels, likely to reflect an active role in spiral artery remodelling essential for embryo implantation and placentation (Rogers and Abberton 2003, Elia et al. 2011). Additionally, during decidual shedding, vasoconstriction is important in limiting blood loss during menstruation (Chan et al. 2004) and as pericytes are contractile cells this could be a primary role in endometrial physiology. Notably in their paper Andersson *et al*, (2014) reported finding low pericyte coverage

of vessels in the endometrium of women suffering from HMB, confirming a role for pericytes in regulating blood loss during menstruation. Finally, if pericytes have MSC functions (Spitzer et al. 2012), high pericyte coverage provides the endometrium with a reliable source of progenitor cells for tissue turnover and regeneration.

4.5.3 Assessing endometrial mesenchymal cell populations

Flow cytometry combined with tissue from the transgenic reporter mice offered a unique opportunity to analyse the numbers of GFP^{bright} pericytes revealing that they were 17.22±1.26% of the total stromal GFP+ cell population (CD31-CD45-GFP+ cells, Figure 4-10) and approximately 8.33±0.36% of total live cells (DAPI- cells, Figure 4-10) present in the tissue. This population of pericytes appears to be higher than the numbers of putative MSC reported by other investigators suggesting not all pericytes are MSC or that there are species differences.

For example, in 2004, Chan *et al* did clonogenic studies on isolated endometrial stromal cells (EpCAM- cells) from human hysterectomy tissues and found that a small population was clonogenic: 1.25%, generating both large (0.02%) and small (1.23%) colonies (Chan et al. 2004). Similarly using the Hoescht exclusion assay on cells isolated from human endometrial tissue, SP cells accounted for between 0-5% of the total cell population, that this was highest in the proliferative phase samples (up to 0.7%) and highly variable between subjects (Kato et al. 2007). Results from other studies using antibodies in combination with flow cytometry reported that Pdgfrβ+CD146+ cells accounted for 1.5±0.2% of the CD45-EpCAM- stromal cell population (Schwab and Gargett 2007). In a separate study screening with antibodies raised against putative MSC identified W5C5 (subsequently found to be encoded by the gene SUSD2) identified a population of clonogenic multipotent cells that were 4.2±0.6% of a purified stromal cells population (Masuda et al. 2012). Finally LRC studies in mice have shown that between 6-9% of the stromal cells can be identified as LRC and that these are mainly located near blood vessels (Chan and Gargett 2006b, Cervelló et al. 2007).

When comparing current results to those gathered in the aforementioned studies it must be appreciated that displayed values are calculated as frequencies of different starting populations. The flow cytometry results discussed in this chapter excludes both

endothelial cells and immune cells from the analysis, then calculates the contribution of pericytes (GFP^{bright}CD146+ cells), confirmed to be EpCAM- and calculated as a percentage of total live cells in the suspension. In contrast, in the clonogenic and SP studies mentioned above the isolation technique does not exclude endothelial or immune cells from the analysis and therefore a more heterogeneous population has been examined. It is of note that the CFU and SP techniques are focussed on identifying a specific MSC population in the endometrial tissue and the difference in value suggests not all Pdgfrβ+CD146+ pericytes are MSC. Similarly when comparing current results with SUSD2/W5C5+ cells as a proportion of stromal cells from human endometrium (Masuda et al. 2012) it is possible that a larger cell population is being captured when analysing co-expression of Pdgfrβ and CD146, while a smaller population expresses SUSD2 alone.

When comparing current results to those by Schwab & Gargett 2007 where they calculated the Pdgfrβ+CD146+ cells as a percentage of CD45-EpCAM- cells, this should be relatively comparable to CD31-CD45- population in this study it is presumed that Pdgfrβ+CD146+ cells are both EpCAM- and CD31-. Discrepancies between these results could be due to differences in the preparation of the single cell suspension, the use of different flow cytometry antibodies, the advantage of the intrinsic GFP reporter protein over the use of an antibody or a true difference in the proportion of pericytes in endometrial tissue in human versus mouse tissue. Interestingly the current results show most similarity to the results gained when using the technique of LRC to identify cells in mouse endometrium (Chan and Gargett 2006b, Cervelló et al. 2007) further highlighting a potential difference in the cellular composition of the endometrium between human and mouse species. Although one caveat is that the LRC method examines all cellular compartments while the current results solely analysed mesenchymal cells.

In summary, the GFP^{bright} cells in the *Pdgfrβ-BAC-eGFP* endometrium were characterised as Pdgfrβ+CD146+ perivascular pericytes by a variety of techniques.

4.5.4 Isolation of endometrial pericytes

Pericytes were purified from endometrial tissue using FACS based on their co-expression of GFP and CD146. Approximately 20,000 GFP^{bright} cells and 400,000

GFP^{dim} cells could be isolated from two naïve *Pdgfrβ-BAC-eGFP* uterine horns using a refined digest protocol (Chapter 2: Section 2.5). A cytospin of the cells was confirmed GFP^{bright} cells were GFP+/Pdgfrβ+/CD146+ while GFP^{dim} cells were negative for CD146. These results were in agreement with the literature where pericytes are Pdgfrβ+CD146+ while stromal fibroblasts are Pdgfrβ+CD146- (Schwab and Gargett 2007, Kaitu'u-Lino et al. 2012, Spitzer et al. 2012).

Different RNA extraction techniques were compared and it was found that for a small cell input, the automated Maxwell extraction method with the SimplyRNA cell kit yielded the best quality RNA. When a molecular characterisation was carried out on RNA extracted from the different cells using primers directed against candidates identified by immunohistochemistry as pericyte/stromal associated GFP^{bright} cells (pericytes) were confirmed as Pdgfrβ+, CD146+, αSMA+ and NG2+ while GFP^{dim} cells (stromal fibroblasts) were Pdgfrβ+, CD146-, αSMA- and NG2-. These results confirmed Pdgfrβ is more highly expressed in pericytes than stromal fibroblasts in the mouse. Notably NG2 was confirmed to be a marker expressed specifically in mouse endometrial pericytes.

Using FACS allowed us to exploit a multi-colour panel of antibodies generating detailed analysis of the expression of multiple cell surface markers in a single sample. In terms of clinical application, magnetic bead sorting has been suggested to be optimal for MSC isolation as it is rapid and simple, yields greater cell numbers, maintains cell viability to a higher degree and results in extracted RNA with better integrity (Masuda et al. 2012). However, the resulting cell population is not 100% pure and multiple cell markers cannot be used and it is dependent upon identification of a cell surface protein that can be bound by antibodies and which is not expressed in other cell types: in human tissue the W5C5 antigen appears to be promising for isolation of stromal clonogenic cells (Masuda et al. 2012).

The current study is the first to describe a robust method to isolate a pure population of pericytes from mouse uterus based on co-expression of Pdgfrβ and CD146. This provided a platform for further molecular characterisation of the cells and an opportunity to expand both the range of pericyte specific genes as well as increase our understanding of their function.

4.5.5 Profiling endometrial pericytes

Next generation sequencing (NGS) was performed on cells isolated from *Pdgfrβ-BAC-eGFP* mouse uterus. In the current study the samples groups compared were total mesenchymal cells (all GFP+ cells) and stromal fibroblasts (GFP^{dim}CD146- cells), as the RNA generated from the GFP^{bright}CD146+ cells had poor quality (determined by LabChip GX Touch technology) and was therefore removed from the initial analysis although RNA from purified pericytes was used in validation experiments. It was postulated that differences in gene expression between the total GFP+ cell population (GFP^{dim}CD146-/GFP^{bright}CD146+) and isolated GFP^{dim}CD146- stromal cells might be due to the presence of the GFP^{bright}CD146+ cells. Anaylsis of results identified 143 putative pericyte associated genes including several previously reported in the literature as being expressed in pericytes including *Mcam* (CD146), *Acta2* (αSMA), *Cspg4* (NG2), *Pdgfrβ*, *Myh11*, *Olfr78*, *Rgs4*, *Rgs5*, *Vcam1*, *Kitl* and *Kcnj8* (Spitzer et al. 2012, Gaafar et al. 2014, Cheng et al. 2017, He et al. 2016).

Spitzer *et al* carried out transcriptomic analysis (by gene array) of human endometrial MSCs isolated by FACS as Pdgfrβ+CD146+ cells in comparison to Pdgfrβ+CD146- stromal fibroblasts which revealed a gene signature they concluded to be similar to that of pericytes (Spitzer et al. 2012). Similarities can be drawn with the current data set and suggest human endometrial MSCs and mouse endometrial pericytes express some of the same genes including: *Pdgfrβ*, *Mcam*, *Acta2*, *Rgs5*, *Angpt2*, *Scl38a*, *Mef2c*, *Serpin1*, *Tagl*, *Abcc9* and *Slit3*. Differences in the results may be because the expression of Pdgfrβ and CD146 identifies slightly different cell populations in human and mouse endometrial tissue, the comparisons drawn in each study were different or the parameters used to filter the resulting data were different. Nevertheless both studies suggest that Pdgfrβ+CD146+ cells in both human and mouse endometrium can be identified as perivascular pericytes.

This conclusion is further supported when comparing current NGS data to a study which analysed the transcriptome of mural cells in the mouse brain. Sequencing of Pdgfrβ+NG2+ cells isolated from brain tissue identified several pericyte-asssociated genes including *Acta2*, *Kcnj8*, *Pdgfrβ*, *Des*, *Abcc9*, *Rgs5* and *Cspg4* (He et al. 2016). However, in that study NG2 (Cspg4) was found to be expressed by both mural cells

(Pdgfrβ+NG2+) and olidodendrocyte progenitor cells (OPCs: Pdgfrβ-NG2+) whereas in the current study detailed analysis showed NG2 was only expressed in endometrial cells that co-expressed Pdgfrβ. Whether this is an important tissue specific difference is yet to be investigated. He *et al* concluded that mural cells (Pdgfrβ+NG2+) in the brain represented a heterogeneous population of cells but this has not yet been investigated in the endometrial pericytes.

Gene Set Enrichment Analysis (GSEA) of genes identified in the current study as being expressed by endometrial pericytes has highlighted several biological processes and signalling pathways relevant to the function of pericytes during homeostasis. Several processes were associated with vascular functioning such as regulation of blood vessel diameter, angiogenesis, vascular smooth muscle contraction and blood vessel morphogenesis which represent the well-known pericyte function of vasculature support, also highlighted by other transcriptomic studies (Spitzer et al. 2012: vasculogenesis, angiogenesis; He *et al*, 2016: angiogenesis, smooth muscle contraction). Additional functions included extracellular matrix assembly, negative regulation of signal transduction, tissue development and regulation of cell proliferation all of which were confirmed in other studies (Spitzer et al. 2012, Gaafar et al. 2014, He et al. 2016). Interestingly, a link to regulation of inflammatory process was also identified such as negative regulation of immune system process, cytokine receptor interactions, regulation of leucocyte migration and regulation of inflammatory response. This function has been identified by others and it has been suggested that endometrial pericytes have immunomodulatory functions which may have therapeutic potential (Spitzer et al. 2012).

Signalling pathways found to be enriched in endometrial perciytes included calcium signalling, Wnt signalling and Hedgehog signalling which have been previously implicated in the MSC properties of self-renewal and multipotency (Spitzer et al. 2012, Gaafar et al. 2014). In a study by Gaafar *et al*, human endometrial MSCs and BM-MSCs were compared by gene expression profiling. They found 52 core genes that were shared including those associated with stemness, self-renewal and members of the TGFβ, Notch and Wnt signalling however differentially expressed genes were associated with vasculogenesis, cell adhesion, smooth muscle contraction and

migration, processes which were identified in endometrial pericytes in the current study by GSEA.

In the current study RNA sequencing confirmed the transcriptomic profile of GFP^{bright}CD146+ cells was consistent with a pericyte phenotype. Notably, when validation of the sequencing data was carried out using RNA purified from isolated cell populations of GFP^{bright}CD146+ and GFP^{dim}CD146- the expression of NG2 (*Cspg4*) was confirmed as being exclusive to GFP^{bright}CD146+ pericytes and not detectable in either stromal or endothelial cells. Building on this information mice in which transcription of a TdTomato fluorescent transgene was induced specifically in mice expressing an NG2 promoter were generated and their uteri recovered for analysis. In addition to confirmation that TdTomato was exclusive to a cell population with a perivascular phenotype Flow cytometry of tissue digests showed tdTomato+ pericytes represented 4.12±0.23% of the total live cells in the endometrial tissue which is comparable to numbers of LRC studies previously identified in mice (Chan and Gargett 2006b, Cervelló et al. 2007). Notably, this proportion was also similar to the numbers of W5C5+ MSCs in human tissues (Masuda et al. 2012). These results were in contrast to those obtained using GFP and CD146 co-expression to identify pericytes in *Pdgfrβ-BAC-eGFP* tissues by flow cytometry which suggested pericytes represented 8.33±0.36% of total live cells. The discrepancy in these values suggests that the co-expression of Pdgfrβ and CD146 may identify a broader population of cells than NG2. These novel findings suggest that the endometrial pericyte population is heterogeneous which may have associated functional heterogeneity. This was further investigated in Chapter 5.

4.5.6 Future prospects

In the current study, in depth characterisation of the cellular and molecular phenotype of endometrial pericytes using IHC, flow cytometry, qPCR and NGS was achieved using various transgenic reporter mice. However functional studies (both *in vitro* and *in vivo*) are required to compliment this data and definitively confirm pericytes as MSCs. To analyse whether endometrial pericytes have true MSC properties both clonogenicity and multilineage differentiation assays need to be performed (Gargett and Masuda 2010), using single expanded cell colonies from isolated cells (Schwab

and Gargett 2007). Additionally, a scratch assay could be performed to study their capacity for migration and potential role in wound healing. Transplanting purified endometrial pericytes ($GFP^{bright}CD146+$) from *Pdgfrβ-BAC-eGFP* mouse endometrium under the kidney capsule of a recipient mouse could be used to compare their capacity to reconstruct endometrial tissue *in vivo* as has been described for human MSC (Masuda et al. 2015). Such analyses are required to further characterise endometrial pericytes before they can be identified as a true stem/progenitor cell population.

4.5.7 Conclusions

$GFP^{bright}CD146+$ cells in *Pdgfrβ-BAC-eGFP* endometrial tissue can be identified as perivascular pericytes which exclusively express NG2. A full characterisation of endometrial pericytes in the mouse uterus has identified novel targets which could be used to specifically target pericytes in future experiments. These results provide a platform for investigating the role of pericytes as progenitor cells in endometrial tissue repair.

Chapter 5 Investigation of the role of mesenchymal progenitor cells in endometrial tissue breakdown and repair

5.1 Introduction

5.1.1 Menstruation and endometrial repair

In women tissue repair of the normal endometrium is relatively rapid being characterised by complete restoration of the epithelial cell layer within 2-3 days (Ferenczy 1976). Recent morphological investigations have revealed that tissue breakdown occurs simultaneously with tissue repair processes which include neoangiogenesis, re-epithelialisation and stabilisation of basal blood vessels (Garry et al. 2009, Garry et al. 2010, Cousins et al. 2016b). It has been postulated that the basal, unshed, endometrial layer can serve as a regenerative compartment from which a new functional layer is generated (Spencer et al. 2005, Gargett and Masuda 2010, Spencer, Dunlap and Filant 2012). Several processes are known to be involved in endometrial tissue repair, however, the precise cellular and molecular mechanisms responsible for 'scarless' healing are yet to be fully elucidated (Jabbour et al. 2006b, Henriet et al. 2012, Garry et al. 2010).

Notably, studies in mice suggest endometrial repair can occur in a steroid hormone depleted environment (Kaitu'u et al. 2005) although the increase in depth recorded during the proliferative phase is oestrogen-dependent. Explant studies in which tissue was cultured in the presence or absence of hormonal support (E2 and P4) have reported that hormone deprived explants increased expression of genes associated with a signature of 'wound healing and inflammation' (Gaide Chevronnay et al. 2012). Progesterone withdrawal is reporter to be associated with tissue-restricted hypoxia and increased biosynthesis of prostaglandins and angiogenic factors including VEGF (Maybin et al. 2011a, Maybin et al. 2011b, Cousins et al. 2016d).

5.1.2 Mechanisms of re-epithelialisation

One of the most fundamental processes of endometrial repair is restoration of the epithelial cell layer after decidual shedding, so-called re-epithelialisation (Cousins et al. 2014). In women this process is reported to begin on day 2 of menses will full epithelial coverage of denuded stromal surfaces achieved by day 5, occurring in

parallel with tissue shedding. Originally it was believed that new epithelial cells arose from glandular epithelium retained in the basal layer (Novak 1946). This hypothesis was updated in the 1970s when Ferenczy suggested that new epithelial cells arose from proliferation of both basal glandular epithelium and intact surface epithelium bordering regions of denuded stromal tissue (Ferenczy 1976, Evans et al. 2011, Kaitu'u-Lino et al. 2010). More recently it has been proposed that three synchronous mechanisms contribute to re-epithelialisation: luminal epithelial cell proliferation, glandular epithelial cell migration and a mesenchymal to epithelial transition (MET) of cells in the endometrial stroma (Garry et al. 2009, Patterson et al. 2013, Cousins et al. 2014).

Key evidence for trans-differentiation of stromal cells so that they gain an epithelial phenotype (MET) has been documented in mouse models of simulated 'menses' using transgenic reporter strains and detailed IHC (Krull et al. 2010, Patterson et al. 2013, Cousins et al. 2014). For example, Cousins *et al*, using the Edinburgh menses mouse model and IHC identified cells in the stromal compartment adjacent to areas of denuded epithelium that expressed both vimentin (stromal marker) and pan cytokeratin (epithelial marker) in samples recovered 12 and 24hrs following P4 withdrawal. This study also highlighted evidence for stromal cell proliferation in regions close to denuded surfaces and found dynamic changes in gene expression implicated in EMT and MET in uterine tissues across a time course of repair including *Wt1, Snai1, Snai2, Snai3, Cdh1, cytokeratin, Wnt1, osteopontin* and *Vim* (Cousins et al. 2014). Although these studies suggest that the stromal cells in the residual unshed endometrium can contribute to reepithelialisation they used total tissue extracts to assess gene expression and did not provide information on what proportion of the stromal cell population are capable of MET.

5.1.3 Myofibroblasts during endometrial repair

During a classical wound healing response, e.g. in the skin, fibroblasts differentiate into myofibroblasts through the fibroblast to myofibroblast transition (FMT) characterised by an increase in the expression of αSMA (Leavitt et al. 2016). Myofibroblasts play a key role in dermal wound contraction however their persistence at a site of injury results in the formation of scar tissue (Hantash et al. 2008, Haldar et

al. 2016, Greenhalgh et al. 2013). Myofibroblasts may also arise through transdifferentiation of epithelial cells into cells with a fibroblast phenotype (EMT) which gives them heightened migration properties (Kothari et al. 2014). The role, if any, of FMT in endometrial repair is unknown.

5.1.4 Stem/progenitor cells and endometrial repair

As discussed in Chapter 4, the striking regenerative capacity of the endometrium has led to the hypothesis that a population of stem/progenitor cells exist that can differentiate into multiple cell lineages in response to 'damage' at the time of menses (Gargett and Masuda 2010, Kaitu'u-Lino et al. 2012). In primates, it was reported an entire endometrium could be regenerated from only a few remaining cells, after performing an experimental endometriectomy (Bickers 1944). Populations of stem/progenitor cells have been identified in the human endometrium using clonogenic stem cell assays (Chan et al. 2004, Dimitrov et al. 2008, Gargett et al. 2009) and Hoechst exclusion assay to identify side population cells (Kato et al. 2007, Hu et al. 2010, Cervelló et al. 2011). In mice, pulse-chase experiments have identified label-retaining cells (LRC) in both epithelial and stromal cell compartments (Chan and Gargett 2006, Cao et al. 2015, Kaitu'u-Lino et al. 2012). The exact contribution of these cells to physiological endometrial repair and remodelling remains unclear (Schwab et al. 2005, Schwab and Gargett 2007, Cervelló et al. 2007).

5.1.5 A role for perivascular pericytes in endometrial repair?

Pericytes are cells that reside in close proximity to blood vessels and there is a growing body of evidence that they have functions in vascular development and stability with a specific role in regulating endothelial cell proliferation and migration (Crocker et al. 1970, Mills et al. 2013, Murray et al. 2014). Pericytes have been shown to have MSC like properties including multilineage differentiation, with the ability to transdifferentiate into chondrocytes, adipocytes and osteocytes *in vitro* (Cervelló et al. 2007, Murray et al. 2014, Ansell and Izeta 2015). Pericytes have also been implicated in the process of wound healing and shown to interact with multiple cell types including platelets, inflammatory cells, connective tissue cells and endothelial cells (Bodnar et al. 2016, Khosrotehrani 2013). It has been shown that pericytes detach from blood vessels and migrate into the surrounding tissue to guide the process of angiogenic sprouting (Stratman et al. 2009): this is reported to be driven by Pdgfrβ-

dependent signalling (Rajkumar et al. 2006). Within the skin it has been found that pericytes promote angiogenesis and epithelial cell proliferation and skin regeneration by modifying their ECM environment (Paquet-Fifield et al. 2009)). Further to this pericytes have been described to play a role in modulating the inflammatory response by secreting chemokines which stimulate the migration of leucocytes through vascular walls (Pober and Tellides 2012, Stark et al. 2013) and in the brain it has even been suggested that pericytes can differentiate into macrophages (Monteiro, Rocha and Marini-Abreu 1996, Sakuma et al. 2016).

Pericytes have also been implicated in pathological fibrosis. Fibrosis is characterised by an excessive accumulation of ECM proteins produced by activated fibroblasts and myofibroblasts (Bodnar et al. 2016). Myofibroblasts are thought to arise from pre-existing fibroblasts, BM-MSCs and pericytes (Hinz 2007). Pericyte-derived myofibroblasts have been implicated in kidney fibrosis as collagen-producing cells (Ballhause et al. 2014, Duffield 2014, LeBleu et al. 2013) and in dermal fibrosis where the majority of collagen producing cells were generated from a Pdgfrβ+NG2+ subpopulation (Dulauroy et al. 2012). It has been suggested that nestin and ADAM12 may be key regulators that determine the pericyte to myofibroblast transition (Bodnar et al. 2016, Dulauroy et al. 2012). However the precise signals that regulate the functions of pericytes in wound healing and fibrosis are yet to be deciphered and additional complexity comes from recent papers that pericytes may represent a heterogeneous population of cells which have functional subclasses (Ansell and Izeta 2015)

Understanding the role of mesenchymal progenitor cells in physiological endometrial repair may inform the mechanisms responsible for gynaecological disorders including heavy menstrual bleeding, endometriosis and Asherman's syndrome (Dimitrov et al. 2008, Deane et al. 2013). These conditions are all associated with abnormal endometrial function which may in part be attributed to abnormalities in the number, function, location and/or regulation of stem/progenitor cells (Gargett and Chan 2006, Du and Taylor 2007, Dimitrov et al. 2008). A better understanding of the role(s) of stem/progenitor cells in endometrial pathologies is seen as a key goal in developing new treatment options.

5.1.6 Summary

The endometrium is a complex multicellular tissue that exhibits ECM remodelling, an inflammatory response, hypoxia, vasculature changes and tissue remodelling in response to menstruation all of which have roles to play in its regeneration without scarring (Spitzer et al. 2012). In Chapter 3 dynamic changes in immune cell populations, including the emergence of a unique population of monocyte-derived macrophages were identified during dynamic shedding and remodelling of endometrium in mice induced to experience artificial 'menses'. Studies described in Chapter 4 have identified a population of putative stem/progenitor cells in the mouse endometrium that were identified as perivascular pericytes. In the studies described in the current Chapter capitalise on the use of the Edinburgh menses mouse model building on previous characterisation of the putative stem cells (pericytes; Chapter 4) as a platform to investigate their role in scar-free tissue healing and restoration of homeostasis.

5.2 Aim

To characterise the phenotype of endometrial pericytes during endometrial tissue repair.

5.3 Experimental Approach

5.3.1 The Edinburgh menses mouse model

To investigate the mesenchymal cell contribution to endometrial tissue repair the Edinburgh menses mouse model was used. The full protocol is outlined in Section 2.2.2 and described in Table 2-4 and Figure 2-5 (Cousins et al. 2014, Cousins et al. 2016b, Cousins et al. 2016d).

5.3.2 Transgenic mouse lines

The results in this chapter were generated using the *Pdgfrβ-BAC-eGFP* reporter mouse line, detailed in Section 2.1.1.1, in which GFP reporter protein is expressed under control of the *Pdgfrβ* promoter element: studies detailed in Chapter 4, demonstrated that GFP/Pdgfrβ was exclusively expressed in the endometrial stromal compartment.

5.3.3 Tissue processing and Immunohistochemistry

Uterine tissue samples were fixed in 4% PFA for 2 hours at 4°C, rinsed in PBS and stored overnight in 18% sucrose at 4°C before being embedded in OCT medium and stored at -80°C, as described in Section 2.3. H&E staining and IHC was carried as in Section 2.4.1 and 2.4.3 respectively using antibodies in Table 5-1.

Table 5-1. Antibodies used to interrogate the role of mesenchymal cells in endometrial repair using the Edinburgh mouse model of endometrial breakdown and repair.

Antibody Name	Supplier and Cat. No. (concentration)	Dilution	Serum block
Polyclonal rabbit anti-GFP	Abcam, ab6556 (0.5mg/ml)	1/1000	Goat
Monoclonal rabbit anti-Pdgfrβ	Abcam, ab32570 (0.15mg/ml)	1/1000	Goat
Monoclonal rabbit anti-CD146 (Mcam)	Abcam, ab75769 (0.123mg/ml)	1/1000	Goat
Polyclonal Rabbit anti-NG2 (Cspg4)	Abcam, ab12905	1/600	Goat
Monoclonal mouse anti-αSMA	Sigma, A-2547	1/10K	Horse
Polyclonal rabbit anti-CD31	Abcam, ab28364 (1mg/ml)	1/500	Goat
Polyclonal rabbit anti-EpCAM	Abcam, ab71916 (1mg/ml)	1/2000	Goat

Picrosirius stain (PSR) was carried out as in Section 2.4.2. Images were obtained using both brightfield and confocal microscopy as in Section 2.4.4.

5.3.4 Flow cytometry and FACS

To interrogate mesenchymal cell populations flow cytometry analysis was performed using protocols detailed in Section 2.5 and flow cytometry antibodies outlined in Table 5-2. FACS was used to isolate specific mesenchymal cell populations from the endometrial tissue as detailed in Section 2.5.3.

Table 5-2. Flow cytometry antibody panel designed to interrogate mesenchymal cell populations in uterine tissue

Antibody name	Supplier Cat. No. (concentration)	Excitation wavelength	Emission wavelength	Dilution
BV421 anti-mouse CD31 (Pecam1)	BioLegend, 102423 (0.2mg/ml)	405nm	421nm	1/200
V450 anti-mouse CD45: 30-F11	Fischer scientific, BDB560501 (0.2mg/ml)	404nm	448nm	1/100
PE anti-mouse CD146 (Mcam)	BioLegend, 134704 (0.2mg/ml)	496nm	578nm	1/200
BV605 anti-mouse CD326 (EpCAM)	BioLegend, 118227 (0.2mg/ml)	405nm	603nm	1/400
APC anti-mouse CD140b (Pdgfrβ)	BioLegend, 136008, (0.2mg/ml)	650nm	660nm	1/100
AF488 anti-mouse NG2	Merck, AB5320A4	495nm	519nm	1/100
APC anti mouse CD146 (Mcam)	BioLegend, 134712, (0.2mg/ml)	650nm	660nm	1/200

5.3.5 RNA extraction and cDNA synthesis

RNA extraction from cells was carried out using the SimplyRNA Cells Maxwell® 16 LEV kit (Section 2.6.3) and run on the automated Maxwell® 16 Instrument (Section 2.6.3.2). The resulting yield of RNA was measured using the LabChip GX Touch Nucleic Acid Analyser (Section 2.6.4) and the RNA Pico Sensitivity Assay (Section 2.6.4.1).

cDNA samples for qPCR were synthesised using the Superscript VILO cDNA Synthesis kit (Section 2.7.1). cDNA samples for NGS were synthesised using the NuGEN Ovation RNA-Seq System V2 (Section 2.7.2) while cDNA samples for single cell sequencing were synthesised using the Chromium™ Single Cell 3' Library & Gel Bead Kit V2 (Section 2.10.2).

5.3.6 Quantitative PCR

qPCR was used to determine mRNA expression of genes specific to endometrial tissue repair as detailed in Section 2.8 using primers detailed in Table 2-17. Quantification of gene expression and statistical analysis was performed as outlined in Section 2.8.3.

5.3.7 Next Generation Sequencing

To complement and extend data detailed in Chapter 4 mesenchymal cells were isolated from *Pdgfrβ-BAC-eGFP* uterine tissues at 24hrs of the mouse model of endometrial breakdown and repair. RNA extraction and cDNA synthesis was carried out as described in Section 2.9.1. Samples were sent to Edinburgh Genomics for sequencing on the HiSeq 4000 75PE platform according to standard protocols at the facility (Section 2.9.2). Bioinformatic analysis of the NGS data was carried out by Jonathan Manning at the Edinburgh Genomics facility, as described in Section 2.9.3. To validate sequencing results qPCR was performed on an independent set of RNA samples generated from cells isolated from *Pdgfrβ-BAC-eGFP* endometrial tissues (Section 2.9.4).

5.3.8 Single Cell Sequencing

Single cell sequencing was carried out on two populations of mesenchymal cells isolated from *Pdgfrβ-BAC-eGFP* uterine tissues: a) at 24hrs of the mouse model of endometrial breakdown and repair and b) from cycling adult females (naïve). Pooled samples (n=4 from either (a) or (b)) were analysed using Single Cell Sequencing technology on the 10x Genomics platform as detailed in Section 2.10. Samples were sent to Edinburgh Genomics (https://genomics.ed.ac.uk/) for sequencing on the Illumina NovaSeq platform (Section 2.10.10) and an in-house bioinformatic analysis was carried out (Section 2.10.11). Loupe files were analysed on the Loupe Cell Browser.

5.4 Results

5.4.1 Dynamic changes in mesenchymal cell populations during endometrial repair

Having identified a population of endometrial stromal pericytes (putative mesenchymal progenitors) in naïve female mice and characterised their gene expression profile (Chapter 4), in the current Chapter their contribution to mechanisms underpinning rapid, synchronous, endometrial breakdown and repair was investigated.

5.4.1.1 Expression of known pericyte markers, Pdgfrβ and CD146, at various time points of endometrial breakdown and repair.

To investigate spatial and temporal changes in location/phenotype of pericyte populations during endometrial breakdown and repair, IHC was used to analyse expression of two known pericyte identification markers (Pdgfrβ and CD146) in endometrial tissues collected at 0, 4, 12 and 24hrs following P4 withdrawal. At 0hrs, before decidual tissue breakdown, Pdgfrβ was immunolocalised to cells throughout the stromal compartment and to decidual cells: in agreement with results in Chapter 4 the myometrial and epithelial cells were immunonegative. CD146+ endothelial cells surrounded blood vessels that were dense in the decidualised tissue and more evenly dispersed in the residual endometrium (Figure 5-1 (A)). Pdgfrβ+/CD146+ pericytes could be identified in perivascular locations consistent with a pericyte phenotype as discussed in depth in Chapter 4 (Figure 5-1 (A) arrows). At 4hrs, during initiation of decidual breakdown, Pdgfrβ+ cells were readily detected in the residual (non-decidualised) endometrium however expression by decidualised cells was decreased (Figure 5-1 (B)). CD146 expressing endothelial cells were abundant throughout the tissue which displayed a dense vasculature in the decidua however there was no association with Pdgfrβ expression in the decidualised tissue (Figure 5-1 (B). Notably, Pdgfrβ+/CD146+ (pericytes) were exclusive to the residual endometrium and could not be detected in the decidualised tissue (Figure 5-1 (B) arrows).

At 12hrs active tissue breakdown was occurring and apoptosis of decidual cells could be detected by altered nuclear morphology (chromatin condensation, nuclear shrinkage, DNA fragmentation as determined by DAPI staining). At this time, Pdgfrβ was expressed predominantly by cells of the residual endometrium with some cells in

the shed tissue expressing Pdgfrβ (Figure 5-1 (C)). CD146 expressing endothelial cells (and vessels) were present throughout the tissue but there was evidence of vessel degeneration in the shed tissue (Figure 5-1 (C) arrow heads). As noted at 4hrs, cells co-expressing Pdgfrβ and CD146 (pericytes) were only located in the residual endometrium and could not be detected in the shed tissue (Figure 5-1 (C) arrows). During active tissue repair (24hrs), Pdgfrβ was exclusively expressed by stromal cells in the residual endometrium and not detected in cells of the shed tissue creating a clear distinction between the two tissue regions (Figure 5-1 (D) dashed line). In contrast to 12hrs, no CD146 expressing endothelial cells were detected in the shed tissue indicating that full vessel degeneration had occurred (Figure 5-1 (D)). In the residual endometrium Pdgfrβ+/CD146+ pericytes were located around blood vessels and in close proximity to edge of the detached shed tissue (Figure 5-1 (D) arrows). In summary, these results demonstrate dynamic changes in both the vasculature and decidual compartments during endometrial tissue breakdown and repair.

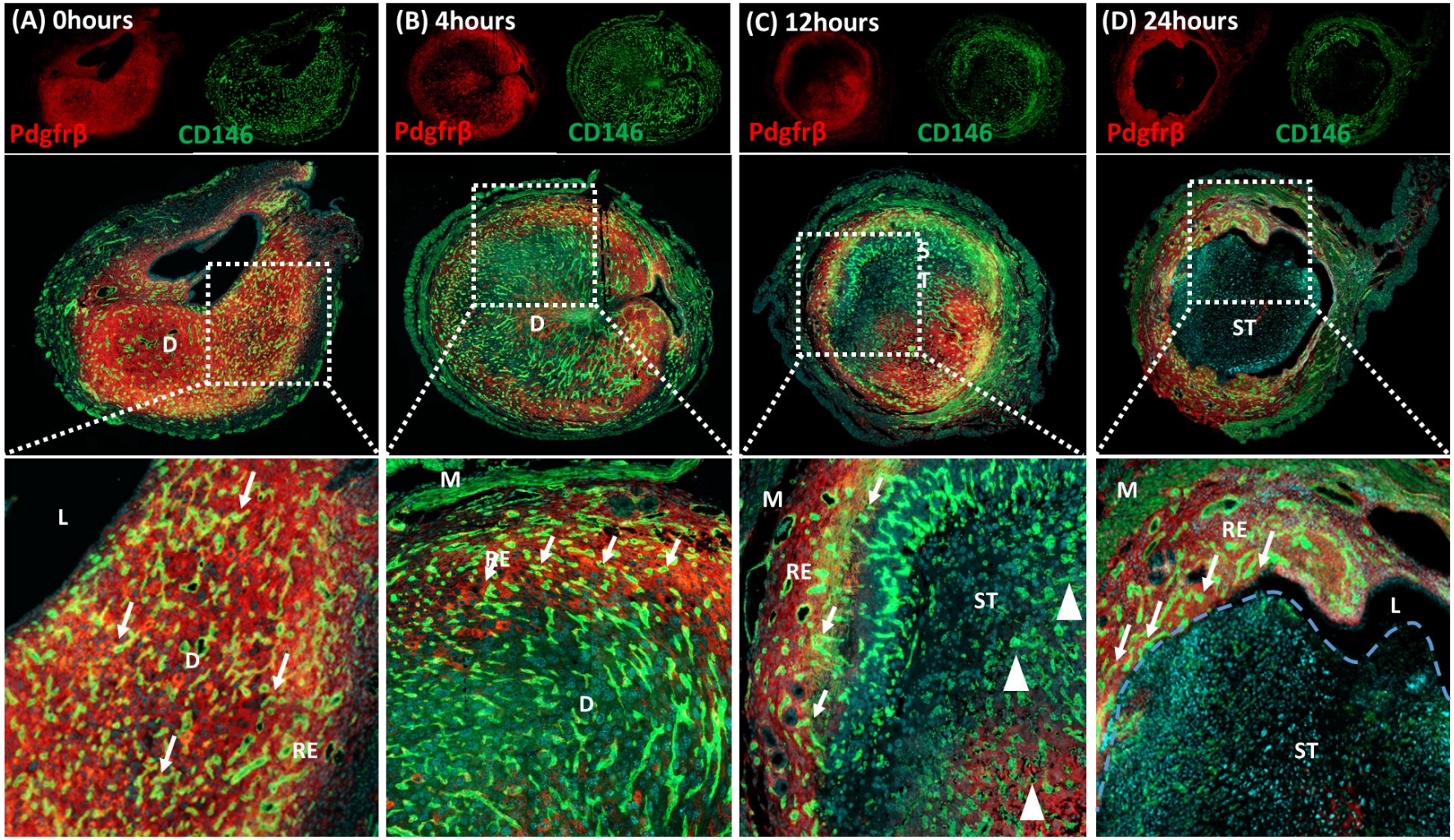
(A) 0hours
Pdgfrβ
CD146
(B) 4hours
Pdgfrβ
CD146
(C) 12hours
Pdgfrβ
CD146
(D) 24hours
Pdgfrβ
CD146
D
D
ST
ST
L
M
RE
D
RE
M
RE
ST
M
RE
L
D
RE
D
ST
ST

Is Figure 5-1. IHC detection of Pdgfrβ and CD146 expression in mouse uterine tissues before (0hrs after P4 withdrawal) and during tissue breakdown (4 and 12hrs) and repair (24hrs). The expression of Pdgfrβ (red) and CD146 (green), co-expression of which identifies pericytes (arrows), was examined in uterine tissues collected from the Edinburgh menses mouse model at various time points of the breakdown and repair phases. Pdgfrβ is expressed by stromal fibroblasts and pericytes while CD146 is expressed by endothelial cells and pericytes. **(A)** At 0hrs Pdgfrβ and CD146 were expressed throughout the decidualised tissue and residual endometrium and double positive cells (arrows) could be detected in association with blood vessel structures. **(B)** At 4hrs, during the initiation of tissue breakdown Pdgfrβ expression was decreased in the decidualised tissue while CD146 was expressed throughout the tissue. Blood vessesl in the decidualised tissue did not have double positive cells (arrows) associated with them. Double positive cells were located in the residual endometrium **(C)** At 12hrs, during active tissue breakdown, Pdgfrβ and CD146 were expressed in the residual endometrium and there was evidence for vascular degeneration in the shed tissue as (arrow heads) where CD146 expressing blood vessels appear smaller and broken. Again double positive cells were confined to the residual endometrium (arrows). **(D)** At 24hrs, during active tissue repair Pdgfrβ and CD146 were exclusively expressed in the residual endometrium while the shed tissue was completely negative. Double positive cells (arrows) were located along the stromal surface denuded of epithelium. Decidua (D), residual endometrium (RE), myometrium (M), lumen (L), shed tissue (ST) blue dashed line= boundary between decidualised/shed tissue and residual endometrium (representative images, n=4 for each time point).

5.4.1.2 Association of pericytes with vasculature in the endometrium during endometrial repair

To better understand the relationship between pericytes and the vasculature during endometrial repair processes, IHC was used to assess the location endothelial cells (CD31+) and NG2+ cells which were previously identified as endometrial pericytes in naïve mice (see results in Chapter 4). Expression was compared between naïve uterine tissue and uterine tissues collected at the 24hrs time point of the Edinburgh menses mouse model (actively repairing).

In naïve samples CD31+ endothelial cells could be identified dispersed throughout the basal endometrial stroma. The NG2+ pericytes were closely associated with these structures (Figure 5-2 (A) yellow arrows) and were not located anywhere else in the tissue. In repairing samples (24hrs) blood vessel structures (CD31+ endothelial cells) were still detected in the residual endometrial stroma with NG2+ pericytes surrounding them (Figure 5-2 (B) yellow arrows) as in naïve tissue. Notably however, in these tissues there were also NG2+ cells that were not associated with CD31+ blood vessel structures (Figure 5-2 (B) white arrows) but were instead located in close proximity to the denuded stromal surface and degrading decidual edge (Figure 5-2 (B), dashed line).

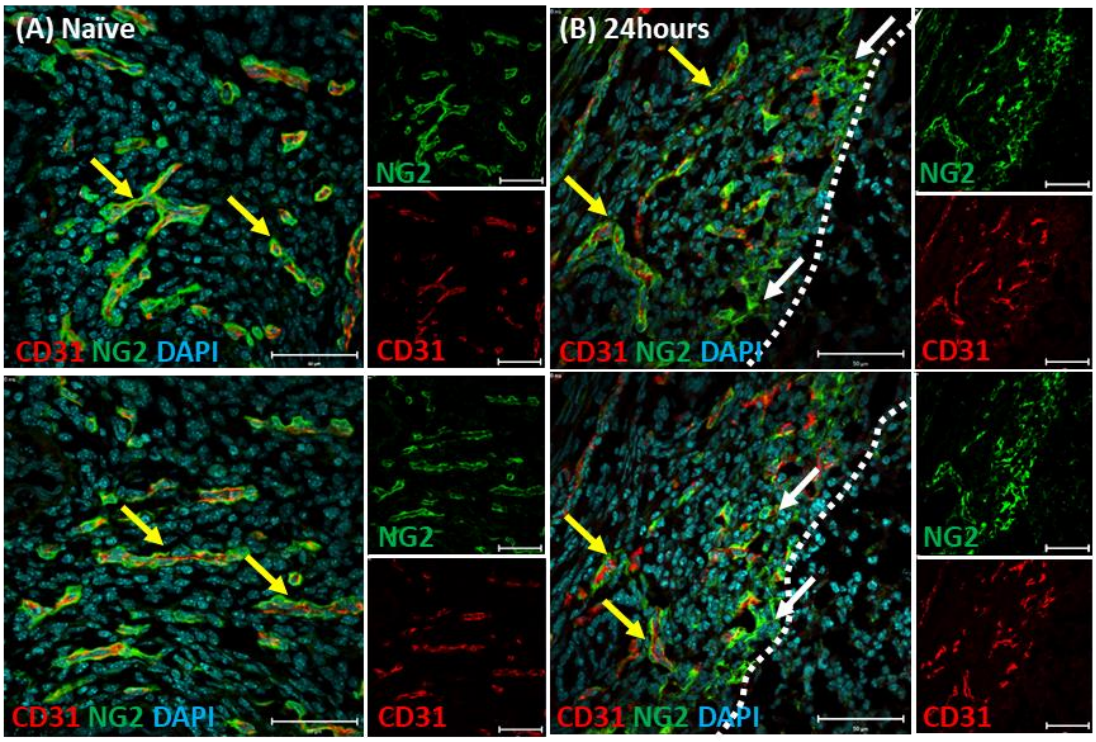

Figure 5-2. Investigation of the distribution of CD31 (red) expressing endothelial cells and NG2 (green) expressing pericytes in naïve uterine tissue (control) and uterine tissue collected at 24hrs following P4 withdrawal (repairing) from C57BL/6 mice. (A) CD31+ endothelial cells are closely surrounded by NG2+ pericytes in naïve tissue. **(B)** CD31+ endothelial cells are closely surrounded by NG2+ pericytes in residual endometrium of repairing tissue while NG2+ cells can also be detected in close proximity to the repairing stromal surface (white dashed line) (representative images, n=6 for each, scale bar = 50µm).

To further analyse these novel findings, cell counting was performed to determine the number of blood vessel structures per field of view (FOV) and then the number of endothelial cells (CD31+ with visible nucleus) and pericytes (NG2+ with visible nucleus) per FOV. Two FOVs were imaged for each tissue section (n=4 mice, n=16 FOV). Representative images of naïve and 24hrs tissue sections can be seen in Figure 5-3 (A-B respectively) outlining the method used to distinguish cell types for counting.

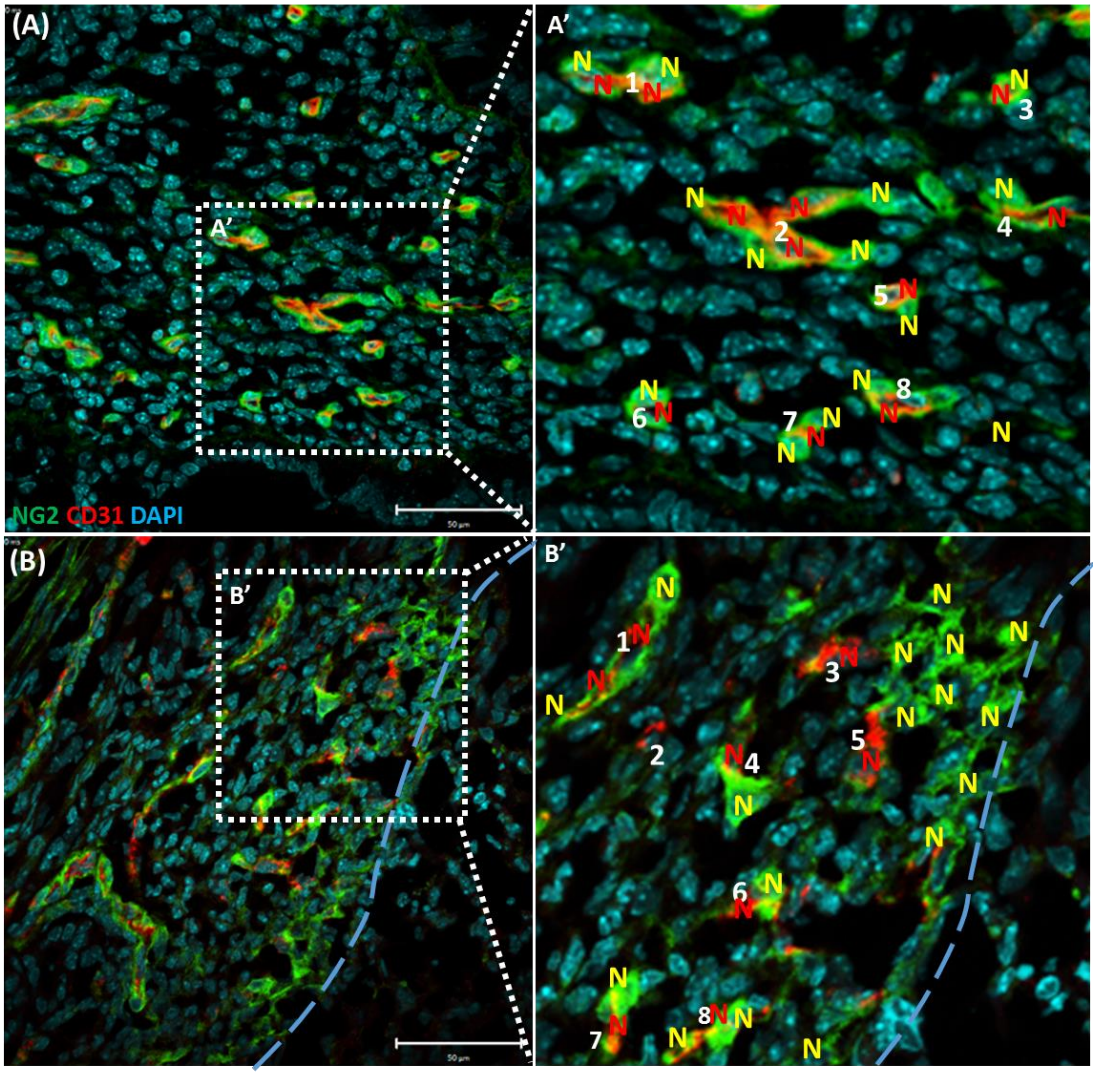

Figure 5-3. Assessment of CD31 (red) expressing endothelial cells and NG2 (green) expressing pericytes in naïve uterine tissue (control) and uterine tissue collected at 24hrs (repairing). Expression of CD31 and NG2 in **(A)** naïve and **(B)** repairing uterine tissues (representative images, n=4). **(A'-B')** Numbers are assigned to each blood vessel structure denoted as having CD31+ endothelial cells present. Red 'N' represent nuclei of CD31+ cells and yellow 'N' represent nuclei of NG2+ cells. Blue dashed line is the border between residual endometrium and shed tissue undergoing breakdown (scale bar = 50µm).

Based on the criteria outlined in Figure 5-3, a number of parameters were counted in both naïve and repairing uterine tissue samples (n=4). There was a significant decrease in the number of blood vessels present in the endometrial stroma at 24hrs (naïve: 26.44±1.39; repairing: 16.25±0.85, unpaired t-test, $p<0.0001$) (Figure 5-4 (A)) consistent with the fact that a large amount of the tissue has been lost during decidual

breakdown and shedding. Similarly the number of CD31+ endothelial cells was reduced while there was a small increase in the number of pericytes (Figure 5-4 (B)). This resulted in a shift in the pericyte:endothelial cell ratio from a mean of 1.27±0.02 in naïve tissues to a mean of 2.03±0.06 in repairing tissues (Figure 5-4 (C)). Notably in the naïve tissue 99.5±0.24% of the NG2+ pericytes were associated with CD31+ blood vessel structures however in the repairing tissue this decreased to 67.48±1.76% (Figure 5-4 (D)) while there was a corresponding increase in the percentage of NG2+ cells located in the endometrial stromal tissue that were not associated with blood vessel structures (0.5±0.24 versus 32.52±1.75) (Figure 5-4 (E)).

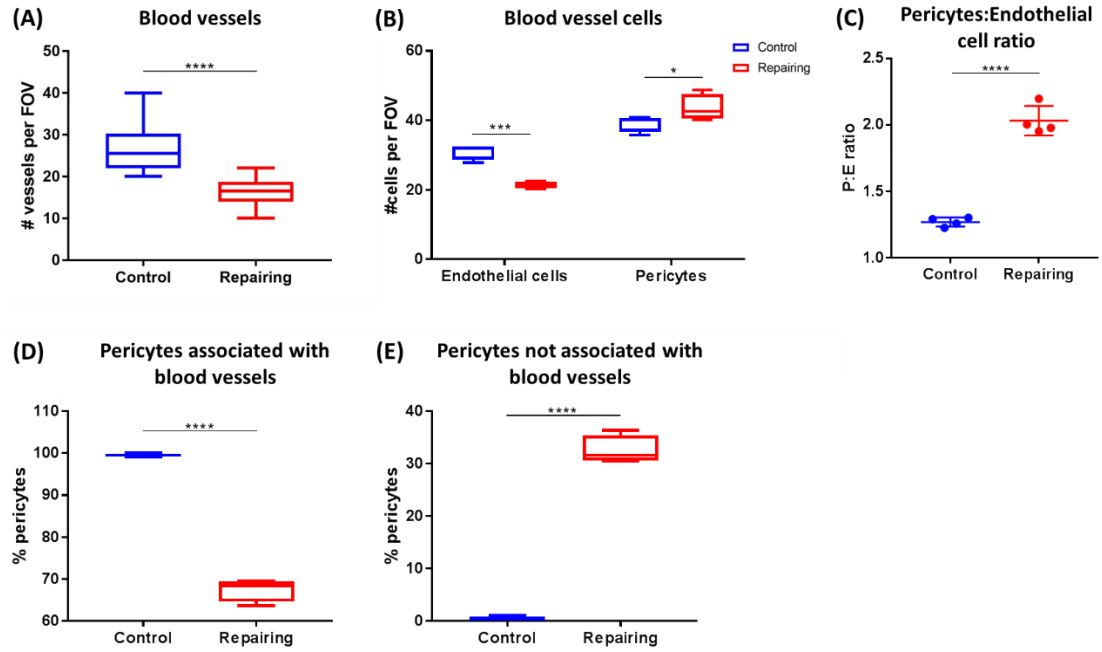

Figure 5-4. Quantification of blood vessels, endothelial cells and pericytes in naïve and repairing uterine tissue. (A) Number of blood vessels per FOV. **(B)** Number of blood vessel associated cells: endothelial cells (CD31+) and pericytes (NG2+) per FOV. **(C)** Pericyte:endothelial cell ratio. **(D)** Number of pericytes associated with blood vessels and **(E)** number of pericytes not associated with blood vessels. # = number (n=4, unpaired t-test, *p<0.05, ***p<0.001 ****p<0.0001).

5.4.1.3 Flow cytometry analysis of GFP+ cell populations *in Pdgfrb-BAC-eGFP* transgenic mouse uterus at various time points of endometrial breakdown and repair

To more accurately assess changes in mesenchymal cell populations during endometrial breakdown and repair, flow cytometry analysis of *Pdgfrb-BAC-eGFP* transgenic mouse uterine tissue was performed. A full characterisation of this transgenic mouse line and associated mesenchymal subpopulations was discussed in Chapter 4. Briefly, in *Pdgfrb-BAC-eGFP* uterus GFP expression is a readout of *Pdgfrβ* promoter activity, and as outlined in Section 4.4.2.3, two GFP expressing subpopulations can be identified in uterine tissue recovered from naïve females using flow cytometry based on both GFP intensity and relative expression of CD146: GFP^{dim}CD146- stromal fibroblasts and GFP^{bright}CD146+ pericytes.

Using parameters validated in Chapter 4 the same subpopulations were quantified in *Pdgfrb-BAC-eGFP* uterine tissue 12hrs (tissue breakdown), 24hrs (tissue repair) and 48hrs (tissue remodelling) after P4 withdrawal using the parameters and analytical gates described in Figure 4-6 and 4-7. As before, GFP+ subpopulations in naïve samples were distinguished by relative expression of CD146: GFP^{dim} cells were CD146- and GFP^{bright} cells were CD146+ (Figure 5-5 (A)). At 12hrs, the same two populations could be detected but there was a further population identified as being $GFP^{dim}CD146^{mid}$ (Figure 5-5 (B)). At 24hrs, these three subpopulations were present with an apparent increase in the numbers of GFP^{dim} $CD146^{mid}$ (intermediate) cells (Figure 5-5 (C)). By 48hrs, the subpopulations once more mirrored those seen in naïve tissues: GFP^{dim}CD146- and GFP^{bright} CD146+ and the third $GFP^{dim}CD146^{mid}$ (intermediate) population (Figure 5-5 (D)) was no longer detectable consistent with the completion of tissue repair and return to homeostasis.

Analysis of the flow cytometry data revealed that there was no significant difference in the proportions of GFP^{dim}CD146- (stromal fibroblasts) at any time point of tissue breakdown and repair, although there was a trend for a decrease at 24hrs (Figure 5-5 (I)). In contrast, there was a significant increase in the number of GFP^{bright}CD146+ (pericytes) at 24hrs when compared to both naïve and 12hrs samples (naïve: 16.84±1.23%; 12hrs: 12.38±1.57% versus 24hrs: 23.97±2.05%, p=0.0299 and p=0.0002 respectively). At 48hrs the proportion of GFP^{bright}CD146+ was comparable

to naïve samples and decreased relative to 24hrs (23.97±2.05% versus 16.98±1.28%, p=0.0343) (Figure 5-5 (J)).

Flow cytometry provided evidence for a population of stromal cells characterised as GFP^{dim} $CD146^{mid}$ (intermediate cells) that were unique to repairing tissue and significantly increased between naïve and 24hrs (1.31±0.15% versus 14.73±2.49%, p<0.0001) and between 12 and 24hrs (4.388±0.97% versus 14.73±2.49%, p=0.0023) but less abundant at 48hrs (24 hours 14.73±2.49%, 48hours 3.536±0.62%, p=0.0009) (Figure 5-5 (K)). Although these novel results identified a population of transient intermediate cells that are specific to repairing endometrial tissue further investigation was required to better understand their location and phenotype.

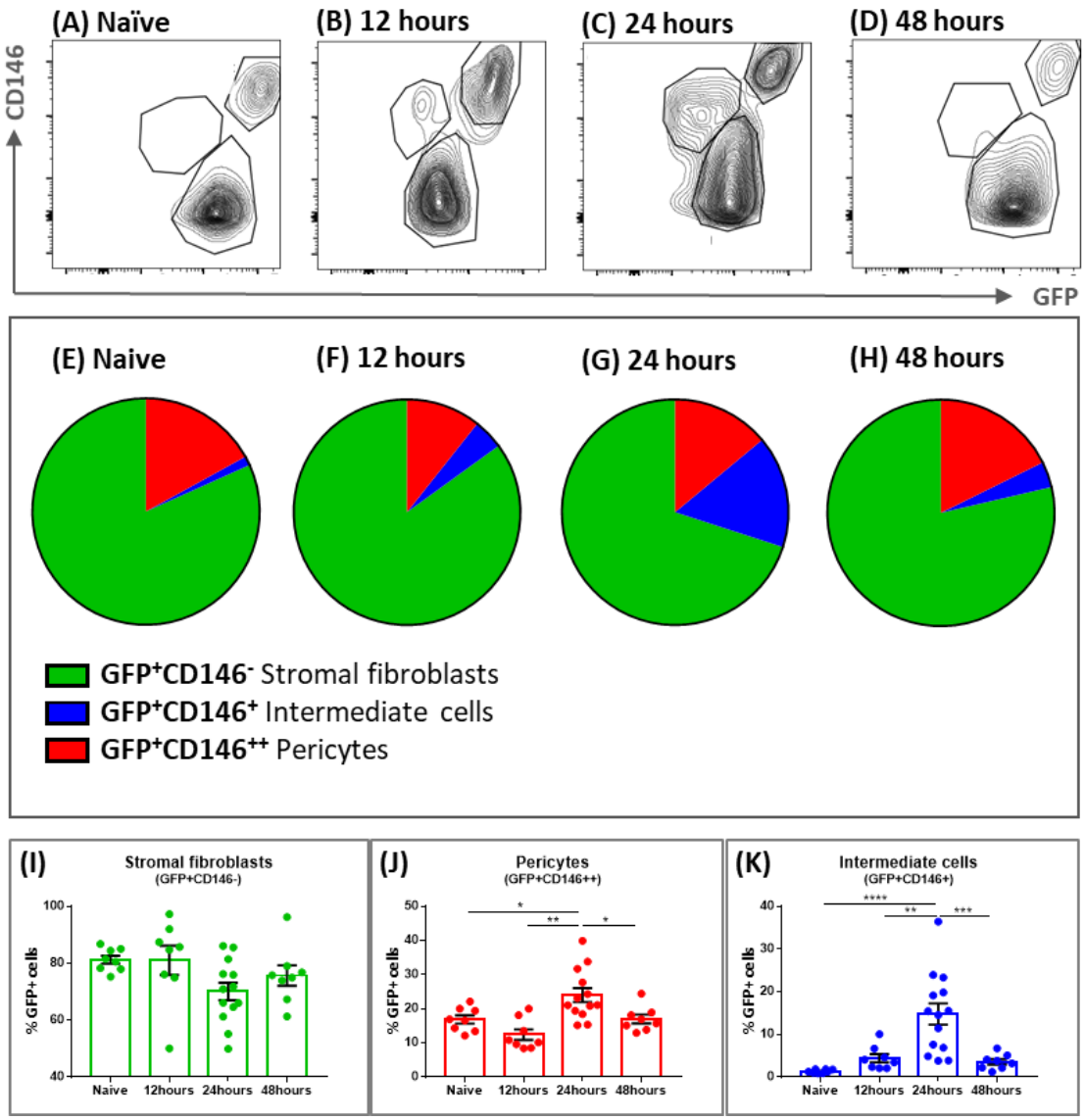

Figure 5-5. Flow Cytometry analysis of GFP+ subpopulations in *Pdgfrβ-BAC-eGFP* uterus at various time points of endometrial tissue breakdown (12hrs), repair (24hrs) and remodelling (48hrs). (A) Flow cytometry plots analysing expression of CD146 (y-axis) in different GFP^+ cell populations (x-axis) in naïve uterine tissue and uterine tissues 12, 24 and 48hrs following P4 withdrawal (*Pdgfrβ-BAC-eGFP*). Parent gates: All cells > Single cells > Live cells > $CD31^-CD45^-$ cells > GFP^+ cells (see Chapter 4, Figure 4-6). **(B)** Pie charts summarising the composition of the GFP+ cell compartment and changes in relative abundance of each GFP+ subpopulation during endometrial breakdown and repair (frequency of total GFP+ cells). **(C)** Quantification of GFP+ subpopulations represented as a frequency of total GFP+ cells in uterine tissue 12, 24 and 48hrs following progesterone withdrawal (naïve: n=8; 12hrs: n=8 , 24hrs: n=13, 48hrs: n=8) (1 way ANOVA, Tukey's multiple comparisons test, *= $p<0.05$, **= $p<0.01$ ***= $p<0.001$ ****= $p<0.0001$).

5.4.2 Investigation of the potential of mesenchymal cells to undergo a mesenchymal to epithelial transition (MET) during endometrial repair

Re-epithelialisation is a fundamental aspect of endometrial tissue repair. Previous results in the Saunders group generated using mice identified three synchronous mechanisms that could contribute to re-establishment of an intact epithelial cell layer: epithelial cell proliferation, epithelial cell migration and a mesenchymal to epithelial transition (MET) (Cousin et al, 2014). Although MET has been identified as a potential mechanism, the contribution of cells in the mesenchymal compartment that may have the ability to trans differentiate as well as the signals that govern METare not known.

5.4.2.1 Flow cytometry analysis of epithelial cell markers by GFP+ cells populations in *Pdgfrβ-BAC-eGFP* transgenic mouse uterus at various time points of endometrial breakdown and repair

To investigate if GFP+ mesenchymal cells in the *Pdgfrb-BAC-eGFP* mouse uterus undergo MET and contribute to re-epithelialisation during endometrial repair, flow cytometry analysis was performed on uterine tissues collected at 12hrs (breakdown), 24hrs (repair) and 48hrs (remodelling) following P4 withdrawal. Flow cytometry histograms in Figure 5-6 (A) display expression of EpCAM in each of the GFP+ subpopulations defined in Figure 5-9 (A): GFP^{dim}CD146- cells (stromal fibroblasts), GFP^{bright}CD146+ cells (pericytes) and $GFP^{dim}CD146^{mid}$ cells (novel intermediate cells). In naïve uterine tissue, the intermediate cell population was not detectable and neither stromal fibroblasts nor pericytes expressed EpCAM consistent with their mesenchymal phenotype, and distinguishing them from epithelial cells in normal tissue (Figure 5-6 (A)).

Assessment of these data has shown changes in the expression of EpCAM by GFP+ mesenchymal cells in naïve; n=8 uterine tissues and uterine tissues at 12hrs; n=8, 24hrs; n=14 and 48hrs; n=8 of the Edinburgh menses mouse model. There was a significant increase in EpCAM expression by stromal fibroblasts at 24hrs when compared to either naïve tissue or samples recovered at 12hrs (naïve: 0.27±0.04%, 12hrs: 1.49±0.44%, 24hrs: 7.73±2.08%, p=0.026 and p=0.045 respectively) (Figure 5-6 (B)). In pericytes there was a significant increase in EpCAM expression when comparing: naive with 12hrs (0.178±0.04% versus 14.93±1.89%, p<0.0001); naïve with 24hrs (0.178±0.04% versus 34.12±2.07%, p<0.0001); and naïve with 48hrs

(0.178±0.04% versus 8.94±1.17%, p=0.017). There was also a significant increase in expression of EpCAM between 12hrs and 24hrs (14.93±1.89% versus 34.12±2.07%, p<0.0001) followed by a significant decrease between 24hrs and 48hrs (34.12±2.07% versus 8.94±1.17%, p<0.0001) (Figure 5-6 (C)). When assessing EpCAM expression by intermediate cells there was a significant increase between naive and 12hrs (0.017±0.01% versus 23.45±1.34%, p<0.0001) and naive and 24hrs (0.017±0.01% versus 34.03±2.27%, p<0.0001); a significant increase between 12hrs and 24hrs (23.45±1.34% versus 34.03±2.27%, p=0.001); and a significant decrease between 12hrs and 48hrs (23.45±1.34% versus 0.434±0.08%, p<0.0001) and 24hrs and 48hrs (34.03±2.27% versus 0.434±0.08%, p<0.0001) (Figure 5-6 (D)). Results demonstrate an increase in EpCAM expression by all three mesenchymal subpopulations, suggesting they can undergo an MET during endometrial repair.

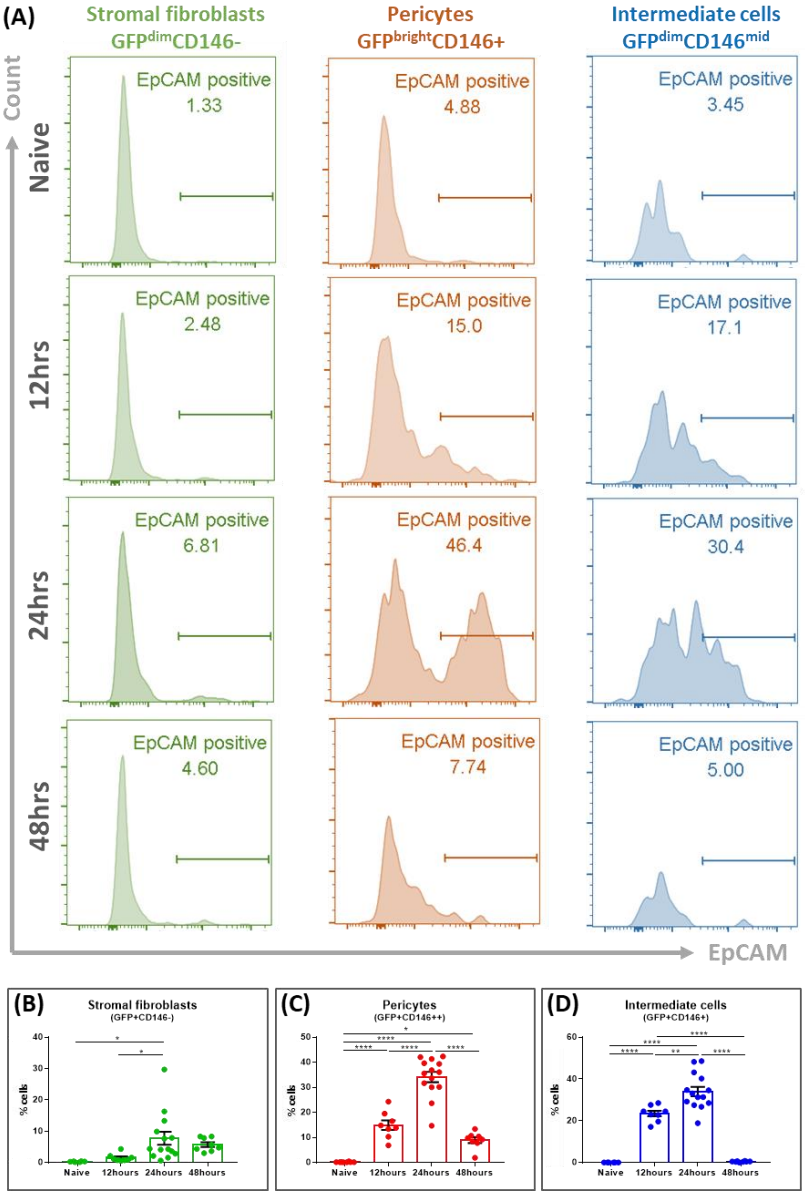

Figure 5-6. Flow Cytometry analysis of the expression of epithelial cell marker EpCAM by GFP$^+$ cell populations in *Pdgfrβ-BAC-eGFP* mouse uterus at various time points endometrial breakdown and repair (12hrs: breakdown, 24hrs: repair, 48hrs: remodelling). Flow cytometry analysis of GFP+ cells was achieved by employing the gating strategy defined in Figure 5-9: All cells > Single cells > Live cells > CD31$^-$CD45$^-$ cells > GFP$^+$ cells. **(A)** Histograms displaying the expression of EpCAM (x-axis) in GFP+ cell populations: GFP^{dim}CD146- stromal fibroblasts; GFP^{bright}CD146+ pericytes and GFP^{dim}CD146^{mid} intermediate cells in naïve *Pdgfrβ-BAC-eGFP* uterine tissue and at 12, 24 and 48hrs of the Edinburgh menses mouse model. Analytical gates to examine each population are defined in Figure 5-9 (A)). Analysis of EpCAM expression calculated as a percentage of each cell subpopulation: **(B)** Stromal fibroblasts (GFP^{dim}CD146-), **(C)** pericytes (GFP^{bright}CD146+) and **(D)** intermediate cells (GFP^{dim}CD146^{mid}) (naïve: n=8; 12hrs: n=8 , 24hrs: n=13, 48hrs: n=8) (one way ANOVA, Tukey's multiple comparisons test, *= p<0.05, **= p<0.01 ***= p<0.001 ****= p<0.0001).

5.4.2.2 Expression of GFP and EpCAM in uterine tissue during endometrial repair determined by IHC

To complement flow cytometry data, IHC was used to generate spatio-temporal information about GFP+EpCAM+ cells in repairing *Pdgfrβ-BAC-eGFP* uterine tissue. In naïve tissue, GFP was expressed exclusively by mesenchymal stromal cells, both GFP^{dim} stromal fibroblasts and GFP^{bright} pericytes (Figure 5-7 (A) white arrows) while EpCAM was expressed exclusively by epithelial cells both luminal and glandular (Figure 5-7 (A), red arrows), distinguishing between the two cellular compartments. Interestingly, in the experimental animals at 24hrs, while the GFP+EpCAM- stromal cells and GFP-EpCAM+ epithelial cells were still present in the tissue (Figure 5-7 (B) white and red arrows respectively), there was also a population of GFP+EpCAM+ cells that were located on the luminal edge of the endometrium that displayed an epithelial-like morphology (Figure 5-7 (B), yellow arrows). At 48hrs no GFP+EpCAM+ cells were detected in the tissue and the two distinct cell compartments were again apparent: GFP+EpCAM- stromal cells and GFP-EPCAM+ epithelial cells (Figure 5-7 (C), white and red arrows respectively).

These results provided further evidence to support our original findings that suggested mesenchymal cells undergo MET to re-instate the epithelial cell layer during endometrial repair (Cousins et al. 2014) however they do not allow us to determine whether these transdifferentiating cells are stromal fibroblasts or pericytes. Specifically, as the reporter in the *Pdgfrβ-BAC-eGFP* transgenic mouse is a knock-in, GFP is only expressed when the *Pdgfrβ* gene promoter is active and GFP is being actively synthesised. This means that when the *Pdgfrβ* gene promoter is no longer active, as will be the case in a fully transdifferentiated 'epithelial' cell, GFP expression will reduce according to the half-life of the protein (~25hrs) with further dilution in actively proliferating cells.

Therefore in follow up studies efforts were made to validate an alternative transgenic strategy to use a lineage tracing system which would allow for persistence of labelling in pericyte derived cell type(s).

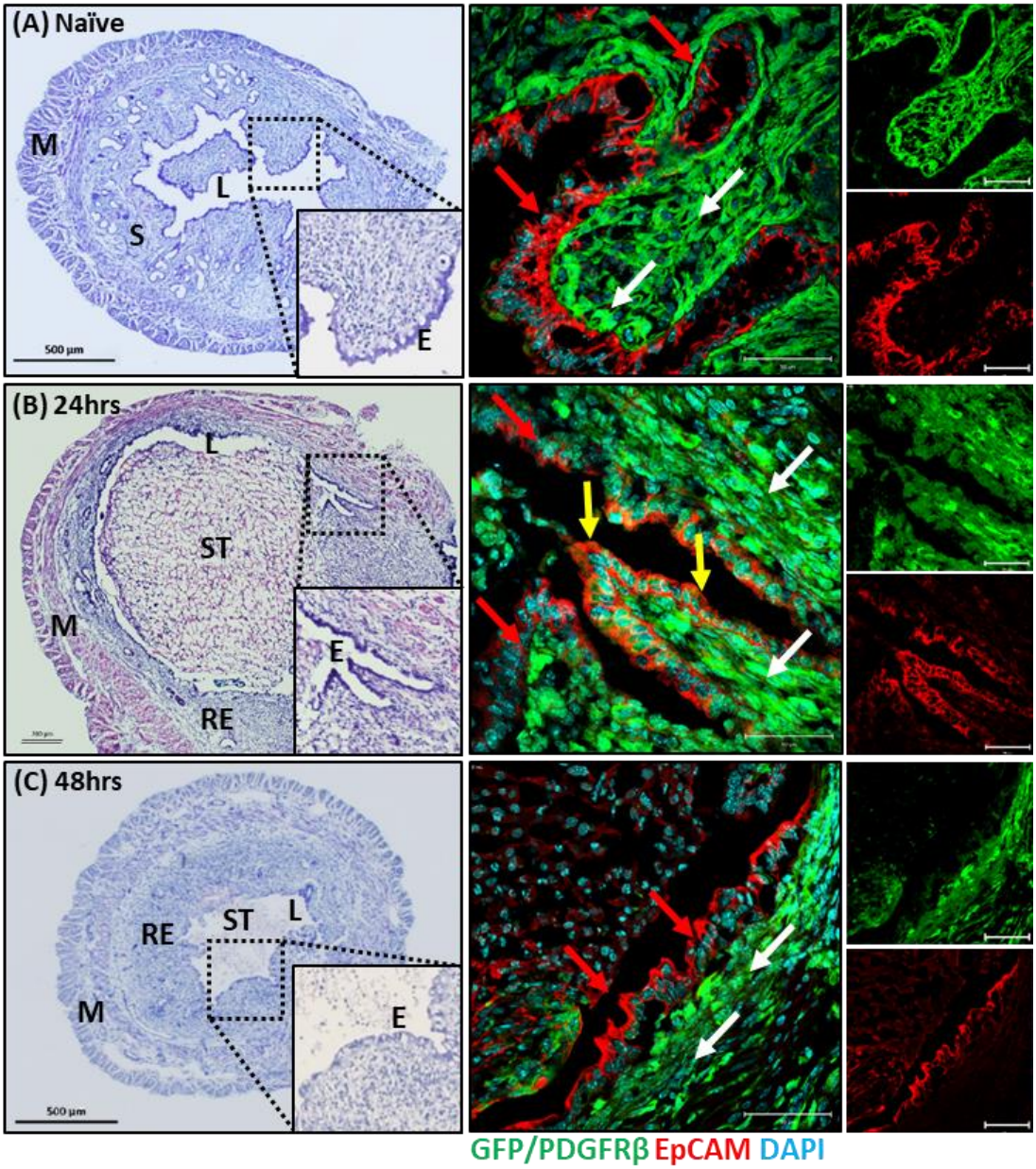

Figure 5-7. Expression of GFP and EpCAM in *Pdgfrβ-BAC-eGFP* uterine tissue during endometrial repair. (A) In naïve tissue there are distinct populations of GFP+ mesenchymal cells (white arrows) and EpCAM+ epithelial cells (red arrows). **(B)** At 24hrs there are GFP+ mesenchymal cells (white arrows), EpCAM+ epithelial cells (red arrows) and GFP+EpCAM+ cells (yellow arrows) located in an area of active re-epithelialisation. **(C)** By 48hrs no GFP+EpCAM+ cells were detected and there are only distinct populations of GFP+ mesenchymal cells (white arrows) and EpCAM+ epithelial cells (red arrows) as in the naïve tissues. Residual endometrium (RE), shed tissue (ST), myometrium (M), epithelium (E), lumen (L) (representative images, n=8-10 mice per group, scale bar H&E=500µm, scale bar IHC=50µm).

5.4.3 Profiling mesenchymal cells from *Pdgfrβ-BAC-eGFP* endometrial tissue during endometrial repair (24hours) by next generation sequencing

Studies using Flow cytometry described above identified dynamic changes in the intensity of GFP and co-expression of EpCAM with the apparent emergence of a transient population at 24hrs after progesterone withdrawal. As this time point has emerged in the studies in both this chapter and Chapter 3 as the most dynamic time in endometrial remodelling/wound repair further transcriptional analysis was undertaken on 24hrs samples.

5.4.3.1 RNA and cDNA sample preparation

To characterise the transcriptomic profile of mesenchymal cells during endometrial repair, total GFP+ cells were isolated from *Pdgfrβ-BAC-eGFP* uterine tissues collected at 24hrs: RNA concentration and quality were analysed using LabChip GX Touch technology (Chapter 2; Section 2.6.4). This sample set was prepared at the same time as the naïve (control/cycling) samples the analysis of which was described in detail in Chapter 4. In the current chapter we sought insights into the transcriptomic phenotype of the different GFP+ cells in the repairing tissue by comparing the previously described dataset (naïve) with the 'repairing' gene set. To provide a direct comparison between these sample sets the naïve samples (Chapter 4) are reproduced in Figure 5-8. The repairing samples had a mean RNA concentration of 0.98±0.13ng/µl and all samples had an RNA Integrity Number (RIN) greater than 8.7 (Figure 5-8 (A)). As described in Chapter 4 these concentrations however did not meet the minimum requirement requested by Edinburgh Genomics (>20ng/µl) therefore cDNA synthesis and amplification was performed (Chapter 2; Section 2.7.2). Following this the repairing samples had a mean cDNA concentration of 86.62±4.61ng/µl and all samples had an A260/280 ratio greater than 1.8 (Figure 5-8 (B)).

5.4.3.2 TruSeq mRNA Sequencing

All samples were sent to Edinburgh Genomics for RNA sequencing within the Genomics Facility (http://genomics.ed.ac.uk/). TruSeq DNA Nano gel free libraries (350bp inserts) were prepared from each of the cDNA samples and sequence data was generated on the HiSeq 4000 75PE platform to yield at least 290M + 290M reads.

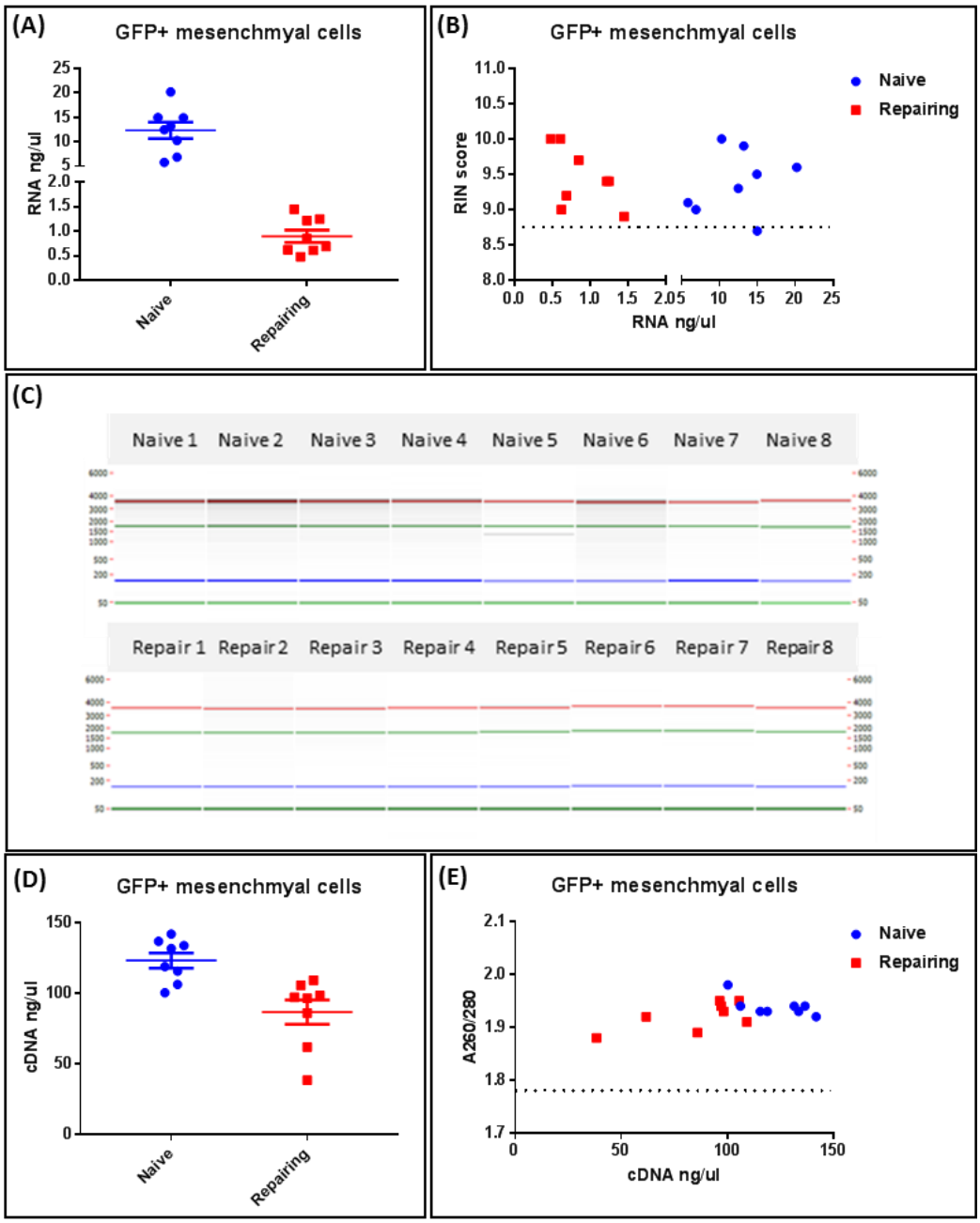

Figure 5-8. LabChip GX Touch analysis of RNA/cDNA quantity and quality for samples generated for RNA sequencing by Edinburgh Genomics. (A) RNA concentrations (ng/ul) of naive and repairing samples. **(B)** RIN score of the naïve and repairing samples, dashed line represents the minimum score required by Edinburgh Genomics (8.7). **(C)** LabChip GX touch read out gel results for the naïve and repairing samples. **(D)** cDNA concentrations (ng/ul) of naïve and repairing samples after performing cDNA amplification using the NuGEN Ovation V2 system. **(E)** A260/A280 ratios of the naïve and repairing samples, dashed line represents the minimum ratio required by Edinburgh Genomics (1.8) (naïve: n=8; repairing: n=8).

5.4.3.3 Bioinformatic data handling

Bioinformatic analysis was performed by Jonathan Manning at Edinburgh Genomics as described in Chapter 2: Section 2.9.3. A summary of the key statistics associated with read pair mapping and counting is outlined in Table 4-3 (Chapter 4).

5.4.3.4 Principle component analysis

As part of the initial analysis, a PCA on normalised and filtered expression data was carried out by Jonathan Manning to explore observed patterns with respect to experimental factors. Briefly, the cumulative proportion of variance associated with each factor was used to study the level of structure in the data, assessed with an ANOVA test. As seen in Figure 5-9 (A), individual naive and repairing samples clustered together showing a large degree of similarity between samples of the same experimental group however when comparing groups there was a large separation on the PCA demonstrating that the transcriptomic profiles of each group were very different (Figure 5-9 (A)). As an extension of the PCA I analysed expression data using BioLayout Express 3D software which determines the correlation between sample groups based on individual gene expression levels. Sample cluster graphs generated (both 2D and 3D) confirmed a high correlation in the transcriptomic profiles of samples within a group but low correlation between naive and repairing groups (each node represents a sample and each line represents similarity between them) (Figure 5-9 (C)).

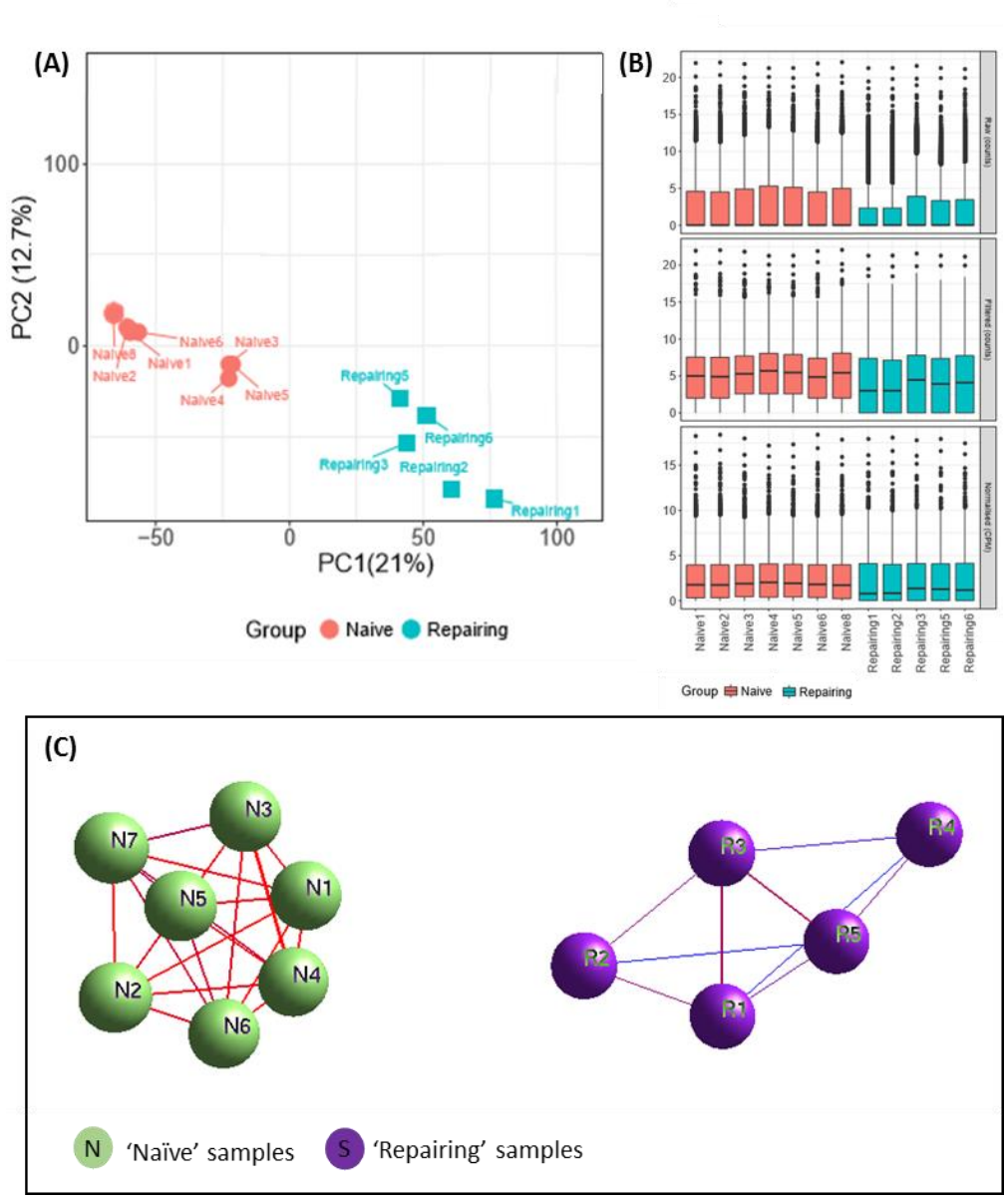

Figure 5-9. Exploratory analysis of the relatedness between naive and repairing sample groups. (A) Principle component plot of the first and second components from PCA analysis using selected naive and repairing samples (n=7 and n=5 respectively). **(B)** Boxplots showing expression distributions among samples at different stages of pre-processing (log2 scale), using selected samples. Note that raw and filtered values are expressed in counts, while normalised values are in counts per million (CPM). Points outside whiskers are outliers at 1.5 x IQR where IQR is the inter-quartile range. **(C)** The correlation of RNASeq datasets between naïve and repairing samples was determined in BioLayout Express3D based on individual gene expression levels and a sample cluster graph generated (Pearson's correlation of R>0.8 and intensity >1 of dataset with fold change >2 or <-2 and FDR <0.05). Nodes represent individual samples and edges represent the degree of correlation between them, colour/thickness is equivalent to how similar the samples are. 3D sample cluster graph displaying a high disparity and little correlation between the groups (naive: n=6; repairing: n=5).

5.4.3.5 Differential gene expression analysis

Differential gene expression analysis was carried out with EdgeR4 (version 3.16.5) and the quasi-likelihood (QL) F-test using the contrast between naïve and repairing sample groups (Jonathan Manning, Edinburgh Genomics). The total numbers of differentially expressed genes are outlined in Table 5-3 according to the thresholds on minimum fold-change (2) and maximum false discovery rate (FDR<0.05).

Table 5-3. Total numbers of differentially expressed genes between naïve and repairing sample groups

Contrast	Upregulated	Downregulated
Naive vs repairing	616	1013

Gene expression data can be visualised as a heatmap, fold change plot and volcano plots which illustrate the most differentially expressed genes between samples (Figure 5-10). Note panel A shows a clear separation between the two datasets based on the top 50 differentially expressed genes. In panels B and C red dots highlight differential expression. As both sample groups were generated following sorting of total GFP+ cells this Figure gives a striking illustration of the changed of patterns of expression in the mesenchymal cell population(s) in response to endometrial 'injury'. Lists of the top 20 most significantly upregulated and downregulated genes in repairing samples, as determined by FDR<0.05, are presented in Tables 5-4 and Table 5-5 respectively. The full list of the top 100 genes is presented in Appendices 5-1; 5-2.

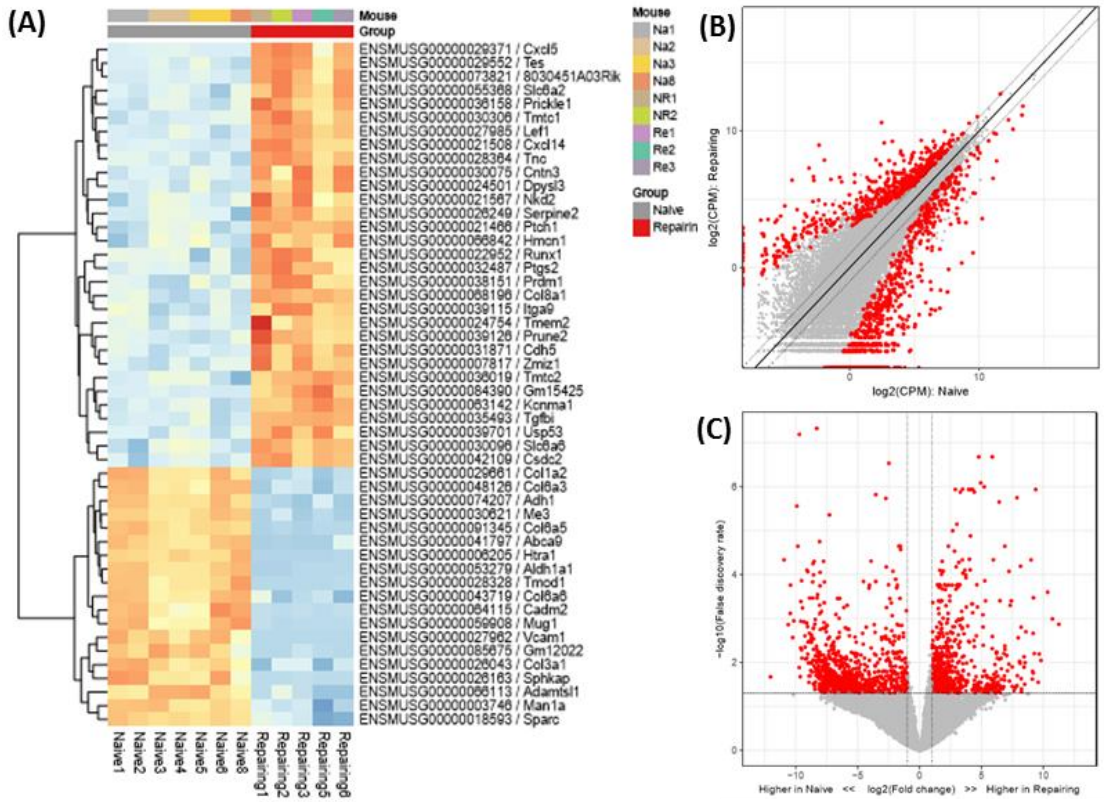

Figure 5-10. Differential gene expression analysis between naïve and 'repairing' sample groups. (A) Heatmap showing the top 50 most differentially expressed genes by false discovery rate (FDR <0.05) between the naïve and repairing groups (616 upregulated genes and 1013 downregulated genes in total. **(B)** Fold change and **(C)** volcano plot illustrating differential expression between groups naive and repairing as defined by group. Volcano plots illustrate log(2) fold change vs –log(10) false discovery rate. The horizontal dashed line represents the specified FDR threshold for significance (0.05), dotted lines in both plots represent the specified fold change threshold (2) in both the positive and negative directions. Points passing both thresholds are coloured red and are differentially expressed.

Table 5-4. Top 20 most significantly upregulated genes in repairing samples when compared to naïve samples as determined FDR <0.05. Table displays the mean CPM for each gene in naïve and repairing tissues and the associated LogFC and p-value.

Gene	Mean CPM Naive	Mean CPM Repairing	LogFC	P-value	FDR <0.05
Mmp10	0.192611314	495.95818	11.2432086	9.71E-06	0.001359377
Erv3	0.045257809	84.0704655	10.71748135	6.49E-06	0.001024937
Mmp12	0.112752673	154.8354046	10.3423004	1.04E-06	0.000252339
Mmp13	0.255816556	231.8863547	9.800783712	0.00017493	0.009061145
Sprr2h	0	7.674410321	9.660603129	9.79E-05	0.006430275
Cd177	0	7.251583962	9.575453439	0.00125461	0.028421027
Jakmip1	0.008520914	11.10935265	9.187891507	1.44E-06	0.000338097
Tnfrsf9	0.01261252	11.4483069	9.164302927	1.98E-05	0.002174383
Slpi	0	5.283499957	9.129152766	0.00043000	0.016091638
Cxcl5	0.145989044	83.00211007	8.998444358	7.58E-08	4.63E-05
Parvb	0.024675058	13.62585254	8.521122087	0.00020797	0.01010534
Onecut3	0.018492264	9.958627792	8.437463465	0.00030168	0.012868605
Gpr55	0	2.800546567	8.204691479	0.00086368	0.023524625
Tnf	0.009246132	5.640869553	8.197978843	1.24E-05	0.001582367
Tnc	5.473751472	1555.833241	8.151385875	1.28E-07	6.48E-05
Abca13	0	2.284936928	7.896652941	0.00064176	0.0201544
Gareml	0	2.03374187	7.727634526	0.00217357	0.037626717
Olfr505-ps1	0	1.715232757	7.487670018	0.00187094	0.035214312
Tph1	0	1.675092592	7.471207085	0.00029689	0.012702769
Lama1	0.579926874	96.79574453	7.402468391	1.94E-06	0.000397164

Table 5-5. Top 20 most significantly downregulated genes in repairing samples when compared to naive samples as determined by FDR <0.05, Table displays the mean CPM for each gene in naïve and repairing tissues and the associated LogFC and p-value.

Gene	Mean CPM Naive	Mean CPM Repairing	LogFC	P-value	FDR <0.05
Vcam1	18.87612	0	-10.9576	7.70E-08	4.63E-05
Ces2g	14.98131	0	-10.6217	1.00E-05	0.001384095
Clca1	13.28959	0	-10.4559	4.51E-06	0.000767291
Asb4	13.12932	0	-10.4326	6.08E-07	0.000174188
Zcchc16	11.60277	0	-10.2586	2.75E-05	0.002711056
Tmod1	25.90097	0.015361301	-9.92398	2.48E-09	2.76E-06
Sphkap	24.39947	0.014478712	-9.84058	2.95E-08	2.26E-05
Crabp1	8.041571	0	-9.73353	0.000312	0.01311522
Aldh1a1	123.7077	0.128831026	-9.72553	5.78E-12	6.43E-08
Ltf	7.409469	0	-9.6104	5.98E-05	0.004668477
Il31ra	7.352368	0	-9.59967	2.02E-06	0.000409847
Ube2t	7.344575	0	-9.59774	7.67E-06	0.001154335
Lgr6	96.94894	0.116242478	-9.53581	3.91E-07	0.000138064
Adamtsl3	6.880863	0	-9.50374	0.000138	0.007983703
Pcdh12	6.161984	0	-9.34644	8.06E-06	0.001196664
Arsi	5.815426	0	-9.27028	2.38E-05	0.002495151
Fhl5	5.00413	0	-9.04249	9.94E-05	0.006472006
Gfra1	32.28628	0.049495506	-9.042	2.12E-07	8.59E-05
Prss23os	4.505037	0	-8.89254	3.64E-05	0.003290656
Olfr78	13.14954	0.019749985	-8.89158	1.51E-06	0.000342751

5.4.3.6 Gene Ontology and Gene Set Enrichment Analysis (GSEA)

To gain insights into the processes that might be altered in the mesenchymal compartment of the repairing endometrium an initial gene ontology analysis was carried out using the online Gene Ontology Consortium platform (http://www.geneontology.org/) inputting the top 100 up and down regulated genes as summarised in Table 5-6. This analysis suggested processes enriched by upregulated genes were associated with smooth muscle cell function, blood vessel function and regulation of the inflammatory response. Interestingly there were a number of genes that have previously been identified as involved in myofibroblast differentiation and smooth muscle contraction consistent with FMT and the morphogenesis of an epithelial sheet consistent with MET which would be in agreement with other data

described in this Chapter. Processes enriched by downregulated genes were associated with collagen organisation, cell adhesion and developmental process.

Table 5-6. Gene Ontology associated with the top 100 up- and down-regulated genes in mesenchymal cells during endometrial repair, fold enrichment scores and associated gene list for each term.

Top 100 upregulated genes in mesenchymal cells during endometrial repair		
Gene Ontology Term	**Fold Enrichment**	**Associated Genes**
Smooth muscle contraction	6.06	*Smad5. Cacna1c, Kcnma1, Rgs2, Ednra, Gatm*
Response to wounding	5.66	*Mmp12, Tnc, Mmp2, Gli1, Serpine2, Notch2, Dpysl3, Cd44*
Relaxation of vascular smooth muscle	5.56	*Kcnma1, Rgs2, Dock5, Ptgs2, Cacna1c, Stc1, Hdac4, Pde4b*
Morphogenesis of an epithelial sheet	5.47	*Mmp12, Notch2, Lama1, Cd44, Hoxd11, Tnc, Ptch1, Lef1, Ednra, Prickle1, Lmo4*
Blood vessel maturation	5.21	*Prickle1, Smad5, Ptgs2, Tmem2, Cdh5, Mmp2, Stra6, Lef1, Ednra, Col8a1, Zmiz1, Notch2, Prdm1, Lama1*
Regulation of vasoconstriction	5.08	*Dock5, Cacna1c, Ptgs2, Mmp2*
Regulation of myoblast differentiation	4.91	*Prickle1, Cxcl14, Tnf, Dock5, Smad5, Neo1, Rgs2, Igf2, Foxp4, Ptgs2*
Smooth muscle cell proliferation	4.79	*Kalrn, Stc1, Tnf, Ptch1, Tgfbi, Ifgbp4, Lef1, Ednra, col8a1, Fst, Nothc2, Prdm1*
Neutrophil chemotaxis	4.53	*Cxcl5, Itga9, Pde4b, Spp1, Neo1, Nav1, Kalrn, Tnf, Cd44, Mmp12*
Regulation of myeloid leucocyte differentiation	4.34	*Tnf, Lef1, Runx1, Notch2, Zmiz1, Prdm1, Inhba*
Top 100 downregulated genes in mesenchymal cells during endometrial repair		
Gene Ontology Term	**Fold Enrichment**	**Associated Genes**
Collagen fibril organisation	5.06	*Col5a1, Col1a2, Adamts2, Col1a1, Col3a1, Tmod1, Gdn, Ccl11, Vim, Gdpd2*
Cell adhesion	4.70	*Pcdh12, Flrt2, Col6a6, Col15a1, Negr1, Cadm2, Col6a1, Col5a1, Col6a5, Bves, Adam12, Cd34, Col6a4, Vcam1, Lsamp*
Regulation of cell localisation	4.26	*Flrt2, Cacnb2, Lgr6, Gpm6b, Olfr78, Sema3b, Dcn, Ptrf, Synpo2, Gsn, Bves, Grin2b, Sparc, Anxa1, Per2, Crp, Npy1r, Vim, Col1a1*
Regulation of developmental process	3.85	*Flrt2, Gpm6b, Negr1, Dcn, Adam12, Ccl11, Vldlr, Dcx, Anxa1, Vim, Col1a1, Asb4, Ptpn5, Gdpd2, Crp, Cd34, Sox5*

Further ontology analysis of the differentially expressed genes dataset was carried out using the Gene Set Enrichment Analysis (GSEA) software to identify pathways enriched in mesenchymal cells during endometrial repair associated with Kyoto Encyclopedia of Genes and Genomes (KEGG) pathways, Biological Process, Canonical Pathways (CP) and Molecular Function (MF) (Figure 5-11 (A-D) respectively).

Signalling pathways identified using this methodology included the Wnt signalling, Hedgehog signalling, TGFβ signalling, Notch signalling and Hippo signalling. Other prominent pathways included the BMP pathway, HDAC Class I pathway, HIF1 pathway and β-catenin pathway.

Biological processes identified were cell junction assembly, adherens junctions, T-cell receptor signalling and processes involving trans-differentiation such as osteoblast differentiation, blood vessel morphogenesis, angiogenesis and epithelial cell morphogenesis. Notably, the data set was also associated with female reproductive processes including maternal process involved in female pregnancy, embryo implantation and decidualisation. These preliminary gene ontology analyses highlighted several processes and pathways that may be essential to regulating endometrial repair several of which are in line with previous results but have generally broadened the range of genes worthy of further study and drive future hypotheses.

Looking in more detail at GO terms of interest, enrichment plots and gene lists were generated to summarise genes in these groups. The top gene targets associated with selected KEGG pathways were identified as follows: Wnt signalling (*Lef1*, *Prkx*, *Prickle* 1), Hedgehog Signalling (*Ptch1*, *Gli1*, *Smo*) and TGFβ signalling (*Fst*, *Smad5*, *Inhba*).

Figure 5-12 summarises the top targets associated with regulation of Biological Processes which were identified as: blood vessel morphogenesis (*Tgfβi*, *Col8a1*, *Lef1*), epithelial cell morphogenesis (*Basp1*, *Wt1*, *Frmd6*) and osteoblast differentiation (*Lef1*, *Hdac9*, *Gli1*) respectively. Examples of canonical pathways included: BMP signalling (*Fst*, *Smad5*, *Ski*), and collagens (*Col8a1*, *Col26a1*, *Col18a1*). Figure 5-13 summarises the top targets associated with molecular functions which included were

all associated with the Wnt signalling pathway: Wnt protein binding (*Sfrp2*, *Fzd1*, *Sfrp1*), Wnt activated receptor activity (*Sfrp2*, *Fzd1*, *Smo*) and β-catenin binding (*Lef1*, *Cdh5*, *Esr1*).

The primary value of this analysis was to identify genes that appeared to play key role(s) in more than one pathway including *Lef1*, *Smo*, *Gli*-1, *Fst* and *Fzd1* which therefore merit further study and validation of their role(s) in regulation of the mesenchymal cell phenotype it was also notable that processes highlighted included those which appeared to reflect previously identified changes in tissue architecture during endometrial repair including blood vessel and epithelial cell morphogenesis.

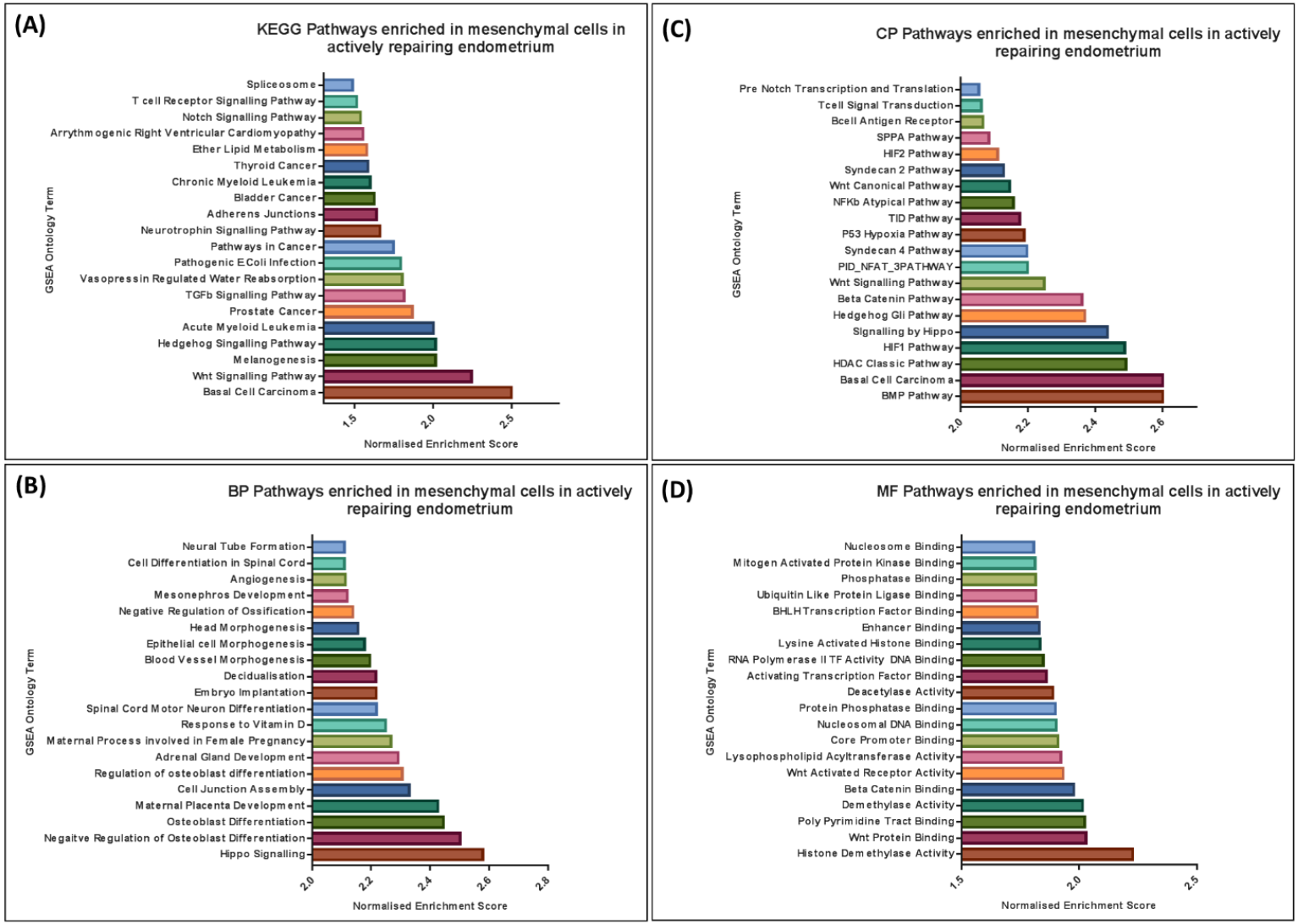

Figure 5-11. Gene Set Enrichment Analysis (GSEA) of genes enriched in mesenchymal cells in the repairing endometrium. Gene ontology analysis as performed using the GSEA software. Analysis of pathways enriched by putative pericyte genes assessing **(A)** Kyoto Encyclopedia of Genes and Genomes (KEGG) pathways **(B)** Biological Process (BP) **(C)** Canonical Pathways (CP) and **(D)** Molecular Function (MF).

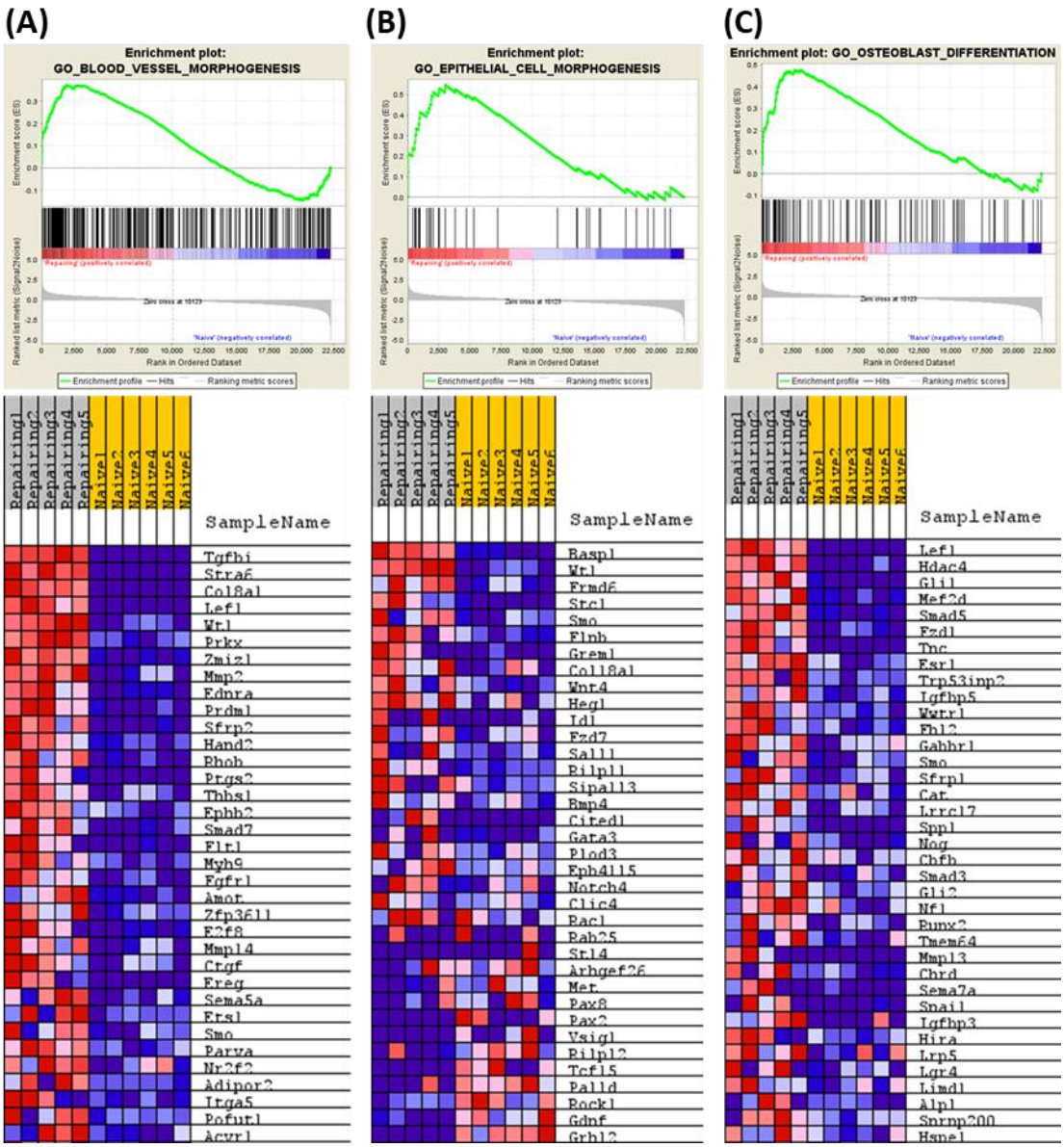

Figure 5-12. Exploration of gene ontology terms enriched by genes upregulated in mesenchymal cells during endometrial repair. Enrichment plots map the relative abundance of each gene associated with a gene ontology term in the dataset (green line). A peak towards the left shows a positive correlation with the repairing samples while a peak towards the right shows a positive correlation with the naïve samples. Heatmaps list the genes associated with each gene ontology term and display expression patterns in naïve and repairing samples. Enrichment plots and heatmaps for the GO terms **(A)** Blood vessel morphogenesis, **(B)** epithelial cell morphogenesis and **(C)** osteoblast differentiation showing strong positive correlation to the repairing samples.

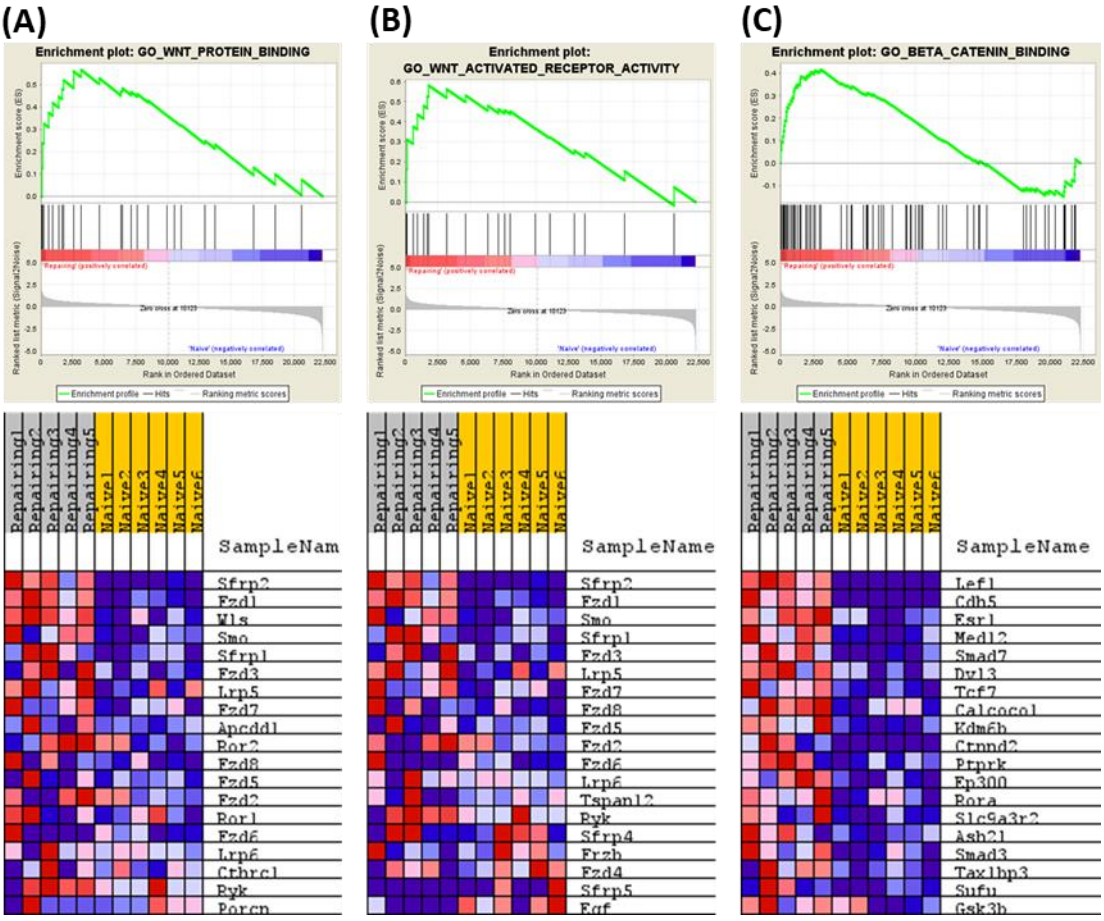

Figure 5-13. Exploration of gene ontology terms enriched by genes upregulated in mesenchymal cells during endometrial repair. Enrichment plots map the relative abundance of each gene associated with a gene ontology term in the dataset (green line). A peak towards the left shows a positive correlation with the repairing samples while a peak towards the right shows a positive correlation with the naïve samples. Heatmaps list the genes associated with each gene ontology term and display expression patterns in naïve and repairing samples. Enrichment plots and heatmaps for the GO terms **(A)** Wnt protein binding, **(B)** Wnt activated receptor activity and **(C)** beta-catenin binding showing strong positive correlation to the repairing samples.

5.4.4 Validation of differentially expressed genes in mesenchymal cells during endometrial repair

To narrow the focus of studies to validate the RNAseq results a ranked gene list was generated using GSEA software to identify the most differentially expressed genes in mesenchymal cells in repairing endometrial tissues when compared to those of naïve tissues (Figure 5-14). This method highlighted 48 genes which were also identified as

differentially expressed by the analysis performed by Edinburgh Genomics (LogFC <-2 and FDR <0.05). Taken together these analyses provide a list of genes which may be essential to endometrial tissue repair.

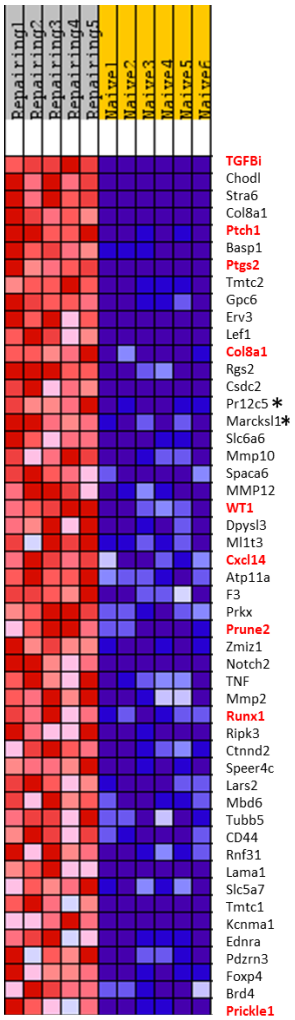

Figure 5-14. Ranked gene list generated using GSEA based on transcript abundance, as determined by CPM, in mesenchymal cells (total GFP+ cells from *Pdgfrβ-BAC-eGFP* uterus) in naïve and repairing samples. Genes, except for those identified with an *, were also found to be differentially expressed in the dataset by Edinburgh Genomics (logFC >2 and FDR <0.05). Genes highlighted in bold/red were chosen for validation studies.

5.4.4.1 Primary validation of mesenchymal cell genes associated with endometrial repair

A new set of RNA samples were generated from cells sorted from naïve and 24 hour repairing uteri to provide a validation of the sequencing dataset: qPCR was performed using the TaqMan method as described in Chapter 2: Section 2.8 using primers designed against nine of the most differentially expressed genes summarised in Table 5-7. In these experiments genes were selected for validation based on the LogFC >2, FDR <0.05, mean CPM in naïve samples >70 and mean CPM in repairing samples <100. The availability of reliable primer sequences and antibodies further vindicated the choice of target.

Table 5-7. List of highly expressed genes that were significantly upregulated by mesenchymal cells (total GFP+ cells from *Pdgfrβ-BAC-eGFP* uterus) in repairing samples when compared to naïve samples as determined by LogFC (>2) in mean counts per million (CPM).

Gene	Expanded Name	Mean CPM Naive	Mean CPM Repairing	LogFC (<-2)
Ptgs2	Prostaglandin-endoperoxide synthase 2	9.702824	598.7562	5.952372
Prune2	Prune homolog 2	64.69977	414.1897	2.671154
Cxcl14	CXC Motif chemokine ligand 14	7.475004	116.655	3.958206
TGFBi	Transforming growth factor beta-induced	1.289687	112.7243	6.421906
Runx1	Runt related transcription factor 1	28.23202	308.234	3.445607
Ptch1	Patched 1	30.71477	341.2435	3.468907
Col8a1	Collagen type VIII alpha 1	4.055594	235.9686	5.868561
Prickle1	Prickle homolog 1	16.32713	115.2596	2.812171
Wt1	Wilms tumor 1	63.55119	159.1044	1.316639

The first validation experiment assessed the amount of mRNA encoded by the selected genes using RNA extracted from GFP+ cells (GFP^{bright}+GFP^{dim}) isolated from normal adult *Pdgfrβ-BAC-eGFP* endometrial tissues ('control') and from *Pdgfrβ-BAC-eGFP* endometrial tissues at 24hrs after progesterone withdrawal ('repairing). Results confirmed that mRNAs encoded by all genes (normalised to reference gene *Actb* and displayed as arbitrary units (AU)) were significantly upregulated in the GFP+ mesenchymal cells isolated from repairing; n=5 endometrial tissue when compared to naïve samples; n=5 (Figure 5-15): *Ptgs2* (0.33±0.04 versus 0.002±0.002, p=0.0001), *Prune2* (0.97±0.04 versus 0.09±0.03, p<0.0001), *Cxcl14* (1.25±0.14 versus 0.37±0.11, p=0.0027), *Tgfβi* (4.16±0.93 versus 0.02±0.01, p=0.0043), *Runx1* (4.58±0.60 versus 0.17±0.05, p=0.0003), *Ptch1* (4.20±0.69 versus 0.37±0.22, p=0.002), *Col8a1* (5.71±0.44 versus 0.004±0.002, p<0.0001), *Prickle1* (4.53±0.67 versus 1.38±0.45, p=0.008), and *Wt1* (1.15±0.09 versus 0.63±0.096, p=0.0073). The results were therefore in agreement with the sequencing data.

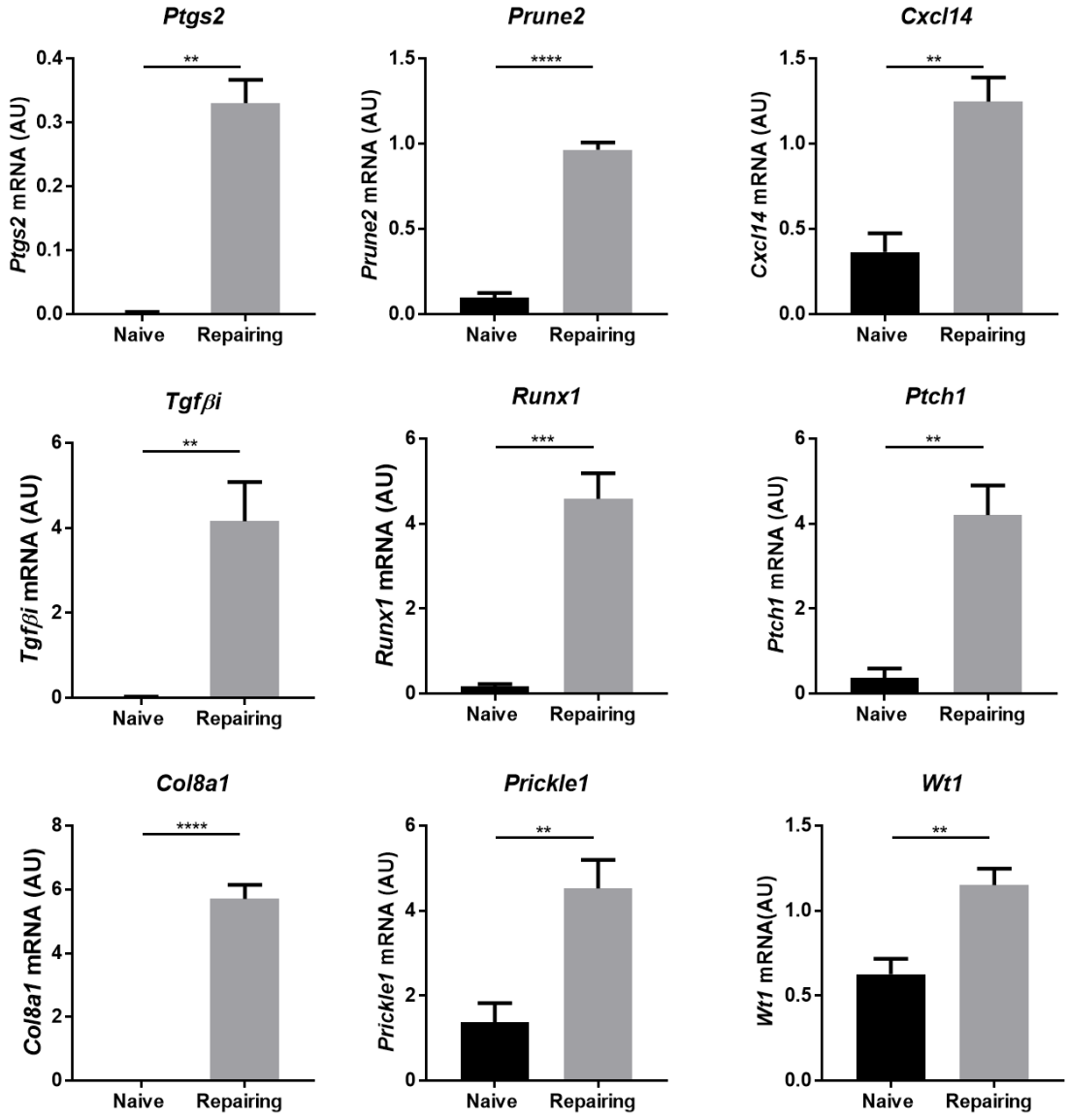

Figure 5-15. Expression of genes upregulated in GFP+ mesenchymal cells generated from *Pdgfrβ-BAC-eGFP* endometrial tissue during homeostasis (naïve) and repair (24hrs; repairing) to validate NGS results. Total GFP+ cells were isolated from naïve *Pdgfrβ-BAC-eGFP* uterine tissues and tissues from 24hrs of the Edinburgh menses mouse model (24hrs; repairing). RNA was extracted and qPCR used to analyse expression of key genes chosen to validate the RNA sequencing results, normalised to *Actb* and displayed as AU. Expression of *Ptgs2*, *Prune2*, *Cxcl14*, *TGFβi*, *Runx1*, *Ptch1*, *Col8a1*, *Prickle1* and *Wt1* were all found to be significantly upregulated in cells of repairing tissue; n=4 when compared to naive tissue; n=4. (unpaired t-test,*p<0.05, **p<0.01, ***p<0.001, ****p<0.0001).

5.4.4.2 Subset validation of mesenchymal cell genes associated with endometrial repair

To extend these findings expression of the same gene set was investigated in RNA extracted from subpopulations of GFP+ cells: GFP^{dim} cells (stromal fibroblasts) and GFP^{bright} cells (pericytes) isolated independently from both control and repairing *Pdgfrβ-BAC-eGFP* endometrial tissues. qPCR revealed that mRNA of some of the genes were significantly upregulated in GFP^{dim} cells isolated from repairing tissues when compared to naïve tissues (Figure 5-16): *Prune2* (0.71±0.08 versus 0.15±0.05, p<0.0001), *Cxcl14* (0.8±0.13 versus 0.27±0.03, p=0.0044), *Tgfβi* (1.96±0.46 versus 0.04±0.03, p=0.0036), *Runx1* (5.52±1.24 versus 0.12±0.003, p=0.0028), *Ptch1* (5.83±0.91 versus 0.58±0.25, p=0.0002), *Col8a1* (14.74±0.92 versus 0.001±0.001, p=0.0009) and *Prickle1* (6.16±0.86 versus 1.17±0.38, p=0.0001), while other genes were not significantly upregulated: *Ptgs2* (0.11±0.03 versus 0.004±0.001, p=0.1592) and *Wt1* (1.39±0.47 versus 0.63±0.18, p=0.1718)

Notably some genes were also significantly upregulated in the GFP^{bright} pericytes cells in repairing tissue when compared to naïve tissue: *Ptgs2* (0.3±0.06 versus 0.05±0.01, p=0.0024), *Tgfβi* (1.9±0.29 versus 0.02±0.005, p=0.0041), *Runx1* (6.21±0.79 versus 2.16±0.15, p=0.0166) and *Col8a1* (20.37±3.33 versus 0.03±0.01, p<0.0001), while other genes were not upregulated: *Prune2* (0.19±0.04 versus 0.04±0.001, p=0.1664), *Cxcl14* (0.29±0.05 versus 0.24±0.08, p=0.9173), *Ptch1* (2.62±0.34 versus 0.65±0.08, p=0.0741), *Prickle1* (1.65±0.18 versus 1.23±0.06, p=0.8389), and *Wt1* (0.17±0.04 versus 0.05±0.01, p=0.9437) (Figure 5-16). These results hihglight different responses in the two cell populations that merited further study.

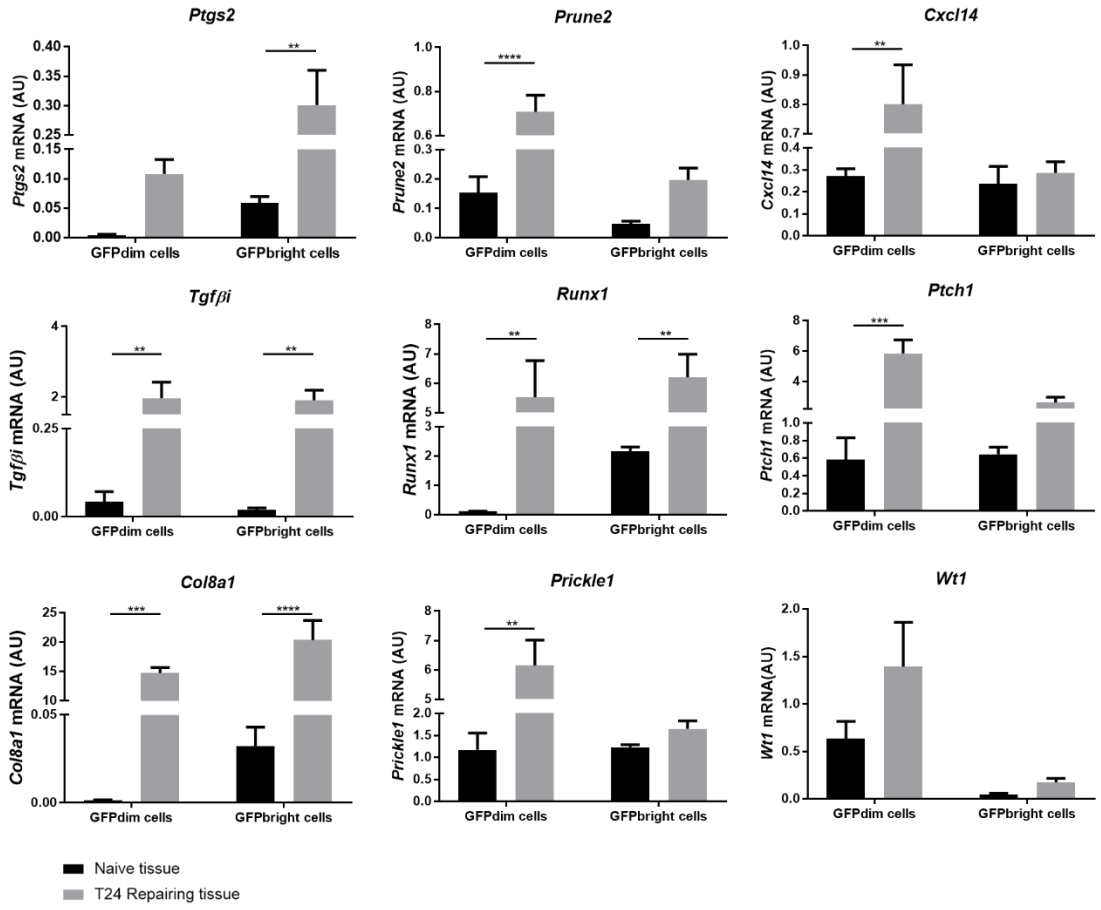

Figure 5-16. Expression of genes upregulated in in isolated subpopulations of mesenchymal cells (GFP^{dim} stromal fibroblasts and GFP^{bright} pericytes) generated from *Pdgfrβ-BAC-eGFP* endometrial tissue during homeostasis (naïve) and repair (24hrs; repairing). GFP^{dim} and GFP^{bright} cells were isolated from naïve *Pdgfrβ-BAC-eGFP* uterine tissues and tissues from 24hrs of the Edinburgh menses mouse model (repairing). RNA was extracted and qPCR used to analyse expression of key genes, normalised to *Actb* and displayed as AU. Expression of *Prune2*, *Cxcl14*, *TGFβi*, *Runx1*, *Ptch1*, *Col8a1*, *Prickle1* and were all found to be significantly upregulated in GFP^{dim} cells of repairing tissue; n=4 when compared to naive tissue; n=4. Expression of *Ptgs2*, *Tgfβi*, *Runx1* and *Col8a1* were significantly upregulated in GFPbright cells of repairing tissue; n=4 when compared to naïve tissue; n=4 (unpaired t-test,*p<0.05, **p<0.01, ***p<0.001, ****p<0.0001).

5.4.5 Profiling mesenchymal cells from *Pdgfrβ-BAC-eGFP* endometrial tissue from controls and during endometrial repair (24hours) by single cell sequencing

Next generation sequencing of RNA extracted from pooled GFP+ endometrial cells identified transcriptomic changes in the total mesenchymal cell population during endometrial repair. To extend these findings, with the specific aim of determining changes in gene signatures of specific mesenchymal subpopulations, single cell sequencing was performed on cells from *Pdgfrβ-BAC-eGFP* uterine tissues.

5.4.5.1 Sample validation

Total GFP+ cells (GFP^{dim} stromal fibroblasts plus GFP^{bright} pericytes) were isolated using FACS from normal adult cycling *Pdgfrβ-BAC-eGFP* (naïve) and from *Pdgfrβ-BAC-eGFP* uterine tissues collected 24hrs after progesterone withdrawal (repairing): cDNA libraries were prepared for single cell sequencing as outlined in Chapter 2; Section 2.10. Each sample was a pool of uterine tissues from four mice to control for variation. For presentation of results the samples are labelled as 'naive and 'repairing'.

Prior to sending the samples, QC was carried out using the LabChip GX Touch instrument (Chapter 2; Section 2.6.4) to assess both the quantity and quality of cDNA. As outlined in Figure 5-17, the naive sample had a concentration of 30.95 ng/µl while the repairing sample had a concentration of 45.56ng/µl, both of which exceeded the minimum QC requirements set by Edinburgh Genomics (https://genomics.ed.ac.uk/).

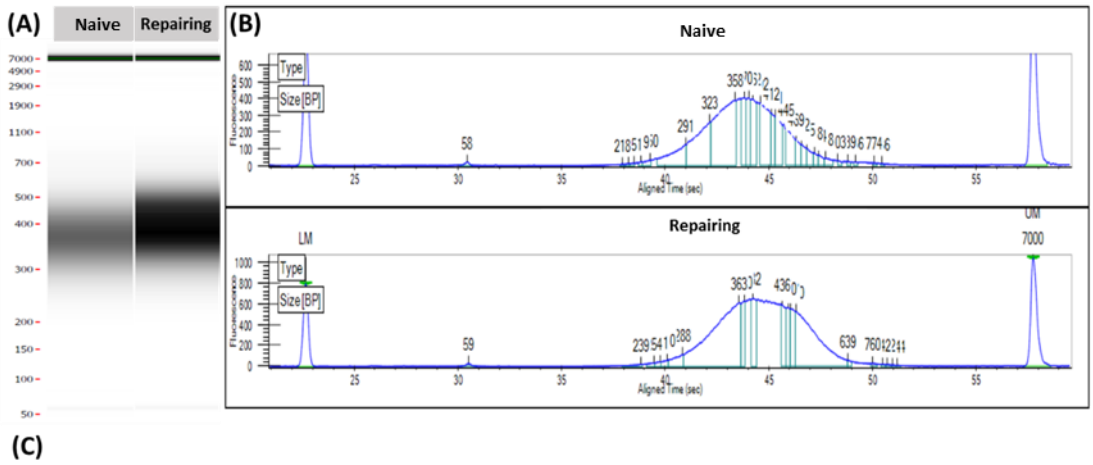

Sample	Concentration (ng/ul)
Naïve	30.95
Repairing	45.56

Figure 5-17. LabChip GX Touch analysis of cDNA quantity and quality for samples generated for single cell sequencing by Edinburgh Genomics. (A) LabChip GX Touch read out gel results for the naive and repairing samples. **(B)** Electrogram results for both naive and repairing samples. **(C)** Concentration of cDNA in both naïve and repairing samples.

5.4.5.2 Bioinformatic data handling

Following generation of the sequence data the initial bioinformatic analysis (as outlined in Chapter 2; Section 2.10.11) was carried out by Frances Turner at the Edinburgh Genomics facility (https://genomics.ed.ac.uk/). Thereafter a secondary analysis was carried out by Dr Richard Taylor affiliated with Professor Neil Henderson's group. A summary of the basic statistics generated by Frances Turner using the Cellranger software can be found in Table 5-8. All values were above threshold for what is considered acceptable cut-off.

Table 5-8. Basic statistics of single cell sequencing data generated for total GFP+ cells isolated from naïve and repairing Pdgfrβ-BAC-eGFP uterine tissue using Cellranger (by Frances Turner). Number of reads, estimated cell number, total genes detected, mean reads per cell, median genes per cell and sequencing saturation values all exceeded threshold requirements, indicating the success of the sequencing.

Sample	No. Reads	Est. No. Cells	Total genes detected	Mean reads per cell	Median genes per cell	Sequencing saturation
Naïve	453,334,959	5,363	18,422	84,530	1,986	84.70%
Repairing	481,132,039	4,515	17,989	106,563	2,773	81.90%

5.4.5.3 t-distributed stochastic neighbour embedding (t-SNE) analysis of control uterine tissue

Loupe files for the naïve and repairing single cell datasets were provided by Frances Turner and Richard Taylor. Subsequent analysis outlined in this Chapter was performed by the author of this thesis. The Cell Loupe Browser software provided by Cellranger (10x Genomics; https://www.10xgenomics.com/) was used to analyse the single cell data sets. The first round of analysis focussed on the results from the naïve uterine tissue to assess heterogeneity within the mesenchymal cell population during homeostasis to extend and complement results detailed in Chapter 4.

The t-SNE analysis is a technique that visualises high-dimensional data by assigning each data point (single cells) a location in a two dimensional space based on similarity to other data points. The Cell Loupe Browser software uses this technique to reveal structures in the data based on similarities and differences in the transcriptomic profiles of each cell. This analysis revealed that the naïve mesenchymal cell population (all GFP+ cells) was composed of five individual clusters based on tSNE-1 and tSNE-2, revealing a high degree of heterogeneity within the population which was a novel finding compared with our previous datasets that had identified 2 populations based only on GFP intensity using IHC, FC and qPCR techniques (Figure 5-18).

As the mesenchymal cell population was isolated from *Pdgfrβ-BAC-eGFP* tissues based on GFP expression (reporter for *Pdgfrβ* promoter activity) it was predicted that all cells should express Pdgfrβ. To confirm this Pdgfrβ expression was mapped onto the t-SNE plot leading to the identification of two populations: cells that had low

Pdgfrβ expression were located in clusters 1 and 4, cells that had high Pdgfrβ expression located in clusters 2 and 3 and cells that had minimal Pdgfrβ expression located in cluster 5 (Figure 5-19). From this analysis it was concluded that Clusters 1 and 4 were the equivalent of the GFP^{dim} stromal cells while Cluster 2 and 3 represented GFP^{bright} cells previously identified as perivascular pericytes. The use of single cell analysis identified heterogeneity within each of these subpopulations that had not previously been detected and further analysis has therefore focused on profiling the five clusters to elucidate their phenotype.

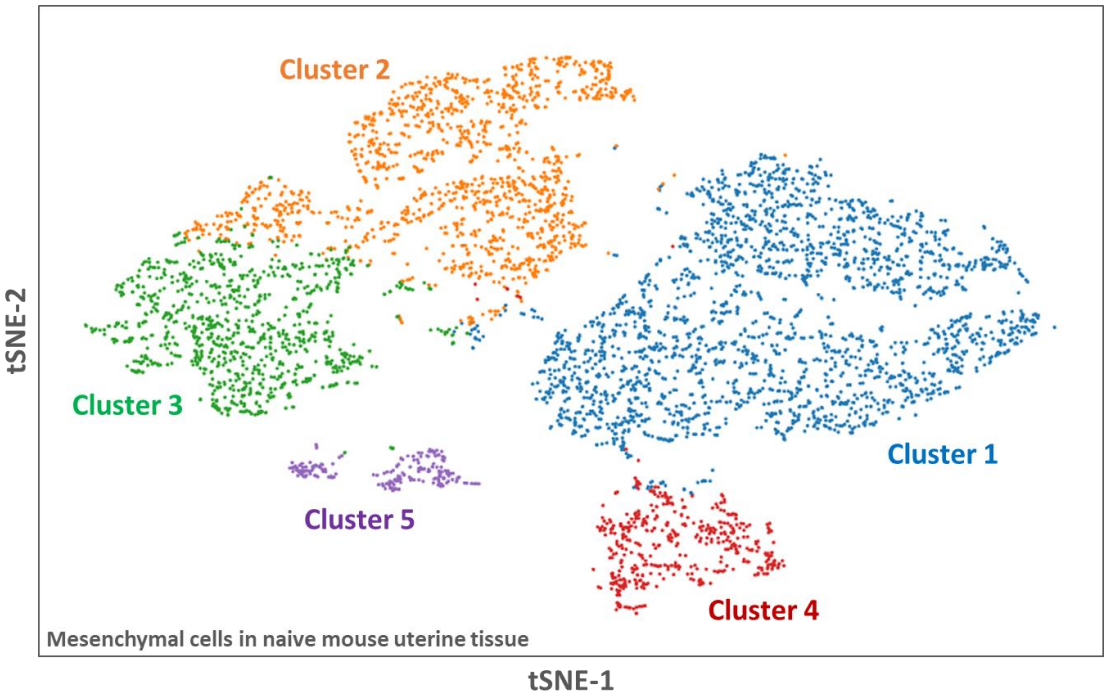

Figure 5-18. Visualisation of the single cell dataset naive uterine mesenchymal cells. A t-SNE plot where each dot represents a single cell. Cells cluster together based on the similarity in their transcriptomic profile: note this software identified 5 discrete cell clusters in the naïve endometrial mesenchymal cell population.

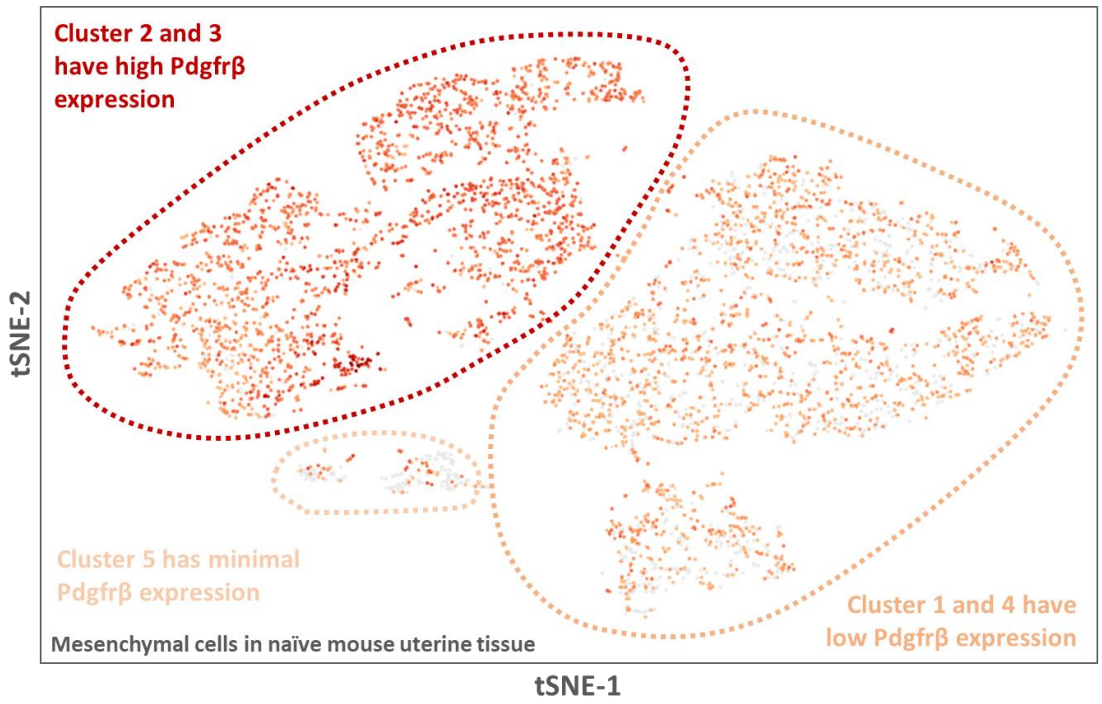

Figure 5-19. Expression of Pdgfrβ in naive uterine mesenchymal cells. Cluster 1 and 4 had low expression of Pdgfrβ while cluster 2 and 3 had high expression of Pdgfrβ and cluster 5 had minimal expression of Pdgfrβ: based on this single gene cluster 1+4 appeared to be representative of GFP^{dim} fibroblasts and 2+3 were GFP^{bright} putative pericytes.

5.4.5.4 Differential gene expression analysis of control uterine tissue

To more thoroughly investigate transcriptomic differences between each cell cluster, a heat map summarising the differential gene expression was generated to identify genes that were more highly expressed in one cell cluster when compared to the others. The heat map in Figure 5-20 displays transcriptomic differences between each cell cluster confirming that there was a degree of similarity between clusters 1 and 4 and between clusters 2 and 3 but a very distinct profile in cluster 5. A list of the top 100 genes differentially expressed by each cell cluster is outlined in Appendix 5-3.

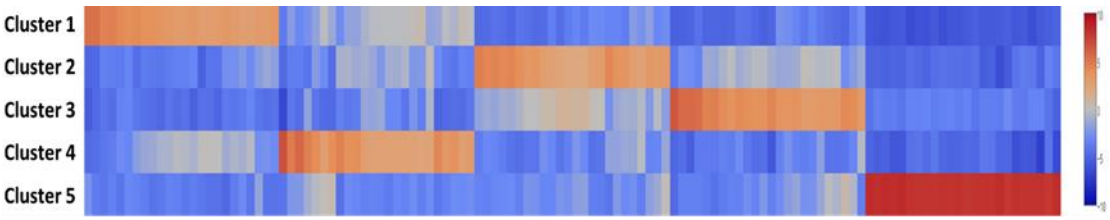

Figure 5-20. Heat map of differentially expressed genes that distinguish five mesenchymal cell clusters in naïve uterine tissue as determined by single cell sequencing. Clusters 1 and 4 show a degree of similarity as do Clusters 2 and 3. Cluster 5 has a very distinct gene signature that does not show a degree of similarity to other cell clusters

To expand the understanding of the differences between clusters, several of the most differentially expressed (DE) genes that distinguished each cluster (identified by bold/highlighting in Appendix 5-3) were mapped to the t-SNE plot to assess their distribution patterns and to start to identify the distinct phenotypes of each cell type, outlined in Figure 5-21.

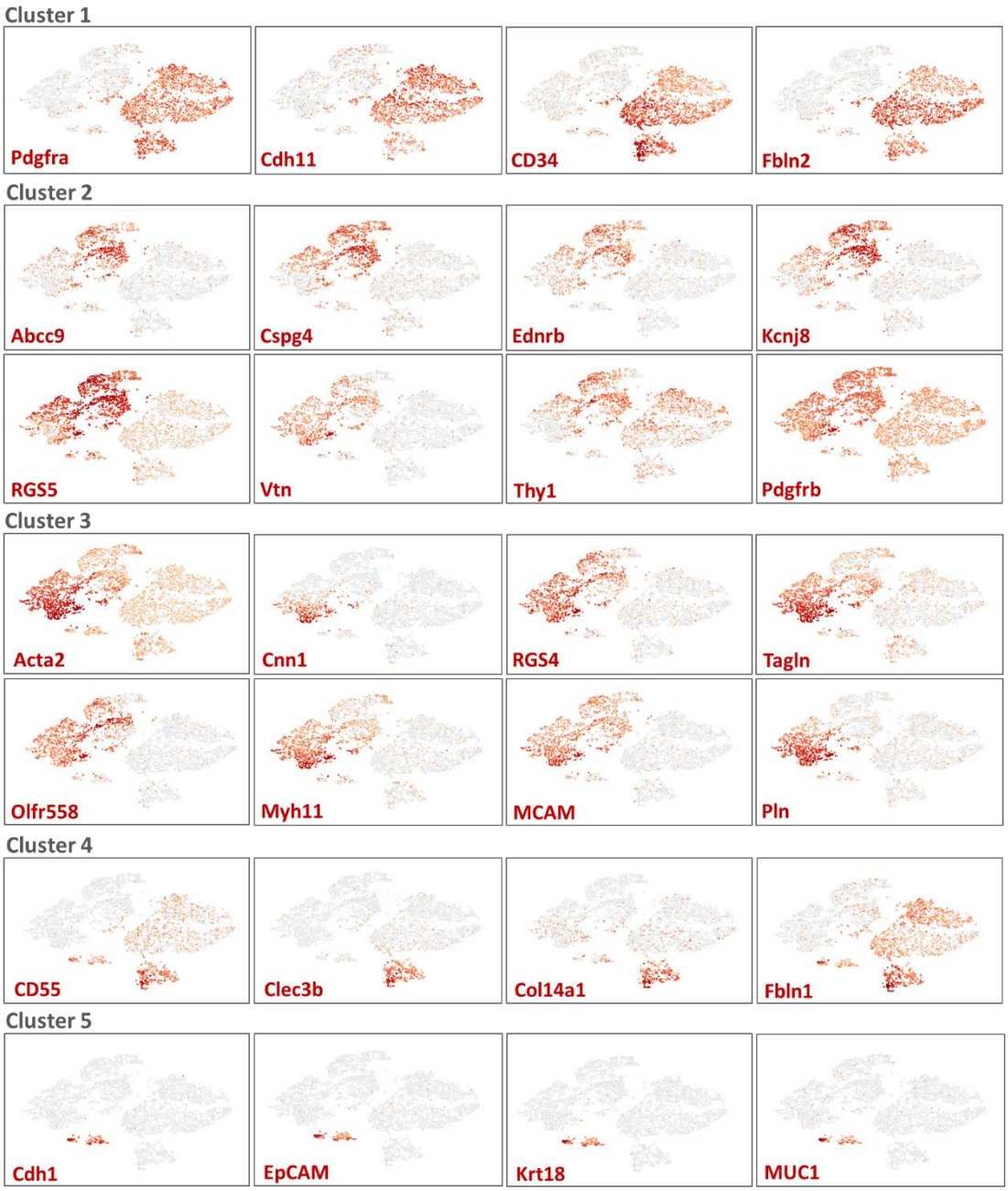

Figure 5-21. tSNE plots exhibiting the distribution of differentially expressed genes that distinguish each cell cluster in the single cell sequencing dataset of naïve endometrial mesenchyme (5 clusters as outlined in Figure 5-18). Gene expression is displayed where increasing intensity of colour (red) correlates to increasing abundance of gene transcripts. Cluster 1 exclusively expressed *Pdgfrα*, *Cdh11*, *Cd34* and *Fbln2*. Cluster 2 expressed *Abcc98*, *Cspg4*, *Endrb*, *Kcnj8*, *Rgs5*, *Vtn*, *Thy1* and *Pdgfrβ* and cluster 3 expressed *Acta2*, *Cnn1*, *Rgs5*, *Tagln*, *Olfr558*, *Myh11*, *Mcam* and *Pln* although there was some overlap between these cell clusters with expression of *Rgs5*, *Vtn*, *Pdgfrβ*, *Rgs4*, *Olfr588* and *Mcam* detected in both cluster 2 and 3. Cluster 5 exclusively expressed *Cdh1*, *EpCAM*, *Krt18* and *Muc1*.

Differential gene expression analysis revealed that Cluster 1 had 439 genes that were significantly up-regulated when compared to other clusters. These up-regulated genes included *Wt1, Cdh11, Fbln2, Pdgfrα, Fn1*, *Igf1* and *CD34*, in line with a stromal fibroblast phenotype. Cluster 4 had 423 significantly upregulated genes some which such as *CD34, Pdgfrα,* and *Igf1* were shared with Cluster 1 (fibroblast-like) whilst others included *CD55, Fbln1, Col14a1, Clec3b,* and *Cald1* (Figure 5-21). Many of the genes that appeared to characterised Cluster 4 encoded collagens suggesting that these cells could be considered as a subpopulations of fibroblast-like cells clustering separately due to a specialised function such as the synthesis of matrix proteins.

Cluster 2 had 577 genes that were significantly upregulated including *Kcnj8, Abcc9, Vtn, Ednrb, Rgs5, Thy1, Olfr588, Pdgfrβ, Cspg4, Rgs3, Rgs4* and *Des.* Cluster 3 had 539 significantly upregulated genes including *Pln, Cnn1, Tagln, Acta2, Myh11, Kitl, Pdgfa, Rgs4, Mcam, Des, Olfr588* and *lmna* (Figure 5-21). Notably Clusters 2 and 3 appeared to express a number of the same genes which including several previously use to identify and characterise perivascular pericytes in endometrial tissue – such as *Mcam, Rgs5* and *Olfr588* (list of top 100 DE genes per cluster in Appendix 5-3). However Cluster 3 also uniquely expressed genes associated with vascular smooth muscle cells.

Finally, Cluster 5 which appeared to have relatively few cells compared with the other clusters had 438 genes that were significantly upregulated including *EpCAM, Krt8, Cdh1, Krt19, Krt18, Kft7* and *MUC1* (Figure 5-21) which were epithelial associated genes suggesting that Cluster 5 is made of epithelial cells.

These results have highlighted complex heterogeneity that has not previously been defined in endometrial stromal cell populations that are summarised in Figure 5-22: Cluster 1 and 4 have been identified as the stromal fibroblast population, composed of subpopulations with discrete functions; Cluster 2 and Cluster 3 have been identified as perivascular pericytes and vascular smooth muscle cells respectively however these populations may represent a spectrum of cells in relation to functions; and Cluster 5 has been identified as a small amount of epithelial cells which is believed to be due to contamination as only GFP+ cells were isolated (usually EpCAM negative) (Figure 5-22).

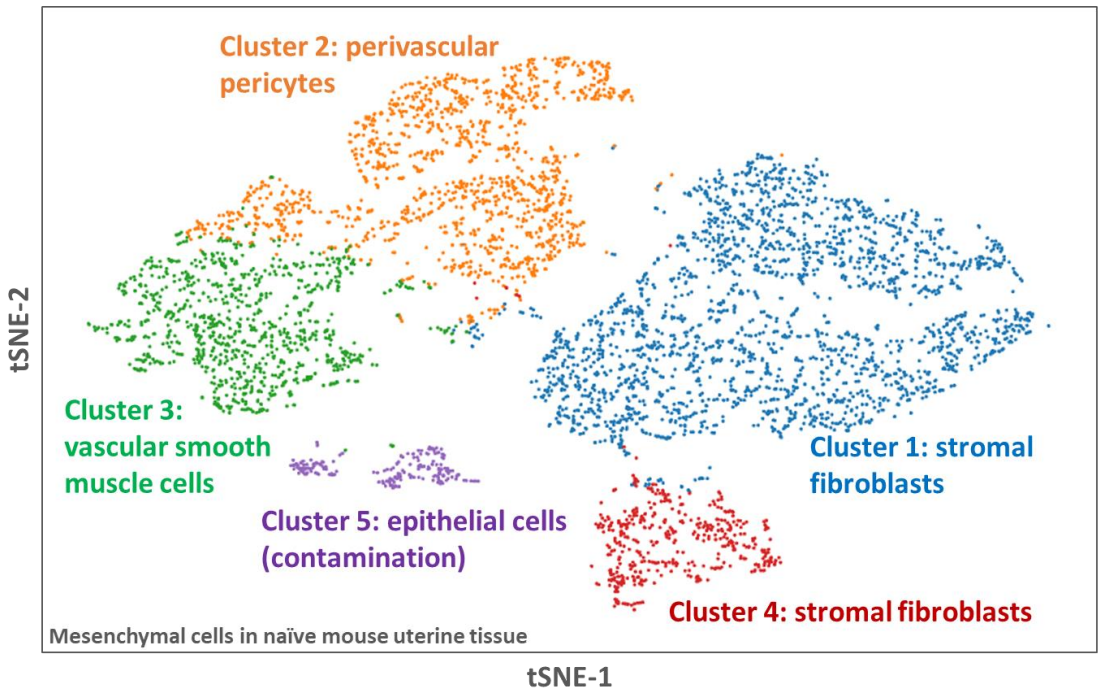

Figure 5-22. Hypothesised phenotypes of each cell cluster identified in the mesenchyme of the naïve mouse endometrium based on differentially expressed genes. Cluster 1 and 4: stromal fibroblasts, Cluster 2: perivascular pericytes, Cluster 3: vascular smooth muscle cells, Cluster 5: epithelial cells (contamination).

5.4.5.5 Comparison between mesenchymal cell populations in naïve and repairing uterine tissue as determined by t-SNE analysis

Having identified complex heterogeneity within the mesenchymal cell population of naive endometrial tissues, the contribution of distinct cell types to the endometrial repair processes was assessed by creating an aggregate file of the single cell sequencing datasets from the naïve and repairing uterine tissues. The tSNE plot generated in Figure 5-23 is colour coded by library ID to identify cells from control (orange) versus repairing (blue) uterine tissues. Two discrete clusters were seen, attributed to global gene expression changes in mesenchymal cells in response to endometrial repair (Figure 5-23, heat map). The t-SNE plot in Figure 5-24 displays the results of cluster analysis on the aggregate file, revealing a striking amount of heterogeneity within the total mesenchymal populations. Nine distinct clusters were identified suggesting that distinct genomic profiles exist in the mesenchymal cells during repair. Combined tSNE analysis showed that Cluster 1, 3, 4 and 8 were cells of control mesenchyme while Cluster 2, 5, 6, 7 and 9 were cells of repairing mesenchyme.

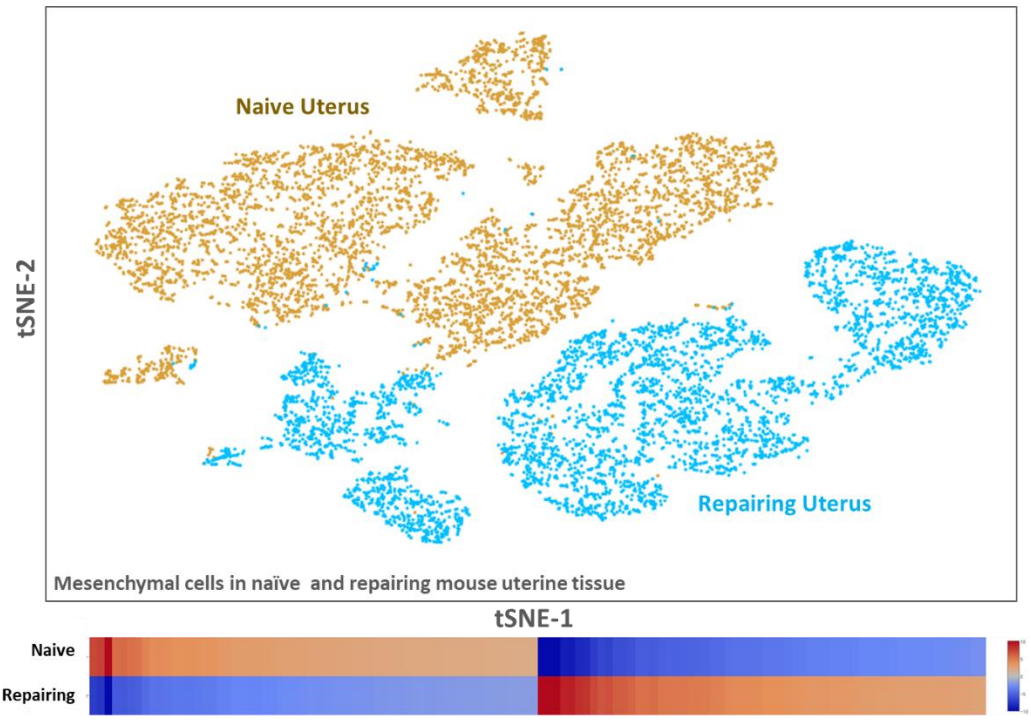

Figure 5-23. Cluster analysis based on Library ID separating mesenchymal cells from naive (orange) and repairing (blue) uterine tissue. Global gene expression changes separate the two experimental datasets distinctly. The heatmap displays striking transcriptomic differences between mesenchymal cells from naïve and repairing endometrium.

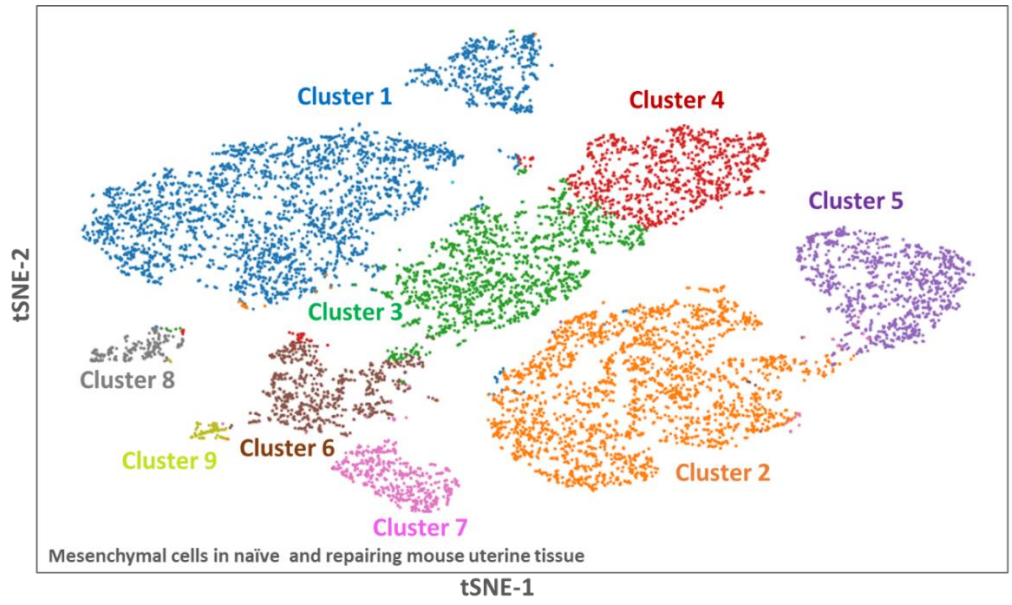

Figure 5-24. Cluster analysis based on DE gene expression profiles of mesenchymal cells in the aggregate file containing both naïve and repairing single cell datasets. A t-SNE plot where each dot represents a single cell and cells cluster together based on the similarity in their transcriptomic profile. Cluster analysis reveals nine distinct cell clusters present in the aggregate file of naïve and repairing endometrial tissues.

Further examining the expression of Pdgfrβ in the aggregate tSNE plot, three prominent populations were once again identified: cells that had high expression of Pdgfrβ (Cluster 3, 4, 6, 7 and 9), cells that had low expression of Pdgfrβ (Cluster 1, 2 and 5), and cells with minimal Pdgfrβ expression (Cluster 8) although it could be argued that Cluster 5 contained some cells with an intermediate expression level (Figure 5-25). Combining the information from Figure 5-23, 5-24 and 5-25 it can be concluded that Cluster 1 represents GFP^{dim} cells and Clusters 3 and 4 represent GFP^{bright} cells from naive uterine tissues, while Clusters 2 and 5 represent GFP^{dim} cells and Clusters 6 and 7 represent GFP^{bright} cells from repairing uterine tissues. Cluster 8 of the naïve data set represents epithelial cells, as previously determined, and cluster 9 of the repairing dataset is unknown.

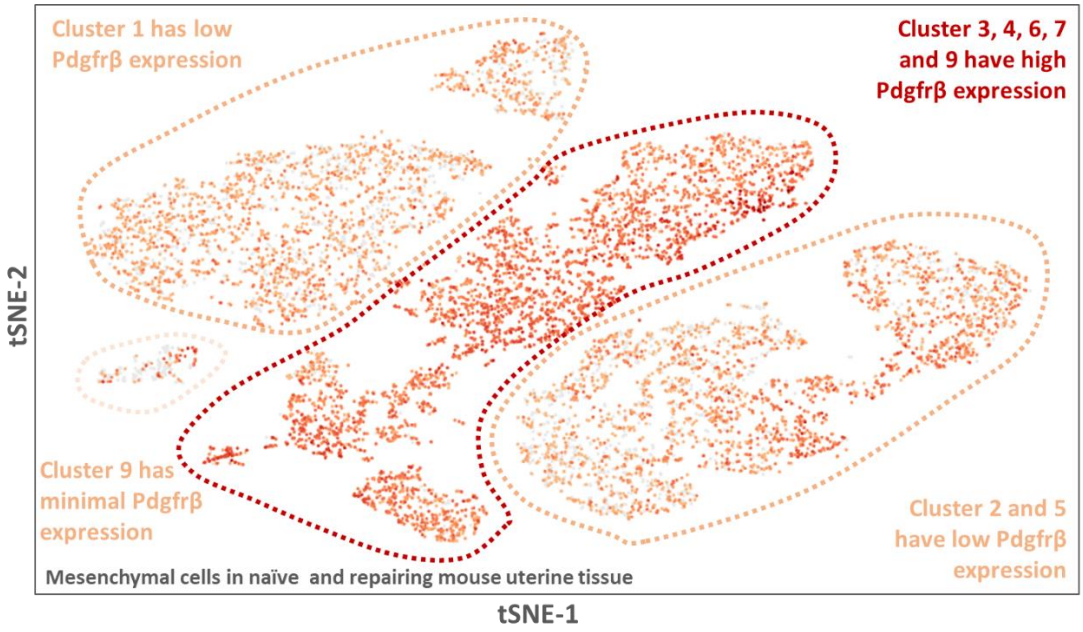

Figure 5-25. Expression of Pdgfrβ mapped onto the t-SNE plot of mesenchymal cells fron naïve and repairing uterine tissue. Pdgfrβ expression is displayed where increasing intensity of colour (red) correlates to increasing abundance of gene transcripts. Cluster 1, 2 and 5 have low expression of Pdgfrβ while Cluster 3, 4, 6, 7 and 9 have high expression of Pdgfrβ. Cluster 8 has minimal expression of Pdgfrβ.

5.4.5.6. Differential gene expression analysis of control and repairing uterine tissue

Differential gene expression analysis was carried out to characterise each cell cluster identified in the tSNE analysis. The heat map in Figure 5-26 displays the most significant transcriptomic differences between each cell cluster when compared to the other clusters. Clusters 1, 2, 5 and 8 have very distinct transcriptomic signatures with their most significantly upregulated genes not expressed in other clusters. In contrast Clusters 3 and 4 have similar expression patterns as do Clusters 6 and 7 which even show some similarities to Clusters 3 and 4. This suggests that there may be a degree of similarity between these cell types. A list of the top 100 genes differentially expressed by each cell cluster are summarised in Appendix 5-5, with previously identified characteristic genes highlighted in bold print.

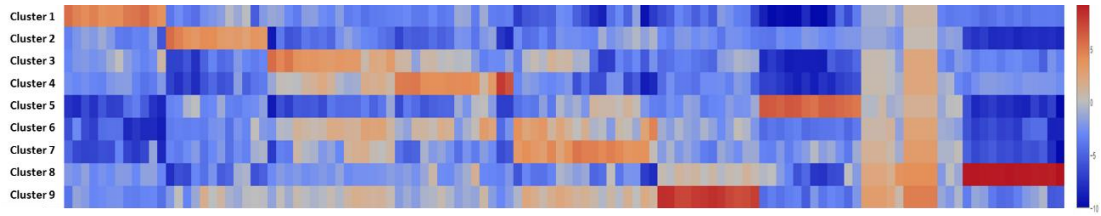

Figure 5-26. Heat map of differentially expressed genes that distinguish the nine cell clusters in the aggregate file containing both naïve and repairing mesenchyme single cell datasets. Striking transcriptomic differences between cell clusters can be detected. Clusters 1, 2, 5 and 8 have very distinct transcriptomic profiles. Clusters 3 and 4 show a high degree of similarity. Clusters 6 and 7 show a high degree of similarity and also share expression of genes in Cluster 3 and 4. Cluster 9 expresses genes associated with all other cell clusters.

To expand analysis beyond cluster analysis, genes previously identified as specific to the five cell clusters in naïve tissue (Section 5.4.5.4) were mapped to the extended merged 9 cluster dataset (Figure 5-27). The stromal fibroblast markers *Cd34*, *Cdh11*, *Fbln2* and *Pdgfrα* mapped to Clusters 1, 2 and 5. Similarly, the expression of *Cd55*, *Clec3b*, *Col14a1* and *Fbln1* prominent in a subset of stromal fibroblasts mapped to a subset of both Clusters 1 and 2. Notably *Cd55* was also expressed by Cluster 5 and *Fbln1* was noticeably upregulated in Cluster 2 when compared with Cluster 1. These results were consistent with the identification of clusters 1, 2 and 5 having low *Pdgfrβ*.

In comparison clusters 3, 4, 6, 7 and 9 had high *Pdgfrβ* and were considered to be putative pericytes. Analysis showed genes identified in control pericytes including *Abcc9*, *Ednrb*, *Kcnj8*, *Thy1* and *Vtn* were expressed predominantly in Clusters 3, 6 and 7 while others including *Cspg4* and *Rgs5* were expressed in Clusters 3, 4, 6 and 7. Notably the expression of vascular smooth muscle cell markers Mcam, *Olfr558* and *Rgs4* mapped to Clusters 3, 4, 6 and 7 while *Acta2*, *Cnn1*, *Mhy1*, *Pln* and *Tagln* were predominantly expressed in Clusters 4 and 6. *Cspg4*, *Thy1*, *Mcam* and *Tagln* were also expressed by Cluster 5 and there was an apparent increase in expression of several genes in Cluster 2 including *Kcnj8*, *Thy1*, *Acta2* and *Tagln*.

Cluster 9 expressed cell associated with progression of the cell cyle such as *Mki67*, *Cdk1* and *Pcna* but also showed similarities to each of the other cell clusters. Therefore this cluster was identified as a mixed population of cells undergoing proliferation. Finally looking at epithelial cell gene expression is was seen that Cluster 8 expressed *Cdh1*, *Epcam*, *Krt8* and Krt18 consistent with a small amount of contamination previously identified in naïve samples (Figure 5-21) and the distinct profile apparent in the heat map.

One of the most interesting Clusters was number 5 which was found to express genes that were otherwise used to identify a range of cells types such as *Cdh11*, *Fbln2*, *Pdgfrα* and *Cd55* used to identify stromal fibroblasts, *Cspg4*, *Pdgfrβ* and *Thy1* used to identify perivascular pericytes and *Acta2* and *Tagln* used to identify vascular smooth muscle cells. Notably Cluster 5 also expressed genes attributable to epithelial cells including *Epcam*, *Krt8* and *Krt18* (Figure 5-27).

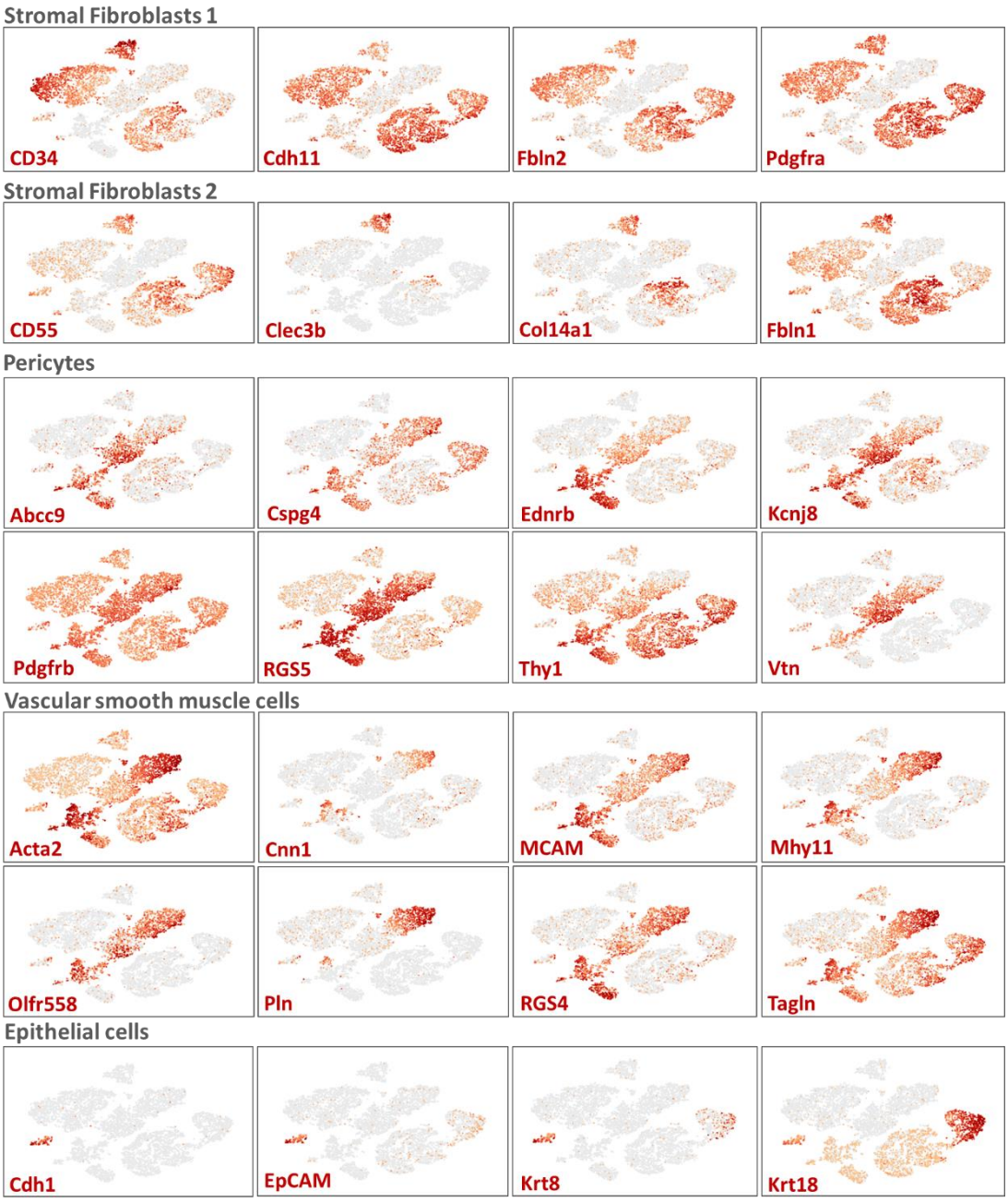

Figure 5-27. tSNE plots exhibiting the distribution of genes used to identify different cell types present in the naïve endometrial mesenchyme (Figure 5-21) amongst cell clusters in the repairing endometrial mesenchyme. To identify the phenotype of the 9 cell clusters in the aggregate single cell dataset (Figure5-24), genes previously found to identify distinct clusters in the naïve uterus were mapped to the t-SNE plot. Genes associated with stromal fibroblasts include *Cd34, Cdh11, Fbln2, Pdgfrα, CD55, Clec3b, Col14a1* and *Fbln1*. Genes associated with pericytes include *Abcc9*, *Cspg4*, *Ednrb*, *Kcnj8, Pdgfrβ, Rgs5, Thy1* and *Vtn*. Genes associated with vascular smooth muscle cells include *Acta2*, *Cnn1*, *Mcam*, *Myh11*, *Olfr558*, *Pln*, *Rgs4* and *Tagln*. Genes associated with epithelial cells include *Cdh1*, *Epcam*, *Krt8* and *Krt18*.

The assessment of gene expression profiles associated with specific cell types in the control uterine tissue clearly identified four clusters of mesenchymal cells (plus minor contamination by epithelial cells) and in the combined analysis these were once more present (although their position in the map produced by the software was slightly altered the stromal fibroblasts appeared as a single cluster) – these are numbered as clusters 1, 3, 4 and 8 in Figure 5-28. Strikingly the gene expression profile of the repairing tissue was sufficiently distinct from the control sample to generate additional clusters – 2, 6, 7 and 5 with cluster 5 having a phenotype that appears unique to the repairing tissue. This provides a platform for the investigation of how each cell population specifically contributes to endometrial repair processes.

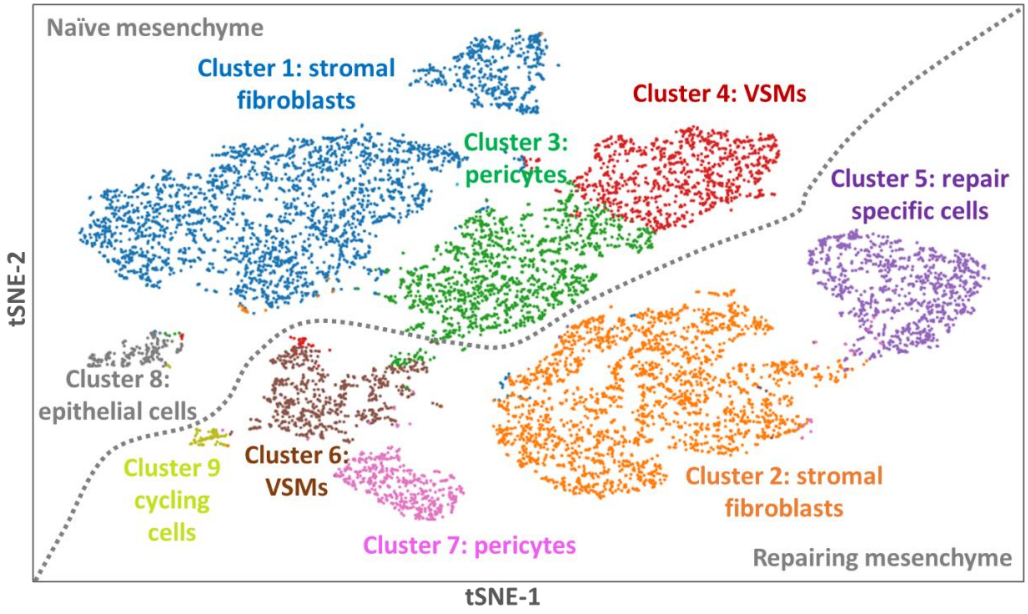

Cell phenotype	Naïve endometrium	Repairing endometrium
Stromal fibroblasts	Cluster 1	Cluster 2
Pericytes	Cluster 3	Cluster 7
Vascular smooth muscle cells	Cluster 4	Cluster 6
Epithelial cells	Cluster 8	N/A
Unknown cells	N/A	Cluster 5

Figure 5-28. Hypothesised phenotypes of each cell cluster identified in the aggregate file containing both naïve and repairing single cell datatsets of endometrial mesenchyme. Identification of cell clusters was determined by the relative expression of DE genes that distinguished cell clusters in the naïve mesenchyme, outlined in the table. Clusters 1 and 2: stromal fibroblasts, Clusters 3 and 7: perivascular pericytes, Clusters 4 and 6: vascular smooth muscle cells, Cluster 8: epithelial cells, Cluster 5: repair-specific cluster of unknown phenotype. Cluster 9: proliferating cells of mixed phenotypes.

5.4.5.7. Investigation of differential gene expression in mesenchymal cell populations during endometrial repair

To augment the initial cluster analysis a comparison was made between expression of genes in the putative stromal fibroblasts, vascular smooth muscle cells and pericytes in the repairing samples and the same cell type in the control samples. For example genes that are upregulate in Cluster 2 when compared to Cluster 1 represent those higher in stromal fibroblasts during endometrial repair. Results for the top 100 genes based on fold change are summarised in (Appendix 5-5).

Gene ontology analysis was carried out using the online Gene Ontology Consortium platform (http://www.geneontology.org/) to investigate processes associated with the top 100 upregulated genes in each cell type during endometrial repair, outlined in Table 5-9. Processes enriched by genes upregulated in stroma cells were associated with ECM production, Wnt signalling and epithelial cell function. Processes enriched by genes upregulated in vascular smooth muscle cells were associated with smooth muscle cell function, regulation of fibroblasts, blood vessel function and the inflammatory response. Processes enriched by genes upregulated in pericytes were associated with ECM production, blood vessel function, regulation of the inflammatory response and mesenchymal cell differentiation. This preliminary analysis suggest some of the processes to which the different cell types might be contributing during the active phase of endometrial repair.

Table 5-9. Gene Ontology associated with the top 100 upregulated genes in mesenchymal cell types during endometrial repair

Stromal Fibroblasts		
Gene Ontology Term	**Fold Enrichment**	**Associated Genes**
Regulation of cGMP-mediated signalling	5.33	Thbs1, Pde10a, Xbp1, Sod2, Hspb1, Pde10a, Mmp3, Sfrp1, Serpine2, Sfrp4, Gsto1, Socs3
Regulation of neutrophil mediated killing	4.06	Cxcl1, Cxcl5, Ccl2, Spp1
Connective tissue replacement involved in inflammatory response	7.97	Timp1, F2r, Cyr61, Sod2, Tpm1, Serpine2, Pdpn, Ccl2, Fbln1, Ighf1,
Regulation of endothelial cell chemotaxis	4.60	Thbs1, Lgn, Hspb1, Rhob, Igf1, Pfn2, Pfn1
Collagen catabolic process	4.72	Mmp10, Mmp13, Mmp3, Mmp14, Mmmp2, Adamts2
TGFβ signalling pathway	5.06	Pdcd5, Col4a1, Fos, Fermt2, Col1a2, Tgfbr2, Jun, Cilp, Zfp36l1, Col3a1, Ccl2, Actr3
VEGFr signalling pathway	4.47	Xbp1, Hsbp1, Ccl2, Pdcd6, Nrp1, Sulf1
Non-canonical Wnt signalling pathway	3.80	Fzd1, Frzb, Sfrp1, Sfrp4, Smo, Ptch1, Rac1, Sfrp2
Regulation of epithelial cell proliferation	3.36	Xbp1, Cepbp, Igfbp4, Col8a1, Fst, Prdx1, Tgfbi, Ptges3
Epithelial tube morphogenesis	4.97	Rhob, Igf1, Tnc, Fzd1, Aldh1a2, Ednra, Sfrp1, Cfl1, Mgp, Pfn1
Vascular Smooth Muscle Cells		
Gene Ontology Term	**Fold Enrichment**	**Associated Genes**
Muscle cell cellular homeostasis	6.52	Hif1a, Lamp2, Cfl2, Il6, Aldoa
Regulation of focal adhesion assembly	5.78	Thy1, Nrp1, Rac1, s100a10, Cfl1, Mmp14, Pten
Angiogenesis	5.36	Trp53, Sod2, Mif, App, Calr, Scp2, Romo1, Picalm, Rwdd1, Serp1, Cisd2, Pebp1
Cellular response to glucocorticoid stimulus	5.34	Eif4ebp1, Hnrnpu, Ssr4, mt-Nd3, Anxa1, Ssr1
Regulation of fibroblast proliferation	4.45	Cdk4, Trp53, Esr1, Anxa2, Sod2, Bax, Mif, pdgfa, Emd, Fth1, Fn1, ndufs4
Regulation of smooth muscle cell migration	4.17	Postn, Mif, Il6st, Igfbp5, Adamts1, Arpc2, Tmsb4x
Regulation of leucocyte migration	4.12	Rhoa, Trp53, Thy1, App, Calr, C1qbp, Selk, Rarres2, Rac1, Mmp14, Ednra, Ccl2
Regulation of cell shape	3.51	Rhoa, Fermt2, myl12a, Wdr1, Ccl1, Rhoc, Cdc42, Anxa1, Il6, Fn1, Cfl1, Rhoj, Aldoa, Msn, Ccl2
Cell matrix adhesion	3.05	Cd63, Rhoa, thy1, Fermt2, Actn1, Ctnnb1, Fn1, Itgb1, Nid1, Col3a1

Perivascular Pericytes		
Gene Ontology Term	**Fold Enrichment**	**Associated Genes**
Negative regulation of plasminogen activation	7.63	Thbs1, Serpine1, MMP14, Serpine2, Ctla2a, Myh9
Wound healing involved in inflammatory response	6.54	Timp1, Hif1a, Hmox1, Sdc1, Mif, Thbs1, Cebpb, Itgav, Ccl11, Cxcl1
Regulation of collagen biosynthetic process	6.07	Errfi1, Got1, Rap1a, Il6, Serpine1, Prdx5, Vim, Itgb1, Ccl2
Regulation of focal adhesion assembly	5.98	Thy1, Lims1, Rac1, Iqgap1, Cfl1, Gpm6b, Mmp14
Positive regulation of endothelial cell apoptotic	5.89	Sop2, Xbp1, Thbs1, Serpine1, Ecscr, Hmox1, Col18a1, Zfp36
Vasoconstriction	5.15	Rhoa, Manf, Acta2, Ednra, Ednrb
Pdgfr signalling pathway	4.99	Plat, Pdgfa, Zfand5, Arid5b, Iqgap1
Regulation of cell migration involved in sprouting angiogenesis	4.75	Rhoa, Thbs1, Hmox1, Anxa1, Rhoj
Regulation of coagulation	4.61	Procr, Anxa2, Cd9, Anxa5, Pdgfa, Serpine2
Positive regulation of smooth muscle cell migration	4.38	Postn, Mif, Pdgfa, Ifgbp5, Serpine1, Arpc2, Tmsb4x, Iqgap1, F3
Cellular response to hypoxia	4.14	Eif4ebp1, P4hb, Higd1a, Gnb1, Fam162a, Hif1a, Bnip3l, Bnip3
Regulation of fibroblast proliferation	3.78	Anxa2, Mmp9, Sod2, Bax, Mif, Pdgfa, Serpine1, Fth1, Fn1, Wnt5a
Positive regulation of leucocyte chemotaxis	3.53	Calr, Thbs1, Hspb1, Rac1, Serpine1, Ednra, Fn1, Wnt5a, Ccl2
Response to TGBβ	3.39	Smad7, Pdcd5, Col4a2, Fermt2, Dbn1, Serpine1, Rock2, Ccl2, Actr3
Mesenchymal cell differentiation	2.88	Loxl2, Ddx5, Hif1a, Ednra, Fn1, Rtn1, Wnt5a, Clf1, Ednrb, Hes1

5.4.5.8. Investigation of the phenotype of the repair-specific cell cluster identified by single cell sequencing

One of the most striking results from the cluster analysis was the identification of a group of cells with a distinct gene signature that appeared to be specific to the repairing uterine tissue. Initial analysis revealed that the cluster expressed a mix of genes consistent with transitory cells with intermediate phenotypes.

The top 16 most differentially expressed genes which discriminated Cluster 5 from all other cell clusters were mapped onto the t-SNE plot to assess their distribution amongst the other clusters (putative cell types) (Figure 5-29). The expression of *Sprr2d*, *Sprr2h*, *Edn1*, *Grem1*, *Pmaip1*, *Tnf* and *Cyp26b1* was exclusive to Cluster 5 while *Slpi*, *Ptgs2* and *Fabp4* were also expressed by putative pericytes in the repairing dataset. Genes including *Tgfbi*, *Tnc* and *Icam1* were expressed by all cells in the repairing dataset while *Cd55* was expressed by stromal fibroblasts in both control and repairing tissues. Interestingly *Des* and *Neat1* were expressed by all mesenchymal cell populations only more highly expressed by Cluster 5 (Figure 5-29)

Gene ontology of these selected genes returned processes such as morphogenesis of an epithelium, regulation of smooth muscle cell contraction and angiogenesis supporting the hypothesis that Cluster 5 may be composed of mesenchymal cells undergoing a transdifferentiation event such as FMT and/or MET.

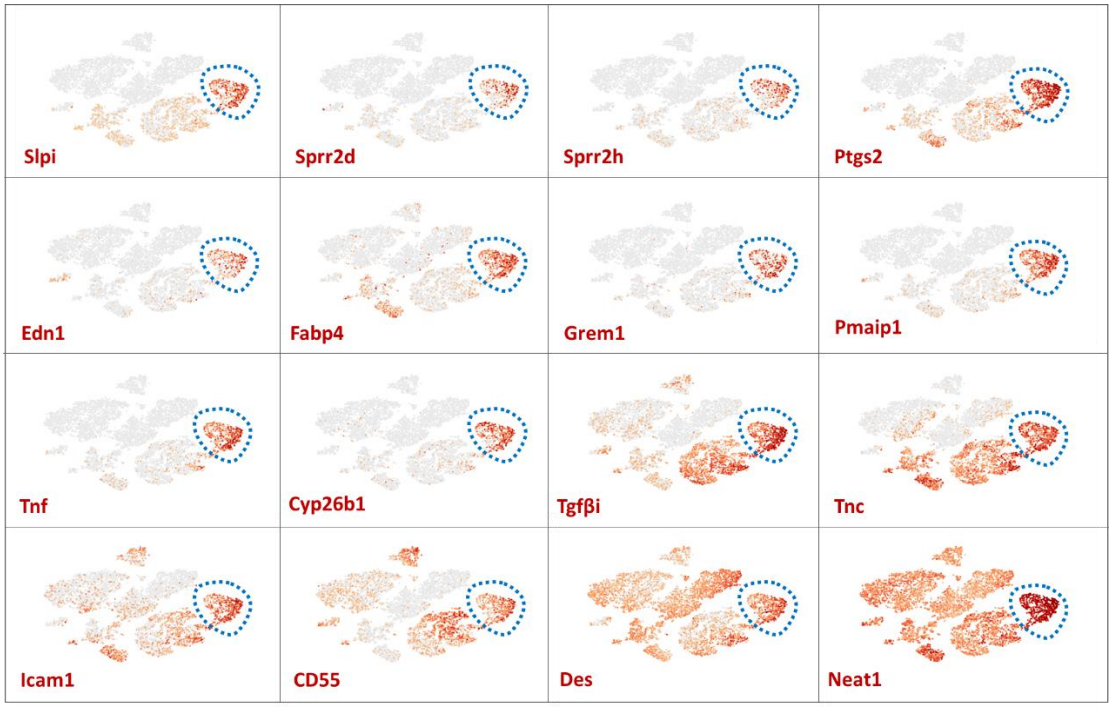

Figure 5-29. The expression of differentially expressed genes that distinguish cluster 5 from all other cell clusters in the aggregate file containing both naïve and repairing single cell datasets of endometrial mesenchyme. The expression of *Spli*, *Sprr2d*, *Sprr2h*, *Ptgs2*, *Edn1*, *Fabp4*, *Grem1*, *Pmaip1*, *Tnf*, and *Cyp26b1* was exclusive to the repair-specific cluster (cluster 5; blue dotted line). *Tgfβ1, Tnc, Icam1, Cd55* were also expressed by other cell types in the repairing mesenchyme while *Des* and *Neat1* were expressed throughout all cell clusters in both naïve and repairing tissues.

5.4.5.9. Gene ontology analysis of differentially expressed genes that distinguish the repair-specific cell cluster from other cell clusters identified by single cell sequencing

The list of differentially expressed genes used to discriminate the repair-specific Cluster 5 from all other cell clusters was analysed using the online Gene Ontology Consortium (http://www.geneontology.org/) in an attempt to identify processes specific to mesenchymal cells in endometrial tissue during repair. Results are displayed as tables outlining the gene ontology terms and associated genes significantly upregulated in repairing tissues. Genes highlighted in bold were mapped onto the t-SNE plot to analyse distribution amongst other cell types/clusters (Figures 5-30 to 5-33).

Gene Ontology Term	Fold Enrichment	Associated Genes
Collagen metabolic process	10.16	***Mmp9***, ***Mmp10***, *Mmp13*, *Mmp3*, *Plod2*
Smooth muscle cell differentiation	7.31	***Mmp9***, ***Ctnn1b***, *Hmox1*, *Itgb3*, *Klf4*, *C3ar1*, *Edn1*, *Sod2*, *Ptgs2*, *Tnf*, *Pbpj*
Regulation of fibroblast proliferation	6.81	***Mmp9***, *Sod2*, *Pmaip*, *Cdkn1a*, *Fth1*, *Pdgfb*, *Fn1*, *Itgb3*
Collagen fibril organisation	5.90	***Lgals3***, ***Mmp9***, ***Fn1***, ***Col5a3,*** *Plod2*, *Mmp13*, *Tnf*, *Tgfbi*, *Ero1l*, *P4ha1*, *Grem1*,
Regulation of stem cell proliferation	5.52	***Ctnnb1***, ***Fgfr1,*** *Pim1*, *Cxcl1*, *Hmga2*
Cell matrix adhesion	5.01	***Ctnn1b***, ***Fn1***, ***Col5a3***, *Bcl2l11*, *Tnfrsf12a*, *Itgav*, *Itgb3*
Mesenchymal cell differentiation	4.80	***Ctnn1b***, ***Fn1***, ***Sema3a***, ***Fgfr1***, *Gja1*, *Edn1*, *Cited2*, *Pbpj*, *plaur*
Stem cell differentiation	4.44	***Sema3a,*** *Msi2*, *Grem1*, *Edn1*, *Cited2*, *Pbpj*, *Fzd1*, *Fn21*

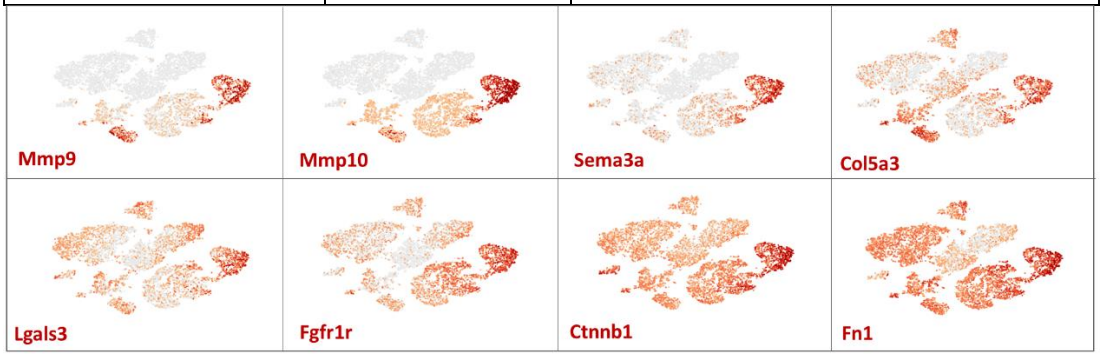

Figure 5-30. GO terms associated with mesenchymal cell function enriched by genes expressed by Cluster 5. Expression of *Mmp9. Mmp10, Sema3a, Col5a3, Lgals3, Fgfr1r, Ctnnb1* and *Fn1* mapped to the aggregate t-SNE plot.

Figure 5-30 outlines GO terms associated with mesenchymal cell function such as collagen metabolic process, fibroblast proliferation, matrix adhesion and mesenchymal cell differentiation. As before many genes were expressed by other cell types (stromal fibroblasts, vascular smooth muscle cells and pericytes) but exclusively in repairing tissue including Mmp9 and Mmp10. In contrast Col5a3, Lgals3, Fgfr1r, Ctnnb1 and Fn1 were also expressed by various cell types in the control tissue at similar or lower levels. Similar levels of expression of Mmp9, and Col5a3 was seen in Cluster 5 and Cluster 7 (pericytes in repairing endometrium) suggesting a level of similarity between these cell types either in phenotype or function. Notably Sema3a was almost exclusively expressed by Cluster 5 and involved in mesenchymal and stem cell differentiation processes (Figure 5-30).

Gene Ontology Term	Fold Enrichment	Associated Genes
Regulation of angiogenesis	7.84	***Ptgs2***, ***Adm***, ***Klf4,*** *Cxcr4, Hmga2, Runx1, Itgb3, Plk, Lgals3, Grem1, Mmp9,*
Endothelial cell chemotaxis	7.61	***Ptgs2***, ***Hmox1***, ***Pdgfb***, ***Klf4,*** *Map2k3, Hspb1, Spred1, Itgb3, Plk2, fgfr1*
Positive regulation of vasoconstriction	6.36	***Edn1***, ***Icam1***, ***Ptgs2***, ***Dusp5***, ***Adm***, ***Pfgfb***, *Tbxas1, Sema3a, Smad7, Mapk2k1*

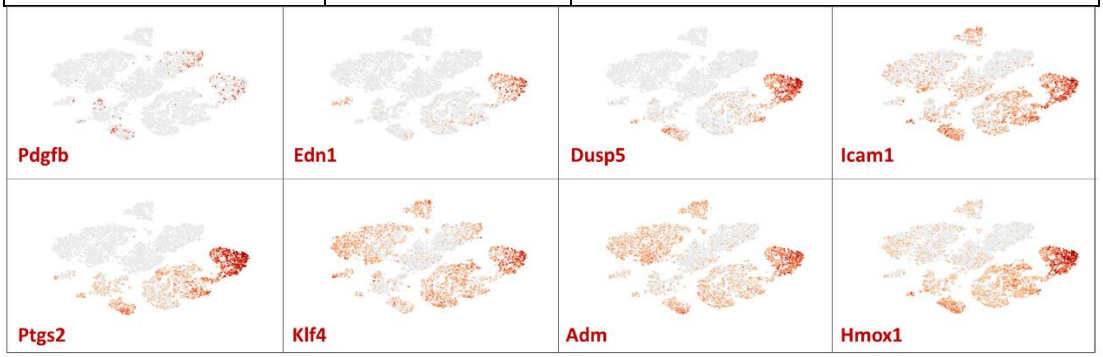

Figure 5-31. GO terms associated with blood vessel function enriched by genes expressed by Cluster 5. Expression of *Pdgfb, Edn1, Dusp5, Icam1, Ptgs2, Klf4, Adm* and *Hmox1* mapped to the aggregate t-SNE plot.

Figure 5-31 outlines GO terms associated with blood vessel function such as angiogenesis and vasoconstriction. Interestingly Pdgfb, Edn1, Dusp5 and Icam1 are exclusively expressed by Cluster 5 and associated with regulation of vasoconstriction suggesting this is a primary function of these cells during endometrial repair. Ptgs2 and Hmox1 are expressed by other cells in the repairing tissue perhaps also involved in endothelial cell chemotaxis, while Klf4 and Adm can be detected predominantly in stromal fibroblasts of the control tissue involved in the regulation of angiogenesis (Figure 5-31).

Gene Ontology Term	Fold Enrichment	Associated Genes
Epithelial tube morphogenesis	11.27	***Grem1***, ***Sprr2d***, ***Ptgs2***, ***Ctnnb1***, *Klf4, Smad7, Mmp12, Tnc, Fgfr1, Basp1, Fzd1,*
Epithelial cell migration	6.19	***Ptgs2***, ***Plk2***, *Fgfr1, Mapk2a3, Mmp9, Hsbp1, Hmox1, Pdgfb, Itgb3,*
Epithelial cell differentiation	5.65	***Grem1***, ***Fem1b***, ***Fndc3a***, ***Sprr2d***, ***Krt18,*** ***Ptgs2***, *Sprr2h, Cebpb, Rbpj, Basp1, Icam1,*
Epithelial cell proliferation	4.03	***Ctnnb1***, *Hmox1, Pdgfb, Itgb3, Fgfr1, Twist2, F3, Mmp12, Hmga2,*
Epithelial cell development	3.80	***Fem1b, Fndc3a***, ***EpCAM, Ctnnb1***, *Pfgfb, Prdm1, Fgfr1, Gja1, Icam1, Cxcr4,*

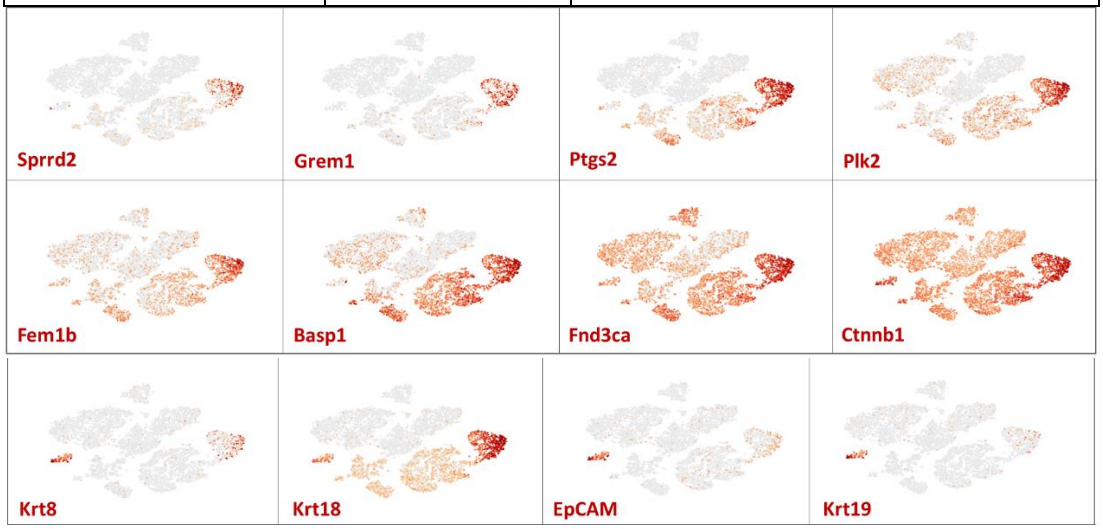

Figure 5-32. GO terms associated with epithelial cell function enriched by genes expressed by Cluster 5. Expression of *Sprrd2, Grem1, Ptgs2, Plk2, Fem1b, Basp1, Fnd3ca, Ctnnb1, Krt8, Krt18, Epcam* and *Krt19* mapped to the aggregate t-SNE plot.

Figure 5-32 outlines GO terms associated with epithelial cell function such as epithelial cell migration, differentiation, proliferation and development. Notably Sprrd2 and Grem1 are exclusively expressed by Cluster 5 and associated with epithelial tube morphogenesis and epithelial cell differentiation in line with these cells undergoing MET. Other genes are expressed but several other cell types/clusters in both control and repairing endometrial tissues. Interestingly, expression of Krt8, Krt18 and EpCAM was seen in regions Cluster 5 and expressed highly by Cluster 8 (epithelial cells in control endometrium) suggesting that a subset of Cluster 5 may infact have an epithelial cell phenotype, further indicating MET (Figure 5-32).

Gene Ontology Term	Fold Enrichment	Associated Genes
Regulation of leucocyte adhesion to endothelium	9.41	***Tnf***, ***Cebpb***, ***Il23a,*** *Klf4, Icam1, Smad7, Lgals3, Sdc4, Arg2, Runx1,*
Regulation of cytokine secretion	9.25	***Il1rap, Csf1r, Tnf,*** *Arg2, Ccl3, Srgn, FN1, Il1r2, Ccr5, MMP12*
Neutrophil chemotaxis	8.76	***Fcer1g***, ***Cxcl2***, ***Cxcl1***, *Lgals3, Ppbp, Ccl7, Il1rn, Ccl3, Pde4b, Spp1*
Negative regulation of immune response	8.51	***Tnf***, ***Bcl1****Smad7, Lgals3, Mmp12, Arg2, Ccr1, Hmox1, Grem1, Sdc4*
Regulation of macrophage differentiation	7.03	***Tnf***, *Prkch, Itgav, Itgb3, Nfkbia, Smad7, Ccr5, Grem1, Ifrd1, Pdgfb*
T cell receptor signalling	6.60	***Bcl10***, *Lgals3, Pvr, Prkch, Elf1*
Leucocyte activation	6.32	***Fcer1g***, ***Cebpb***, ***Bcl10***, *Fpr2, Icam1, Itgav, Cyp26b1, Rbpj, Cxcr4, Ctnnb1*
Myeloid leucocyte activation	5.85	***Fcer1g***, ***Bcl10***, *Fpr2, Rbpj, Ndrg1, Clu, Tlr7*
Regulation of myeloid leucocyte differentiation	4.34	***Cebpb***, ***Csf1r***, ***Tnf***, ***Il23a***, *Ccr1, Fam213a, Ctnnb1, Ccl3, Runx1, Itgb3,*
Cytokine production	4.23	***Fcer1g***, ***Il1rap,*** *Fabp4, , Itgav, Ptgs2, Pbpj, Fgfr1*

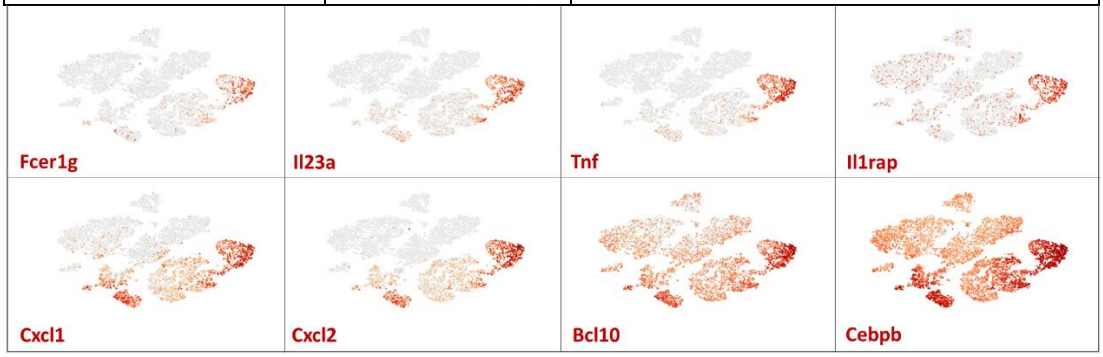

Figure 5-33. GO terms associated with an inflammatory response enriched by genes expressed by Cluster 5. Expression of *Fcer1g, Il23a, Tnf, Il1rap, Cxcl1, Cxcl2, Bcl10* and *Cebpb* mapped to the aggregate t-SNE plot.

Figure 5-33 outlines GO terms associated with an inflammatory response including regulation of leucocyte adhesion to endothelium, neutrophil chemotaxis and regulation of macrophage differentiation. Notably Fcer1g, Il23a, Tnf and Il1rap were exclusively expressed by Cluster 5 genes attributed to leucocyte activation, adhesion and differentiation and cytokine production, functions perhaps attributed to cells of Cluster 5. Similar levels of expression of Cxcl1, Cxcl2, Bcl10 and Cebpb was seen in Cluster 5 and Cluster 7 (pericytes in repairing endometrium) further suggesting a level of similarity between these cell types either in phenotype or function. (Figure 5-33).

Gene ontology analysis of differentially expressed genes associated with the repair-specific Cluster 5 has identified key roles in wound healing, regeneration, mesenchymal cell function, blood vessel function, epithelial cell function and the inflammatory response. It has also identified key genes that can be exclusively attributed to cells of Cluster 5 including Cyp26b1, Pdgfb, Edn1, Dusp5, Icam1 Sprrd2, Grem1 Fcer1g, Il23a, Tnf and Il1rap. It is hypothesised that Cluster 5 represents mesenchymal cells undergoing a transdifferentiation event (FMT and/or MET) however the precise origin of these cells remains unknown. Further bioinformatic trajectory analysis and *in vivo* lineage tracing studies are required to compliment and extend this data.

5.5 Discussion

The human endometrium is a highly dynamic tissue that has a unique and remarkable capacity for scarless tissue repair during the 'wounding' stimulus of menstruation. The restoration of endometrial tissue homeostasis requires rapid reepithelialisation, stromal and vascular remodelling with a number of studies suggesting that a population of stem/progenitor cells that reside in the basal layer of the endometrium may play a key role in endometrial repair processes (Schwab and Gargett 2007, Cervelló and Simón 2009, Cervelló et al. 2011, Masuda et al. 2012). In the current study the Edinburgh menses mouse model that recapitulates key features of human menstrual repair including focal hypoxia, tissue breakdown, reepithelialisation and inflammation (Cousins et al. 2014, Cousins et al. 2016b, Cousins et al. 2016c, Cousins et al. 2016d, Gibson et al. 2015) was used. In conjunction with the *Pdgfrβ-BAC-eGFP* transgenic mouse line, the dynamics of mesenchymal cell populations, in particular putative pericytes were investigated during endometrial repair. The results in this chapter expanded on those in Chapter 4 which had generated a gene expression profile of endometrial pericytes in endometrium from adult female mice (naïve).

5.5.1 Dynamic changes in mesenchymal cell populations during endometrial repair

IHC identified Pdgfrβ, CD146 and NG2 in endometrial tissues over the time course of repair (0, 12, 24, 48hrs after progesterone withdrawal). Detailed analysis using co-staining of endothelial cells (CD31) and pericytes (NG2) revealed that in normal (naïve) endometrium CD31+ blood vessels were surrounded by NG2+ pericytes however during active repair (24hrs) pericyte coverage appeared reduced and there were some NG2+ cells in close proximity to the denuded stromal surface. Assessment of the results confirmed a significant decrease in the percentage of pericytes associated with blood vessels with a corresponding increase in the percentage of pericytes located in the stroma tissue irrespective of blood vessels. Pericytes detaching from blood vessels and migrating into the surrounding tissue is well documented in studies of development, wound healing and tumorigenesis (Stratman et al. 2009, Abramsson, Lindblom and Betsholtz 2003, Ansell and Izeta 2015) and during development (Gerhardt and Betsholtz 2003) where is it shown they guide the angiogenic sprout during angiogenesis. Evidence also suggests that during skin wound healing when pericytes dissociate from vasculature this can induce a differentiation event from a smooth muscle phenotype to a mesenchymal phenotype (Zebardast, Lickorish and Davies 2010). However, studies have also demonstrated that pericytes migrate away from blood vessels and differentiate into myofibroblasts in response to injury and are therefore effector cells in fibrosis (Humphreys 2012). Current results suggest that pericytes may be mobilised from their normal perivascular location to contribute to endometrial repair processes following menstruation although the functional significance remains unknown and further studies are needed to confirm this. Indeed pericytes residing in the vascular niche have been described as well positioned to respond to signals accompanying endometrial breakdown, modulate the inflammatory response and migrate through tissue to the site of damage (Spitzer et al. 2012).

Analysis of GFP+ cell populations in *Pdgfrβ-BAC-eGFP* uterine tissues at 12, 24 and 48hrs following progesterone withdrawal suggested that the stromal fibroblast population was relatively unchanged throughout endometrial breakdown and repair. In contrast, at 24hrs there were significantly more GFP+CD146+ pericytes in the tissue. Pericytes have been shown to proliferate in response to Pdgfrβ signalling and

TGFβ signalling, during development, angiogenesis and fibrosis (Humphreys 2012). These two pathways may well be in effect during endometrial repair. Unexpectedly, a phenotypically distinct transient population of cells characterised as $GFP^{dim}CD146^{mid}$ was identified in 24hrs samples. The origin of this cell population remains unknown but we postulate two possible origins: they derive from stromal fibroblasts ($GFP^{dim}CD146^{-}$cells) that have increased expression of CD146; or they derive from pericytes ($GFP^{bright}CD146^{+}$) that have decreased expression of Pdgfrβ and CD146. It is also notable that at 24hrs data analysis of monocyte cell populations (Chapter 3) identified a rapid increase in monocytes at the same time point and these appeared to have a unique phenotype compared with tissue resident macrophages.

MSCs have heterogeneity in expression of CD146 however it has been demonstrated that this does not affect CFU-F number, the osteogenic, chondrogenic and adipogenic differentiation ability or the ability for haematopoietic support (Espagnolle et al. 2014). Interestingly MSCs with high CD146 expression have a lower proliferation rate but a better potential for contraction of collagen matrix and it was therefore suggested that CD146 expression by MSCs is characteristic of commitment towards the vSMC lineage (Espagnolle et al. 2014). Another study indicates however that CD146 expression defines MSCs with high multipotency (Feng et al. 2011) which suggests CD146 expression may be decreased by MSCs as they undergo transdifferentiation events. Fibroblasts and myofibroblasts do not express CD146 (Akamatsu et al. 2013) but pericytes are reported to have the ability to differentiate into fibroblasts and myofibroblasts (Humphreys 2012, Kramann and Humphreys 2014, Greenhalgh et al. 2013, Hosaka et al. 2016). With this in mind it seems sensible to suggest that the transient, intermediate, mesenchymal cell population discovered in repairing endometrial tissues has arisen from the pericyte population (CD146+) and may be undergoing a trandifferentiation event to either become part of the CD146- fibroblast population or indeed the Pdgfrβ-CD146- cell population. Further lineage tracing studies are required to investigate the true origin of the intermediate cell population.

5.5.2 Investigation of the potential of mesenchymal cells to undergo a mesenchymal to epithelial transition (MET) during endometrial repair

EpCAM was expressed exclusively by epithelial cells and not found to co-express with GFP in naïve *Pdgfrβ-BAC-eGFP* uterine tissue but GFP+EpCAM+ cells were identified by flow cytometry in tissue digests during the endometrial shedding/repair time window. This result was supported by IHC with a population of GFP+EpCAM+ cells detected both in regions of decidual detachment and also lining the luminal surface. Both results appear in agreement with our previous studies reporting evidence for MET in the Edinburgh menses mouse model (Cousins et al. 2014). The suggestion that MET occurs during endometrial repair was first put forward by Garry *et al*, who used detailed SEM of menstrual phase human endometrium to provide evidence that stromal cells residing close to the luminal surface could contribute to the new epithelial cell layer (Garry et al. 2009, Garry et al. 2010). Restoration of the epithelial cell layer is essential for uterine function. When the epithelial-specific gene *Cdh1* (E-cadherin) is knocked out in mice this is associated with abnormal epithelial development and reduced expression of epithelial markers including cytokeratin 8 and occludin (Reardon et al. 2012). Interestingly these genes were found to be upregulated during endometrial repair in mice with a corresponding decrease in stromal associated genes (Cousins et al. 2014). It must be kept in mind however that in this study whole uterine tissues were examined which cannot rule out the contribution of epithelial cells as well as remaining stromal cells to the transcriptomic signature. Furthermore, genetic fate mapping has been used to examine endometrial remodelling following parturition which showed that stromal derived cells (anti-Mullerian hormone (AMH) receptor type II expressing cells) incorporated into the luminal and glandular epithelium through MET (Huang et al. 2012). Using the same tools Patterson *et al* investigated endometrial repair in a mouse model and showed a population of cells exhibiting both stromal and epithelial cell markers in the myometrial epithelial border (Patterson et al. 2013).

It has been reported that the protein 'smoothened' a GPCR (encoded by *Smo*) is a master regulator of hepatic epithelial regeneration based on its ability to promote MET in hepatic stellate cells through Hedgehog, TGFβ and Wnt signalling pathways

(Michelotti et al. 2013). In the endometrium it is believed that a balance in EMT and MET is important to repair processes: partial EMT may occur in epithelial cells to allow them to obtain a migratory phenotype; while MET may occur in stromal cells to allow them both to contribute to reepithelialisation (Cousins et al. 2014, Maybin and Critchley 2015) although the particular cell types which have this potential remain unknown.

Cells that express both Pdfrβ and CD146 have been identified in human endometrium and classified as pericytes with MSC properties. Although their role in human menstrual physiology has not yet been investigated, they have been shown to give rise to both endometrial stromal and epithelial cell compartments *in vitro* and by xenografting studies *in vivo* (Schwab and Gargett 2007). In general, MSCs (pericytes) have been found to differentiate into various epithelial cell types after systemic administration *in vivo* such as airway epithelial cells, retinal pigment epithelial cells, skin epithelial cells, sebaceous duct cells, tubular epithelial cells in the kidney (Phinney and Prockop 2007) however little evidence exists to support pericytes giving rise to epithelial cells in the endometrium.

It has been reported that CD146 is an important regulator of EMT with overexpression of CD146 in non-invasive epithelial breast cancer cells repressing the epithelial cell phenotype, inducing a mesenchymal cell phenotype and increasing migratory and invasive behaviour. (Zeng et al. 2012). Purified endometrial CD146+ cells cultured in a collagen-matrigel scaffold gave rise to epithelial-like cells which expressed genes including Spp1, Mmp2, ZO-1, Laminin alpha 2 and collagen type IV (Fayazi, Salehnia and Ziaei 2017). Applying this knowledge to the current results supports the theory that pericytes ($Pdgfr\beta^{bright}CD146+$) can undergo MET and may downregulate CD146 as they do so, giving rise to the newly identified intermediate cells ($Pdgfr\beta^{dim}CD146^{mid}$) which we postulate are novel transient population of transdifferentiating pericytes.

Some previous evidence of MET transition has been identified in endometrial tissues using lineage tracing methods (Huang et al. 2012, Patterson et al. 2013) however as these studies were carried out using constitutive-Cre systems they do not discount MET that may have occurred during development. Pilot experiments using the

NG2-CreER^{TM} BAC tamoxifen-inducible mouse line, detailed in Chapter 4, have provided a novel way of tracking the fate of pericytes by lineage tracing but the use of the anti-oestrogen tamoxifen to induce the transgene requires some further refinement of methods before these mice can be used in the Edinburgh menses mouse model.

5.5.3 Profiling of mesenchymal cells during endometrial repair by next generation sequencing and single cell sequencing revealed heterogeneity within the stromal compartment

GFP+ cells purified from *Pdgfrβ-BAC-eGFP* endometrial tissue recovered during active breakdown/repair 24hrs after progesterone withdrawal were analysed by both RNAseq and single cell sequencing with their resulting transcriptional profiles compared to those previously generated using a similar population of GFP+ cell recovered from normal, cycling adult mouse endometrium (see Chapter 4). Profiling mesenchymal cells during endometrial repair by NGS revealed a wide range of transcriptomic changes with 616 significantly upregulated genes and 1013 significantly downregulated genes. Gene ontology terms enriched by the significantly upregulated genes were largely associated with smooth muscle cell function, blood vessel function and regulation of the inflammatory response. Gene ontology terms enriched by the significantly downregulated genes included collagen fibril organisation, cell adhesion and regulation of cell localisation. Various studies have highlighted similar genes and pathways during endometrial breakdown and repair including ECM proteolysis, cell migration, haemostasis, vasoconstriction, inflammation, chemotaxis and wound healing (Spitzer et al. 2012, Talbi et al. 2006, Critchley et al. 2006a).

Interestingly, in the current study some of the upregulated genes were associated with smooth muscle contraction, regulation of myoblast differentiation and smooth muscle cell proliferation (e.g. *Tnc, Smad5, Tnf, Rgs2, Kcnma1, Ptgs2, Prickle1, Ifg2, Stc1, Ptch1, Ednra, Prdm1*), which would be consistent with stromal cells undergoing FMT. Tenascin-C (Tnc) was highly upregulated in the repairing endometrial tissue. This gene encodes a glycoprotein that specifically attracts fibroblasts and promotes their differentiation into myofibroblasts in response to injury in a rat model of cardiac injury (Tamaoki et al. 2005). In knockout mice the appearance of myofibroblasts was delayed even though cardiac repair was achieved (Tamaoki et al. 2005). These results highlight

potential parallels between regulatory molecules involved in cardiac and endometrial repair. Interestingly lineage tracing experiments in mice have shown that injury-induced ADAM12 (a disintegrin and metalloprotease 12) positive cells are a pro-inflammatory subset of collagen-overproducing cells that differentiate into myofibroblasts and either ablating these cells or knocking down ADAM12 has been shown to be sufficient to decrease fibrosis and scarring in muscle and skin (Dulauroy et al. 2012). In the current data set ADAM12 was significantly downregulated in the repairing endometrial mesenchyme which appears to further support the hypothesis that endometrial repair involves a unique FMT response so that there is less ECM deposition and a fibrotic response does not occur. Further lineage tracing and gene profiling experiments will establish whether this response is specific to pericytes.

Changes in genes associated with the morphogenesis of an epithelial sheet such as *Mmp12, Notch2, Lama1, Spp1, Cdh1, Cd44, Hoxd11, Mmp9, Sani1, Tnc, Ptch1, Lef1, Ednra, Prickle1* and *Lmo1* appear consistent with the evidence for EMT from this and other studies. For example, using tissues from the same mouse model system Cousins *et al* used a focussed gene array that contained a small selection of EMT/MET regulators: their results highlighted significant increases in several genes involved in the process including *Krt7*, *Cdh1 Dcsc2*, *Spp1*, *Dsp*, *Mmp3*, *Mmp9*, *Snai1*, *Slug* and *Wt1* (Cousins *et al*, 2014). Bioinformatic analysis of the new dataset identified changes in genes associated with a number of signalling pathways including Wnt signalling, Hedgehog signalling, TGFβ signalling, BMP signalling, all of which have previously been implicated in regulation of wound healing and in both FMT and EMT.

Single cell sequencing was used to complement NGS and further investigate transcriptomic changes within discrete mesenchymal cell populations. Single cell sequencing revealed novel heterogeneity of the endometrial mesenchyme that had not previously been described. Strikingly in normal endometrium cluster analysis identified 5 individual clusters of cells whereas cell sorting based on GFP intensity suggested there are only two (GFP^{dim} stromal fibroblasts and GFP^{bright} pericytes). When differential gene expression analysis was carried out to generate lists of genes specific to each cluster Clusters 1 and 4 were revealed as stromal fibroblasts with a high degree of similarity between their gene expression signatures. However as the

cells in cluster 4 appeared to be associated with collagen biosynthesis and ECM assembly it is possible they represent a population of stromal myofibroblast-like cells that are involved in maintaining tissue architecture. In contrast Clusters 2 and 3 appeared to be subpopulations of the cells previously identified as GFP^{bright} pericytes. However as Cluster 3 had higher expression of genes associated with vascular smooth muscle cells (*Myh11*, *Acta2*, *Tagln*) while Custer 2 had higher expression of genes associated with pericytes (*Kcnj8*, *Abcc9*, *Rgs5*) it is hypothesised that they share a common phenotype but may differ in function.

A comparison of the datasets generated from single cells recovered from naïve uterine tissues with those from endometrium undergoing active tissue repair (24hrs) revealed global gene expression changes in all mesenchymal cell populations in response to wounding which have not previously been described. Cluster analysis identified 9 distinct clusters of cells which were identified using gene signatures detected in the analysis of normal uterine tissue. Gross gene changes could be detected in each cell compartment: stromal fibroblasts, vascular smooth muscle cells and perictyes, associated with repair processes. Strikingly, there was a population of cells specific only to the repairing tissue that could not be identified based on the previously identified characteristic gene signatures. Notably, genes upregulated in this cell cluster were enriched for biological processes associated with reproductive function, wound healing, mesenchymal cell function, blood vessel function, epithelial cell function and the inflammatory response. Signalling pathways identified included Pdgfr signalling, Tnf signalling, response to glucocorticoid and response to growth factors.

It has been described that signalling by Cxcl12 through Cxcr4 and the expression of multiple MMPs is essential to the migration of MSCs during tissue repair (Spitzer et al. 2012, Son et al. 2006, Rafii et al. 2015). Interestingly the repair-specific cluster exclusively expressed Cxcr4 although Cxcl12 was not detected in the data set. This suggests that this cluster may represent migrating MSC-like cells responding to paracrine signalling via Cxcl12 generated by cells out with the mesenchymal compartment (immune cells). Notably the repair-specific cluster also expressed higher levels of Mmp3, Mmp9, Mmp10 and Mmp12 consistent with an important role for this cell cluster and the secretion of MMP proteins in tissue breakdown during

menstruation which has been highlighted in previous reports based on human (Gaide Chevronnay et al. 2012, Marbaix et al. 1996b, Marbaix et al. 1996a) and mouse tissues (Cousins et al. 2014, Kaitu'u et al. 2005).

The repair-specific cluster also exclusively expressed *Sprrd2*, *Grem1*, *Ptgs2*, *Plk2*, *Fem1b*, *Basp*, *Fnd3ca*, *Bmp7* and *Ctnnb1* all of which are regulatory genes implicated in the morphogenesis of an epithelium. The expression of *Krt8*, *Krt18*, *Krt19*, *Cdh1* and *Epcam* was detected in a contaminating epithelial cell cluster in the naïve tissue but notably some of these genes were also present in the repair-specific cluster (Kalluri and Weinberg 2009). The transcription factor Klf4 has been demonstrated to drive the expression of epithelial genes including *Cdh1* (Li et al. 2010) and *Pax2*, *Bmp7* and *Wt1* are all well-known drivers of the conversion of mesenchymal cells to epithelial cells through MET (Kalluri and Weinberg 2009). *Klf4*, *Bmp7* and *Wt1* were significantly upregulated in the repair-specific cluster with all the data above consistent with cells in this cluster undergoing MET.

Cells in the repairing cluster also expressed *Pdgfrβ* and *Mcam* (CD146) (although to a lesser extent than the pericyte cluster) and were also genes expressed by pericytes and the stromal fibroblast cluster. Collectively this suggests that a 'repair-unique' cluster includes the cells identified by flow cytometry and defined as Pdgfrβ^{dim}CD146^{mid}. The origin of this cell population remains to be fully validated but is clearly important in defining a cell phenotype with an apparently important role in scarless endometrial tissue repair.

In other studies single cell sequencing technologies have been used to analyse human endometrial biopsies highlighting transcripts including *FOS*, *APOD* and *DCN* implicated in decidualisation and *SERPINF1* and *LUM* involved in the immune response (Krjutškov et al. 2016). Similarly uterine epithelial cells from neonatal to sexually mature mice have been analysed by single cell sequencing which has revealed a subpopulation of stem/progenitor cells and redefined a hierarchal map during epithelial development (Wu et al. 2017). To the best of my knowledge this is the first single cell dataset that specifically interrogates mesenchymal cells during endometrial repair using a defined and validated mouse model. This study has identified complex heterogeneity within the endometrial mesenchyme that has not previously been

reported allowing the landscape of the endometrial mesenchyme to be redefined which may change perspectives on the results of many studies. Identifying definitive molecular signatures for each subpopulation is an important future goal as this will drive in greater understanding of how the endometrial mesenchyme responds during scarless tissue repair.

5.5.4 Future prospects

The novel results presented in this chapter have revealed a dynamic role for endometrial pericytes in repair processes with a potential to undergo MET to contribute to reepithelialisation. To complement and extend these studies lineage tracing experiments are required to more thoroughly interrogate dynamics of mesenchymal and epithelial cell populations. In further experiments inducible Cre lines will be employed under control of cell specific markers to specifically trace the contribution of pericytes (NG2) and stromal fibroblasts (Pdgfrα) individually to endometrial repair. Initial results using NG2 immunohistochemistry have already suggested these cells become mobilised during the repair process. With such genetic tools further ablation studies could be carried out whereby the lines would be crossed with a floxed DTR line and upon administration of diphtheria toxin the cells would be ablated. This would determine how essential specific cell populations are to endometrial repair. Furthermore, conditional gene knockout studies could be carried out by crossing the cre lines with floxed mouse lines around various genes of interest allowing for the identification of therapeutic targets.

Single cell sequencing analysis identified previously undetected heterogeneity within the endometrial mesenchyme. With the current single cell dataset it would be interesting to run bioinformatic comparisons to data sets generated in uninjured and injured kidney/liver/heart such as those already generated by the Henderson lab group (unpublished data). This would highlight any significant transcriptomic differences between a scarless wound healing response seen in the endometrium and a scarring response seen during liver/kidney/cardiac fibrosis. Such cross disciplinary studies may identify therapeutic approaches to target fibrosis in the kidney/liver/heart. Additionally, if pericytes are identified as a key player in scarless healing they could be manipulated in other tissues to alleviate fibrosis. The use of adoptive transfer studies

using endometrial pericytes as a cell-based therapy may also provide an experimental approach to alleviate fibrotic disease in other tissues.

5.5.5 Concluding remarks

These studies which have focussed on the role of perivascular pericytes in scarless endometrial tissue repair, have provided new and compelling evidence that endometrial pericytes have the ability to undergo MET and thereby contribute to both stromal remodelling and reepithelialisation. To complement and extend the current data, lineage tracing studies are planned building on identification of NG2 as a specific pericyte marker in endometrial tissues.

Chapter 6 Final Discussion

The endometrium is a dynamic steroid-dependent tissue that exhibits a unique 'wound healing' response that is both inflammatory and completely regenerative with complete restoration of a complex tissue architecture following menstruation without development of any scar tissue. The aim of this thesis was to use the endometrium as a paradigm for scarless tissue repair in which to interrogate the phenotype and function of both myeloid immune cells and mesenchymal progenitors and investigate their role during post-menstrual endometrial repair. As it is difficult to obtain human samples of menstrual endometrium, a previously established mouse model of endometrial breakdown and repair (Cousins et al. 2014), referred to in this thesis as the 'Edinburgh menses mouse model'. The Edinburgh model has previously been characterised and shown to successfully recapitulate key processes of menstruation in women including focal hypoxia, tissue breakdown, immune cell influx and re-epithelialisation. In this model the mouse endometrium exhibits complete restoration of tissue integrity within 48hours, recapitulating the rapid healing process observed in the human endometrium. In conjunction with different transgenic mouse lines the contribution of both myeloid immune cells (MacGreen, MacApple, CD68-eGFP) and mesenchymal progenitors (Pdgfrβ-BAC-eGFP, NG2-CreER^{TM} BAC) has been thoroughly investigated. The studies presented in this thesis have revealed novel mechanisms contributing to scar-free endometrial repair processes, which are discussed below.

6.1 A heterogeneous monocyte/macrophage population can be identified in endometrial tissue during repair

Menstruation is associated with the sequential recruitment of neutrophils and macrophages that are believed to play key roles in the controlled break down of the tissue and its subsequent shedding (Evans and Salamonsen 2012). The studies outlined in this thesis have focussed on the contribution of macrophages to the regulation of endometrial inflammation and tissue breakdown. Evidence shows that macrophage numbers peak in the human endometrium during menstruation where they represent up to 15% of the leucocyte population (Salamonsen and Woolley 1999). As macrophages are able to acquire a pro- or anti-inflammatory phenotype in response to signals from the microenvironment (Mantovani et al. 2013) it is likely

that discrete signals from the endometrial microenvironment affect macrophage phenotype and function. In Chapter 3, the aim was to determine the phenotype and spatial localisation of mononuclear phagocytes in endometrial tissue during homeostasis and endometrial repair.

The MacGreen transgenic mouse was used to focus investigations on the monocyte/macrophage lineage as GFP is expressed specifically in cells under control of the CSF1R, a protein essential to the proliferation, differentiation and survival of monocytes and macrophages (Sasmono and Williams 2012). Results obtained demonstrated that numbers of GFP+ immune cells rapidly increased in the endometrial tissue in response to the 'wounding' stimulus of tissue breakdown. These cells were most abundant in the residual endometrium and shed tissue 24hrs following P4 withdrawal and by 48hrs were much reduced seemingly in line with the resolution of inflammation and completion of repair. Further characterisation of immune cells using the mature macrophage marker F4/80 identified a heterogeneous population of immune cells of the monocyte/macrophage lineage present in repairing endometrial tissues with novel evidence for three subpopulations based on their expression of GFP and/or F4/80. The three populations showed discrete spatial localisation within the tissue: GFP+F4/80- inflammatory monocytes located most prominently in the shed tissue undergoing breakdown and in regions of residual endometrium undergoing repair; GFP+F4/80+ monocyte-derived macrophages localised to residual endometrium undergoing repair and not associated with shed tissue undergoing breakdown nor regions of endometrium where repair was complete; and GFP-F4/80+ presumptive tissue-resident macrophages which appeared relatively stable and unchanged during endometrial repair, and were dispersed throughout the tissue irrespective of areas of tissue breakdown and repair. It is reasonable to postulate that these distinct locations of monocyte/macrophage subpopulations in the endometrium may have significant impacts on their phenotype and function as has been shown in other studies (Schulz et al. 2012) but this will require further study to unravel. Taken together, my novel results support a dynamic spatio-temporal role for monocytes and macrophages in regulating endometrial repair which are summarised in Figure 6-1.

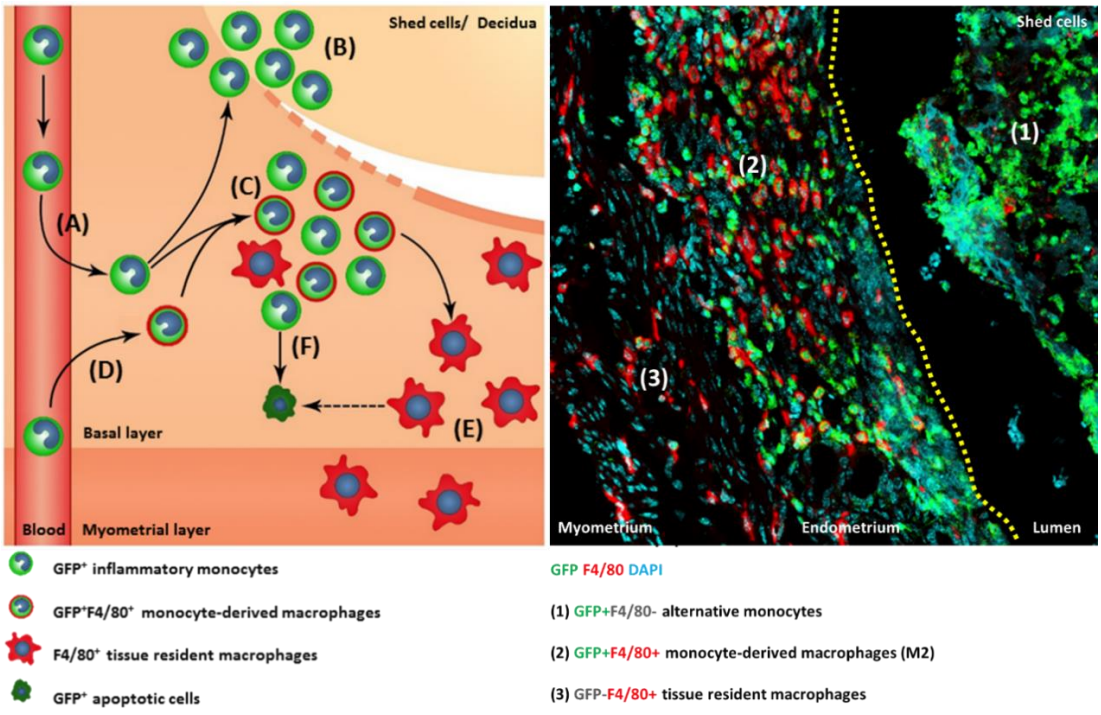

Figure 6-1. Schematic representation of the fate of mononuclear phagocytes during scar-free endometrial tissue repair (left) in relation to three distinct phenotypes identified by IHC (right). (A) Endometrial repair is associated with a dynamic influx of monocytes from the circulation in response to the 'wounding' stimulus of menses which differentiate in response to spatially distinct signals within the tissue. **(B)** GFP+F4/80- monocytes (**(1)** green) cluster in the shed tissue undergoing active tissue breakdown, peaking at 24hrs after P4 withdrawal. **(C)** A mixed population of GFP+F4/80- monocytes and GFP+F4/80+ monocyte-derived macrophages (**(2)** green/red) cluster in areas of active repair and remodelling in close proximity to denuded stromal surfaces (yellow dotted line). **(D)** It is currently undetermined whether GFP+F4/80+ cells arise from an independent population of monocytes that influx independently of the GFP+F4/80- monocytes. **(E)** Tissue resident macrophages are located throughout the endometrial tissue and remain homeostatic during repair (**(3)** red). Upon completion of repair GFP+F480- monocytes may undergo differentiation to become part of the tissue resident macrophage population or **(F)** undergo apoptosis and be cleared from the tissue following resolution of inflammation.

One of the major questions arising from this data was the identification of a macrophage population that was seemingly persisting independently of CSF1 signalling (GFP-F4/80+ cells) which appeared at odds with reports that macrophages require CSF1 signalling to survive (Sasmono and Williams 2012, Jones and Ricardo 2013). To address whether this result was in part a reflection of the site of insertion of the transgene in the MacGreen line two further transgenic mouse lines were utilised:

the MacApple line where mCherry (RFP) is expressed under control of the CSF1R promoter (Hawley et al. 2018) although the locus of insertion varies to that of the MacGreen line; and the CD68-eGFP line where eGFP is expressed under control of the CD68 promoter, a protein expressed by myeloid cells, specifically monocytes and macrophages (Iqbal et al. 2014). Using these different transgenic lines similar results were obtained when analysing the expression of the intrinsic reporter and F4/80. As in MacGreen tissues three subpopulations of labelled cells were always identified: Reporter+F4/80- cells, Reporter+F4/80+ cells and Reporter-F4/80+ cells and these all showed similar tissue distribution patterns in the endometrium during repair. When triple IHC was used to concurrently examine expression of GFP, CSF1R and F4/80 in MacGreen tissues the presence of an F4/80+ cell population that did not express either GFP or CSF1R was confirmed and this was backed up by gene expression analysis confirming isolated GFP-F4/80+ cells had very low expression levels of CSF1R mRNA when compared to GFP+F4/80- and GFP+F4/80+ cells.

The experiments described above confirmed that three subpopulations of monocyte/macrophages exist in endometrium the numbers of which change dynamically during shedding/repair and further investigations have begun to explore the functional significance of this result. The expression of key candidate genes associated with currently 'known' monocyte/macrophage phenotypes was assessed by qRTPCR. This revealed that the different subpopulations expressed genes associated with alternatively activated, anti-inflammatory and pro-repair monocyte and macrophage phenotypes. Notably the GFP+F4/80+ cell population exhibited markers usually assigned to both monocytes and macrophages suggesting further heterogeneity in this population. As these cells are specifically located to regions of repairing tissue and only present in abundance during the repair phase (24hrs in this study) we believe further studies on this population should be undertaken as they may help to decipher the role(s) played by macrophages in scar-free endometrial repair.

Although the current studies were focussed on the myeloid lineage, the inflammatory response in the endometrium is believed to involve a complex interplay not only between the various immune cells but also cross-talk with other

cells in the tissue microenvironment which will inevitably influence phenotype and function. To broaden current knowledge an interrogation of the other immune cell populations and their relationship to monocyte/macrophages is required. As described in detail in Chapter 5, single cell sequencing can be used to simultaneously examine a heterogeneous cell population and gene expression changes that may be relevant to different experimental conditions. To apply this technology to immune cells in the endometrial repair, a single cell sequencing dataset for total CD45+ cells in both naïve mouse endometrium and endometrium from mice at the 24hrs time point of the mouse model of endometrial breakdown and repair, has very recently been generated. Analysis is currently underway to interrogate the new dataset so as to better understand the different immune cell phenotypes present in the tissue, their relative proportions and how they interact to control the inflammatory response associated with endometrial repair.

As the studies in this thesis were designed to explore the roles of both immune cells and mesenchymal cells in the endometrial repair processes, new hypotheses can be generated by comparing different sets of the data: one such example is summarised in Figure 6-2. Interestingly by examining endometrial pericytes (Figure 6-2 (A) white arrows) and immune cells (Figure 6-2 (B) yellow arrows) separately (Chapters 3 and 4), both cell types were found to be clustering in close proximity to the denuded stromal surface (Figure 6-2 (A-B) yellow dotted line) in tissue regions undergoing active tissue repair. Without performing a double stain for these two cell types a definitive conclusion cannot be drawn, however it seems possible that these different cell populations may interact at the interface of endometrial repair. Whether pericytes govern immune cell function or the other way around or both, and how these regulatory mechanisms influence endometrial repair is an important future line of study that can increase our knowledge of the mechanisms underpinning scar-free tissue repair.

Data mining of the bulk RNA sequencing dataset generated from tissues recovered from Pdgfrβ+ mice during repair has revealed changes in expression of mRNAs for cytokines and chemokines (summarised in Figure 6-2 (C)) indicating a substantial role for these cells in regulating immune cell trafficking and function. By analysing

the single cell dataset of mesenchymal cells generated in the studies described in Chapter 5 further detail can be obtained. Many molecules that regulate the inflammatory response were identified and a few have been discussed as examples below. Specifically, it appears that the upregulation of *Cxcl1* and *Cxcl2* in the total tissue sample can be specifically attributed to the pericyte population during repair (Figure 6-2 (D-E) red dotted line) and to the new repair-specific mesenchymal cell cluster currently of unknown identity (Figure 6-2 (D-E) green dotted line). CXCL1 has mitogenic properties and is involved in several wound healing processes including angiogenesis, and inflammation, specifically neutrophil recruitment (Vries et al. 2015). CXCL1 has also been shown to be important for the migration of progenitor cells in the spinal cord (Tsai et al. 2002) and signals through the CXCR2 receptor. CXCL2 is a related chemokine to CXCL1 also signalling through CXCR2 and is chemotactic for both polymorphonuclear leucocytes and haematopoietic stem cells (Pelus and Fukuda 2006). CXCL2 has also been shown to be implicated in the migration of smooth muscle cells in the airways (Al-Alwan et al. 2013). Similarly, the expression of *Il123a* and *Tnf* was most abundant in the new 'repair-specific' cell cluster (Figure 6-2 (F-G) green dotted line) and appeared not to be expressed by other cell types. IL23a is a cytokine which has been shown to promote the upregulation of MMP9, increase angiogenesis and regulate T cell functions specifically T_h17 responses (Kikly et al. 2006) and TNF is a well described pro-inflammatory cytokine which has various roles in regulating immune cells. This suggests that both cells identified by their profile as pericytes as well as the newly identified population of 'repair specific' cells can play critical roles in regulating the inflammatory response, signalling to immune cell subtypes and stimulating stem cell responses. Interactions between mesenchymal cells and immune cells require further investigation.

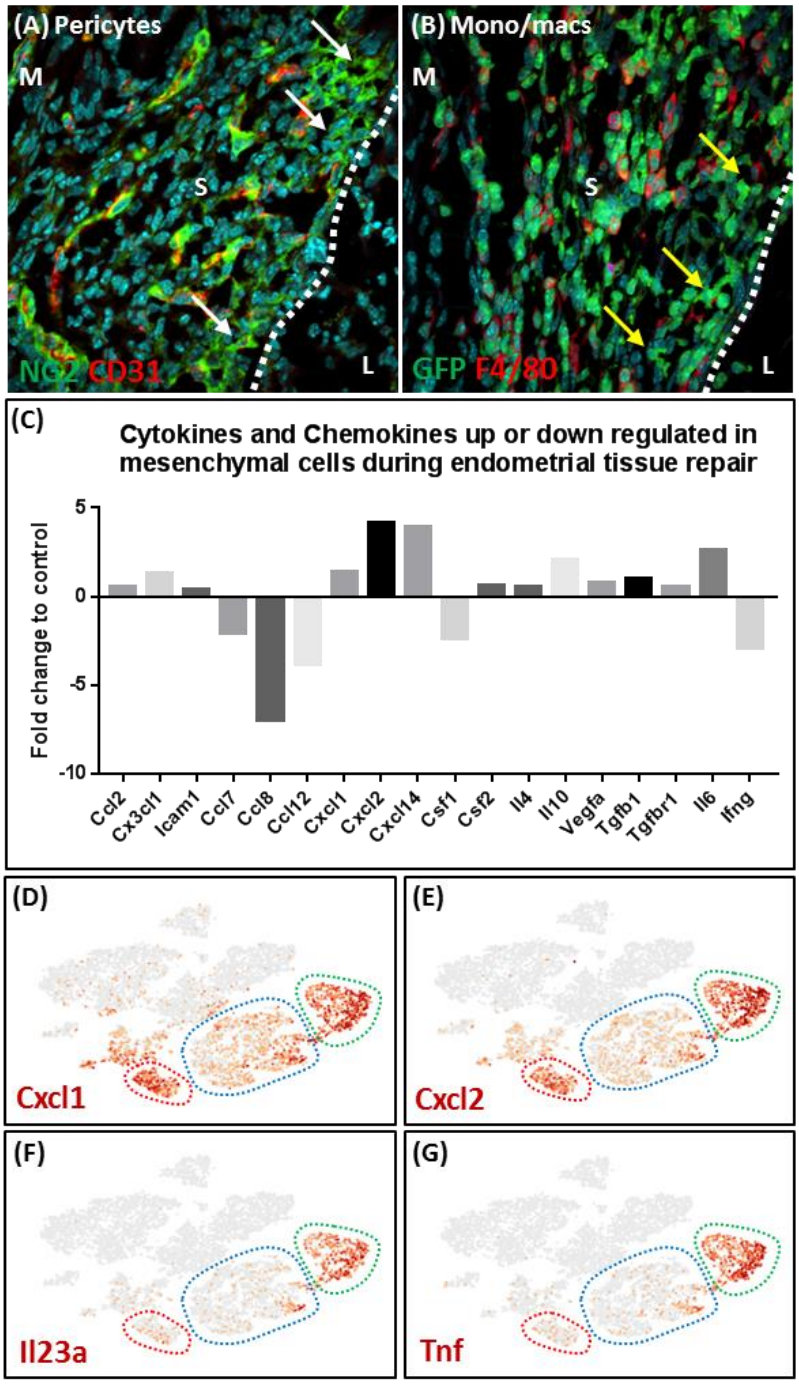

Figure 6-2. Expression of factors that regulate the inflammatory response by mesenchymal cells during active endometrial repair (24h after P4 withdrawal). (A) IHC for NG2+ pericytes (green) and CD31+ endothelial cells (red) showing pericytes clustering near to the denuded stromal surface (white dotted line). (B) IHC for GFP (green) and F480 (red) expressing immune cells showing clusters near to the denuded stromal surface (white dotted line). Myometrium = M, Stroma =S, lumen = L. (C) The expression of various cytokines and chemokines by mesenchymal cells during endometrial repair as determined by RNA sequencing. (D-G) expression of Cxcl1, Cxcl2, Il23a and Tnf by mesenchymal cells during endometrial repair as determined by single cell sequencing.

6.2 Identification of a pericyte specific marker in mouse endometrial tissues

As the endometrium exhibits an unparalleled regenerative capacity many studies including this one, have hypothesised that a population of mesenchymal stem/progenitor cells exist in the tissue that are in part responsible for the rapid and scar-free tissue repair (Gargett et al. 2016). This concept was first introduced in 1978 by Prainishnikov however evidence for the existence of endometrial stem cells only came about in 2004 when Chan *et al* identified populations of clonogenic cells in both the epithelial and stromal cell compartment (Chan et al. 2004). Since then, various studies have identified stem/progenitor cells in the endometrium (both human and rodent) which have been shown to have functions in maintaining tissue homeostasis (Gargett and Masuda 2010). However, the majority of current knowledge on the characterisation of endometrial stem/progenitor cells has been gathered using *in vitro* studies on a heterogeneous populations of stromal cells which does not exclude contamination from other cell types or effects of different culture conditions (Masuda et al. 2012). Therefore there was a need for a more robust characterisation of these cells which has been addressed by the studies in this thesis which have used transgenic mice combined with extensive image, flow and genomic analyses.

Studies in the human endometrium have used PDGFRβ and CD146 co-expression to identify a population of endometrial MSCs (Schwab and Gargett 2007). Notably these markers were also found to be expressed by stromal LRC in mouse tissue hypothesised to represent the MSC population in mice (Chan and Gargett 2006a). Stromal LRCs are located near CD31+ endothelial cells and express various stem cell markers including c-kit/CD117 and Oct4 (Cervelló et al. 2007). A further study has confirmed that Pdgfrβ and CD146 are co-expressed in a population of perivascular cells in the mouse endometrium, as well as mouse embryonic stem cells and therefore it is believed that these cells may possess stem cell activity (Parasar et al. 2017). Investigations carried out in this thesis utilised the *Pdgfrβ-BAC-eGFP* transgenic reporter mouse line in which GFP is expressed under the control of the *Pdgfrβ* promoter (Henderson et al. 2013). This mouse has been already been used in a number of studies to identify mesenchymal cells in various tissues including liver, kidney and brain (Henderson et

al. 2013, Zhang et al. 2018, Vanlandewijck et al. 2018, Martin et al. 2016) but has not previously been used to study mesenchymal cells in the endometrium. Robust reporting by GFP provided a reliable and reproducible way to target endometrial mesenchymal cells and an additional novel finding was that the two subpopulations of mesenchymal cells, stromal fibroblasts and pericytes could be easily separated based on the intensity of GFP expression. Having an intrinsic reporter to identify and isolate cells by flow cytometry and FACS methods has bypassed the difficulties encountered when relying purely on antibody detection including cross reactivity, unspecific staining and cleaved epitopes.

IHC, flow cytometry and sequencing methods were employed to show that the two subpopulations of Pdgfrβ expressing cells could be further distinguished by discrete localisation and gene expression profiles. Of particular interest was the identification of GFP^{bright} cells which expressed CD146, αSMA and NG2 and were located in close proximity to CD31 expressing endothelial cells therefore occupying a perivascular niche. In line with phenotypes described by other studies (Schwab and Gargett 2007, Spitzer et al. 2012, Crisan et al. 2009, Murray et al. 2014), these new results confirmed that the mouse endometrium houses a population of perivascular cells that express both Pdgfrβ and CD146. Further characterisation using a panel of markers commonly used to identify perivascular pericytes in various tissues (Crisan et al. 2008, Crisan et al. 2009) identified these cells as endometrial pericytes. As GFP expression in the *Pdgfrβ-BAC-eGFP* transgenic mouse line is a readout of Pdgfrβ gene promoter activity (Henderson et al. 2013) this indicates that GFP^{bright} pericytes in the endometrium may specifically upregulate expression of *Pdgfrβ* which may be of functional importance, although this is still to be investigated.

The IHC and gene expression studies have highlighted that Pdgfrβ is also expressed by stromal fibroblasts while CD146 is also expressed by endothelial cells, therefore neither is an exclusive marker of pericytes. Similarly upon validation of top hits from the RNA sequencing study the majority of genes were also expressed by other mesenchymal populations as summarised in Figure 6-3. Notably this detailed anlaysis demonstrated that expression of NG2 was exclusive to GFP^{bright} pericytes and the mRNA was not detected in GFP^{dim} stromal fibroblasts nor in CD31+ endothelial cells.

These results showed that NG2 fulfilled the criteria to be a pericyte-specific identification marker in mouse endometrium and may be useful in targeting these cells in downstream applications (Figure 6-3).

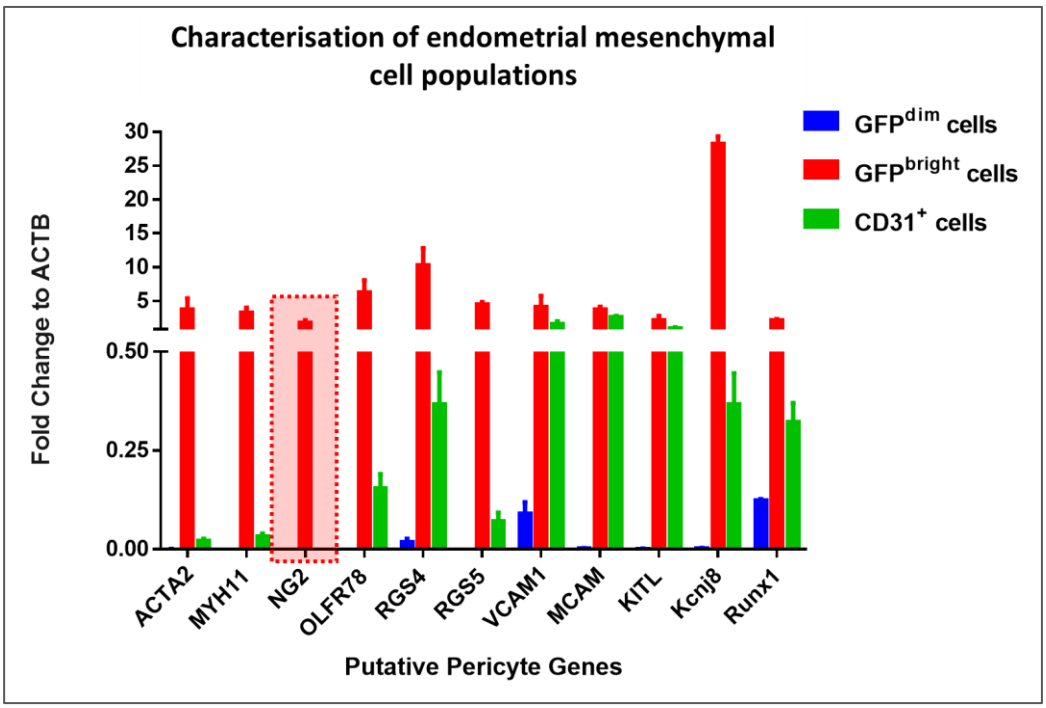

Figure 6-3. qPCR gene expression analysis of putative pericyte genes in mesenchymal cell populations isolated from naïve *Pdgfrβ-BAC-eGFP* uterus. All genes were expressed by GFP^{bright} pericytes, while VCAM1, MCAM (CD146) and Kitl were also expressed by CD31+ endothelial cells. Minimal expression of RGS4, VCAM1 and Runx1 was detected in GFP^{dim} stromal fibroblasts. NG2 (encoded by *Cspg4*) was exclusively expressed by GFP^{bright} pericytes as highlighted by the red dotted line (n=5).

As NG2 was determined to be a pericyte specific marker for endometrial tissues the NG2-CreER^{TM} BAC transgenic mouse line, where TdTomato is expressed under control of the NG2 promoter when induced with tamoxifen, was purchased from JAX®. Preliminary results using these transgenic mice have shown promise as TdTomato positive cells were shown to co-express NG2, CD146 and Pdgfrβ and were located in close association with CD31+ endothelial cells, consistent with results obtained using the *Pdgfrβ-BAC-eGFP* mouse line and those reported in the literature (Schwab and Gargett 2007, Spitzer et al. 2012, Crisan et al. 2009, Murray et al. 2014).

Several interesting comparisons can be drawn when identifying endometrial pericytes using different transgenic lines, as summarised in Figure 6-4. Immunohistochemistry demonstrates that both GFP^{bright} cells in *Pdgfrβ-BAC-eGFP* and TdTomato+ cells in *NG2-CreER^{TM} BAC* uterine tissues have a perivascular location and similar morphology with rounded cell bodies and long membranous processes that wrap around blood vessels (Figure 6-4 (A-B)). Quantification by flow cytometry revealed that GFP^{bright} cells in the adult *Pdgfrβ-BAC-eGFP* uterus represent 8.33±0.36% live cells while TdTomato+ cells in uterine tissues recovered from *NG2-CreER^{TM} BAC* adult female mice represented only 4.12±0.23% of live cells (Figure 6-4 (C-D)). The discrepancy in these values may be due to the fact that Pdgfrβ and CD146 co-expression identifies a larger population of cells than NG2 does. Interestingly this hypothesis can be explored by analysing the single cell sequencing dataset discussed in Chapter 5, where 4 clusters of mesenchymal cells were identified in the GFP+ cell population (all mesenchymal cells). Clusters 1 and 4 had low expression of Pdgfrβ representing the GFP^{dim} stromal fibroblasts while clusters 2 and 3 had high expression of Pdgfrβ representing the GFP^{bright} pericytes (Figure 6-4 (E)). Notably when analysing NG2 (Cspg4) expression in this dataset, cluster 2 was highly positive while cluster 3 was less so (Figure 6-4 (F)), indicating that Pdgfrβ/CD146 identify a heterogeneous population of cells (clusters 2 and 3) of which NG2 expressing cells represent a subset (Cluster 2).

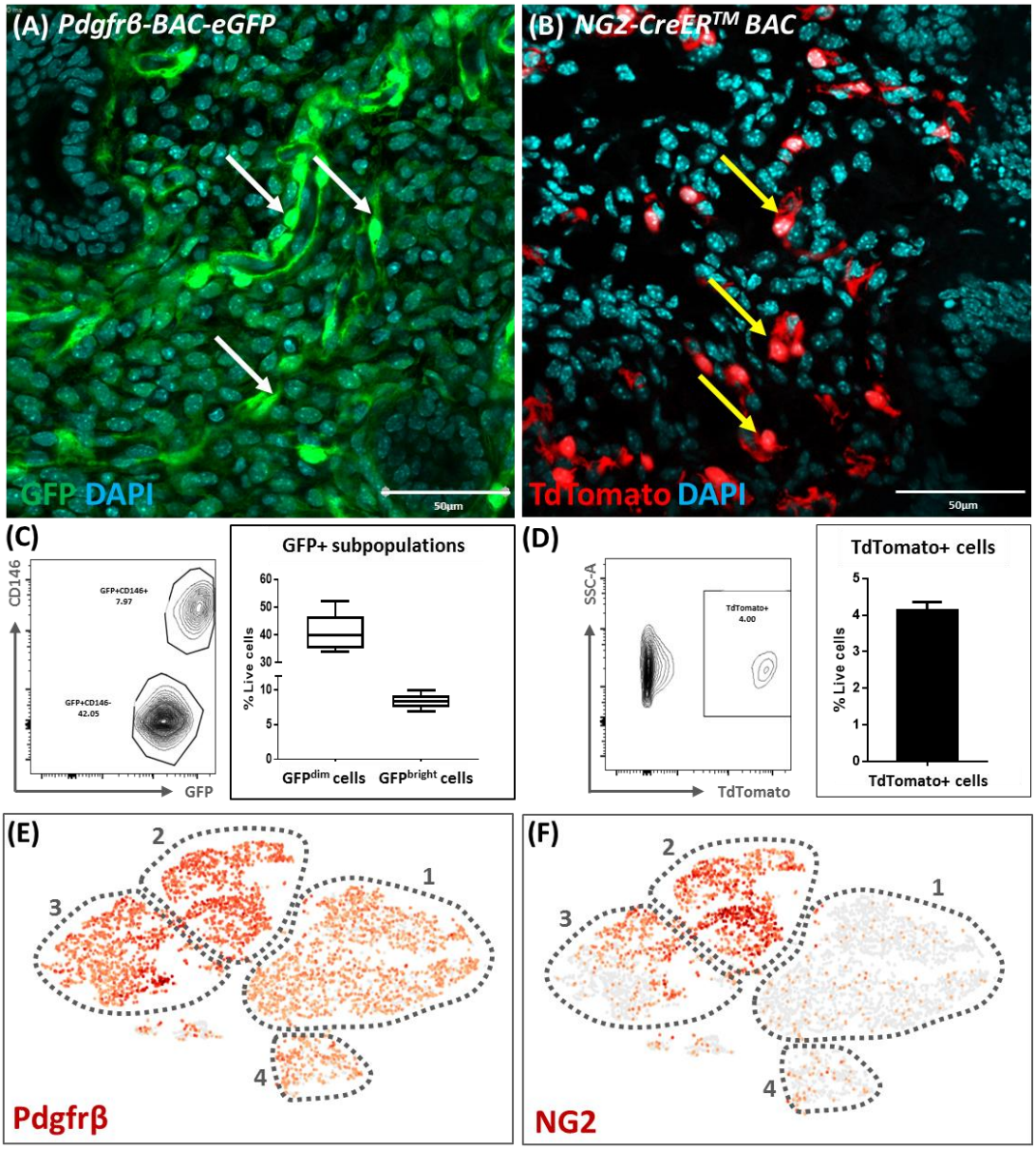

Figure 6-4. Comparison of data generated from *Pdgfrβ-BAC-eGFP* and *NG2-CreER^{TM} BAC* transgenic mice. (A) GFP expression in *Pdgfrβ-BAC-eGFP* uterine tissue indicating Pdgfrβ expressing cells, white arrows. **(B)** TdTomato expression in *NG2-CreER^{TM} BAC* uterine tissue indicating NG2 expressing cells, yellow arrows. Flow cytometry analysis of **(C)** GFP+ cell populations in *Pdgfrβ-BAC-eGFP* uterine tissue displaying both GFP+CD146+ and GFP+CD146- subpopulations representing 8.33±0.36% and 40.05±2.25% of live cells respectively and **(D)** NG2+ cell population in *NG2-CreER^{TM} BAC* uterine tissue representing 4.12±0.23% of live cells. **(E-F)** Single cell sequencing analysis of GFP+ cells from naive *Pdgfrβ-BAC-eGFP* uterine tissue identified 4 unique clusters of mesenchymal cells distinguished by dotted lines, all of which express Pdgfrβ and some of which express NG2.

Further bioinformatic analysis of the single cell sequencing dataset revealed that the two clusters identified within the GFP^{bright} cell population isolated from the *Pdgfrβ-BAC-eGFP* uterus have discrete genetic signatures (illustrated in Figure 6-5). This analysis identified clusters 2 and 3 as pericytes and vSMCs respectively. In various studies it has been concluded that adult MSCs in human tissues share common markers and characteristics with vSMCs, pericytes and endothelial cells (Rastegar et al. 2010, Bianco et al. 2001, Perkins and Fleischman 1990, Kinner, Zaleskas and Spector 2002) however in light of the current findings it may be that markers used in these studies do not definitively identify MSCs. Notably the new single cell sequencing dataset generated in the current study has shown that the commonplace markers used to identify pericytes (Pdgfrβ and CD146) also identify vSMCs in mouse endometrial tissue. Uncovering such heterogeneity will allow for future studies to be designed appropriately in order to target each population separately and avoid results that are due to a mixed cell response. In this study, the expression of NG2 was homogenous throughout the pericyte population (Figure 6-4 (F)) further confirming NG2 as a pericyte specific marker in mouse endometrium and verifying the use of the NG2-CreER^{TM} BAC transgenic mouse line to specifically target endometrial pericytes in future investigations.

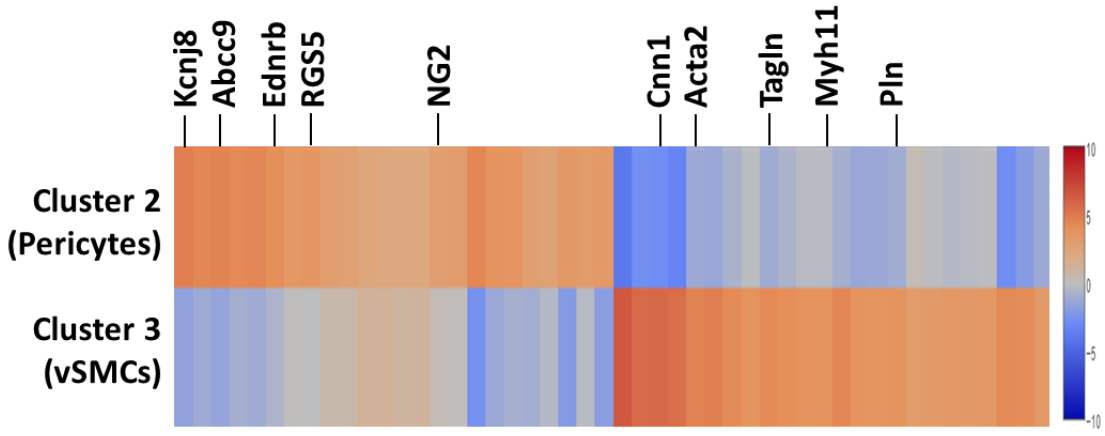

Figure 6-5. Heatmap of differentially expressed genes between clusters 2 and 3 from the single cell sequencing study on GFP+ mesenchymal cells isolated from naive *Pdgfrβ-BAC-eGFP* uterine tissue. Cluster 2 expressed genes associated with a pericyte phenotype including Kcnj8, Abcc9, Ednrb, RGS5 and NG2. Cluster 3 expressed genes associated with a vascular smooth muscle cell phenotype including Cnn1, Acta2, Tagln, Myh11 and Pln.

6.3 Endometrial pericytes undergo an MET during endometrial repair to contribute to rapid re-epithelialisation

The *Pdgfrβ-BAC-eGFP* transgenic mouse line has been invaluable in investigating mesenchymal dynamics during endometrial repair which was the aim of Chapter 5. Flow cytometry demonstrated that there was an increase in pericytes in endometrial tissue during repair (24hrs) which would be in agreement with other studies where pericytes have been shown to proliferate in response to Pdgfrβ and TGFβ signalling during development, angiogenesis and fibrosis in various tissues (Humphreys et al., Humphreys 2012). What was more exciting was the identification of a new population of cells present only in endometrial tissue during repair, of an intermediate phenotype between that of pericytes and stromal fibroblasts characterised as $GFP^{dim}CD146^{mid}$. This transient cell population could either originate from stromal fibroblasts ($GFP^{dim}CD146^{-}$cells) that have increased expression of CD146, or from pericytes ($GFP^{bright}CD146^{+}$) that have decreased expression of Pdgfrβ and CD146, or indeed from both. One study has shown that CD146 expression is varied amongst MSCs and that MSCs with high expression of CD146 show lower proliferative potential and greater contractile properties and therefore may be of the vSMC phenotype (Espagnolle et al. 2014), while another study has demonstrated that CD146 expression correlates with increased multipotency (Feng et al. 2011). Although the origin of the intermediate cell population is at present unknown I would speculate that they have arisen from CD146+ pericytes which have multipotent potential and that they represent cells undergoing trans-differentiation to either become part of the CD146- stromal fibroblast population or indeed the Pdgfrβ-CD146- cell population. This cannot be definitively determined without employing robust lineage tracing methods.

Previous work in the Saunders' laboratory demonstrated that during endometrial repair cells of the stromal compartment are able to undergo an MET to differentiate into new epithelial cells and aid in re-epithelialisation of the denuded stromal surface (Cousins et al. 2014). This phenomenon has also been reported in endometrial tissues following artificial menstruation or parturition in mice using elegant lineage tracing strategies where cells of mesenchymal origin become established in the new epithelial cell layer

(Patterson et al. 2013, Huang et al. 2012). However, without a targeted approach, these studies failed to identify which cell populations in the stromal compartment have the ability to respond and undergo MET. With this in mind the current study aimed to look in more detail at stromal fibroblasts and pericytes specifically using the *Pdgfrβ-BAC-eGFP* mouse line and various techniques to interrogate MET during endometrial repair (summaried in Figure 6-6). Interestingly it was found that during repair cells expressing both stromal and epithelial cell markers could be identified by flow cytometry, most predominantly seen in the pericyte and novel intermediate cell population at 24hrs following P4 withdrawal (Figure 6-6 (A-C)). IHC confirmed the existence of these cells during endometrial repair and localised them to regions of denuded stroma and in regions of newly synthesised epithelium (Figure 6-6 (D-E) yellow arrows). Taken together these results suggest that endometrial pericytes have the ability to undergo MET during endometrial repair in order to enhance rapid re-epithelialisation, and that the intermediate cell population identified only in repairing tissues may represent the MET transitioning cells.

This hypothesis can also be addressed by investigating epithelial cell marker expression in the single cell sequencing dataset of total mesenchymal cells in repairing endometrial tissues (Figure 6-6 (F-I)). Notably epithelial cell markers *Cdh1*, *Epcam, Krt8* and *Krt18* were expressed by the population of epithelial cells identified in the naive dataset as contamination (Figure 6-6 (F-I) cluster 9, blue dotted line), but what was interesting to see was that *Epcam*, *Krt8* and *Krt18* were expressed in the repair-specific cluster at 24hrs which otherwise expressed mesenchymal identification markers (Figure 6-6 (G-I) cluster 5, red dotted line). These data therefore appear consistent with idenfication of the 'repair specific' cluster as MET transitioning cells. Of note these cells did not express *Cdh1* (Figure 6-6 (F) cluster 5, red dotted line), an epithelial cell adhesion molecule, indicating that at 24hrs, transitioning cells do not yet have the capacity to establish the cell adhesion contacts required to form an intact epithelial cell layer, but are instead of a migratory phenotype.

Although the human MSC population has not been investigated in menstrual tissue samples, MSCs isolated based on expression of Pdgfrβ and CD146 have been shown to give rise to both stromal and epithelial cells *in vitro* and *in vivo* in xenografting

techniques (Schwab and Gargett 2007). The studies outlined in this thesis are the first to demonstrate that endometrial pericytes have the ability to undergo an MET during endometrial repair to reinstate the epithelial cell layer, which may be re-named as a pericyte-to-epithelial transition (PET).

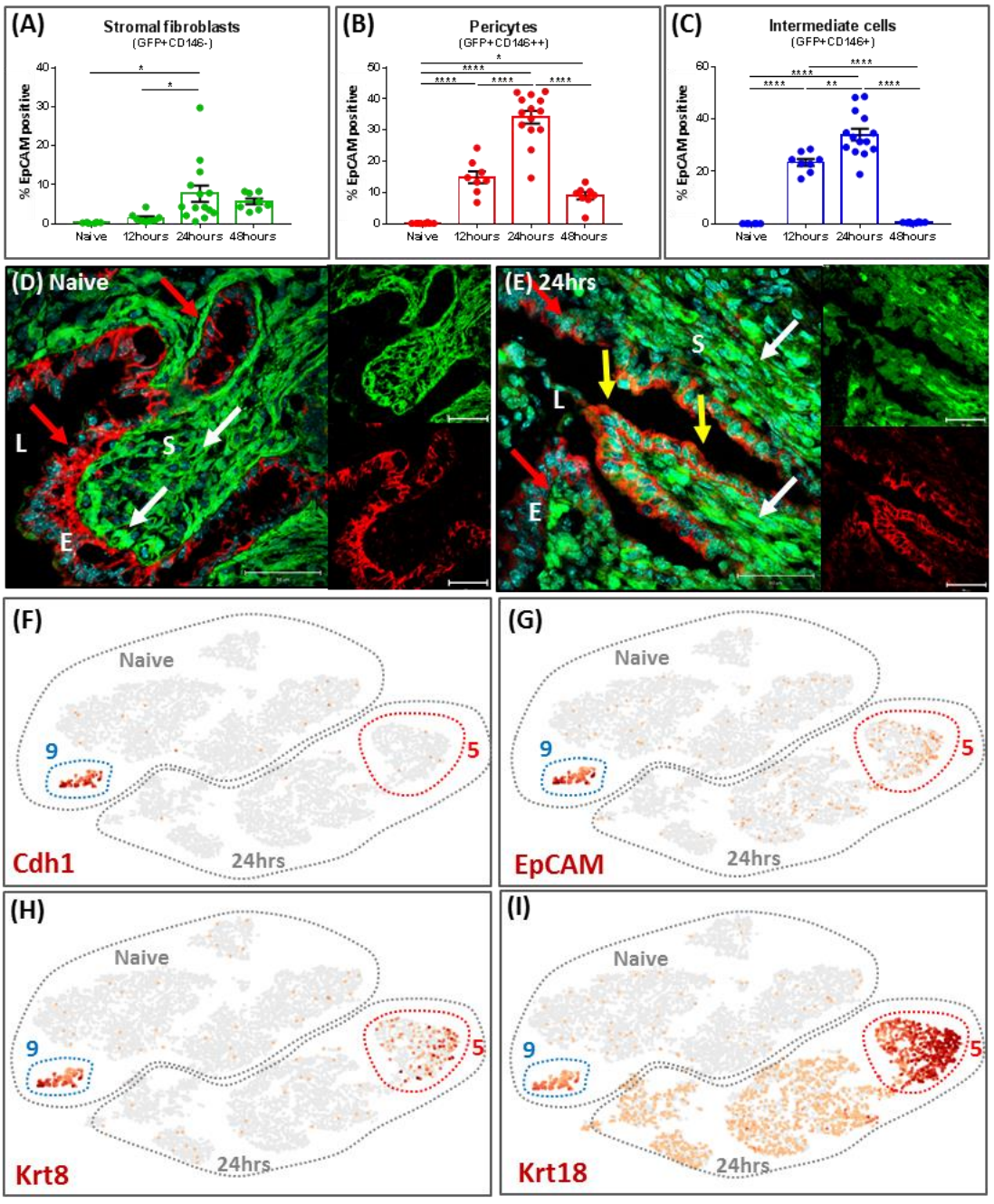

Figure 6-6. Summarised data supporting a role for MET during endometrial repair identified using the *Pdgfrβ-BAC-eGFP* transgenic mouse line. Expression of the epithelial cell marker EpCAM by **(A)** stromal fibroblasts, **(B)** pericytes and **(C)** repair-specific intermediate cells in naive endometrial tissues and during various phases of endometrial repair. IHC detection of cells expressing GFP (white arrows) and EpCAM (red arrows) in **(D)** naive endometrial tissues and **(E)** endometrial tissue during repair at 24hrs of the mouse model. GFP+EpCAM cells are denoted by yellow arrows. Lumen= L, stroma= S and epithelium= E. **(F-I)** Expression of *Cdh1*, *Epcam*, *Krt8* and *Krt18* in the single cell sequencing dataset examining total mesenchymal cells from naive endometrial tissues and from endometrial tissue during repair at 24hrs of the mouse model, separated by grey dotted lines. Cluster 9 (blue dotted line) represents epithelial cell contamination in the naive subset while cluster 5 (red dotted line) represents the repair-specific cell population.

In general MSCs (identified by Pdgfrβ and CD146, indicative of a pericyte phenotype) have been shown to differentiate into various epithelial cell types after systemic administration *in vivo* (Phinney and Prockop 2007) however this has not previously been investigated in endometrial tissues. Furthermore, CD146 has been identified as an important regulator of EMT as overexpression of CD146 in non-invasive epithelial breast cancer cells represses the epithelial cell phenotype and induces migratory and invasive behaviour indicative of a mesenchymal cell phenotype. Conversely, downregulation of CD146 in mesenchymal breast cancer cells reversed the migratory phenotype and reinstated an epithelial one (Zeng et al. 2012). Additionally, CD146+ cells purified from human endometrium and cultured in a collagen-matrigel scaffold gave rise to epithelial-like cells which expressed genes including Spp1, Mmp2, ZO-1, Laminin alpha 2 and collagen type IV (Fayazi et al. 2017). Pericytes have been found to influence the progression of EMT in cancer (Cooke et al. 2012) and it has also been postulated that mesenchymal products generated by EMT in cancer progression often express multiple pericyte markers (αSMA, NG2) and associate with blood vessels thus phenotypically and functionally resembling pericytes. Therefore some cancer-associated EMT may represent an epithelial-to-pericyte transition (Shenoy and Lu 2017, Lu and Shenoy 2017) and as EMT is a reversible process, a pericyte-to-epithelial transition (PET) may also be contributing to the malignant phenotype.

Applying this knowledge to the current results supports the theory that pericytes (Pdgfrβ^{bright}CD146+) can undergo MET and may downregulate CD146 as they do so.

This supports previous evidence for MET by the stromal compartment during endometrial repair (Cousins et al. 2014) however this is the first study to demonstrate the ability of pericytes to undergo PET during endometrial repair. As the phenotype of the intermediate cells ($Pdgfr\beta^{dim}CD146^{mid}$) is currently unknown it can be postulated that they are transdifferentiating pericytes. It cannot be ruled out however that stromal fibroblasts may also undergo an MET and contribute to the intermediate cell population. Figure 6-7 outlines the proposed contribution of mesenchymal stromal fibroblasts and pericytes to re-epithelialisation during endometrial repair.

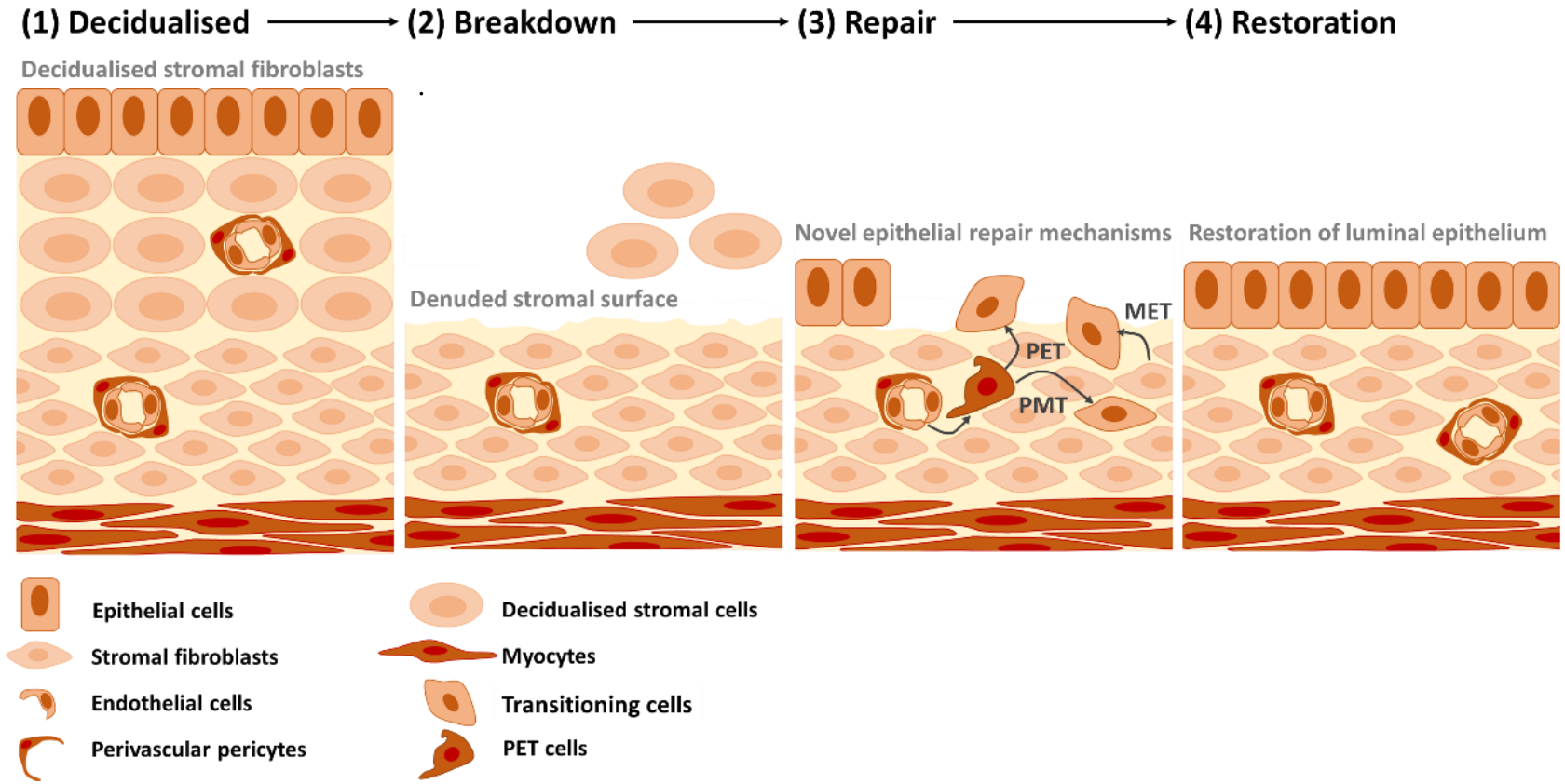

Figure 6-7. Schematic representation of the contribution of mesenchymal cell populations to endometrial repair processes. (1) Prior to tissue breakdown stromal cells of the endometrium have undergone decidualisation during the secretory phase of the menstrual cycle. **(2)** P4 withdrawal initiates menstruation and decidualised stromal tissue undergoes tissue breakdown and shedding leaving behind a denuded stromal surface. **(3)** Mesenchymal cells in the basal endometrium are stimulated to respond: stromal fibroblasts undergo MET and pericytes undergo PET to contribute to rapid re-epithelialisation. Pericytes may also undergo a pericyte-to-mesenchymal transition to replenish lost fibroblasts and regain tissue integrity. **(4)** Upon completion of repair, endometrial tissue is fully restored and cell populations return to homeostasis in preparation for the subsequent menstrual cycle

6.4 Future prospects of the studies outlined in this thesis

6.4.1 Lineage tracing mesenchymal cells in endometrial repair

Although evidence for MET during endometrial repair has been gathered the tools used in this thesis are inadequate to definitively conclude that this mechanisms takes place. When analysing *Pdgfrβ-BAC-eGFP* uterine tissue 48hrs after P4 withdrawal, cells that express both stromal and epithelial cell markers were not detected by either flow cytometry or IHC. This is because the *Pdgfrβ-BAC-eGFP* transgenic line is a knock-in reporter system and therefore if the Pdgfrβ gene promoter is 'switched off' as it would be in a fully transformed epithelial cell, GFP expression is lost. This means there is no historic evidence of the origin of new epithelial cells if they have in fact arisen from the mesenchymal cell compartment. A definitive conclusion therefore cannot be drawn without employing an inducible-Cre system to specifically target each mesenchymal subpopulation individually and solidify current results. The principles of inducible Cre technology is outlined in Figure 6-8 (A-C).

As discussed above in chapter 4, NG2 was identified as a pericyte specific marker and the *NG2-CreER^{TM} BAC* transgenic mouse line has already been acquired and initial investigations have highlighted it as a promising tool with which to lineage trace pericytes in particular. Further analysis of the single cell sequencing has confirmed that NG2 is most highly expressed in the pericyte population, making it an ideal candidate for lineage tracing (Figure 6-8 (D)). To further decipher the origin of the intermediate cells a lineage tracing strategy for the stromal fibroblasts is also required. Analysis of the single cell sequencing dataset has identified that Pdgfrα is expressed exclusively by the stromal fibroblasts (Figure 6-8 (E)). Through a collaboration with Professor Neil Henderson an inducible *Pdgfrα-CreERT* line has also been acquired and will be used in future lineage tracing experimentation to determine the specific contribution of stromal fibroblasts to endometrial repair.

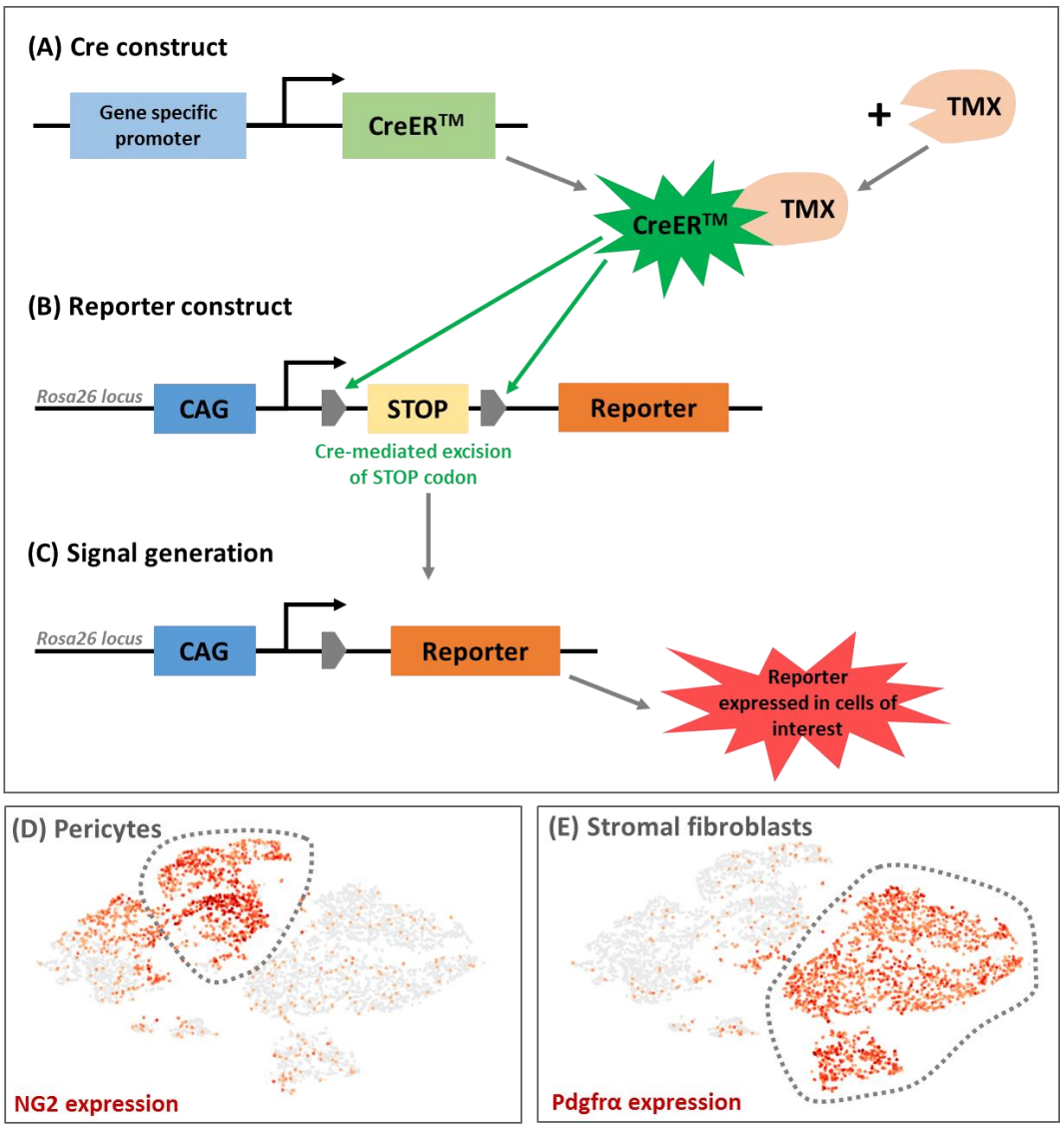

Figure 6-8. Schematic representation of the principles behind the inducible-cre system for lineage tracing. (A) The Cre construct is composed of CreER^{TM} that contains the mouse oestrogen receptor ligand binding domain with a mutation that only allows the ligand tamoxifen to bind, under control of the promoter region of a gene of interest. When this promoter is active and the GOI is transcribed this gives gene-specific expression of CreER^{TM}. CreER^{TM} is only activated when tamoxifen (TMX) is administered and binds, translocating the CreER^{TM}:TMX complex to the nucleus. **(B)** The reporter construct is located in the broadly expressed ROSA26 locus and contains a loxP-flanked STOP codon upstream of a reporter gene (fluorescent protein) under control of the ubiquitously expressed CAG promoter. Following TMX administration, activated Cre recombines the loxP-flanked STOP codon leading to its excision and **(C)** downstream expression of the reporter protein and signal generation. This technique allows for the spatio-temporal control of reporter proteins that then 'tattoo' the cells of interest indefinitely. The single cell sequencing dataset of mesenchymal cells from naïve endometrial tissue can be analysed to show exclusive expression of **(D)** NG2 by pericytes and **(E)** Pdgfrα by stromal fibroblasts highlighting these genes as promising reporter systems for each cell type for use in downstream lineage tracing experiments.

Lineage tracing has been used to demonstrate MET in the endometrium following artificially induced menstruation and natural parturition in mice (Huang et al. 2012, Patterson et al. 2013) however these studies made use of the constitutive-Cre system (*Amhr2-Cre: R26R*) and therefore this strategy does not rule out the effects of Cre expression that may have occurred during development. Similarly constitutive-Cre expression may have toxic side effects associated with prolonged Cre activity which should be taken into account when examining these tissues. The advantages of employing an inducible-Cre system is it allows for strict spatial and temporal control over Cre activity which results in irreversible labelling of a cell population of interest and it is very fast acting upon Tamoxifen administration. Disadvantages must also be noted: the transgene may be influenced by the integration site and there is potential toxicity of both the Cre and Tamoxifen which should be accounted for as well as potential leakiness of the Cre (Feil, Valtcheva and Feil 2009). What is more, Tamoxifen is an antagonist for the oestrogen receptor which will therefore impact on oestrogen-dependent endometrial tissue growth (Goodsell 2002) and the ability to upregulate PR expression in response to E2. Bearing this in mind, before using the inducible-Cre lines outlined above (*NG2-CreER^{TM} BAC*, *Pdgfrα-CreERT*), various optimisation experiments will need to be undertaken to confirm specificity of each line and ensure side effects are controlled for. Once control experiments are completed it is hoped these two transgenic lines will allow for discrimination between two potential origins of MET transformed epithelial cells identified in endometrial repair.

Such genetic tools would also allow for genetic ablation studies whereby the Cre lines are crossed with a floxed DTR line and upon administration of diptheria toxin the cells would be ablated. This approach would allow for new insights into how essential specific cell populations are to endometrial repair. Furthermore, conditional gene knockout studies could be carried out by crossing the Cre lines with floxed mouse lines targeting genes of interest to facilitate the identification of new therapeutic targets. With these tools in place various unanswered questions could be addressed: do pericytes represent a true progenitor cell population in the endometrium? Do all pericytes/stromal cells have the ability to undergo PET/MET during endometrial repair or is a specific subset responsible? What signals are important in regulating this

response? Can the endometrial healing response be further enhanced? Such studies would further advance our understanding of the scarless healing response.

6.4.2 Analysis of a fibrotic response in endometrial tissues

Another interesting aspect to this work is the relationship between cell phenotype and development of fibrosis. In other tissues pericytes and fibroblasts are reported to undergo a FMT during wound healing which is essential for the synthesis of ECM proteins and contraction of the wound: in the case of aberrant repair the persistence of myofibroblasts results in ECM accumulation and formation of persistent scar tissue (Leavitt et al. 2016, Hinz et al. 2012). Both bulk mRNA sequencing and single cell sequencing studies outlined in this thesis highlighted drastic changes in the expression of collagens during endometrial repair. To complement and extend the main studies in this thesis a preliminary investigation of the expression of collagens in endometrial tissues was conducted using PSR staining, and the myofibroblast phenotype was investigated by IHC looking at the well described MF marker (αSMA). Interestingly there was a striking change in the pattern of collagen deposition whereby in normal endometrium the myometrium was composed of dense collagen I fibres and the stroma composed of loose collage III fibres, while in the repairing endometrium the myometrium was still composed of dense collagen I fibres however, the regions of stroma undergoing repair and underlying new epithelium were collagen negative (Figure 6-9).

In addition, a population GFP+αSMA+ cells were located in endometrial tissue at 24hrs, predominantly located in regions of stroma adjacent to the denuded surface and undergoing active repair, indicative of a myofibroblast phenotype (Figure 6-10). As endometrial repair shares common features with wound healing it is not unexpected to identify an FMT occurring here. Interestingly however, myofibroblast-like cells (GFP+αSMA+) were located in collagen negative regions of tissue. These results together suggest that an FMT is taking place during endometrial repair however the resulting myofibroblast-like cells do not display the functional characteristics of true myofibroblasts in that they have decreased ECM synthesis properties. The phenotype of adult skin myofibroblasts has been shown to be altered by application of UCMSC-conditioned media whereby they displayed characteristics of foetal

fibroblasts: a decreased expression of αSMA, decreased TGFβ1:3 ratio and increased expression of MMPs. Wounds treated with the same media were shown to heal faster and have decreased collagen accumulation (Li et al. 2017). Myofibroblasts in the endometrium therefore may exhibit similar properties to foetal myofibroblasts, A host of cytokines, growth factors, hypoxia and ECM components have been implicated in the regulation of FMT (Leavitt et al. 2016) it is therefore proposed that strict control of these factors in the human endometrium may alter myofibroblast phenotype therefore underpin its ability to restrict deposition of collagen which may be integral the endometrium's ability to heal month on month without scarring. This area of research warrants further investigation once the new transgenic lines have been established.

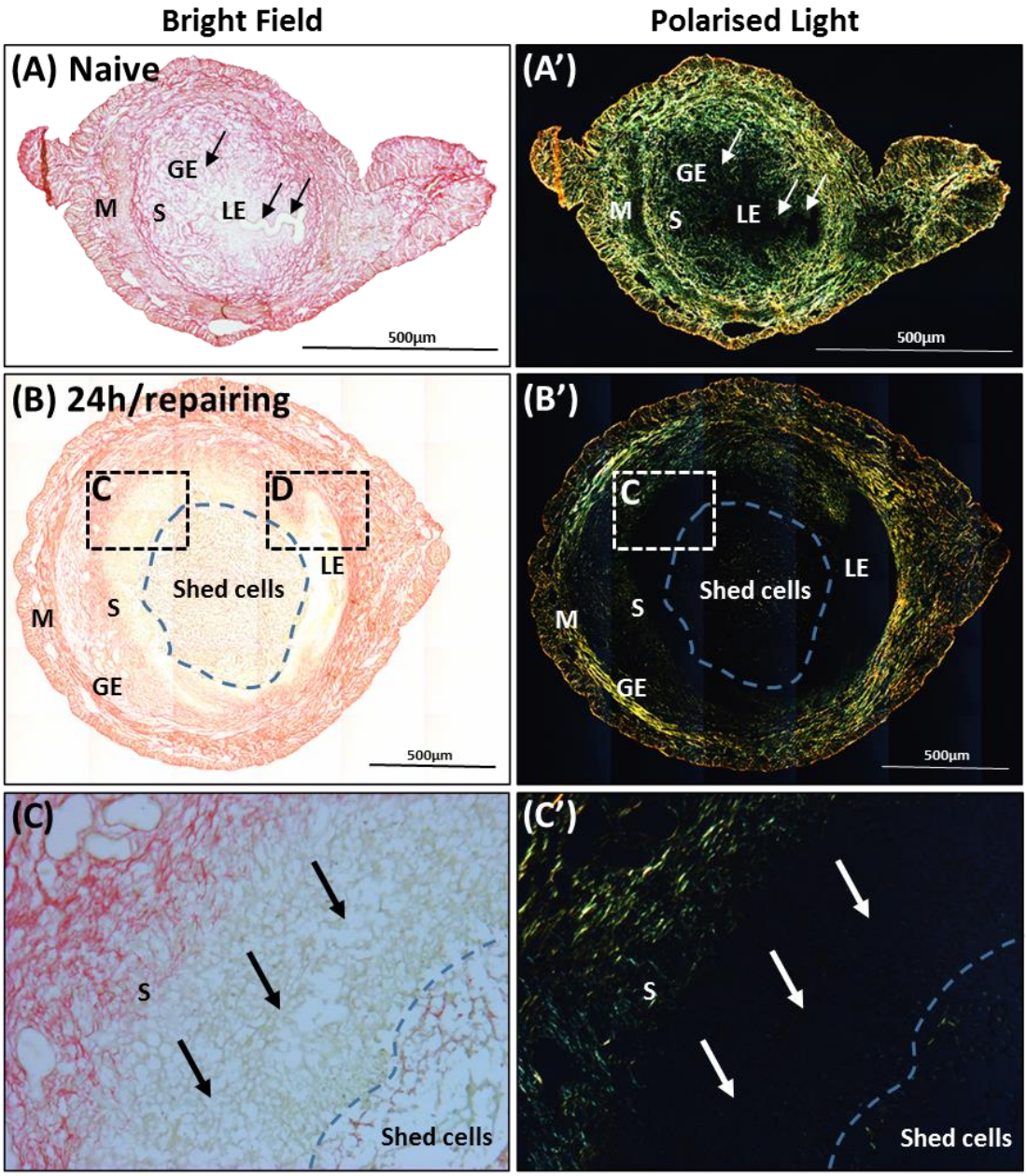

Figure 6-9. PSR staining to visualise collagen content of both naïve and repairing (24hrs) uterine tissues. Brightfield images of **(A)** naïve uterus and **(B)** repairing 24hrs uterus showing collagen positive regions in red/pink and collagen negative regions in yellow/white. Polarised light images of **(A')** naïve uterus and **(B')** repairing 24hrs uterus showing collagen I bundles in yellow/orange and collagen III bundles in green. **(C-C')** Brightfield and polarised light images of regions of endometrium undergoing active tissue repair (arrows). Myometrium (M), Stroma (S), Luminal Epithelium (LE), Glandular Epithelium (GE) and shed cells (blue dashed line) (representative images, n=5, scale bar = 500µm).

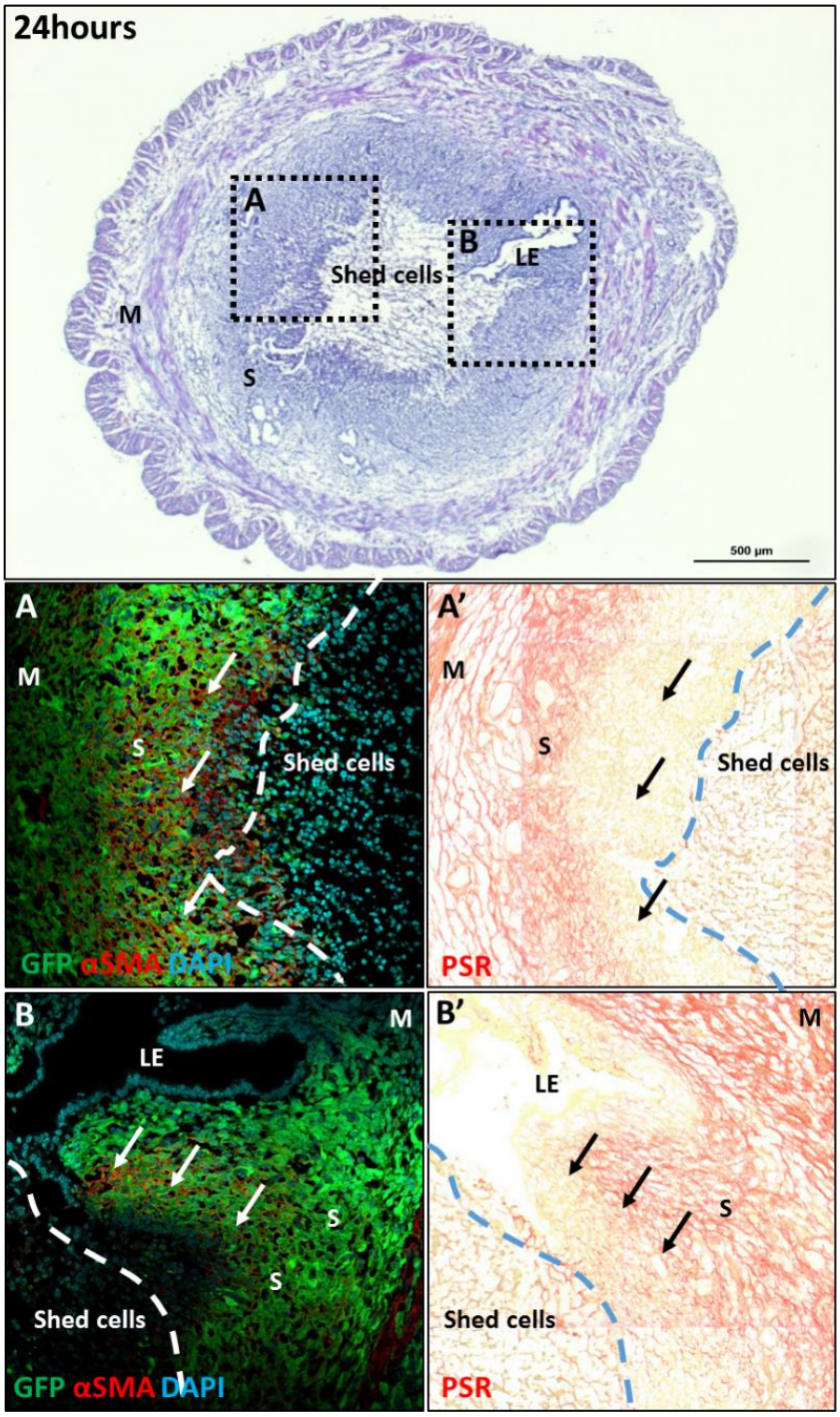

Figure 6-10. The expression of GFP and αSMA in *Pdgfrβ-BAC-eGFP* uterine tissues at 24hrs and the association with collagen deposition. (A-B) IHC staining for GFP (green) and αSMA (red) showing GFP+aSMA+ cells (white arrows) in the functional stromal region close to the degrading decidua (dashed line). **(A'-B')** PSR stain showing collagen positive regions (red/pink) in the myometrium and endometrial stroma adjacent to this and collagen negative regions (yellow/white) of the endometrial stroma in close proximity to the denuded stromal surface and shed tissue. Myometrium (M), stroma (S), luminal epithelium (LE) (representative images, n=5, scale bar = 500µm)

6.4.3 How can these results inform our understanding of the mechanisms of postpartum endometrial repair?

In the initial planning stages of this project it was hoped to investigate the repair processes that occur in the postpartum uterus and compare these to mechanisms of post-menstrual repair, however due to time constraints this work was not started. It is believed that the menstrual cycle is an evolutionary mechanism that has arisen in order to precondition the uterine tissues to the physiological stresses associated with placentation and pregnancy (Brosens et al. 2009, Emera, Romero and Wagner 2012b). The degree of physiological tissue injury experienced by the uterus following parturition is much greater than that during menstruation as the placenta and membranes are completely shed exposing much larger area of denuded stroma. Despite this major difference it has been proposed that repair mechanisms are broadly similar (Brosens et al. 2009). In women the postpartum period begins immediately after delivery of the infant and placenta and continues for 6-8 weeks as physiological changes return to baseline (Plunk et al. 2013). This period is known as uterine involution which requires ECM remodelling, cellular proliferation and apoptosis to allow the uterus to return to its pre-pregnant state (Takamoto, Leppert and Yu 1998).

Due to the difficulties in sampling tissues from these time phases, the molecular mechanisms underlying postpartum repair and uterine involution in women remain relatively unknown (Salamonsen 2003b) although a number of studies have been carried out in animal models that highlight a role for myometrial contraction, hypoxia, ECM remodelling, inflammation and progenitor cells (Sharman 1952, Thomson et al. 1999, Yoshii et al. 2014, Hsu et al. 2014, Huang et al. 2012, Cao et al. 2015). Studying postpartum repair in rodents has the potential to inform human biology as the mouse and rat also have a haemochorial type of placentation and go through similar dramatic changes in cellular organisation during pregnancy and following parturition (Yoshii et al. 2014, Cao et al. 2015). Defects in postpartum repair may underlie issues such as postpartum haemorrhage, subfertility, miscarriage and recurrent pregnancy loss. The new understanding and genomic datasets developed in the current thesis could easily be translated to studies investigating postpartum endometrial repair in mice and offer the potential to inform our understanding of postpartum endometrial repair in women.

6.4.4 Cross disciplinary research studies

The human endometrium represents the only adult tissue to undergo regular and repeated cycles of degeneration and regeneration under normal physiological conditions (Gargett and Masuda 2010). Similarities exist between menstrual endometrial tissue repair and scar-free wound healing observed in both foetal skin and the oral mucosa including extensive cellular proliferation, matrix deposition and re-epithelialisation, however in these tissues it is believed that a diminished inflammatory response and altered fibroblast phenotype are responsible for the scar-free healing response, two mechanisms which have not been definitively observed in the endometrium (Szpaderska et al. 2003, Martin and Leibovich 2005, Leavitt et al. 2016). Parallels can also be drawn with the wound healing response of the epidermis including the migration of fibroblasts, inflammation, re-epithelialisation and tissue remodelling, the biggest difference being that the endometrium does not synthesise scar tissue during repair (Shaw and Martin 2009, Leavitt et al. 2016, Critchley et al. 2006a). The endometrium therefore may represent a tissue that employs a mix of mechanisms characteristic of scarless and scarring tissue repair and could therefore be used as model system to inform both processes.

The research outlined in this thesis has scope for developing into further cross-disciplinary studies, in particular comparing mechanisms of endometrial repair with mechanisms that contribute to the progression of fibrosis in response to repeated injury in other tissues such as the skin, liver and kidney. If we can understand the relationship between cell types in the endometrium and how they work together to ensure scarless healing this knowledge could be applied to other tissue systems: comparing intrinsic properties of different cell types and the signals from the microenvironment which influences cell phenotype and function. These studies would highlight targets that might allow for *in situ* manipulation of cellular responses during fibrosis and scarring or maybe identify a cell population that could be used in adoptive transfer experiments to alleviate fibrosis (endometrial pericytes?). In particular the single cell dataset generated using mesenchymal cells from naive and repairing endometrial tissues, can be directly compared with similar datasets generated by Professor Neil Henderson's laboratory using comparable techniques to investigate mesenchymal cell changes in the liver, kidney and heart. Bioinformatic data analysis

may reveal differences in mesenchymal cell phenotype or function specific to each wound healing/non-healing response and therefore identify targets for future use. Of particular interest is to identify a factor which when manipulated may alleviate fibrosis in the liver/kidney or induce a fibrotic response in the endometrium. Cross disciplinary studies comparing the endometrium to other tissues will also help to reliably place the endometrium in the wound healing continuum and validate its use as a model in which to uncover mechanisms of scarless tissue repair.

6.5 Translational aspects for patient benefit

Restoration of uterine tissue homeostasis following menstruation must be rapid and complete to ensure continued functional success of the uterus. It is believed that aberrant endometrial repair may predispose to several gynaecological conditions including heavy menstrual bleeding, Asherman's syndrome and endometriosis (Dimitrov et al. 2008). Despite the prevalence and health burden that these conditions pose, and extensive research their aetiology and pathogenesis remain poorly understood (Gargett and Chan 2006). For each condition a link to dysregulated macrophage function has been suggested. Careful characterisation of macrophage phenotype and function in physiological endometrial repair and proliferative disorders therefore may inform the development of therapies to treat such conditions. Similarly, because MSCs/stem/progenitor cells are believed to play a key role in physiological endometrial repair it has been suggested that abnormalities in the location and/or function of endometrial stem/progenitor cells may contribute to both the development and persistence of various gynaecological conditions (Deane et al. 2013, Dimitrov et al. 2008). Understanding the role of stem/progenitor cells in endometrial physiology and the pathogenesis of these diseases is considered as a key opportunity in the discovery of new treatment options.

As previously discussed, cross disciplinary studies may highlight important similarities and differences between wound healing responses of the endometrium and other tissues. Further investigation of the contribution of stem/progenitor cells and/or macrophages to the scar-free repair process exhibited by endometrial tissue may identify these cells as targets in conditions where chronic inflammation and excessive fibrosis are a problem. Such knowledge would inform the development of cell-based

therapies or treatments chronic inflammation, fibrosis and excessive scarring that effects many adult tissues including the liver, kidney, skin and heart. These conditions present a huge burden on public health and are believed to be due to aberrant wound healing and although recent advances have been made with regards to stem cell biology, a lack of a standardised model hinders translation of this knowledge (Leavitt et al. 2016). Defining which cells and signals truly promotes scarless endometrial wound healing *in vivo* will improve translatability of findings and aid in discovery of treatment options for various fibrotic conditions.

Stem cell based therapies have been found to accelerate wound closure and encourage tissue regeneration of the skin and other tissues (Lee, Ayoub and Agrawal 2016), through both differentiation and production of pro-repair and anti-inflammatory factors (Wu et al. 2007, Leavitt et al. 2016). For example, amniotic fluid-derived MSCs have been shown to rescue renal function and resolve fibrosis when injected into the renal artery in a preclinical porcine model of renal transplantation (Baulier et al. 2014). In addition, transplantation of BM-MSCs on collagen scaffolds have shown promise in enhancing regeneration of injured uterine tissue in rats (Ding et al. 2014). A more recent study in which umbilical cord MSC-conditioned media was applied to dermal fibroblasts induced a phenotype that was reminiscent of foetal fibroblasts believed to be consistent with scar-free wound healing. When mouse full-thickness skin wounds were treated with this media they showed enhanced wound healing and decreased collagen formation (Li et al. 2017). MSCs are multipotent and can differentiate into various mesodermal cell lineages and have potential use in both autologous and allogenic transplantation as they are immunologically silent (Tamama and Kerpedjieva 2012) making them ideal candidates in the development of various cell-based therapies to tackle scarring in disease.

If the endometrial pericytes identified and characterised in this thesis are found to have regenerative MSC-like properties then they could be used in future cell-based therapies. Notably endometrial pericytes can be obtained from routine endometrial biopsies or menstrual effluent in an outpatient setting and without the need for anaesthetic (Masuda et al. 2010, Maybin and Critchley 2015) offering the potential that they could replace the need for painful bone marrow biopsies currently used to

obtain haematopoietic stem cells (Maybin and Critchley 2015). To support this idea it is worth noting, the application of human umbilical cord pericytes embedded in a fibrin gel to full thickness cutaneous wounds showed improved re-epithelialisation, greater tensile strength, more organised collagen fibres and enhanced angiogenesis (Zebardast et al. 2010). Similarly pericytes from adipose tissue have been shown to increase vascularisarion, promote collagen deposition and enhance remodelling in an excisional wound model (Paquet-Fifield et al. 2009). Finally pericytes have been shown to enhance epidermal regeneration in an organotypic skin culture model (Zamora et al. 2013). Endometrial MSCs/pericytes are highly proliferative (Gargett et al. 2009) so would be ideal candidates for *in vitro* expansion and use in cell-based therapies, the endometrium therefore provides a readily accessible source of cells that could have widespread clinical applications in the future.

6.6 Concluding remarks

Using transgenic mouse lines and the robust Edinburgh mouse model of endometrial breakdown and repair the contribution of both myeloid immune cells and mesenchymal progenitor cells to endometrial repair has been investigated. New data identified dynamic changes in the number and localisation of mononuclear phagocytes in regions of endometrial tissue undergoing active repair, with a previously unknown role for alternative monocytes. Furthermore complex heterogeneity in the monocyte/macrophage population has been revealed associated with discrete regions of the repairing tissue, which may have functional implications for endometrial repair processes. Additional characterisation of these monocyte/macrophage subpopulations may give insight into the role of unique heterogeneity in scar-free tissue repair.

This is also the first study to characterise a perivascular pericyte population in the mouse endometrium and define NG2 as a pericyte specific marker in this tissue. It is suggested that endometrial pericytes represent a mesenchymal progenitor cell population that have important roles in re-epithelialisation during endometrial repair, undergoing a pericyte-to-epithelial transition (PET) in concert with other mechanisms to rapidly reinstate the epithelial cell layer. Progenitor cells are the immediate progeny of tissue stem cells and the true stem cell population that gives rise to pericytes in the endometrium remains to be determined. Single cell sequencing had identified novel

heterogeneity within the endometrial pericyte population revealing that methods commonly used to target mesenchymal stem cells (MSCs) may in fact be identifying both MSCs/pericytes and vSMCs. More definitive markers are therefore required to discriminate between cell populations. Having determined robust methods of identification and isolation, future studies will focus on functional characteristics of these cells, lineage tracing and targeted inhibition/stimulation studies to more thoroughly understand their role in endometrial breakdown and repair.

The endometrium provides a robust physiological model in which to study various mechanisms associated with tissue repair including inflammation, angiogenesis and differentiation. Studies like those presented in this thesis are important to inform future work and fill gaps in the knowledge so that one day we can uncover mechanisms essential to scarless tissue repair and use these as the basis for novel therapies.

References

Van der Horst Abramsson, A., P. Lindblom & C. Betsholtz (2003) Endothelial and nonendothelial sources of PDGF-B regulate pericyte recruitment and influence vascular pattern formation in tumors. *J Clin Invest,* 112**,** 1142-51.

Acharya, K. R. & S. J. Ackerman (2014) Eosinophil granule proteins: form and function. *J Biol Chem,* 289**,** 17406-15.

Acosta, A. A., L. Elberger, M. Borghi, J. C. Calamera, H. Chemes, G. F. Doncel, H. Kliman, B. Lema, L. Lustig & S. Papier (2000) Endometrial dating and determination of the window of implantation in healthy fertile women. *Fertil Steril,* 73**,** 788-98.

Adams, R. H. & K. Alitalo (2007) Molecular regulation of angiogenesis and lymphangiogenesis. *Nat Rev Mol Cell Biol,* 8**,** 464-78.

Aerts, J. L., M. R. Christiaens & P. Vandekerckhove (2002) Evaluation of progesterone receptor expression in eosinophils using real-time quantitative PCR. *Biochim Biophys Acta,* 1571**,** 167-72.

Agarwal, S., N. P. Piesco, L. P. Johns & A. E. Riccelli (1995) Differential expression of IL-1 beta, TNF-alpha, IL-6, and IL-8 in human monocytes in response to lipopolysaccharides from different microbes. *J Dent Res,* 74**,** 1057-65.

Aghajanova, L., S. Houshdaran, S. Balayan, E. Manvelyan, J. C. Irwin, H. G. Huddleston & L. C. Giudice (2018) In vitro evidence that platelet-rich plasma stimulates cellular processes involved in endometrial regeneration. *J Assist Reprod Genet*.

Ahmed, T. A. & N. El-Badri (2017) Pericytes: The Role of Multipotent Stem Cells in Vascular Maintenance and Regenerative Medicine. *Adv Exp Med Biol.*

Akamatsu, T., Y. Arai, I. Kosugi, H. Kawasaki, S. Meguro, M. Sakao, K. Shibata, T. Suda, K. Chida & T. Iwashita (2013) Direct isolation of myofibroblasts and fibroblasts from bleomycin-injured lungs reveals their functional similarities and differences. *Fibrogenesis Tissue Repair,* 6**,** 15.

Akoum, A., C. N. Metz, M. Al-Akoum & R. Kats (2006) Macrophage migration inhibitory factor expression in the intrauterine endometrium of women with endometriosis varies with disease stage, infertility status, and pelvic pain. *Fertil Steril,* 85**,** 1379-85.

Al-Alwan, L. A., Y. Chang, A. Mogas, A. J. Halayko, C. J. Baglole, J. G. Martin, S. Rousseau, D. H. Eidelman & Q. Hamid (2013) Differential roles of CXCL2 and CXCL3 and their receptors in regulating normal and asthmatic airway smooth muscle cell migration. *J Immunol,* 191**,** 2731-41.

Alawadhi, F., H. Du, H. Cakmak & H. S. Taylor (2014) Bone Marrow-Derived Stem Cell (BMDSC) transplantation improves fertility in a murine model of Asherman's syndrome. *PLoS One,* 9**,** e96662.

Allen, E. (1922) The oestrous cycle in the mouse. *American Journal of Anatomy,* 30**,** 297-371.

Anders, H. J. & M. Ryu Renal microenvironments and macrophage phenotypes determine progression or resolution of renal inflammation and fibrosis.

Andersson, E., E. Zetterberg, I. Vedin, K. Hultenby, J. Palmblad & M. Mints (2015) Low pericyte coverage of endometrial microvessels in heavy menstrual bleeding correlates with the microvessel expression of VEGF-A. *Int J Mol Med,* 35**,** 433-8.

Andreotti, J. P., A. E. Paiva, P. H. D. M. Prazeres, D. A. P. Guerra, W. N. Silva, R. S. Vaz, A. Mintz & A. Birbrair (2018) The role of natural killer cells in the uterine microenvironment during pregnancy. *Cell Mol Immunol*.

Ansell, D. M. & A. Izeta (2015) Pericytes in wound healing: friend or foe? *Exp Dermatol,* 24**,** 833-4.

Arantes, R. M., S. Lourenssen, C. R. Machado & M. G. Blennerhassett (2000) Early damage of sympathetic neurons after co-culture with macrophages: a model of neuronal injury in vitro. *Neuroreport,* 11**,** 177-81.

Armstrong, G. M., J. A. Maybin, A. A. Murray, M. Nicol, C. Walker, P. T. K. Saunders, A. G. Rossi & H. O. D. Critchley (2017) Endometrial apoptosis and neutrophil infiltration during menstruation exhibits spatial and temporal dynamics that are recapitulated in a mouse model. *Sci Rep,* 7**,** 17416.

Armulik, A., G. Genové & C. Betsholtz (2011) Pericytes: developmental, physiological, and pathological perspectives, problems, and promises. *Dev Cell,* 21**,** 193-215.

Arnal, J. F., C. Fontaine, A. Billon-Galés, J. Favre, H. Laurell, F. Lenfant & P. Gourdy (2010) Estrogen receptors and endothelium. *Arterioscler Thromb Vasc Biol,* 30**,** 1506-12.

Ashcroft, G. S., T. Greenwell-Wild, M. A. Horan, S. M. Wahl & M. W. Ferguson (1999) Topical estrogen accelerates cutaneous wound healing in aged humans associated with an altered inflammatory response. *Am J Pathol,* 155**,** 1137-46.

Ashcroft, G. S. & S. J. Mills (2002) Androgen receptor-mediated inhibition of cutaneous wound healing. *J Clin Invest,* 110**,** 615-24.

Ashcroft, G. S., S. J. Mills, K. Lei, L. Gibbons, M. J. Jeong, M. Taniguchi, M. Burow, M. A. Horan, S. M. Wahl & T. Nakayama (2003) Estrogen modulates cutaneous wound healing by downregulating macrophage migration inhibitory factor. *J Clin Invest,* 111**,** 1309-18.

Bacci, M., A. Capobianco, A. Monno, L. Cottone, F. Di Puppo, B. Camisa, M. Mariani, C. Brignole, M. Ponzoni, S. Ferrari, P. Panina-Bordignon, A. A. Manfredi & P. Rovere-Querini (2009) Macrophages are alternatively activated in patients with endometriosis and required for growth and vascularization of lesions in a mouse model of disease. *Am J Pathol,* 175**,** 547-56.

Bach, S. P., A. G. Renehan & C. S. Potten (2000) Stem cells: the intestinal stem cell as a paradigm. *Carcinogenesis,* 21**,** 469-76.

Baggish, M. S., C. J. Pauerstein & J. D. Woodruff (1967) Role of stroma in regeneration of endometrial epithelium. *Am J Obstet Gynecol,* 99**,** 459-65.

Bahou, W. F. & D. V. Gnatenko (2004) Platelet transcriptome: the application of microarray analysis to platelets. *Semin Thromb Hemost,* 30**,** 473-84.

Balic, A., C. Garcia-Morales, L. Vervelde, H. Gilhooley, A. Sherman, V. Garceau, M. W. Gutowska, D. W. Burt, P. Kaiser, D. A. Hume & H. M. Sang (2014) Visualisation of chicken macrophages using transgenic reporter genes: insights into the development of the avian macrophage lineage. *Development,* 141**,** 3255-65.

Ballhause, T. M., R. Soldati & P. R. Mertens (2014) Sources of myofibroblasts in kidney fibrosis: all answers are correct, however to different extent! *Int Urol Nephrol,* 46**,** 659-64.

Bartelmez, G. W. (1957) The phases of the menstrual cycle and their interpretation in terms of the pregnancy cycle. *Am J Obstet Gynecol,* 74**,** 931-55.

Bates, G. W. & M. Bowling (2013) Physiology of the female reproductive axis. *Periodontol 2000,* 61**,** 89-102.

Battersby, S., S. C. Boddy, H. O. Critchley & H. N. Jabbour (2002) Expression and localization of endothelial monocyte-activating polypeptide II in the human endometrium across the menstrual cycle: regulation of expression by prostaglandin E(2). *J Clin Endocrinol Metab,* 87**,** 3928-35.

Baulier, E., F. Favreau, A. Le Corf, C. Jayle, F. Schneider, J. M. Goujon, O. Feraud, A. Bennaceur-Griscelli, T. Hauet & A. G. Turhan (2014) Amniotic fluid-derived mesenchymal stem cells prevent fibrosis and preserve renal function in a preclinical porcine model of kidney transplantation. *Stem Cells Transl Med,* 3**,** 809-20.

Beckman, D. A. & M. Feuston (2003) Landmarks in the development of the female reproductive system. *Birth Defects Res B Dev Reprod Toxicol,* 68**,** 137-43.

Bellofiore, N., F. Cousins, P. Temple-Smith, H. Dickinson & J. Evans (2018) A missing piece: the spiny mouse and the puzzle of menstruating species. *J Mol Endocrinol,* 61**,** R25-R41.

Bellofiore, N., S. J. Ellery, J. Mamrot, D. W. Walker, P. Temple-Smith & H. Dickinson (2017) First evidence of a menstruating rodent: the spiny mouse (Acomys cahirinus). *Am J Obstet Gynecol,* 216**,** 40.e1-40.e11.

Berbic, M., C. H. Ng & I. S. Fraser (2014) Inflammation and endometrial bleeding. *Climacteric,* 17 Suppl 2**,** 47-53.

Berbic, M., L. Schulke, R. Markham, N. Tokushige, P. Russell & I. S. Fraser (2009) Macrophage expression in endometrium of women with and without endometriosis. *Hum Reprod,* 24**,** 325-32.

Bergers, G. & S. Song (2005) The role of pericytes in blood-vessel formation and maintenance. *Neuro Oncol,* 7**,** 452-64.

Bhartiya, D. (2016) An update on endometrial stem cells and progenitors. *Human Reproduction Update,* 22**,** 529-531.

Bianco, P., M. Riminucci, S. Gronthos & P. G. Robey (2001) Bone marrow stromal stem cells: nature, biology, and potential applications. *Stem Cells,* 19**,** 180-92.

Bickers, W. (1944) Regeneration of the monkey uterus after surgical removal of the endometrium and accidental endometriosis. *American Journal of Obstetrics & Gynecology,* 48**,** 440.

Biswas Shivhare, S., J. N. Bulmer, B. A. Innes, D. K. Hapangama & G. E. Lash (2015) Menstrual cycle distribution of uterine natural killer cells is altered in heavy menstrual bleeding. *J Reprod Immunol,* 112**,** 88-94.
Biswas, S. K., M. Chittezhath, I. N. Shalova & J. Y. Lim (2012) Macrophage polarization and plasticity in health and disease. *Immunol Res,* 53**,** 11-24.
Bodnar, R. J., L. Satish, C. C. Yates & A. Wells (2016) Pericytes: A newly recognized player in wound healing. *Wound Repair Regen,* 24**,** 204-14.
Bonasio, R. & U. H. von Andrian (2006) Generation, migration and function of circulating dendritic cells. *Curr Opin Immunol,* 18**,** 503-11.
Bonatz, G., M. L. Hansmann, F. Buchholz, L. Mettler, H. J. Radzun & K. Semm (1992) Macrophage- and lymphocyte-subtypes in the endometrium during different phases of the ovarian cycle. *Int J Gynaecol Obstet,* 37**,** 29-36.
Brasted, M., C. A. White, T. G. Kennedy & L. A. Salamonsen (2003) Mimicking the events of menstruation in the murine uterus. *Biol Reprod,* 69**,** 1273-80.
Brenner, R. M., L. Rudolph, L. Matrisian & O. D. Slayden (1996) Non-human primate models; artificial menstrual cycles, endometrial matrix metalloproteinases and s.c. endometrial grafts. *Hum Reprod,* 11 Suppl 2**,** 150-64.
Brenner, R. M. & O. D. Slayden (2012) Molecular and functional aspects of menstruation in the macaque. *Rev Endocr Metab Disord,* 13**,** 309-18.
Brosens, J. J., M. G. Parker, A. McIndoe, R. Pijnenborg & I. A. Brosens (2009) A role for menstruation in preconditioning the uterus for successful pregnancy. *Am J Obstet Gynecol,* 200**,** 615.e1-6.
Bulmer, J. N. & G. E. Lash (2005) Human uterine natural killer cells: a reappraisal. *Mol Immunol,* 42**,** 511-21.
Burghardt, R. C. & R. Droleskey (2006) Transmission electron microscopy. *Curr Protoc Microbiol,* Chapter 2**,** Unit 2B.1.
Butts, C. L., E. Bowers, J. C. Horn, S. A. Shukair, E. Belyavskaya, L. Tonelli & E. M. Sternberg (2008) Inhibitory effects of progesterone differ in dendritic cells from female and male rodents. *Gend Med,* 5**,** 434-47.
Byers, S. L., M. V. Wiles, S. L. Dunn & R. A. Taft (2012) Mouse estrous cycle identification tool and images. *PLoS One,* 7**,** e35538.
Bühring, H. J., V. L. Battula, S. Treml, B. Schewe, L. Kanz & W. Vogel (2007) Novel markers for the prospective isolation of human MSC. *Ann N Y Acad Sci,* 1106**,** 262-71.
Calandra, T. & R. Bucala (1995) Macrophage migration inhibitory factor: a counter-regulator of glucocorticoid action and critical mediator of septic shock. *J Inflamm,* 47**,** 39-51.
Caligioni, C. S. (2009) Assessing reproductive status/stages in mice. *Curr Protoc Neurosci,* Appendix 4**,** Appendix 4I.
Campbell, L., E. Emmerson, F. Davies, S. C. Gilliver, A. Krust, P. Chambon, G. S. Ashcroft & M. J. Hardman (2010) Estrogen promotes cutaneous wound healing via estrogen receptor beta independent of its antiinflammatory activities. *J Exp Med,* 207**,** 1825-33.
Campbell, S., M. W. Seif, J. D. Aplin, S. J. Richmond, P. Haynes & T. D. Allen (1988) Expression of a secretory product by microvillous and ciliated cells of the human endometrial epithelium in vivo and in vitro. *Hum Reprod,* 3**,** 927-34.
Cano, E., V. Gebala & H. Gerhardt (2017) Pericytes or Mesenchymal Stem Cells: Is That the Question? *Cell Stem Cell,* 20**,** 296-297.
Canosa, S., A. Moggio, A. Brossa, G. Pittatore, G. L. Marchino, S. Leoncini, C. Benedetto, A. Revelli & B. Bussolati (2017) Angiogenic properties of endometrial mesenchymal stromal cells in endothelial co-culture: an in vitro model of endometriosis. *Mol Hum Reprod,* 23**,** 187-198.
Cao, M., R. W. Chan & W. S. Yeung (2015) Label-retaining stromal cells in mouse endometrium awaken for expansion and repair after parturition. *Stem Cells Dev,* 24**,** 768-80.
Cao, W., K. Mah, R. S. Carroll, O. D. Slayden & R. M. Brenner (2007) Progesterone withdrawal up-regulates fibronectin and integrins during menstruation and repair in the rhesus macaque endometrium. *Hum Reprod,* 22**,** 3223-31.
Caplan, A. I. (2008) All MSCs are pericytes? *Cell Stem Cell,* 3**,** 229-30.
Cash, J. L. & P. Martin (2016) Myeloid Cells in Cutaneous Wound Repair. *Microbiol Spectr,* 4.
Castella, L. F., L. Buscemi, C. Godbout, J. J. Meister & B. Hinz (2010) A new lock-step mechanism of matrix remodelling based on subcellular contractile events. *J Cell Sci,* 123**,** 1751-60.
Catalano, R. D., H. O. Critchley, O. Heikinheimo, D. T. Baird, D. Hapangama, J. R. Sherwin, D. S. Charnock-Jones, S. K. Smith & A. M. Sharkey (2007) Mifepristone induced progesterone

withdrawal reveals novel regulatory pathways in human endometrium. *Mol Hum Reprod,* 13**,** 641-54.
Cecchini, M. G., M. G. Dominguez, S. Mocci, A. Wetterwald, R. Felix, H. Fleisch, O. Chisholm, W. Hofstetter, J. W. Pollard & E. R. Stanley (1994) Role of colony stimulating factor-1 in the establishment and regulation of tissue macrophages during postnatal development of the mouse. *Development,* 120**,** 1357-72.
Cervelló, I., J. A. Martínez-Conejero, J. A. Horcajadas, A. Pellicer & C. Simón (2007) Identification, characterization and co-localization of label-retaining cell population in mouse endometrium with typical undifferentiated markers. *Hum Reprod,* 22**,** 45-51.
Cervelló, I., A. Mas, C. Gil-Sanchis, L. Peris, A. Faus, P. T. Saunders, H. O. Critchley & C. Simón (2011) Reconstruction of endometrium from human endometrial side population cell lines. *PLoS One,* 6**,** e21221.
Cervelló, I. & C. Simón (2009) Somatic stem cells in the endometrium. *Reprod Sci,* 16**,** 200-5.
Chan, R. W. & C. E. Gargett (2006) Identification of label-retaining cells in mouse endometrium. *Stem Cells,* 24**,** 1529-38.
Chan, R. W., T. Kaitu'u-Lino & C. E. Gargett (2012) Role of label-retaining cells in estrogen-induced endometrial regeneration. *Reprod Sci,* 19**,** 102-14.
Chan, R. W., K. E. Schwab & C. E. Gargett (2004) Clonogenicity of human endometrial epithelial and stromal cells. *Biol Reprod,* 70**,** 1738-50.
Chen, Y. T., F. C. Chang, C. F. Wu, Y. H. Chou, H. L. Hsu, W. C. Chiang, J. Shen, Y. M. Chen, K. D. Wu, T. J. Tsai, J. S. Duffield & S. L. Lin (2011) Platelet-derived growth factor receptor signaling activates pericyte-myofibroblast transition in obstructive and post-ischemic kidney fibrosis. *Kidney Int,* 80**,** 1170-81.
Cheng, Y., L. Li, D. Wang, Q. Guo, Y. He, T. Liang, L. Sun, X. Wang & G. Zhang (2017) Characteristics of Human Endometrium-Derived Mesenchymal Stem Cells and Their Tropism to Endometriosis. *Stem Cells Int,* 2017**,** 4794827.
Cho, N. H., Y. K. Park, Y. T. Kim, H. Yang & S. K. Kim (2004) Lifetime expression of stem cell markers in the uterine endometrium. *Fertil Steril,* 81**,** 403-7.
Christiaens, G. C., J.J. Sixma & A. A. Haspels (1980) Morphology of haemostasis in menstrual endometrium. *Br J Obstet Gynaecol.* 87: 425-39.
Christiaens, G. C., J.J. Sixma & A. A. Haspels (1983) Fibrin and platelets in menstrual discharge before and after the insertion of an intrauterine contraceptice device. *Am J Obstet Gynaecol.* 140:793-98.
Church, H. J., L. M. Vićovac, J. D. Williams, N. A. Hey & J. D. Aplin (1996) Laminins 2 and 4 are expressed by human decidual cells. *Lab Invest,* 74**,** 21-32.
Clancy, K. B. (2009) Reproductive ecology and the endometrium: physiology, variation, and new directions. *Am J Phys Anthropol,* 140 Suppl 49**,** 137-54.
Clark, D. A., S. Wang, P. Rogers, G. Vince & B. Affandi (1996) Endometrial lymphomyeloid cells in abnormal uterine bleeding due to levonorgestrel (Norplant). *Hum Reprod,* 11**,** 1438-44.
Clausen, B. E., C. Burkhardt, W. Reith, R. Renkawitz & I. Förster (1999) Conditional gene targeting in macrophages and granulocytes using LysMcre mice. *Transgenic Res,* 8**,** 265-77.
Cooke, V. G., V. S. LeBleu, D. Keskin, Z. Khan, J. T. O'Connell, Y. Teng, M. B. Duncan, L. Xie, G. Maeda, S. Vong, H. Sugimoto, R. M. Rocha, A. Damascena, R. R. Brentani & R. Kalluri (2012) Pericyte depletion results in hypoxia-associated epithelial-to-mesenchymal transition and metastasis mediated by met signaling pathway. *Cancer Cell,* 21**,** 66-81.
Coons, A. H., H. J. Creech & R. N. Jones (1941) Immunological Properties of an Antibody Containing a Fluorescent Group. *Proceedings of the Society for Experimental Biology and Medicine,* 47**,** 200-202.
Corwin, E. J. (1997) Endometriosis: pathophysiology, diagnosis, and treatment. *Nurse Pract,* 22**,** 35-8, 40-2, 45-6, passim; quiz 56-7.
Coudyzer, P., P. Lemoine, B. F. Jordan, B. Gallez, C. Galant, M. Nisolle, P. J. Courtoy, P. Henriet & E. Marbaix (2013) Hypoxia is not required for human endometrial breakdown or repair in a xenograft model of menstruation. *FASEB J,* 27**,** 3711-9.
Coudyzer, P., P. Lemoine, C. Po, B. F. Jordan, P. Van Der Smissen, P. J. Courtoy, P. Henriet & E. Marbaix (2015) Induction of post-menstrual regeneration by ovarian steroid withdrawal in the functionalis of xenografted human endometrium. *Hum Reprod,* 30**,** 1156-68.
Couse, J. F. & K. S. Korach (1999) Estrogen receptor null mice: what have we learned and where will they lead us? *Endocr Rev,* 20**,** 358-417.

Cousins, F. L., P. M. Kirkwood, A. a. Murray, F. Collins, D. a. Gibson & P. T. K. Saunders (2016b) Androgens regulate scarless repair of the endometrial "wound" in a mouse model of menstruation. *FASEB Journal,* 30**,** 2802-2811.

Cousins, F. L., P. M. Kirkwood, P. T. Saunders & D. A. Gibson (2016c) Evidence for a dynamic role for mononuclear phagocytes during endometrial repair and remodelling. *Sci Rep,* 6**,** 36748.

Cousins, F. L., A. Murray, A. Esnal, D. A. Gibson, H. O. Critchley & P. T. Saunders (2014) Evidence from a mouse model that epithelial cell migration and mesenchymal-epithelial transition contribute to rapid restoration of uterine tissue integrity during menstruation. *PLoS One,* 9**,** e86378.

Cousins, F. L., A. A. Murray, J. P. Scanlon & P. T. Saunders (2016d) Hypoxyprobe™ reveals dynamic spatial and temporal changes in hypoxia in a mouse model of endometrial breakdown and repair. *BMC Res Notes,* 9**,** 30.

Crisan, M., C. W. Chen, M. Corselli, G. Andriolo, L. Lazzari & B. Péault (2009) Perivascular multipotent progenitor cells in human organs. *Ann N Y Acad Sci,* 1176**,** 118-23.

Crisan, M., M. Corselli, W. C. Chen & B. Péault (2012) Perivascular cells for regenerative medicine. *J Cell Mol Med,* 16**,** 2851-60.

Crisan, M., S. Yap, L. Casteilla, C. W. Chen, M. Corselli, T. S. Park, G. Andriolo, B. Sun, B. Zheng, L. Zhang, C. Norotte, P. N. Teng, J. Traas, R. Schugar, B. M. Deasy, S. Badylak, H. J. Buhring, J. P. Giacobino, L. Lazzari, J. Huard & B. Péault (2008) A perivascular origin for mesenchymal stem cells in multiple human organs. *Cell Stem Cell,* 3**,** 301-13.

Critchley, H. O., R. L. Jones, R. G. Lea, T. A. Drudy, R. W. Kelly, A. R. Williams & D. T. Baird (1999) Role of inflammatory mediators in human endometrium during progesterone withdrawal and early pregnancy. *J Clin Endocrinol Metab,* 84**,** 240-8.

Critchley, H. O., R. W. Kelly, D. T. Baird & R. M. Brenner (2006a) Regulation of human endometrial function: mechanisms relevant to uterine bleeding. *Reprod Biol Endocrinol,* 4 Suppl 1**,** S5.

Critchley, H. O., R. W. Kelly, R. M. Brenner & D. T. Baird (2001a) The endocrinology of menstruation--a role for the immune system. *Clin Endocrinol (Oxf),* 55**,** 701-10.

Critchley, H. O., J. Osei, T. A. Henderson, L. Boswell, K. J. Sales, H. N. Jabbour & N. Hirani (2006b) Hypoxia-inducible factor-1alpha expression in human endometrium and its regulation by prostaglandin E-series prostanoid receptor 2 (EP2). *Endocrinology,* 147**,** 744-53.

Critchley, H. O. & P. T. Saunders (2009) Hormone receptor dynamics in a receptive human endometrium. *Reprod Sci,* 16**,** 191-9.

Critchley, H. O. D., R. M. Brenner, T. A. Henderson, K. Williams, N. R. Nayak, O. D. Slayden, M. R. Millar & P. T. K. Saunders (2001b) Estrogen receptor beta, but not estrogen receptor alpha, is present in the vascular endothelium of the human and nonhuman primate endometrium. *Journal of Clinical Endocrinology & Metabolism,* 86**,** 1370-1378.

Crocker, D. J., T. M. Murad & J. C. Geer (1970) Role of the pericyte in wound healing. An ultrastructural study. *Exp Mol Pathol,* 13**,** 51-65.

Dai, X. M., G. R. Ryan, A. J. Hapel, M. G. Dominguez, R. G. Russell, S. Kapp, V. Sylvestre & E. R. Stanley (2002) Targeted disruption of the mouse colony-stimulating factor 1 receptor gene results in osteopetrosis, mononuclear phagocyte deficiency, increased primitive progenitor cell frequencies, and reproductive defects. *Blood,* 99**,** 111-20.

Daley, J. M., A. A. Thomay, M. D. Connolly, J. S. Reichner & J. E. Albina (2008) Use of Ly6G-specific monoclonal antibody to deplete neutrophils in mice. *J Leukoc Biol,* 83**,** 64-70.

Dalmas, E., K. Clément & M. Guerre-Millo (2011) Defining macrophage phenotype and function in adipose tissue. *Trends Immunol,* 32**,** 307-14.

Das, A., M. Sinha, S. Datta, M. Abas, S. Chaffee, C. K. Sen & S. Roy (2015) Monocyte and macrophage plasticity in tissue repair and regeneration. *Am J Pathol,* 185**,** 2596-606.

Davis, G. E. & W. B. Saunders (2006) Molecular balance of capillary tube formation versus regression in wound repair: role of matrix metalloproteinases and their inhibitors. *J Investig Dermatol Symp Proc,* 11**,** 44-56.

De Leo, B., A. Esnal-Zufiaurre, F. Collins, H. O. D. Critchley & P. T. K. Saunders (2017) Immunoprofiling of human uterine mast cells identifies three phenotypes and expression of ERβ and glucocorticoid receptor. *F1000Res,* 6**,** 667.

de Souza, L. E., T. M. Malta, S. Kashima Haddad & D. T. Covas (2016) Mesenchymal Stem Cells and Pericytes: To What Extent Are They Related? *Stem Cells Dev,* 25**,** 1843-1852.

de Ziegler, D., R. Fanchin, B. de Moustier & C. Bulletti (1998) The hormonal control of endometrial receptivity: estrogen (E2) and progesterone. *J Reprod Immunol,* 39**,** 149-66.

Deane, J. A., R. C. Gualano & C. E. Gargett (2013) Regenerating endometrium from stem/progenitor cells: is it abnormal in endometriosis, Asherman's syndrome and infertility? *Curr Opin Obstet Gynecol,* 25**,** 193-200.
Deane, J. A., Y. R. Ong, J. E. Cain, W. S. Jayasekara, A. Tiwari, D. L. Carlone, D. N. Watkins, D. T. Breault & C. E. Gargett (2016) The mouse endometrium contains epithelial, endothelial and leucocyte populations expressing the stem cell marker telomerase reverse transcriptase. *Mol Hum Reprod,* 22**,** 272-84.
DeLoia, J. A., A. M. Stewart-Akers, J. Brekosky & C. J. Kubik (2002) Effects of exogenous estrogen on uterine leukocyte recruitment. *Fertil Steril,* 77**,** 548-54.
Demers, L. M., G. J. Macdonald, A. T. Hertig, N. W. King & J. J. Mackey (1972) The cervix uteri in Macaca mulatta, Macaca arctoides, and Macaca fascicularis--a comparative anatomic study with special reference to Macaca arctoides as a unique model for endometrial study. *Fertil Steril,* 23**,** 529-34.
Deonarine, K., M. C. Panelli, M. E. Stashower, P. Jin, K. Smith, H. B. Slade, C. Norwood, E. Wang, F. M. Marincola & D. F. Stroncek (2007) Gene expression profiling of cutaneous wound healing. *J Transl Med,* 5**,** 11.
Desmoulière, A., M. Redard, I. Darby & G. Gabbiani (1995) Apoptosis mediates the decrease in cellularity during the transition between granulation tissue and scar. *Am J Pathol,* 146**,** 56-66.
Diegelmann, R. F. & M. C. Evans (2004) Wound healing: an overview of acute, fibrotic and delayed healing. *Front Biosci,* 9**,** 283-9.
Dimitrov, R., T. Timeva, D. Kyurkchiev, M. Stamenova, A. Shterev, P. Kostova, V. Zlatkov, I. Kehayov & S. Kyurkchiev (2008) Characterization of clonogenic stromal cells isolated from human endometrium. *Reproduction,* 135**,** 551-8.
Ding, L., X. Li, H. Sun, J. Su, N. Lin, B. Péault, T. Song, J. Yang, J. Dai & Y. Hu (2014) Transplantation of bone marrow mesenchymal stem cells on collagen scaffolds for the functional regeneration of injured rat uterus. *Biomaterials,* 35**,** 4888-900.
Drudy, L., B. Sheppard & J. Bonnar (1991) Mast cells in the normal uterus and in dysfunctional uterine bleeding. *Eur J Obstet Gynecol Reprod Biol,* 39**,** 193-201.
Du, H. & H. S. Taylor (2007) Contribution of bone marrow-derived stem cells to endometrium and endometriosis. *Stem Cells,* 25**,** 2082-6.
Duffield, J. S. (2014) Cellular and molecular mechanisms in kidney fibrosis. *J Clin Invest,* 124**,** 2299-306.
Duffield, J. S., M. Lupher, V. J. Thannickal & T. A. Wynn (2013) Host responses in tissue repair and fibrosis. *Annu Rev Pathol,* 8**,** 241-76.
Duffield, J. S., P. G. Tipping, T. Kipari, J. F. Cailhier, S. Clay, R. Lang, J. V. Bonventre & J. Hughes (2005) Conditional ablation of macrophages halts progression of crescentic glomerulonephritis. *Am J Pathol,* 167**,** 1207-19.
Dulauroy, S., S. E. Di Carlo, F. Langa, G. Eberl & L. Peduto (2012) Lineage tracing and genetic ablation of ADAM12(+) perivascular cells identify a major source of profibrotic cells during acute tissue injury. *Nat Med,* 18**,** 1262-70.
Dunn, C. L., R. W. Kelly & H. O. Critchley (2003) Decidualization of the human endometrial stromal cell: an enigmatic transformation. *Reprod Biomed Online,* 7**,** 151-61.
Dunster, J. L. (2016) The macrophage and its role in inflammation and tissue repair: mathematical and systems biology approaches. *Wiley Interdiscip Rev Syst Biol Med,* 8**,** 87-99.
Elia A., F. Charalambous & P. Georgiades 2011. New phenotypic aspects of the decidual spiral artery wall during early post-implantation mouse pregnancy. *Biochem Biophys Res Commun.* 416:211-6.
Emera, D., C. Casola, V. J. Lynch, D. E. Wildman, D. Agnew & G. P. Wagner (2012a) Convergent evolution of endometrial prolactin expression in primates, mice, and elephants through the independent recruitment of transposable elements. *Mol Biol Evol,* 29**,** 239-47.
Emera, D., R. Romero & G. Wagner (2012b) The evolution of menstruation: a new model for genetic assimilation: explaining molecular origins of maternal responses to fetal invasiveness. *Bioessays,* 34**,** 26-35.
Eming, S. A., T. Krieg & J. M. Davidson (2007) Inflammation in wound repair: molecular and cellular mechanisms. *J Invest Dermatol,* 127**,** 514-25.
Espagnolle, N., F. Guilloton, F. Deschaseaux, M. Gadelorge, L. Sensébé & P. Bourin (2014) CD146 expression on mesenchymal stem cells is associated with their vascular smooth muscle commitment. *J Cell Mol Med,* 18**,** 104-14.

Evans, J., T. Kaitu'u-Lino & L. A. Salamonsen (2011) Extracellular matrix dynamics in scar-free endometrial repair: perspectives from mouse in vivo and human in vitro studies. *Biol Reprod,* 85**,** 511-23.
Evans, J. & L. A. Salamonsen (2012) Inflammation, leukocytes and menstruation. *Rev Endocr Metab Disord,* 13**,** 277-88.
Fan, J. M., X. R. Huang, Y. Y. Ng, D. J. Nikolic-Paterson, W. Mu, R. C. Atkins & H. Y. Lan (2001) Interleukin-1 induces tubular epithelial-myofibroblast transdifferentiation through a transforming growth factor-beta1-dependent mechanism in vitro. *Am J Kidney Dis,* 37**,** 820-31.
Fan, X., S. Krieg, J. Y. Hwang, S. Dhal, C. J. Kuo, B. L. Lasley, R. M. Brenner & N. R. Nayak (2012) Dynamic regulation of Wnt7a expression in the primate endometrium: implications for postmenstrual regeneration and secretory transformation. *Endocrinology,* 153**,** 1063-9.
Fan, X., S. Krieg, C. J. Kuo, S. J. Wiegand, M. Rabinovitch, M. L. Druzin, R. M. Brenner, L. C. Giudice & N. R. Nayak (2008) VEGF blockade inhibits angiogenesis and reepithelialization of endometrium. *FASEB J,* 22**,** 3571-80.
Fata, J. E., V. Chaudhary & R. Khokha (2001) Cellular turnover in the mammary gland is correlated with systemic levels of progesterone and not 17beta-estradiol during the estrous cycle. *Biol Reprod,* 65**,** 680-8.
Fayazi, M., M. Salehnia & S. Ziaei (2017) In-vitro construction of endometrial-like epithelium using CD146. *Reprod Biomed Online,* 35**,** 241-252.
Feil, S., N. Valtcheva & R. Feil (2009) Inducible Cre mice. *Methods Mol Biol,* 530**,** 343-63.
Felix, J. C. & S. Farahmand (1997) Endometrial glandular proliferation and estrogen receptor content during the normal menstrual cycle. *Contraception,* 55**,** 19-22.
Feng, J., A. Mantesso, C. De Bari, A. Nishiyama & P. T. Sharpe (2011) Dual origin of mesenchymal stem cells contributing to organ growth and repair. *Proc Natl Acad Sci U S A,* 108**,** 6503-8.
Ferenczy, A. (1976) Studies on the cytodynamics of human endometrial regeneration. I. Scanning electron microscopy. *Am J Obstet Gynecol,* 124**,** 64-74.
Ferenczy, A., G. Bertrand & M. M. Gelfand (1979) Proliferation kinetics of human endometrium during the normal menstrual cycle. *American Journal of Obstetrics and Gynecology,* 133**,** 859-67.
Fernandes, K. J., I. A. McKenzie, P. Mill, K. M. Smith, M. Akhavan, F. Barnabé-Heider, J. Biernaskie, A. Junek, N. R. Kobayashi, J. G. Toma, D. R. Kaplan, P. A. Labosky, V. Rafuse, C. C. Hui & F. D. Miller (2004) A dermal niche for multipotent adult skin-derived precursor cells. *Nat Cell Biol,* 6**,** 1082-93.
Ferrante, C. J. & S. J. Leibovich (2012) Regulation of Macrophage Polarization and Wound Healing. *Adv Wound Care (New Rochelle),* 1**,** 10-16.
Fettke, F., A. Schumacher, S. D. Costa & A. C. Zenclussen (2014) B cells: the old new players in reproductive immunology. *Front Immunol,* 5**,** 285.
Figueira, P. G., M. S. Abrão, G. Krikun, H. S. Taylor & H. Taylor (2011) Stem cells in endometrium and their role in the pathogenesis of endometriosis. *Ann N Y Acad Sci,* 1221**,** 10-7.
Fimmel, S., R. Kurfurst, F. Bonté & C. C. Zouboulis (2007) Responsiveness to androgens and effectiveness of antisense oligonucleotides against the androgen receptor on human epidermal keratinocytes is dependent on the age of the donor and the location of cell origin. *Horm Metab Res,* 39**,** 157-65.
Finn, C. A. & P.M. Keen (1963) The induction if deciduomata in the rat. *J Embryol. exp. Morphl,* 11, 673-682.
Finn, C. A. (1987) Why do women and some other primates menstruate? *Perspect Biol Med,* 30**,** 566-74.
Finn, C. A. & M. Pope (1984) Vascular and cellular changes in the decidualized endometrium of the ovariectomized mouse following cessation of hormone treatment: a possible model for menstruation. *J Endocrinol,* 100**,** 295-300.
--- (1986) Control of leucocyte infiltration into the decidualized mouse uterus. *J Endocrinol,* 110**,** 93-6.
Fischer, A. H., K. A. Jacobson, J. Rose & R. Zeller (2008) Hematoxylin and eosin staining of tissue and cell sections. *CSH Protoc,* 2008**,** pdb.prot4986.
Flynn, L., B. Byrne, J. Carton, P. Kelehan, C. O'Herlihy & C. O'Farrelly (2000) Menstrual cycle dependent fluctuations in NK and T-lymphocyte subsets from non-pregnant human endometrium. *Am J Reprod Immunol,* 43**,** 209-17.

Gaafar, T., O. Osman, A. Osman, W. Attia, H. Hamza & R. El Hawary (2014) Gene expression profiling of endometrium versus bone marrow-derived mesenchymal stem cells: upregulation of cytokine genes. *Mol Cell Biochem,* 395**,** 29-43.
Gaide Chevronnay, H. P., C. Selvais, H. Emonard, C. Galant, E. Marbaix & P. Henriet (2012) Regulation of matrix metalloproteinases activity studied in human endometrium as a paradigm of cyclic tissue breakdown and regeneration. *Biochim Biophys Acta,* 1824**,** 146-56.
Gargett, B. E. & R. W. Chan (2006) Endometrial stem/progenitor cells and proliferative disorders of the endometrium. *Minerva Ginecol,* 58**,** 511-26.
Gargett, C. E., R. W. Chan & K. E. Schwab (2007) Endometrial stem cells. *Curr Opin Obstet Gynecol,* 19**,** 377-83.
--- (2008) Hormone and growth factor signaling in endometrial renewal: role of stem/progenitor cells. *Mol Cell Endocrinol,* 288**,** 22-9.
Gargett, C. E. & D. L. Healy (2011) Generating receptive endometrium in Asherman's syndrome. *J Hum Reprod Sci,* 4**,** 49-52.
Gargett, C. E. & H. Masuda (2010) Adult stem cells in the endometrium. *Mol Hum Reprod,* 16**,** 818-34.
Gargett, C. E., K. E. Schwab & J. a. Deane (2016) Endometrial stem/progenitor cells: The first 10 years. *Human Reproduction Update,* 22**,** 137-163.
Gargett, C. E., K. E. Schwab, R. M. Zillwood, H. P. Nguyen & D. Wu (2009) Isolation and culture of epithelial progenitors and mesenchymal stem cells from human endometrium. *Biol Reprod,* 80**,** 1136-45.
Garry, R., R. Hart, K. A. Karthigasu & C. Burke (2009) A re-appraisal of the morphological changes within the endometrium during menstruation: a hysteroscopic, histological and scanning electron microscopic study. *Hum Reprod,* 24**,** 1393-401.
--- (2010) Structural changes in endometrial basal glands during menstruation. *BJOG,* 117**,** 1175-85.
Gellersen, B. & J. J. Brosens (2014) Cyclic decidualization of the human endometrium in reproductive health and failure. *Endocr Rev,* 35**,** 851-905.
Gerhardt, H. & C. Betsholtz (2003) Endothelial-pericyte interactions in angiogenesis. *Cell Tissue Res,* 314**,** 15-23.
Germeyer, A., A. E. Hamilton, L. S. Laughlin, B. L. Lasley, R. M. Brenner, L. C. Giudice & N. R. Nayak (2005) Cellular expression and hormonal regulation of neuropilin-1 and -2 messenger ribonucleic Acid in the human and rhesus macaque endometrium. *J Clin Endocrinol Metab,* 90**,** 1783-90.
Gibson, D. A., E. Greaves, H. O. Critchley & P. T. Saunders (2015) Estrogen-dependent regulation of human uterine natural killer cells promotes vascular remodelling via secretion of CCL2. *Hum Reprod,* 30**,** 1290-301.
Gilliver, S. C., J. J. Ashworth, S. J. Mills, M. J. Hardman & G. S. Ashcroft (2006) Androgens modulate the inflammatory response during acute wound healing. *J Cell Sci,* 119**,** 722-32.
Gilliver, S. C., J. P. Ruckshanthi, M. J. Hardman, L. A. Zeef & G. S. Ashcroft (2009) 5alpha-dihydrotestosterone (DHT) retards wound closure by inhibiting re-epithelialization. *J Pathol,* 217**,** 73-82.
Ginhoux, F., M. Greter, M. Leboeuf, S. Nandi, P. See, S. Gokhan, M. F. Mehler, S. J. Conway, L. G. Ng, E. R. Stanley, I. M. Samokhvalov & M. Merad (2010) Fate mapping analysis reveals that adult microglia derive from primitive macrophages. *Science,* 330**,** 841-5.
Giudice, L. C. (2010) Clinical practice. Endometriosis. *N Engl J Med,* 362**,** 2389-98.
Giudice, L. C. & L. C. Kao (2004) Endometriosis. *Lancet,* 364**,** 1789-99.
Glim, J. E., R. H. Beelen, F. B. Niessen, V. Everts & M. M. Ulrich The number of immune cells is lower in healthy oral mucosa compared to skin and does not increase after scarring.
Goffin, F., C. Munaut, F. Frankenne, S. Perrier D'Hauterive, A. Béliard, V. Fridman, P. Nervo, A. Colige & J. M. Foidart (2003) Expression pattern of metalloproteinases and tissue inhibitors of matrix-metalloproteinases in cycling human endometrium. *Biol Reprod,* 69**,** 976-84.
Goodsell, D. S. (2002) The molecular perspective: tamoxifen and the estrogen receptor. *Stem Cells,* 20**,** 267-8.
Goren, I., N. Allmann, N. Yogev, C. Schürmann, A. Linke, M. Holdener, A. Waisman, J. Pfeilschifter & S. Frank (2009) A transgenic mouse model of inducible macrophage depletion: effects of diphtheria toxin-driven lysozyme M-specific cell lineage ablation on wound inflammatory, angiogenic, and contractive processes. *Am J Pathol,* 175**,** 132-47.

Greaves, E., F. L. Cousins, A. Murray, A. Esnal-Zufiaurre, A. Fassbender, A. W. Horne & P. T. Saunders (2014) A novel mouse model of endometriosis mimics human phenotype and reveals insights into the inflammatory contribution of shed endometrium. *Am J Pathol,* 184**,** 1930-9.

Greenhalgh, S. N., J. P. Iredale & N. C. Henderson (2013) Origins of fibrosis: pericytes take centre stage. *F1000Prime Rep,* 5**,** 37.

Guimarães-Camboa, N., P. Cattaneo, Y. Sun, T. Moore-Morris, Y. Gu, N. D. Dalton, E. Rockenstein, E. Masliah, K. L. Peterson, W. B. Stallcup, J. Chen & S. M. Evans (2017) Pericytes of Multiple Organs Do Not Behave as Mesenchymal Stem Cells In Vivo. *Cell Stem Cell,* 20**,** 345-359.e5.

Guo, Y., B. He, X. Xu & J. Wang (2011) Comprehensive analysis of leukocytes, vascularization and matrix metalloproteinases in human menstrual xenograft model. *PLoS One,* 6**,** e16840.

Gurevich, D. B., C. E. Severn, C. Twomey, A. Greenhough, J. Cash, A. M. Toye, H. Mellor & P. Martin (2018) Live imaging of wound angiogenesis reveals macrophage orchestrated vessel sprouting and regression. *EMBO J,* 37.

Gurtner, G. C., S. Werner, Y. Barrandon & M. T. Longaker (2008) Wound repair and regeneration. *Nature,* 453**,** 314-21.

Gurung, S., J. A. Deane, S. Darzi, J. A. Werkmeister & C. E. Gargett (2018) In Vivo Survival of Human Endometrial Mesenchymal Stem Cells Transplanted Under the Kidney Capsule of Immunocompromised Mice. *Stem Cells Dev,* 27**,** 35-43.

Götte, M., M. Wolf, A. Staebler, O. Buchweitz, R. Kelsch, A. N. Schüring & L. Kiesel (2008) Increased expression of the adult stem cell marker Musashi-1 in endometriosis and endometrial carcinoma. *J Pathol,* 215**,** 317-29.

Haldar, D., N. C. Henderson, G. Hirschfield & P. N. Newsome (2016) Mesenchymal stromal cells and liver fibrosis: a complicated relationship. *FASEB J,* 30**,** 3905-3928.

Hampton, A. L., P. A. Rogers, B. Affandi & L. A. Salamonsen (2001) Expression of the chemokines, monocyte chemotactic protein (MCP)-1 and MCP-2 in endometrium of normal women and Norplant users, does not support a central role in macrophage infiltration into endometrium. *J Reprod Immunol,* 49**,** 115-32.

Hanna, J., D. Goldman-Wohl, Y. Hamani, I. Avraham, C. Greenfield, S. Natanson-Yaron, D. Prus, L. Cohen-Daniel, T. I. Arnon, I. Manaster, R. Gazit, V. Yutkin, D. Benharroch, A. Porgador, E. Keshet, S. Yagel & O. Mandelboim (2006) Decidual NK cells regulate key developmental processes at the human fetal-maternal interface. *Nat Med,* 12**,** 1065-74.

Hantash, B. M., L. Zhao, J. A. Knowles & H. P. Lorenz (2008) Adult and fetal wound healing. *Front Biosci,* 13**,** 51-61.

Hapangama, D. K. & J. N. Bulmer (2016) Pathophysiology of heavy menstrual bleeding. *Womens Health (Lond),* 12**,** 3-13.

Hapangama, D. K., H. O. Critchley, T. A. Henderson & D. T. Baird (2002) Mifepristone-induced vaginal bleeding is associated with increased immunostaining for cyclooxygenase-2 and decrease in prostaglandin dehydrogenase in luteal phase endometrium. *J Clin Endocrinol Metab,* 87**,** 5229-34.

Hardman, M. J., A. Waite, L. Zeef, M. Burow, T. Nakayama & G. S. Ashcroft (2005) Macrophage migration inhibitory factor: a central regulator of wound healing. *Am J Pathol,* 167**,** 1561-74.

Harris, L., H. Fritsche, R. Mennel, L. Norton, P. Ravdin, S. Taube, M. R. Somerfield, D. F. Hayes, R. C. Bast & A. S. o. C. Oncology (2007) American Society of Clinical Oncology 2007 update of recommendations for the use of tumor markers in breast cancer. *J Clin Oncol,* 25**,** 5287-312.

Hashimoto, R. (2003) Development of the human Müllerian duct in the sexually undifferentiated stage. *Anat Rec A Discov Mol Cell Evol Biol,* 272**,** 514-9.

Hass, R., C. Kasper, S. Böhm & R. Jacobs (2011) Different populations and sources of human mesenchymal stem cells (MSC): A comparison of adult and neonatal tissue-derived MSC. *Cell Commun Signal,* 9**,** 12.

Hawley, C. A., R. Rojo, A. Raper, K. A. Sauter, Z. M. Lisowski, K. Grabert, C. C. Bain, G. M. Davis, P. A. Louwe, M. C. Ostrowski, D. A. Hume, C. Pridans & S. J. Jenkins (2018) -mApple Transgene Expression and Ligand Binding In Vivo Reveal Dynamics of CSF1R Expression within the Mononuclear Phagocyte System. *J Immunol,* 200**,** 2209-2223.

He, L., M. Vanlandewijck, E. Raschperger, M. Andaloussi Mäe, B. Jung, T. Lebouvier, K. Ando, J. Hofmann, A. Keller & C. Betsholtz (2016) Analysis of the brain mural cell transcriptome. *Sci Rep,* 6**,** 35108.

Hedlund, E. & Q. Deng (2018) Single-cell RNA sequencing: Technical advancements and biological applications. *Mol Aspects Med,* 59**,** 36-46.

Henderson, N. C., T. D. Arnold, Y. Katamura, M. M. Giacomini, J. D. Rodriguez, J. H. McCarty, A. Pellicoro, E. Raschperger, C. Betsholtz, P. G. Ruminski, D. W. Griggs, M. J. Prinsen, J. J. Maher, J. P. Iredale, A. Lacy-Hulbert, R. H. Adams & D. Sheppard (2013) Targeting of αv integrin identifies a core molecular pathway that regulates fibrosis in several organs. *Nat Med,* 19**,** 1617-24.

Henderson, T. A., P. T. Saunders, A. Moffett-King, N. P. Groome & H. O. Critchley (2003) Steroid receptor expression in uterine natural killer cells. *J Clin Endocrinol Metab,* 88**,** 440-9.

Henriet, P., H. P. Gaide Chevronnay & E. Marbaix (2012) The endocrine and paracrine control of menstruation. *Mol Cell Endocrinol,* 358**,** 197-207.

Herzog, E. L. & R. Bucala (2010) Fibrocytes in health and disease. *Exp Hematol,* 38**,** 548-56.

Hesketh, M., K. B. Sahin, Z. E. West & R. Z. Murray (2017) Macrophage Phenotypes Regulate Scar Formation and Chronic Wound Healing. *Int J Mol Sci,* 18.

Hestdal, K., F. W. Ruscetti, J. N. Ihle, S. E. Jacobsen, C. M. Dubois, W. C. Kopp, D. L. Longo & J. R. Keller (1991) Characterization and regulation of RB6-8C5 antigen expression on murine bone marrow cells. *J Immunol,* 147**,** 22-8.

Hewitt, K. J., Y. Shamis, E. Knight, A. Smith, A. Maione, A. Alt-Holland, S. D. Sheridan, S. J. Haggarty & J. A. Garlick (2012) PDGFRβ expression and function in fibroblasts derived from pluripotent cells is linked to DNA demethylation. *J Cell Sci,* 125**,** 2276-87.

Hickey, M., D. a. Doherty, I. S. Fraser, D. M. Sloboda & L. a. Salamonsen (2008) Why does menopausal hormone therapy lead to irregular uterine bleeding? Changes to endometrial blood vessels. *Human reproduction (Oxford, England),* 23**,** 912-918.

Hickey, M. & I.S. Fraser 2000. The structure of endometrial microvessels. *Human Reproduction.* 15: 57-66

Hickey, M., G. Pillai, J. M. Higham, M. Sullivan, D. Horncastle, D. Doherty & G. Stamp (2003) Changes in endometrial blood vessels in the endometrium of women with hormone replacement therapy-related irregular bleeding. *Hum Reprod,* 18**,** 1100-6.

Hinz, B. (2007) Formation and function of the myofibroblast during tissue repair. *J Invest Dermatol,* 127**,** 526-37.

Hinz, B., S. H. Phan, V. J. Thannickal, M. Prunotto, A. Desmoulière, J. Varga, O. De Wever, M. Mareel & G. Gabbiani (2012) Recent developments in myofibroblast biology: paradigms for connective tissue remodeling. *Am J Pathol,* 180**,** 1340-55.

Ho, S., H. Marçal & L. J. Foster (2014) Towards scarless wound healing: a comparison of protein expression between human, adult and foetal fibroblasts. *Biomed Res Int,* 2014**,** 676493.

Hogan, S. P., H. F. Rosenberg, R. Moqbel, S. Phipps, P. S. Foster, P. Lacy, A. B. Kay & M. E. Rothenberg (2008) Eosinophils: biological properties and role in health and disease. *Clin Exp Allergy,* 38**,** 709-50.

Holmgren, L., A. Glaser, S. Pfeifer-Ohlsson & R. Ohlsson (1991) Angiogenesis during human extraembryonic development involves the spatiotemporal control of PDGF ligand and receptor gene expression. *Development,* 113**,** 749-54.

Hosaka, K., Y. Yang, T. Seki, C. Fischer, O. Dubey, E. Fredlund & J. Hartman (2016) Pericyte – fibroblast transition promotes tumor growth and metastasis. *Proceedings of the National Academy of Sciences of the United States of America*.

Hou, X. X., W. J. Zhou, X. Q. Wang & D. J. Li (2016) Fractalkine/CX3CR1 is involved in the pathogenesis of endometriosis by regulating endometrial stromal cell proliferation and invasion. *Am J Reprod Immunol,* 76**,** 318-25.

Houser, B. L., T. Tilburgs, J. Hill, M. L. Nicotra & J. L. Strominger (2011) Two unique human decidual macrophage populations. *J Immunol,* 186**,** 2633-42.

Hsu, K. F., H. A. Pan, Y. Y. Hsu, C. M. Wu, W. J. Chung & S. C. Huang (2014) Enhanced myometrial autophagy in postpartum uterine involution. *Taiwan J Obstet Gynecol,* 53**,** 293-302.

Hu, F. F., Jing Xu, Y. G. Cui, X. Q. Qian, Y. D. Mao, L. M. Liao & J. Y. Liu (2010) Isolation and characterization of side population cells in the postpartum murine endometrium. *Reprod Sci,* 17**,** 629-42.

Huang, C. C., G. D. Orvis, Y. Wang & R. R. Behringer (2012) Stromal-to-epithelial transition during postpartum endometrial regeneration. *PLoS ONE*.

Hufnagel, D., F. Li, E. Cosar, G. Krikun & H. S. Taylor (2015) The Role of Stem Cells in the Etiology and Pathophysiology of Endometriosis. *Semin Reprod Med,* 33**,** 333-40.

Humphreys, B. D. (2012) Targeting pericyte differentiation as a strategy to modulate kidney fibrosis in diabetic nephropathy. *Semin Nephrol,* 32**,** 463-70.

Humphreys, B. D., A. Lin Sl Fau - Kobayashi, T. E. Kobayashi A Fau - Hudson, B. T. Hudson Te Fau - Nowlin, J. V. Nowlin Bt Fau - Bonventre, M. T. Bonventre Jv Fau - Valerius, A. P. Valerius Mt Fau - McMahon, J. S. McMahon Ap Fau - Duffield & J. S. Duffield Fate tracing reveals the pericyte and not epithelial origin of myofibroblasts in kidney fibrosis.

Hunt, J. S., L. Miller & J. S. Platt (1998) Hormonal regulation of uterine macrophages. *Dev Immunol,* 6**,** 105-10.

Hurskainen, R., J. Teperi, J. Paavonen & B. Cacciatore (1999) Menorrhagia and uterine artery blood flow. *Hum Reprod,* 14**,** 186-9.

Hwang, N. S., C. Zhang, Y. S. Hwang & S. Varghese (2009) Mesenchymal stem cell differentiation and roles in regenerative medicine. *Wiley Interdiscip Rev Syst Biol Med,* 1**,** 97-106.

Ilina, O. & P. Friedl (2009) Mechanisms of collective cell migration at a glance. *J Cell Sci,* 122**,** 3203-8.

Inaba, K. & M. Inaba (2005) Antigen recognition and presentation by dendritic cells. *Int J Hematol,* 81**,** 181-7.

Indumathi, S., R. Harikrishnan, J. S. Rajkumar, D. Sudarsanam & M. Dhanasekaran (2013) Prospective biomarkers of stem cells of human endometrium and fallopian tube compared with bone marrow. *Cell Tissue Res,* 352**,** 537-49.

Ino, K., M. Masuya, I. Tawara, E. Miyata, K. Oda, Y. Nakamori, K. Suzuki, K. Ohishi & N. Katayama (2014) Monocytes infiltrate the pancreas via the MCP-1/CCR2 pathway and differentiate into stellate cells. *PLoS One,* 9**,** e84889.

Iqbal, A. J., E. McNeill, T. S. Kapellos, D. Regan-Komito, S. Norman, S. Burd, N. Smart, D. E. Machemer, E. Stylianou, H. McShane, K. M. Channon, A. Chawla & D. R. Greaves (2014) Human CD68 promoter GFP transgenic mice allow analysis of monocyte to macrophage differentiation in vivo. *Blood,* 124**,** e33-44.

Irwin, J. C., L. de las Fuentes, B. A. Dsupin & L. C. Giudice (1993) Insulin-like growth factor regulation of human endometrial stromal cell function: coordinate effects on insulin-like growth factor binding protein-1, cell proliferation and prolactin secretion. *Regul Pept,* 48**,** 165-77.

Ito, I., T. Hayashi, K. Yamada, M. Kuzuya, M. Naito & A. Iguchi (1995) Physiological concentration of estradiol inhibits polymorphonuclear leukocyte chemotaxis via a receptor mediated system. *Life Sci,* 56**,** 2247-53.

Ito, M., Y. Liu, Z. Yang, J. Nguyen, F. Liang, R. J. Morris & G. Cotsarelis (2005) Stem cells in the hair follicle bulge contribute to wound repair but not to homeostasis of the epidermis. *Nat Med,* 11**,** 1351-4.

Jabbour, H. N., R. W. Kelly, H. M. Fraser & H. O. Critchley (2006) Endocrine regulation of menstruation. *Endocrine Reviews,* 27**,** 17-46.

Jaffe, E. A., J. T. Ruggiero & D. J. Falcone (1985) Monocytes and macrophages synthesize and secrete thrombospondin. *Blood,* 65**,** 79-84.

Jensen Dv Fau - Andersen, K. B., G. Andersen Kb Fau - Wagner & G. Wagner Prostaglandins in the menstrual cycle of women. A review.

Jeziorska, M., H. Nagase, L. A. Salamonsen & D. E. Woolley (1996) Immunolocalization of the matrix metalloproteinases gelatinase B and stromelysin 1 in human endometrium throughout the menstrual cycle. *Journal of Reproduction and Fertility,* 107**,** 43-51.

Johannisson, E., B. M. Landgren, H. P. Rohr & E. Diczfalusy (1987) Endometrial morphology and peripheral hormone levels in women with regular menstrual cycles. *Fertil Steril,* 48**,** 401-8.

Jolicoeur, C., M. Boutouil, R. Drouin, I. Paradis, A. Lemay & A. Akoum (1998) Increased expression of monocyte chemotactic protein-1 in the endometrium of women with endometriosis. *Am J Pathol,* 152**,** 125-33.

Jones, C. V. & S. D. Ricardo (2013) Macrophages and CSF-1: implications for development and beyond. *Organogenesis,* 9**,** 249-60.

Jones, R. L., N. J. Hannan, T. J. Kaitu'u, J. Zhang & L. A. Salamonsen (2004) Identification of chemokines important for leukocyte recruitment to the human endometrium at the times of embryo implantation and menstruation. *J Clin Endocrinol Metab,* 89**,** 6155-67.

Kaitu'u, T. J., J. Shen, J. Zhang, N. B. Morison & L. A. Salamonsen (2005) Matrix metalloproteinases in endometrial breakdown and repair: functional significance in a mouse model. *Biol Reprod,* 73**,** 672-80.

Kaitu'u-Lino, T. J., L. A. Morison Nb Fau - Salamonsen & L. A. Salamonsen Estrogen is not essential for full endometrial restoration after breakdown: lessons from a mouse model.

Kaitu'u-Lino, T. J., N. B. Morison & L. A. Salamonsen (2007) Neutrophil depletion retards endometrial repair in a mouse model. *Cell Tissue Res,* 328**,** 197-206.
Kaitu'u-Lino, T. J., D. J. Phillips, N. B. Morison & L. A. Salamonsen (2009) A new role for activin in endometrial repair after menses. *Endocrinology,* 150**,** 1904-11.
Kaitu'u-Lino, T. J., L. Ye & C. E. Gargett (2010) Reepithelialization of the uterine surface arises from endometrial glands: evidence from a functional mouse model of breakdown and repair. *Endocrinology,* 151**,** 3386-95.
Kaitu'u-Lino, T. J., L. Ye, L. A. Salamonsen, J. E. Girling & C. E. Gargett (2012) Identification of label-retaining perivascular cells in a mouse model of endometrial decidualization, breakdown, and repair. *Biol Reprod,* 86**,** 184.
Kalinina, N. I., V. Y. Sysoeva, K. A. Rubina, Y. V. Parfenova & V. A. Tkachuk (2011) Mesenchymal stem cells in tissue growth and repair. *Acta Naturae,* 3**,** 30-7.
Kalluri, R. & R. A. Weinberg (2009) The basics of epithelial-mesenchymal transition. *J Clin Invest,* 119**,** 1420-8.
Kamat, B. R. & P. G. Isaacson (1987) The immunocytochemical distribution of leukocytic subpopulations in human endometrium. *Am J Pathol,* 127**,** 66-73.
Kao, L. C., A. Germeyer, S. Tulac, S. Lobo, J. P. Yang, R. N. Taylor, K. Osteen, B. A. Lessey & L. C. Giudice (2003) Expression profiling of endometrium from women with endometriosis reveals candidate genes for disease-based implantation failure and infertility. *Endocrinology,* 144**,** 2870-81.
Kao, L. C., S. Tulac, S. Lobo, B. Imani, J. P. Yang, A. Germeyer, K. Osteen, R. N. Taylor, B. A. Lessey & L. C. Giudice (2002) Global gene profiling in human endometrium during the window of implantation. *Endocrinology,* 143**,** 2119-38.
Kato, K. 2012. Stem cells in human normal endometrium and endometrial cancer cells: Characterization of side population cells.
Kato, K., M. Yoshimoto, S. Adachi, A. Yamayoshi, T. Arima, K. Asanoma, S. Kyo, T. Nakahata & N. Wake (2007) Characterization of side-population cells in human normal endometrium. *Hum Reprod,* 22**,** 1214-23.
Kats, R., M. Al-Akoum, S. Guay, C. Metz & A. Akoum (2005) Cycle-dependent expression of macrophage migration inhibitory factor in the human endometrium. *Hum Reprod,* 20**,** 3518-25.
Kelly, R. W., A. E. King & H. O. Critchley (2002) Inflammatory mediators and endometrial function--focus on the perivascular cell. *J Reprod Immunol,* 57**,** 81-93.
Khosrotehrani, K. (2013) Mesenchymal stem cell therapy in skin: why and what for? *Exp Dermatol,* 22**,** 307-10.
Kikly, K., L. Liu, S. Na & J. D. Sedgwick (2006) The IL-23/Th(17) axis: therapeutic targets for autoimmune inflammation. *Curr Opin Immunol,* 18**,** 670-5.
King, A. E. & H. O. Critchley (2010) Oestrogen and progesterone regulation of inflammatory processes in the human endometrium. *J Steroid Biochem Mol Biol,* 120**,** 116-26.
King, A. E., H. O. Critchley, J. M. Sallenave & R. W. Kelly (2003) Elafin in human endometrium: an antiprotease and antimicrobial molecule expressed during menstruation. *J Clin Endocrinol Metab,* 88**,** 4426-31.
Kinner, B., J. M. Zaleskas & M. Spector (2002) Regulation of smooth muscle actin expression and contraction in adult human mesenchymal stem cells. *Exp Cell Res,* 278**,** 72-83.
Kita, H. (2011) Eosinophils: multifaceted biological properties and roles in health and disease. *Immunol Rev,* 242**,** 161-77.
Kobayashi, A. & R. R. Behringer (2003) Developmental genetics of the female reproductive tract in mammals. *Nat Rev Genet,* 4**,** 969-80.
Kodaman, P. H. & A. Arici (2007) Intra-uterine adhesions and fertility outcome: how to optimize success? *Curr Opin Obstet Gynecol,* 19**,** 207-14.
Koh, T. J. & L. A. DiPietro (2011) Inflammation and wound healing: the role of the macrophage. *Expert Rev Mol Med,* 13**,** e23.
Konrad, L., J. Gronbach, F. Horné, E. O. Mecha, E. Berkes, M. Frank, S. Gattenlöhner, C. O. A. Omwandho, F. Oehmke & H. R. Tinneberg (2018) Similar Characteristics of Endometrial and Endometriotic Epithelial Cells. *Reprod Sci***,** 1933719118756745.
Konrad, L., J. Kortum, R. Nabham, J. Gronbach, R. Dietze, F. Oehmke, E. Berkes & H. R. Tinneberg (2017) Composition of the Stroma in the Human Endometrium and Endometriosis. *Reprod Sci***,** 1933719117734319.

Kothari, A. N., Z. Mi, M. Zapf & P. C. Kuo (2014) Novel clinical therapeutics targeting the epithelial to mesenchymal transition. *Clin Transl Med,* 3**,** 35.
Kramann, R. & B. D. Humphreys (2014) Kidney pericytes: roles in regeneration and fibrosis. *Semin Nephrol,* 34**,** 374-83.
Krjutškov, K., S. Katayama, M. Saare, M. Vera-Rodriguez, D. Lubenets, K. Samuel, T. Laisk-Podar, H. Teder, E. Einarsdottir, A. Salumets & J. Kere (2016) Single-cell transcriptome analysis of endometrial tissue. *Hum Reprod,* 31**,** 844-53.
Krull, A. L., L. Zhang, N. A. Arango, J. Teixeira & J. K. Pru (2010) A Potential Role for Mesenchymal-to-Epithelial Transition During Endometrial Regeneration. *Biology of Reproduction,* 83**,** 156-156.
Kukurba, K. R. & S. B. Montgomery (2015) RNA Sequencing and Analysis. *Cold Spring Harb Protoc,* 2015**,** 951-69.
Kyo, S., Y. Maida & M. Inoue (2011) Stem cells in endometrium and endometrial cancer: accumulating evidence and unresolved questions. *Cancer Lett,* 308**,** 123-33.
Kämmerer, U., K. Marzusch, S. Kröber, P. Ruck, R. Handgretinger & J. Dietl (1999) A subset of CD56+ large granular lymphocytes in first-trimester human decidua are proliferating cells. *Fertil Steril,* 71**,** 74-9.
Lai, J. J., K. P. Lai, K. H. Chuang, P. Chang, I. C. Yu, W. J. Lin & C. Chang (2009) Monocyte/macrophage androgen receptor suppresses cutaneous wound healing in mice by enhancing local TNF-alpha expression. *J Clin Invest,* 119**,** 3739-51.
Larson, B. J., M. T. Longaker & H. P. Lorenz (2010) Scarless fetal wound healing: a basic science review. *Plast Reconstr Surg,* 126**,** 1172-80.
Lathbury, L. J. & L. A. Salamonsen (2000) In-vitro studies of the potential role of neutrophils in the process of menstruation. *Mol Hum Reprod,* 6**,** 899-906.
Lea, R. G. & D. A. Clark (1991) Macrophages and migratory cells in endometrium relevant to implantation. *Baillieres Clin Obstet Gynaecol,* 5**,** 25-59.
Leavitt, T., M. S. Hu, C. D. Marshall, L. A. Barnes, H. P. Lorenz & M. T. Longaker (2016) Scarless wound healing: finding the right cells and signals. *Cell Tissue Res,* 365**,** 483-93.
LeBleu, V. S., G. Taduri, J. O'Connell, Y. Teng, V. G. Cooke, C. Woda, H. Sugimoto & R. Kalluri (2013) Origin and function of myofibroblasts in kidney fibrosis. *Nat Med,* 19**,** 1047-53.
Lee, D. E., N. Ayoub & D. K. Agrawal (2016) Mesenchymal stem cells and cutaneous wound healing: novel methods to increase cell delivery and therapeutic efficacy. *Stem Cell Res Ther,* 7**,** 37.
Leyendecker, G., M. Herbertz, G. Kunz & G. Mall (2002) Endometriosis results from the dislocation of basal endometrium. *Hum Reprod,* 17**,** 2725-36.
Leyendecker, G., L. Wildt & G. Mall (2009) The pathophysiology of endometriosis and adenomyosis: tissue injury and repair. *Arch Gynecol Obstet,* 280**,** 529-38.
Li, M., F. Luan, Y. Zhao, H. Hao, J. Liu, L. Dong, X. Fu & W. Han (2017) Mesenchymal stem cell-conditioned medium accelerates wound healing with fewer scars. *Int Wound J,* 14**,** 64-73.
Li, R., J. Liang, S. Ni, T. Zhou, X. Qing, H. Li, W. He, J. Chen, F. Li, Q. Zhuang, B. Qin, J. Xu, W. Li, J. Yang, Y. Gan, D. Qin, S. Feng, H. Song, D. Yang, B. Zhang, L. Zeng, L. Lai, M. A. Esteban & D. Pei (2010) A mesenchymal-to-epithelial transition initiates and is required for the nuclear reprogramming of mouse fibroblasts. *Cell Stem Cell,* 7**,** 51-63.
Li, X. F., D. S. Charnock-Jones, E. Zhang, S. Hiby, S. Malik, K. Day, D. Licence, J. M. Bowen, L. Gardner, A. King, Y. W. Loke & S. K. Smith (2001) Angiogenic growth factor messenger ribonucleic acids in uterine natural killer cells. *J Clin Endocrinol Metab,* 86**,** 1823-34.
Liu, Y., C. Meyer, A. Müller, F. Herweck, Q. Li, R. Müllenbach, P. R. Mertens, S. Dooley & H. L. Weng (2011) IL-13 induces connective tissue growth factor in rat hepatic stellate cells via TGF-β-independent Smad signaling. *J Immunol,* 187**,** 2814-23.
Longaker, M. T., R. J. Rohrich, L. Greenberg, H. Furnas, R. Wald, V. Bansal, H. Seify, A. Tran, J. Weston, J. M. Korman, R. Chan, D. Kaufman, V. R. Dev, J. A. Mele, M. Januszyk, C. Cowley, P. McLaughlin, B. Beasley & G. C. Gurtner (2014) A randomized controlled trial of the embrace advanced scar therapy device to reduce incisional scar formation. *Plast Reconstr Surg,* 134**,** 536-46.
Lu, J. & A. K. Shenoy (2017) Epithelial-to-Pericyte Transition in Cancer. *Cancers (Basel),* 9.
Ludwig, H. & U. M. Spornitz (1991) Microarchitecture of the human endometrium by scanning electron microscopy: menstrual desquamation and remodeling. *Ann N Y Acad Sci,* 622**,** 28-46.
Luo, J., F. Elwood, M. Britschgi, S. Villeda, H. Zhang, Z. Ding, L. Zhu, H. Alabsi, R. Getachew, R. Narasimhan, R. Wabl, N. Fainberg, M. L. James, G. Wong, J. Relton, S. S. Gambhir, J. W.

Pollard & T. Wyss-Coray (2013) Colony-stimulating factor 1 receptor (CSF1R) signaling in injured neurons facilitates protection and survival. *J Exp Med,* 210**,** 157-72.
Lupher, M. L. & W. M. Gallatin (2006) Regulation of fibrosis by the immune system. *Adv Immunol,* 89**,** 245-88.
MacDonald, K. P., J. S. Palmer, S. Cronau, E. Seppanen, S. Olver, N. C. Raffelt, R. Kuns, A. R. Pettit, A. Clouston, B. Wainwright, D. Branstetter, J. Smith, R. J. Paxton, D. P. Cerretti, L. Bonham, G. R. Hill & D. A. Hume (2010) An antibody against the colony-stimulating factor 1 receptor depletes the resident subset of monocytes and tissue- and tumor-associated macrophages but does not inhibit inflammation. *Blood,* 116**,** 3955-63.
Mackler, A. M., L. M. Green, P. J. McMillan & S. M. Yellon (2000) Distribution and activation of uterine mononuclear phagocytes in peripartum endometrium and myometrium of the mouse. *Biol Reprod,* 62**,** 1193-200.
Makabe, S. & P. M. Motta (1989) Migration of human germ cells and their relationship with the developing ovary: ultrastructural aspects. *Prog Clin Biol Res,* 296**,** 41-54.
Malik, S., K. Day, I. Perrault, D. S. Charnock-Jones & S. K. Smith (2006) Reduced levels of VEGF-A and MMP-2 and MMP-9 activity and increased TNF-alpha in menstrual endometrium and effluent in women with menorrhagia. *Hum Reprod,* 21**,** 2158-66.
Mamrot, J., R. Legaie, S. J. Ellery, T. Wilson, T. Seemann, D. R. Powell, D. K. Gardner, D. W. Walker, P. Temple-Smith, A. T. Papenfuss & H. Dickinson (2017) De novo transcriptome assembly for the spiny mouse (Acomys cahirinus). *Sci Rep,* 7**,** 8996.
Manaster, I., S. Mizrahi, D. Goldman-Wohl, H. Y. Sela, N. Stern-Ginossar, D. Lankry, R. Gruda, A. Hurwitz, Y. Bdolah, R. Haimov-Kochman, S. Yagel & O. Mandelboim (2008) Endometrial NK cells are special immature cells that await pregnancy. *J Immunol,* 181**,** 1869-76.
Mandl, M., S. Schmitz, C. Weber & M. Hristov (2014) Characterization of the CD14++CD16+ monocyte population in human bone marrow. *PLoS One,* 9**,** e112140.
Mann, A., K. Breuhahn, P. Schirmacher & M. Blessing (2001) Keratinocyte-derived granulocyte-macrophage colony stimulating factor accelerates wound healing: Stimulation of keratinocyte proliferation, granulation tissue formation, and vascularization. *J Invest Dermatol,* 117**,** 1382-90.
Mantovani, A., S. K. Biswas, M. R. Galdiero, A. Sica & M. Locati (2013) Macrophage plasticity and polarization in tissue repair and remodelling. *J Pathol,* 229**,** 176-85.
Marbaix, E., I. Kokorine, J. Donnez, Y. Eeckhout & P. J. Courtoy (1996a) Regulation and restricted expression of interstitial collagenase suggest a pivotal role in the initiation of menstruation. *Hum Reprod,* 11 Suppl 2**,** 134-43.
Marbaix, E., I. Kokorine, P. Moulin, J. Donnez, Y. Eeckhout & P. J. Courtoy (1996b) Menstrual breakdown of human endometrium can be mimicked in vitro and is selectively and reversibly blocked by inhibitors of matrix metalloproteinases. *Proc Natl Acad Sci U S A,* 93**,** 9120-5.
Markee, J. E. (1978) Menstruation in intraocular endometrial transplants in the Rhesus monkey. *Am J Obstet Gynecol,* 131**,** 558-9.
Marquez-Curtis, L. A., A. Janowska-Wieczorek, L. E. McGann & J. A. Elliott (2015) Mesenchymal stromal cells derived from various tissues: Biological, clinical and cryopreservation aspects. *Cryobiology,* 71**,** 181-97.
Marshall, J. C., A. C. Dalkin, D. J. Haisenleder, S. J. Paul, G. A. Ortolano & R. P. Kelch (1991) Gonadotropin-releasing hormone pulses: regulators of gonadotropin synthesis and ovulatory cycles. *Recent Prog Horm Res,* 47**,** 155-87; discussion 188-9.
Martin, K., J. Pritchett, J. Llewellyn, A. F. Mullan, V. S. Athwal, R. Dobie, E. Harvey, L. Zeef, S. Farrow, C. Streuli, N. C. Henderson, S. L. Friedman, N. A. Hanley & K. Piper Hanley (2016) PAK proteins and YAP-1 signalling downstream of integrin beta-1 in myofibroblasts promote liver fibrosis. *Nat Commun,* 7**,** 12502.
Martin, P. & S. J. Leibovich (2005) Inflammatory cells during wound repair: the good, the bad and the ugly. *Trends Cell Biol,* 15**,** 599-607.
Martinez, F. O., S. Gordon, M. Locati & A. Mantovani (2006) Transcriptional profiling of the human monocyte-to-macrophage differentiation and polarization: new molecules and patterns of gene expression. *J Immunol,* 177**,** 7303-11.
Masuda, H., S. S. Anwar, H. J. Bühring, J. R. Rao & C. E. Gargett (2012) A novel marker of human endometrial mesenchymal stem-like cells. *Cell Transplant,* 21**,** 2201-14.

Masuda, H., T. Maruyama, C. E. Gargett, K. Miyazaki, Y. Matsuzaki, H. Okano & M. Tanaka (2015) Endometrial side population cells: potential adult stem/progenitor cells in endometrium. *Biol Reprod,* 93**,** 84.

Masuda, H., T. Maruyama, E. Hiratsu, J. Yamane, A. Iwanami, T. Nagashima, M. Ono, H. Miyoshi, H. J. Okano, M. Ito, N. Tamaoki, T. Nomura, H. Okano, Y. Matsuzaki & Y. Yoshimura (2007) Noninvasive and real-time assessment of reconstructed functional human endometrium in NOD/SCID/gamma c(null) immunodeficient mice. *Proc Natl Acad Sci U S A,* 104**,** 1925-30.

Masuda, H., Y. Matsuzaki, E. Hiratsu, M. Ono, T. Nagashima, T. Kajitani, T. Arase, H. Oda, H. Uchida, H. Asada, M. Ito, Y. Yoshimura, T. Maruyama & H. Okano (2010) Stem cell-like properties of the endometrial side population: implication in endometrial regeneration. *PLoS One,* 5**,** e10387.

Matsumoto, H., K. Sakai & M. Iwashita (2008) Insulin-like growth factor binding protein-1 induces decidualization of human endometrial stromal cells via alpha5beta1 integrin. *Mol Hum Reprod,* 14**,** 485-9.

Matsuura-Sawada, R., T. Murakami, Y. Ozawa, H. Nabeshima, J. Akahira, Y. Sato, Y. Koyanagi, M. Ito, Y. Terada & K. Okamura (2005) Reproduction of menstrual changes in transplanted human endometrial tissue in immunodeficient mice. *Hum Reprod,* 20**,** 1477-84.

Matsuzaki, S. & C. Darcha (2012) Epithelial to mesenchymal transition-like and mesenchymal to epithelial transition-like processes might be involved in the pathogenesis of pelvic endometriosis. *Hum Reprod,* 27**,** 712-21.

Maybin, J. A. & H. O. Critchley (2011) Progesterone: a pivotal hormone at menstruation. *Ann N Y Acad Sci,* 1221**,** 88-97.

--- (2012) Steroid regulation of menstrual bleeding and endometrial repair. *Rev Endocr Metab Disord,* 13**,** 253-63.

--- (2015) Menstrual physiology: implications for endometrial pathology and beyond. *Hum Reprod Update,* 21**,** 748-61.

Maybin, J. A., N. Hirani, P. Brown, H. N. Jabbour & H. O. Critchley (2011a) The regulation of vascular endothelial growth factor by hypoxia and prostaglandin F_2 α during human endometrial repair. *J Clin Endocrinol Metab,* 96**,** 2475-83.

Maybin, J. A., N. Hirani, H. N. Jabbour & H. O. Critchley (2011b) Novel roles for hypoxia and prostaglandin E2 in the regulation of IL-8 during endometrial repair. *Am J Pathol,* 178**,** 1245-56.

Maybin, J. A., A. A. Murray, P. T. K. Saunders, N. Hirani, P. Carmeliet & H. O. D. Critchley (2018) Hypoxia and hypoxia inducible factor-1α are required for normal endometrial repair during menstruation. *Nat Commun,* 9**,** 295.

McLennan, C. E. & A. H. Rydell (1965) Extent of endometrial shedding during normal menstruation. *Obstet Gynecol,* 26**,** 605-21.

McNeil, P. L. & T. Kirchhausen (2005) An emergency response team for membrane repair. *Nat Rev Mol Cell Biol,* 6**,** 499-505.

Menning, A., A. Walter, M. Rudolph, I. Gashaw, K. H. Fritzemeier & L. Roese (2012) Granulocytes and vascularization regulate uterine bleeding and tissue remodeling in a mouse menstruation model. *PLoS ONE*.

Menzies, F. M., M. C. Shepherd, R. J. Nibbs & S. M. Nelson (2011) The role of mast cells and their mediators in reproduction, pregnancy and labour. *Hum Reprod Update,* 17**,** 383-96.

Merlo, S., G. Frasca, P. L. Canonico & M. A. Sortino (2009) Differential involvement of estrogen receptor alpha and estrogen receptor beta in the healing promoting effect of estrogen in human keratinocytes. *J Endocrinol,* 200**,** 189-97.

Michelotti, G. A., G. Xie, M. Swiderska, S. S. Choi, G. Karaca, L. Krüger, R. Premont, L. Yang, W. K. Syn, D. Metzger & A. M. Diehl (2013) Smoothened is a master regulator of adult liver repair. *J Clin Invest,* 123**,** 2380-94.

Mills, S. J., A. J. Cowin & P. Kaur (2013) Pericytes, mesenchymal stem cells and the wound healing process. *Cells,* 2**,** 621-34.

Miyazaki, K., T. Maruyama, H. Masuda, A. Yamasaki, S. Uchida, H. Oda, H. Uchida & Y. Yoshimura (2012) Stem cell-like differentiation potentials of endometrial side population cells as revealed by a newly developed in vivo endometrial stem cell assay. *PLoS One,* 7**,** e50749.

Moffett, A. & C. Loke (2006) Implantation, embryo-maternal interactions, immunology and modulation of the uterine environment -- a workshop report. *Placenta,* 27 Suppl A**,** S54-5.

Monteiro, R. A., E. Rocha & M. M. Marini-Abreu (1996) Do microglia arise from pericytes? An ultrastructural and distribution study in the rat cerebellar cortex. *J Submicrosc Cytol Pathol,* 28**,** 457-69.
Morelli, S. S., P. Rameshwar & L. T. Goldsmith (2013) Experimental evidence for bone marrow as a source of nonhematopoietic endometrial stromal and epithelial compartment cells in a murine model. *Biol Reprod,* 89**,** 7.
Morris, M. W., M. Allukian, B. J. Herdrich, R. C. Caskey, C. Zgheib, J. Xu, W. Dorsett-Martin, M. E. Mitchell & K. W. Liechty (2014) Modulation of the inflammatory response by increasing fetal wound size or interleukin-10 overexpression determines wound phenotype and scar formation. *Wound Repair Regen,* 22**,** 406-14.
Mosser, D. M. & J. P. Edwards (2008) Exploring the full spectrum of macrophage activation. *Nat Rev Immunol,* 8**,** 958-69.
Motta, P. M., S. Makabe & S. A. Nottola (1997) The ultrastructure of human reproduction. I. The natural history of the female germ cell: origin, migration and differentiation inside the developing ovary. *Hum Reprod Update,* 3**,** 281-95.
Mueller, M. D., D. I. Lebovic, E. Garrett & R. N. Taylor (2000) Neutrophils infiltrating the endometrium express vascular endothelial growth factor: potential role in endometrial angiogenesis. *Fertil Steril,* 74**,** 107-12.
Munro, M. G., K. Dickersin, M. A. Clark, P. Langenberg, R. W. Scherer, K. D. Frick & S. T. O. P. f. D. U. B. Group (2011) The Surgical Treatments Outcomes Project for Dysfunctional Uterine Bleeding: summary of an Agency for Health Research and Quality-sponsored randomized trial of endometrial ablation versus hysterectomy for women with heavy menstrual bleeding. *Menopause,* 18**,** 445-52.
Murakami, K., Y. H. Lee, E. S. Lucas, Y. W. Chan, R. P. Durairaj, S. Takeda, J. D. Moore, B. K. Tan, S. Quenby, J. K. Chan, C. E. Gargett & J. J. Brosens (2014) Decidualization induces a secretome switch in perivascular niche cells of the human endometrium. *Endocrinology,* 155**,** 4542-53.
Murray, I. R., C. C. West, W. R. Hardy, A. W. James, T. S. Park, A. Nguyen, T. Tawonsawatruk, L. Lazzari, C. Soo & B. Péault (2014) Natural history of mesenchymal stem cells, from vessel walls to culture vessels. *Cellular and Molecular Life Sciences,* 71**,** 1353-1374.
Naftalin, J. & D. Jurkovic (2009) The endometrial-myometrial junction: a fresh look at a busy crossing. *Ultrasound Obstet Gynecol,* 34**,** 1-11.
Nagase, H., R. Visse & G. Murphy (2006) Structure and function of matrix metalloproteinases and TIMPs. *Cardiovasc Res,* 69**,** 562-73.
Nagori, C. B., S. Y. Panchal & H. Patel (2011) Endometrial regeneration using autologous adult stem cells followed by conception by in vitro fertilization in a patient of severe Asherman's syndrome. *J Hum Reprod Sci,* 4**,** 43-8.
Nahrendorf, M., F. K. Swirski, E. Aikawa, L. Stangenberg, T. Wurdinger, J. L. Figueiredo, P. Libby, R. Weissleder & M. J. Pittet (2007) The healing myocardium sequentially mobilizes two monocyte subsets with divergent and complementary functions. *J Exp Med,* 204**,** 3037-47.
Nayak, N. R. & R. M. Brenner (2002) Vascular proliferation and vascular endothelial growth factor expression in the rhesus macaque endometrium. *J Clin Endocrinol Metab,* 87**,** 1845-55.
Nguyen, H. P. T., L. Xiao, J. A. Deane, K. S. Tan, F. L. Cousins, H. Masuda, C. N. Sprung, A. Rosamilia & C. E. Gargett (2017) N-cadherin identifies human endometrial epithelial progenitor cells by in vitro stem cell assays. *Hum Reprod,* 32**,** 2254-2268.
Niklaus, A. L., C. R. Murphy & A. Lopata (2001) Characteristics of the uterine luminal surface epithelium at preovulatory and preimplantation stages in the marmoset monkey. *Anat Rec,* 264**,** 82-92.
Niswender, G. D., J. L. Juengel, P. J. Silva, M. K. Rollyson & E. W. McIntush (2000) Mechanisms controlling the function and life span of the corpus luteum. *Physiol Rev,* 80**,** 1-29.
Nitsch, S. M., F. Wittmann, P. Angele, M. W. Wichmann, R. Hatz, T. Hernandez-Richter, I. H. Chaudry, K. W. Jauch & M. K. Angele (2004) Physiological levels of 5 alpha-dihydrotestosterone depress wound immune function and impair wound healing following trauma-hemorrhage. *Arch Surg,* 139**,** 157-63.
Novak, E. (1946) Functional uterine bleeding; a summarizing review. *Obstet Gynecol Surv,* 1**,** 682-98.
Nowak, J., B. Borkowska & B. Pawlowski (2016) Leukocyte changes across menstruation, ovulation, and mid-luteal phase and association with sex hormone variation. *Am J Hum Biol,* 28**,** 721-8.

Noyes, R. W., A. T. Hertig & J. Rock (1975) Dating the endometrial biopsy. *Am J Obstet Gynecol,* 122**,** 262-3.
Nurden, A. T., P. Nurden, M. Sanchez, I. Andia & E. Anitua (2008) Platelets and wound healing. *Front Biosci,* 13**,** 3532-48.
Okada, S., H. Kita, T. J. George, G. J. Gleich & K. M. Leiferman (1997) Migration of eosinophils through basement membrane components in vitro: role of matrix metalloproteinase-9. *Am J Respir Cell Mol Biol,* 17**,** 519-28.
Oróstica, L., I. Astorga, F. Plaza-Parrochia, C. Vera, V. García, R. Carvajal, F. Gabler, C. Romero & M. Vega (2016) Proinflammatory environment and role of TNF-α in endometrial function of obese women having polycystic ovarian syndrome. *Int J Obes (Lond),* 40**,** 1715-1722.
Ozerdem, U., E. Monosov & W. B. Stallcup (2002) NG2 proteoglycan expression by pericytes in pathological microvasculature. *Microvasc Res,* 63**,** 129-34.
P. Hess, A., N. R. Nayak & L. Giudice. 2006. *Oviduct and EndometriumCyclic Changes in the Primate Oviduct and Endometrium*.
Padykula, H. A., L. G. Coles, W. C. Okulicz, S. I. Rapaport, J. A. McCracken, N. W. King, C. Longcope & I. R. Kaiserman-Abramof (1989) The basalis of the primate endometrium: a bifunctional germinal compartment. *Biol Reprod,* 40**,** 681-90.
Paquet-Fifield, S., H. Schlüter, A. Li, T. Aitken, P. Gangatirkar, D. Blashki, R. Koelmeyer, N. Pouliot, M. Palatsides, S. Ellis, N. Brouard, A. Zannettino, N. Saunders, N. Thompson, J. Li & P. Kaur (2009) A role for pericytes as microenvironmental regulators of human skin tissue regeneration. *J Clin Invest,* 119**,** 2795-806.
Parasar, P., C. R. Sacha, N. Ng, E. R. McGuirk, S. Chinthala, P. Ozcan, J. Lindsey, S. Salas, M. R. Laufer, S. A. Missmer & R. M. Anchan (2017) Differentiating mouse embryonic stem cells express markers of human endometrium. *Reprod Biol Endocrinol,* 15**,** 52.
Patterson, A. L. & J. K. Pru (2013) Long-term label retaining cells localize to distinct regions within the female reproductive epithelium. *Cell Cycle,* 12**,** 2888-98.
Patterson, A. L., L. Zhang, N. A. Arango, J. Teixeira & J. K. Pru (2013) Mesenchymal-to-epithelial transition contributes to endometrial regeneration following natural and artificial decidualization. *Stem Cells Dev,* 22**,** 964-74.
Peake, M. A., M. Caley, P. J. Giles, I. Wall, S. Enoch, L. C. Davies, D. Kipling, D. W. Thomas & P. Stephens (2014) Identification of a transcriptional signature for the wound healing continuum. *Wound Repair Regen,* 22**,** 399-405.
Pelus, L. M. & S. Fukuda (2006) Peripheral blood stem cell mobilization: the CXCR2 ligand GRObeta rapidly mobilizes hematopoietic stem cells with enhanced engraftment properties. *Exp Hematol,* 34**,** 1010-20.
Perkins, S. & R. A. Fleischman (1990) Stromal cell progeny of murine bone marrow fibroblast colony-forming units are clonal endothelial-like cells that express collagen IV and laminin. *Blood,* 75**,** 620-5.
Peterson, A. P., L. C. Altman, J. S. Hill, K. Gosney & M. E. Kadin (1981) Glucocorticoid receptors in normal human eosinophils: comparison with neutrophils. *J Allergy Clin Immunol,* 68**,** 212-7.
Phan, S. H., K. Zhang, H. Y. Zhang & M. Gharaee-Kermani (1999) The myofibroblast as an inflammatory cell in pulmonary fibrosis. *Curr Top Pathol,* 93**,** 173-82.
Phinney, D. G. & D. J. Prockop (2007) Concise review: mesenchymal stem/multipotent stromal cells: the state of transdifferentiation and modes of tissue repair--current views. *Stem Cells,* 25**,** 2896-902.
Pietryga, E. & W. Woźniak (1992) The growth and topography of the human fetal uterus. *Folia Morphol (Warsz),* 51**,** 165-80.
Platz, E. A. & E. Giovannucci (2004) The epidemiology of sex steroid hormones and their signaling and metabolic pathways in the etiology of prostate cancer. *J Steroid Biochem Mol Biol,* 92**,** 237-53.
Plunk, M., J. H. Lee, K. Kani & M. Dighe (2013) Imaging of postpartum complications: a multimodality review. *AJR Am J Roentgenol,* 200**,** W143-54.
Pober, J. S. & G. Tellides (2012) Participation of blood vessel cells in human adaptive immune responses. *Trends Immunol,* 33**,** 49-57.
Prianishnikov, V. A. (1978) On the concept of stem cell and a model of functional-morphological structure of the endometrium. *Contraception,* 18**,** 213-23.
Punyadeera, C., V. L. Thijssen, S. Tchaikovski, R. Kamps, B. Delvoux, G. A. Dunselman, A. F. de Goeij, A. W. Griffioen & P. G. Groothuis (2006) Expression and regulation of vascular

endothelial growth factor ligands and receptors during menstruation and post-menstrual repair of human endometrium. *Mol Hum Reprod,* 12**,** 367-75.
Qian, L. W., A. B. Fourcaudot, K. Yamane, T. You, R. K. Chan & K. P. Leung (2016) Exacerbated and prolonged inflammation impairs wound healing and increases scarring. *Wound Repair Regen,* 24**,** 26-34.
Radzun, H. J. (2015) History and perspectives of the monocyte-macrophage system. *Pathologe,* 36**,** 432-441.
Rafii, S., Z. Cao, R. Lis, I. I. Siempos, D. Chavez, K. Shido, S. Y. Rabbany & B. S. Ding (2015) Platelet-derived SDF-1 primes the pulmonary capillary vascular niche to drive lung alveolar regeneration. *Nat Cell Biol,* 17**,** 123-136.
Raica, M. & A. M. Cimpean (2010) Platelet-Derived Growth Factor (PDGF)/PDGF Receptors (PDGFR) Axis as Target for Antitumor and Antiangiogenic Therapy. *Pharmaceuticals (Basel),* 3**,** 572-599.
Rajkumar, V. S., X. Shiwen, M. Bostrom, P. Leoni, J. Muddle, M. Ivarsson, B. Gerdin, C. P. Denton, G. Bou-Gharios, C. M. Black & D. J. Abraham (2006) Platelet-derived growth factor-beta receptor activation is essential for fibroblast and pericyte recruitment during cutaneous wound healing. *Am J Pathol,* 169**,** 2254-65.
Ramos-Vara, J. A. & M. A. Miller (2014) When tissue antigens and antibodies get along: revisiting the technical aspects of immunohistochemistry--the red, brown, and blue technique. *Vet Pathol,* 51**,** 42-87.
Rastegar, F., D. Shenaq, J. Huang, W. Zhang, B. Q. Zhang, B. C. He, L. Chen, G. W. Zuo, Q. Luo, Q. Shi, E. R. Wagner, E. Huang, Y. Gao, J. L. Gao, S. H. Kim, J. Z. Zhou, Y. Bi, Y. Su, G. Zhu, J. Luo, X. Luo, J. Qin, R. R. Reid, H. H. Luu, R. C. Haydon, Z. L. Deng & T. C. He (2010) Mesenchymal stem cells: Molecular characteristics and clinical applications. *World J Stem Cells,* 2**,** 67-80.
Rasweiler, J. J. (1991) Spontaneous decidual reactions and menstruation in the black mastiff bat, Molossus ater. *Am J Anat,* 191**,** 1-22.
Rasweiler, J. J., N. K. Badwaik & K. V. Mechineni (2011) Ovulation, fertilization, and early embryonic development in the menstruating fruit bat, Carollia perspicillata. *Anat Rec (Hoboken),* 294**,** 506-19.
Rasweiler, J. J. & H. de Bonilla (1992) Menstruation in short-tailed fruit bats (Carollia spp.). *J Reprod Fertil,* 95**,** 231-48.
Reardon, S. N., M. L. King, J. A. MacLean, J. L. Mann, F. J. DeMayo, J. P. Lydon & K. Hayashi (2012) CDH1 is essential for endometrial differentiation, gland development, and adult function in the mouse uterus. *Biol Reprod,* 86**,** 141, 1-10.
Ribatti, D., B. Nico & A. Vacca (2015) Multiple myeloma as a model for the role of bone marrow niches in the control of angiogenesis. *Int Rev Cell Mol Biol,* 314**,** 259-82.
Riesewijk, A., J. Martín, R. van Os, J. A. Horcajadas, J. Polman, A. Pellicer, S. Mosselman & C. Simón (2003) Gene expression profiling of human endometrial receptivity on days LH+2 versus LH+7 by microarray technology. *Mol Hum Reprod,* 9**,** 253-64.
Rogers A.W. & K.M. Abberton 2003. Endometrial arteriogenesis: Vascular smooth muscle cell proliferation and differentiation during the menstrual cycle and changes associated with endometrial bleeding disorders. *Microsc Res Tech.* 1:412-9
Rosas, M., B. Thomas, M. Stacey, S. Gordon & P. R. Taylor (2010) The myeloid 7/4-antigen defines recently generated inflammatory macrophages and is synonymous with Ly-6B. *J Leukoc Biol,* 88**,** 169-80.
Rose, S., A. Misharin & H. Perlman (2012) A novel Ly6C/Ly6G-based strategy to analyze the mouse splenic myeloid compartment. *Cytometry A,* 81**,** 343-50.
Rudolph, M., W. D. Döcke, A. Müller, A. Menning, L. Röse, T. M. Zollner & I. Gashaw (2012) Induction of Overt menstruation in intact mice. *PLoS ONE*.
Ryan, A. J., B. Susil, T. W. Jobling & M. K. Oehler (2005) Endometrial cancer. *Cell Tissue Res,* 322**,** 53-61.
Sahin Ersoy, G., M. M. Zolbin, E. Cosar, I. Moridi, R. Mamillapalli & H. S. Taylor (2017) CXCL12 Promotes Stem Cell Recruitment and Uterine Repair after Injury in Asherman's Syndrome. *Mol Ther Methods Clin Dev,* 4**,** 169-177.
Sakuma, R., M. Kawahara, A. Nakano-Doi, A. Takahashi, Y. Tanaka, A. Narita, S. Kuwahara-Otani, T. Hayakawa, H. Yagi, T. Matsuyama & T. Nakagomi (2016) Brain pericytes serve as

microglia-generating multipotent vascular stem cells following ischemic stroke. *J Neuroinflammation,* 13**,** 57.
Salamonsen, L. A. (1998) Current concepts of the mechanisms of menstruation: a normal process of tissue destruction. *Trends Endocrinol Metab,* 9**,** 305-9.
--- (2003a) Review Tissue injury and repair in the female human reproductive tract. 301-311.
--- (2003b) Tissue injury and repair in the female human reproductive tract. *Reproduction,* 125**,** 301-11.
Salamonsen, L. a. & L. J. Lathbury (2000) Endometrial leukocytes and menstruation. *Human reproduction update,* 6**,** 16-27.
Salamonsen, L. A., M. M. Marsh & J. K. Findlay (1999) Endometrial endothelin: regulator of uterine bleeding and endometrial repair. *Clin Exp Pharmacol Physiol,* 26**,** 154-7.
Salamonsen, L. A. & D. E. Woolley (1999) Menstruation: induction by matrix metalloproteinases and inflammatory cells. *J Reprod Immunol,* 44**,** 1-27.
Salamonsen, L. A., J. Zhang & M. Brasted (2002) Leukocyte networks and human endometrial remodelling. *J Reprod Immunol,* 57**,** 95-108.
Salamonsen, L. A., J. Zhang, A. Hampton & L. Lathbury (2000) Regulation of matrix metalloproteinases in human endometrium. *Hum Reprod,* 15 Suppl 3**,** 112-9.
Salker, M., G. Teklenburg, M. Molokhia, S. Lavery, G. Trew, T. Aojanepong, H. J. Mardon, A. U. Lokugamage, R. Rai, C. Landles, B. A. Roelen, S. Quenby, E. W. Kuijk, A. Kavelaars, C. J. Heijnen, L. Regan, N. S. Macklon & J. J. Brosens (2010) Natural selection of human embryos: impaired decidualization of endometrium disables embryo-maternal interactions and causes recurrent pregnancy loss. *PLoS One,* 5**,** e10287.
Sampson, J. A. (1927) Metastatic or Embolic Endometriosis, due to the Menstrual Dissemination of Endometrial Tissue into the Venous Circulation. *Am J Pathol,* 3**,** 93-110.43.
SantaLucia, J. (2007) Physical principles and visual-OMP software for optimal PCR design. *Methods Mol Biol,* 402**,** 3-34.
Sasmono, R. T., D. Oceandy, J. W. Pollard, W. Tong, P. Pavli, B. J. Wainwright, M. C. Ostrowski, S. R. Himes & D. A. Hume (2003) A macrophage colony-stimulating factor receptor-green fluorescent protein transgene is expressed throughout the mononuclear phagocyte system of the mouse. *Blood,* 101**,** 1155-63.
Sasmono, R. T. & E. Williams (2012) Generation and characterization of MacGreen mice, the Cfs1r-EGFP transgenic mice. *Methods Mol Biol,* 844**,** 157-76.
Schneikert, J., P. A. Peterziel H Fau - Defossez, H. Defossez Pa Fau - Klocker, Y. Klocker H Fau - de Launoit, A. C. de Launoit Y Fau - Cato & A. C. Cato Androgen receptor-Ets protein interaction is a novel mechanism for steroid hormone-mediated down-modulation of matrix metalloproteinase expression.
Schulke, L., F. Manconi, R. Markham & I. S. Fraser (2008) Endometrial dendritic cell populations during the normal menstrual cycle. *Hum Reprod,* 23**,** 1574-80.
Schulz, C., E. Gomez Perdiguero, L. Chorro, H. Szabo-Rogers, N. Cagnard, K. Kierdorf, M. Prinz, B. Wu, S. E. Jacobsen, J. W. Pollard, J. Frampton, K. J. Liu & F. Geissmann (2012) A lineage of myeloid cells independent of Myb and hematopoietic stem cells. *Science,* 336**,** 86-90.
Schwab, K. E., R. W. S. Chan & C. E. Gargett (2005) Putative stem cell activity of human endometrial epithelial and stromal cells during the menstrual cycle. *Fertility and sterility,* 84**,** 1124-30.
Schwab, K. E. & C. E. Gargett (2007) Co-expression of two perivascular cell markers isolates mesenchymal stem-like cells from human endometrium. *Hum Reprod,* 22**,** 2903-11.
Sellin Jeffries, M. K., A. J. Kiss, A. W. Smith & J. T. Oris (2014) A comparison of commercially-available automated and manual extraction kits for the isolation of total RNA from small tissue samples. *BMC Biotechnol,* 14**,** 94.
Semenza, G. L. (1998) Hypoxia-inducible factor 1: master regulator of O2 homeostasis. *Curr Opin Genet Dev,* 8**,** 588-94.
Sensky, T. E. & D. T. Liu (1980) Endometriosis: associations with menorrhagia, infertility and oral contraceptives. *Int J Gynaecol Obstet,* 17**,** 573-6.
Shapouri-Moghaddam, A., S. Mohammadian, H. Vazini, M. Taghadosi, S. A. Esmaeili, F. Mardani, B. Seifi, A. Mohammadi, J. T. Afshari & A. Sahebkar (2018) Macrophage plasticity, polarization, and function in health and disease. *J Cell Physiol,* 233**,** 6425-6440.
Sharman, A. (1952) An experimental study of post-partum endometrial repair in the guinea-pig and rat. *J Endocrinol,* 8**,** 162-8.
Shaw, T. J. & P. Martin (2009) Wound repair at a glance. *J Cell Sci,* 122**,** 3209-13.
--- (2016) Wound repair: a showcase for cell plasticity and migration. *Curr Opin Cell Biol,* 42**,** 29-37.

Shenoy, A. K. & J. Lu (2017) Relevance of epithelial-to-pericyte transition in cancer. *Mol Cell Oncol,* 4**,** e1260672.
Shi, S. & S. Gronthos (2003) Perivascular niche of postnatal mesenchymal stem cells in human bone marrow and dental pulp. *J Bone Miner Res,* 18**,** 696-704.
Shimada-Hiratsuka, M., M. Naito, C. Kaizu, J. Shuying, G. Hasegawa & L. D. Shultz (2000) Defective macrophage recruitment and clearance of apoptotic cells in the uterus of osteopetrotic mutant mice lacking macrophage colony-stimulating factor (M-CSF). *J Submicrosc Cytol Pathol,* 32**,** 297-307.
Shinzawa, H., A. Takeda, Y. Sone, K. Murashita & E. Uchinuma (2007) Wound healing process of a full-thickness skin wound model in rats. *Int Surg,* 92**,** 63-72.
Sivridis, E., A. Giatromanolaki, P. Anastasiadis, L. Georgiou, K. C. Gatter, A. L. Harris, R. Bicknell, M. I. Koukourakis & T. a. A. R. Group (2002) Angiogenic co-operation of VEGF and stromal cell TP in endometrial carcinomas. *J Pathol,* 196**,** 416-22.
Slayden, O. D. & R. M. Brenner (2006) A critical period of progesterone withdrawal precedes menstruation in macaques. *Reprod Biol Endocrinol,* 4 Suppl 1**,** S6.
Smith, O. P., H. N. Jabbour & H. O. Critchley (2007) Cyclooxygenase enzyme expression and E series prostaglandin receptor signalling are enhanced in heavy menstruation. *Hum Reprod,* 22**,** 1450-6.
Smith, S. K., M. H. Abel, R. W. Kelly & D. T. Baird (1981) Prostaglandin synthesis in the endometrium of women with ovular dysfunctional uterine bleeding. *Br J Obstet Gynaecol,* 88**,** 434-42.
Son, B. R., L. A. Marquez-Curtis, M. Kucia, M. Wysoczynski, A. R. Turner, J. Ratajczak, M. Z. Ratajczak & A. Janowska-Wieczorek (2006) Migration of bone marrow and cord blood mesenchymal stem cells in vitro is regulated by stromal-derived factor-1-CXCR4 and hepatocyte growth factor-c-met axes and involves matrix metalloproteinases. *Stem Cells,* 24**,** 1254-64.
Son, E. D., J. Y. Lee, S. Lee, M. S. Kim, B. G. Lee, I. S. Chang & J. H. Chung (2005) Topical application of 17beta-estradiol increases extracellular matrix protein synthesis by stimulating tgf-Beta signaling in aged human skin in vivo. *J Invest Dermatol,* 124**,** 1149-61.
Sorg, H., D. J. Tilkorn, S. Hager, J. Hauser & U. Mirastschijski (2017) Skin Wound Healing: An Update on the Current Knowledge and Concepts. *Eur Surg Res,* 58**,** 81-94.
Spencer, T. E., K. A. Dunlap & J. Filant (2012) Comparative developmental biology of the uterus: insights into mechanisms and developmental disruption. *Mol Cell Endocrinol,* 354**,** 34-53.
Spencer, T. E., K. Hayashi, J. Hu & K. D. Carpenter (2005) Comparative developmental biology of the mammalian uterus. *Curr Top Dev Biol,* 68**,** 85-122.
Spitzer, T. L., A. Rojas, Z. Zelenko, L. Aghajanova, D. W. Erikson, F. Barragan, M. Meyer, J. S. Tamaresis, A. E. Hamilton, J. C. Irwin & L. C. Giudice (2012a) Perivascular human endometrial mesenchymal stem cells express pathways relevant to self-renewal, lineage specification, and functional phenotype. *Biol Reprod,* 86**,** 58.
Stark, K., A. Eckart, S. Haidari, A. Tirniceriu, M. Lorenz, M. L. von Brühl, F. Gärtner, A. G. Khandoga, K. R. Legate, R. Pless, I. Hepper, K. Lauber, B. Walzog & S. Massberg (2013) Capillary and arteriolar pericytes attract innate leukocytes exiting through venules and 'instruct' them with pattern-recognition and motility programs. *Nat Immunol,* 14**,** 41-51.
Starkey, P. M., L. M. Clover & M. C. Rees (1991) Variation during the menstrual cycle of immune cell populations in human endometrium. *Eur J Obstet Gynecol Reprod Biol,* 39**,** 203-7.
Stout, R. D. & J. Suttles (2004) Functional plasticity of macrophages: reversible adaptation to changing microenvironments. *Journal of Leukocyte Biology,* 76**,** 509-13.
Strassmann, B. I. (1996) The evolution of endometrial cycles and menstruation. *Q Rev Biol,* 71**,** 181-220.
Stratman, A. N., K. M. Malotte, R. D. Mahan, M. J. Davis & G. E. Davis (2009) Pericyte recruitment during vasculogenic tube assembly stimulates endothelial basement membrane matrix formation. *Blood,* 114**,** 5091-101.
Sugino, N., A. Karube-Harada, S. Kashida, S. Takiguchi & H. Kato (2002) Differential regulation of copper-zinc superoxide dismutase and manganese superoxide dismutase by progesterone withdrawal in human endometrial stromal cells. *Mol Hum Reprod,* 8**,** 68-74.
Sugino, N., A. Karube-Harada, T. Taketani, A. Sakata & Y. Nakamura (2004) Withdrawal of ovarian steroids stimulates prostaglandin F2alpha production through nuclear factor-kappaB activation via oxygen radicals in human endometrial stromal cells: potential relevance to menstruation. *J Reprod Dev,* 50**,** 215-25.

Szpaderska, A. M., J. D. Zuckerman & L. A. DiPietro (2003) Differential injury responses in oral mucosal and cutaneous wounds. *J Dent Res,* 82**,** 621-6.
Tagliani, E. & A. Erlebacher (2011) Dendritic cell function at the maternal-fetal interface. *Expert Rev Clin Immunol,* 7**,** 593-602.
Takahashi, A., H. Nakajima, K. Uchida, N. Takeura, K. Honjoh, S. Watanabe, M. Kitade, Y. Kokubo, W. E. B. Johnson & A. Matsumine (2018) Comparison of Mesenchymal Stromal Cells Isolated from Murine Adipose Tissue and Bone Marrow in the Treatment of Spinal Cord Injury. *Cell Transplant***,** 963689718780309.
Takamoto, N., P. C. Leppert & S. Y. Yu (1998) Cell death and proliferation and its relation to collagen degradation in uterine involution of rat. *Connect Tissue Res,* 37**,** 163-75.
Taketani, Y. & M. Mizuno (1988) Cyclic changes in epidermal growth factor receptor in human endometrium during menstrual cycle. *Endocrinol Jpn,* 35**,** 19-25.
Talbi, S., A. E. Hamilton, K. C. Vo, S. Tulac, M. T. Overgaard, C. Dosiou, N. Le Shay, C. N. Nezhat, R. Kempson, B. A. Lessey, N. R. Nayak & L. C. Giudice (2006) Molecular phenotyping of human endometrium distinguishes menstrual cycle phases and underlying biological processes in normo-ovulatory women. *Endocrinology,* 147**,** 1097-121.
Tamama, K. & S. S. Kerpedjieva (2012) Acceleration of Wound Healing by Multiple Growth Factors and Cytokines Secreted from Multipotential Stromal Cells/Mesenchymal Stem Cells. *Adv Wound Care (New Rochelle),* 1**,** 177-182.
Tamaoki, M., K. Imanaka-Yoshida, K. Yokoyama, T. Nishioka, H. Inada, M. Hiroe, T. Sakakura & T. Yoshida (2005) Tenascin-C regulates recruitment of myofibroblasts during tissue repair after myocardial injury. *Am J Pathol,* 167**,** 71-80.
Tan, S. C. & B. C. Yiap (2009) DNA, RNA, and protein extraction: the past and the present. *J Biomed Biotechnol,* 2009**,** 574398.
Taylor, H. S. (2004) Endometrial cells derived from donor stem cells in bone marrow transplant recipients. *JAMA,* 292**,** 81-5.
Tetlow, R. L., I. Richmond, D. J. Manton, J. Greenman, L. W. Turnbull & S. R. Killick (1999) Histological analysis of the uterine junctional zone as seen by transvaginal ultrasound. *Ultrasound Obstet Gynecol,* 14**,** 188-93.
Thannickal, V. J. & J. C. Horowitz (2006) Evolving concepts of apoptosis in idiopathic pulmonary fibrosis. *Proc Am Thorac Soc,* 3**,** 350-6.
Theilgaard-Mönch, K., S. Knudsen, P. Follin & N. Borregaard (2004) The transcriptional activation program of human neutrophils in skin lesions supports their important role in wound healing. *J Immunol,* 172**,** 7684-93.
Thiruchelvam, U., I. Dransfield, P. T. Saunders & H. O. Critchley (2013) The importance of the macrophage within the human endometrium. *J Leukoc Biol,* 93**,** 217-25.
Thiruchelvam, U., J. A. Maybin, G. M. Armstrong, E. Greaves, P. T. Saunders & H. O. Critchley (2016) Cortisol regulates the paracrine action of macrophages by inducing vasoactive gene expression in endometrial cells. *J Leukoc Biol,* 99**,** 1165-71.
Thomas, W. E. (1999) Brain macrophages: on the role of pericytes and perivascular cells. *Brain Res Brain Res Rev,* 31**,** 42-57.
Thomson, A. J., J. F. Telfer, A. Young, S. Campbell, C. J. R. Stewart, I. T. Cameron, I. A. Greer & J. E. Norman (1999) Leukocytes infiltrate the myometrium during human parturition: Further evidence that labour is an inflammatory process. *Human Reproduction*.
Tikare, S. N., K. K. Das & S. A. Dhundasi (2008) Blood leukocyte profile in different phases of menstrual cycle. *Indian J Physiol Pharmacol,* 52**,** 201-4.
Timonen, S., J. Tuominen, K. Irjala & J. Mäenpää (2002) Ovarian function and regulation of the hypothalamic-pituitary-ovarian axis after tubal sterilization. *J Reprod Med,* 47**,** 131-6.
Tintut, Y., Z. Alfonso, T. Saini, K. Radcliff, K. Watson, K. Boström & L. L. Demer (2003) Multilineage potential of cells from the artery wall. *Circulation,* 108**,** 2505-10.
Tomasek, J. J., G. Gabbiani, B. Hinz, C. Chaponnier & R. A. Brown (2002) Myofibroblasts and mechano-regulation of connective tissue remodelling. *Nat Rev Mol Cell Biol,* 3**,** 349-63.
Tremellen, K. P. & P. Russell (2012) The distribution of immune cells and macrophages in the endometrium of women with recurrent reproductive failure. II: adenomyosis and macrophages. *J Reprod Immunol,* 93**,** 58-63.
Tsai, H. H., E. Frost, V. To, S. Robinson, C. Ffrench-Constant, R. Geertman, R. M. Ransohoff & R. H. Miller (2002) The chemokine receptor CXCR2 controls positioning of oligodendrocyte precursors in developing spinal cord by arresting their migration. *Cell,* 110**,** 373-83.

Tsuji, S., M. Yoshimoto, K. Takahashi, Y. Noda, T. Nakahata & T. Heike (2008) Side population cells contribute to the genesis of human endometrium. *Fertil Steril,* 90**,** 1528-37.

Turner, K. J., S. Macpherson, M. R. Millar, A. S. McNeilly, K. Williams, M. Cranfield, N. P. Groome, R. M. Sharpe, H. M. Fraser & P. T. Saunders (2002) Development and validation of a new monoclonal antibody to mammalian aromatase. *J Endocrinol,* 172**,** 21-30.

Tushinski, R. J. & E. R. Stanley (1985) The regulation of mononuclear phagocyte entry into S phase by the colony stimulating factor CSF-1. *J Cell Physiol,* 122**,** 221-8.

Ulrich, M. M., M. Verkerk, L. Reijnen, M. Vlig, A. J. van den Bogaerdt & E. Middelkoop (2007) Expression profile of proteins involved in scar formation in the healing process of full-thickness excisional wounds in the porcine model. *Wound Repair Regen,* 15**,** 482-90.

Van Furth, R. & J. Thompson (1971) Review of the origin and kinetics of the promonocytes, monocytes, and macrophages and a brief discussion of the mononuclear phagocyte system. *Ann Inst Pasteur (Paris),* 120**,** 337-55.

Vanlandewijck, M., L. He, M. A. Mäe, J. Andrae, K. Ando, F. Del Gaudio, K. Nahar, T. Lebouvier, B. Laviña, L. Gouveia, Y. Sun, E. Raschperger, M. Räsänen, Y. Zarb, N. Mochizuki, A. Keller, U. Lendahl & C. Betsholtz (2018) A molecular atlas of cell types and zonation in the brain vasculature. *Nature,* 554**,** 475-480.

Vannella, K. M. & T. A. Wynn (2017) Mechanisms of Organ Injury and Repair by Macrophages. *Annu Rev Physiol,* 79**,** 593-617.

Vassilev, V., C. M. Pretto, P. B. Cornet, D. Delvaux, Y. Eeckhout, P. J. Courtoy, E. Marbaix & P. Henriet (2005) Response of matrix metalloproteinases and tissue inhibitors of metalloproteinases messenger ribonucleic acids to ovarian steroids in human endometrial explants mimics their gene- and phase-specific differential control in vivo. *J Clin Endocrinol Metab,* 90**,** 5848-57.

Vercellini, P., P. Viganò, E. Somigliana & L. Fedele (2014) Endometriosis: pathogenesis and treatment. *Nat Rev Endocrinol,* 10**,** 261-75.

Vries, M. H., A. Wagenaar, S. E. Verbruggen, D. G. Molin, I. Dijkgraaf, T. H. Hackeng & M. J. Post (2015) CXCL1 promotes arteriogenesis through enhanced monocyte recruitment into the peri-collateral space. *Angiogenesis,* 18**,** 163-71.

Walker, M. P., R. P. Diaugustine, E. Zeringue, M. K. Bunger, M. Schmitt, T. K. Archer & R. G. Richards (2010) An IGF1/insulin receptor substrate-1 pathway stimulates a mitotic kinase (cdk1) in the uterine epithelium during the proliferative response to estradiol. *J Endocrinol,* 207**,** 225-35.

Wallace, A. E., K. J. Sales, R. D. Catalano, R. A. Anderson, A. R. Williams, M. R. Wilson, J. Schwarze, H. Wang, A. G. Rossi & H. N. Jabbour (2009) Prostaglandin F2alpha-F-prostanoid receptor signaling promotes neutrophil chemotaxis via chemokine (C-X-C motif) ligand 1 in endometrial adenocarcinoma. *Cancer Res,* 69**,** 5726-33.

Wang, H., H. O. Critchley, R. W. Kelly, D. Shen & D. T. Baird (1998) Progesterone receptor subtype B is differentially regulated in human endometrial stroma. *Molecular Human Reproduction,* 4**,** 407-12.

Wang, Q., X. Xu, B. He, Y. Li, X. Chen & J. Wang (2013) A critical period of progesterone withdrawal precedes endometrial breakdown and shedding in mouse menstrual-like model. *Hum Reprod,* 28**,** 1670-8.

Wang, Z., M. Gerstein & M. Snyder (2009) RNA-Seq: a revolutionary tool for transcriptomics. *Nat Rev Genet,* 10**,** 57-63.

Wang, Z., X. Liu, D. Zhang, X. Wang, F. Zhao, T. Zhang, R. Wang, X. Lin, P. Shi & X. Pang (2015) Phenotypic and functional modulation of 20-30 year old dermal fibroblasts by mid- and late-gestational keratinocytes in vitro. *Burns,* 41**,** 1064-75.

Watson, H., S. Franks & R. C. Bonney (1996) Regulation of epidermal growth factor receptor synthesis by ovarian steroids in human endometrial cells in culture. *J Reprod Fertil,* 107**,** 199-205.

Wei, S., S. Nandi, V. Chitu, Y. G. Yeung, W. Yu, M. Huang, L. T. Williams, H. Lin & E. R. Stanley (2010) Functional overlap but differential expression of CSF-1 and IL-34 in their CSF-1 receptor-mediated regulation of myeloid cells. *J Leukoc Biol,* 88**,** 495-505.

Winuthayanon, W., S. C. Hewitt, G. D. Orvis, R. R. Behringer & K. S. Korach (2010) Uterine epithelial estrogen receptor α is dispensable for proliferation but essential for complete biological and biochemical responses. *Proc Natl Acad Sci U S A,* 107**,** 19272-7.

Wong, V. W., K. C. Rustad, S. Akaishi, M. Sorkin, J. P. Glotzbach, M. Januszyk, E. R. Nelson, K. Levi, J. Paterno, I. N. Vial, A. A. Kuang, M. T. Longaker & G. C. Gurtner (2011) Focal adhesion

kinase links mechanical force to skin fibrosis via inflammatory signaling. *Nat Med,* 18**,** 148-52.
Wu, B., C. An, Y. Li, Z. Yin, L. Gong, Z. Li, Y. Liu, B. C. Heng, D. Zhang, H. Ouyang & X. Zou (2017) Reconstructing Lineage Hierarchies of Mouse Uterus Epithelial Development Using Single-Cell Analysis. *Stem Cell Reports,* 9**,** 381-396.
Wu, Y., L. Chen, P. G. Scott & E. E. Tredget (2007) Mesenchymal stem cells enhance wound healing through differentiation and angiogenesis. *Stem Cells,* 25**,** 2648-59.
Wynn, T. A. (2008) Cellular and molecular mechanisms of fibrosis. *J Pathol,* 214**,** 199-210.
Wynn, T. A. & L. Barron (2010) Macrophages: master regulators of inflammation and fibrosis. *Semin Liver Dis,* 30**,** 245-57.
Wynn, T. A., A. Chawla & J. W. Pollard (2013) Macrophage biology in development, homeostasis and disease. *Nature,* 496**,** 445-55.
Wynn, T. A. & K. M. Vannella (2016) Macrophages in Tissue Repair, Regeneration, and Fibrosis. *Immunity,* 44**,** 450-462.
Xiong, Y., Y. Liu, W. Xiong, L. Zhang, H. Liu, Y. Du & N. Li (2016) Hypoxia-inducible factor 1α-induced epithelial-mesenchymal transition of endometrial epithelial cells may contribute to the development of endometriosis. *Hum Reprod,* 31**,** 1327-38.
Yang, J., L. Zhang, C. Yu, X. F. Yang & H. Wang (2014) Monocyte and macrophage differentiation: circulation inflammatory monocyte as biomarker for inflammatory diseases. *Biomark Res,* 2**,** 1.
Yen, S. S. (1977) Regulation of the hypothalamic--pituitary--ovarian axis in women. *J Reprod Fertil,* 51**,** 181-91.
Yoshii, A., S. Kitahara, H. Ueta, K. Matsuno & T. Ezaki (2014) Role of uterine contraction in regeneration of the murine postpartum endometrium. *Biol Reprod,* 91**,** 32.
Zamora, D. O., S. Natesan, S. Becerra, N. Wrice, E. Chung, L. J. Suggs & R. J. Christy (2013) Enhanced wound vascularization using a dsASCs seeded FPEG scaffold. *Angiogenesis,* 16**,** 745-57.
Zebardast, N., D. Lickorish & J. E. Davies (2010) Human umbilical cord perivascular cells (HUCPVC): A mesenchymal cell source for dermal wound healing. *Organogenesis,* 6**,** 197-203.
Zeng, Q., W. Li, D. Lu, Z. Wu, H. Duan, Y. Luo, J. Feng, D. Yang, L. Fu & X. Yan (2012) CD146, an epithelial-mesenchymal transition inducer, is associated with triple-negative breast cancer. *Proc Natl Acad Sci U S A,* 109**,** 1127-32.
Zhang, J., G. Nie, W. Jian, D. E. Woolley & L. A. Salamonsen (1998) Mast cell regulation of human endometrial matrix metalloproteinases: A mechanism underlying menstruation. *Biol Reprod,* 59**,** 693-703.
Zhang, Y., N. Daubel, S. Stritt & T. Mäkinen (2018) Transient loss of venous integrity during developmental vascular remodeling leads to red blood cell extravasation and clearance by lymphatic vessels. *Development,* 145.
Zhao, R., H. Liang, E. Clarke, C. Jackson & M. Xue (2016) Inflammation in Chronic Wounds. *Int J Mol Sci,* 17.
Zhu, L. & J. W. Pollard (2007) Estradiol-17beta regulates mouse uterine epithelial cell proliferation through insulin-like growth factor 1 signaling. *Proc Natl Acad Sci U S A,* 104**,** 15847-51.
Zhu, X., R. A. Hill, D. Dietrich, M. Komitova, R. Suzuki & A. Nishiyama (2011) Age-dependent fate and lineage restriction of single NG2 cells. *Development,* 138**,** 745-53.

Appendices

Appendix 5.1. Top 100 most significantly upregulated genes in repairing samples when compared to naive samples. RNAseq. FDR <0.05.

Gene	Mean CPM Naive	Mean CPM Repairing	LogFC	P-value	FDR <0.05
Mmp10	0.192611314	495.95818	11.2432086	9.71E-06	0.001359377
Erv3	0.045257809	84.0704655	10.71748135	6.49E-06	0.001024937
Mmp12	0.112752673	154.8354046	10.3423004	1.04E-06	0.000252339
Mmp13	0.255816556	231.8863547	9.800783712	0.000174931	0.009061145
Sprr2h	0	7.674410321	9.660603129	9.79E-05	0.006430275
Cd177	0	7.251583962	9.575453439	0.001254616	0.028421027
Jakmip1	0.008520914	11.10935265	9.187891507	1.44E-06	0.000338097
Tnfrsf9	0.01261252	11.4483069	9.164302927	1.98E-05	0.002174383
Slpi	0	5.283499957	9.129152766	0.000430007	0.016091638
Cxcl5	0.145989044	83.00211007	8.998444358	7.58E-08	4.63E-05
Parvb	0.024675058	13.62585254	8.521122087	0.000207972	0.01010534
Onecut3	0.018492264	9.958627792	8.437463465	0.000301689	0.012868605
Gpr55	0	2.800546567	8.204691479	0.000863689	0.023524625
Tnf	0.009246132	5.640869553	8.197978843	1.24E-05	0.001582367
Tnc	5.473751472	1555.833241	8.151385875	1.28E-07	6.48E-05
Abca13	0	2.284936928	7.896652941	0.000641762	0.0201544
Gareml	0	2.03374187	7.727634526	0.002173574	0.037626717
Olfr505-ps1	0	1.715232757	7.487670018	0.001870948	0.035214312
Tph1	0	1.675092592	7.471207085	0.000296895	0.012702769
Lama1	0.579926874	96.79574453	7.402468391	1.94E-06	0.000397164
Ctnnd2	0.091362769	15.24264456	7.317967332	2.68E-06	0.000502385
Nccrp1	0	1.426811239	7.247691261	0.001112081	0.026711533
Ptprn	0.189028612	30.53674021	7.217093422	2.05E-07	8.44E-05
Il23a	0.027056728	5.151658687	7.094824017	0.000404091	0.015555815
Pmaip1	0.099100306	13.3496406	6.883746254	6.71E-05	0.005085459
Cntn3	0.645734597	77.5487802	6.879002008	2.72E-08	2.26E-05
Slc5a7	0.08492125	10.4059451	6.878734677	5.08E-05	0.00424783
Gdap1	0.051731786	7.410215138	6.859942119	0.00100242	0.025163336
Fam167a	0.010990292	2.264316352	6.845431489	0.000652647	0.020324261
Hs3st3b1	0.017767046	3.169080274	6.813610433	9.49E-05	0.006324106
Myom2	0.028507163	4.265241857	6.800887906	0.00189685	0.035451495
Dusp9	0	0.981838393	6.707551213	0.002448828	0.040062893
Fam83b	0.011511855	1.965549243	6.641733679	0.002111108	0.037100182
Wnt2	0.032269843	3.930703856	6.60074578	0.000345267	0.013952278
Ereg	0.170861444	16.23735086	6.575360719	0.000143461	0.008012998
Cyp11a1	0	0.856621351	6.511805974	0.0019001	0.035462706
H19	0.266592985	24.75493067	6.488998264	1.84E-06	0.000394339
Chodl	6.307622148	556.4212	6.452630926	0.000157756	0.008450687
Tgfbi	1.289687263	112.7243018	6.42190615	1.90E-09	2.23E-06
Acap1	0.049597048	4.725477929	6.328794257	0.001239234	0.028253536
Pcdha2	0.055447945	5.140268045	6.287716435	0.001529205	0.031560155
Cldn2	0.023023711	2.344733067	6.261255821	0.001743987	0.033884487
Kcna1	0.047852459	4.107454455	6.251085281	0.000665798	0.020430076
Lck	0.034133682	3.468850806	6.244429792	0.003377213	0.047348629
Ifitm7	0.037759161	3.503917574	6.166029699	0.002233477	0.037933326
Pigyl	0.109336808	8.167876868	6.145896137	0.001458012	0.030878956
Cbx8	0.017041829	1.831500939	6.046137994	0.002352953	0.039126851
Grip1os1	0.017729362	1.819502617	6.016589866	0.001281406	0.028761884
Lcp2	0.075305478	5.337675619	6.012669288	0.001171804	0.027484175
Stk32c	0.037071627	3.027779459	5.975553825	0.001880296	0.035303233
Ptgs2	9.702823909	598.7562275	5.952372343	7.29E-08	4.63E-05

Cited1	0	0.573839986	5.933452633	0.003080496	0.045137899
Rims3	0.145216769	9.129001601	5.900509684	0.003101315	0.045281236
Wipf3	0.403969416	24.44235098	5.872696452	2.49E-05	0.002562769
Col8a1	4.05559421	235.9685682	5.868560643	3.59E-11	2.09E-07
Hmga2	1.291790599	75.27728177	5.861928965	6.29E-05	0.00484825
Kcnf1	0.021005192	1.722071559	5.848035423	0.001939503	0.035719588
Zfp689	0.164362571	10.08563616	5.843818515	0.001524977	0.031527509
Btnl10	0.040019019	2.677160601	5.765446073	0.003737749	0.049686401
Tac2	0.208796274	11.64610947	5.726976092	0.000816265	0.02294268
Agtr1b	0.078791256	4.617888521	5.721685685	0.002375288	0.039322051
Dctpp1	0.211290089	11.30445497	5.692210995	0.002095899	0.037008149
Fen1	0	0.480500739	5.681039796	0.00239913	0.039597304
Cd83	0.102476219	5.820461529	5.656359795	0.001678218	0.033393391
Fam189a1	0.105186078	6.096885183	5.653464523	0.002527575	0.04087073
Plek2	0.023949841	1.761410869	5.628287709	0.002046526	0.036661622
Rasal1	0.037759161	2.294284313	5.588792342	0.003338353	0.047105056
Parvg	0	0.418257602	5.487938679	0.003757897	0.049781747
Cdh4	0.010014899	0.859356514	5.482826807	0.002262638	0.038282592
Stxbp5l	0.033745954	1.815376721	5.47304435	0.001475294	0.03106005
Snord16a	0.009246132	0.787738492	5.379176963	0.003687891	0.049347705
Speer4e	0.043329789	2.268355109	5.366670377	0.001801281	0.034426895
Spp1	0.976727048	39.91647584	5.324052535	1.91E-06	0.000397164
Gatm	2.506420699	96.46750681	5.258381893	3.99E-07	0.000138925
Ttc9	0.009246132	0.720873278	5.249347278	0.002747969	0.042638522
Tes	5.04646613	188.3008376	5.212457819	3.17E-10	1.01E-06
Arc	0.020757987	1.074238591	5.187794139	0.002445198	0.04003293
Stra6	5.178319584	181.6579177	5.123092735	1.20E-05	0.001557026
Tead4	0.16926942	5.982473511	5.072744527	0.000693768	0.020874912
Clu	0.348424863	11.28564111	4.961939136	0.001272274	0.028671605
Lef1	2.760784681	84.80746962	4.926968918	2.21E-10	8.19E-07
Kcnma1	8.190361893	225.4057473	4.777558072	3.75E-11	2.09E-07
Kcnmb2	0.975602016	25.86511302	4.715229976	0.001584778	0.0322112
Fst	1.750804875	45.01400457	4.665004163	2.97E-06	0.000547235
Gipc2	0.383264024	9.785216578	4.646179499	0.00288926	0.043556041
Tmem108	0.238592911	6.238433431	4.643349184	0.001485626	0.03106005
Slc2a1	3.1787423	78.07519056	4.618926085	5.42E-07	0.00017096
Sfrp2	15.22049027	366.4942383	4.576420328	2.36E-05	0.002489778
Hs3st3a1	0.368896416	8.664094723	4.538270824	0.001817746	0.034622698
A3galt2	0.448943992	10.14310494	4.463464345	0.002348032	0.039103429
Cemip	3.59742022	77.79093471	4.427304874	0.00029278	0.012609377
Kif26b	1.448743902	31.08524067	4.418503053	5.32E-05	0.004384043
Serpine2	15.16047351	325.4502619	4.417608455	8.57E-10	1.32E-06
Speer4c	0.122593117	2.81395094	4.39782471	0.002282596	0.038474097
Ddit4	0.281725655	6.138860813	4.393635137	0.002737998	0.042558719
Flt1	2.806311108	58.9919908	4.390577855	3.43E-05	0.003153821
Igsf11	0.714456362	15.2592845	4.389197547	0.001644359	0.032837039
Sprr1a	0.789691581	15.56273462	4.284011234	0.002512543	0.040746016
Cdh5	5.018368436	98.23442448	4.28009585	6.74E-10	1.15E-06
Igf2	4.036994981	78.45678141	4.278489932	4.33E-06	0.000741028

Appendix 5-2. Top 100 most significantly downregulated genes in repairing samples when compared to naive samples: RNAseq. FDR <0.05

Gene	Mean CPM Naive	Mean CPM Repairing	LogFC	P-value	FDR <0.05
Vcam1	18.87612	0	-10.9576	7.70E-08	4.63E-05
Ces2g	14.98131	0	-10.6217	1.00E-05	0.001384095
Clca1	13.28959	0	-10.4559	4.51E-06	0.000767291
Asb4	13.12932	0	-10.4326	6.08E-07	0.000174188
Zcchc16	11.60277	0	-10.2586	2.75E-05	0.002711056
Tmod1	25.90097	0.015361301	-9.92398	2.48E-09	2.76E-06
Sphkap	24.39947	0.014478712	-9.84058	2.95E-08	2.26E-05
Crabp1	8.041571	0	-9.73353	0.000312	0.01311522
Aldh1a1	123.7077	0.128831026	-9.72553	5.78E-12	6.43E-08
Ltf	7.409469	0	-9.6104	5.98E-05	0.004668477
Il31ra	7.352368	0	-9.59967	2.02E-06	0.000409847
Ube2t	7.344575	0	-9.59774	7.67E-06	0.001154335
Lgr6	96.94894	0.116242478	-9.53581	3.91E-07	0.000138064
Adamtsl3	6.880863	0	-9.50374	0.000138	0.007983703
Pcdh12	6.161984	0	-9.34644	8.06E-06	0.001196664
Arsi	5.815426	0	-9.27028	2.38E-05	0.002495151
Fhl5	5.00413	0	-9.04249	9.94E-05	0.006472006
Gfra1	32.28628	0.049495506	-9.042	2.12E-07	8.59E-05
Prss23os	4.505037	0	-8.89254	3.64E-05	0.003290656
Olfr78	13.14954	0.019749985	-8.89158	1.51E-06	0.000342751
Gbp11	4.385322	0	-8.85822	0.000645	0.020191026
Chst13	4.168863	0	-8.78885	0.000221	0.010423267
Slc38a4	4.042288	0	-8.73851	2.84E-05	0.002776442
Esco2	4.023685	0	-8.72881	0.000206	0.01006253
Pitpnm3	3.69344	0	-8.61623	0.000168	0.008881228
Mug1	128.0082	0.320167773	-8.61413	1.09E-07	5.64E-05
Cfap100	10.53778	0.019655492	-8.57479	2.74E-07	0.000101675
Slc6a13	10.01382	0.015361301	-8.56925	3.06E-05	0.002924838
Fermt1	3.509144	0	-8.54144	0.000265	0.011905013
Cadm2	22.59851	0.049589999	-8.53049	9.25E-08	5.02E-05
Gdpd2	9.910633	0.021545657	-8.47081	9.63E-06	0.001357456
Ppp2r2c	3.298611	0	-8.46676	0.00258	0.041301723
Nrk	730.4203	2.119082988	-8.43557	6.78E-06	0.0010563
Gpr87	3.249793	0	-8.43084	0.000333	0.013632465
Slc28a3	3.245888	0	-8.42659	0.000115	0.007064455
Ebf2	3.229965	0	-8.41555	0.001226	0.02821222
Gm14329	3.138684	0	-8.37012	0.000623	0.019954732
Dtwd1	3.069308	0	-8.3446	5.17E-05	0.004280818
Cd300a	3.072398	0	-8.34309	0.000456	0.016495096
Htra1	58.21763	0.171009257	-8.31438	2.11E-12	4.70E-08
Tmem229a	399.825	1.267626953	-8.28853	1.49E-06	0.000342751
Ugt1a5	2.928183	0	-8.27548	7.78E-05	0.005695067
Ramp3	18.0807	0.045201315	-8.25341	1.19E-06	0.000285572
Cdnf	2.90462	0	-8.25284	0.00033	0.01360408
Adh7	2.71271	0	-8.16817	0.000132	0.007707299
Plppr4	18.0637	0.054672286	-8.16394	0.000745	0.021798813
Spock3	7.874384	0.019655492	-8.15624	0.000662	0.020430076
Slitrk6	2.680745	0	-8.14744	0.000791	0.022581451
Slc44a3	2.682988	0	-8.14616	0.000279	0.012196067
Ugt1a7c	2.675706	0	-8.14429	0.000511	0.017511175
Grip2	2.618624	0	-8.11012	0.000513	0.017535384
Ccdc81	2.594924	0	-8.1069	9.48E-05	0.006324106

Pdzrn4	2.595921	0	-8.10241	0.000394	0.015369726
Rgs1	2.549462	0	-8.08908	0.001617	0.032503906
Col6a5	17.30204	0.056562451	-8.08122	2.00E-08	1.78E-05
Ptpn5	16.65389	0.050378095	-8.07881	2.63E-06	0.000499967
Ano5	23.29262	0.086182629	-8.07461	4.65E-06	0.000778881
Crtac1	21.02661	0.071041163	-8.04413	2.24E-07	8.92E-05
Ehf	2.481379	0	-8.04057	0.000686	0.02071257
Klhl4	2.46747	0	-8.02932	0.00019	0.009466803
Tmprss11g	2.453125	0	-8.01698	0.000489	0.017037895
Pcolce2	2.404193	0	-8.00192	0.000169	0.008890506
Naip1	2.372204	0	-7.97096	0.000192	0.00955267
Mmp27	2.2391	0	-7.88793	0.000399	0.015449665
Six1	2.205024	0	-7.85986	0.00033	0.01360408
Lrrc23	2.18217	0	-7.85334	0.0023	0.038482515
Grin2b	78.18713	0.329686532	-7.81461	1.36E-05	0.001686751
Adh1	198.0982	0.920533228	-7.76303	8.75E-08	4.99E-05
Krt84	2.027137	0	-7.75985	0.002532	0.040917416
P2ry13	2.023485	0	-7.74914	0.003151	0.045582272
Trem2	2.001787	0	-7.73264	0.002135	0.037254293
Hs3st5	13.24499	0.05388419	-7.72942	8.43E-06	0.001234746
Hoxc6	1.997399	0	-7.72412	0.000188	0.00944629
Uqcc3	1.986676	0	-7.7197	0.000193	0.00955351
Cd163	1.986359	0	-7.71787	0.000722	0.0214293
Fam26e	9.987311	0.043091314	-7.71573	2.23E-06	0.000439667
Frmd7	1.975673	0	-7.7052	0.000889	0.023784175
Pm20d1	16.84421	0.073728669	-7.70133	4.51E-07	0.000147589
Prrx2	1.944704	0	-7.6983	0.000273	0.012103498
Ptprb	1.958816	0	-7.69357	0.000908	0.024061664
Scin	1.9531	0	-7.69183	0.000153	0.008360403
Plxna4os2	1.953175	0	-7.68435	0.003552	0.048414103
Uroc1	1.900605	0	-7.6588	0.001649	0.032877045
Zakit	1.904787	0	-7.65459	0.000451	0.016446942
Dhrs9	1.900491	0	-7.65114	0.000396	0.015404211
Map10	1.869318	0	-7.62923	0.000137	0.007983703
Npy1r	5.118415	0.014478712	-7.62154	1.31E-05	0.001646277
Xirp1	1.809889	0	-7.58148	0.002358	0.039181877
Tspan15	1.808048	0	-7.57739	0.000464	0.016687778
BC050972	1.798502	0	-7.57396	0.000168	0.008890506
Nrip3	5.296504	0.019749985	-7.57361	4.70E-05	0.003977595
BC037032	1.788751	0	-7.55997	0.001331	0.029438967
Smim6	1.743011	0	-7.54165	0.000536	0.018019646
Oxct2a	1.720906	0	-7.51314	0.000973	0.024635942
Slc5a9	1.713305	0	-7.50415	0.001234	0.028253536
Kcnv2	1.70686	0	-7.497	0.000289	0.012526957
Sema3b	5.107127	0.021545657	-7.49533	1.10E-05	0.001475267
F2rl2	1.65763	0	-7.4681	0.001041	0.025796999
Efcab1	1.663464	0	-7.46543	0.000479	0.016839053
Vcam1	18.87612	0	-10.9576	7.70E-08	4.63E-05

Appendix 5-3: Top 100 differentially expressed genes that identify each cell cluster in the naïve endometrial mesenchyme, singe cell sequencing.

Cluster 1	Cluster 2	Cluster 3	Cluster 4	Cluster 5
Saa3	***Kcnj8***	*Rergl*	*Clec3b*	*Fcgbp*
Wnt16	***Abcc9***	***Pln***	*Mmp3*	*Prap1*
Cxcl14	*Higd1b*	*Sncg*	*Ly6c1*	*Lcn2*
Dio2	***Vtn***	***Cnn1***	***Col14a1***	*Tmem213*
Smoc2	*Akr1cl*	***Tagln***	*Inmt*	*Tspan1*
Ccl8	*Sept4*	***Acta2***	*Igfbp3*	***Epcam***
Aspg	***Ednrb***	*Map3k7cl*	*Cxcl16*	*Pigr*
Hsd11b2	*Id4*	*Sorbs2*	*Slc43a3*	*Arg1*
Ngfr	*Art3*	*Cdc42ep3*	***Cd55***	*S100g*
Mfap4	***Rgs5***	*Lmod1*	*Penk*	*Plet1*
Aldh1a2	*Ndufa4l2*	*Hspb1*	*Adh1*	*Aqp5*
Wt1	*Fhl2*	***Myh11***	*Lum*	*Sftpd*
Gxylt2	*Ifitm1*	*Pcp4l1*	*Efemp1*	***Krt8***
Cdh11	*Myo1b*	*Nrip2*	***Fbln1***	*BC048679*
Wnt5a	*Adap2os*	*Crim1*	*Mgp*	*Serpina1e*
Rbp4	*Slc11a1*	*Mustn1*	*Col15a1*	*Clca1*
Ramp2	*Nrp1*	*Rcan2*	*Plpp3*	*Pdzk1ip1*
Steap3	*Adap2*	*Mob2*	***Col3a1***	*Ltf*
Ccl11	*Gucy1b3*	*Rasd1*	*Figf*	*Wfdc2*
Twist2	*Rem1*	*Crip1*	*Hpgd*	*Aoc1*
Fbln2	*Esam*	*Bcam*	*Gsn*	*4833423E24Rik*
Mfap5	*Klhl23*	*Rbpms2*	*Postn*	*Fxyd3*
Dkk3	*Slc7a2*	*Klf2*	*Lama4*	***Cdh1***
Tmem119	*Btbd3*	*Ptp4a3*	***Col1a1***	*Alox15*
Srgn	*Pten*	*Net1*	*Ms4a4d*	*Sprr2f*
Sema3c	***Thy1***	*Ptgis*	***Fbln1***	*Slc39a4*
Rorb	*Gjc1*	*Tpm1*	*Akap12*	*Smim22*
Rev3l	***Olfr558***	*Tpm2*	*Ctsh*	*Urah*
Dpep1	*Notch3*	*Kcnab1*	*Loxl1*	*Padi2*
Igfbp4	*Timp3*	*Csrp2*	*Scara5*	*Cxcl17*
Pla1a	*Tinagl1*	***Kitl***	*Cd248*	***Krt19***
Chchd10	*Gucy1a3*	*Crtc3*	*Lamc1*	***Krt18***
Mmp11	*Vstm4*	*Myl9*	*Apoe*	*Cldn7*
Htra1	*Mfge8*	***Pdgfa***	*Dpt*	*Ckmt1*
Islr	***Pdgfrb***	*Tbx3os1*	*Col1a2*	*Rmst*
F3	*Aspn*	*Tm4sf1*	*Meg3*	*Krt7*
Sfrp2	*1810011O10Rik*	*Hspb2*	*Fxyd5*	*Rnf128*
Ctla2a	*Maged2*	*Rrad*	*S100a16*	*Mecom*
Col6a4	*Ebf1*	*Mir143hg*	***CD34***	***Fxyd4***
Spon2	*Ier5*	***Rgs4***	*S100a6*	*Tspan8*
Acot1	***Cspg4***	***Mcam***	*S100a10*	*Car2*
Cped1	*Sept7*	*Crip2*	*Rcn3*	*Elf3*
Gja1	*Tmem176a*	*Ppp1r12b*	*Adamts2*	*Trpv6*
Maf	*Gm13889*	*Pdlim3*	***Sparc***	*Sult1d1*
Ahnak2	*Pkig*	*AI838599*	***Col5a1***	*Plekhs1*
Mdk	*Ndrg2*	*Cd200*	*Pcolce*	*Cbr2*
Sfrp4	*Mgst3*	*Zak*	*Serpinh1*	*Fut9*
Lsp1	*Hes1*	*Cryab*	*C1qtnf3*	*Prom1*
Nbl1	*Zeb2*	*Ltbp1*	*Ly6a*	*Pglyrp1*
Dcn	*Rasl11a*	*Ckb*	*Mgst1*	*Bcat1*
Rnase4	*P2ry14*	*Pi15*	*Htra3*	***Muc1***
Pdgfra	*Rasl12*	*Epas1*	*Abi3bp*	*Dgat2*
Scpep1	*Nudt4*	*Rasl12*	***Col5a2***	*Cfb*
Rin2	*Atp1b2*	*Actn1*	*Cxcl12*	*Cd24a*

Aebp1	*Gnb4*	*Cav1*	*Rbp1*	*Alcam*
Pamr1	*Fxyd6*	*Dstn*	*Gpx7*	*Atp1b1*
Fn1	*Dtx3*	*Lims1*	*Celf2*	*Gsto1*
Serpinf1	***Rgs3***	*Lbh*	*Nfib*	*Msx1*
Mmp14	*Tmem176b*	*Itpr1*	*Tnxb*	*Gstm7*
Ramp3	*Gng11*	*Mef2c*	*C3*	*Fam213a*
Cd164	*Fam162a*	*Zfhx3*	*Pdia6*	*Tmc4*
Mettl7a1	*Mndal*	*Cyr61*	*Ltbp4*	*C3*
Antxr1	*Isg15*	*Gm13889*	*Matn2*	*Clu*
Gadd45g	*Tmem100*	*Flna*	***Col6a3***	*Ezr*
Olfml3	*Serping1*	*Csrp1*	*Vkorc1*	*Lbp*
Itih5	*Junb*	*Atp1b2*	*Man1a*	*Anpep*
Igfbp6	*Vasp*	*Anxa11*	*Igfbp6*	*Cndp2*
Gpx3	*Limd1*	*Rasl11a*	*Thbd*	*Cldn10*
Vat1	*Mef2c*	*Rap1a*	*Lpl*	*Spint2*
Mmp2	*Nr2f2*	*Map1b*	*Galnt15*	*Rdh10*
Igf1	*Epas1*	*Myl6*	*Gas1*	*Ivns1abp*
Ifit3	*Fxyd5*	*Ccdc107*	*Calr*	*Sec23b*
Ogn	*Mat2a*	*Ptrf*	*Tmed3*	*Tmem158*
Pltp	*Btg2*	*Serpine2*	*Gpm6b*	*Cp*
Pgrmc1	*Gyg*	*Iqgap1*	*Lamb1*	*Fuom*
Oasl2	*Slc38a2*	*Prkcdbp*	*Ecm1*	*1110008P14Rik*
Angptl2	*AI838599*	*Des*	*Ccdc80*	*Sec11c*
Ctsk	*Serinc3*	*Utrn*	*Serpinf1*	*Ier3*
Lox	*Eif1b*	*Msrb1*	*Hmgcs2*	*Atp1a1*
Hmgcs2	*Col4a1*	*Ppp1r12a*	***Igf1***	*Mt2*
Osr2	*Col4a2*	*Pde3a*	***Col6a2***	*Gng12*
Slc3a2	*Ech1*	***Olfr558***	*S100a1*	*Sat1*
Marcks	*Gnas*	*Calm1*	*Pdia4*	*Slc1a5*
Pbx1	***Mcam***	*Filip1l*	*Fuca1*	*Tmem176a*
Prnp	***Rgs4***	*Rras*	*Rcn1*	*Mt1*
Nid1	*Id3*	*Uba2*	*Fndc3a*	*Rnaset2b*
Npc2	*Ifitm3*	*Aspn*	*Mt2*	*Cystm1*
Lgals3bp	*Lhfp*	*Calm2*	*Maged2*	*Slc40a1*
Thbd	*Uba2*	*Blmh*	*Ppib*	*Gadd45a*
Dap	*Pkm*	*Rock1*	*Spon1*	*Rbbp7*
Zbtb20	*Serpine2*	*Mgst3*	*Hsp90b1*	*Rnaset2a*
Tsc22d1	*Ypel3*	*Tinagl1*	*Itih5*	*2810474O19Rik*
Lrp1	*Tnfrsf1a*	*Mylk*	*Kdelr2*	*mt-Atp8*
Mmp23	*Ifi203*	*Pls3*	*Fkbp7*	*Cd2ap*
Mfap2	*Acaa2*	*Gucy1a3*	***Pdgfra***	*Fkbp4*
Prpf19	*Des*	*Pdcl3*	***Col6a1***	*Tmem176b*
Htra3	*Ndufs2*	*Ppp1cb*	*Fstl1*	*Ndufa4*
Bcl2	*Prkar1a*	*Notch3*	*Ptgis*	*Mien1*
Col18a1	*Fgl2*	*Mrvi1*	*Tspo*	*Nfib*
CD34	*Tbx3os1*	***Lmna***	***Cald1***	*Taldo1*

Appendix 5-4. Top 100 differentially expressed genes in the 8 clusters identified in the combined dataset of control and repairing endometrial mesenchyme, single cell sequencing.

1	2	3	4	5	6	7	8	9
Rps2	*Chodl*	*Akr1cl*	*Rergl*	*Slpi*	*Ren1*	*Clec4e*	*Prap1*	*Ccnb1*
Ndufs7	*Cilp*	***Vtn***	***Pln***	***Krt18***	*Akr1b7*	*Arhgdi*	*Arg1*	*Hmmr*
Fastk	*Sfrp1*	*Art3*	*Gm37800*	*Sprr2h*	*Procr*	*Cx3cr1*	*Tspan1*	*Prc1*
Kcnq1ot	*Fst*	*Gm1347*	*Sncg*	*Ccr1*	*S100a4*	*Flt1*	*Fcgbp*	*Nusap1*
Cetn2	*Nnat*	*Higd1b*	*Hspb7*	*Sprr2d*	*Ednrb*	*Tnfrsf9*	*Pdzk1ip1*	*Ccna2*
Lamp1	***Col8a1***	*Cox4i2*	*Nrip2*	***Mmp12***	*AI662270*	*Hp*	*Pigr*	*Top2a*
Zfp511	*Cxcl5*	*Adap2*	*Mob2*	*Grem1*	*Lair1*	*Gpr35*	*Serpina1*	*Ube2c*
Ilk	*Mgp*	*Id4*	*Lmod1*	*Pmaip1*	***Mcam***	*Klk8*	*Clca1*	*Birc5*
Ndufa7	*Frzb*	*Adap2os*	*Rcan2*	*Cyp26b1*	*Il6*	*Serpine*	*BC04867*	*2810417*
mt-Nd4l	*Serpinb*	*Inpp4b*	*Pcp4l1*	*Tnf*	*Gpr65*	*Cxcl3*	*Tmem213*	*Cenpf*
Cox14	*Sfrp4*	***Abcc9***	*Map3k7cl*	***Edn1***	*Mrgpra2b*	*Cd300l*	*Sftpd*	*Cenpe*
Atp5e	***Fbln1***	***Kcnj8***	*Bcam*	***Mmp10***	*Nxpe5*	*Arhgap*	*Sprr2f*	*Tpx2*
Nktr	*F2r*	*Clec4d*	*Sorbs2*	*Cemip*	*F630028*	*Apold1*	*Ltf*	*Racgap1*
Cst3	*Aldh1a2*	*Alox5ap*	*Rasd1*	***Ptgs2***	*Notch3*	*Il6*	*Spink1*	*Cdca3*
Anp32a	*Itm2a*	*Ndufa4l*	*Mustn1*	*Il23a*	*Apold1*	*Tfpi2*	*Wfdc2*	*Cdc20*
Zfp36l2	***Cxcl14***	*Slc11a1*	***Myh11***	*Hmga2*	*Emid1*	*Sema6d*	*Cxcl17*	*Ccnb2*
Btf3	***Igf1***	*Gca*	*AI838599*	*Dusp5*	***Cnn1***	*Stc1*	*Aqp5*	*Cdca8*
Rnaset2	*Mfap4*	*Klhl23*	*Rgs7bp*	*Fam84a*	*Fabp5*	*Slc16a3*	*4833423*	***Mki67***
Col5a2	*Timp1*	*Gucy1b*	*Mir143hg*	*Egln3*	***Acta2***	***Ednrb***	*Smim22*	*Cenpa*
Fbln2	*Lbp*	*Gucy1a*	***Kitl***	*Arg2*	*Ccnd2*	*Chst2*	*S100g*	*Knstrn*
Gpx8	*Csf2rb2*	*Sept4*	*Tbx3os1*	*Fcer1g*	*Nes*	*Akr1b7*	*Ckmt1*	***Cdk1***
Mif	*Pcsk5*	*Myo1b*	*Gm13861*	*Cryab*	*Actg2*	*Gpr65*	***Cdh1***	*Wfdc17*
Snrpb2	*Dclk1*	***Rgs5***	*Rrad*	***Mmp3***	*Sorl1*	*Mrgpra*	***Fxyd3***	*Lockd*
Sidt2	*Loxl1*	*Rem1*	*Crtc3*	*Fabp4*	*Nr4a3*	*Nxpe5*	*Muc4*	*Rrm2*
Sf3b5	*Pde10a*	*Slco2b1*	*Ptgis*	*Aldh1a3*	***Rgs5***	*F63002*	*Rab25*	*Gpr65*
Snx16	*Mfap5*	*Ndrg2*	*Entpd1*	*Hcar2*	*Ptp4a3*	*Got1*	*Cldn3*	*Itgb2*
Rc3h1	*Vcan*	***Olfr558***	*Kcnab1*	*Cd33*	*B930036N*	*Aplp1*	*Padi2*	*Mrgpra2*
Rbm39	*Fxyd6*	*Nrp1*	***Tagln***	*Hmox1*	*Id3*	*Ddit4*	*Slc39a4*	*Nxpe5*
Bcas2	*Sulf1*	*Gm4955*	*Crim1*	*Ero1l*	*Nr4a1*	*Il11*	*Trpv6*	*F630028*
Rnf187	*C1qtnf7*	*Aspn*	*Fry*	*Cxcl2*	*Gm13889*	*Rgs16*	*Elf3*	*Smc2*
Snx17	*Igfbp4*	*Mfge8*	*Wtip*	*Mt2*	*Sept4*	*Procr*	*Lcn2*	*Gm20406*
Zmat2	*Sfrp2*	***Rgs3***	*Hspb2*	*Plk2*	*Ctsc*	*Ecscr*	*Cldn7*	*Fpr2*
mt-Cytb	*Lpl*	*Slc7a2*	*Cnn1*	*Ppbp*	*Fpr2*	*993002*	*Itgam*	*AF25170*
Mrpl33	*Lgmn*	*Gpr65*	*Crip1*	*Ndrg1*	*AF251705*	*Errfi1*	*Mecom*	*Gpr183*
Npdc1	*Mmp2*	*Mrgpra*	*Ppp1r12b*	*Tnfrsf23*	*Gpr183*	*Tnip1*	*Sult1d1*	*Mcemp1*
Hjurp	*Pfn2*	*Pirb*	***Acta2***	*Mt1*	*Mcemp1*	*Nudt4*	*Urah*	*Lrch4*
Pdgfra	*Nxn*	*Nxpe5*	*Crip2*	***Mmp13***	*Lrch4*	*Fpr2*	*Cbr2*	*Arhgap30*
Rnf139	***Col3a1***	*F63002*	*Rasl12*	*Lmcd1*	*Arhgap30*	*AF2517*	*Gpx2*	*Fcgr4*
Fig4	*Sulf2*	*Rsad2*	*Rgs1*	*Sema3a*	*Fcgr4*	*Gpr183*	*Aoc1*	*Smc4*
Mpc2	***Cdh11***	*AI83859*	*Mef2c*	*Glipr1*	*Slc11a1*	*Mcemp*	*Tspan8*	*Ms4a7*
Matr3	*Meis2*	*Catip*	*Pdlim3*	*Mapk6*	*Myl9*	*Lrch4*	*Rmst*	*AI662270*
Gnai2	*Serpine*	*Pten*	*Itpr1*	*Sgk1*	*Rgs7bp*	*Fcgr4*	*Ceacam1*	*Lmnb1*
Ap2s1	*Stra6*	*Tinagl1*	*Ptrf*	*Slc2a1*	*Crip1*	*Ets1*	*Plekhs1*	*Hmgb2*
Mpp1	*Tes*	*P2ry14*	*Pi15*	*Coch*	*Id4*	*Hilpda*	*Padi1*	*Tyms*
Anxa6	*Dpysl3*	*Cpe*	*Ltbp1*	*Slc2a3*	***Myh11***	***Rgs4***	*Blnk*	*H2afx*
Cd63	***Col1a1***	*Hmha1*	*Ckb*	*Il1rn*	*Slc12a2*	*Cystm1*	*Pglyrp1*	*Wfdc21*
Ctla2a	*Eln*	*Ebf1*	*Atp1b2*	***Inhba***	*Olfml2b*	*Mxd1*	*Fxyd4*	*Slfn4*
mt-Co2	*Tspan6*	*Emid1*	*Cdc42ep3*	*Tnfrsf11b*	*Ifngr2*	*Traf1*	*Napsa*	*Pirb*
Naca	*Serpinf1*	*Mgst3*	*Zak*	*Pfkfb3*	***Olfr558***	*Irf5*	*Lrg1*	*Tlr7*
Smim14	*Thbs1*	*Dennd1*	*Rbpms2*	*Csf1r*	*Coro1a*	*Fabp5*	*Dlx5*	*Gm13479*
Steap4	*Gli2*	*Atp1b2*	*Sept6*	*Glrx*	*C1qc*	*Coro1a*	***Krt7***	*Cks1b*
Cdk12	***Cd55***	*Rasl12*	*Ptp4a3*	*Igsf6*	*Crispld2*	*Gcnt2*	***Krt19***	*Cks2*

Bag1	*Nme1*	***Pdgfrb***	*Gucy1a3*	***Mmp9***	*Map3k7cl*	*Ankrd3*	*Rnf128*	*Gas2l3*
Prpf39	*Pld4*	*Pck2*	*Myl9*	*Tlr7*	*Esam*	*Sdc1*	*Car2*	*9930022*
Trmt112	*AF2517*	*Pla2r1*	*Zfhx3*	*Ptges*	***Rgs4***	***Pdgfa***	***Muc1***	*Bst1*
Pet100	*Fcgr4*	*Esam*	*Tm4sf1*	*Ier3*	*Cd151*	*Itga1*	*Prom1*	*Fcgr3*
mt-Co3	*Fcgr3*	*Isg15*	*Ndrg2*	*Tbxas1*	*Tpm2*	*Phlda1*	***Epcam***	*Cdc25b*
Rpl13a	*Lsp1*	*Notch3*	*Epas1*	*Katnbl1*	*Cd44*	*Pdlim1*	*Alox15*	*Trem1*
Smdt1	***Fbln1***	*Ccrl2*	*Ehd4*	*1810011O*	*Tinagl1*	*Bhlhe4*	*Hdc*	*Pld4*
Rab9	*Pam*	*Tmem17*	*Ccdc107*	*Adm*	*Epas1*	*Ms4a7*	*Tlr1*	*Cd300lb*
Atp5g1	*Bok*	*Mef2c*	*Aspn*	*Gja1*	*Rftn1*	*Dennd1*	*Ifitm6*	*Lilrb4a*
mt-Nd2	*Tgfbr2*	*Snrk*	*Atp1a2*	*Bnip3*	*Nexn*	*AI6622*	*Plet1*	*Lilr4b*
Ppp1cc	*Fscn1*	*Timp3*	***Olfr558***	*Mmd*	*Ehd2*	*Csf3r*	*Lyz2*	*Lair1*
Secisbp	*Fkbp10*	*Cygb*	*Lbh*	*Ptpre*	*Tm4sf1*	*Nfkbia*	*Ctss*	*Cd84*
Por	*Pcolce*	*Vstm4*	*Hip1*	*Il1rap*	***Pdgfa***	*Mmp9*	*Laptm5*	*Stmn1*
Ndufb5	*Ccl2*	*Dtx3*	*Klf2*	*Gas2l3*	*Hacd1*	*Col5a3*	*Dgat2*	*Hmgn2*
Golgb1	*Cd83*	*Mndal*	*Mgst3*	*Uck2*	*Ms4a7*	*Esam*	*Cfb*	*C1qc*
Rcn1	*Tuba1a*	*Gjc1*	*Mical1*	*Smox*	*Retnlg*	*Maff*	*Hpgds*	*Dennd1c*
Pabpc1	*S100a16*	*Zeb2*	*4930523C*	*Sat1*	*C5ar1*	*Cd44*	*Lcp1*	*Retnlg*
Fis1	*Mtch1*	*Rrad*	*Mrvi1*	*Usp53*	*Cald1*	*Stab1*	*Slfn4*	*Csf2rb2*
Map1lc	*Saa3*	*Fpr2*	*Pdgfb*	*Abhd17c*	*Cycs*	*Rftn1*	*Fut9*	*Cd33*
Slc25a2	*Lgals9*	*Pld4*	*Gpr65*	*Neat1*	*Gcnt2*	*Apobec*	*Bcat1*	*C1qa*
Sytl2	***Col5a2***	*AF2517*	*Mrgpra2b*	*Hilpda*	*Flt1*	*Atf3*	*Msx1*	*Csf3r*
Tfpi	*Ier2*	*Gpr183*	*Nxpe5*	*Ifrd1*	*Cav1*	*Cxcl1*	*Gstm7*	*Dut*
Shisa5	*Penk*	*Mcemp1*	*F630028*	*Sdc4*	*Il6st*	*Mcl1*	***Krt8***	***Pcna***
Napa	*Dnajc25*	*Lrch4*	*Ccrl2*	***Tgfbi***	*Tpm1*	*Trim47*	*Tmc4*	*H2afz*
Vps18	*Txndc5*	*C1qb*	*Csrp2*	*Dhfr*	*Crem*	*Morf4l*	*Atp1b1*	*Ube2s*
Ccnt2	*Ppp3ca*	*Arhgap3*	*Blmh*	*Gadd45a*	*Slc25a5*	*Smad7*	*Cldn10*	*Arl6ip1*
Crebzf	*Fbln2*	*Fcgr4*	*Tpm2*	*Tnfaip2*	*Itga1*	*Tpi1*	*Ptpn18*	*Tubb4b*
Drap1	*Dennd4*	*Txnip*	*Mylk*	*Fem1b*	*Rgs16*	*Sept4*	*Spint2*	*2700094*
mt-Nd4	*Mfap2*	*Tbx3os1*	*Cd200*	*Clcn5*	*Anxa3*	*Ifngr2*	*Slc15a2*	*Tuba1b*
Cd34	*Pdia6*	*Nr2f2*	*Adamts5*	*Nrg1*	*Mustn1*	***Pdgfb***	*Sorl1*	*Tmpo*
Adam8	***Col12a1***	*Gm1388*	*Net1*	*Dcbld2*	*Cd300lb*	*Ptges*	*C3*	*Osm*
G0s2	*Fxyd5*	*Rasl11a*	*Cst3*	*Serpinb6b*	*Lmod1*	*Loxl2*	*C1qb*	*C3ar1*
Tcf4	***Pdgfra***	*Apobec1*	***Rgs4***	*Gsr*	*Clec4d*	*Plin2*	*Ucp2*	*C1qb*
Cmtm3	*Mdk*	*Gm1386*	*Rasl11a*	*Cxcl1*	*Col18a1*	*Pkm*	*Cd24a*	*Apold1*
Rpgrip1	*Ly6a*	*Tmem86*	*Tinagl1*	*Klf6*	*Emd*	*Igsf6*	*Anpep*	*Fabp5*
1810058	*Marcksl*	*Slc12a2*	*B930036N*	*Plaur*	*Got1*	*Wfdc21*	*Slc7a11*	*Hjurp*
Mkln1	*Rbp1*	*Arhgap1*	*Klhl23*	*Fam213a*	*Kcnab1*	*Slfn4*	*Cd14*	*Stab1*
Atp5g2	*Tmem16*	*Ddit4l*	*Cav1*	*Atp13a3*	*Ecscr*	*Itgb2*	*Ccl6*	*Nucks1*
Eif4a2	*Parva*	*Klhdc8b*	*Catip*	*Ankrd37*	*Rasl12*	*Pirb*	*Ezr*	*Cxcr4*
Uqcrh	***Col1a2***	*Rxfp1*	*Gm13889*	*Smad7*	*Igfbp7*	*Tlr7*	*Cd68*	*Ccdc34*
Ndufs2	*Slc6a6*	*Mrvi1*	*Tpm1*	*Akr1b8*	***Kcnj8***	*Gm134*	*Gpr65*	*C5ar1*
Cox5b	*Ostc*	*Cebpa*	*Spint2*	*Prdm1*	*Gng11*	*Birc3*	*Mrgpra2*	*Tlr1*
Anxa3	*Serpinh*	*Ech1*	*Inpp4b*	*Pdpn*	*Eln*	*Slc2a1*	*Nxpe5*	*Dhfr*
Snrpg	*Nr4a3*	*Ifi203*	*Bst1*	*Ccl3*	*Cyr61*	*Lrrfip1*	*F630028*	*Lsm2*
Ankrd11	*Igfbp6*	*Mpeg1*	*Fxyd1*	*Slc39a14*	*Tmem38b*	*Anxa1*	*Mapkapk*	*Il6*
Scamp3	*Sytl2*	*Gyg*	*Ncf2*	*Cks2*	*Plat*	*Pvr*	*Gsto1*	*Anp32e*
Mbtps2	*Ramp1*	*Etfb*	*Klhdc8b*	*Clu*	*Tubb4b*	*Plaur*	*Dennd1c*	*Tuba1c*
Rap2b	*Tubb6*	*Tmem10*	*Anxa11*	*Fam46a*	***Abcc9***	*Gng11*	*Cndp2*	*Dek*

Appendix 5-5. Top 100 upregulated genes in different mesenchymal cell types during endometrial repair.

Stromal	Vascular smooth muscle cells	Pericytes
Spp1	*Ren1*	*Mmp13*
Mmp10	*Il6*	*Hp*
Mmp13	*Cxcl1*	*Mmp9*
Col8a1	*Akr1b7*	*Cxcl2*
Chodl	*Ccl2*	*Mmp10*
Cxcl5	*Procr*	*Il6*
Nnat	*Postn*	*Il11*
Tnc	*Vcan*	*Inhba*
Serpine2	*Sdc1*	*Tnfrsf9*
Mmp3	*Ednrb*	*Stc1*
Cilp	*Fabp5*	*Mmp3*
Tgfbi	*Ccl11*	*Tnc*
Sfrp1	*Saa3*	*Serpine1*
Cxcl1	*Tnc*	*Saa3*
Fst	*Ctsc*	*Slc2a1*
Ifitm1	*Olfml2b*	*Tfpi2*
Col12a1	*Apold1*	*F3*
Itm2a	*Loxl2*	*Ddit4*
Ier3	*Tubb6*	*Ptges*
Mgp	*Fhl2*	*Hilpda*
Hspb1	*Hspa5*	*Cxcl1*
Timp1	*Thy1*	*Maff*
Tes	*Manf*	*Slc16a3*
Frzb	*Adamts2*	*Cks2*
Saa3	*Ifitm1*	*Ier3*
Ednra	*Fn1*	*Mt2*
Sod2	*Nid1*	*Arhgdib*
Fam213a	*Marcks*	*Basp1*
C1qtnf7	*Meg3*	*Flt1*
Mt2	*Tpm4*	*Ero1l*
Id3	*Col1a1*	*Ecscr*
Tagln	*Pdia6*	*Itgav*
Pdpn	*Actg2*	*Sod2*
Tubb4b	*Hsp90b1*	*Hmox1*
Pde10a	*Nme1*	*P4ha2*
F2r	*Crispld2*	*Nfkbia*
Fxyd5	*Phlda1*	*Apold1*
Eln	*Pdlim1*	*Bhlhe40*
Acta2	*Gas1*	*Lmcd1*
Basp1	*Fstl1*	*Sdc1*
Cyr61	*Pdia4*	*Tubb6*
Hspa5	*Dnajb11*	*Ndrg1*
Serpinb1a	*Col18a1*	*Chst2*

Nme1	*Kdelr3*	*Hspb1*
Socs3	*Sparc*	*Srgn*
Thy1	*Plac8*	*Timp1*
Actn1	*Serpinh1*	*Higd1a*
Manf	*Sep-04*	*Serpinb6b*
Tubb6	*Kcnj8*	*Got1*
Pdgfrl	*Morf4l2*	*Twist2*
Vcan	*Tmem167*	*Rgs16*
Pmepa1	*Pdia3*	*Akr1b8*
Cycs	*Cnn3*	*Smad7*
Fxyd6	*Calr*	*Hspa1a*
Aldh1a2	*Cycs*	*Morf4l2*
Tspan6	*Ostc*	*Cebpb*
Igfbp4	*Vmp1*	*Lrrfip1*
Pam	*S100a4*	*Procr*
Fzd1	*Rcn1*	*Mcl1*
Tpm4	*Xbp1*	*Plin2*
Mmd	*Cebpb*	*Hif1a*
Lgmn	*Plat*	*Thbs1*
Gsto1	*Col4a2*	*Manf*
Klf2	*Col4a1*	*Pdgfa*
Hsp90aa1	*Ckap4*	*Bnip3*
Emp1	*Hspa1a*	*Ednrb*
Ckap4	*Id3*	*Rhoc*
Morf4l2	*Dnajc3*	*Phlda1*
Thbs1	*Col5a2*	*Mgp*
Ran	*Kdelr2*	*Mt1*
Hsp90b1	*Tuba1a*	*Wnt5a*
Srsf3	*Igfbp4*	*Sat1*
Ldha	*Calu*	*Znrf1*
Sec13	*Sec61b*	*Pdlim1*
Loxl1	*Cmtm7*	*Ctsc*
Dclk1	*Ran*	*Loxl2*
Golga7	*Rpn2*	*Col5a3*
Higd1a	*Tagln2*	*Oaf*
Ranbp1	*Maged2*	*Msn*
Calm1	*Sod2*	*Pgam1*
Ccl2	*Socs3*	*Anxa2*
Vimp	*Anxa2*	*Hspa5*
Sfrp4	*Tubb4b*	*Cystm1*
Arpc1b	*Higd1a*	*Ldha*
Cacybp	*Col3a1*	*Tpi1*
Ier2	*Sec13*	*Errfi1*
Eif1a	*Ifitm3*	*Adamts4*
Fkbp10	*Arf4*	*Actg1*
Ostc	*Rgs5*	*Cyr61*
Nfkbia	*Tram1*	*Vmp1*

Serp1	*Cd302*	*S100a6*
Tuba1a	*Nfkbia*	*Fstl1*
Vmp1	*Serp1*	*Tpm4*
Xbp1	*Canx*	*Nid1*
Ostf1	*Shisa5*	*Snx18*
Dnajb11	*Vimp*	*P4ha1*
Tpm1	*Mmp14*	*Anxa1*
Pdlim1	*Ctsb*	*Id3*
Man2a1	*Ifngr2*	*Emp1*
Pdia6	*Hsp90aa1*	*Pkm*

Appendix 6. Publications relating to this thesis.

Cousins, F. L. & Kirkwood, P. M., Saunders, P. T. & Gibson, D. A. (2016) Evidence for a dynamic role for mononuclear phagocytes during endometrial repair and remodelling. *Sci Rep,* 6, 36748 (Appendix 6).

Cousins, F.L., Kirkwood, P. M., Murray, A. A., Collins, F. Gibson, D.A. & Saunders, P.T (2016) Androgens regulate scarless repair of the endometrial "wound" in a mouse model of menstruation. *FASEB J,* 30, 2802-11.